Photocatalytic Tryptophan Alkylation for Chemoselective Peptide Modification

Joanna Lee

14249733

Dr James Cuthbertson

Dr Nicholas Mitchell

Declaration

I hereby declare that I am the author of this thesis, and the work described therein was carried out by myself, unless otherwise indicated in the text. The following thesis contains results reported in the publication: Chemoselective Late-Stage Functionalization of Peptides via Photocatalytic C2-Alkylation of Tryptophan.[1]

Acknowledgments

I would like to begin the report by thanking everyone who has helped me throughout my PhD. First, I would like to thank my supervisors Dr James Cuthbertson and Dr Nicholas Mitchell for providing me with constant support and guidance over the years. They have taught me a lot and I am truly grateful for how they have helped develop my career as a scientist. An additional thanks goes to Dr Liam Ball for being my internal assessor offering me great advice and feedback which aided my research and prepared me for the thesis submission and viva.

I would also like to thank the Mitchell research group members and members of C17: Rhys, Andrea, Salwa, Lola, Tom, Sarah and Enrico who created a fun and supportive lab environment. I'd especially like to thank Dr Fran Smith for her daily support in and out the lab, scientifically and mentally, I'm lucky to have made a friend for life.

The PhD would not have been possible without funding, so a special thank you goes to the EPSRC CDT and University of Nottingham and to all the staff who keep the lab running: Jim and Eric made sure we never ran out of consumables. Also, a thank you is owed to all the technical staff: Kev, Shaz, Huw, Ben, Tong and Lola for maintaining the instruments which was crucial for acquiring data throughout this research.

Finally, a massive thank you to my family who have supported me not only through my PhD but my whole life! I am so appreciative of them especially for putting up with me when I'm high on caffeine and low on sleep, this milestone is as much their achievement as my own.

Abstract

A chemoselective peptide functionalisation strategy *via* photocatalytic tryptophan (Trp) modification has been developed. The versatility of the reaction is demonstrated by tethering a variety of difluoroalkyl groups to Trp using an organic photocatalyst and short irradiation times with visible light (**Scheme 1A**). Due to the mild and biocompatible reaction conditions, a range of complex peptides have been successfully functionalised to give a diverse library of small molecule-peptide conjugates. Results have confirmed site-selectivity for Trp in the presence of other amino acids, illustrating that this transformation can expand the field of chemoselective photo-bioconjugation. Applications of the methodology have been explored including protein modification and peptide stapling. For the latter, incorporation of the bromodifluorocarbonyl moiety into the peptide sequence during solid phase peptide synthesis (SPPS), enabled the synthesis of macrocyclic peptides (**Scheme 1B**).

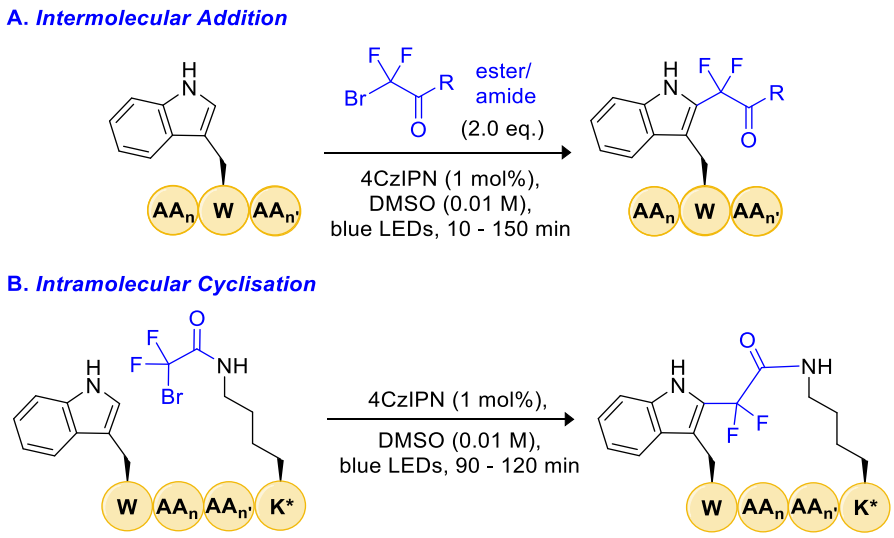

Scheme 1. Photocatalytic difluoroalkylation of Trp: A. Intermolecular addition to give small molecule-peptide conjugates. B. Intramolecular cyclisation to give peptide macrocycles.

Abbreviations

Å	angstrom(s)
Ac	acetyl
aq	aqueous
Ar	aryl
atm	atmosphere(s)
Bn	benzyl
bpy	2,2′-bipyridyl
Boc	*tert*-butoxycarbonyl
n-Bu	butyl
Bz	benzoyl
°C	degrees Celsius
calcd	calculated
CD	circular dichroism
cm	centimeter(s)
cm^{-1}	wavenumber(s)
COSY	correlation spectroscopy
4CzIPN	1,2,3,5-tetrakis(carbazol-9-yl)-4,6-dicyanobenzene
CFL	compact fluorescent lamp
CV	cyclic voltammetry
δ	chemical shift in parts per million downfield from tetramethylsilane
3DPAFIPN	2,4,6-tris(diphenylamino)-5-fluoroisophthalonitrile
DMA	dimethylacetamide
DMF	dimethylformamide

DMSO	dimethyl sulfoxide
EI	electron impact
eq.	equivalent
ESI	electrospray ionization
Et	ethyl
Fmoc	9-fluorenylmethoxycarbonyl
g	gram(s)
GSH	glutathione
h	hour(s)
HAA	hydrogen atom abstraction
HMQC	heteronuclear multiple quantum correlation
HOMO	highest occupied molecular orbital
HPLC	high-performance liquid chromatography
HRMS	high-resolution mass spectrometry
HSQC	heteronuclear single quantum correlation Hz hertz
$Ir(ppy)_3$	*tris*[2-phenylpyridinato-C^2,*N*]iridium(III)
IR	infrared
J	coupling constant (in NMR spectrometry)
k	kilo
LED	light-emitting diode
lit.	literature value
LUMO	lowest unoccupied molecular orbital
μ	micro
m	multiplet (spectral); meter
M	molar (moles per litre)

M^+	parent molecular ion
MALDI	matrix-assisted laser desorption ionization
Me	methyl
MHz	megahertz
min	minute(s)
mM	millimolar (millimoles per litre)
MO	molecular orbital
mol	mole(s)
mp	melting point
MS	mass spectrometry
MW	molecular weight
m/z	mass-to-charge ratio
nm	nanometer(s)
NOE	nuclear Overhauser effect
NOESY	nuclear Overhauser effect spectroscopy
ppm	part(s) per million
PDC	peptide drug conjugate
PK	pharmacokinetics
Pr	propyl
i-Pr	isopropyl
TEEDA	*N*,*N*,*N*′,*N*′-tetraethylethylenediamine
TFT	α,α,α-trifluorotoluene
rel	relative
Rt	retention time (in chromatography)
rt	room temperature

SET	single electron transfer
SN_1	unimolecular nucleophilic substitution
SN_2	bimolecular nucleophilic substitution
SOMO	single-occupied molecular orbital
T	temperature in units of degrees Celsius (ºC)
TFA	trifluoroacetic acid
THF	tetrahydrofuran
TOF	time-of-flight
UV	ultraviolet

Contents

1 Introduction 1
1.1 Applications of Modified Peptides 3
1.2 Bioconjugation 18
1.3 Peptide Cyclisation 30
1.4 Photocatalysis 44
1.5 Photochemical Modification of Trp 45
1.6 Project Aims 55
2 Reaction Optimisation 56
2.1 Photocatalytic Difluoroalkylation 56
2.2 Photocatalytic Difluoroalkylation Analysis 59
2.3 Photocatalytic Difluoroalkylation Conditions 63
3 Reaction Development and Application 90
3.1 Probe Scope 90
3.2 Photocatalytic Diflluoroalkylation of Ac-Trp-OEt 100
3.3 Reaction Rate 110
3.4 Difluoroalkylation of Ac-WHISKEY-NH_2 127
3.5 Chemoselectivity for Trp 145
3.6 Difluoroalkylation of Other Trp-Containing Peptides 152
3.7 Photocatalytic Modification of β-Casein 170
4 Peptide Stapling 185
4.1 Reaction Development 186
4.2 Synthesis of macrocycles 194
5 Overall Conclusions and Future Work 212
6 Experimental 217
6.1 Optimisation studies with Ac-Trp-OEt 223
6.2 Synthesis of Radical Precursors 225
6.3 Biomolecule Synthesis 236

6.4 Photochemical Alkylation of Ac-Trp-OEt 255

6.5 Photochemical Alkylation of Trp-containing Peptides and Protein 269

6.6 Photochemical Stapling of Trp-Containing Peptides 308

7 References 316

8 Appendix 332

1 Introduction

Over the past two decades, peptides have gained increasing attention from the pharmaceutical industry by bridging the gap between small molecule and protein therapeutics.[2] Commercial drugs can be split into two categories: traditional 'small molecule' drugs (<500 Da) or the much larger 'biologics' (>5000 Da) including therapeutic proteins and antibodies. Peptides fall in between these two categories, combining the advantages of each: membrane permeability and oral bioavailability plus selective binding to cell surface receptors with high affinity.[3] Peptides also avoid some drawbacks such as the high cost associated with larger biologic production, and side-effects resulting from reduced target selectivity associated with small molecules.[4]

Unfortunately, peptides have limitations including poor metabolic stability and short half-lives, resulting in rapid clearance through the body.[3] However, non-proteinogenic modifications of peptides i.e. covalent addition of functional groups after peptide synthesis,[5] have been successful at overcoming these downfalls. Polyethylene glycol (PEG) conjugation is the most common strategy employed for half-life extension,[6] and glycosylation (attachment of a sugar group) can improve membrane permeability, therefore in both cases pharmacokinetic (PK) activity is enhanced compared to the natural peptide analogue.[7,8]

Alternatively, peptide conjugation can be utilised as a drug delivery strategy for small molecules which lack specificity. Peptide-drug conjugates (PDCs) transport the cytotoxic small molecule to a specific peptide receptor, which avoids side effects resulting from the drug interacting with healthy tissues.

Certain peptide receptors are overexpressed in tumour cells and absent in healthy cells, which allows the selective delivery to diseased cells and subsequent receptor-mediated endocytosis (**Figure 1A**).[7] Additionally, the peptides can be easily synthesised due to their small chain length using well established solid phase peptide synthesis (SPPS): many are only 2-20 amino acids long.[9,10]

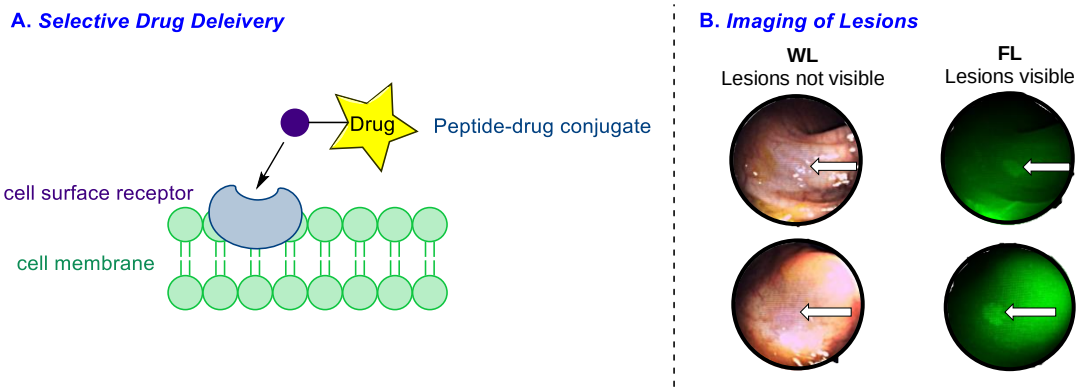

Figure 1. Applications of functionalised peptides: A. Receptor selective drug delivery of a drug conjugated to a peptide. B. White light (WL) and fluorescent light (FL) images of lesions highlighting how the use of a peptide-fluorophore conjugate enhanced the visibility of these lesions.[11]

Drugs are not the only type of small molecule that can benefit from selective delivery: certain clinical imaging techniques rely on fluorophores covalently bonded to peptides.[12] Similarly to PDCs, the peptide targets a receptor that is overexpressed on diseased cells, but instead of triggering cell death, the fluorophore presents a signal at the desired site. Following visualisation using fluorescence microscopy, this non-invasive technique can be used to detect diseases, hence identify the most appropriate treatment, aiding therapy success.[12] For example, a peptide-fluorophore conjugate is used to detect colon cancer lesions by targeting the overexpressed receptor c-Met, whereas alternative imaging techniques such as white-light endoscopic procedures can often miss these early signs because the receptor is not easily visible (**Figure 1B**).[11]

Therefore peptide modification can contribute to different fields within the pharmaceutical industry acting as therapeutics, carriers for selective delivery of a 'payload' or as biological tools.[13] Following this overview, reported below are specific examples of modified peptides highlighting their importance and impact on society.

1.1 Applications of Modified Peptides

Peptide functionalisation relies on the selective targeting of the canonical amino acids which can be challenging due to the vast array of amino acid functionality. However successful strategies are available allowing the synthesis of: therapeutic peptides with enhanced pharmacokinetic and dynamic properties, peptide-drug conjugates (PDCs) for targeted delivery and peptide-fluorophore conjugates for visualisation and diagnostic imaging.[14] Cyclised peptides and fluorinated biomolecules will also be discussed because these examples highlight the potential applications of products generated using the methodology developed in this PhD.

Therapeutic Peptides

Therapeutic peptides generally have molecular weights between 500-5000 Da and have been used in a diverse range of medicinal areas including respiratory, pain and cardiovascular.[4,15,16] Natural or modified peptides can be used as therapeutics, but the latter is generally more successful, and their synthesis can be achieved chemically (SPPS), biologically (recombinant expression) or semi-synthetically.[17] From a 2022 review outlining current applications of therapeutic peptides there are more than 170 peptides in active clinical development and many more in preclinical studies.[4]

Insulin was the first therapeutic peptide isolated and subsequently became the first commercial peptide drug which manages blood glucose levels in diabetic patients.[4] Since then other peptide hormones have been used as therapeutics including glucagon-like peptide Exenatide **1**, brand name Byetta, which was approved in 2005 as a treatment for patients with type 2 diabetes. This peptide acts as a GLP-1RA receptor agonist, administered as either a short- or long-term formulation (daily or weekly) to provide remarkable improvements in blood glucose and weight control.[18] The peptide sequence consists of 39 amino acids and was derived from Gila Monster venom.[4]

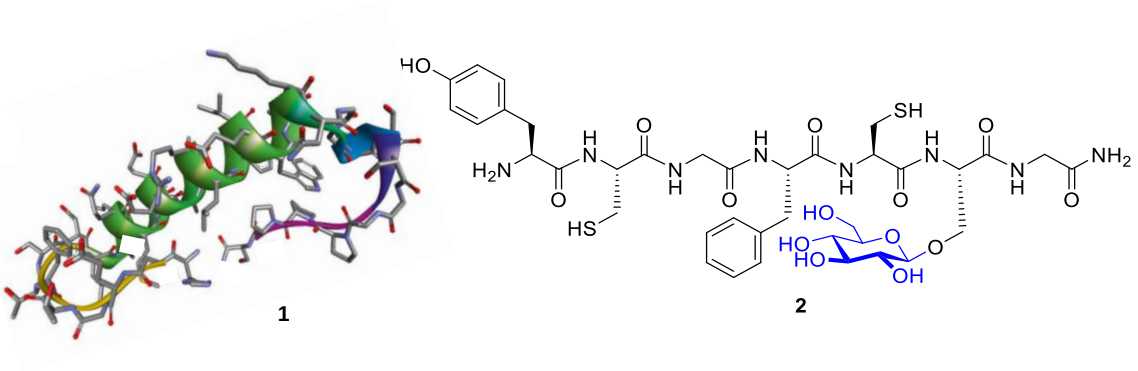

Figure 2. Structures of therapeutic peptides: Exenatide **1** and glycosylated peptide **2**.

More recently, peptide drugs have been extended beyond hormone mimics, but this usually requires modification to improve their PK properties. For example, small peptide drugs often have inadequate membrane permeability preventing them from reaching the desired target. This is especially challenging for neurological targets due to the blood-brain barrier (BBB).[7] Hruby and co-workers combatted this by attaching β-D-glucose to peptide sequences because the sugar is actively transported into the brain.[19] Analogues of enkephalin (a pentapeptide involved in regulating the pain sensation) were successfully glycosylated through the incorporation of a serine residue bonded to glucose (Ser(Glc)). Peptide **2** showed increased

PK activity *in vivo*, resulting from the attachment of the glycoside but also its specific placement. It was revealed that the most active glycosylated peptides showed comparable antinociceptive effects to morphine.[19]

Therapeutic peptides are not expected to replace small molecule drugs, instead they will help expand the toolbox of therapies available to successfully treat diseases. Additionally, peptides and cytotoxic small molecules can work together *via* conjugation to combine the best properties of each: peptide-drug conjugates (PDCs).

Peptide-Drug Conjugates

Small molecules are undeniably important in therapeutic and diagnostic applications as their small nature generally allows passage across cell membranes *via* diffusion from an area of high concentration (outside the cell) to an area of low concentration (inside the cell).[20] On the other hand often short half-lives and widespread distribution is observed,[13] which is where biologics possess the more favourable properties.[21] Another contributing factor to drug development is cost and small molecules are considerably easier and cheaper to manufacture owing to their less complex structures, a greater number of competitors in the market and readily accessible drug availability in pharmacies. Whereas biologics tend to have very sensitive, specific manufacturing processes and administration is generally as an injection in a hospital.[21] An investigation into ten pharmaceutical companies was carried out by Boston Consulting Group who disclosed that the average production cost per pack differed by $55 between small molecules and biologics ($5 and $60 respectively).[22]

One strategy to combine the favourable properties of both small molecules and biologics is through peptide conjugation synthesising peptide-drug conjugates. Due to the affinity and specificity of the peptide for a particular target, therapeutic agents can be delivered more selectively, reducing off-target side reactions and overall providing a highly potent medicine with fewer side-effects.[23] Furthermore peptide conjugation can enable delivery to sites which are inaccessible to bulky proteins.[13]

Somatostatin is a peptide growth hormone inhibiting hormone (GHIH), produced by paracrine cells, which can suppress the growth of many different cancer cells. However, somatostatin analogues are more commonly used as clinical treatments for pancreatic and vasoactive intestinal peptide-secreting tumours,[24] due to their enhanced selectivity. Octreotide is an analogue of interest because it has been successfully conjugated to the radioactive isotope 177Lu: a chemotherapeutic agent which induces tumour death by peptide receptor radionuclide therapy (PRRT).[25] The name of this conjugated product is 177Lu-Dotatate **3** (**Figure 3**) which achieved high potency with greater than a hundredfold selectivity through targeted radioisotope therapy,[26] hence has been approved for the treatment of gastroenteropancreatic neuroendocrine tumors.[27] This peptide-drug conjugate combined the inherent anticancer property of somatostatin but lowered the radioactive toxicity, enhancing the therapeutic efficacy and safety of somatostatin or radiotherapy individually.[23]

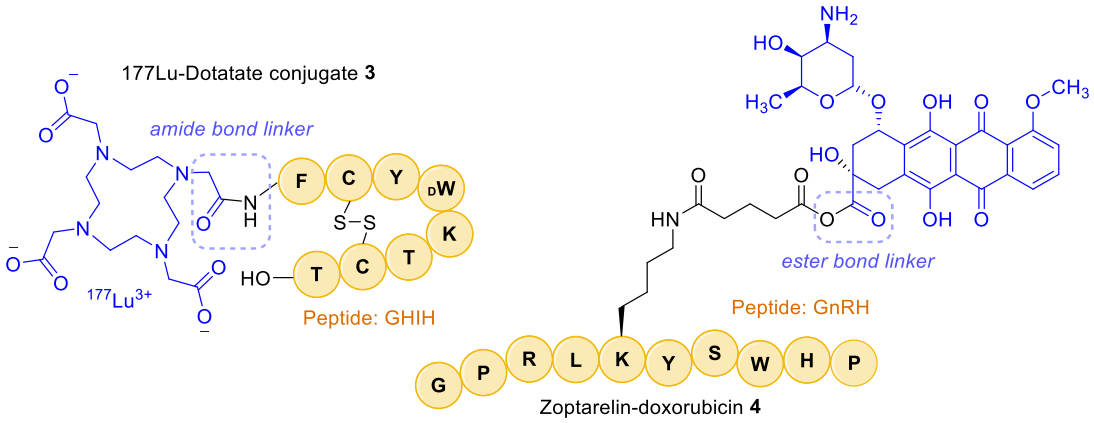

Figure 3. Peptide drug conjugates 177Lu-Dotatate **3** and Zoptarellin-doxorubicin **4**.

Another example involves a hypothalamic peptide hormone conjugated to the small molecule drug doxorubicin *via* an ester bond and glutaric acid spacer: Zoptarelin-doxorubicin **4** (**Figure 3**).[13] This peptide hormone is a gonadotropin-releasing hormone (GnRH) and a variety of endocrine cancers such as ovarian, breast and prostate express the GnRH receptor, therefore these cancer cells present a target for oncolytic drugs.[28] Studies carried out on mouse tumour models revealed that the peptide-drug conjugate inhibited cell proliferation more effectively than doxorubicin alone, and was more potent than either individual component of the conjugate.[23,29]

Natural product peptides are continuously being discovered providing a library of bioactive peptides with known receptor targets, aiding the development of peptide-drug conjugates.[30] Due to variety of available conjugation methods,[7] the combination of peptide and drug is not limited to only one therapeutic product, in fact combining octreotide from peptide-drug conjugate (PDG) **3** with doxorubicin from PDG **4** provided a new PDG **5** which can be used as a potent and selective antitumor agent (**Figure 4**).[9]

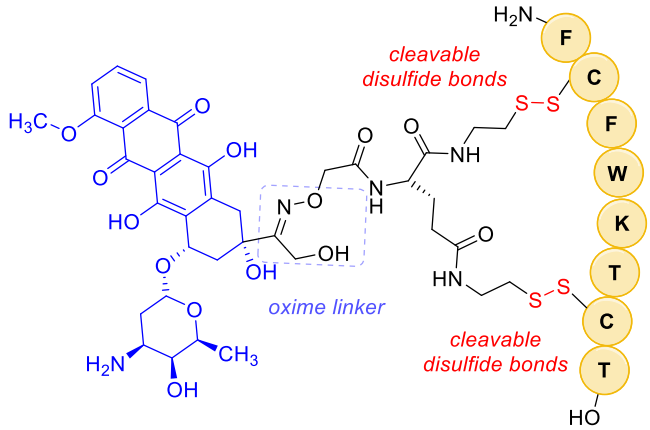

Figure 4. Cyclic peptide drug conjugate octreotide-doxorubicin **5**.

Peptide Cyclisation

A novel feature of the octreotide-doxorubicin conjugate **5**, reported by Lelle and co-workers, is the linker reagent which forms two cleavable disulfide bonds, *via* the terminal cysteines on octreotide.[9] As mentioned previously, tumour cells overexpress somatostatin receptors and octreotide has a high affinity for these receptors.[7] However, using peptides as drug delivery agents can be challenging because their small size can allow facile degradation by proteases in the blood.[7] Notably, the octreotide-doxorubicin conjugate contains a macrocyclic peptide and generally cyclic structures have a greater resistance to proteolytic cleavage compared to their acyclic counterparts.[31] Preventing premature cleavage allows doxorubicin to be delivered selectively to the target cancer cells and successful reduction of the disulfide bonds (under intracellular conditions) allows efficient release of the drug molecule. Therefore when cytotoxicity assays were carried out on pancreatic and breast cancer cell lines, as expected, the hybrid was more selective and potent than the octreotide or drug alone.[9] This peptide

macrocycle was synthesised chemically, whereas there is an abundance of naturally occurring macrocyclic peptides with biological activities.

Bioactive peptides can be extracted from numerous sources including marine sponges or meat and milk products. Focusing on marine sources such as sponges and mollusks, a wide variety of bioactive peptides have been discovered, with anticancer and anti-inflammatory properties.[30] For the former, cell death is stimulated by, but not limited to, apoptosis, cytotoxic effects and antiproliferative effects.[32] Three examples of cyclic, anticancer peptides are shown in Figure 5.

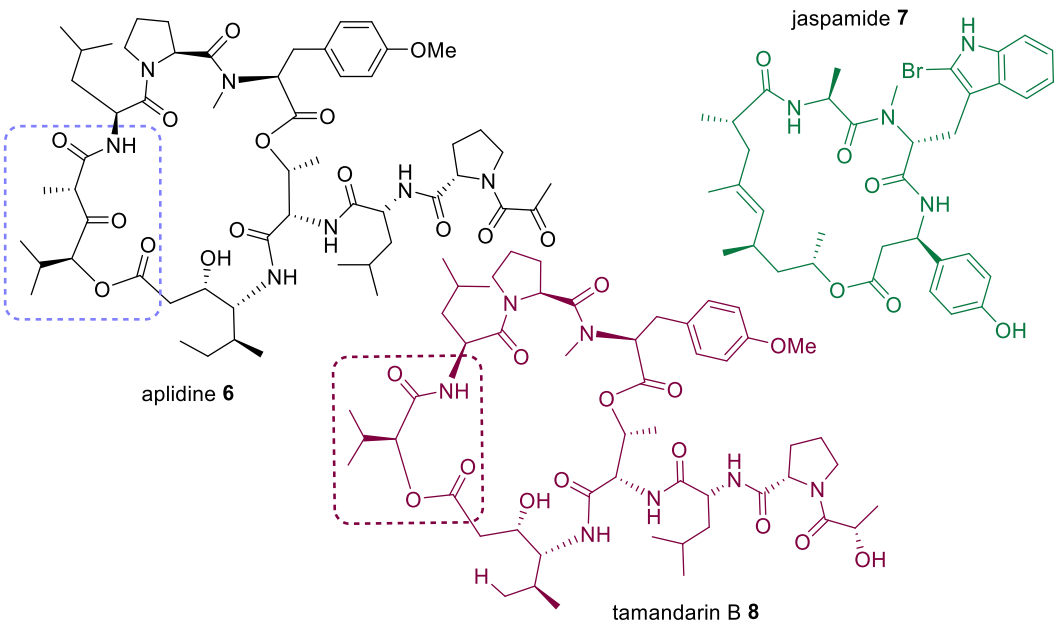

Figure 5. Structures of three cyclic anticancer peptides: aplidine **6**, jaspamide **7** and tamandarin B **8**.

Aplidine (also known as plitidepsin) **6** has been shown to inhibit cell growth and induce apoptosis in human leukemia cell line MOLT-4.[33] More recently, aplidine has been studied as a potential treatment of COVID-19, demonstrating potent efficacy against SARS-CoV-2.[34] This highlights that one cyclic peptide may have the potential to provide multiple therapeutic treatments. Secondly, jaspamide **7** can also induce apoptosis in human

leukemia cells HL-60.[35] Despite the therapeutic potential of bioactive peptides, it is challenging to extract sufficient quantities required for testing and their purification is often difficult.[36]

Considering they are small peptides usually ranging between 2 and 20 amino acids,[37] chemical synthesis can provide an alternative route to these bioactive peptides. However, such routes can be long and complex limiting the development of analogues which is the case for aplidine particularly because of the moiety highlighted by the blue box in figure 5.[38] Alternatively, tamandarin B **8**, exhibiting a very similar structure, hence antitumour activity comparable to aplidine,[39] is more easily synthesised. Joullié and co-workers carried out the total synthesis of four analogues of the marine cyclic peptide tamandarin B **8** and investigated their anticancer properties.[40] With this strategy, structure-activity relationship can be evaluated potentially providing more potent or selective analogues, along with the opportunity for scale up chemistry to be carried out when commercialising a successful drug.

Peptide-Fluorophore Conjugates

Like peptide-drug conjugates, linear or cyclized peptides can be used to transport fluorophores to a specific receptor for disease detection either for early diagnosis or for monitoring biological processes.[12] A variety of techniques can be used to visualize the fluorophore including near-infrared fluorescence imaging,[41] and for the example discussed later, single molecule array (SiMoA) technology.[42]

Fluorophores can be split into four categories: organic dyes, metal complexes, biological fluorophores and quantum dots; the organic dye BODIPY has been used for the imaging of bacteria and fungi (**Figure 6**).[12]

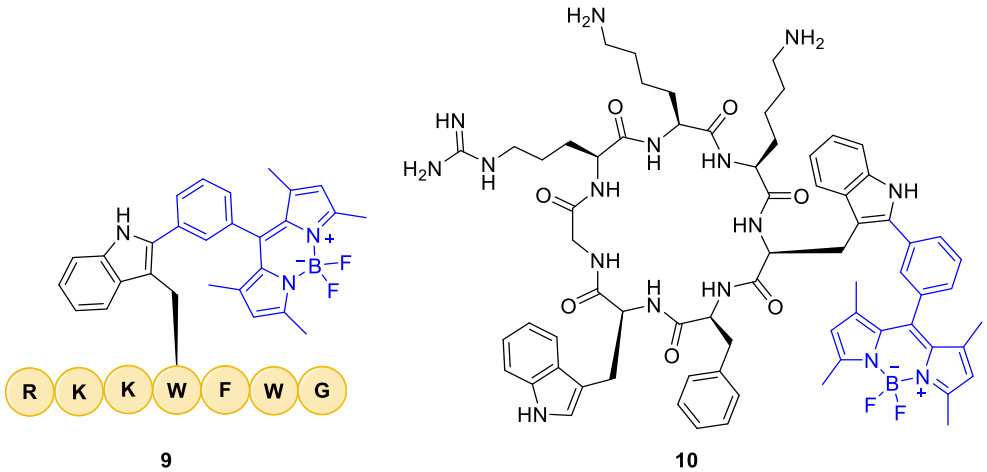

Figure 6. Linear **9** and cyclised **10** analogues of Trp-BODIPY peptide.

The pathogen responsible for the fungal infection invasive pulmonary aspergillosis can be detected using an antimicrobial heptapeptide conjugated to the dye (**Figure 6**) combined with multi-photon fluorescence microscopy.[43] Vendrell and co-workers carried out numerous assays comparing the linear peptide-BODIPY conjugate **9** and the cyclised example **10**. It was reported that macrocyclic peptide **10**, showed a high selectivity for bacterial cells over human cells and a greater affinity for fungal cells compared to the linear analogue **9**.[43] A peptide's conformational flexibility is often restricted by cyclisation, which can enhance affinity and activity.[44] Additionally the full potential of peptide-fluorophore conjugate **10** was explored by investigating the staining of different fungal strains. Most receptors were stained successfully, although a variation in fluorescence was observed demonstrating that macrocycle **10** has the potential to detect numerous fungal infections.[43]

Instead of fluorescence microscopy, Walt and co-workers used a modified version of their SiMoA assay as a non-invasive technique to detect thrombosis, a disease with few available biomarkers.[42,45] Current diagnosis relies on blood or urine samples containing byproducts from the clotting cascade but often clinically useful results are not obtained.[46,47] This research was driven by the aim to achieve detection at microdose levels for early detection (**Figure 7**).

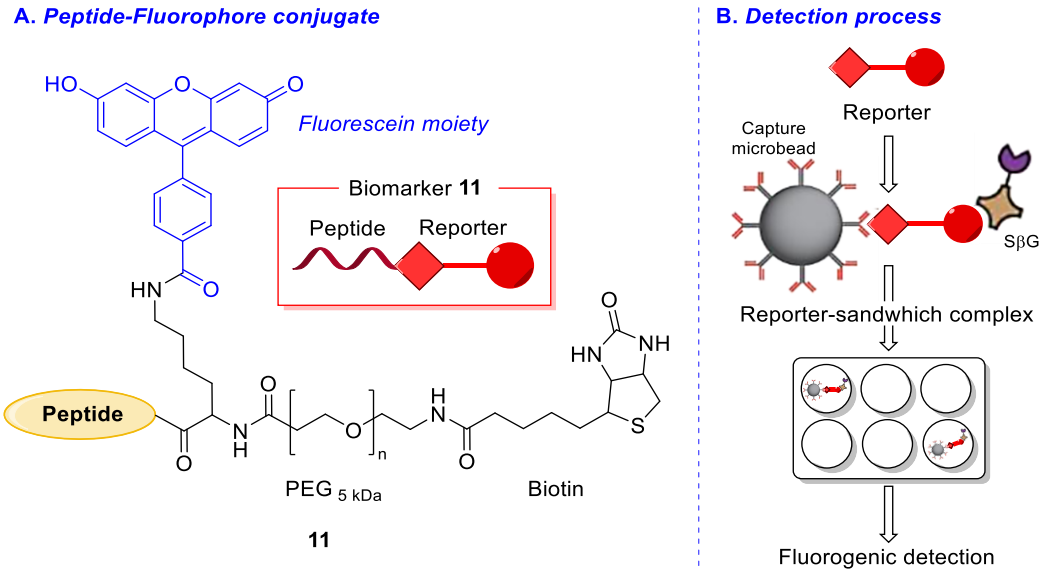

Figure 7. A. Structure of the synthetic biomarker **11**. B. A simplified overview of the steps in which the reporter undergoes to enable detection. Figure adopted from Walt and co-workers'.[42]

This was achieved by combining their existing technology (SiMoA) with synthetic biomarkers: a mouse was injected with the synthetic biomarker **11**, which in the presence of disease-associated proteases would release reporters allowing their removal by urine excretion.[42] Key features of the reporter include a non-degradable PEG spacer to provide favourable pharmacokinetics and the fluorescein is used to immobilize the reporter for capture through the attachment on antibody-coated beads (**Figure 7**). Also, biotin is crucial for femtomolar-scale detection following conjugation with the enzyme streptavidin β-galactosidase (SβG) creating a reporter-

sandwich complex. The antibody beads and enzyme are added to the urine sample which is then loaded into arrays of ~50,000 wells for fluorogenic detection (**Figure 7**).

Owing to the ultrasensitive nature of the SiMoA assay (sensitive enough to detect a single sandwich complex), a simple, low cost and safe diagnosis of thrombosis was achieved. The possibility of targeting other disease-specific proteases is possible providing femtomolar detection of cancers, fibrosis, and inflammatory disorders.[42]

Fluorination of biomolecules

Instead of detecting fluorescence, an alternative imaging technique is positron emission tomography (PET) which uses radioactive molecules to visualise abnormalities resulting from diseases. Mentioned previously was the radioactive isotope lutetium-177 (177Lu),[25] but fluorine-18 can also be used: [^{18}F]fluoro-2-deoxyglucose (FDG) **12**. One standard practice for staging cancers of the esophagus is FDG-PET imaging, either for detection alone or for measuring the tumour volume which can aid radiotherapy treatment.[48] Specifically when combined with CT imaging (FDG-PET/CT) the detection of proximal gastric cancer was achieved (**Figure 8**) and more importantly occult liver metastasis was observed which is not often seen using conventional CT imaging.[48] A PET scan shows molecular activity and is more sensitive than a CT scan, therefore can generally identify lesions at earlier stages.

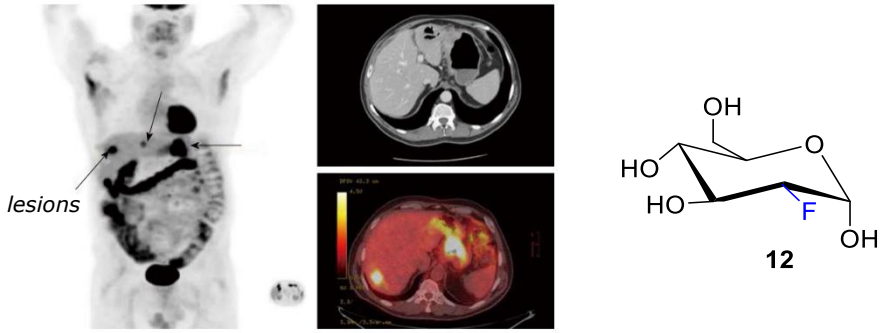

Figure 8. FDG-PET/CT image of a patient with proximal gastric cancer and occult liver metastasis,[48] and the structure of FDG.

The radioisotope fluorine-18 has to be synthesised using a cyclotron with proton irradiation of the naturally occurring oxygen isotope: ^{18}O,[49] whereas naturally occurring fluorine-19 also has its merits when using fluorine NMR spectroscopy.[50]

Fluorine is an important probe for evaluating biological systems: protein conformational changes, enzyme mechanisms, and various protein interactions can be analysed using NMR spectroscopy.[50] Owing to the high sensitivity of the ^{19}F nucleus and the much greater chemical shift span compared to the ^{1}H nucleus (~400 ppm and ~15 ppm respectively),[51] peaks have a greater dispersion in chemical shift resulting from changes affecting the local environment of a peptide or protein. The incredibly low abundance of ^{19}F in biological systems reduces the chances of signals overlapping in the spectrum, which is a problem for NMR spectroscopy experiments using ^{1}H, ^{13}C and ^{15}N nuclei. A disadvantage of this technique, however, is line broadening which weakens the signals; however, this is not exclusive to ^{19}F and is also an issue for other nuclei. In order to study these interactions, the incorporation of at least one fluorine atom is required, usually at a specific position within the biomolecule. One of the most common ways to install a fluorine is by utilising commercially available fluorinated amino

acids (**Figure 9**). However, addition of fluorine as a late-stage functionalisation strategy would provide a beneficial alternative.

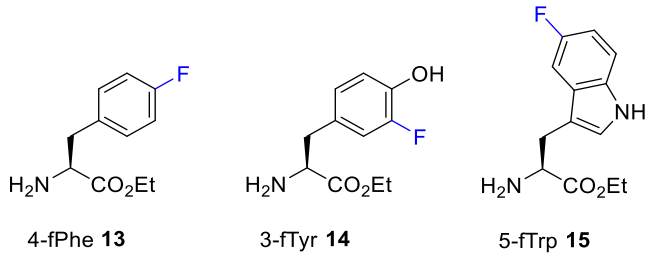

Figure 9. A selection of commercially available fluorinated amino acids.[50]

Vogel and co-workers took advantage of *para*-fluoro-Phe (pfF) **13** and 3-fluoro-Tyr (3fY) **14**, in their research to synthesise analogues of tritrpticin, an antimicrobial peptide (AMP), and study their effects on peptide-membrane interactions.[52] Because bacterial membrane surfaces have been identified as targets for this AMP,[53] these interactions could relate to the activity of tritrpticin; however, a simplified alternative to bacterial membranes was used for their experiments: SDS micelles.

Fluorine NMR spectroscopy first revealed conformation differences between AMPs in aqueous solution or when bound to SDS micelles (**Figure 10**). Tritrpticin (bearing no fluorine atoms) would not be visible in the ^{19}F spectrum therefore an analogue was synthesised replacing its phenylalanine residues with pfF: GTVRR(**pfF**)PWWWP(**pfF**)LRR **16**. Interestingly in an aqueous solution four intense peaks were observed for **16** (**Figure 10A**), instead of the expected two. This can be attributed to peptide conformers: when Pro residues are present cis/trans insomerisation can occur.[54] This was eliminated when the peptide was bound to SDS micelles (**Figure 10B**) highlighting how peptide conformation can be influenced by interactions and how NMR spectroscopic analysis had the ability to show this. [52]

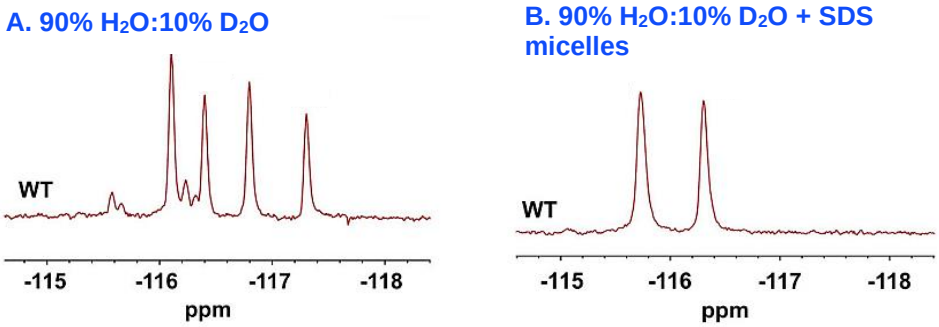

Figure 10. ^{19}F NMR spectra, zoomed in to the region between −115 and −119 ppm, for the wild type (WT) AMP **16** in A. aqueous solution and B. when bound to SDS micelles.[52]

Furthermore, evaluating the changes in chemical shift values between 10% D_2O compared to 90% D_2O can be used to identify the location of residues with respect to the SDS micelles.[55] For this study tritrpticin analogues GTVRRYPWWWP(**pfF**)LRR **17** with one pfF and GTVRRFPWWWP(**3fY**)LRR **18** incorporating 3fY were assessed (**Figure 11**).

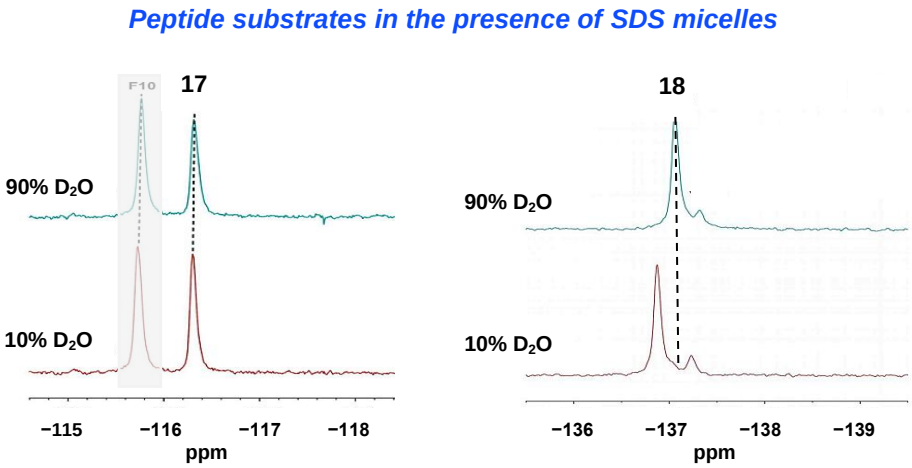

Figure 11. ^{19}F NMR spectra, zoomed in to specific ppm ranges, for pfF peptide **17** and 3fY peptide **18** in the presence of SDS micelles. The black dashed line highlights how the chemical shift value is affected when altering the percentage of D_2O. An additional peptide was shown in the original paper but this was not discussed in this text therefore has been greyed out to avoid confusion.[52]

Due to a negligible chemical shift change observed for **17** (Δδ peak ppm = 0.01 ppm) it was suggested that pfF residues are embedded within the hydrophobic region. On the other hand, **18** had a greater shift (Δδ peak ppm = 0.19 ppm) implying solvent exposure for the 3fY residues, which implied these were at the surface of the micelles. This agreed with their

activity data, which showed that antimicrobial potency was greater for Phe analogues compared to Tyr, demonstrating that the antimicrobial mechanism of action relies on membrane interactions.[56]

Other than using fluorine as a biological tool for imaging or assessing biological interactions, its selective incorporation can alter the binding affinity and specificity of peptides or proteins *via* indirect fluorine electronic effects and direct intermolecular fluorine−hydrogen bonding: C−F···H−X (X = N, O).[57] The existence of such interactions has been proven using NMR spectroscopy experiments which identify the through space coupling between the fluorine and hydrogen nuclei,[58] and the influence of physical parameters such as dilution and temperature on hydrogen bonding can be monitored.

Additionally inserting a single fluorine atom into a peptide sequence can increase the hydrophobicity of the biomolecule, which can hinder proteolytic cleavage and enhance activity.[59] This was studied by Wang and co-workers using the honeybee peptide jelleine-1 **19** which is an antimicrobial peptide.[60] Numerous assays were carried out to investigate the effects of halogenation on activity, cytotoxicity and proteolytic stability. When Phe was replaced with pfF the resulting peptide **19a** had improved protease stability without increasing toxic effects to mammalian cells.[61] This led to a small improvement in activity against Gram-(+) and Gram-(−) bacteria was observed for **19a** compared to the unmodified peptide **19**. Interestingly other halogenated derivatives showed a greater increase in the *in vitro* activity, especially the iodinated analogue **19d** which gave a four- to eightfold increase depending on the bacteria strain (**Table 1**).[60]

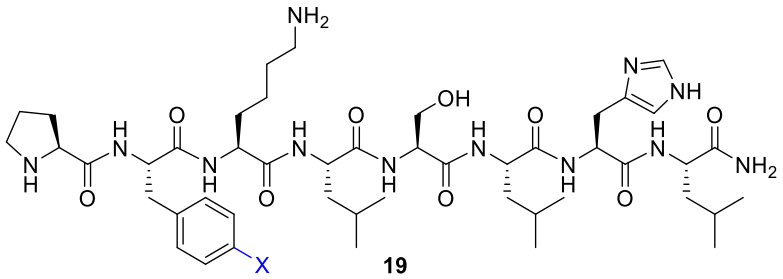

Entry	Peptide	MBIC (µM) *S.aureus*
1	X = H Jelleine-1 **19**	512
2	X = F **19a**	256
3	X = Cl **19b**	64
4	X = Br **19c**	64
5	X = I **19d**	64

Table 1. MBIC values of Jelleine-1 **19** and its halogenated derivates against *S.aureus.*[60]

The start of this chapter has highlighted the application of modified peptides in the pharmaceutical industry. Selective peptide functionalisation is usually crucial for improved PK-PD properties such as activity and stability enhancing their therapeutic and diagnostic ability.[13] This next section will discuss a variety of reactions which have been developed to produce such functionalised peptides through bioconjugation.[62]

1.2 Bioconjugation

Bioconjugation involves the coupling of a molecule to a biomolecule (**Scheme 2**), in the case of peptide functionalisation this is achieved *via* amino acid modification. Important features of a successful bioconjugation strategy include robust and mild conditions which achieve site-selectivity and ultimately, conservation of the biomolecule's structure and function.[62] Most of the currently available chemoselective methods target cysteine (Cys)[63,64] and lysine (Lys)[65] due to their intrinsic nucleophilicity and the wide variety of known electrophiles that can react with these residues. Maleimide reagents (**21**) are frequently used due to their facile synthesis, ability to incorporate various 'tags' including drug molecules, fluorophore labels or

biotin and commercial availability.[66] However the conjugation products can often have poor stability, hydrolysing in aqueous media, limiting the biological application.[67]

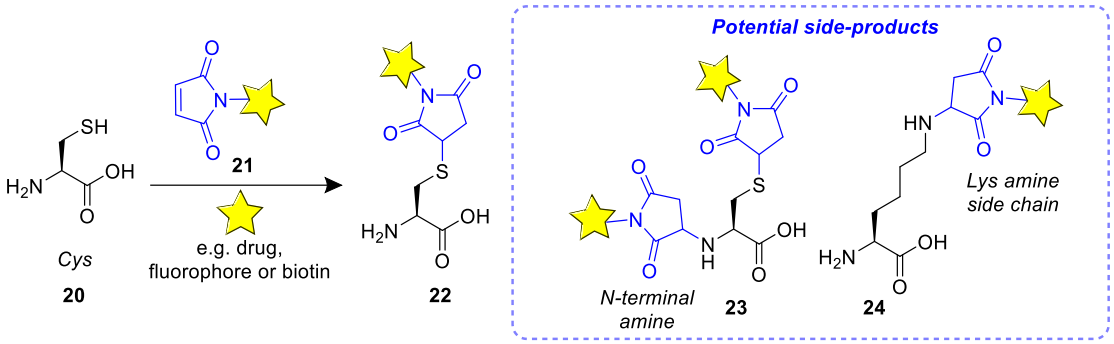

Scheme 2. A simple representation of a bioconjugation reaction showing maleimide conjugated products.

Selective amino acid modification within a peptide or protein depends on both the inherent chemical reactivity of the residue (chemoselectivity) and its relative proteinogenic abundance or accessibility. Achieving high chemoselectivity for a reaction can be difficult due to the vast array of functionality present on the amino acid side chains within peptides. These can interfere with the desired transformation resulting in side-products, over modification or reaction inhibition. As mentioned previously both the thiol and amine side chains on Cys and Lys respectively have similar nucleophilic reactivities resulting in a mixture of products in a proteinaceous environment (**Scheme 2**).[67,68] However, chemoselective bioconjugation strategies within peptides and proteins are continuously being developed and a selection of successful Cys modification techniques are outlined in figure 12.[66] Activated Michael acceptors are the most common reagents used and 3-bromo-5-methylene pyrrolone (3Br-5MP) **25** (**Figure 12A**),[69] comparable to maleimide **21**, was shown to enhance product **26** stability.[69,70] Alternatively, the acrylamide-based Michael acceptor **27**

(**Figure 12B**),[71] also demonstrated similar reactivity to maleimide reagents but generated linear conjugation products (**28**) with greater stability toward hydrolysis and thiol-exchange in plasma leading to successful *in vivo* applications.[71] More recently, hypervalent iodine reagents such as tetrafluoroalkyl benziodoxole (TFBX) **29** have displayed compatibility in aqueous media, allowing the synthesis of tetrafluorinated Cys-conjugation products **30** (**Figure 12C**).[72] The final selected example (**Figure 12D**) utilises the strain-releasing reagent **31**, which is highly reactive, demonstrated by the rapid reaction time of 15 minutes, due to the combination of a strained cyclopropenyl moiety and an activated Michael acceptor (α,β-unsaturated ketone).[73]

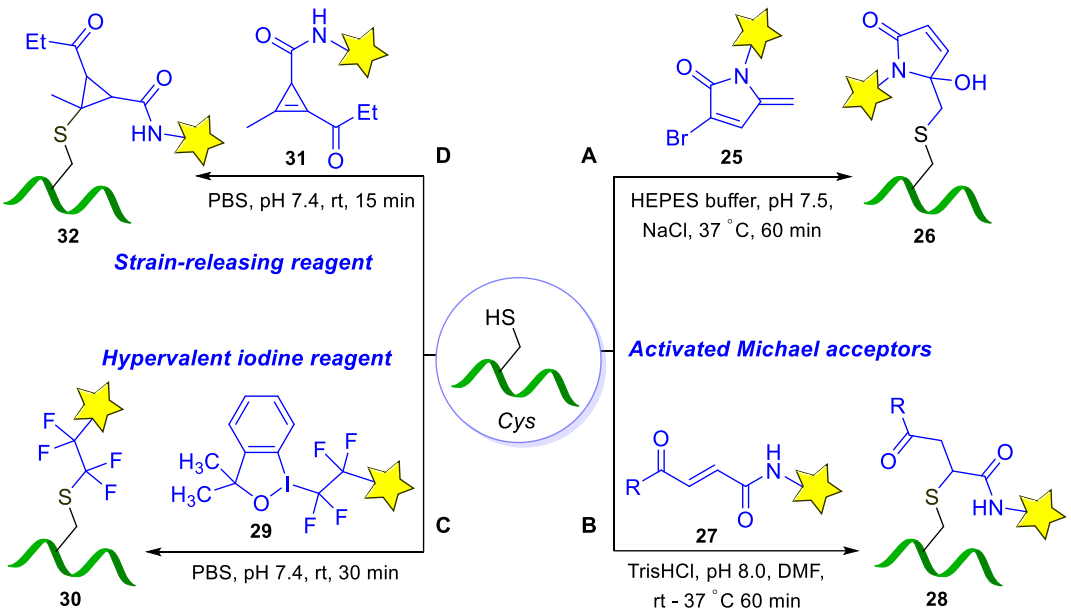

Figure 12. A selection of fast Cys-selective bioconjugation strategies. A. Bioconjugation *via* Michael addition to 5-Methylene Pyrrolones.[69] B. Bioconjugation using carbonylacrylic reagents.[71] C. Fluoroalkylation.[72] D. Conjugate addition of cyclopropenyl ketones.[73]

While the methods described above use mild conditions: near neutral pH, low temperature (rt → 37 °C) and aqueous media, due to the presence of other thiol containing species in cells such as glutathione, proteins and free Cys, selectivity for peptide/protein bioconjugation can be challenging.[74] This

is not a unique disadvantage of Cys functionalisation, in fact specific targeting of any natural amino acid intracellularly is impossible, highlighting the difficulty of amino acid modification. Often this is overcome when carrying out *in vitro* bioconjugation to avoid the complexity of natural systems.

For Lys modification, competition for selectivity can arise on the peptide/protein itself because there are often multiple Lys residues, and another primary amine functional group is present: the *N*-terminal amine. Nonetheless there are procedures which achieve selectivity for Lys by ensuring that the reaction solvent falls within a specific pH range. At near physiological pH the Lys side chain is more likely to be protonated, hence a slightly basic pH is optimal for Lys modification (8.5 – 9.5)[75] presenting the free amine which is more nucleophilic. Lys is marginally more basic than the N-terminal amine (pKa 10 and 8 respectively),[14] which to some degree enhances the reactivity of Lys side chains, but overall these chemical handles are likely equivalent. Selective Lys modification reagents include glycoside **33** which was used to successfully prepare glycoproteins for the study of targeted drug delivery (**Figure 13A**),[76] and unsaturated aldehyde derivatives such as reagent **35** (**Figure 13B**).[77] Rapid functionalisation was achieved after 30 minutes for the latter, compared to other reaction times > 12 h, synthesising products with a cyclic amine moiety **36**. Large-scale synthesis was carried out for the aldehyde reagents **35** to provide a lysine labelling kit named "Stella+" utilised for molecular imaging.[79,80]

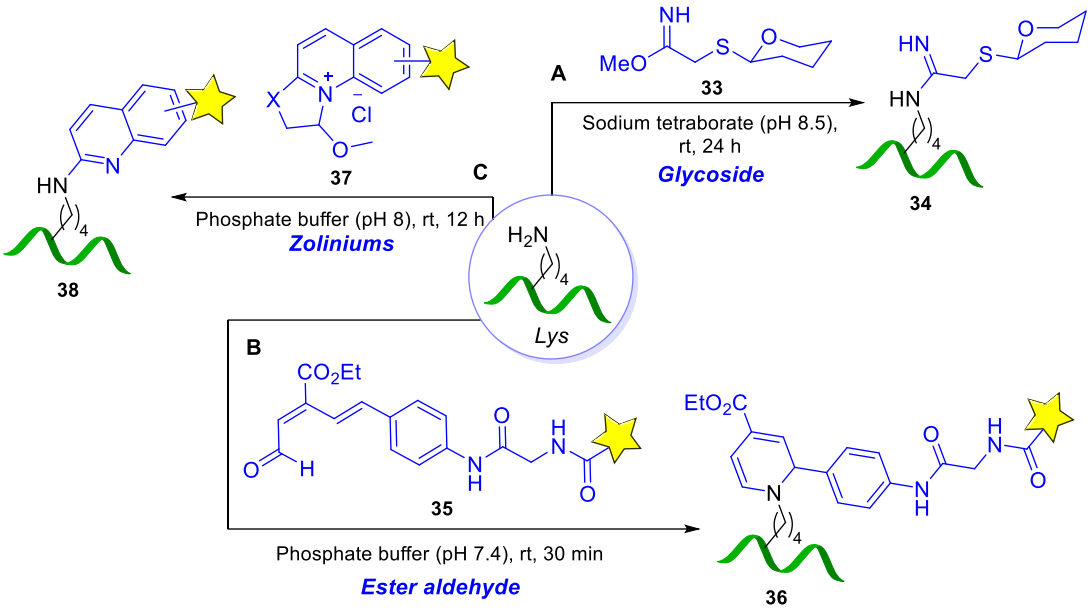

Figure 13. A selection of Lys-selective bioconjugation strategies. A. Glycosylation with sugar-IME reagents.[76] B. Lys labelling *via* 6π-azaelectrocyclization.[77] C. Quinolylation using zoliniums.[78]

In 2022, Zhu and co-workers reported the use of zoliniums **37** for quinolylation of Lys (**Figure 13C**) within peptides and proteins.[78] The products detailed in figure 13 were obtained as mixtures containing numerous functionalised Lys residues (1-20), depending on the number present and accessibility on the biomolecule. This isn't unexpected because Lys is one of the most prevalent amino acids in the human proteome,[75] however over-modification is not desirable because it can disrupt the peptide's function preventing future applications. Additionally, purification of the desired product from the di- and tri- modified analogues is challenging, especially as the peptide increases in size, highlighting why site-selective modification is beneficial.

Ideally bioconjugation reactions would employ reagents in stoichiometric quantities however this is rarely the case: Cys functionalisation required 50 eq. of cyclopropenyl reagent **31**,[73] and for Lys bioconjugation, 7-500 eq. of unsaturated aldehyde **35** was used.[77] As long and complex synthetic routes

may be required to prepare such reagents, further improvements are required to deliver cost- and time-efficient bioconjugation strategies.[66] While reactions have been developed over the past few decades to target alternative canonical amino acids, generally these have substrate limitations and are less effective or inapplicable for complex peptide conjugation.[62,81] Therefore, novel chemoselective bioconjugation strategies which target other residues are in high demand.

The electron-rich indole side chain of Trp has a different reactivity profile compared to Cys and Lys, which opens up the possibility of developing mechanistically distinct bioconjugation methods. Additionally, Trp has a low occurrence (~ 1.4%) within native peptides and proteins, the lowest of the 20 proteinogenic amino acids.[82] This suggests that any given biomolecule target is likely to have only one Trp reside, inherently avoiding over modification, and validating Trp as an ideal chemical handle. Despite the low abundance, Trp is present in 90% of native proteins,[83] or alternatively can be installed *via* mutagenesis. One potential drawback of targeting Trp is that the indole moiety is considered non-polar, preferring to be buried in biomolecule hydrophobic cores. These regions are not surface exposed which could hinder functionalisation due to poor accessibility.

Trp C–H functionalisation

An alternative approach to utilising functional group chemistry for peptide modification is C–H functionalisation which has been carried out using a variety of transition metal (TM) catalysed procedures as well as photocatalysed approaches (the latter of which will be discussed in 1.5 Photochemical Modification of Trp). Each TM strategy successfully modified

Trp at the C–2 position on the indole ring including manganese C2-allylation,[84] palladium C2-arylation,[85] and palladium-catalyzed macrocyclization.[86]

Ackermann and co-workers developed an unprecedented manganese(I)-catalyzed C–H allylation strategy for the functionalisation of modified Trp within peptides (**Scheme 3**).[87] Regarding the conditions a relatively high catalyst loading (10 mol%) was used with NaOAc (30% mol%), followed by heating the biomolecule to 80 °C for 16 h which is unlikely to be biocompatible for larger peptide systems. For this reaction, it was crucial that the indole nitrogen was functionalised with pyridine (2-py) in order to form substrate-manganese complex **42**, which reduces the applicability of this methodology to be used on native peptide sequences.

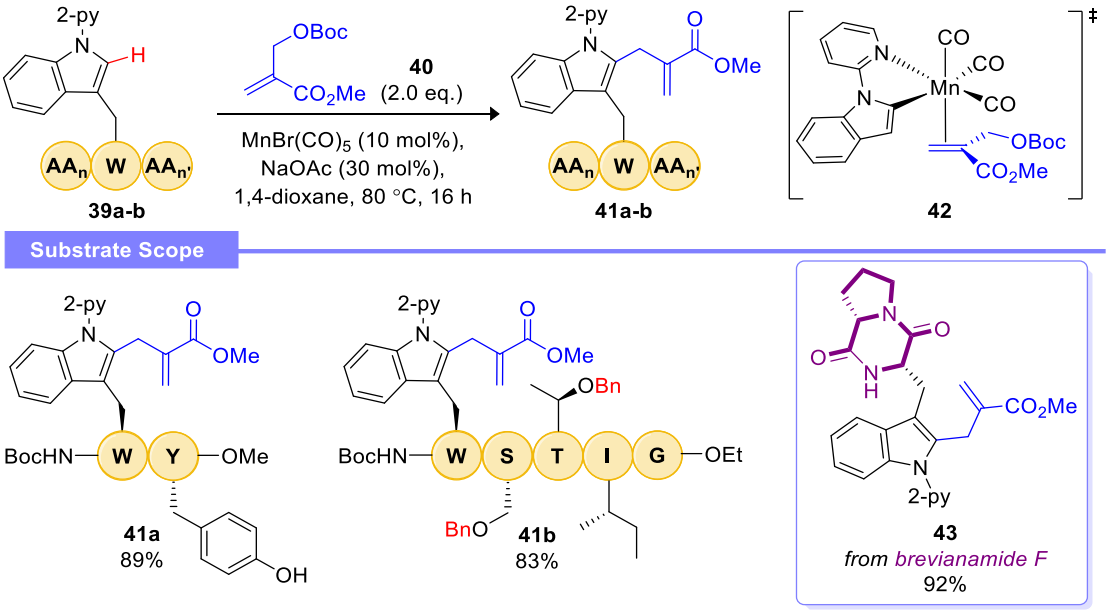

Scheme 3. Trp C–H allylation using conditions developed by Ackermann and co-workers.[87]

Mostly high product yields were obtained for their 19 peptide examples ranging from 53-98%, a couple of which have been shown in scheme 3. The peptide sequences varied in length (di- to pentapeptides) and amino acid

sequence to investigate the reaction robustness. The presence of serine (Ser), tyrosine (Tyr) and methionine (Met) presenting hydroxyl and thio-ether functional groups were tolerated giving high product yields between 81-89% (**Scheme 3**). However, most peptide sequences contained hydrophobic residues and/or featured protecting groups on amino acid side chains (**41b**) which suggested poor functional group tolerance. Finally, the successful conjugation of steroids and natural products (**43**) was reported highlighting the effectiveness of this manganese(I) catalysed transformation for fusing various complex scaffolds.[87]

Fairlamb and co-workers developed three complimentary conditions each using Pd catalysis and low temperatures (≤40 °C) to arylate Trp-containing peptides.[85] The importance of this modification is to enhance the photophysical properties of the indole through extending the π-system by arylation.[88] This direct C–H functionalisation does not require any Trp pre-functionalisation i.e. protecting or directing groups which is a major advantage allowing application to natural products. However, the use of organic solvents are not ideal from a biocompatibility perspective because the native structure of a protein can be disrupted, specifically the hydrophobic interactions between non-polar amino acid residues.[89] The following brief overview will focus on the comparison of most recent conditions B[90] and C[85] (**Scheme 4**). The use of Cu(II) as the co-catalyst for conditions B led to successful arylation of Ac-Trp-OMe **44** in good conversions up to 93% (analytical HPLC), however the aryl scope was limited consisting of only five examples: all *para* substituted benzene derivatives.

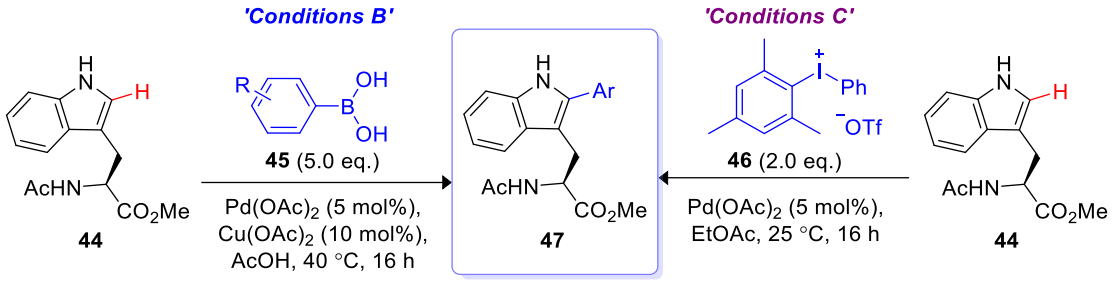

Scheme 4. Overview of conditions B and C developed Fairlamb and co-workers for Trp-arylation.[90]

The peptide substrate scope was also small (< 10), and some examples required a very high catalyst loading of $Pd(OAc)_2$ (30 mol%): six times greater than the amount used for the amino acid substrate (**Scheme 5**).[90] Additionally using these conditions caused the formation of dihydroxylated side products **49b**** and **49c**** (hydroxylation of the aryl group) when peptide substrates contained a C-terminal alanine neighbouring Trp. Therefore the poor product selectivity gave rise to the development of conditions C, where the Cu(II) co-catalyst was replaced by two equivalents of [MesPhI]OTf.[85]

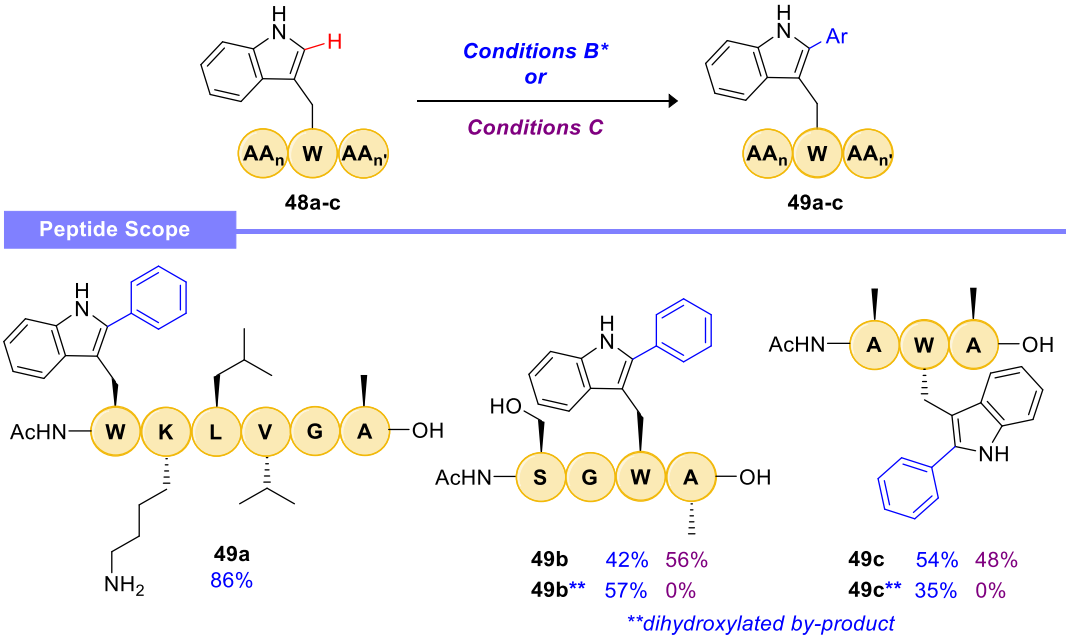

Scheme 5. Analytical HPLC conversions for Trp-arylation products. Conditions B*: $Pd(OAc)_2$ (30 mol%), $Cu(OAc)_2$ (60 mol%), $PhB(OH)_2$ (5.0 eq.), AcOH, 40 °C, 16h (blue conversion). Conditions C: [MesPhI]OTf (2.0 eq.), $Pd(OAc)_2$ (10 mol%), ^{i}PrOH, 25 °C, 16 h (purple conversion).[90]

Pleasingly, using this diaryliodonium salt completely prevented the formation of oxidised aromatic side products (**Scheme 5**). Other advantages of conditions C compared to B include the lower reaction temperature (25 °C) and catalyst loading (10 mol%) and a smaller excess of aryl reagent reducing material waste. However, the arylation reagent scope was not explored and the peptide substrate scope was very limited (mostly hydrophobic amino acids) because the focus was on examples previously oxidised using conditions B. Varied success was reported using alternative conditions C for product formation: arylated product **49c** gave a poorer product yield whereas peptide **49b** showed a small improvement. Therefore, it was suggested that these conditions were only used when milder conditions were preferable (EtOAc and lower temperatures) and/or purification of the desired arylation product from the oxidised side product was challenging.

From a green chemistry perspective, the use of transition metal catalysts, especially in high loadings, is not ideal therefore metal-free procedures have been explored. However, despite ongoing work in this area, there are still few transformations available for Trp functionalisation: sulfenylation,[91] trifluoromethylation[92] and bioconjugation using persistent radical traps.[93]

Trp bioconjugation using persistent radical traps is rare, but Kanai and co-workers demonstrated great applicability of their TM-free method for the synthesis of protein conjugation products.[93] The radical reagent keto-ABNO **50** was favourable in terms of reactivity and versatility allowing the incorporation of various functional molecules such as fluorescent probes **51** and anticancer drugs **52**.

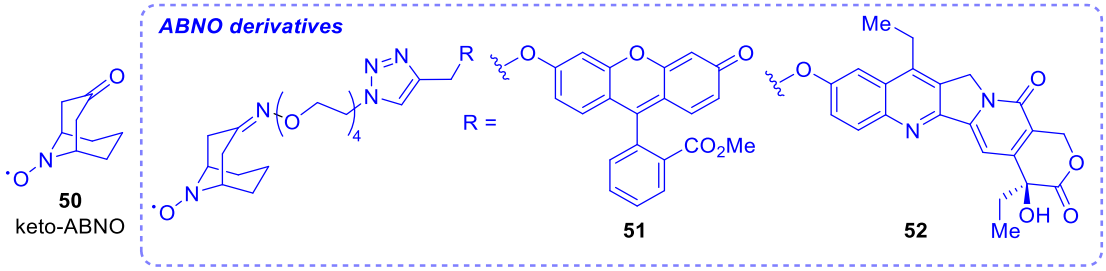

Figure 14. Structure of keto-ABNO reagent **50** and its derivates **51** and **52**.

Numerous small peptide substrates (5-10 amino acids) were exposed to the optimised conditions with favourable parameters such as stoichiometric amounts of organo-radical reagent **50**, ambient temperature, and rapid 30-minute reaction times (**Table 2**). Peptides **53a-d** containing oxidation sensitive amino acids: Ser (alcohol), Lys (amine), Tyr (phenol) and Met (sulfide) were unaffected and the yields obtained for Trp-conjugation were high (**Table 2**, entry 1-4). However, these yields are HPLC yields based on starting peptide, which is not a quantitative technique, and it is a combination of (at least) two products: **54** and the dehydrated analogue **55** showcasing that the reaction did not exclusively deliver one product.

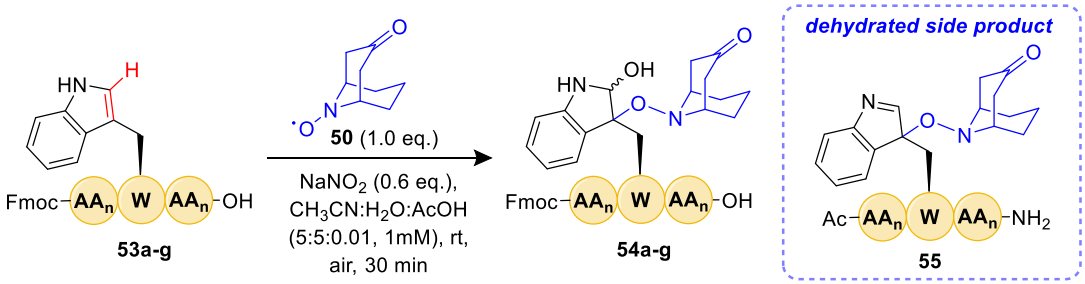

Entry	Peptide	Yield[a] (%)
1	Fmoc-Gly-Ser-Asn-Trp-Gly-OH (**54a**)	95
2	Fmoc-Gly-Lys-Asn-Trp-Gly-OH (**54b**)	85
3	Fmoc-Gly-Tyr-Asn-Trp-Gly-OH (**54c**)	95
4	Fmoc-Gly-Met-Asn-Trp-Gly-OH (**54d**)	96
5[b]	Ala-Asn-Leu-Trp-Ala-Thr-Gly-His-Phe-Met-NH_2 (**54e**)	84
6[b]	Pyr-His-Trp-Ser-Tyr-Gly-Leu-Arh-Pro-Gly-NH_2 (**54f**)	91
7[b]	Tyr-Asn-TrpAsn-Ser-Phe-Gly-Leu-Arg-Phe-NH_2 (**54g**)	83

Table 2. A selection of peptide substrates used for Trp-oxidation. [a]HPLC combined yield of **54** and dehydrated **55** based on the starting peptide.[b]H_2O/AcOH (1:0.001).[93]

An alternative solvent system, without CH_3CN, was used for biologically relevant peptides, neuromedin B **53e**, luteinizing hormone-releasing hormone **53f**, and kisspeptin-10 **53g** which provided equally high yields and is desirable for protein bioconjugation. Hence these conditions were applied to a native protein lysozyme, but greater equivalents of keto-ABNO **50** and $NaNO_2$ were employed (5.0 and 3.0 respectively). Successful mono-conjugation was observed despite the presence of six Trp residues within the 129 amino acid sequence. Analysis using X-ray diffraction revealed Trp62 as being the major modification site for functionalised lysozyme product **56** demonstrating high Trp-selectivity (**Figure 15**).

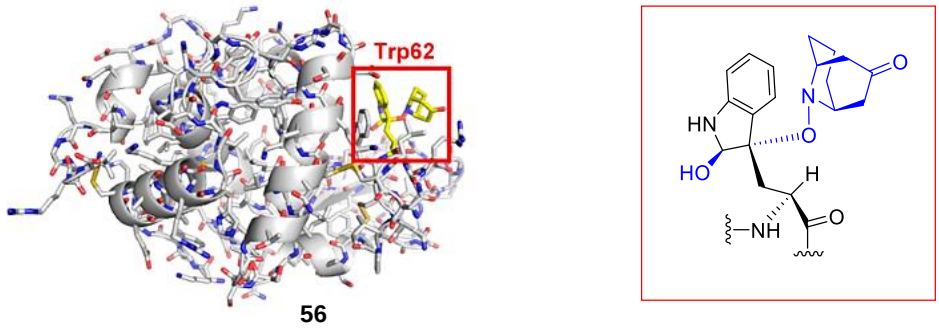

Figure 15. The crystal structure of functionalised lysozyme **56** showing selective modification of Trp62 using the conditions reported by Kanai and co-workers.[93]

Despite the development of TM-catalysed and catalyst free Trp modification procedures, literature precedent is sparse. Limitations include the use of protecting groups on amino acid residues, even Trp itself, and a low number of complex peptide substrates limiting the application of such methods for native peptide functionalisation. Furthermore, most examples utilised organic solvents which commonly denature proteins at high concentrations through the disruption of hydrophobic interactions resulting in molecular unfolding.[89] This effect is often concentration dependent and protein specific, for example Schwartz and co-workers found that alcohols, in low

concentrations, stabilised sickle haemoglobin and other solvents such as pentane and formamide had no overall effect.[89]

1.3 Peptide Cyclisation

In addition to the peptide functionalisation strategies discussed previously which were used to generate linear peptide conjugation products, methodologies which can produce cyclic and stapled peptides are also in demand. Cyclised peptides often have improved properties (from a pharmaceutical perspective) compared to the linear analogue such as a greater resistance to proteolytic cleavage and a higher receptor binding capacity (due to a larger surface area).[31,94] A selection of biologically active cyclic peptides, out of the large number of commercialized peptides,[95] were discussed previously in 1.1 Applications of Modified Peptides, highlighting the importance of these products. Additionally, short peptides are ideal drug candidates because they can disrupt protein-protein interactions (PPIs) in diseased cells providing they have an α-helical segment.[96] However, sometimes a predicted α-helical structure may exist as a random coil instead which would not possess the same properties, therefore peptide stapling strategies have been developed over recent decades to lock the α-helical shape in place.[7]

General Peptide Stapling Techniques

A brief overview of common peptide stapling techniques is shown in scheme 6, highlighting a variety of different macrocyclisation chemistries.[96] Naturally within peptides/proteins, Cys side chains cross-link to form disulfide bridges which can stabilise the secondary structure providing greater resistance toward proteases and enhancing activity,[97] however

disulfide stapled peptides are unstable in reducing environments which can inhibit their use for intracellular targeting.[96] To overcome this more stable thioether products **58** are synthesised which continue to utilise the Cys thiol functionality in a reaction with external electrophiles such as α,α'-dibromo-*m*-xylene **57** (**Scheme 6A**).[98]

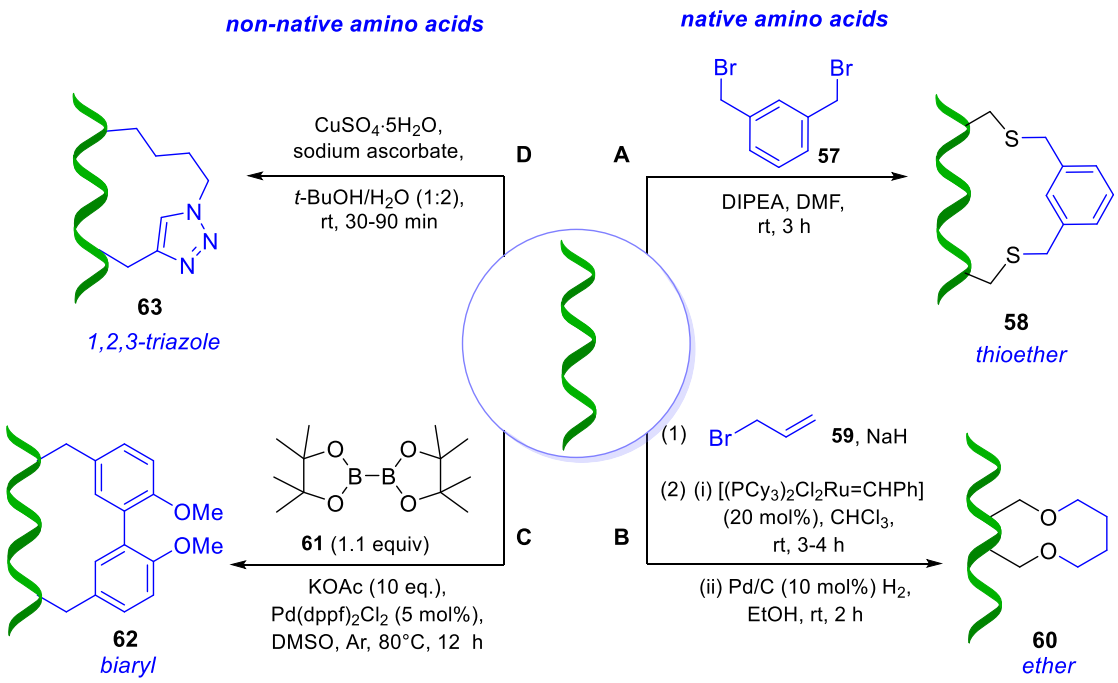

Scheme 6. A selection of peptide stapling techniques utilising different macrocyclisation chemistries.[98,99,100,101]

Serine (Ser) residues can be functionalised to incorporate olefin moieties and an intermediate peptide diene can undergo ring closing metathesis (RCM) to yield macrocycles (**Scheme 6B**).[99] Alternatively, non-native amino acids can be installed into the peptide sequence such as aryl iodides (**Scheme 6C**) taking advantage of Pd-catalysed biaryl coupling *via* borylated phenylalanine intermediates,[100] or azide and alkyne moieties for cyclisation using click chemistry (**Scheme 6D**).[101]

Generally, the peptide stapling strategies reviewed above are expensive, utilising palladium chemistry, and long stepwise syntheses are involved.[96]

A variety of linkers are available which is advantageous as this can affect the properties of the stapled peptide; for example lactam stapled peptides have been particularly successful for extracellular and membrane-bound targeting.[96] Expanding the scope of peptide substrates tolerated in stapling reactions along with the development of new linkers will broaden the field of peptide-based therapeutics for a variety of targets.

Peptide Stapling via the Trp Residue

With regard to Trp, there are very few available stapling techniques despite the fact that it is an ideal chemical handle as the residue has the lowest relative abundance in eukaryotic proteomes: approximately 1% out of the canonical amino acids.[102] This inherently minimises the production of undesired isoforms therefore development of strategies that target Trp would be of high impact.

Currently, multiple peptide stapling techniques were inspired by Larrosa's work in 2008: C–2 indole arylation using aryl iodides and palladium catalysis in acidic media (**Scheme 7**).[103] Moderate to excellent product yields were obtained using $Pd(OAc)_2$ (5 mol%), Ag_2O (0.75 eq.) and 2-nitrobenzoic acid (1.5 eq.) in DMF at room temperature for 15 h (**66a-c**), but longer reaction times and a greater excess of iodoarene was required for ortho-substituted aryl substrates **66d** and **66e**. Most examples were carried out using *N*-methyl indole, though the protecting group was not crucial as a moderate product yield of 61% was obtained for **67** albeit with more forcing conditions (38 h, 50 °C).

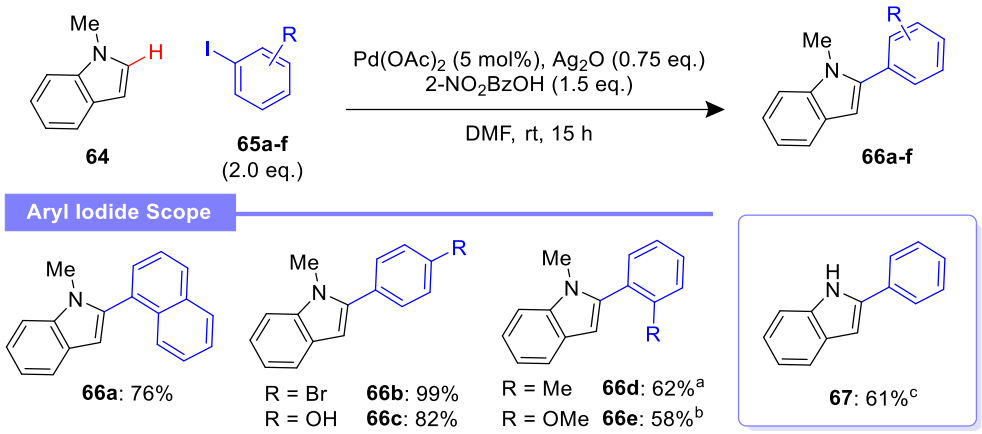

Scheme 7. Isolated yields obtained for a selection of C–2 arylated indole products synthesised by Larrosa and co-workers.[103] [a]24 h. [b]5.0 eq. of iodoarene **65e**, 38 h. [c]50°C for 38 h.

Following this, in 2012, James and co-workers applied the palladium-catalysed C–H arylation methodology to peptidic substrates to synthesise 15- to 25- membered biaryl macrocycles.[86] The conditions for peptidic stapling were similar to Larrosa's indole arylation conditions,[103] but with a different silver salt ($AgBF_4$), a solvent swap to DMA from DMF and microwave heating (130 °C) which provided rapid reaction times of 30 minutes instead of 15-38 h at room temperature (**Scheme 8**). Drawbacks of this strategy included the relatively high loading of a rare transition metal catalyst (5 mol% Pd), a high reaction temperature (130 °C) and the use of an acid additive. Additionally, the substrates, hence products, were not 'true' peptides i.e. some amino acids were joined by a linker not a peptide backbone.

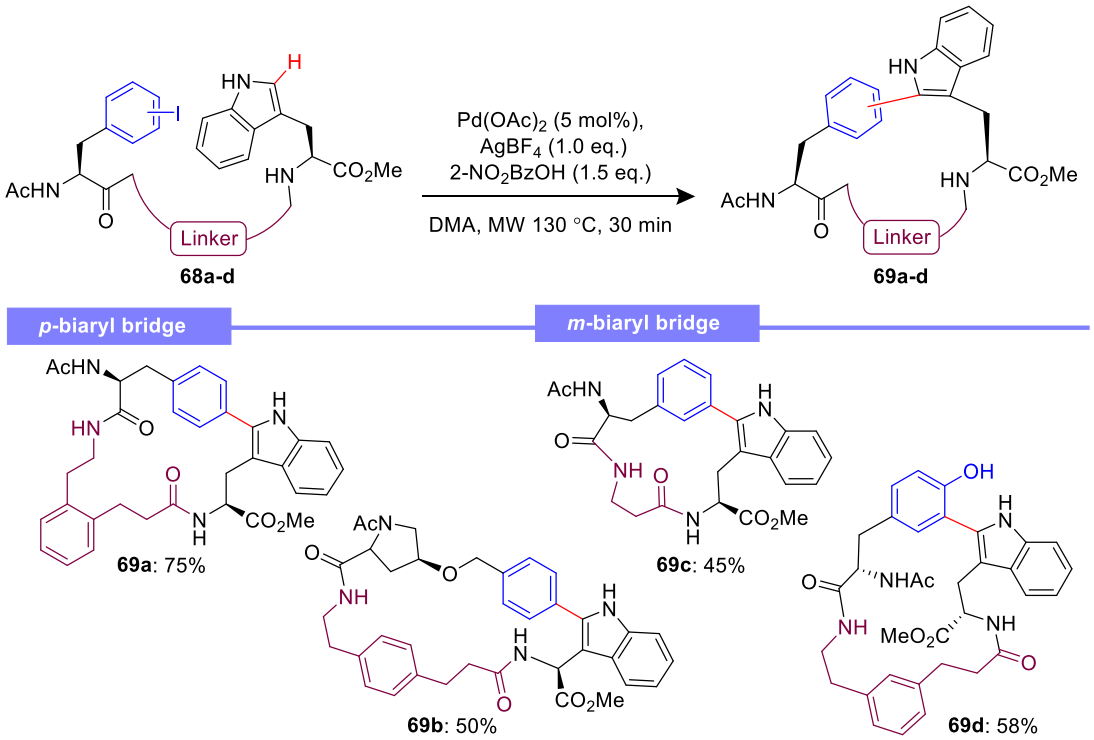

Scheme 8. Isolated yields obtained a selection of macrocycles synthesised by James and co-workers showing both *para*- and *meta*-bridged aryl groups.[86]

A variety of macrocycles were synthesised (**69a-d**) bearing a new 2-aryl-indole linkage in moderate to good yields between 40-75%. Most examples utilised iodo-phenylalanine (I-Phe) showing both *para*- and *meta*-iodo derivatives as successful reagents and there was one example where the indole-aryl bridged macrocycle **69d** was formed using iodo-Tyr (**Scheme 8**). Importantly, the indole nitrogen was unprotected in all cases, avoiding additional synthetic steps for protection and deprotection, however very few functional groups were present in the substrate scope which may suggest potential complications for application to peptide substrates.

More recently in 2015, Lavilla and co-workers in 2014 also utilised the palladium-catalysed C–H arylation strategy with the novelty being formation of stapled peptides.[95] As mentioned previously a covalent C–C bond is formed *via* intramolecular cyclisation between Trp and a

prefunctionalised iodinated Phe/Tyr residue (**Scheme 9**). Numerous unique studies were carried out in this research including investigation into the distance between Trp and *meta*-I-Phe/Tyr, application to bioactive peptides along with potency and peptide stability studies, highlighting the full potential of this technique and the value of macrocyclic peptides.

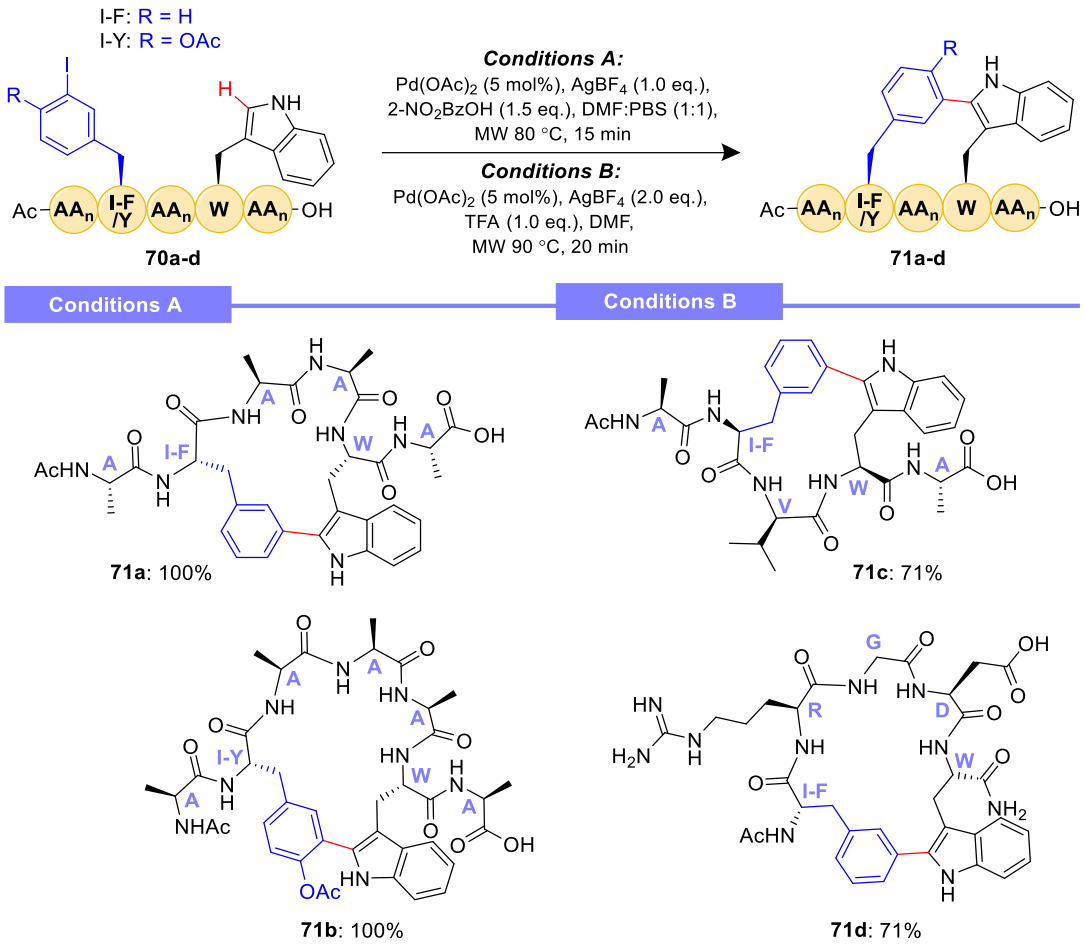

Scheme 9. Conversion estimated yields (HPLC-MS) for a selection of peptide macrocycles synthesised by Lavilla and co-workers using either conditions A or B.[95]

A series of 11 linear peptides were initially investigated, where the number of amino acids between Trp and aryl iodide varied between one (i, i+2) and three (i, i+4) forming different sized macrocycles (**Scheme 9**). Reaction conditions (conditions A) used for simple peptide substrates Ac-A^{I}FAAWA-OH **70a** and Ac-A^{I}YAAAWA-OH **70b** were similar to James' discussed above ($Pd(OAc)_2$, $AgBF_4$ and 2-nitrobenzoic acid with microwave heating),[86] and

provided excellent conversions of 100% (HPLC-MS estimated yields) for cyclised products **71a** and **71b**. However, these peptide sequences mostly contained Ala residues with little functionality and when sterically bulky or electronically charged amino acids were present in the peptide chain such as Ac-A^{I}FVWA-OH **70c** and Ac-^{I}FRGDW-NH_2 **70d**, alternative conditions were required. Even with modified conditions B using a different acid (TFA) and solvent (DMF), lower (more variable) conversions were obtained between 39-77%, presumably due to the increased substrate complexity. Furthermore, isolated yields were considerably lower than the HPLC-MS estimated yields ranging between 1 and 32%, highlighting the fact that HPLC is not a quantitative technique and that losses resulting from purification can become significant at a small scale.

Peptides containing tumour-targeting signaling sequences: Arg-Gly-Asp (-RGD-) and Asn-Gly-Arg (-NGR-) were included in their peptide scope to give macrocyclic peptides **71d** and **71e**. Preliminary studies were carried out on both **71d** and the analogous linear peptide Ac-^{I}FRGDW-NH_2 **70d** which showed that the stapling technique improved the peptide's potency against αvβ3 in front of αvβ5 integrin receptors.[95] Additionally proteolytic stability was measured and stapled peptides **71d** and **71e** were unchanged after 5-6 h under enzyme degradation conditions, whereas the comparable linear peptides Ac-^{I}FRGDW-NH_2 **70d** and Ac-^{I}FNGRW-NH_2 **70e**, underwent rapid cleavage completely degrading in the same time frame (**Figure 16**). These results (improved potency and stability) highlight the impact cyclisation can have for medicinal chemistry peptide development.

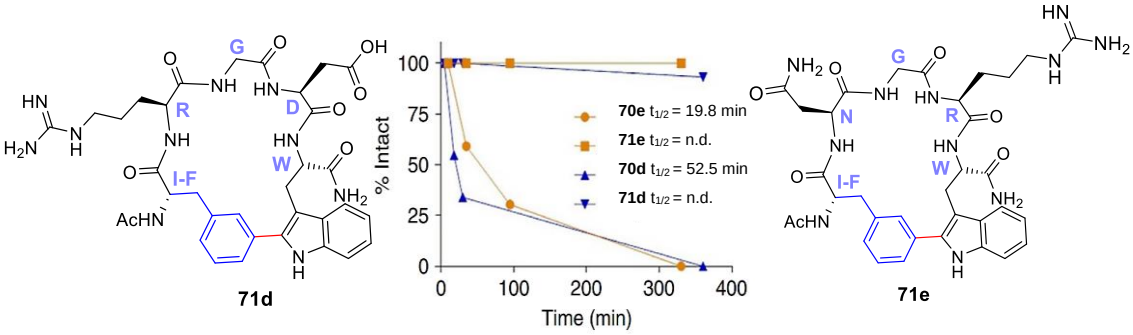

Figure 16. Macrocyclic peptide products containing tumour-homing signaling sequences -RGD- and -NGR- along with the proteolytic degradation assay.[95]

Known linear bioactive peptides have been successfully stapled using this methodology such as a potent dipeptidyl peptidase III inhibitor: valorphin analogue **70f** and baratin, a neurostimulating peptide, **70g** generating peptide macrocycles **71f** and **71g** (**Figure 17**).[104,105]

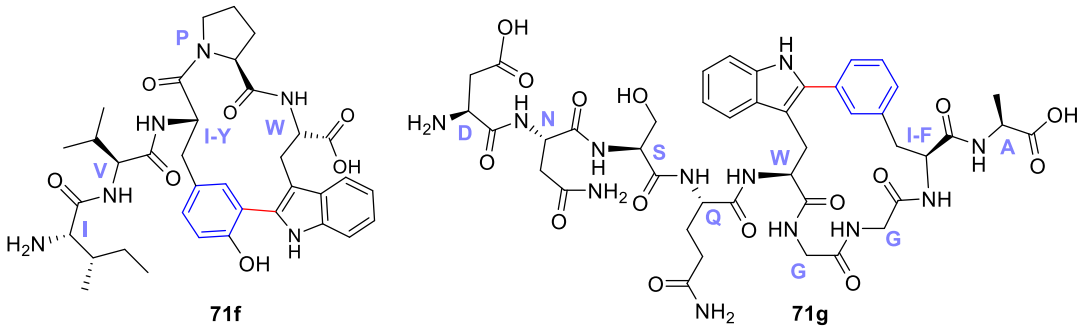

Figure 17. Macrocycles **71f** and **71g** synthesised from known bioactive linear peptides: valorphin and baratin analogues.

In conclusion, Pd-catalysed arylation was used to synthesise stapled peptides using Trp-containing peptide sequences with the incorporation of a non-native iodo-phenylalanine (or Tyr) residue. A wide variety of canonical (unprotected) amino acids were tolerated and different ring sizes were displayed by a thorough peptide scope including application to bioactive peptide substrates. The next example, developed by Ackermann and co-workers in 2019, involved a previously unprecedented cobalt-catalysed C–H activation strategy, however the overall procedure was

multi-catalytic and complex (**Scheme 10**).[106] One of the unique drivers of this research was the use of Co as a cost-effective,[107] earth abundant metal in comparison to expensive and toxic Pd which currently dominates the field, however their final step used 10-20% Pd/C.

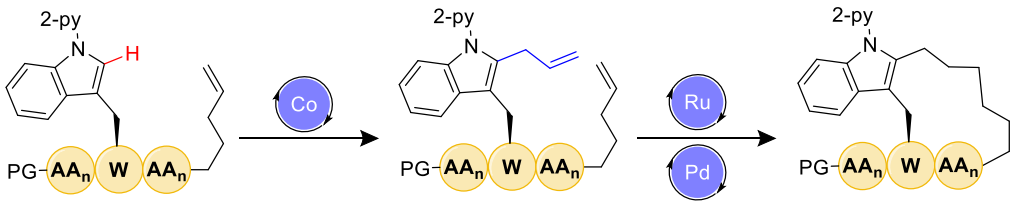

Scheme 10. Overall scheme for the stapling technique developed by Ackermann and co-workers involving C–H activation, alkene metathesis and hydrogenation.[106]

This cyclisation technique involved 3 steps undergoing C–H activation, alkene metathesis and hydrogenation, and 2 purifications which is not ideal based on the number of processes required. Additionally, it was essential that the indole nitrogen on Trp was protected and to obtain the free indole product, deprotection involved two steps, two days and the use of palladium highlighting numerous drawbacks of this cyclisation strategy.

Optimisation of conditions was carried out for the Co-catalysed C–H allylation of Trp, investigating catalyst and solvent and the final conditions are reported in scheme 11. The catalyst $[Cp^*Co(MeCN)_3](SbF_6)_2$ is air and moisture stable however, drawbacks of this transformation include the use of TFE which has serious hazards associated with it along with the use of a protecting group on the indole nitrogen which is unavoidable because this coordinates with the catalyst **75**.

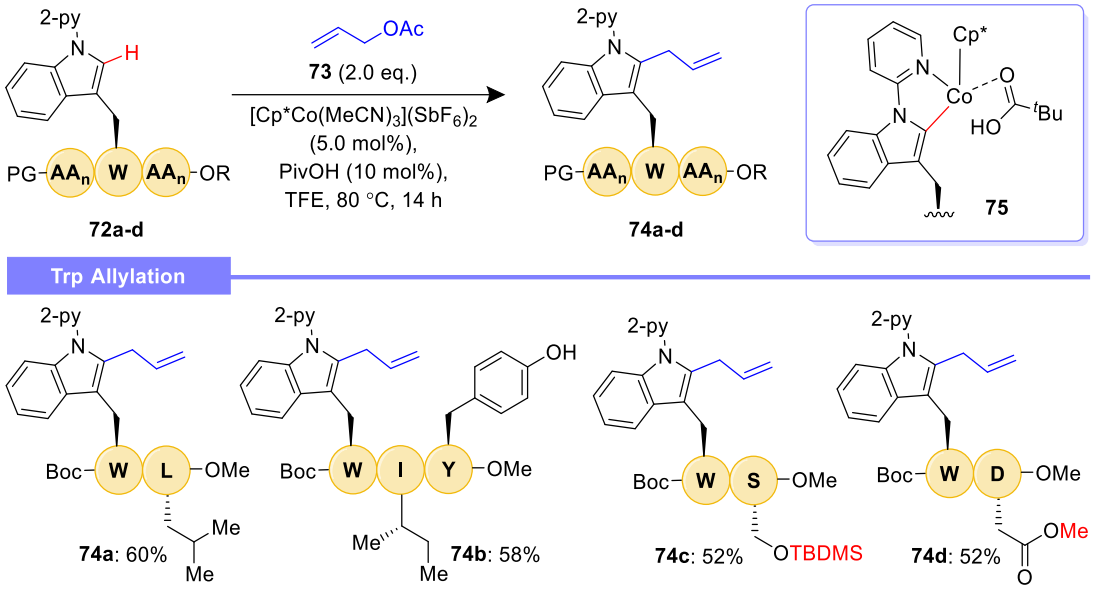

Scheme 11. Isolated yields obtained by Ackermann and co-workers for a selection of allylated Trp peptide products along with the co-ordination structure between 2-py Trp and the Co catalyst.[106]

In terms of reaction versatility, a range of Trp-containing di- and tripeptides were explored, but mostly aliphatic amino acids were present such as **74a**. For amino acids bearing functionality such as Tyr (**74b**) and Met good product yields were obtained, however protecting groups were required for Ser **74c** and Asp **74d**. Following purification of the allylated peptides, ring closing olefin metathesis followed by hydrogenation on the crude product was carried out (**Scheme 12**). A range of 11- to 18-membered macrocycles were tolerated but the amino acid complexity was poor, only containing Phe **73b** or Ala **73d** residues, instead the focus appeared to be on extending the alkyl chain.

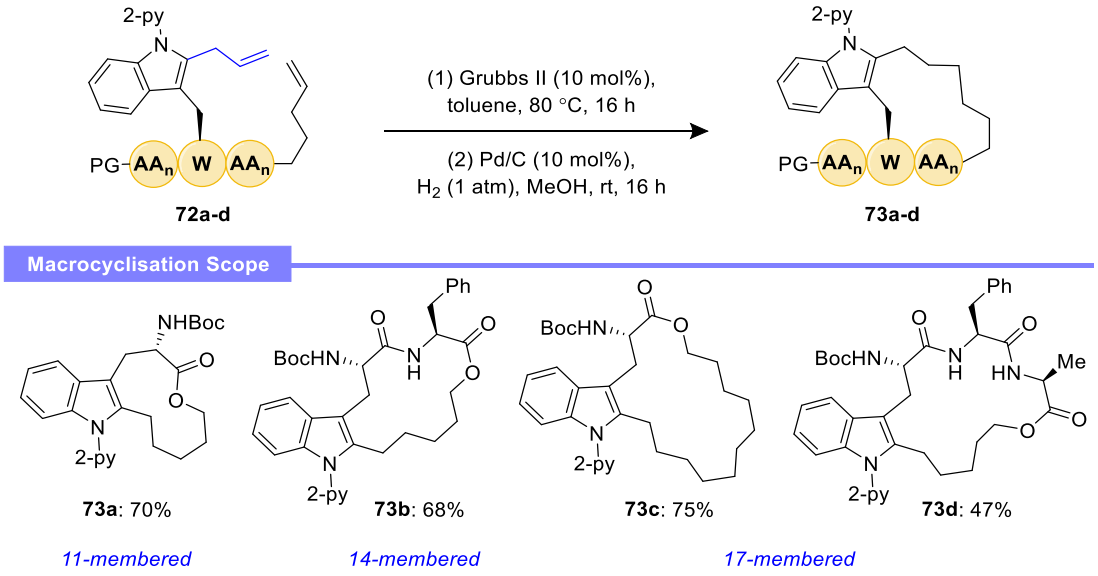

Scheme 12. Isolated yields for a selection of cyclic peptides synthesised using multimetallic metathesis/hydrogenation.[106]

As a native peptide cyclisation strategy there are several limitations which require addressing, five days minimum would be required to isolate an unprotected cyclised peptide product along with three purifications, three metal catalysts (with loadings between 5-20%) and the amino acid tolerance was not fully explored. Despite the novelty of the initial Co-catalysed Trp allylation, further development to streamline the process is necessary if this was to be used as a peptide stapling strategy.

The final example to be discussed is catalyst free, avoiding the possibility of trace toxic metals being present in final peptide products. An acid-mediated condensation reaction using an aryl aldehyde was developed by Johannes and co-workers to fuse two indole (Trp) residues together forming various stapled peptide products (**Scheme 13**).[94] Optimisation studies, using 3-methyl indole **74** and 4-bromobenzaldehyde **75** (**Scheme 13A**), explored a variety of acids, temperatures and times. Both sulfuric acid and (1S)-(+)-camphor-10-sulphonic acid (CSA) provided **76** in good yields (85% and

72% respectively) but due to the harsh nature of sulfuric acid, which could cause complications for peptide substrates, CSA was chosen going forward.

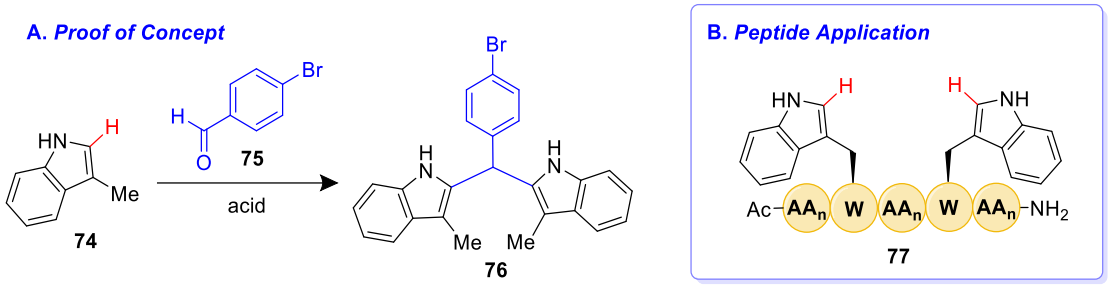

Scheme 13. A. Intramolecular indole-condensation B. A representative linear peptide substrate to enable peptide stapling.[94]

For peptide cyclisation, reactions were carried out on resin which can be advantageous as it avoids isolating the peptide starting material hence a purification step i.e. peptide synthesis was telescoped through to the indole condensation reaction. However, regarding reaction conditions, 1,2-dichloroethane (DCE) was used as the solvent, which is toxic, and the reagents are employed in large excess: 6 eq. of CSA and 10 eq. of aldehyde **75** (**Table 3**). The size of peptide macrocycle was investigated by methodically varying the distance between Trp residues (i, i+n where n = 1 – 4) and good to excellent conversions were reported: 81-100% (determined by analytical HPLC). Entries 1-4 in table 3 suggest that the distance between Trp amino acids had little influence on the reaction with a maximum difference of 7% conversion as the macrocycle increased in size. Additionally, the scope of peptide substrates displayed a good range of functional group complexity (**Table 3**, entry 5-9) including amide (N), iminium (R), carboxylic acids (D,E), phenol (Y) and thiol (S) moieties along with the incorporation of fragments commonly observed in biologically active peptides -NGR- **77h** and -RGD- **77i**.[108,109]

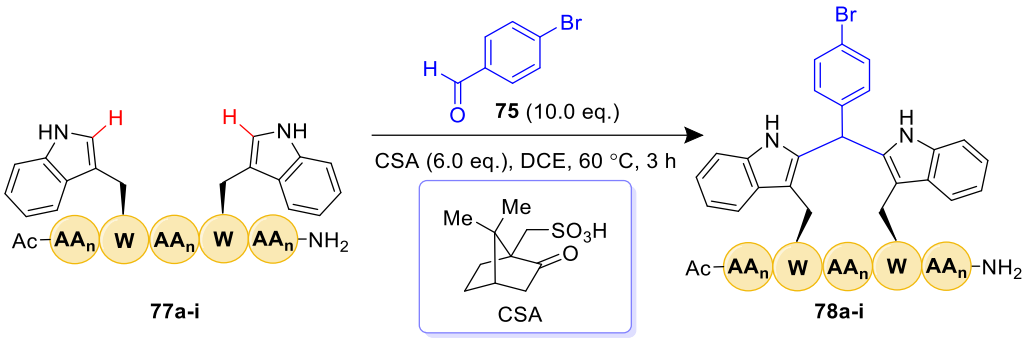

Entry	i, i+n	Linear peptide	Cyclic peptide	% Conv.[a]
1	i, i+1	Ac-WWALL-NH_2 (**77a**)	**78a**	100
2	i, i+2	Ac-WAWLL-NH_2 (**77b**)	**78b**	98
3	i, i+3	Ac-WALWL-NH_2 (**77c**)	**78c**	93
4	i, i+4	Ac-WALLW-NH_2 (**77d**)	**78d**	93
5	i, i+4	Ac-EYWALLW-NH_2 (**77e**)	**78e**	95
6	i, i+4	Ac-YWALLWS-NH_2 (**77f**)	**78f**	95
7	i, i+4	Ac-ALWALLW-NH_2 (**77g**)	**78g**	100
8	i, i+4	Ac-WNGRW-NH_2 (**77h**)	**78h**	81
9	i, i+4	Ac-WRGDW-NH_2 (**77i**)	**78i**	94

Table 3. Scope of stapled peptides using CSA and 4-bromobenzaldehyde. [a]Determined by estimating the consumption of the linear peptide **77** using HPLC.[94]

Similarly to Lavilla and co-workers,[95] the proteolytic stability of tryptophan-linked stapled peptide **78d** and its linear counterpart **77d** was investigated. Following treatment with chymotrypsin (a digestive enzyme), analytical HPLC identified rapid degradation for linear peptide **77d** whereas stapled peptide **78d** showed resistance (**Figure 18**). Therefore, this new intramolecular Trp stapling strategy tolerated a wide variety of amino acid functional groups showcasing the robustness of the methodology but also the enhanced stability of cyclised products against proteolytic cleavage can aid the development of peptide-conjugates for targeted delivery of a drug or imaging agent.

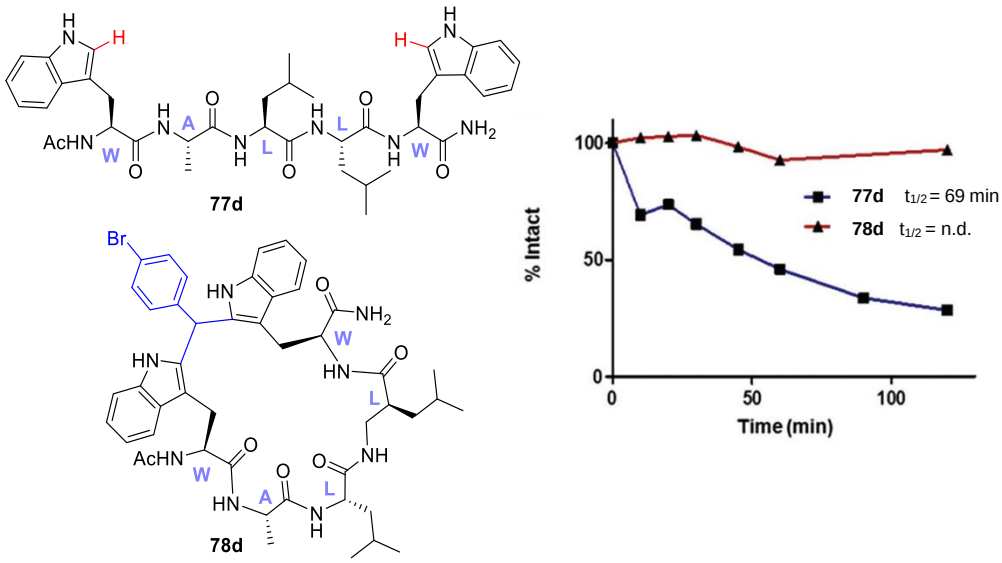

Figure 18. Chymotrypsin proteolysis highlighting the stability difference toward degradation between linear **77d** and cyclised peptide **78d** analogues.[94]

Conclusion

In conclusion, there are few available methods for peptide stapling utilising the Trp residue and drawbacks are often associated with each technique. Most examples require the use of expensive, rare metal catalysts with high loadings along with additives or reagents in high excess. In some cases, protecting groups are required either on other amino acid side chains or Trp itself and exploration into functional group compatibility was limited, which lowers the chance of successful application to peptide modification. Once again organic solvents dominate this field, potentially limiting the applicability to certain biomolecules. Ideally multiple synthetic steps and toxic solvents would be avoided therefore, peptide stapling *via* Trp modification would benefit considerably from development, with the aim of a more sustainable approach, encouraging application to industry to aid the advancement of peptide therapeutics.

Over the last decade, photochemical C–H functionalisation has emerged as an important synthetic strategy that can overcome some of the drawbacks associated with the previously discussed methods. The use of single-electron processes, under mild conditions, can unlock transformations previously unattainable *via* 2-electron mechanisms, opening up new methods for biomolecule bioconjugation.

1.4 Photocatalysis

Photocatalysis, especially utilising light in the visible region, has gained increasing attention over the last decade as an operationally simple method for carrying out novel transformations under mild conditions.[110] A photocatalyst (PC) harvests the light to access a photoexcited state which can engage in single electron transfer (SET) processes with organic substrates. As a result, reactive radical intermediates are formed which can participate in a range of reactions (**Scheme 14**).[111]

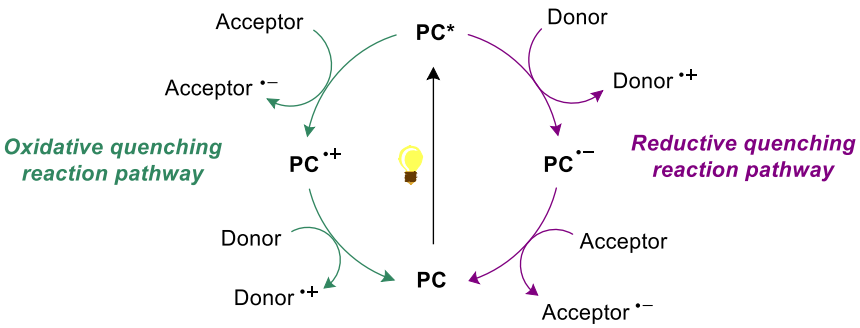

Scheme 14. An overview of two possible quenching pathways for an excited photocatalyst.[111]

PCs employed are typically transition metal complexes containing ruthenium, iridium and sometimes palladium,[110] all of which have limited availability or are at a rising threat due to increased use. Alternatively organic PCs have been employed such as 4CzIPN and 3DPAFIPN,[111] which can be readily synthesised and avoid the use of precious metals.

The use of visible light as the energy source to drive a reaction instead of heat is favourable from a practical perspective by the instant control of reaction kinetics, whereas with temperature-controlled reactions, time and energy is wasted through heating and cooling. Light can also be supplied at a single wavelength (or at least a narrow range) which corresponds to a specific energy for each photon. Tuning the wavelength to match the energy gap between the PC and its photoexcited state favours successful photon absorption hence reaction efficiency.

Photobioconjugation, the photochemical modification of biomolecules, is an underdeveloped area of chemical biology, which has gained increased attention over the past decade.[81] With ongoing development into this field the number of amino acids acting as chemical handles is expanding; in 2018 only six amino acids were plausible targets for photocatalytic modification, whereas just four years on, 15 residues have shown at least one successful photocatalytic transformation.[112] The type of biomolecule substrate varies in complexity from amino acid to protein with the latter being much less common.[110,112] Cys is the most explored residue presumably due to its low abundance and ability to form radical cations,[110] followed by His and Tyr. Chemoselective methodologies developed for these amino acids have been successfully applied to protein substrates (> 50 amino acid residues).[112]

1.5 Photochemical Modification of Trp

Because this research revolves around Trp modification, an overview of the most relevant photo-induced transformations applied to Trp will be discussed, all of which have been used to synthesise at least 10 small molecule-peptide conjugation products. Chemoselectivity for Trp was

generally observed, however, a wide range of yields (20 – 80%) were reported due to cross-reactivity with certain amino acids.

Fluoroalkylation

Protein modification *via* fluoroalkylation is useful for understanding the protein's function and dynamics within cells using ^{19}F NMR spectroscopy (discussed previously).[51,113] Chiang and co-workers reported visible light induced trifluoromethylation of tryptophan-containing peptides using sodium trifluoromethanesulfinate ($NaSO_2CF_3$, 2 eq.), $Ir[dF(CF_3)ppy]_2(dtbbpy)PF_6$, (2 mol%) and blue LED irradiation (**Scheme 15**).[114] This is a significant improvement with regards to efficiency compared to previous literature conditions reported by Krska in 2018: $Ir[dFCF_3ppy]$ (15 mol%), $NaSO_2CF_3$ (20 eq.) and 20 h.[115]

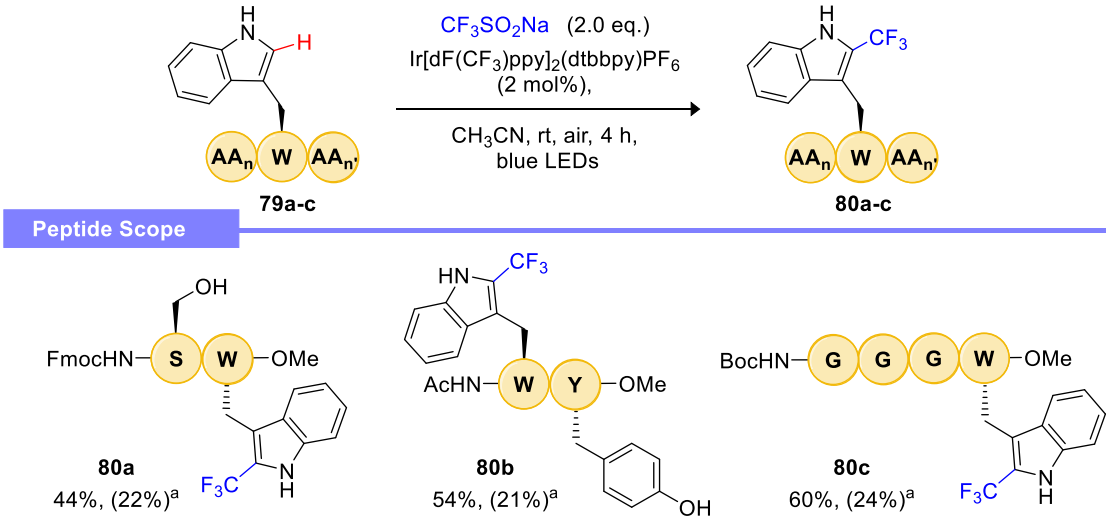

Scheme 15. Trifluoromethylation of Trp-containing peptides.[114] [a]CH_3CN/H_2O (1:1), 14 h.

To determine the functional group compatibility of the reaction twelve peptides were exposed to the photocatalytic conditions in both CH_3CN and $CH_3CN:H_2O$ (1:1). Moderate yields (44 - 60%) were obtained in the presence of readily oxidisable (**80a**), aromatic (**80b**), and relatively inert

(**80c**) amino acids when CH_3CN was used as the solvent. However, when replaced with the more biocompatible solvent system (CH_3CN:H_2O) a longer reaction time of 14 h was required and a significant drop in yield was observed in all cases (**Scheme 15[a]**).

In general, chemoselectivity for Trp was achieved despite other amino acids being susceptible to trifluoromethylation including Tyr, Phe and Cys (observed using ^{19}F NMR spectroscopy). Competition assays revealed that Trp was preferentially functionalised however when equimolar mixtures of amino acids were used as substrates for the reaction. Interestingly His did not form trifluoromethylated products yet inhibited the desired reaction on Trp, therefore Cys and His were deliberately excluded from the peptide scope.

Carbamate Insertion

In 2020, Taylor and co-workers reported the addition of carbamates to Trp residues using UV light in the absence of a PC (**Scheme 16**).[116] The higher energy associated with UV-B light (λ = 280 – 315 nm), compared to visible, enables the functionalisation mechanism to proceed *via* indole excitation. This facilitates chemoselectivity for Trp within peptides because Trp is the most photochemically active of the aromatic residues,[117] with a greater capacity for absorbing photons in the UV-B range.[118]

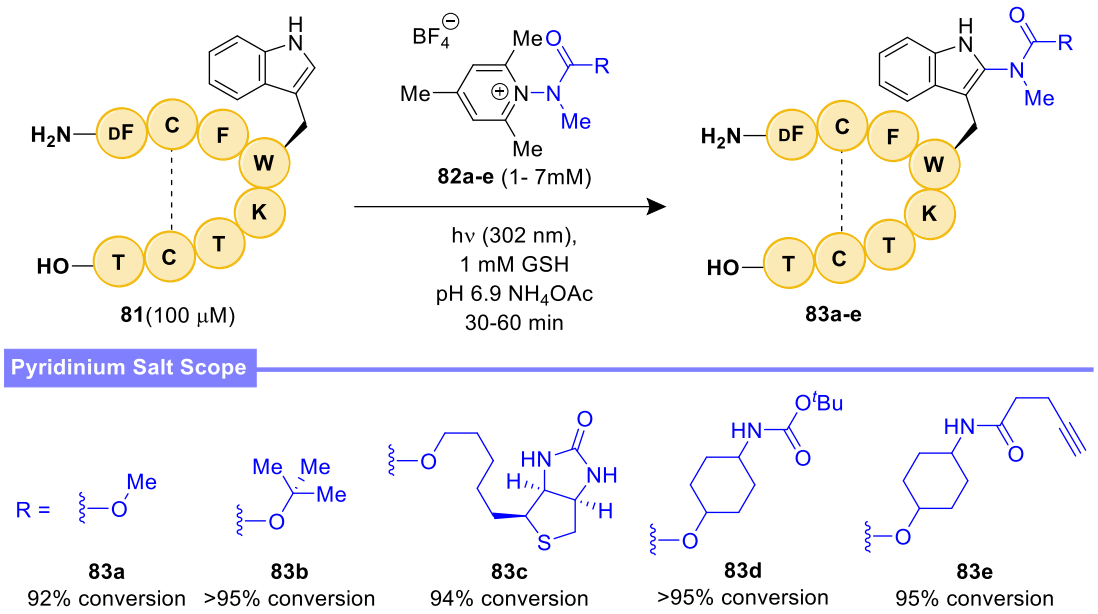

Scheme 16. Estimated LCMS TIC conversions for a range of products synthesised by photochemical carbamate insertion using pyridinium salts.[116]

An additive glutathione (GSH) was crucial for achieving complete conversions (>95%), by acting as a reactive oxygen species (ROS) scavenger, and a large excess (10-70 eq.) of the pyridinium salt reagent **82a-e** was used which is inefficient and wasteful. Despite these drawbacks, this procedure is the only example with the following appealing features: buffered solution (pH 6.9 NH_4OAc), short irradiation times (15 and 60 min) and successful application to a protein substrate.

The versatility of the *N*-carbamoyl pyridinium salt was displayed through simple and convenient derivatization of the carbomyl moiety, even for the incorporation of biologically relevant small molecules including biotin **83c** and alkyne **83e**. When applied to their model octreotide **81** reaction profiles showed clean conversion (HPLC analysis), with little or no side-product formation, however **83a** was isolated with a 68% yield (> 20% less than the estimated conversion).

A further four peptides of increasing weight (1.2 – 3.4 kDa) were selectively functionalised on the Trp residue, three of which are shown in figure 19. Very high conversions (85 - >95%) were reported with the lowest being 85% for the peptide Mellittin product **85**. It should be noted that oxidation, degradation, or di-labelled side products were observed for certain substrates, however this was very minor with the poorest selectivity being 9:1 mono- to di-labelling for the antibiotic daptomycin **84**. Excellent selectivity for Trp was observed when lysozyme (14.3 kDa) was exposed to the conditions for as little as 15 min. Despite the presences of six Trp residues in the sequence, a 6:1 mono:di labelled conjugate **86** was obtained *via* Trp-62 functionalisation.

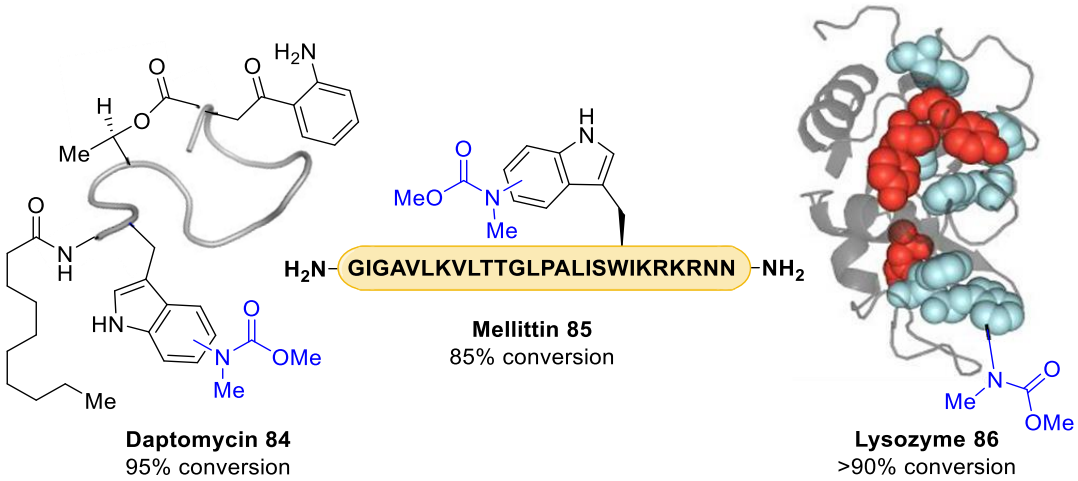

Figure 19. Photochemically modified biomolecules and their % conversion estimated by LCMS TIC.[116]

Alkylation

The final photoinduced transformation reported for Trp modification is alkylation, specifically α-carboxyalkylation. This has been achieved using α-bromo-carbonyl reagents with the aid of $Ir(dF(CF_3)ppy)_2(bpy)]PF_6$,[119] or alternatively in the absence of a photocatalyst using Katritzky salts.[120]

(a) Alkylation with α-Bromo-Carbonyl Compounds

In 2021 Paixão and co-workers reported a photoredox mediated alkylation of Trp-containing peptides (**Scheme 17**).[121] A low loading of the Ir PC was used and a wide substrate scope for both the alkylating agent and the peptide was reported, showcasing excellent functional group tolerance.

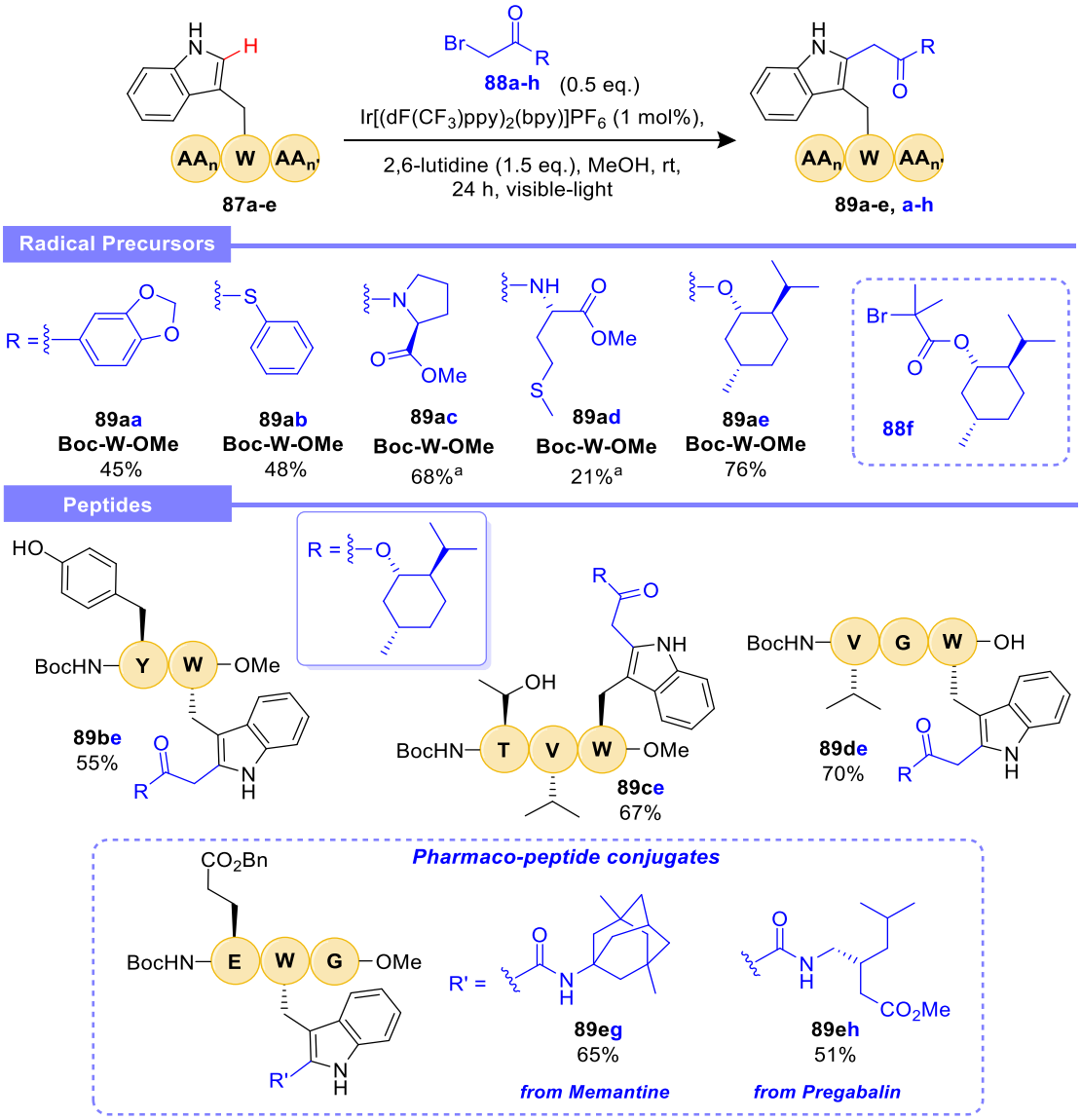

Scheme 17. Photocatalytic alkylation of Ac-W-OMe **87a** and peptide substrates **88b-e** using a range of α-bromo-carbonyl compounds. [a]2 mol% Ir[(dF(CF$_3$)ppy)$_2$(bpy)]PF$_6$.[121]

Several drawbacks to this procedure included the use of an additive (2,6-lutidine) along with long irradiation times of 24 h with two visible-light lamps

(90 W each). Additionally, 2 equivalents of the peptide were required with respect to the α-bromo-carbonyl reagents meaning half of the usually precious peptide is wasted. Despite these minor limitations, using the amino acid substrate Boc-Trp-OMe **87a**, a variety of α-bromo acetophenones, esters, thioesters, amides and amino acids proved to be successful alkylating reagents (**Scheme 17**). The desired products were synthesised in generally good yields (40 - 76%) with a couple of exceptions including **89ad** (21%). An increase in PC loading (2 mol%) was required when amide alkylating reagents were used and tertiary radical precursor **88f** was unsuccessful**.**

The regio- and chemoselective potential of the photocatalytic alkylation was investigated using Trp-containing di-, tri- and tetrapeptides providing moderate to good yields of the alkylated peptides (26 - 70%). Most proteinogenic amino acid side chains were tolerated: aromatic **89be**, polar **89ce** and aliphatic **89de**. The free C-terminal on the latter also demonstrated negligeable interference. However, a robustness study revealed that L-Glu, L-Lys and L-Met all decreased product yield and L-His inhibited the reaction.

Pharmaco-peptide conjugates **89dg** and **89dh** were synthesised using standard conditions and radical precursors derived from drugs (**Scheme 17**). The drug memantine is used to treat Alzheimer's disease and pregabaline is used to treat epilepsy, highlighting not only the versatility of the reaction but the pharmaceutical value as potential PDGs.

(b) Alkylation with Katritzky Salts

An alternative photo-induced method for Trp alkylation in the absence of a photocatalyst was reported by Melchiorre and co-workers, exploiting the formation of an electron donor–acceptor (EDA) complex (**Scheme 18**).[120]

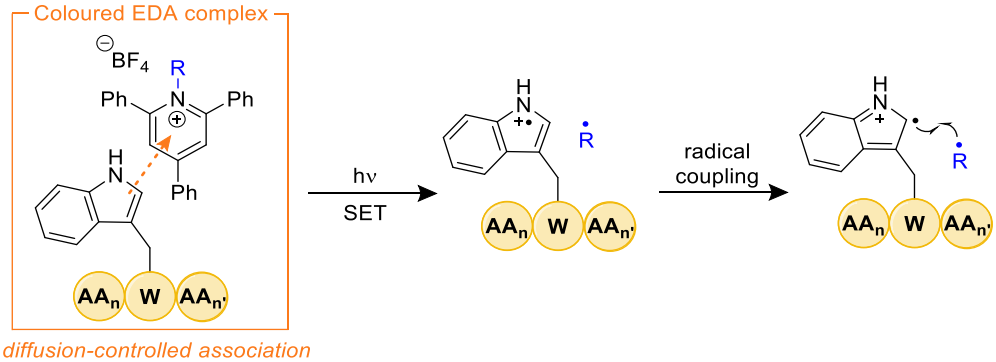

Scheme 18. Photochemical EDA complex strategy to generate radicals in close proximity of tryptophan.[120]

Formation of this complex is achieved *via* diffusion in solution between the electron rich indole ring of Trp (the donor) and the Katritzky salt which bears a pyridinium moiety (the acceptor).[120] Like with the carbamate insertion procedure,[116] higher energy irradiation (λ = 390 nm) exploits the photoactivity of the EDA complex allowing excitation. Subsequent SET generates a radical ion pair within close proximity for facile radical recombination (**Scheme 18**).

A methodical investigation regarding the selectivity for Trp was carried out using 14 dipeptides with the sequence Boc-W-AA-OMe, and generally moderate to good yields were obtained (45 - 84%) (**Scheme 19**). In particular, the protocol tolerated oxidizable amino acids **92aa**, a thioether **92ba** and the imidazole ring on His **92da**, albeit for the latter a much lower isolated yield was obtained (20%). This is advantageous over the alkylation with α-bromo-carbonyl reagents discussed above,[119] where His completely

inhibited product formation and the presence of a thioether moiety caused a significant 30% drop in product yield.

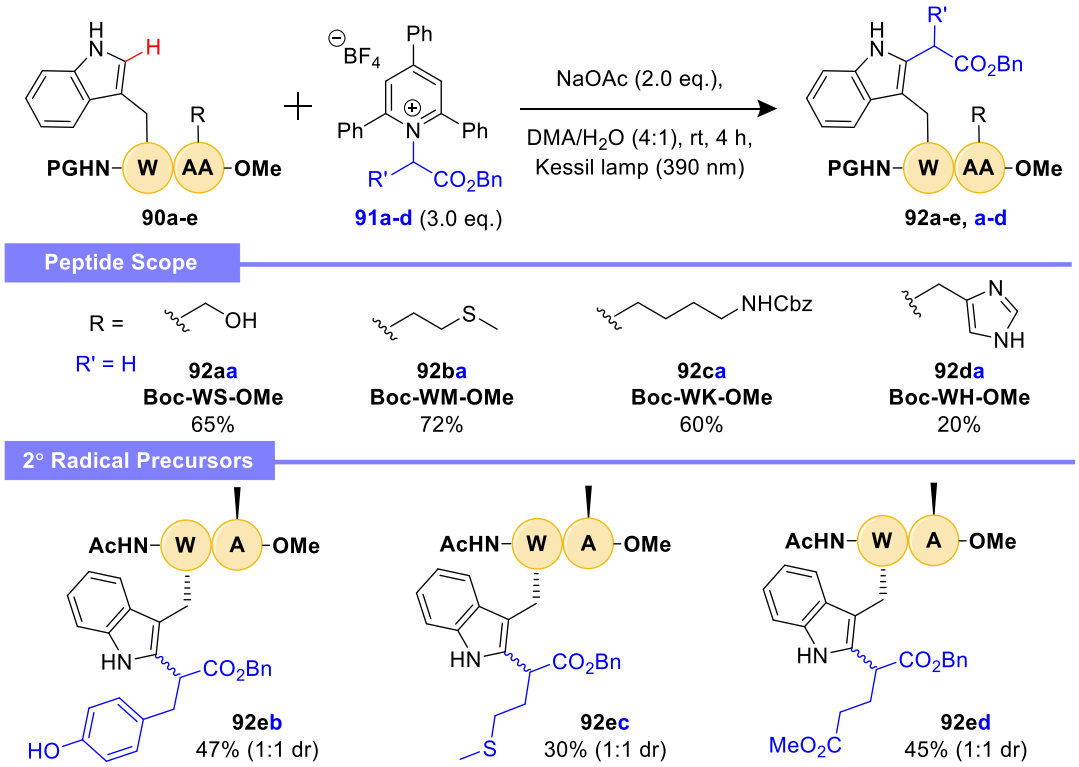

Scheme 19. Photocatalytic alkylation of dipeptides using Katritzky salts as both primary and secondary radical precursors.[120]

Tri- and tetrapeptides were also successfully alkylated (41% and 51% yields), however they both contained relatively inert aliphatic residues (Gly and Leu). Unprotected amino acid residues (H-Trp-OH and Boc-Trp-Asp-OH) and the free thiol on Cys however, were not tolerated and their reactions were not discussed further.

Alternative Katritzky salts were readily prepared from amino acids creating secondary radical precursors for Trp alkylation, however these generally resulted in lower yields compared to the primary salts (**Scheme 19**). A variety of functional groups were chemoselectively conjugated to Boc-Trp-Ala-OMe including a phenol **92eb**, thioether **92ec** and ester **92ed** in moderate yields (27 - 50%). In all cases, the newly generated stereocenter

could not be controlled resulting in inseparable mixtures of diastereoisomers.

Conclusion

Evidently, there are a small number of available photochemical strategies for Trp C–H functionalisation specifically within peptides, highlighting this under-explored class of bioconjugation chemistry. Discussed above was the formation of a new C–X bond (X = C or N) at the C–2 position on Trp and high chemoselectivity was achieved for a variety of peptide substrates. Operationally simple photochemical set-ups were used with generally mild conditions, however long reaction times, organic solvents, rare metal PCs and excess reagents were also commonly used. Most methodologies were impacted negatively or completely inhibited by the free thiol of Cys, the imidazole ring of His or other functionalities incorporated in amino acid side chains hence protecting groups were frequently employed.[87] Alternatively, peptide substrates featuring mostly hydrophobic residues, such as dipeptides containing only Trp and Ala,[120] or a tetrapeptide containing three Gly residues were often employed to avoid side reactions and lower product yields.[114] Consequently, these functionality concerns or hindrances could prevent broad application to natural peptide substrates. Therefore, the development of strategies which can chemoselectively modify complex Trp-containing peptides in the presence of all native amino acids are required.

1.6 Project Aims

The aim of the project is to develop a more sustainable photocatalytic alkylation strategy targeting Trp. The transformation would provide a novel method for accessing modified peptides, supporting the discovery of new therapeutic peptides and photo-bioconjugation (**Scheme 20**). The objectives of the project are to:

- Develop a photocatalytic alkylation strategy (**Scheme 20A**) which overcomes limitations present in the current literature by aiming for more sustainable conditions: an organic photocatalyst, stoichiometric reagents and the absence of additives.
- Ensure conditions are progressed which allow application of the methodology to peptides and investigate chemoselectivity for Trp.
- Investigate the versatility of the reaction through the synthesis of a range of small molecules to conjugate to the peptides. Different moieties should be explored for different product applications.
- Explore potential applications of the methodology including protein modification (**Scheme 20B**) and/or peptide stapling to form macrocyclic peptide products.

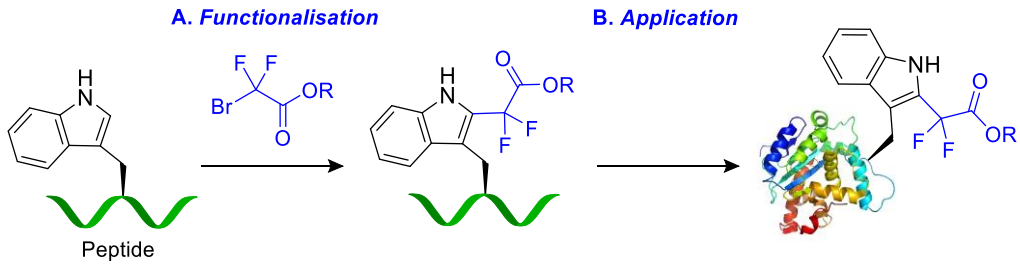

Scheme 20. Photocatalytic alkylation of Trp and a potential application of the methodology.[122]

2 Reaction Optimisation

Research began with the development and optimisation of photocatalytic alkylation conditions using Ac-Trp-OEt **93** as the biomolecule and ethyl bromodifluoroacetate **94a** as the radical precursor. Difluoroalkylation was the modification of choice because this chemical handle (CF_2FG) has been shown to form the desired radical intermediate using a range of photocatalytic conditions.[123,124] Variations of reagent **94a** such as α-bromo carbonyl compounds (without fluorine atoms), often require additives to form a reactive radical species.[121] This was an unfavourable stipulation because aside from aiming for a high product yield, a key objective was to overcome some of the sustainability limitations associated with current literature methods: using additives or excess reagents and rare metal catalysts. Furthermore, because the methodology will be applied to biomolecules it was important to aim for biocompatible conditions: temperatures below 37 °C, pH 6-8, and an aqueous/ aqueous:organic solvent system.[125]

2.1 Photocatalytic Difluoroalkylation

Cho and co-workers reported the photocatalytic difluoroalkylation of aromatic and heteroaromatic compounds: two of which were indole substrates.[123] A high product yield was obtained for the difluoroalkylation of 3-methylindole **74** using an Ir photocatalyst and ethyl bromodifluoroacetate **94a** (**Scheme 21**).

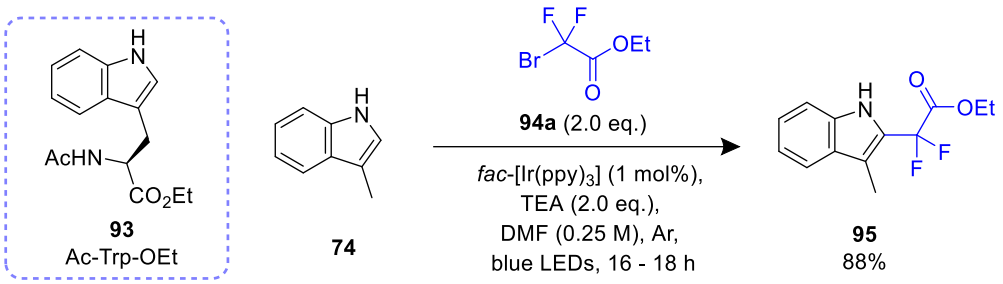

Scheme 21. Photocatalytic alkylation of 3-methylindole reported by Cho.[123]

It was hypothesised that this method could be used as a peptide modification strategy using Trp as the chemical handle. Both substrate **74** and Ac-Trp-OEt **93** contain the crucial indole moiety; however, the conditions would require adjustment aiming for biocompatibility.

The reaction is photon-mediated; it begins when the PC (in this case *fac*-[Ir(ppy)$_3$]) absorbs a photon to reach the photoexcited state (**Scheme 22**).

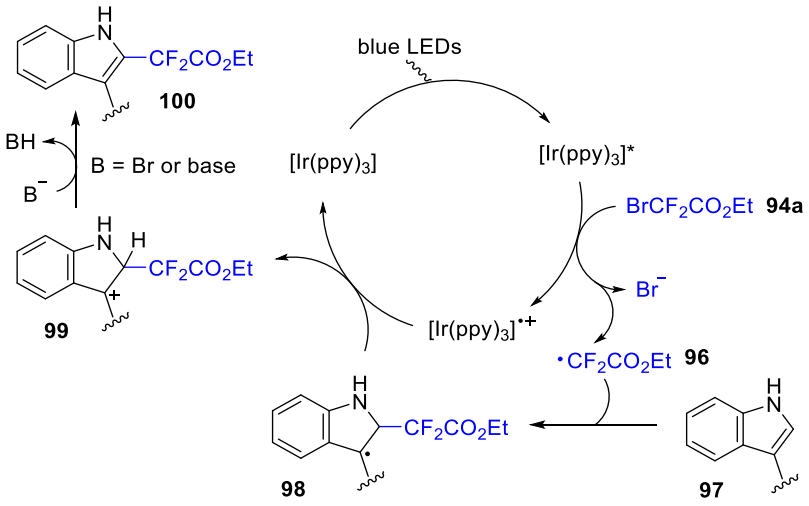

Scheme 22. Proposed catalytic cycle based on literature precedent.[123]

The excited PC ([Ir(ppy)$_3$]*) reduces bromodifluoroacetate **94a** forming the alkyl radical **96** which reacts favourably with the electron rich indole ring to give the radical intermediate **98**. This newly formed indole radical **98** is oxidised by [Ir(ppy)$_3$]$^{\cdot+}$, generating the carbocation **99** while simultaneously regenerating ground state [Ir(ppy)$_3$], closing the

photocatalytic cycle. Finally, cation **99** undergoes rearomatisation to give the product **100**.

Cho's research (**Scheme 23**) revealed that the reaction was most successful with electron-rich aromatic substrates including substituted benzene derivatives **101a** and **101b** and heteroaromatics **103a** and **103b**. However, over half of their aromatic substrate scope gave a mixture of alkylated products e.g. **102b**, which showed that even though the regioselectivity followed the expected trend for radical mediated aromatic substitution, it could not be controlled to give a single product selectively.[123]

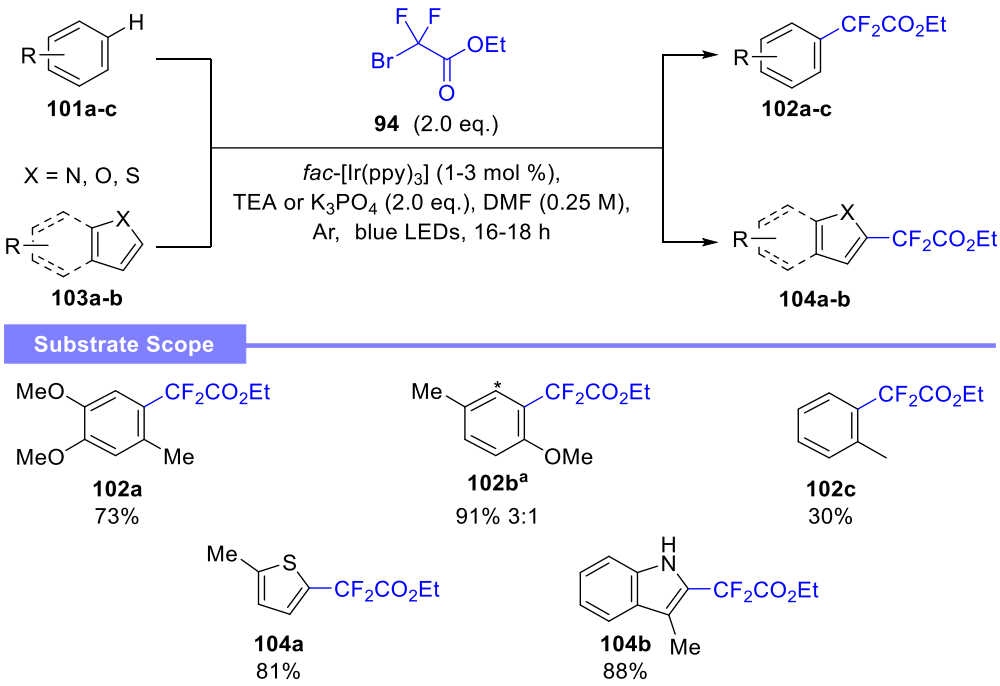

Scheme 23. Photocatalytic alkylation of aromatics and heteroaromatics showing isolated yields. [a]The minor regioisomeric position is labelled with "*", and the ratio was determined by ^{19}F NMR spectroscopy, gas chromatography, and nOe experiments.[123]

Furthermore, less electron rich substrates gave much lower product yields (**102c**) because the reaction utilises an electron-deficient carbon-centred radical (·CF_2R). A favourable polarity match is observed between this radical **96** and the electron rich substrates which can enhance the stabilisation of radical/cationic intermediates, through electron delocalisation and

induction, therefore promoting product formation.[126] In contrast, these advantageous mechanistic features are not achieved for electron poor compounds, hence lower or negligible product yields were obtained. The innate reactivity of an electron deficient radical presents the opportunity for selective Trp modification within a peptide because Trp is the most electron rich aromatic amino acid.

2.2 Photocatalytic Difluoroalkylation Analysis

For the optimisation studies Ac-Trp-OEt **93** was chosen as the model substrate. Both *N*– and *C*–termini were initially protected to avoid any potential side reactions or solubility issues. Cho's literature conditions were applied to amino acid **93** (**Scheme 24**) which gave a 55% isolated product yield when a blue LED light strip (iNextStation, 24 W) wrapped inside a Pyrex dish was used as the irradiation source.

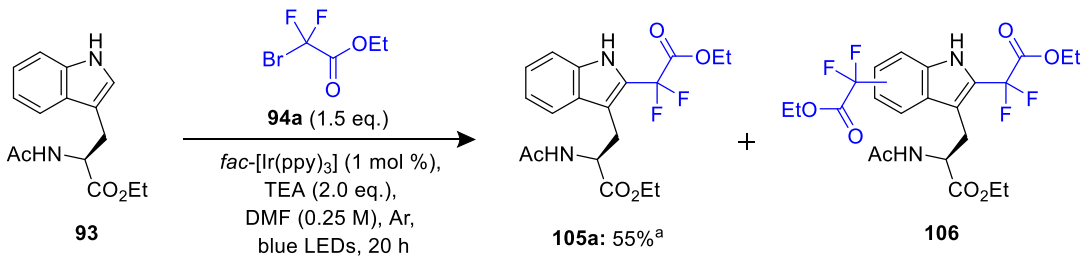

Scheme 24. Photocatalytic alkylation of Ac-Trp-OEt using slightly modified conditions reported by Cho and co-workers.[123] [a]Isolated yield.

For this initial reaction, 1.5 equivalents of bromodifluoroacetate **94a** were used instead of 2.0 which was reported in the literature.[123] Preliminary studies by Dr James Cuthbertson showed that a significant amount of dialkylated product **106** was observed when a greater excess of alkylating agent **94a** was used. This side product was briefly mentioned in the literature; however, it was stated that the desired product had a lower reactivity toward alkylation compared to the starting material, therefore it

was not a concerning problem as monoalkylation was favoured. Having shown that Trp could be alkylated the reaction was then optimised, throughout which the reaction mixtures were analysed by both quantitative fluorine NMR spectroscopy and analytical HPLC. Both techniques were utilized to gain a better understanding of the reaction mixture: the fluorine NMR spectrum allowed quantitative ^{19}F spectroscopic yields to be obtained for the desired product and the analytical HPLC trace identified any starting material (SM) remaining. Regarding fluorine NMR spectroscopy, the longitudinal relaxation time constants (T1) were measured by Dr Kevin Butler using inversion recovery experiments on the model system (Ac-Trp-OEt **93** and $BrCF_2CO_2Et$ **94a**). It was identified that both compounds had completely relaxed after 2.5 seconds (T1 = 2.5 secs) and to allow quantitative analysis of NMR spectra, the repetition time (delay) between consecutive excitation pulses (scans) must be ≥5 × T1 to allow ≥99.3% relaxation.[127] Therefore the parameters for the fluorine NMR spectroscopy experiments were set: 15 sec delay with 32 scans, where the latter aided signal intensity. With the addition of an internal standard, α,α,α-trifluorotoluene (TFT), the integral of the product **105a** signal(s) could be used to determine quantitative ^{19}F NMR (qNMR) spectroscopic yields. In figure 20 this is 79%: 85% integral for product doublet a with the deduction of a 6% impurity signal b which was present between the doublet peaks. The second doublet has been labelled as a' for completion.

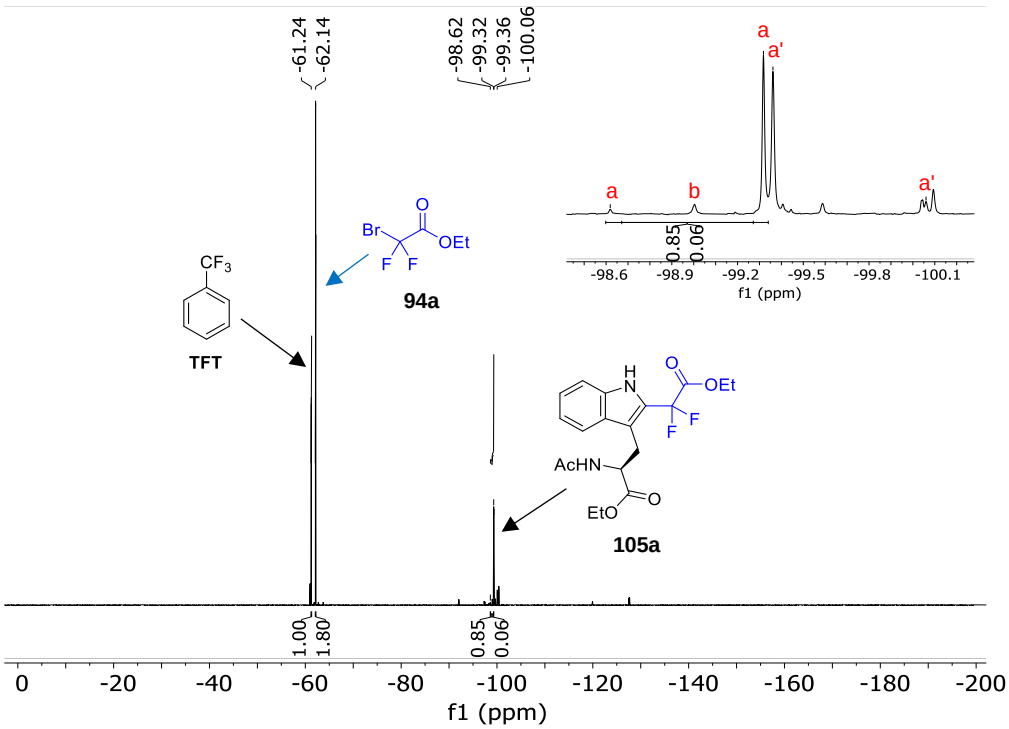

Figure 20. A representative fluorine NMR spectrum of a reaction mixture during optimization.

Both analytical techniques showed evidence of side product formation by the appearance of additional signals. Unfortunately, due to the minor quantities formed, it was challenging to interpret these signals quantitatively using ^{19}F NMR spectroscopy. Whereas utilizing analytical HPLC allowed the number of side products (3 - 4) to be identified (**Figure 21**). Another advantage of HPLC analysis was starting material (SM) **93** observation. An analytical HPLC chromatogram shows UV absorbance (mAU) against time, and the distinct retention times (Rt) of the compounds

with minor signal overlap, allowed clear identification of each signal (**Figure 21**).

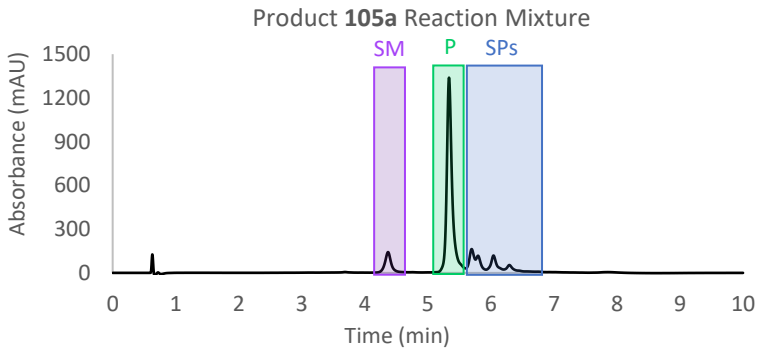

Figure 21. Analytical HPLC chromatogram for an example reaction mixture showing starting material (SM), product (P) and side products (SPs) on analytical gradient 20-80% B over 5 min, 280 nm.

Integrating each compound signal gave a value for its relative intensity which was used for basic comparative purposes: minor or major signal / more or less of a specific compound. It should be noted that this was not a quantitative approach due to differences in extinction coefficient between the different species, however, instead was used as a complementary technique to support and potentially explain the yields determined by ^{19}F NMR spectroscopy and isolated yields obtained for specific examples.

HPLC-MS was carried out on the reaction mixture and three side product signals had the same mass associated with them, the mass which corresponded to dialkylated Trp **106**. This can be explained by the formation of regioisomers: same mass but presumably slightly different polarities, hence distinct retention times on the reverse phase column. However, similar retention times were apparent on a normal phase column, therefore isolation of pure products was not achieved. Co-elution was observed for the side products along with some desired product contamination therefore the ^{1}H NMR spectrum consisted of many overlapped signals (especially in the aromatic region). Despite this, additional signals were observed in the aliphatic region and in the ^{19}F spectrum (within close range of the

monoalkylated product signals: −97 → −104 ppm). Even though the specific site of a subsequent alkylation was not identified, with the available NMR and MS data, it can be speculated that the side products are regioisomers of dialkylated Ac-Trp-OEt **106**.

Similarly, Gillaizea and co-workers observed a mixture of products when indole **107** was exposed to iron-catalysed trifluoromethylation, showing that electrophilic radicals (·CF_3) can insert onto the benzene ring of indole (**Scheme 25**).[128]

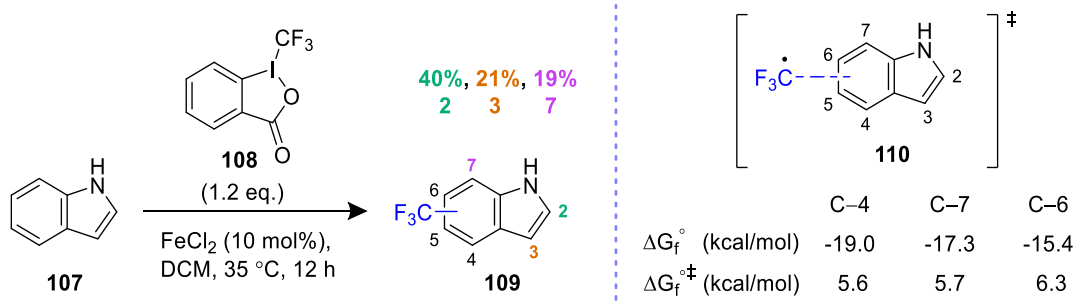

Scheme 25. Iron-catalysed trifluoromethylation of indole (left)[128] Energetics of calculated structures at B3LPY/6-311G** (right).[129]

Furthermore, separate DFT studies revealed that the difference in energy barrier for trifluoromethyl radical addition to positions C–4, C–6 and C–7 on the benzene ring of indole **107** is very small ($\Delta G_f^{\circ\ddagger}$ 5.6 kcal/mol, 5.7 kcal/mol and 6.3 kcal/mol, respectively).[129] Therefore, in theory radical addition could be observed for such positions and it was important, throughout optimisation, to minimise the formation of these regioisomeric side-products.

2.3 Photocatalytic Difluoroalkylation Conditions

The most coherent way to discuss the results obtained throughout optimisation is to introduce the final optimised conditions first, followed by reaction deviations. The reason for this is because a lot of the earlier

experiments were carried out using only HPLC analysis, hence quantitative data was not obtained. This resulted in inconsistent data being recorded as optimisation studies progressed and became difficult to compare certain reactions to subsequently draw conclusions with confidence. Therefore, significant experiments were repeated using ^{19}F NMR spectroscopy which allowed accurate spectroscopic yields to be obtained for the products providing a more concise and comprehensible discussion.

Numerous optimisation studies were carried out exploring reaction parameters such as solvent, base, photocatalyst, time and equivalents of reagents, along with the photoreactor set-up, presence of air and scalability of the process. The final conditions for the photocatalytic alkylation of Ac-Trp-OEt **93** are reported in table 4 entry 1.

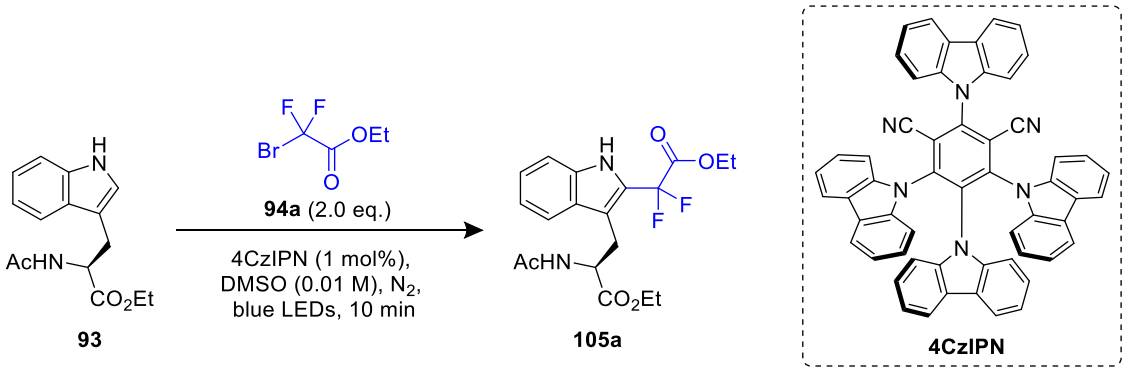

Entry	Deviation from standard conditions	% Yield[a]
1	none	71
2	*fac*-[Ir(ppy)$_3$] (1 mol%), TEA (2 eq.), DMF (0.25 M), blue LEDs, 17 h[123]	30[b]
3	Stirred	67
4	Standard set-up blue LED strip: 10 min, 60 min	25, 53
5	No PC/ no light	0

Table 4. Reactions carried out on a 60.0 μmol scale in position A of the PhotoRedOx box using EvoluChem™ LED spotlights (455 nm). [a]Yields determined by ^{19}F NMR spectroscopy using TFT as the internal standard. [b]120 μmol scale.

Unlike the initial, proof of concept experiment (**Scheme 24**) in which a blue LED light strip wrapped inside a Pyrex dish was used as the irradiation source, a different photoredox setup was used for most of the optimisation

reactions: Hepatochem's PhotoRedOx Box equipped with an 18W, 34 mW•cm^{-2} LED 455 nm bulb (**Table 4**).

Throughout the optimisation studies, yields were determined by quantitative fluorine NMR spectroscopy instead of isolated yields for speed and accuracy. Due to the reactions being carried out on a 60 μmol scale, small scale errors when weighing the product and inherent loses through work-up and purification techniques could result in less reliable isolated yields for comparison purposes. Subsequently this could lead to the inaccurate identification of the optimal conditions.

Notably in table 4 entry 2, when applying Cho and co-workers' literature conditions again to Ac-Trp-OEt **93**, there is a significant drop in product yield to 30% compared to the 55% yield obtained for the proof-of-concept experiment in scheme 24. This is because a different photoredox set-up and 2.0 eq. of TEA was used to obtain an initial product yield as a pre-optimisation yield, using literature conditions. Stirring was found to have no impact on the reaction. Therefore, to avoid potential complications (insufficient mixing and small losses on the stir bar), when low reaction volumes are used for peptide substrates, all further reactions were carried out without stirring.

Standard Set-Up vs PhotoRedOx Box

As mentioned previously, two photoredox set-ups were available: a cheaper, more readily available set-up using an iNextStation blue LED light strip wrapped inside a Pyrex dish (standard set-up), or a commercial PhotoRedOx box produced by HepatoChem (**Figure 22**).

Figure 22. Photos of the different photoredox setups showing the standard set-up (left) and the PhotoRedOx box with 8 mL and 20 mL vial holders (right).

For the standard set-up a longer reaction time (60 min) was required, and a lower yield was obtained compared to the reaction carried out in the PhotoRedOx box (53% and 71% respectively). This longer reaction time presumably resulted from the light intensity: a greater light intensity causes an increase in the concentration of excited state PC due to the proportional increase in photon-capture events.[130] Therefore a greater concentration of excited PC will lead to more radical formation at a given time, hence enhanced product formation. The EvoluChem™ LED spotlights used in the PhotoRedOx box, provided a visibly greater intensity of light compared to the LED strip, however the specific light intensity (lumens per square foot) was not measured.

Similar trends were observed by König and co-workers when they investigated the effects of four commercial photoreactors on numerous photochemical reactions.[131] They found that the initial reaction rate for the trifluoromethylation of arenes reported by MacMillan and co-workers (**Scheme 26**),[132] was dependent on light intensity. The highest rate was obtained for TAK120 reactors with an average power output of 28 W, followed by the PennOC photoreactor and the HepatoChem box each with average power outputs of 21 W and 18 W respectively.[131]

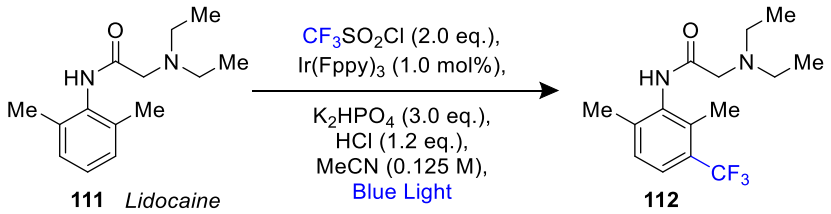

Scheme 26. Photocatalytic trifluoromethylation of arenes and heteroarenes.[132]

With that in mind, leaving the reaction for longer in the standard set-up was believed to eventually give the same product yield as the PhotoRedoxBox, just at a lower rate. However, this was not the case, the highest yield obtained using the less intense blue LED strip was approximately 20% lower than the EvoluChem™ LED spotlight and there are multiple factors that could account for this. First, a longer reaction time allows further generation of radical **96** (·CF_2CO_2Et) for the desired product formation, but also for side product formation (**Scheme 27B**).

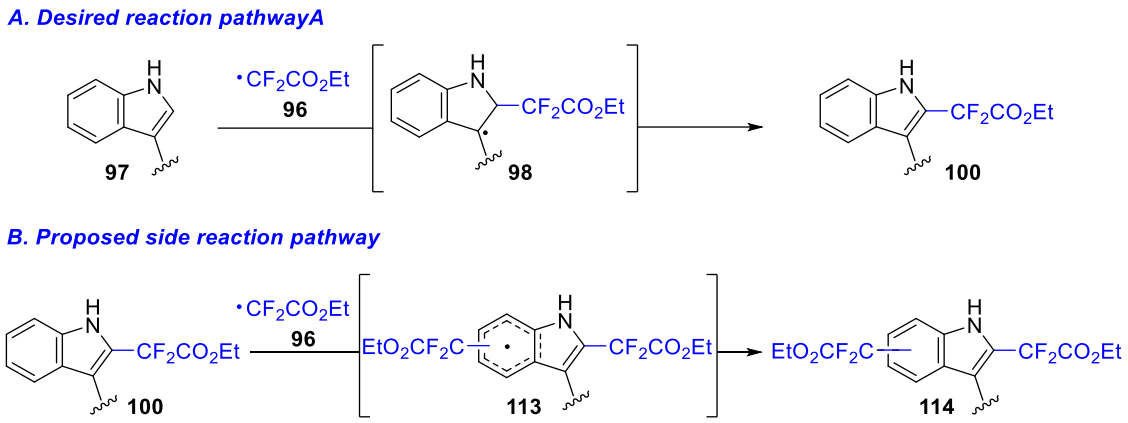

Scheme 27. Reaction pathways for desired product and side product formation.

Instead of stopping the reaction efficiently after product **100** had formed, it remained in the solution for up to 60 minutes increasing the probability of reaction with radical **96** and subsequent alkylation. Secondly, the standard set-up is not equipped with a fan so higher temperatures (up to

45 °C) were observed which could encourage thermally induced side reactions, decreasing selectivity for the desired product.

Along with light intensity, König and co-workers also assessed the effects of temperature on the photocatalysed trifluoromethylation of arenes and heteroarenes (**Scheme 26**).[132] Initially, hotter temperatures led to a higher product conversion giving yields of 97% and 64% with the corresponding reaction temperatures of 35 °C and 25 °C. However, this was only beneficial to a point and above this temperature a lower yield was obtained. This was discovered when the temperature was set to 55 °C, providing a reduced product yield of 58%,[131] which could be due to heat increasing the number of and/or rate of undesired side reactions.

Similarly, to the comparison between the PhotoRedOx box and the standard set-up, there was also a discrepancy between product yields depending on which position the reaction vial was placed in; position A or C (**Figure 23**). Despite the PhotoRedOx box being designed to ensure even light distribution and efficient cooling for each sample,[133] when simultaneous reactions were carried out in position A and C a 20% lower product yield was obtained for the latter. This drop in yield was accompanied by greater probe (radical precursor) consumption (and side product formation); therefore, it can be assumed that position C had a higher rate of reaction. The two reaction vials could have been exposed to differences with respect to light intensity and/or heat, the effects of which were discussed previously. Position C is located more centrally in the PhotoRedOx box (**Figure 23**), allowing maximum surface area exposure to the light, however position A is at the edge, potentially reducing the available amount of light intensity received. Also, the location of the fan (employed to offset

the heat released by the LEDs) is adjacent to position A. During the 10-minute reaction time, vial A remained at room temperature however reaction vial C increased by 10 °C, potentially due to vial A blocking the air flow.

Figure 23. PhotoRedOx box with 8 mL vials in position A and C.

Therefore the photocatalytic alkylation reaction appeared to be sensitive to light intensity, temperature and time, which is not uncommon for these types of reactions,[131] but does highlight the importance of reaction set-up and a potential challenge for replicating exact results. The PhotoRedOx box is advantageous over the standard set-up because it enabled standardization and acceleration of the photocatalytic reaction as a result of the built-in fan, mirrors and a higher intensity bulb,[133] hence going forward all reactions were carried out in position A of the PhotoRedOx box.

Aerobic Conditions

A reaction run in the presence of air gave a similar yield to the reaction run under anaerobic conditions (61% and 71% respectively, **Table 5**). However, aerobic conditions could potentially be detrimental to the yield for peptide substrates especially when oxidizable amino acids are present e.g. Cys,[134] therefore, to be consistent for all substrates (amino acid and peptide), anaerobic conditions were chosen. The experimental procedure is operationally simple because the requirement for a glove box or Schlenk

line is not necessary, instead the reaction solution was sparged with nitrogen for 5 minutes, after all the reagents were added.

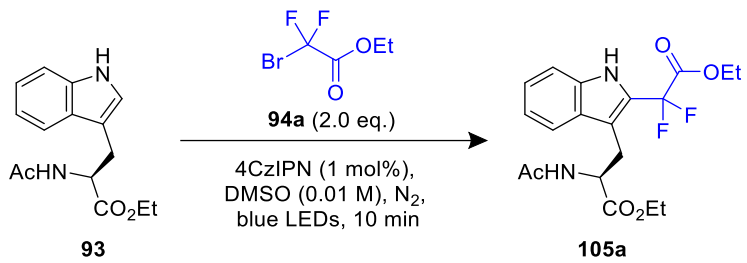

Entry	Deviation from standard conditions	% Yield[a]
1	none	71
2	Aerobic	61
3	0.2 mmol 'scale up'	65 [64[b]]

Table 5. Reactions carried out on a 60.0 μmol scale in position A of the PhotoRedOx box using EvoluChem™ LED spotlights (455 nm). [a]Yields determined by ^{19}F NMR spectroscopy using TFT as the internal standard. [b]Isolated yields.

'Scale Up'

Repeating the optimised conditions on a 200 μmol scale allowed an isolated yield to be obtained which was consistent with the qNMR yield (64% and 65% respectively). This confirmed that the yields obtained by ^{19}F NMR spectroscopy in the analytical scale reactions (20.0/60.0 μmol) were accurate. This also suggested that the reaction was not sensitive to vial size even though light penetration of the larger 20 mL vial could have been limited compared to the usual 8 mL vial. Photonic flux decreases exponentially with depth in a given reaction medium,[130] therefore a greater volume for the scale up reaction would in theory have been impenetrable, resulting in a smaller concentration of excited PC, however fortunately this was not the case here.

Solvent Screen

The initial reaction solvent was DMF (used in the literature),[123] however one of the goals of this research was to make a conscious effort toward more

sustainable conditions. This would not be achieved using DMF because it is in the red region of GSK's solvent sustainability guide,[135] and has serious hazards associated with it, in contrast to DMSO which lies in the green region. Another requirement for the solvent choice was solubility: it must solubilise the biomolecule to allow the reaction to occur which limited the number of solvents available to investigate. Despite DMSO often achieving biomolecule dissolution, in doing so this commonly disrupts hydrophobic interactions resulting in molecular unfolding,[89] which may have limitations when substrates are biologically relevant targets. Protein refolding can be carried out using dialysis and it is possible to fold into their native structures, when specific organic solvents or buffers are used,[136] however folding rates are variable, depending on the solvent, and difficult to predict.

When solubilising biomolecules, the concentration of the reaction is important. Generally, the more dilute the better: 0.01 M (**Table 6**, entry 1) is acceptable for peptide substrates whereas further dilution is desirable for protein substrates. Peptides and proteins are often precious materials where for example only 1 mg can be used for a reaction, and when accounting for the high molecular weight of these biomolecules, this would result in a very small solvent volume for reaction concentrations > 1 - 10 mM. For example, a common reaction concentration for organic chemistry is 0.25 M and this could result in a solvent volume as little as 4 μL which will unlikely dissolve all components of the reaction. Furthermore, increasing the concentration can cause the protein to aggregate,[137] which would likely hinder the desired reaction by potentially reducing the accessibility of amino acid residues.

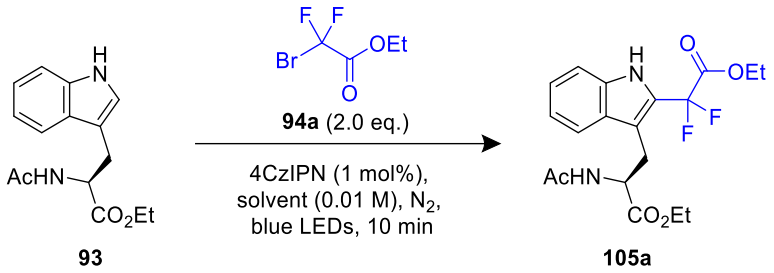

Entry	Solvent	% Yield[a]
1	DMSO	71
2	DMSO (0.25 M)	45[b]

Table 6. Reactions carried out on a 60.0 µmol scale in position A of the PhotoRedOx box using EvoluChem™ LED spotlights (455 nm). [a]Yields determined by ^{19}F NMR spectroscopy using TFT as the internal standard. [b]120 µmol scale, 60 min.

Interestingly, a more concentrated reaction solution (0.25 M) gave a lower product yield (**Table 6**, entry 2). At 10 minutes only an 8% product yield was obtained by ^{19}F NMR, and whilst extending the reaction time to 60 minutes gave an improved product yield of 45%, there was still a significant amount of unreacted starting material left (**Figure 24**). This is considerably lower than the reaction carried out in 0.01 M DMSO which gave a 71% spectroscopic yield after only 10 minutes of blue light irradiation (**Table 6**, entry 1).

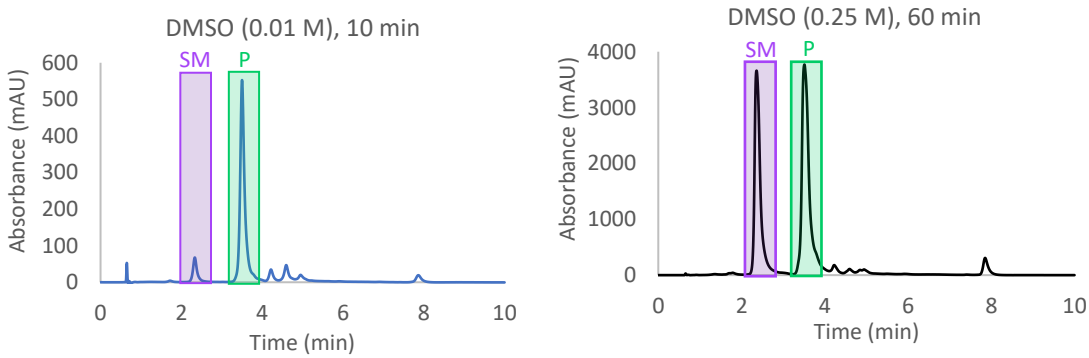

Figure 24. Analytical HPLC chromatograms for crude reaction mixtures: 0.01 M and 0.25 M DMSO with reaction times of 10 and 60 minutes respectively on analytical gradient 40-80% B over 5 min, 280 nm.

This contradicts the expected trend between concentration and reaction rate for an intermolecular addition mechanism where a higher concentration generally increases the rate of reaction due to a greater number of collisions in a given volume. Comparing crude HPLC chromatograms for the reactions

carried out in DMSO at different concentrations (**Figure 24**), it was suggested that no additional impurity signals were observed which was also supported by the ^{19}F NMR spectra. One hypothesis for the lower yield obtained when the reaction was performed as a 0.25 M concentration is that 4CzIPN dimerization may occur due to the more concentrated solution positioning molecules closer together. Two neighbouring 4CzIPN molecules can experience $\pi - \pi$ intermolecular interactions *via* full overlap (FO) or partial overlap (PO) of the aromatic groups of the carbazole units (**Figure 25**).[138]

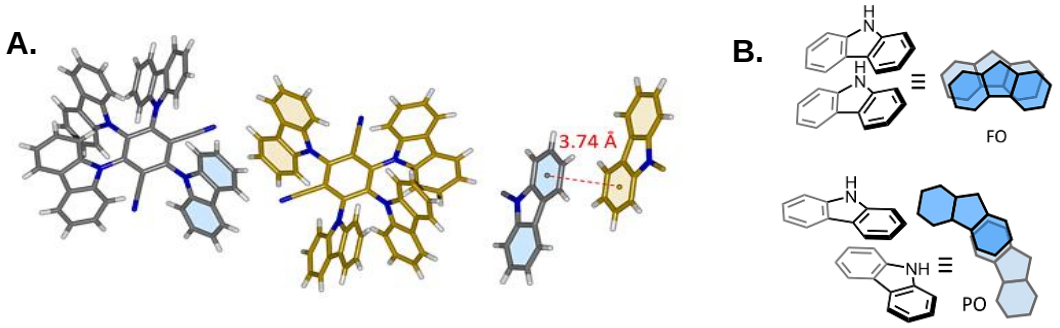

Figure 25. A. Crystal structure of 4CzIPN obtained by sublimation showing two neighbouring molecules interacting through the carbazole units and the distance between those molecules. B. Fully overlapped (FO) and partially overlapped (PO) carbazole units.[138]

When the reaction concentration is 0.25 M (in contrast to 0.01 M) some molecules presumably underwent this $\pi - \pi$ stacking, likely altering the photochemical properties of 4CzIPN and/or its availability to undergo excitation.[139] However, because the catalyst is employed in a low concentration (1 mol%), it can be assumed that other molecules were dispersed far enough apart to remain as the monomer. Therefore, less than 1 mol% of 4CzIPN was available to reduce $BrCF_2CO_2Et$ **94a** for the desired reaction, hence product **105a** formation was considerably lower but not completely inhibited.

Alternatively, increasing the photocatalyst concentration can reduce the photon penetration depth into the solution shown by the rearranged Beer-Lambert law (**Equation 1**). This inversely proportional relationship between 4CzIPN's concentration and path length can cause lower product yields due to a lower concentration of [4CzIPN]* being generated but also the distribution of these molecules relative to the quenching species $BrCF_2CO_2Et$ **94a**.[140]

$$L = \frac{-\log(T)}{\varepsilon c}$$

L = path length
T = transmittance
c = concentration of absorbing species
ε = molar extinction coefficent

Equation 1. Rearrangement of the Beer–Lambert law in terms of path length L.

After discovering that 0.01 M was the better concentration, a range of other solvents were investigated (**Table 7**). DMF provided a similar product yield to DMSO, however MeCN gave a significantly lower 22% yield.

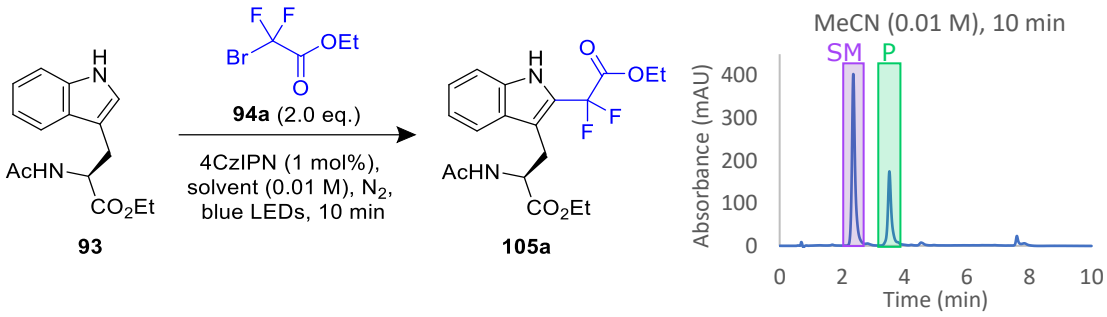

Entry	Solvent	% Yield[a]
1	DMSO	71
2	DMF	61
3	MeCN	22
4	9:1 DMSO:H_2O	71
5	1:1 DMSO:H_2O	2

Table 7. Reactions carried out on a 60.0 μmol scale in position A of the PhotoRedOx box using EvoluChem™ LED spotlights (455 nm). [a]Yields determined by ^{19}F NMR spectroscopy using TFT as the internal standard.

Likewise with other underperforming reactions, additional side products were not observed (by ^{19}F NMR spectroscopy or HPLC), instead a large amount of unreacted starting material was visible in the HPLC chromatogram. The relative intensity of starting material **93** (SM) and product **105a** (P) signals after irradiation in MeCN was 64:30 (by HPLC) whereas for DMSO and DMF the amount of Ac-Trp-OEt **93** remaining was significantly lower. Similar to the concentration effects on 4CzIPN dimerization, different solvents can promote or break the carbazole interactions, affecting the success of Trp difluoroalkylation.[138] However the formation of dimers is speculative, especially at low concentrations of 4CzIPN. Interestingly, the reaction mixture in MeCN was distinctively paler in colour compared to the other solvents. Visibly the reaction mixture was homogeneous therefore perhaps the accuracy of 4CzIPN (0.5 mg) addition was poor, hence < 1 mol% of catalyst may have been added to the mixture, resulting in a lower product yield.

The ideal biocompatible solvent would be water, however using an aqueous:organic solvent system (water/DMSO 1:1) hindered the reaction with near negligible product formation (2% yield determined by NMR spectroscopy). Additional signals were not observed by analytical HPLC (only unreacted starting material **93**), however a previously unseen signal at −56.3 ppm was present in the ^{19}F NMR spectrum. Presumably the new signal was probe related because compounds containing Trp are visible in the HPLC spectrum and usually have signals around −100 ppm in the ^{19}F NMR spectrum. Identification was unsuccessful, however a reasonable prediction would be hydrolysis of the ester bond to give the carboxylic acid

115 because this is similar to the shift reported by Hu and co-workers for $BrCF_2CO_2Na$: −57.98 ppm.[141]

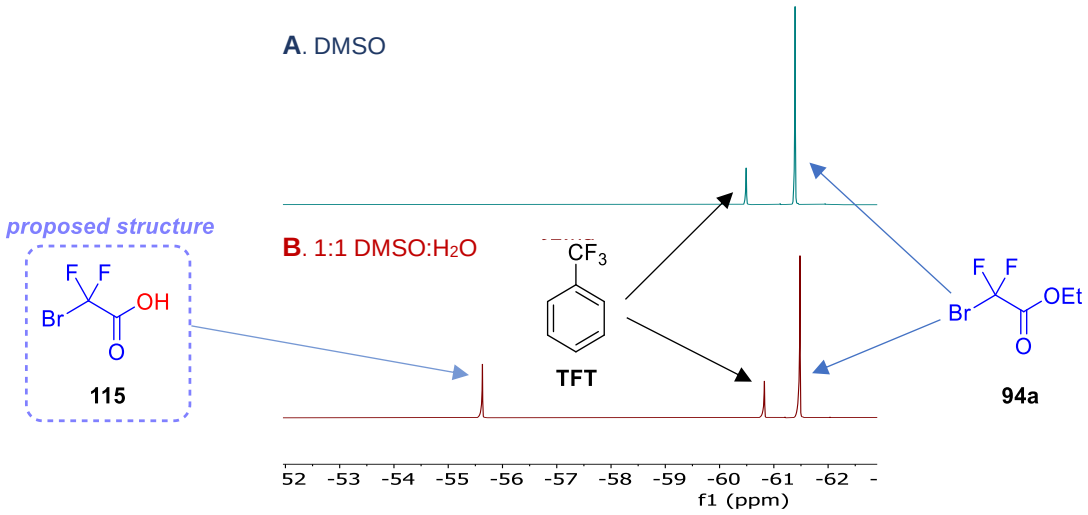

Figure 26. ^{19}F NMR spectra for probe **94a** and TFT in 100% DMSO and 1:1 DMSO:H_2O.

Running the ^{19}F NMR experiment of bromodifluoroacetate **94a** alone in 1:1 DMSO:H_2O with TFT, generated the same new signal −55.6 ppm (**Figure 26**) confirming that this compound was formed by a reaction between probe and water. Neutral ester hydrolysis can occur through water autoionization: ionization of the water molecule followed by attack of the ester. This can be either acid or base initiated but in the case of ester **94a** with an electron withdrawing $BrCF_2$− group, it would more likely proceed *via* a base initiation pathway ($W_{AI}B$) reported by Pliego and co-workers (**Scheme 28**).[142]

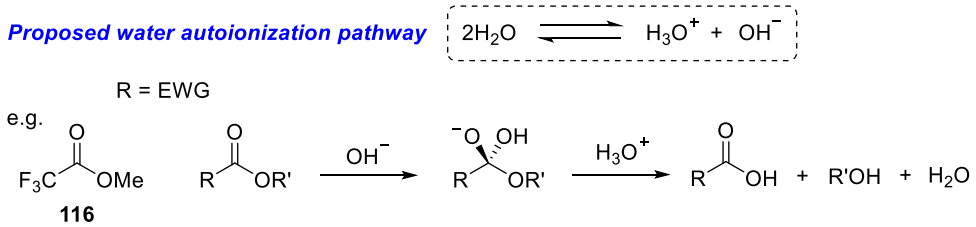

Scheme 28. Proposed water autoionization pathway.[142]

However, this gave rise to a new question resulting from the signal integrations because in 1:1 DMSO:H_2O there was approximately 1.7 eq. of bromodifluoroacetate **94a** left. In theory this excess reagent should be able

to undergo the desired reaction giving the product in a moderate yield, based on the successful preliminary studies in which 1.5 eq. of **94a** was used. Therefore, the reaction inhibition was unlikely due to the lack of available alkyl reagent **94a** initially. Instead, it is proposed that the hydrogen bromide by-product formed during photocatalytic difluoroalkylation can act as an acid catalyst, mediating further ester hydrolysis of the probe **94a**. This was supported by the increased amount of $BrCF_2CO_2H$ **115** observed at the end of the reaction (determined by ^{19}F NMR spectroscopy). Therefore, desired product formation was inhibited because presumably little or no alkyl radical was able to form due to this competing side reaction.

Interestingly in 9:1 DMSO:H_2O, the desired reaction was unaffected giving a product yield of 71%, suggesting that water is tolerated in the reaction up to somewhere between 10 and 50% v/v. Notably, $BrCF_2CO_2H$ **115** remained in the reaction mixture i.e. was not reduced by the excited state of the photocatalyst hence could not undergo the desired indole alkylation reaction. This was supported by reduction potentials reported by Luxen and co-workers which suggest it is much harder to reduce the carboxylic acid analogue of bromodifluoroacetate **94a**: −1.27 V and −0.89 V vs SCE respectively.[124] This higher value is outside the reduction potential of 4CzIPN $E_{1/2}$ ($PC^{\bullet+}/PC^*$) = −1.18 V,[112] and it therefore cannot be reduced.

Base Screen

In Cho's reported literature procedure, 2.0 eq. of triethylamine (TEA) were used for the photocatalytic difluoroalkylation of 3-methyl indole, however

they also showed that the base employed could have a big influence on reaction success (**Table 8**).[123]

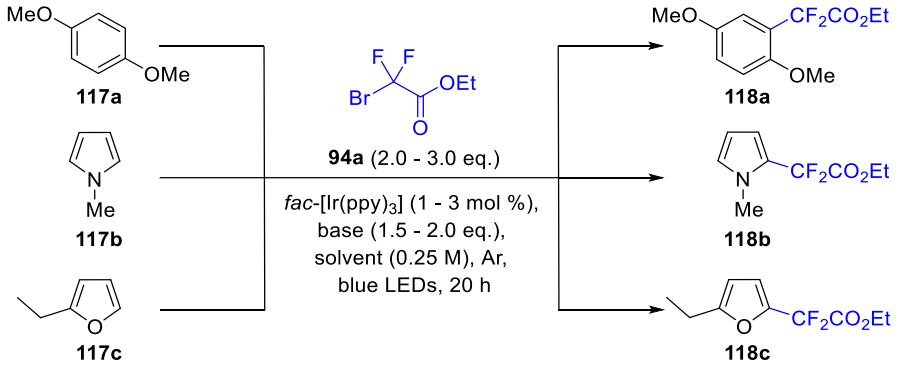

Entry	Aromatic substrate	Base	Solvent	% Yield[a]
1	**117a**	K_3PO_4	DMSO	52
2	**117a**	KO^{t}Bu	DMSO	81
3	**117b**	KO^{t}Bu	DMSO	trace
4	**117b**	TEA	DMF	95
5	**117c**	TEA	DMF	30
6	**117c**	K_3PO_4	DMF	83

Table 8. Reactions carried out by Cho and co-workers on a 0.1 mmol scale of aromatic substrate.[123] [a]The yields were determined by gas chromatography and ^{19}F NMR spectroscopy with internal standards of dodecane and 4-fluorotoluene, respectively.[123]

This was dependent on the aromatic or heteroaromatic substrate, for example difluoroalkylation of 1,4-dimethoxybenzene **117a** with KO^{t}Bu provided the product **118a** in a 30% higher yield compared to K_3PO_4 (**Table 8**, entry 1 and 2). Unfortunately, when those conditions were applied to *N*-methylpyrrole **117b** only trace amounts of product **118b** were reported, whereas switching to TEA, along with a solvent swap to DMF, the product was obtained in a 95% yield. Once again when applying these newly optimised conditions to furan analogue **117c**, only a 30% product yield was obtained for **118c**, but this was improved greatly by substituting the base for K_3PO_4 (**Table 8**, entry 5 and 6). Therefore, this highlighted the variability in yields reported by Cho and co-workers depending on the base used, hence a selection of bases would likely be required for screening against every substrate undergoing difluoroalkylation, which is not ideal.

Mechanistically the base is not involved in the photocatalytic step, shown by phosphorescence decay investigations carried out by Cho and co-workers: the presence of base did not affect the reductive quenching of photoexcited *fac*-[Ir(ppy)$_3$]*.[123] This result suggested that base is not required to initiate the desired reaction, therefore the importance of base was questioned.

The equivalents of TEA were investigated (**Table 9**) and showed that product formation was almost completely inhibited when 2.0 eq. were used giving a 6% spectroscopic yield of **105a**. This was marginally improved to 12% when only 1.0 eq. of TEA was added (**Table 9**, entry 3), however a better yield (68%) was observed when TEA was completely omitted. Analysis of the reaction mixtures containing TEA revealed that significant amounts of Ac-Trp-OEt **93** and bromodifluoroacetate **94a** remained in the solution unreacted, specifically 1.8 eq. of the latter. These results were unexpected, usually after 10 minutes of irradiation 0.6 – 0.8 eq. of **94a** is left unreacted; therefore, the presence of TEA negatively affect product formation by inhibiting radical formation.

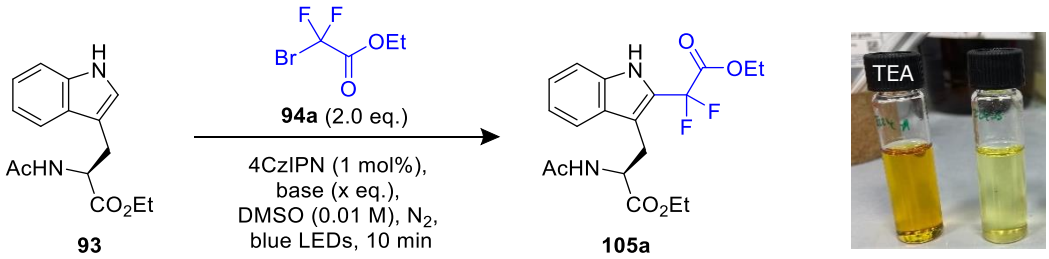

Entry	Base (x eq.)	% Yield[a]
1	-	68
2	TEA (2.0)	6
3	TEA (1.0)	12

Table 9. Reactions carried out on a 60.0 μmol scale in position A of the PhotoRedOx box using EvoluChem™ LED spotlights (455 nm). [a]Yields determined by ^{19}F NMR spectroscopy using TFT as the internal standard.

One way in which the desired radical formation could be prevented is through the reaction of TEA and 4CzIPN, hence competing with bromodifluoroacetate **94a** and limiting the amount of catalyst available for Trp alkylation. Based on oxidation potentials TEA can be oxidised by excited 4CzIPN ([4CzIPN]*): +0.78 V and +1.43 V vs SCE in MeCN respectively.[143,111] Once oxidised the TEA radical **119** can undergo numerous reaction pathways, a few of which are shown in scheme 29.[143]

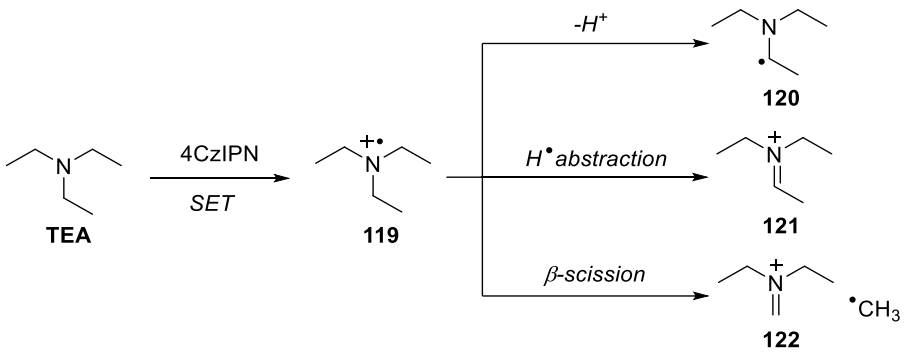

Scheme 29. Formation of TEA radical **119** and a selection of subsequent reaction pathways.[143]

Similar amine bases (*N*,*N*-diisopropylethylamine and *N*,*N*-diisopropylmethylamine) have been shown to react with cyanoarene-based photocatalysts under blue LED irradiation (455 nm).[144] The resulting photodegradation product 4Cz-Me-BN (**Scheme 30**) will likely exhibit different photocatalytic properties to 4CzIPN (if any), because structural changes are known to alter a compounds absorption spectra.[139] After irradiation in the presence of TEA, a previously unseen colour change was observed for the reaction mixture, from yellow to orange which could support 4CzIPN degradation and the lower product yields obtained.

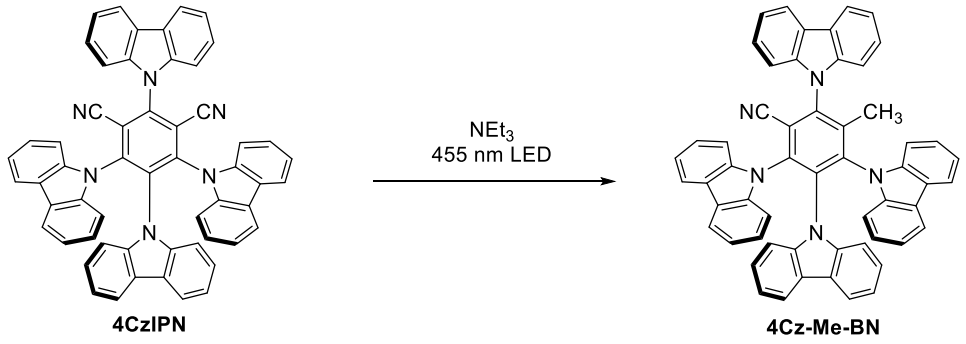

Scheme 30. Photodegradation of 4CzIPN to 4Cz-Me-BN in the presence of TEA.[144]

For completeness a variety of inorganic bases were investigated as additives for the photocatalytic difluoroalkylation reaction, to ensure that the reaction performed favourably without a base. Overall similar yields for product **105a** were obtained with the addition of K_2CO_3, K_3PO_4 or NaOH compared to the absence of base (**Table 10**, entry 1-4).

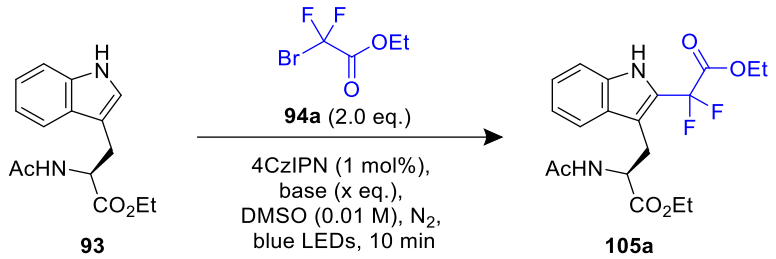

Entry	Base (x eq.)	% Yield[a]
1	-	68
2	K_2CO_3 (1.0)	62
3	K_3PO_4 (1.0)	66
4	NaOH (1.0)	65

Table 10. Reactions carried out on a 60.0 μmol scale in position A of the PhotoRedOx box using EvoluChem™ LED spotlights (455 nm). [a]Yields determined by ^{19}F NMR spectroscopy using TFT as the internal standard.

Presumably K_3PO_4 had minimal effect on the desired reaction because the phosphate salt was insoluble in DMSO and visibly settled on the bottom of the vial. Similarly, K_2CO_3 did not fully dissolve, and solid particles were dispersed throughout the solution. Whereas NaOH was soluble, yet equally had minimal effect on the desired reaction, suggesting that a base additive is not crucial in this reaction mechanism. Therefore, omitting the base was

more beneficial not only in terms of the highest yield obtained but also increased atom economy and reduced waste, affording more sustainable conditions.

Photocatalyst Screen

Alternative photocatalysts to 4CzIPN were investigated including *fac*-[Ir(ppy)$_3$] (employed by Cho and co-workers),[124] 3CzClIPN, Ru(bpy)$_3$Cl$_2$·6H$_2$O and Eosin Y. The function of the photocatalyst, as mentioned previously, is to form the alkyl radical ·CF$_2$CO$_2$Et **96** *via* reduction of BrCF$_2$CO$_2$Et **94a** which has a reduction potential of −0.886 V.[124] The following excited state reduction potentials $E_{½}$ ($PC^{\cdot+}/PC^{*}$) have been reported for each photocatalyst in table 11, and generally any photocatalyst with a more negative reduction potential than −0.886 V should have the ability to form the desired radical, hence form product **105a** (**Table 11**, entry 1-3). This expectation was mostly followed hence product formation was not observed for Ru(bpy)$_3$Cl$_2$·6H$_2$O as a result of its reduction potential being approximately 0.07 V more positive (**Table 11,** entry 4). Surprisingly the organic dye Eosin Y did not form any desired product despite having a more negative reduction potential than bromodifluoroacetate **94a** (−1.13 V and −0.886 V respectively). This can be explained by the absorbance spectrum of the dye which has a peak maximum at 520 nm in DMSO and very little absorbance at 455 nm,[145] hence the LED bulb used for the difluoroalkylation reaction would not provide the correct amount of energy to form the excited photocatalyst state.

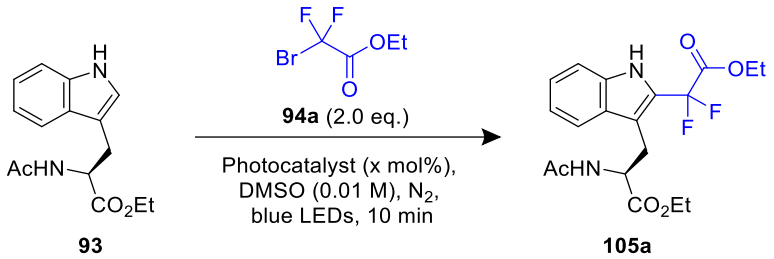

Entry	Photocatalyst (x mol%)	$E_{½}$ ($PC^{\cdot+}$/PC*) vs SCE (V)	% Yield[a]
1	4CzIPN (1.0)	−1.18[111]	70
2	*fac*-[Ir(ppy)$_3$] (1.0)	−1.73[146]	56
3	3CzClIPN (1.0)	−0.93[111]	44
4	Ru(bpy)$_3$Cl$_2$·6H$_2$O (1.0)	−0.81[146]	0
5	Eosin y (1.0)	−1.13[147]	0

Table 11. Reactions carried out on a 60.0 μmol scale in position A of the PhotoRedOx box using EvoluChem™ LED spotlights (455 nm). [a]Yields determined by ^{19}F NMR spectroscopy using TFT as the internal standard. The reduction potentials reported are literature values.[111,146,147]

Both *fac*-[Ir(ppy)$_3$] and 3CzClIPN gave lower product yields compared to 4CzIPN. For 3CzClIPN this is potentially because it is a weaker reducing agent. However, with the addition of a stir bar, the yield can be improved by 20% to give a 65% product yield, comparable with 4CzIPN. Nonetheless, this argument doesn't apply for *fac*-[Ir(ppy)$_3$], as this was the strongest photocatalyst tested. Originally it was predicted that the lower yield was due to more side reactions e.g., further alkylation on Trp, however analysis of the reaction mixture disproved this showing unreacted starting material. Instead, this lower product conversion was potentially due to solubility: a stock solution was made for each photocatalyst in DMSO and for *fac*-[Ir(ppy)$_3$] this was the least soluble giving an opaque solution. Therefore, if the catalyst was not fully dissolved, when a sample was taken for the reaction, it could have been less than 1 mol% resulting in a reduced product conversion. Overall, a range of photocatalysts can be utilised for the photocatalytic alkylation transformation of Trp (**Figure 27**), affording acceptable yields but 4CzIPN was carried forward due to its organic nature

and ease of synthesis; nucleophilic aromatic substitution using commercially available reagents (tetrafluoroisophthalonitrile and carbazole).

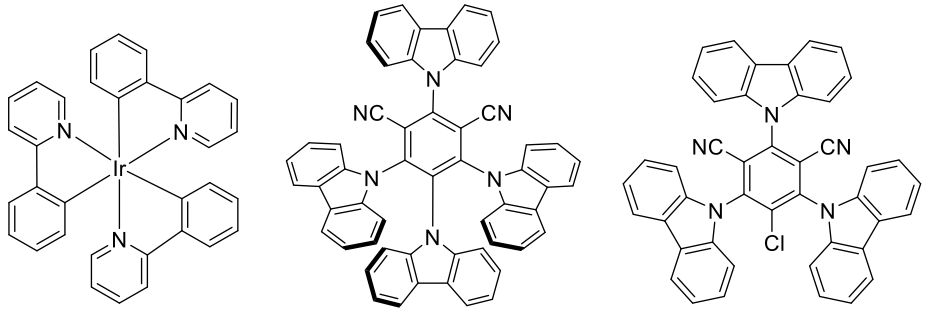

	fac-[Ir(ppy)$_3$]	4CzIPN	3CzClIPN
$E_{½}$ (PC$^{•+}$/PC*) *vs* SCE (V)	–1.732	–1.182	–0.932

Figure 27. Photocatalysts which successfully initiated photocatalytic alkylation with their corresponding reduction potential values.[111,146]

To ensure 1 mol% was the optimum catalyst loading, investigations were carried out using 0.5, 2.0 and 5.0 mol%. As expected, increasing the photocatalyst concentration led to slightly higher product yields (**Table 12**, entry 1-3), but the difference between 2 and 5 mol% was negligible.

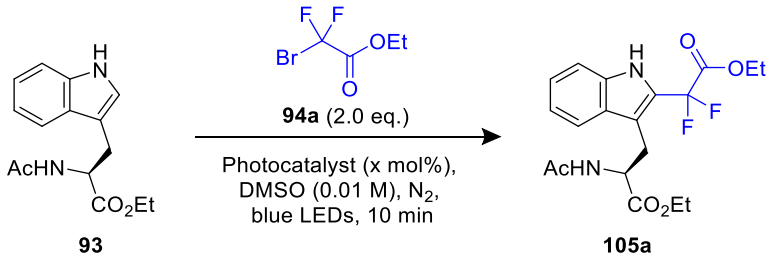

Entry	Photocatalyst (x mol%)	% Yield[a]
1	4CzIPN (1.0)	70
2	4CzIPN (2.0)	79
3	4CzIPN (5.0)	78
4	4CzIPN (0.5)	62
5	-	0

Table 12. Reactions carried out on a 60.0 μmol scale in position A of the PhotoRedOx box using EvoluChem™ LED spotlights (455 nm). [a]Yields determined by ^{19}F NMR spectroscopy using TFT as the internal standard.

Pleasingly a loading as low as 0.5 mol% performed well giving a 62% product yield in 10 minutes (**Table 12**, entry 4). The difference between 1 and 2 mol% of 4CzIPN is minor, therefore, to keep the loading as low as

possible without the expense of product yield, it was hypothesised that extending the reaction time could give the same enhanced yield as 2 mol%.

Reaction Time and Ethyl Bromodifluoroacetate Equivalents

One of the most important discoveries during optimisation was the sensitivity of photocatalytic difluoroalkylation to reaction time. Unfortunately, to obtain the highest product yield it was not as simple as extending the irradiation time to ensure full consumption of Ac-Trp-OEt **93** had occurred. Reaction mixture analysis was carried out at multiple time points between 10- and 45 minutes shown in figure 28.

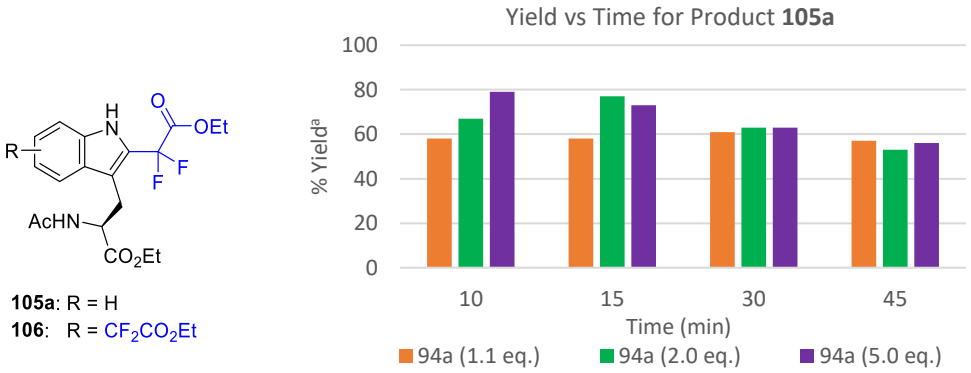

Figure 28. Bar chart to show how the yield of product **105a** is affected by time when using 1.1, 2.0 and 5.0 equivalents of bromodifluroacetate **94a**. [a]Yields determined by fluorine NMR spectroscopy using TFT as the internal standard.

Increasing the reaction time actually decreased product yield because it led to the consumption of desired product **105a** to form the over alkylated product **106**. As discussed previously dialkylation of Ac-Trp-OEt **93** can be formed by the reaction between desired product **105a** and $\cdot CF_2CO_2Et$ **96**, which is enhanced by prolonged reaction times. When the reaction was left for 60 minutes using 2.0 eq. of bromodifluoroacetate **94a** a large 30% reduction in product yield was observed compared to 15 minutes: 45% and 77% respectively.

Most optimisation studies were carried out using 2.0 eq. of **94a** because preliminary studies showed that using almost stoichiometric equivalents (1.1) gave a 10% lower yield after 10 minutes (**Figure 28**, orange bar). Because of the enhanced yield using 2.0 eq., a greater excess of 5.0 eq. was also explored (**Figure 28**, purple bar). Once again increasing the equivalents of **94a** increased the product yield after 10 minutes giving a 79% yield for **105a**. With one of the aims of this research being to consciously design a more sustainable reaction, using 5.0 equivalents of a reagent was not preferable. Pleasingly a comparably high yield of 77% was obtained using 2.0 eq. by leaving the reaction for an extra 5 minutes: 15 minutes total. Understanding the balance between probe equivalents and reaction time was crucial to obtain a high yield: excess probe combined with longer reaction times was detrimental to product yield causing a 10 to 30% reduction, however a slight excess can be favourable under short irradiation times by allowing greater consumption of Ac-Trp-OEt **93**. This is why 2.0 eq. of bromodifluoroacetate **94a** became beneficial; in contrast to the start of the chapter. Previously, significant dialkylation was observed due to the irradiation time being 16 h, whereas in this study the reaction was stopped after 15 minutes, limiting this side reaction and providing the desired product in an excellent yield.

It was unlikely that increasing probe equivalents greater than 5.0 could enhance the product yield further because a negligible difference was observed between product yields when using 3.0 eq. and 5.0 eq. of **94a** (**Table 13**, entry 3-4). This suggested that, even though it had previously been shown that increased probe equivalents resulted in a higher product yield, above 3.0 eq. the alkyl reagent was no longer influencing product

conversion. Instead, perhaps it would be the concentration of photocatalyst: 1 mol% can only initiate a certain amount of radical formation at any given time.

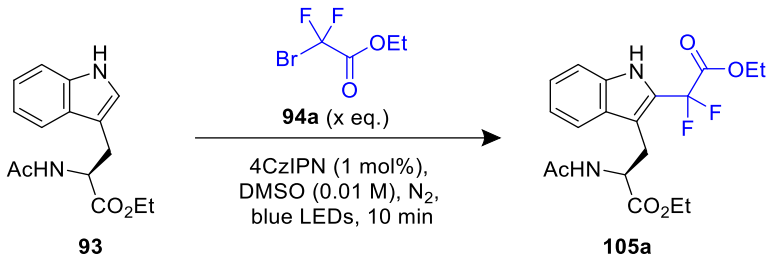

Entry	$BrCF_2CO_2Et$ 94a (x eq.)	% Yield[a]
1	1.0	69
2	2.0	68
3	3.0	75
4	5.0	76[b]

Table 13. Reactions carried out on a 60.0 μmol scale in position A of the PhotoRedOx box using EvoluChem™ LED spotlights (455 nm). [a]Yields determined by ^{19}F NMR spectroscopy using TFT as the internal standard. [b]Average yield after two experiments.

Interestingly repeating the experiment using 1.0 eq. of **94a**, in the same study as 2.0, 3.0 and 5.0 eq., gave a comparable yield to 2.0 eq. after 10 minutes: 69% (**Table 13**, entry 1). This contradicted the yield obtained during preliminary investigations (58%, **Figure 28**) likely due to the use of a different starting material batch and changes to the purification method, potentially altering the purity of Ac-Trp-OEt **93**.

It has already been shown how the product yield is affected significantly by $BrCF_2CO_2Et$ **94a** equivalents between 1.0 and 5.0 (**Figure 28**). It can be challenging to measure the probe equivalents exactly, particularly on small scales associated with peptide chemistry, where a difference of 1 mg could correspond to 1.0 eq.. Therefore, the risk of using stoichiometric amounts of **94a** is that inherent small-scale errors could lead to the addition of less than the desired amount which would result in a significant amount of unreacted starting material. Therefore, before each reaction was irradiated

with light an aliquot of only the bromodifluoroacetate **94a** and internal standard (TFT) was analysed by quantitative NMR spectroscopy. This allowed the identification of exact probe equivalents added to the reaction which would provide an insight into how long to leave the reaction for. Nonetheless to avoid unnecessary amounts of unreacted SM or small-scale complications, 2.0 eq. of alkyl bromide **94a** with an irradiation time of 15 minutes was chosen for the optimised conditions.

Conclusion

This concludes the optimisation studies carried out, where the final conditions used bromodifluoroacetate **94a** (2.0 eq.) and 4CzIPN (1 mol%) in DMSO (0.01 M) with 15 minutes of blue LED irradiation (**Scheme 31**).

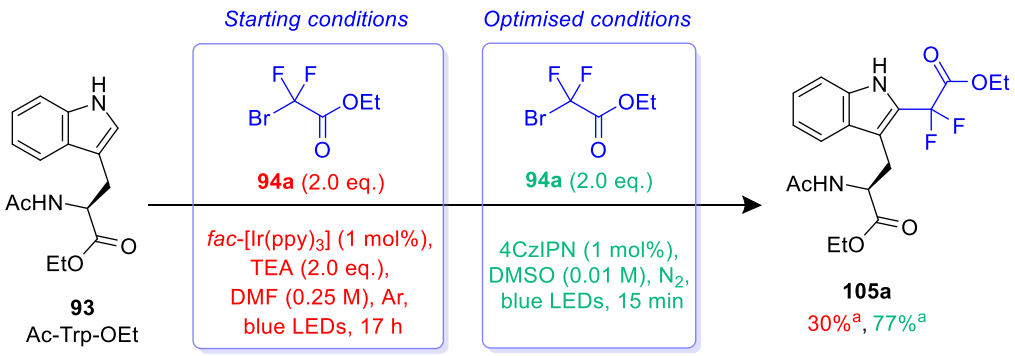

Scheme 31. Comparison of phototcatalytic alkylation conditions. Starting conditions in red were reported by Cho and co-workers.[123] Optimised conditions are shown in green. [a]Yields determined by ^{19}F NMR spectroscopy using TFT as the internal standard.

Compared to the initial literature conditions,[123] the reaction is rapid (15 min), additive free and the rare transition metal catalyst was replaced by an organic alternative: 4CzIPN. Therefore, more sustainable conditions were developed using safer chemicals (DMSO instead of DMF)[135] and providing a greater atom economical and energy efficient process.

Importantly, regioselectivity was achieved hence Trp was alkylated at the C–2 position with a good yield. A significant increase in product **105a** yield was obtained using the optimised conditions compared to the starting conditions (77% and 30% respectively) and this was predominantly due to the reduction of side-products (SPs) **106** eluting between 4 and 6 minutes in the HPLC chromatogram (**Figure 29**).

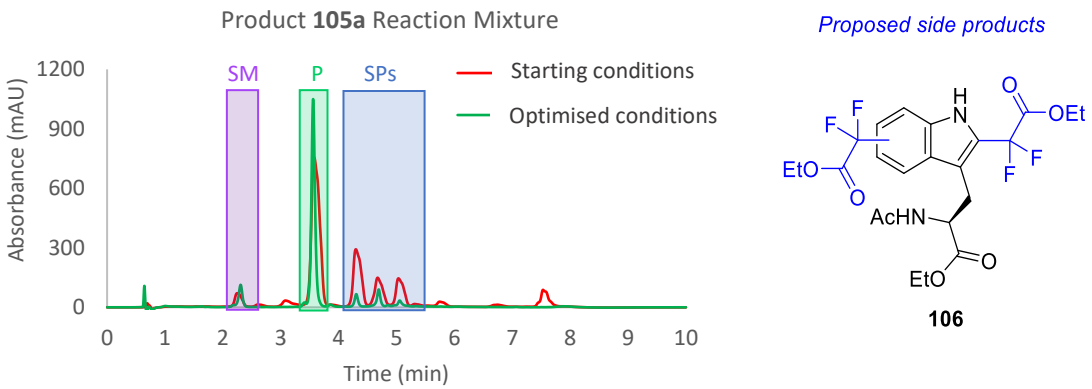

Figure 29. Overlap of crude reaction mixture HPLC chromatograms for product **105a** using starting and optimised conditions on analytical gradient 40-80% B over 5 min, 280 nm.

3 Reaction Development and Application

With optimised conditions in hand, the full potential of the reaction was investigated. There were two areas to explore: the alkyl bromide scope and the peptide substrate compatibility.

3.1 Probe Scope

To begin this chapter, a variety of alkylating reagents (probes) were synthesised to subsequently react with Ac-Trp-OEt **93**, investigating the versatility of the photocatalytic strategy. The probes of choice contained ester or amide linkers (bromodifluoro-acetates and acetamides respectively, **Figure 30**) covalently bonded to moieties which differed in steric and electronic properties. Additionally probes important to chemical biology were included in the scope, for example a PEG chain and a sugar moiety (**Figure 30**), to enable potential therapeutic applications of the products.

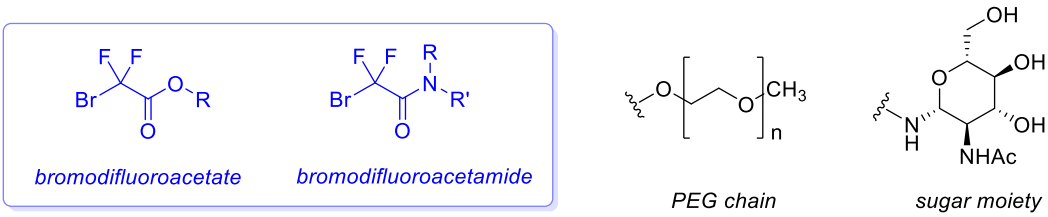

Figure 30. Structures of bromodifluoroacetates, bromodifluoroacetamides and biologically relevant molecules.

Bromodifluoroacetates

A variety of bromodifluoroacetate compounds **94b-g** (ester probes) were readily synthesised *via* an esterification reaction starting from the commercial acid chloride **123** using a modification of the procedure reported by Jin and co-workers (**Scheme 32**).[148]

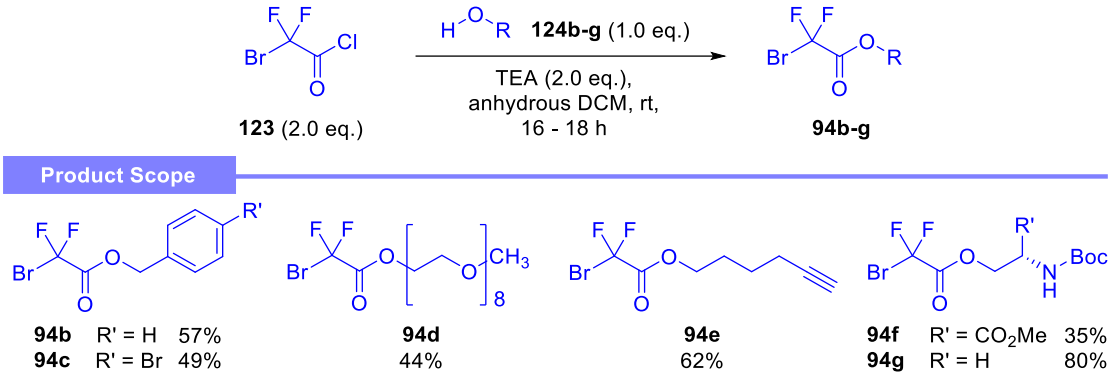

Scheme 32. Synthesis of bromodifluroacetates.

A range of aromatic **94b**, **94c** and aliphatic moieties were tolerated including ether **94d**, ester **94f** and amide **94g** functional groups. Two of these examples incorporated functionalities important to chemical biology such as a PEG chain **94d** and an alkyne **94e**. A PEG group, once conjugated to a peptide, has been shown to enhance pharmaceutically relevant properties: decreased accessibility for degradation enzymes as a result of increased steric hindrance.[149] Whereas the alkyne can act as a bio-orthogonal linker: a subsequent reaction with an azide substrate could exploit click chemistry.[150]

Mostly moderate to good yields were obtained for the ester probes with the lowest being 35% for carbamate **94f**, whereas the analogous probe without the ester functional group (**94g**) provided a much greater yield of 80%. Before the serine (Ser) derived probe **94f** could be exposed to the photocatalytic alkylation reaction, stability problems arose. Mass spectrometry data revealed that within a week the product signal had vanished and instead the major signal corresponded to methyl L-serinate **125a** (**Scheme 33**). This suggested that probe **94f** was susceptible to degradation at room temperature, highlighting the lability of the ester bond. A new, broad signal at −54.0 ppm was observed in the ^{19}F NMR spectrum

along with a minor signal at −60.8 ppm corresponding to ester **94f** (**Scheme 33**). Comparable values of −58.0 ppm (CD_3OD) reported in the literature,[141] and −51.5 ppm (DMSO-d_6) obtained after the synthesis of $BrCF_2COONa$ **126** supported the occurrence of probe hydrolysis.

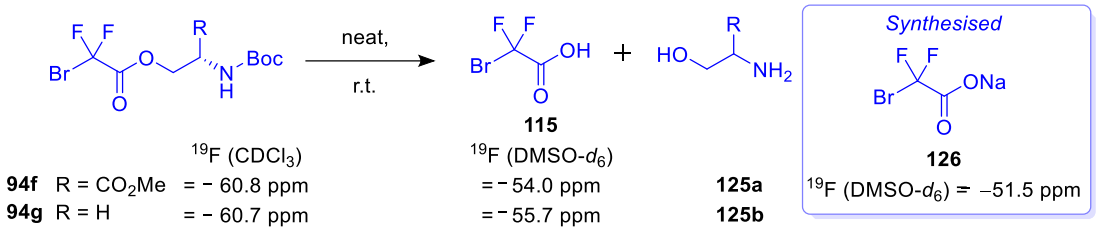

Scheme 33. A potential decomposition pathway for unstable probes along with the corresponding ^{19}F NMR spectroscopy signals.

Due to these instability issues associated with probe **94f**, a similar probe **94g** was synthesised without the ester. However, the same trend was observed: instability in DMSO and when stored at room temperature over time. Consequently, these Ser derived probes could not be investigated in the photocatalytic reaction.

Bromodifluoroacetamides

Bromodifluoroacetamides were also synthesised which provided alternative linkers for photochemical bioconjugation. The linker connects the biomolecule to the payload (small molecule/drug/fluorophore etc) in peptide conjugates and they can be cleavable or non-cleavable. The former is more common in peptide drug conjugates (PDCs): stable at neutral pH in the blood but more susceptible to hydrolysis inside diseased cells delivering the payload selectively.[151] Therefore including both ester and amide linkers within the small molecule scope could allow numerous applications depending on the required bond cleavage susceptibility.

Using solvent free literature conditions reported by Ohshima and co-workers,[152] cheap, readily available starting materials were used to synthesise a range of 'amide probes' in good yields between 54% and 84% (**Scheme 34**). A lower 34% yield was obtained for the pyridine amide probe **94j**, potentially due to the challenging purification as the product slowly eluted over many fractions, nonetheless sufficient material was obtained for photocatalytic difluoroalkylation studies.

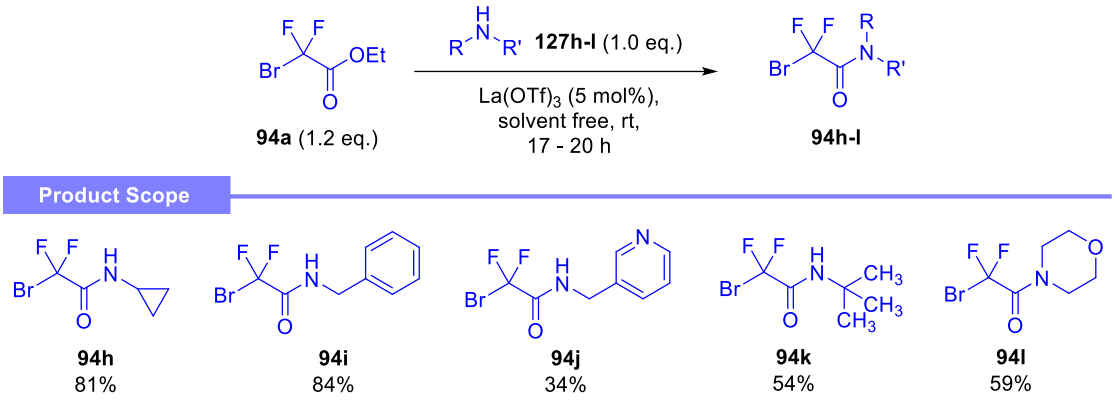

Scheme 34. Synthesis of bromodifluroacetamides using conditions reported by Ohshima.[152]

The scope predominantly consisted of secondary amides bearing cyclic **94h**, aryl **94i**, **94j** and alkyl **94k** moieties, however a heterocyclic tertiary amide **94l** was also synthesised successfully (**Scheme 34**). The moieties attached to the amide differ in steric and electronic properties, chosen deliberately to determine whether this influenced the outcome of the photocatalytic alkylation. Additionally, the nature of the carbonyl group could affect the reaction performance, therefore the benzyl amide probe **94i** was synthesized for a direct comparison with benzyl ester probe **94b**.

To further explore moieties important to chemical biology, amide probes incorporating a biotin reporter tag **94m** and a sugar **94n** were also synthesised (**Scheme 35**). Biomolecules conjugated to biotin can be used

for many applications including targeted delivery,[153] selective purification and chemical labelling.[154] Additionally, mentioned in the introduction chapter, incorporating a sugar onto a peptide can improve their absorption across biological membranes improving PK properties.[8]

The previous synthetic route to amide probes took advantage of the fact that many amine reagents are liquids at room temperature, allowing for solvent free conditions. However, the amine reagents required to synthesise biologically relevant probes are solids: biotin-ethylenediamine (biotin-EDA) **127m** and 2-acetamido-2-deoxy-beta-D-glucopyranosylamine **127n**, hence a solvent was required. Additionally, due to the steric bulk of these reagents, carrying out the acylation reaction with acid chloride **123** (**Scheme 35**) was likely to be more favourable than ethyl bromodifluoroacetate **94a** because the carbonyl is more electrophilic. Therefore, for these amide probes the method used to prepare the ester probes was followed.

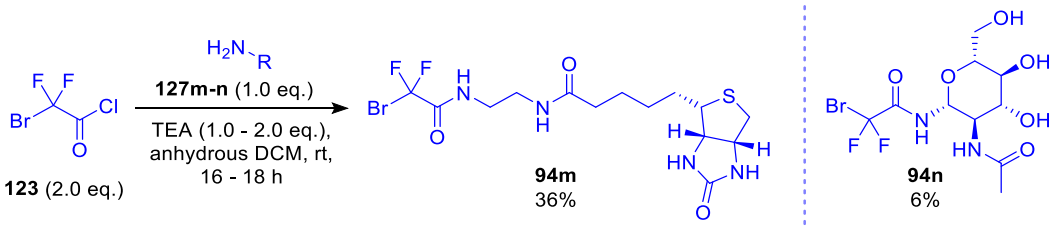

Scheme 35. Proposed pathway to synthesise the desired biotin **94m** and sugar probe **94n**.

Prior to this, ester and amide probe synthesis had been relatively simple: following literature conditions and isolating ample material, however these two substrates provided a few challenges. For biotin conjugation, an amide linker wasn't the first choice, instead the synthesis of ester probe **94o** was initially attempted. Following the synthesis of known compound biotin 2-

hydroxyethyl ester **130**, and subsequent esterification with bromodifluoroacetyl chloride **123**, the desired biotin ester probe **94o** would be synthesised in two steps (**Scheme 36**).

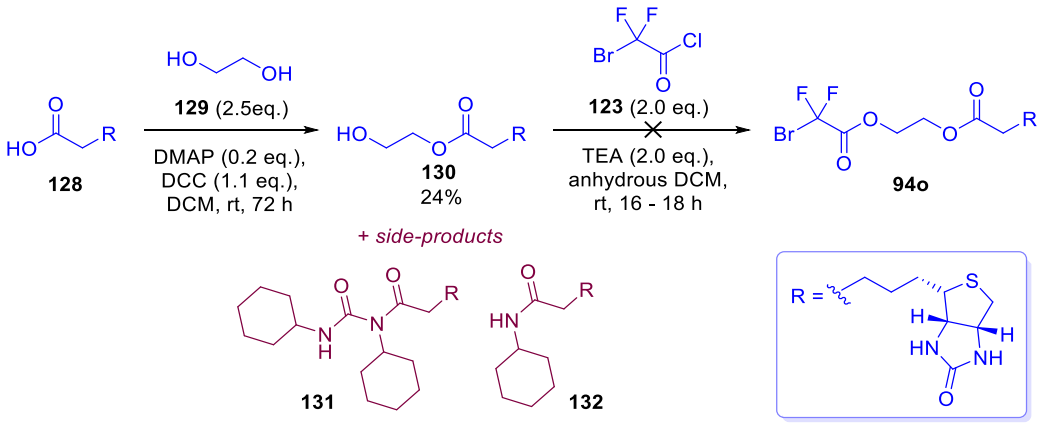

Scheme 36. Reaction pathway attempted to synthesise biotin ester probe **94o** along with proposed side product structures.

Unfortunately, the carboxylic acid activating agents 4-dimethylaminopyridine (DMAP) and *N*,*N'*-dicyclohexylcarbodiimide (DCC) created side products **131** and **132** which were preferentially formed over the desired product, causing the disappointing 24% yield. Despite the low yield, it was consistent with literature precedence: a 29% yield was obtained by Marchetti and co-workers using similar conditions with a different carbodiimide reagent.[155] Importantly, enough material was obtained to carry out the subsequent step, however, isolation of material was poor. Analysis of the reaction mixture and purified compounds was challenging as mass spectrometry data did not show desired product ions, instead the presence of $BrCF_2CO_2H$ was clearly observed, but this could result from sample preparation and analysis conditions. Additionally, the corresponding fluorine NMR spectra were not informative; either multiple baseline signals were observed, or signals were not visible. This suggested that the desired transformation was not occurring, or that the new ester bond was unstable

under the reaction or analysis conditions, immediately hydrolysing. Consequently, this synthetic route was abandoned, and an alternative three-step route was proposed to synthesise the amide analogue (**Scheme 37**).

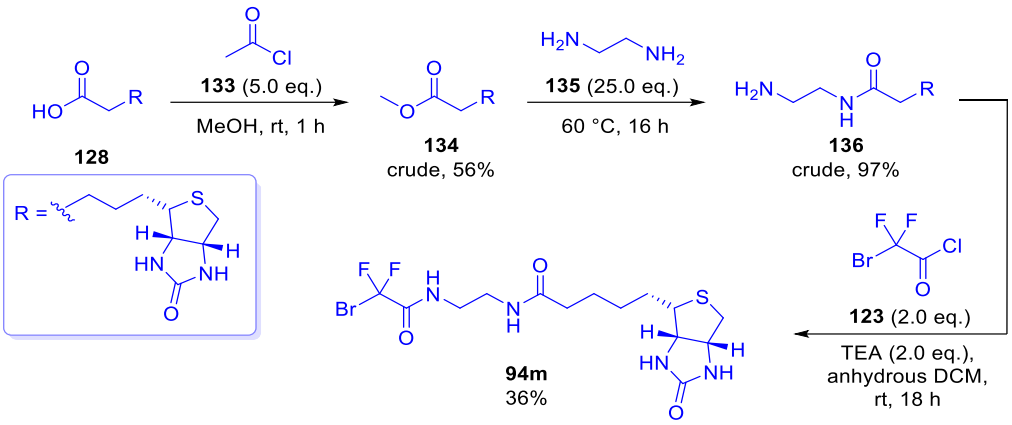

Scheme 37. Reaction pathway used to synthesise biotin amide probe **94m**.

The literature conditions used to synthesise biotin methyl ester (biotin-OMe) **134** and biotin-EDA **136** were more promising as a previous member of the group had successfully carried out these transformations.[156] Pleasingly moderate to good yields were obtained for these intermediate compounds and even though two steps are required, the set-up is simple and purification is not necessary. The final amidation step allowed the desired probe **94m** to be synthesised in a moderate yield (36%) which, on a 2.18 mmol scale, provided sufficient material for peptide conjugation.

Conversely, the synthesis of sugar probe **94n** was only one step, much like the other probes and the selectivity for amide bond formation, over an ester bond, was promising based on literature procedures. For example the reaction between sugar substrate **137** with either an ester **138** or carboxylic acid **140** reagent provided amide products with yields of 52% and 99%

respectively (**Scheme 38**).[157,158] This is presumably because primary amines are generally more nucleophilic than the corresponding alcohol.

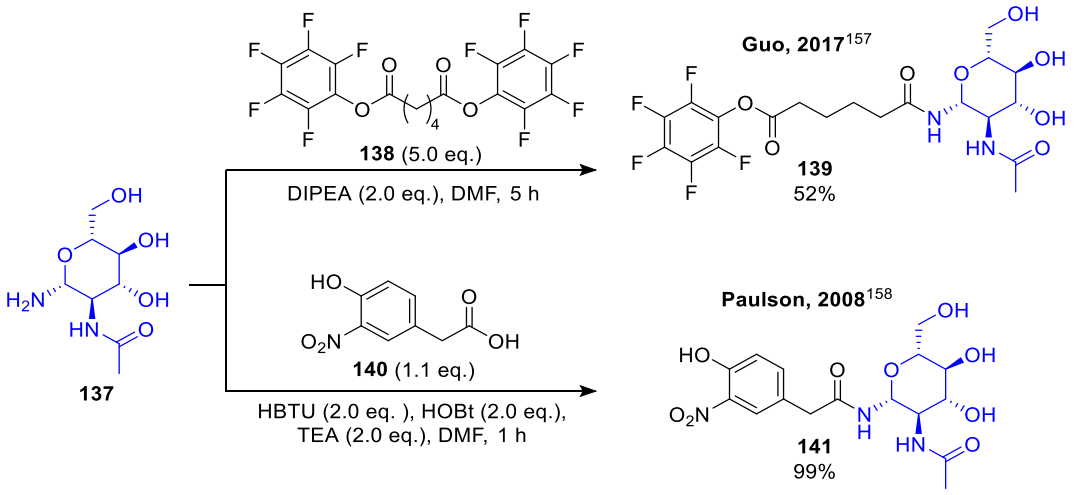

Scheme 38. A selection of literature procedures which showed successful amide bond formation using sugar **137** as the amine source.[157,158]

For this research the acid chloride **123** was used as the electrophile mostly for consistency because it was previously used for probe syntheses, but as a precaution, the number of TEA equivalents was reduced to 1.0 (beforehand 2.0 eq.) to limit any competing nucleophilic attack (**Scheme 39**).

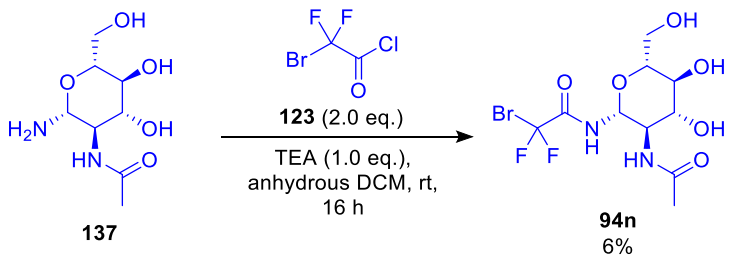

Scheme 39. Modified literature conditions used to synthesise sugar probe **94n**.[148]

Analysis of the reaction mixture was challenging due to the poor absorbance of **137**, hence limited visibility in HPLC chromatograms. Despite this, products resulting from the reaction were visible by HPLC analysis, however the reaction mixture chromatograms were very impure: at least 5 side

product (SP) signals were observed, suggesting poor selectivity of the acylation (**Figure 31**).

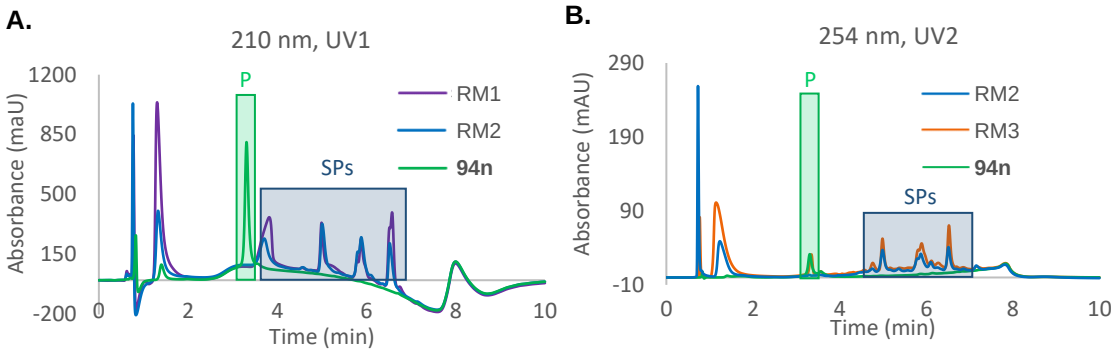

Figure 31. Analytical HPLC chromatograms overlaying multiple traces. A. RM1, RM2 and pure sugar probe **94n**. B. RM2, RM3 and pure sugar probe **94n**. 2-95% B over 5 mins, 210 nm or 254 nm.

The reaction was analysed at three time points: after 3 h (RM1), after 16 h (RM2) and 3 h after additional reagents ($BrCF_2COCl$ 1.0 eq. and TEA 0.5 eq.) were added (RM3). Following the isolation of desired product **94n**, the chromatograms were compared: figure 31B contains RM2 (blue line), RM3 (orange line) and pure sugar probe **94n** (green line) at 254 nm. The product signal at 3.34 minutes was observed for the latter two but not for RM2 highlighting the fact that absorbance signals were inconsistent, complicating interpretations. Hence reaction monitoring by analytical HPLC, combined with the low absorption intensity observed at 254 nm (**Figure 31B**), was not the most reliable technique for the synthesis of probe **94n**.

Unsurprisingly, the crude reaction mixture ^{19}F NMR spectrum also revealed the presence of multiple fluorine containing products (**Figure 32**): a mixture of singlet and doublet signals were observed along with a range in coupling constants: small 6.5 - 7.6 Hz and large 163 Hz. As observed by analytical HPLC, the intensity of signals in the ^{19}F NMR spectrum were similar, supporting the lack of reaction selectivity.

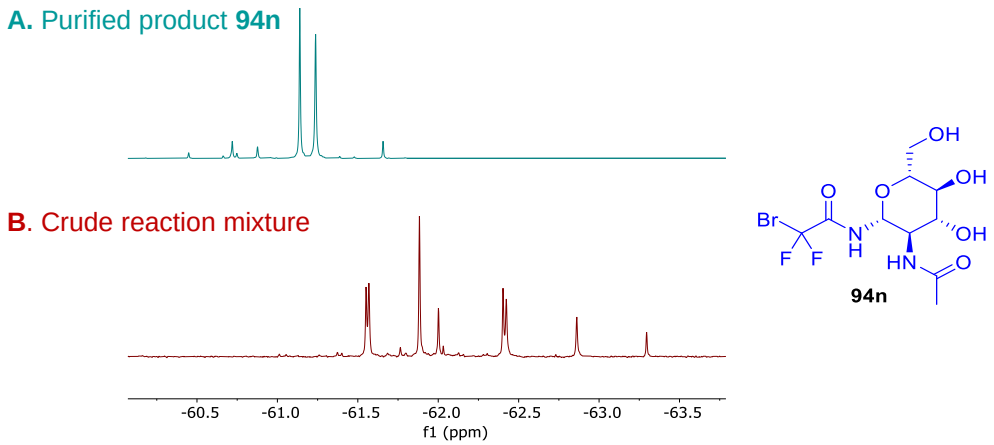

Figure 32: Stacked ^{19}F NMR spectra for purified product **94n** the crude reaction mixture.

Purification was also challenging, and despite efforts to promote its success (dissolving the crude material in a higher volume of polar diluent and beginning the purification with a 95-98% H_2O concentration) often material eluted with the solvent front, requiring additional purification. Because the synthesis of sugar probe **94n** was carried out toward the end of the PhD, time was limited and the priority was to obtain material, therefore reaction/ purification optimisation was not investigated. After initial studies were carried out on 0.5 mmol of sugar **137**, this was scaled up to 1 mmol which subsequently required six purification runs, mostly because there is a maximum loading on the preparative HPLC column of 100 mg, to obtain only a 6% yield for probe **94n**.

In hindsight, after further research into the literature, use of an acid chloride as the electrophile was likely too reactive causing poor selectivity and the reaction may have been more successful with the carboxylic acid analogue and coupling agents. Additionally normal phase silica gel column chromatography could have been further explored using DCM:MeOH 4:1 as the eluent, as this was used for similar literature products.[157,158] Nonetheless, a 6% yield corresponded to approximately 24 mg, which

provided material for peptide studies, but unfortunately had to be absent from the amino acid small molecule scope.

This concludes the synthesis of variety of ester and amide probes varying in steric and electronic properties along with the incorporation of diverse functionalities. A library of 12 small molecules were available for use in the photocatalytic conjugation, firstly with Trp amino acid followed by more complex peptide substrates as a late-stage functionalisation strategy.

3.2 Photocatalytic Diflluoroalkylation of Ac-Trp-OEt

Proof of concept experiments were first carried out using Ac-Trp-OEt **93** and bromodifluoro- acetates/acetamides assessing their ability as alkylating agents under photocatalytic conditions. Because the principle focus of this research was peptide modification, yields were mostly obtained by ^{19}F NMR spectroscopy for Trp amino acid conjugation products, however three examples were scaled up to enable isolation and full characterization of the products.

Conjugation with Probes - Analytical Scale

Bioconjugation reactions were carried out using Ac-Trp-OEt **93** on a 20 μmol scale for two reasons: to enable consistent starting material masses with peptide substrates (~ 5 mg), hence similar weighing errors associated with all samples and to avoid using unnecessarily large amounts of probe. Additionally, this 'analytical' scale provided accurate ^{19}F NMR yields, whereas isolated yields could be less reliable. It was observed during the optimisation studies that the desired product can co-elute with the side-products; therefore, some isolated fractions were contaminated resulting in material loss and reduced yields. Mentioned previously, weighing errors

associated with small scale chemistry can be significant especially when combined with inherent losses through workup and purification. Therefore, it was desirable to determine yields by ^{19}F NMR spectroscopy for these reactions to accurately assess how substrate complexity affected the reaction success. Usually, these minor product losses would not be consequential for the more common organic chemistry reaction scales (0.2 mmol), which is why a selection of scale up reactions were carried out to obtain isolated yields which will be discussed later.

For the photocatalytic difluoroalkylation of Ac-Trp-OEt **93** using 4CzIPN (1 mol%) and radical precursor (2.0 eq.) in DMSO (0.01 M), all bromodifluoroacetates **94a-e** and bromodifluoroacetamides **94h-n** were tolerated providing generally moderate to good product yields after short irradiation times (**Scheme 40**). Cyclic **105h** and heterocyclic **105l** moieties were compatible along with aromatic **105b-c**, **105i-j** and biologically relevant functional groups **105m**. The conjugation of bromobenzyl ester **105c** gave a pleasing 62% product yield, and the presence of this halogen allows the potential for subsequent reactions.[159] Additionally, a good yield was obtained for the difluoroalkylated product bearing an octa-PEG moiety **105d** after 15 minutes, which was consistent with the other ester conjugated products despite the potential steric hindrance associated with this long chain.

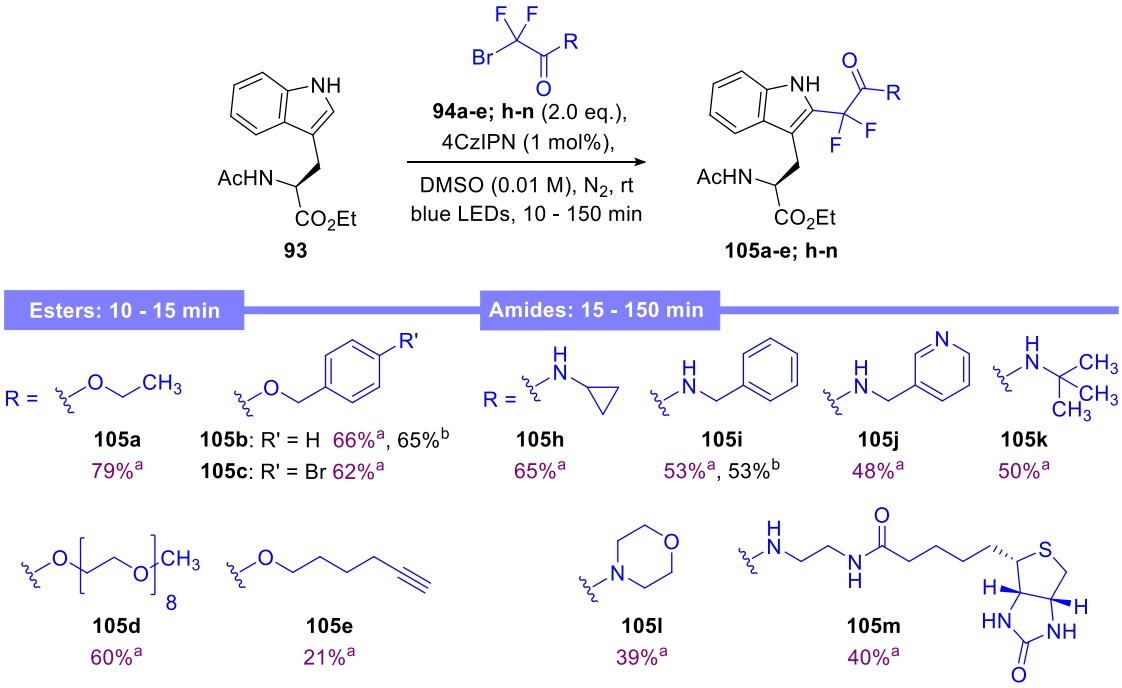

Scheme 40. Photochemical alkylation of Ac-Trp-OEt **93**; Reactions performed on a 20.0 μmol scale. [a]Yields determined by ^{19}F NMR spectroscopy using TFT as the internal standard. [b]Isolated yield on a 200 μmol scale.

For amide conjugation reactions, however, significant amounts of starting material had not reacted after 10–15 minutes of irradiation (shown by HPLC analysis). Hence for the amide probes, prolonged reaction times were required which enhanced starting material consumption and product yield, in contrast to the ester conjugation reactions. For example, the product yield for cyclopropyl-Trp conjugate **105h** improved by 12% after a reaction time of 60 minutes instead of 30 minutes. Potential explanations and further discussion into ester and amide reaction rates will be discussed in more detail in 3.3 Reaction Rates.

Despite the overall broad range in product yields (21-79%), within each class of carbonyl these were more consistent. Ester conjugation reactions were rapid affording product yields between 60% and 79% with reaction times as little as 10-15 minutes. Whereas the amide conjugation reactions required longer and more varied reaction times between 15 and 150

minutes to produce slightly lower product yields of 40-65%. The longest reaction time was required for biotin conjugation which provided the product **105m** in a modest yield (40%), despite the chemical complexity associated with the probe **94m**. However, despite the prolonged irradiation time a significant amount of unmodified Ac-Trp-OEt **93** (SM) was observed at the end of the reaction (**Figure 33**).

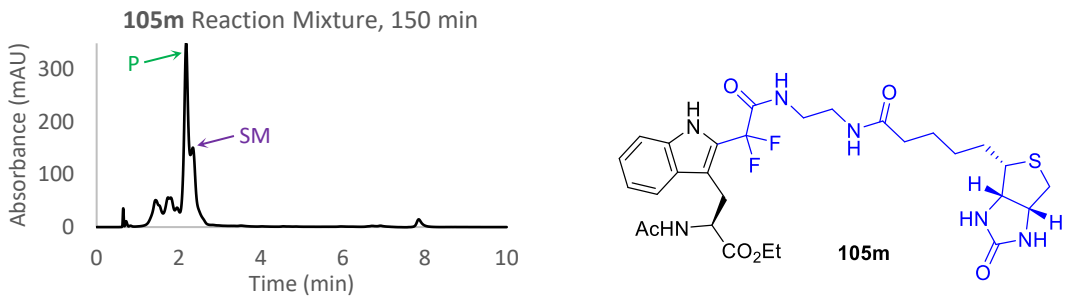

Figure 33. Reaction mixture HPLC chromatogram for **105m**, 40-80% B over 5 min, 280 nm.

Exceptions to the General Reaction Trends

The most significant outlier to the general trends was hexyne ester probe **94e** which performed poorly compared to other examples affording product **105e** in the lowest yield 21%. Typically, the reaction mixtures (RMs) had one major signal and a few minor signals in both the ^{19}F NMR spectrum and HPLC chromatogram highlighting reaction selectivity. As mentioned previously HPLC analysis is not quantitative; however, it can provide a complementary insight into the reaction mixture when combined with results from ^{19}F NMR spectroscopy i.e., a low product yield could be rationalised by the presence of a large SM signal which was the case for small-molecule Trp conjugate **105e** bearing the alkyne moiety (**Figure 34**).

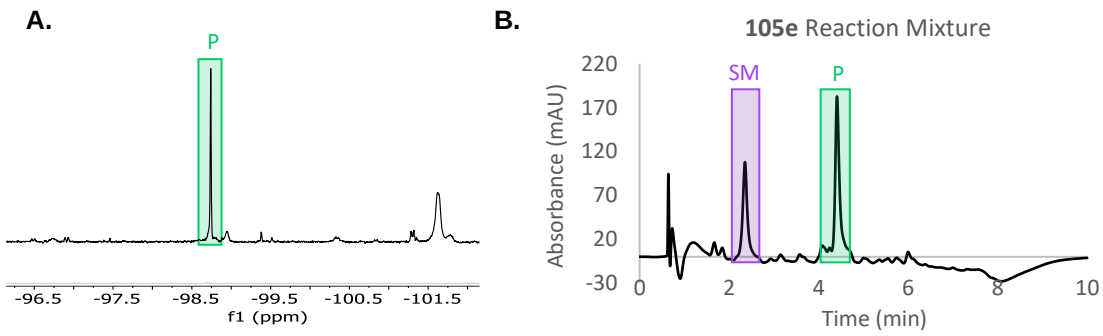

Figure 34. Reaction mixture data collected for **105e**. A. ^{19}F NMR spectrum. B. HPLC chromatogram, 20-80% B over 5 min, 280 nm.

As for an explanation into the unusually high intensity of the starting material signal, it was identified using ^{19}F NMR spectroscopy that a greater consumption of probe had occurred (qNMR) along with the formation of a new broad signal at −103 ppm (**Figure 35**, red spectrum), which was unseen for other examples. This suggested that the probe was potentially undergoing a side reaction, preventing the desired radical addition to Trp.

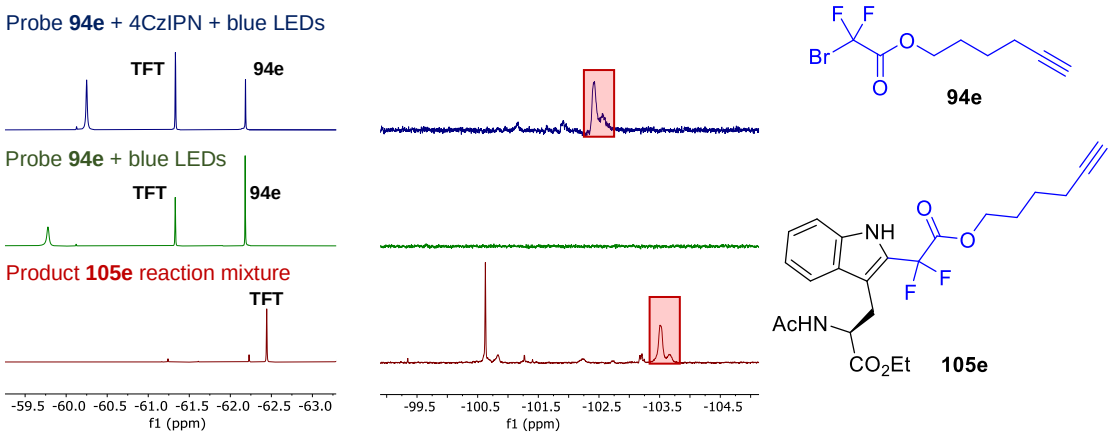

Figure 35. Stacked ^{19}F NMR spectra highlighting the impurity signal formed when hexyne probe **94e** is exposed to 4CzIPN and blue LEDs.

Therefore, two new reactions were carried out: one being the reaction mixture with the absence of Ac-Trp-OEt **93** and the other consisting of only probe **94e** i.e., removing **93** and 4CzIPN (**Figure 35,** blue and green spectra respectively). It was concluded that the formation of this new impurity signal highlighted by the red boxes in figure 35, was 4CzIPN mediated and formed in the absence of Ac-Trp-OEt **93**. Despite efforts

including scale up and carrying out the reaction in DMSO-d_6, isolation or identification was unsuccessful. However, there is literature precedence for a similar α-ester radical having the ability to add into a double bond.[123]

Cho and co-workers reported that for the difluoroalkylation of 1-methoxy-4-vinylbenzene **142** using $BrCF_2CO_2Et$ **94a**, the alkene was susceptible to radical addition forming a mixture of products (**Scheme 41**).[123]

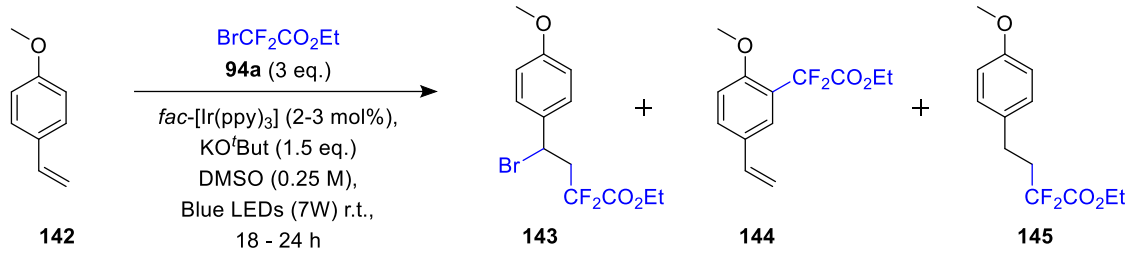

Scheme 41. Photocatalytic alkylation of 1-methoxy-4-vinylbenzene **142** with $BrCF_2CO_2Et$ **94a** revealing a mixture of products.[123]

It can be assumed that electrophilic radical addition to an alkyne is possible, because this is more electron rich than an alkene. Therefore, it is likely that the impurity resulted from probe **94e** reacting with itself: difluoroalkylation of the alkyne and/or bromodifluoroalkylation,[160] which would account for the enhanced probe consumption and significant amount of unreacted Ac-Trp-OEt **93** observed.

Unfortunately, a disappointing result was also obtained using morpholine probe **94l**. Although a modest yield was obtained for product **105l** (39%), it was 10-15% lower than other amide conjugation products despite the reaction mixture chromatogram suggesting relatively pure conversion to product **105l** (**Figure 36**). An unusually rapid reaction time was also observed for this amide conjugation reaction: after 5 minutes the relative intensity of starting material **93** to product **105l** was almost 1:1 (**Figure 36**).

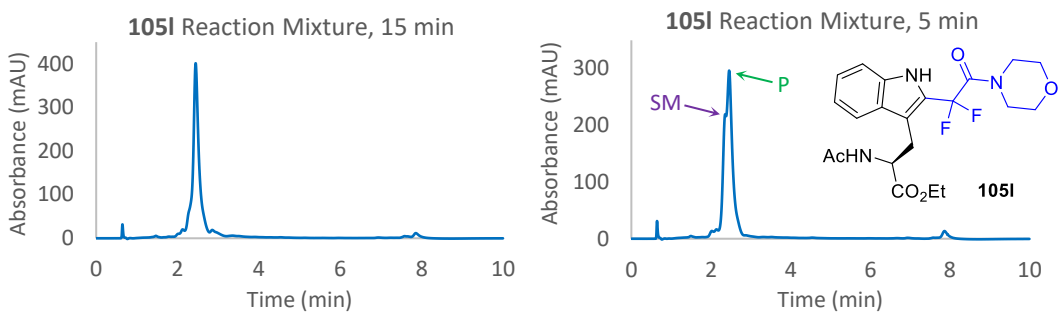

Figure 36. Reaction mixture HPLC chromatograms for **105l**, 40-80% B over 5 min, 280 nm.

Attention was turned to the fluorine NMR spectrum to identify any anomalies which could account for the below average yield obtained for **105l**. Overall, there were more signals observed in the reaction mixture spectrum compared to other amide conjugation products, which implied that fluorine containing side products had formed. Within the spectrum there were two areas of interest: the product region around −88 → −91 ppm and a region which is usually associated with probe side reactions such as hydrogen atom abstraction (HAA) more upfield at −109 → −125 ppm (**Figure 37**). First the desired product doublets were assigned by identifying the largest roofing doublets with matching J values and these are highlighted in green on figure 36. The formation of numerous impurity signals were apparent after only 5 minutes of irradiation, therefore likely unavoidable. Despite the impurity signals being enhanced by a longer irradiation time of 60 minutes, a similar product yield was obtained as that for 5 minutes (33% and 30% respectively). This highlighted the significance of unreacted starting material and the balance between starting material consumption and impurity formation. Based on the chemical shift values of these impurity signals it was predicted that they corresponded to Ac-Trp-OEt alkylation side products.

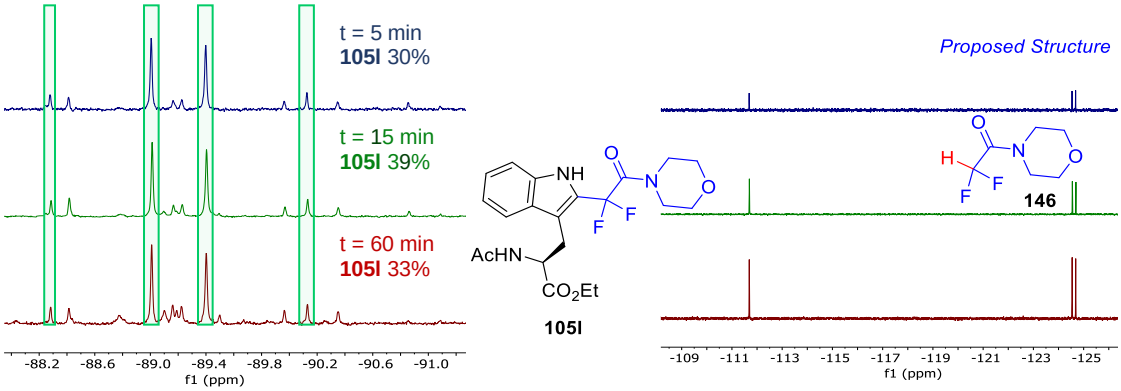

Figure 37. Stacked reaction mixture ^{19}F NMR spectra for morpholine conjugation after different irradiation times: 5 min (blue), 15 min (green) and 60 min (red). Product doublets are highlighted in green and proposed side product structures are shown.

A potential explanation for the increased side product formation arises from the electron withdrawing effect of the oxygen atom in the morpholine ring. This would lower the electron density on the nitrogen atom, subsequently causing poor donation into the C=O π* system compared to the other amide examples. Therefore, a more similar comparison is made with the ester probes i.e. rapid starting material consumption and a tendency of the product to undergo dialkylation, the mass ion of which was observed in the mass spectrum.

The second region of interest in the reaction mixture ^{19}F NMR spectrum at −109 → −125 ppm (**Figure 37**) suggested probe side reactions had also ocurred. A doublet signal at −124.6 ppm was present with a coupling constant of 52.6 Hz which is similar to literature data for compound **146** (−120.9 ppm, J = 53.6 Hz).[161] This product corresponds to a side reaction where radical intermediate ·CF_2COR abstracts a hydrogen atom instead of alkylating Ac-Trp-OEt **93** to give HCF_2COR.

The yield for morpholine conjugation may be improved by reducing the equivalents of probe **94l** from two to one, potentially hindering

overalkylation, or adding a base. Liu and co-workers obtained moderate to excellent yields for their photocatalytic difluoroacetamidation of unactivated arenes and heteroarenes using morpholine probe **94l**, *fac*-[Ir(ppy)$_3$] as the photocatalyst and KOAc (3.0 eq.) (**Scheme 42**).[162] Similarly Cho and co-workers also added bases to their photocatalytic difluoroalkylation reactions (TEA or K_3PO_4), obtaining good product yields despite long irradiation times (> 16 h).[123] Additionally, in scheme 42 the heterocycle has been added in a large excess (10 eq.) which would inherently disfavour overalkylation.

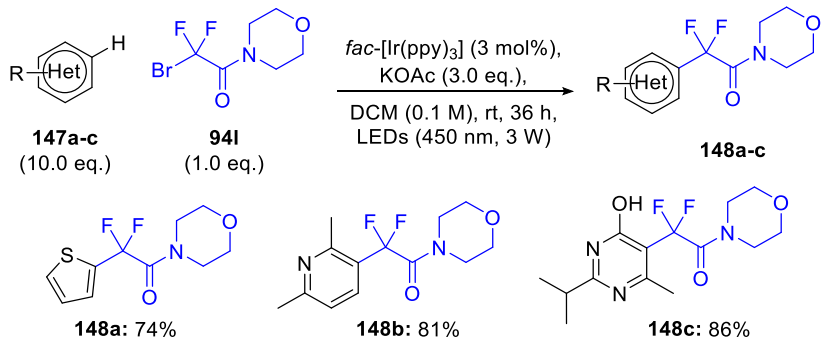

Scheme 42. A selection of difluoroacetamidated heteroarenes reported by Liu and co-workers.[162]

This concludes the discussion regarding analytical scale Trp difluoroalkylation reactions, but to validate the accuracy of the yields determined by ^{19}F NMR spectroscopy and to ensure that the desired transformation had occurred, three scale up reactions were carried out.

Conjugation with Probes - 'Scale Up'

Scale up is used as a loose term for these studies because even though the reaction scale was increased tenfold to 200 μmol, corresponding to approximately 55 mg, this is generally classed as a small scale reaction (1 – 25 mmol) in terms of synthetic organic chemistry.[163] The reaction scale was limited by the vial sizes compatible with the PhotoRedOx box, and the concentration of the reaction: 0.01 M is reasonably dilute and corresponded

to a solvent volume of 20 mL. Nevertheless, successful purification of three small molecule-Trp products was achieved which allowed characterisation to be carried out (**Scheme 43**).

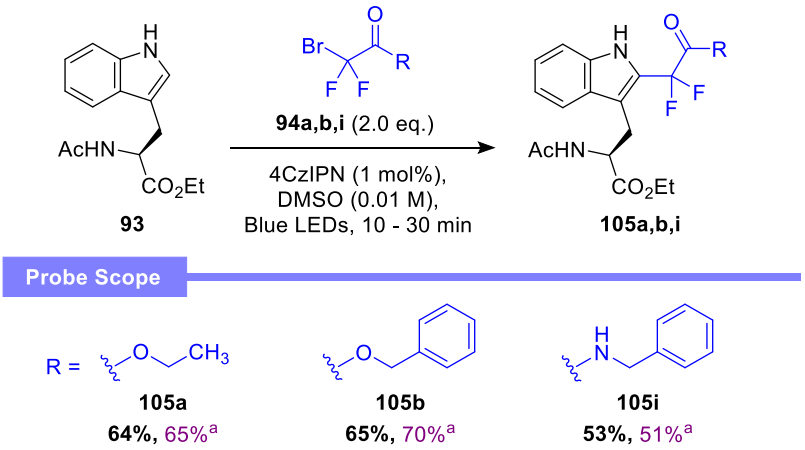

Scheme 43. Isolated yields for small molecule-Trp products. [a]Yields determined by ^{19}F NMR spectroscopy using TFT as the internal standard.

Pleasingly, the optimised conditions were compatible with the larger reaction scale and provided ^{19}F NMR yields consistent with the analogous small-scale reactions: **105a** = 64%, **105b** = 67% and **105i** = 50%. Following isolation, the product yields were within 5% of the yields determined by ^{19}F NMR spectroscopy, confirming the accuracy of these quantitative values (**Scheme 43**). ^{1}H NMR spectroscopy was used to identify the site of alkylation through the loss of a starting material C–H proton signal, which was the desired indole C–2 singlet signal confirming regioselective difluoroalkylation on the indole ring.

Comparing the reaction mixtures for benzyl ester **105b** and benzyl amide **105i** products highlighted the effects of the carbonyl used in the reaction. Not only was a shorter reaction time required for the ester conjugation reaction (10 vs 30 minutes), but it also provided a higher product yield (12% increase by ^{19}F NMR spectroscopy). It was unclear whether this

enhanced yield was due to greater Ac-Trp-OEt **93** consumption, fewer/less favoured impurities or a combination of the two as the HPLC chromatograms were very similar. Potential explanations for these differences observed will be discussed below and a more thorough comparison between benzyl ester and benzyl amide reaction mixtures will be carried out in the following section: 3.4 Photocatalytic Difluoroalkylation of Ac-WHISKEY-NH_2.

It should be noted that the above scale up reactions were carried out early on in the PhD and since then a significant number of analytical scale reactions were repeated assessing reproducibility along with further investigation into reaction rates. Therefore, the scale up reaction using ethyl ester probe **94a** provided a lower 65% NMR yield compared to the previously mentioned 79% yield, because 10 and 15-minute reaction times were used respectively, as well as different starting material batches. To maintain validity, yields can only be compared when reaction parameters are consistent such as reagent batches, reaction times, temperature etc. When this was the case the ^{19}F NMR yields obtained for the analytical scale and scale up reactions were between 1-3% of each other, demonstrating reaction consistency.

Conversely, increasing the reaction time to 60 minutes using benzyl amide probe **94i** (20 μmol scale) only marginally improved the product yield to 53% from 50%. This was because even though starting material consumption was enhanced, so were the side product signals.

3.3 Reaction Rate

Optimum product yields were obtained for ester-based probes in 10-15 minutes whereas amide probes required 15-150 minutes. Surprisingly

morpholine amide probe **94l**, provided an outlier reaction time of 15 minutes which was more comparable with ester conjugation reactions: other amides required at least 30 minutes. Therefore, the following questions arose and will be discussed below: why were longer reaction times required for α-amide radical precursors compared to α-ester radical precursors? and why does morpholine amide probe **94l** have a more comparable reaction time with ester conjugation?

Reaction Rates for Amide and Ester Radical Precursors

As observed the reaction rate was generally influenced by the type of carbonyl involved and, for the amide probes, the moiety present further along the molecule. Therefore, benzyl ester **94b** and benzyl amide **94i** probes provided a reliable comparison to purely assess the carbonyl affect. The ester analogue gave product **105b** in a 67% yield after 10 minutes, whereas the amide conjugation product **105i** was synthesised in a slightly lower 53% yield after 60 minutes of irradiation.

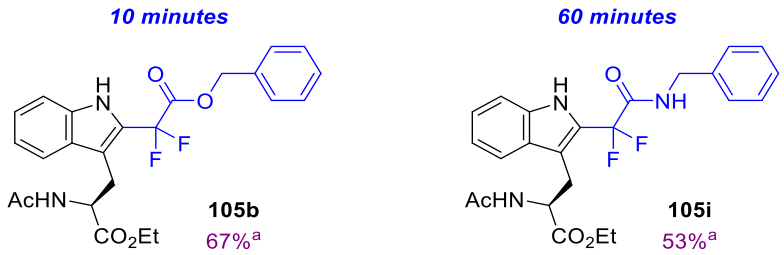

Figure 38. Benzyl ester and amide conjugated Trp products synthesised using optimised photocatalytic difluoroalkylation conditions on a 20.0 μmol scale. [a]Yields determined by ^{19}F NMR spectroscopy using TFT as the internal standard.

Numerous factors can affect the rate of radical addition including sterics, bond strength, stabilization and polar effects of the probe,[164] along with the rate of radical formation itself. One contributing factor for the difference observed between these α-ester and α-amide radicals is their polarity

difference: the partial positive character of the carbonyl carbon is smaller in amides than in esters due to the delocalisation of the nitrogen lone pair into the π-system (**Figure 39**). This would result in α-amide radicals being less electrophilic, therefore presumably weaker electrostatic forces were present for radical addition to the electron rich indole **97**.

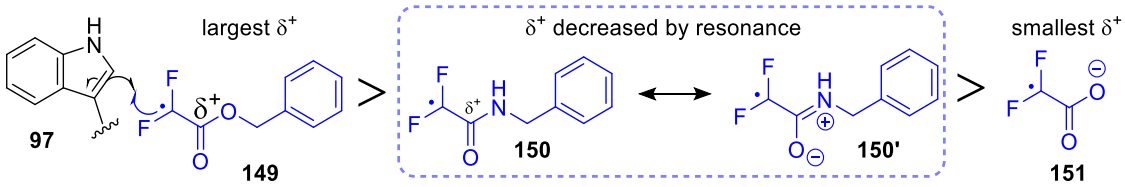

Figure 39. The proposed influence of radical polarity on the rate of radical addition.

Michigan and co-workers discussed the absolute rate constants resulting from a variety of radical precursors reacting with tributyltin hydride (Bu_3SnH).[126] Greater rate constants were observed for α-ester **152a** and α-amide radicals **152b** compared to radicals substituted with electron donating groups: alkyl **152c** and methoxy **152d** (**Figure 40A**). This demonstrated a favourable polarity match between electron deficient radicals in particular the α-ester radical **152a** and the electron rich tin substrate, as expected.

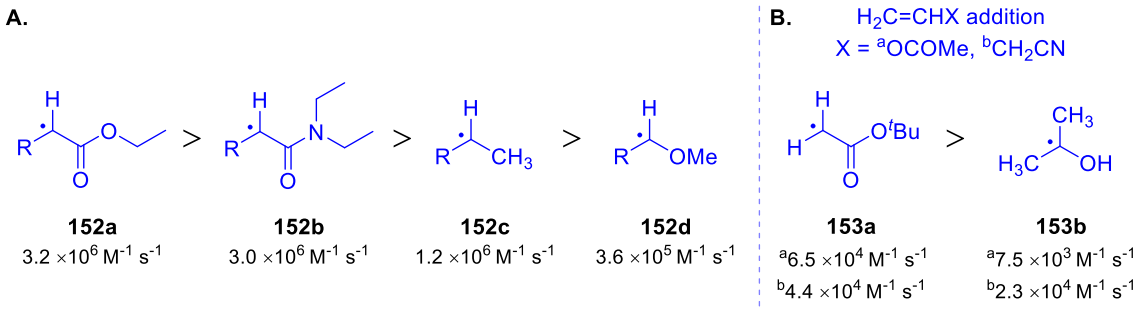

Figure 40. A. Rate constants for the reaction between radical intermediates and Bu_3SnH.[126] B. Rate constants for radical addition to alkenes.[165,166]

Despite this being a hydrogen atom transfer (HAT) mechanism, similar rate trends have been observed for intermolecular radical addition reactions (**Figure 40B**). Radical addition to simple alkenes was more rapid for α-ester radical **153a** than 1,1-dimethyl-1-hydroxyl radical **153b** which presented electron-donating groups alpha to the radical,[165,166] highlighting how a polarity match can enhance the reaction rate for numerous radical reactions.

Electronic Effects on Radical Reactivity

Other than α-amide radicals having longer reaction times compared to the corresponding α-ester radicals, this was also much more variable depending on the moiety attached to the nitrogen (**Figure 41**). Ester conjugation reaction times differed by only 5 minutes whereas amide difluoroalkylation spanned a 135-minute time window. Potentially this trend reflects the electronics associated with the substituents and whether they donate or withdraw electron density from the amide nitrogen. This subsequently affects the polarity of the α-amide radical hence the rate of radical addition.

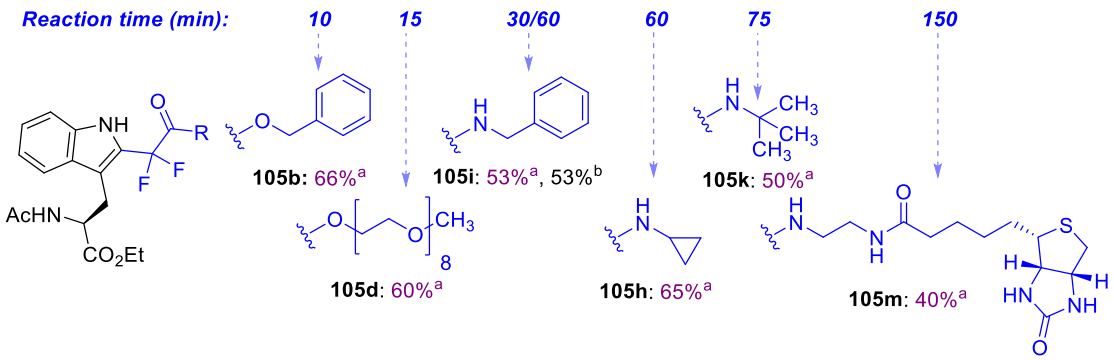

Figure 41. Reaction times for the products synthesised using optimised photocatalytic difluoroalkylation conditions on a 20.0 μmol scale. [a]Yields determined by ^{19}F NMR spectroscopy using TFT as the internal standard.

Hydrogen-Bonding Effects on Radical Reactivity

Another effect which may influence the rate of radical addition is hydrogen-bonding. Bietti and co-workers predicted that the formation of a hydrogen bonded complex between benzyloxy radical **154** and DMSO (**Figure 42**) promoted hydrogen atom abstraction. This was based on measured rate constants for this transformation which showed that a considerably greater value was obtained for radical **154** compared to cumyloxyl radical **155** which cannot undergo H–bonding (2.88 x10^8 and 1.8 x10^4 M^{-1} s^{-1} respectively).[167]

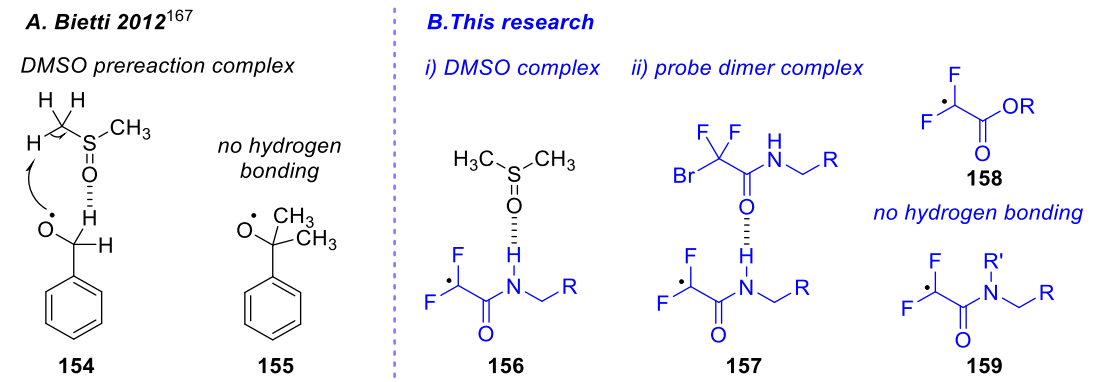

Figure 42. A. Proposed hydrogen bonded pre-reaction complex between BnO· and DMSO.[167] B. Suggested hydrogen bond interactions in reaction mixtures involving amide radicals.

Because of the delocalisation of the nitrogen lone pair, secondary amides have an acidic proton which can readily undergo hydrogen bonding. Therefore, a similar DMSO coordination complex could be suggested for amide radicals **156** which could encourage hydrogen atom abstraction to form side-products and lower the rate of radical addition. Alternatively, the same effect on reaction rate i.e. poorer radical addition may be observed if the amide probes hydrogen-bonded with each other (**157**) forming dimer complexes.[168] For example, biotin's affinity to proteins results from hydrogen-bonding interactions within the binding pocket,[169] therefore is

potentially susceptible to complexes and dimers such as **160** and **161**. Due to the large number of amide bonds present on the molecule, hence availability to H−bond, this could contribute to the longer reaction times observed for photocatalytic difluoroalkylation along with the significant formation of a HAA side product.

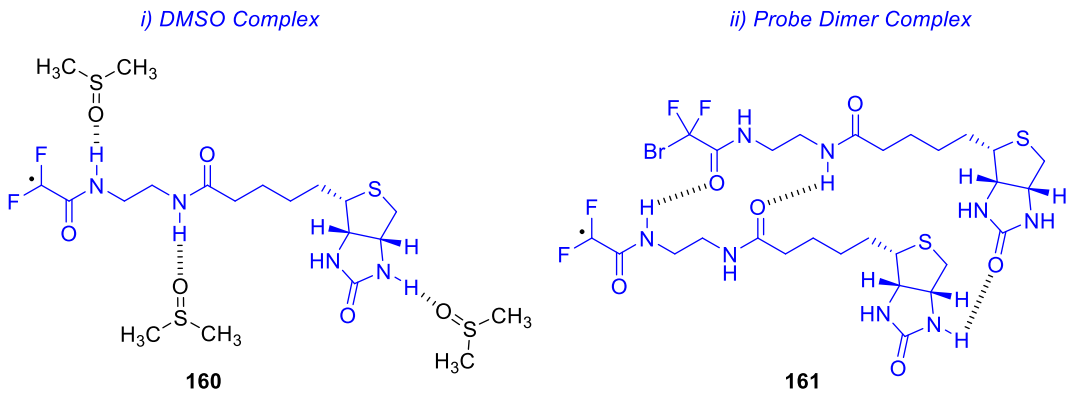

Figure 43. Suggested hydrogen bond interactions for biotin probe **94m**.

Therefore, two factors have been discussed that could influence the rate of radical addition: electronic effects of the electron deficient radicals resulting from the type of carbonyl and substituents present and potential hydrogen-bond complex formations. However, these are all suggestions and hypotheses based on the data collected and theory available. Conversely, the rate of radical formation i.e. how easy it is to reduce the probe would also influence the overall reaction rate.

Cyclic Voltammetry to Gain Insight into Probe Reduction Potentials

Reduction potentials can be acquired providing values indicative of how easily radical formation will occur. These can be measured using cyclic voltammetry and a more negative value corresponds to more energy being required to reduce the analyte. Cyclic voltammetry experiments were carried out using a selection of probes. Four examples were chosen that

presented different reaction trends (**Figure 44**), including the initial ethyl ester probe **94a** and three amides. Amide conjugation reactions showed more variety in terms of reaction endpoints and how the product yield changed over time: increased product yield (cyclopropyl **94h**), decreased product yield (picolyl **94j**) and unusually low product conversion (morpholine **94l**), hence the examples selected represented each trend.

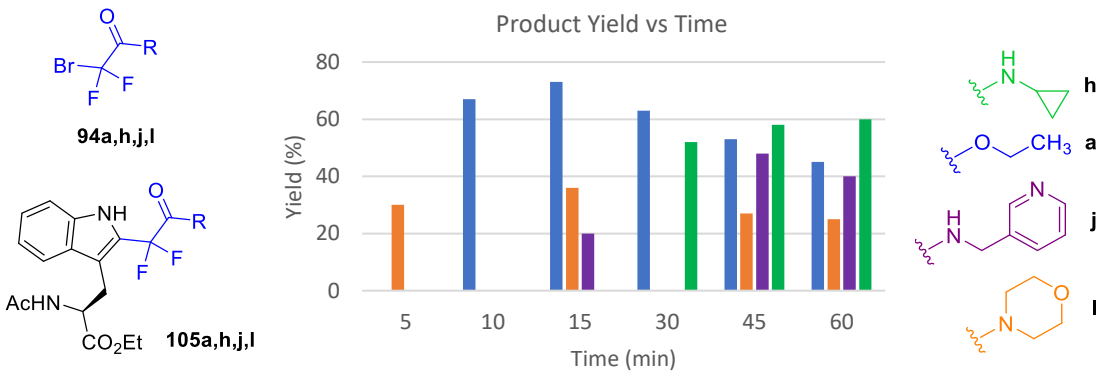

Figure 44. Bar chart to show how product yields varied over time depending on the probe used. Yields determined by ^{19}F NMR spectroscopy using TFT as the internal standard.

CV experiments use an external power source (potentiostat) to provide electrons for single electron transfer (SET) reactions. As a brief introduction, the set-up includes three electrodes: a working electrode (WE) which undergoes the electrochemical event under investigation, a reference electrode (RE) which provides a well-defined equilibrium potential and a counter electrode (CE) which completes the electrical circuit (**Figure 45A**).[170]

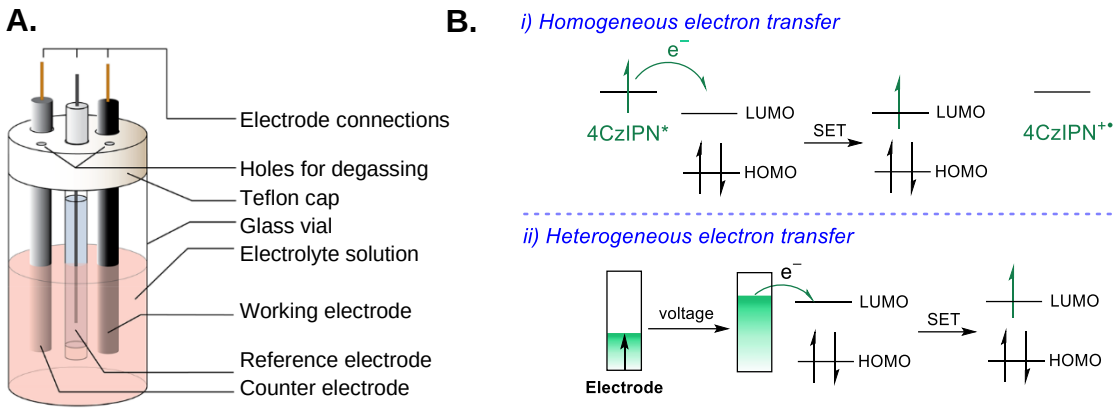

Figure 45. A. Diagram of an electrochemical cell for CV experiments.[170] B. A representation of homogeneous and heterogeneous electron transfer for compound reduction.

The substrate undergoing the electrochemical transformation (analyte) must be dissolved in an electrolyte solution which contains a salt to help decrease solution resistance as ions move in the solution.[170] In terms of the electrochemical reaction the power source provides a voltage to the WE which modulates the energy of electrons. For this research the probes **94a-n** undergo a reduction, therefore when the energy of the electrons becomes greater than the LUMO energy of these compounds, SET can occur from the electrode to the analyte (**Figure 45B**).[170] This is comparable to homogeneous SET from 4CzIPN*: how the radical is generated in the desired reaction.

For this study electrochemistry was carried out on a 5.0 mM solution of probe (analyte) in anhydrous MeCN using $TBAPF_6$ as the electrolyte. The electrodes used were glassy carbon, $Ag/AgNO_3$ and platinum (Pt) as the working, reference and counter electrodes respectively and a potential width of 2.5 V to −3.5 V was scanned to obtain the cyclic voltammogram (CV) for ethyl ester probe **94a** (**Figure 46**).

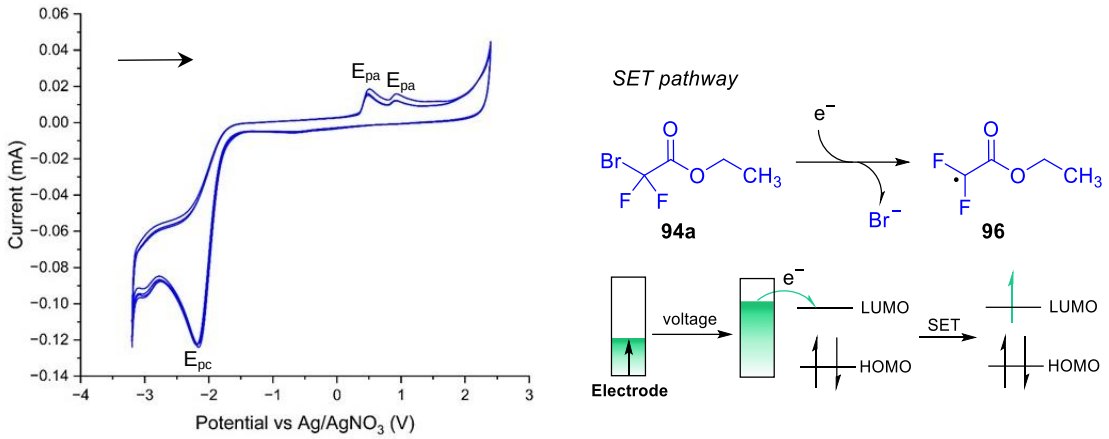

Figure 46. Cyclic voltammogram of ethyl ester probe **94a** showing two anodic peak potentials and one cathodic peak potential.

The IUPAC convention was followed for the CV data recorded where the forward scan represents oxidation (right), hence the reverse scan corresponds to reduction process (left).[170] The x-axis represents the applied potential whilst the y-axis measured the response as current. The arrow on the CV indicates the initial sweep direction: the potential was swept positively from the starting potential (E = 0 V) showing an anodic trace then at 2.5 V the scan direction is reversed, and the potential is swept negatively providing a cathodic trace.

Similar voltammograms were observed for each probe with the following key features: an electrochemically irreversible reduction, and two anodic peaks. The cathodic peak (E_{pc}) (**Figure 46**) was believed to correspond to the reduction of ethyl ester probe **94a** giving the desired radical intermediate **96**, and the two anodic peaks (E_{pa}) are characteristic of Br^- oxidation.[171] The initial forward sweep did not show these distinctive peaks highlighting that bromide ions were formed by the reduction of **94a**, agreeing with the proposed mechanism. Because single waves are observed, instead of the more common 'duck shape', it suggested that an

irreversible electron transfer had occurred, which was also expected because elimination of Br^- is an irreversible chemical reaction.

To identify any differences in reduction potentials between the four radical precursors investigated, their corresponding cyclic voltammograms were overlapped in figure 47. Pleasingly the cathodic peak observed for each probe, highlighted by the zoomed in region, mostly complemented their reaction rates: ethyl ester probe **94a** had the least negative value followed by morpholine **94l** then cyclopropyl **94h** and picolyl **94j**. A more negative E_{pc} value demonstrated that more energy was required to undergo SET due to a higher energy LUMO orbital. However, the reaction rate associated with picolyl probe **94j** was not the lowest therefore affording the lowest E_{pc} was unexpected. Another value which can be obtained from CV data is the reduction onset potential (E_{onset}), which is the potential that can reduce the analyte at the surface of the working electrode,[172] and in this case, this value is more positive than cyclopropyl probe **94h**, agreeing more so with the rate trend.

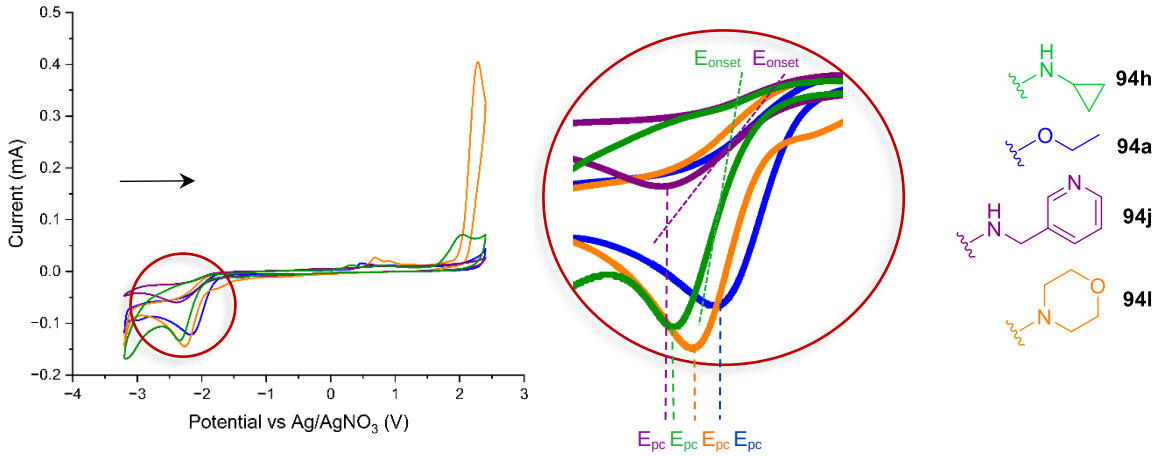

Figure 47. Overlapped cyclic voltammograms of probes showing their cathodic peak potentials between −2.0 and −2.5 V and the reduction onset potential for **94h** and **94j**.

Unfortunately, the potential values were around −2 to −2.5 V which had to be incorrect because the reduction potential of 4CzIPN is $E_{1/2}$ ($PC^{\bullet+}/PC^*$) =

−1.18 V vs SCE,[111] which means that the excited state of the photocatalyst can only reduce compounds with a reduction potential more positive than this value. Additionally, these values deviate significantly from literature values reported for ethyl ester probe **94a** (−0.886 V vs SCE) and a similar amide probe **162** (−0.900 V vs SCE) (**Figure 48**).[173]

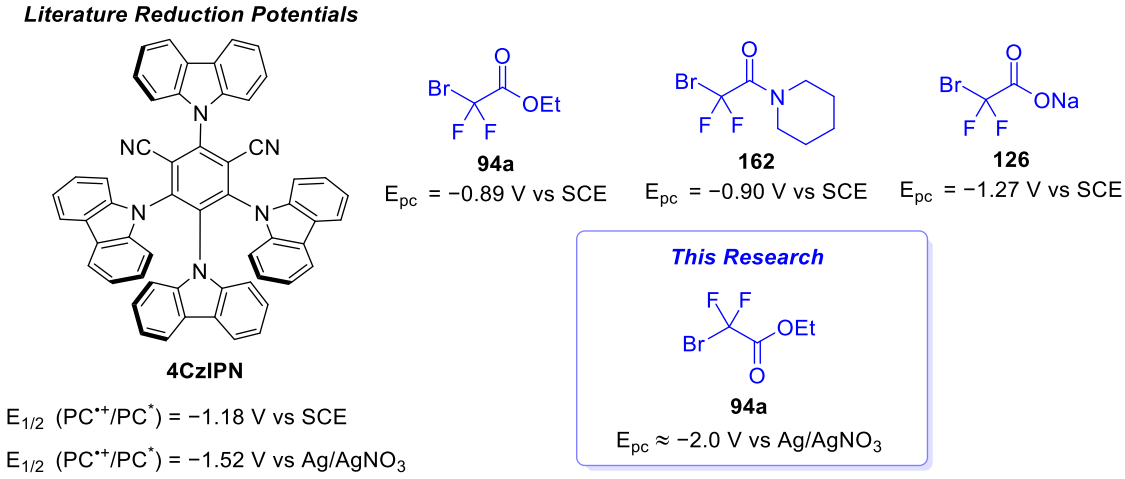

Figure 48. Reported reduction potentials for a range of compounds.[111,173,174]

It's important to note that the reference electrode (saturated calomel or Ag/$AgNO_3$) used for carrying out CV experiments can influence potential values significantly therefore Addison and co-workers have provided conversion constants to enable a more accurate comparison of redox potentials.[174] Accordingly the reduction potential for 4CzIPN vs Ag/$AgNO_3$ becomes $E_{1/2}$ ($PC^{\bullet+}$/PC*) = −1.52 V, which is closer to the experimental probe reduction values but still insufficient. Furthermore, the reduction potentials reported by Xu and co-workers in figure 48 also used a saturated calomel electrode, therefore the values would require converting (−343 mV),[174] however the resulting reduction potentials are still far from the measured − 2.0 V.

Previously, during optimisation studies, the α-carboxylate radical precursor **126** ($BrCF_2CO_2Na$) was synthesised and did not form a radical under photocatalytic conditions shown by the absence of product and presence of unreacted Ac-Trp-OEt **93**. The reduction potential (E_{pc}) for this compound is reported as −1.27 V vs SCE,[124] which would convert to −1.61 V vs $Ag/AgNO_3$,[174] hence cannot be reduced by 4CzIPN, supporting the fact that the values must be less than or equal to −1.52 V. In hindsight, it would have been beneficial to run the CV for carboxylate radical precursor **126** to determine whether the cathodic peak was comparable with the current literature value or equally more negative than expected (like the other probes).

Potentially the very negative reduction potentials observed resulted from a shift caused by experimental parameters, but this was disproved by the anodic peaks observed which were associated with Br^- formation, because the oxidation potentials were similar to the literature values: 694 mV and 1033 mV.[171] Additionally, ferrocene was added to the last experiment as an internal standard which also showed the expected ferrocene couple (Fc^+/Fc) at 0 V.[172]

Interestingly, when the CV is zoomed in to the potential range where probe reduction is expected around −0.9 V,[173] low intensity cathodic peaks are observed (**Figure 49**). The peak potentials (E_{pc} vs $Ag/AgNO_3$) were collected and once again correlated with the observed reaction rates: **94a** (ethyl) = −0.685 V, **94l** (morpholine) = −0.769 V, **94j** (picolyl) = −1.113 V, **94h** (cyclopropyl) **=** −1.383 V. These values were within the reduction ability of 4CzIPN (−1.52 V), albeit low intensity.

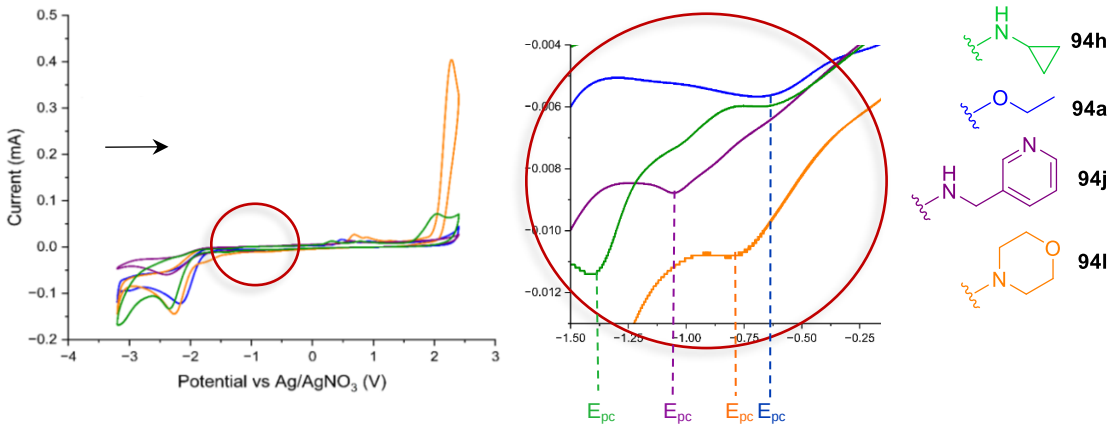

Figure 49. Overlapped cyclic voltammograms of probes showing their cathodic peak potentials between −0.5 and −1.5 V.

Attempts were made to increase the intensity/current of the cathodic peak using ethyl ester probe **94a**, such as reducing the potential width, changing the number of scans and increasing the probe concentration (**Figure 50**). The potential width was cut off at −1.5 V, to avoid the formation of the more intense cathodic peak which was masking the desired peak when looking at the complete CV. Additionally, this would identify whether the reduction at −0.685 V (**Figure 49**) corresponded to α-ester radical formation by the subsequent observation of Br^- anodic peaks.

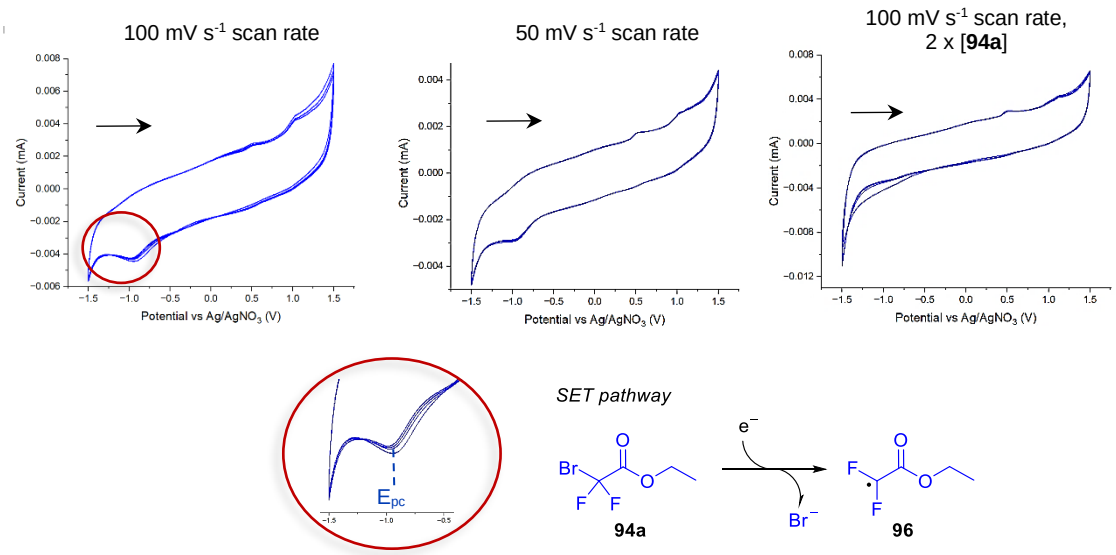

Figure 50. Cyclic voltammograms of ethyl ester probe **94a** varying the scan rate and concentration.

The scan rate can also affect the size of current measured where higher rates tend to exhibit higher currents therefore 50- , 100- and 1000 mV s^{-1} were explored. Finally, the concentration of ethyl ester probe was doubled, due to the hypothesis that more compound would enable more radical formation and a higher current would be the outcome, but in all cases the CVs were not vastly improved.

These 'optimisation' studies were carried out on a different day to the initial CVs obtained using the four probe examples, which highlighted the sensitivity of this technique: a significantly lower E_{pc} value was obtained for the ethyl ester probe **94a** differing by 266 mV: −0.951 V. This poor reproducibility is consistent with the limited and inconsistent cyclic voltammograms available for $BrCF_2CO_2Et$ **94a** (**Figure 51**).

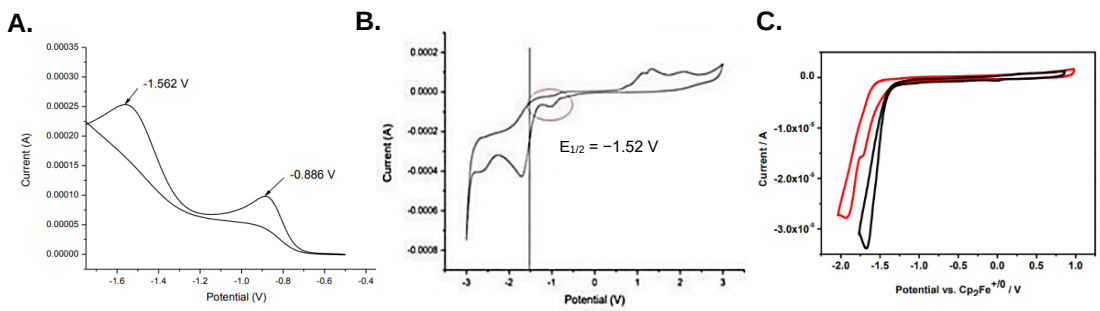

Figure 51. Reported cyclic voltammograms for $BrCF_2CO_2Et$ **94a**. A. Saturated calomel electrode, $[Bu_4N][BF_4]$ in MeCN, 100 mV s^{-1}.[175] B. Ag/AgCl electrode, $[Bu_4N][PF_6]$ in MeCN, 100 mV s^{-1}.[176] C. Ag/$AgNO_3$ electrode, $[Bu_4N][PF_6]$ in MeCN, 50 mV s^{-1}.[177]

Similarly, to the CV obtained in this research, two cathodic peaks are observed in the CVs displayed in figure 51A and B,[175,176] however, a more distinct peak is observed for the reduction potential around −1.0 V. Interestingly Yang and co-workers quoted −1.52 V as the onset reduction potential for **94a**,[176] even though there is a high chance this is incorrect based on the previous discussions. The CV in figure 51C used conditions

similar to those employed in our research i.e. $Ag/AgNO_3$ reference electrode with the same electrolyte and solvent, but once again a more negative cathodic peak than expected is obtained.[177] The main difference between CVs which clearly showed a reduction peak around −0.9 V used different reference electrodes: SCE or Ag/AgCl and a review by Dempsey and co-workers highlighted how $Ag/AgNO_3$ reference electrodes can vary easily which can interfere with electrochemical measuremets.[170]

In conclusion, unfortunately the CV studies were more complicated than expected and didn't provide the absolute values desired. However, more negative reduction potentials were observed for the probes which required longer irradiation times, which does suggest that these radicals are more difficult to form requiring more energy. Interestingly, the reduction potential for morpholine amide **94l** was closer to ethyl ester **94a**, compared to the other amide examples **94h** and **94j**, only differing by 0.084 V which supported the rapid experimental reaction time of 15 minutes associated with each.

Morpholine Amide - An Outlier to the Probe Reactivity Trends

The unusually short reaction time (15 minutes) associated with morpholine amide probe **94l**, considering other amide conjugation reactions required at least 30 minutes of irradiation, can be due to a combination of numerous factors discussed previously. The electron withdrawing effect of the oxygen atom in the morpholine ring would lower the electron density on the nitrogen atom subsequently causing poor donation into the C=O π^* system. This would provide a more favourable polarity match with the electron rich indole ring compared to the other amide examples. Additionally, being a

tertiary amide morpholine probe **94l** cannot undergo hydrogen bonding, which potentially reduces the rate of difluoroalkylation, further enhancing the reactivity compared to the secondary amide probes. Therefore, it is suggested that electronic effects and lack of H−bond interactions could account for the enhanced starting material consumption observed for morpholine conjugation.

For Trp photocatalytic difluoroalkylation, the reaction time was the most varied parameter, which was important to understand, because this effected the product yield obtained. Generally, the reaction was influenced by electronic effects of the probe where the more electron deficient radicals displayed enhanced reactivity, hence increased starting material consumption, but it was crucial to stop irradiation before overalkylation was also amplified.

Reaction Rate Control

It was observed that the reaction can be stopped, stored in the absence of light, and re-started the following day demonstrating the instant control of the reaction. Using picolyl amide probe **94j**, a reaction time of 30 minutes provided a 48% yield for product **105j** and a second reaction mixture was made but was exposed to only 15 minutes of blue LED irradiation. For the latter a HPLC chromatogram was obtained immediately after irradiation (instant) and at t = 19 h (after being stored in a cupboard overnight) (**Figure 52A**). Comparable SM:P relative intensity ratios (49:36) were obtained confirming that the reaction had not progressed in the absence of light. This was also supported by ^{19}F NMR spectroscopy which revealed a 20% and 22% quantitative yield for **105j** at each respective time point. The

reaction mixture was then irradiated for another 15 minutes, and the data were compared to the reaction mixture after 30 minutes of continuous LED irradiation (**Figure 52B**).

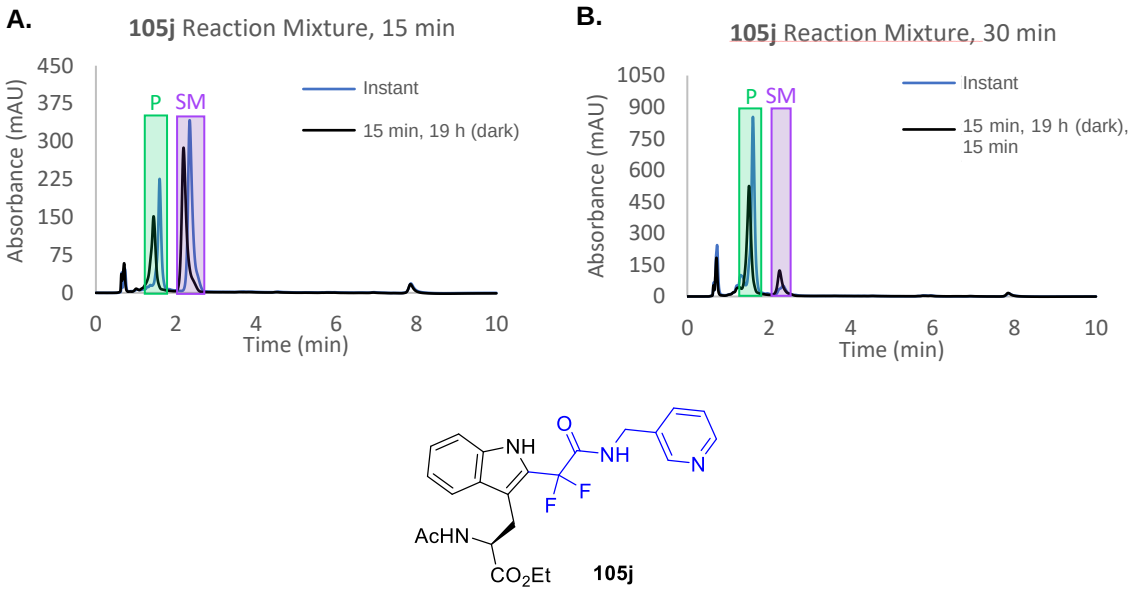

Figure 52. Overlapped reaction mixture HPLC chromatograms for product **105j** after instant radiation and 'paused' irradiation. 40-80% B over 5 min, 280 nm. A. After 15 min. B. After 30 min.

In both cases, similar starting material consumption (Ac-Trp-OEt **93**) was observed and importantly increased compared to the 15-minute time point providing a greater relative intensity of product 15:63 (SM:P). Unfortunately, the presence of TFT in the reaction mixture during irradiation likely underwent a side reaction or decomposition because a 62% product yield was estimated for the reaction with intermittent irradiation. This was 14% higher than the yield usually obtained after 30 minutes even though the analytical HPLC chromatographs looked comparable.

This study also provided crucial information going forward: once TFT had been added to the reaction mixture, it would not be beneficial to undergo further irradiation because the NMR yield obtained would not be reliable. Instead HPLC analysis was run first, and the chromatogram was interpreted to determine whether the amount of unreacted starting material was

acceptable or whether further irradiation was required, before TFT was added to the reaction mixture.

This concludes the photocatalytic difluoroalkylation studies carried out on Ac-Trp-OEt **93** demonstrating the reaction's versatility by the synthesis of 11 small molecule-Trp conjugation products with yields between 21-79%. Conditions developed during optimisation were compatible with a variety of small molecule probes and three reactions were scaled up ten-fold producing consistent yields with those obtained for the analytical scale reactions. Product isolation was successful and characterisation using ^{1}H NMR spectroscopy confirmed that the desired transformation took place. Finally, the difference in reaction rate observed for α-amide and α-ester radical precursors was discussed including potential explanations and attempted cyclic voltammetry studies.

3.4 Difluoroalkylation of Ac-WHISKEY-NH_2

After successful difluoroalkylation of Ac-Trp-OEt **93** was demonstrated, investigation into chemoselective peptide modification was carried out using the model peptide Ac-WHISKEY-NH_2 **163** (**Figure 53**).

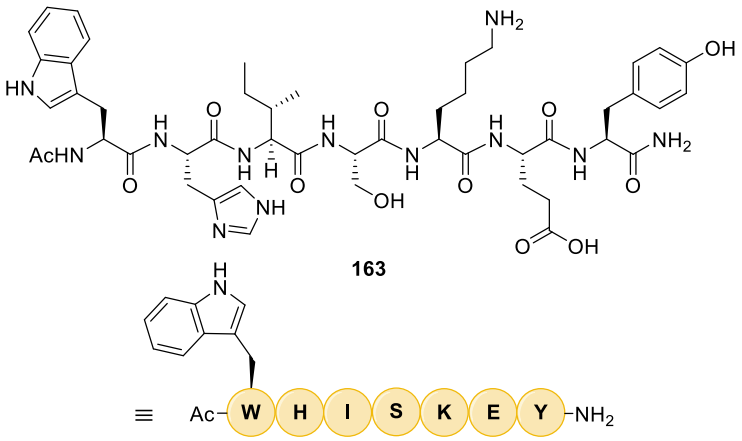

Figure 53. The structure of Ac-WHISKEY-NH_2 **163** and its simplified representation.

A variety of complex peptides were synthesised using solid phase peptide synthesis (SPPS), including examples based on biologically relevant sequences. Across the seven peptide examples, every native amino acid was incorporated ensuring that the reactions capability against all proteinogenic functionality was explored.

First Ac-WHISKEY-NH_2 **163** was synthesised *via* Fmoc-SPPS, in a 20% overall yield, with the presence of aromatic residues and unprotected functional groups: alcohol, amine, and carboxylic acid. This 7-mer Trp-containing peptide substrate is complex: displaying a range of functionality which is unique compared to a lot of other photocatalytic Trp modification strategies reported in the literature. Most exploration has previously been carried out on di- and tripeptides with little functional group scope such as Boc-YAVW-OMe **164** and Boc-GWL-OMe **165**.[119,120]

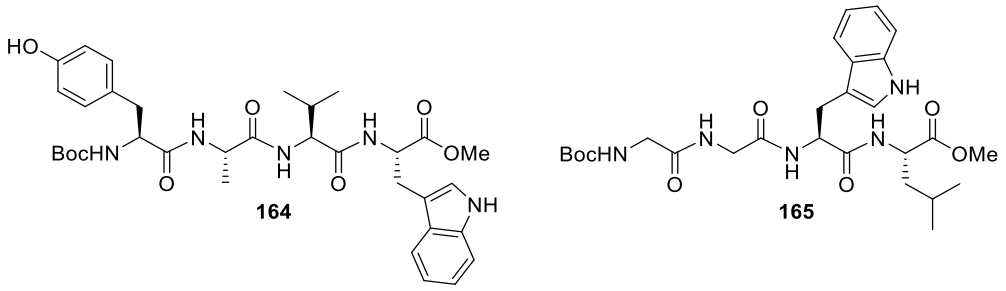

Figure 54. Peptide substrates used in the literature for photocatalytic Trp functionalisation.[119,120]

Reactions were carried out on a 5.00 μmol scale using Ac-WHISKEY-NH_2 **163**; and despite this small scale, product isolation was successfully carried out using semi-preparative HPLC purification. This allowed a variety of analysis techniques to be carried out on the small molecule-WHISKEY conjugation products, including proton NMR spectroscopy which was used to identify the site of alkylation and determine the reaction's chemoselectivity. After a discussion on probe compatibility and peptide

conjugation product yields, the NMR evidence proving regio- and chemoselective difluoroalkylation will be covered in 3.5 Chemoselectivity for Trp.

For the photocatalytic difluoroalkylation of Ac-WHISKEY-NH_2 **163**, all the ester and amide probes were compatible with the substrate giving moderate to good product yields considering the complexity of the peptide substrate (**Scheme 44**). The same conditions were used as those developed during optimisation, with a minor alteration for probe **94m**, highlighting the applicability of this functionalisation strategy for peptide modification.

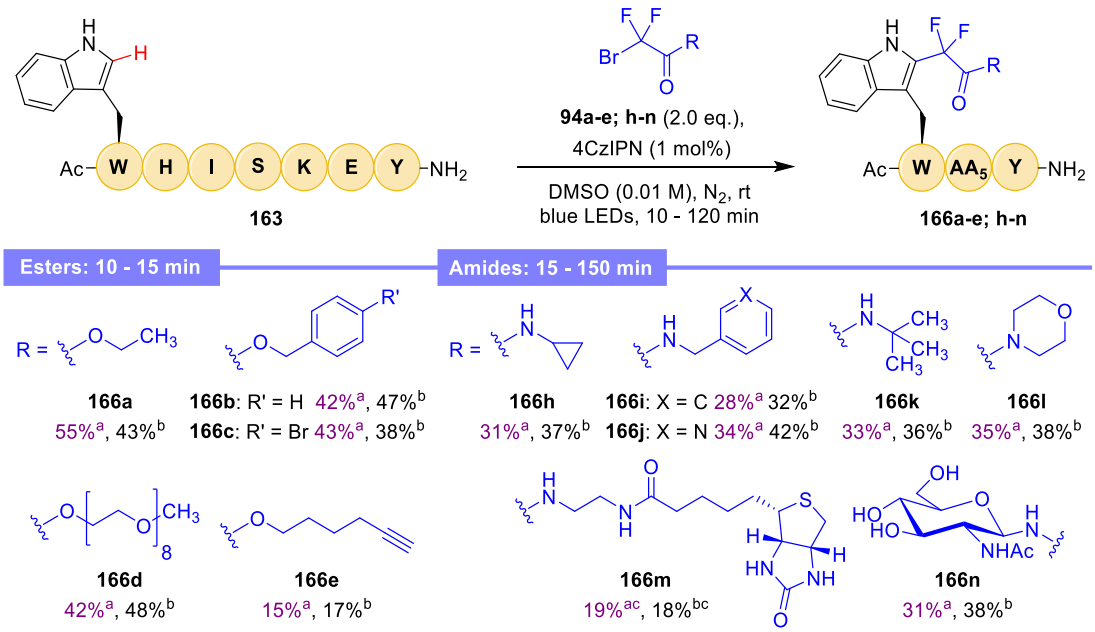

Scheme 44. Photochemical chemoselective alkylation of Ac-WHISKEY-NH_2 **163**; reactions performed on a 5.00 μmol scale. [a]Yields determined by ^{19}F NMR spectroscopy using TFT as the internal standard. [b]Isolated yields. [c]4CzIPN (5 mol%), bromodifluoroacetamide **94m** (1.5 eq).

Beginning with ethyl ester probe **94a**, HPLC analysis revealed that the conjugation reaction was complete within 10 minutes and gave product **166a** in a pleasing 55% yield: determined by quantitative ^{19}F NMR spectroscopy. Despite this being approximately 25% lower than the corresponding amino acid conjugation product, it remained a positive result:

the reactions' compatibility with a wide range of unprotected functional groups was demonstrated. This peptide model carries the majority of chemical diversity found across the proteome which is crucial for the successful application to other biomolecular substrates.

Similarly, to the more straight-forward Ac-Trp-OEt **93** conjugation reactions, exposing the library of small molecules probes to Ac-WHISKEY-NH_2 **163** difluoroalkylation revealed that aliphatic **166a**, aromatic **166b-c**; **166i-j**, cyclic **166h** and biologically relevant **166m-n** moieties were all incorporated onto the peptide highlighting a robust methodology (**Scheme 44**). The highest isolated yield was 48% which was achieved for PEG-conjugated WHISKEY product **166d** with a rapid reaction time of 10 minutes, highlighting the utility of this methodology to potentially aid the growth of PEGylated therapeutics.[6]

Additionally, for WHISKEY-conjugation a new amide probe was synthesised bearing a sugar moiety **94n** (with three unprotected hydroxyl groups) for peptide glycosylation which can improve a biomolecules' absorption across biological membranes enhancing PK properties.[8] The corresponding glycosylated WHISKEY product **166n** was synthesised in a 38% isolated yield after 90 minutes of irradiation. A similar post-translational modification (PTM) of Trp is synthesised by the action of C-mannosyltransferases in the endoplasmic reticulum (ER) type to give C−2 mannosylation of Trp (C-Man-Trp **167**).[178] Proteins with this PTM have various functions including the formation of sugar bridges to aid intracellular transport and protein folding, highlighting the importance of this modification.

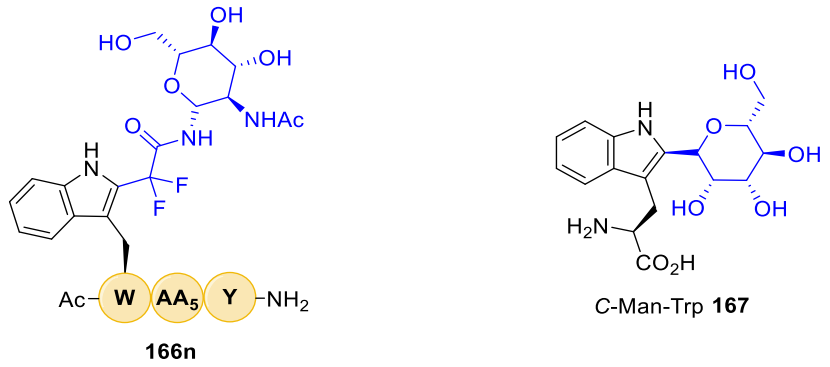

Figure 55. Examples of C−2 glycosylated Trp in nature.

Analysis of Ac-WHISKEY-NH_2 **163** conjugation reaction mixtures by analytical HPLC was mostly informative, displaying distinct signals in the chromatograms for starting material, product, and side products (**Figure 56A**). However, similarly to a few amino acid conjugation reactions, some examples provided an ambiguous chromatogram due to significant overlap of signals.

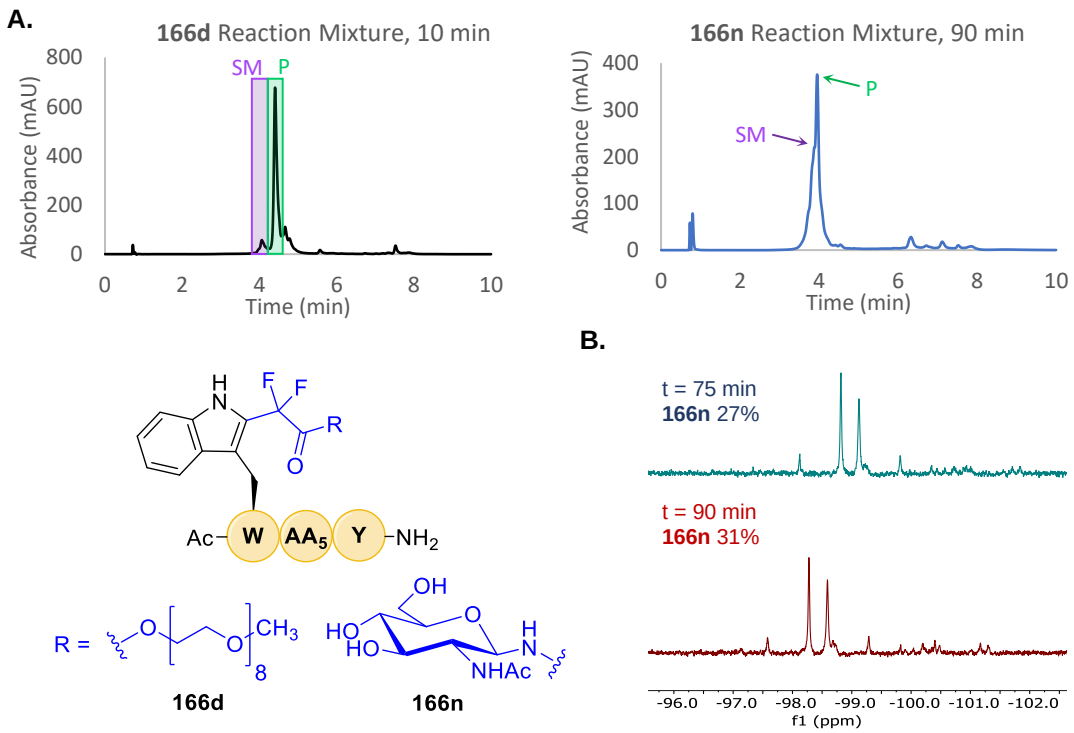

Figure 56. A. Reaction mixture HPLC chromatograms for **166d** and **166n**. 2-95% B over 5 min, 280 nm. B. Crude ^{19}F NMR spectra for **166n** after different reaction times; yields determined by using TFT as the internal standard.

It is common in the literature to report HPLC conversions as estimated yields for peptide transformations, but often these are remarkably higher than the subsequently obtained isolated yields,[116,95] and would likely be inaccurate if/when signals overlap. Therefore, obtaining additional data using ^{19}F NMR spectroscopy (**Figure 56B**), offered an uncommon advantage of this work and provided further insight into the reaction. For example, although minor, increasing the reaction time from 75- to 90 minutes for WHISKEY glycosylation improved the product yield for **166n** by 4% (**Figure 56**), whereas the corresponding HPLC chromatograms were unclear as to whether this increased time was beneficial or detrimental due to an overlap between starting material (SM) and product (P) signals.

Generally, a 10-20% drop in yield was observed when comparing the peptide alkylation products to the corresponding amino acid products, as a consequence of substrate complexity. Nonetheless, most small molecule-WHISKEY product yields were between 30% and 50%, which is encouraging especially because similar photocatalytic Trp alkylation transformations in the literature could not tolerate,[121] or provided a low product yield (20%) in the presence of a histidine residue.[120] Surprisingly morpholine probe **94l**, gave a 35% spectroscopic product yield which was only 4% lower than the corresponding product resulting from Ac-Trp-OEt difluoroalkylation. Comparing reaction mixture ^{19}F NMR spectra for these substrates (**Figure 57**), revealed that some of the additional side product impurity signals observed for amino acid alkylation (between −87 and −92 ppm) had been inhibited.

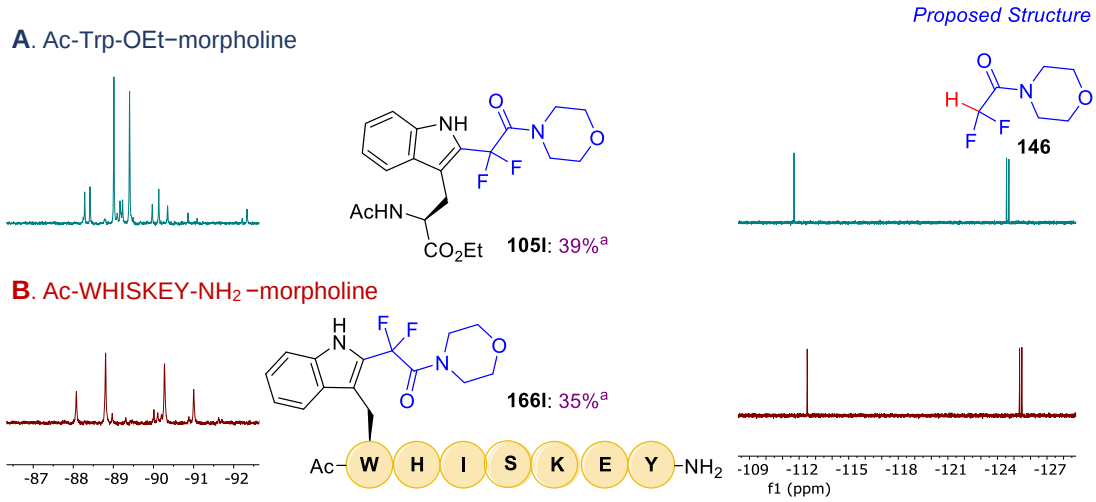

Figure 57. Reaction mixture ^{19}F NMR spectra for **105l** and **166l** showing the regions of interest. Yields determined by using TFT as the internal standard.

The region on the spectrum between −109 and −127 ppm showed two signals (−112 ppm (s) and −125 ppm (d)) which are believed to result from morpholine probe **94l** side reactions unrelated to the indole ring on Trp such as HAA to give amide **146**. This was supported by the fact that comparable integrations for these signals were obtained for both the amino acid and peptide reaction. Probe side reactions would likely be influenced by differences in probe equivalents and reaction concentration but because these are constant parameters for each reaction mixture, regardless of the biomolecule substrate, it is to be expected that these side reactions were unaffected.

The ester conjugation reactions were rapid and consistent with those reported for Ac-Trp-OEt **93** difluoroalkylation: complete within 10-15 minutes which provided product ^{19}F NMR spectroscopic yields between 42-43% (**166b-d**). Conversely, the amide conjugation reactions required a broader range of reaction times from 15-120 minutes, affording product yields between 28-35% (**166h-n**). As discussed previously (3.3 Reaction Rates), the more variable reaction times for α-amide radical precursors

presumably resulted from electronic effects associated with moieties substituted on the nitrogen.

Due to the reaction's sensitivity to time and to ensure the highest product yield was obtained, most Ac-WHISKEY-NH_2 **163** conjugation reactions were carried out using two different irradiation times, albeit the difference was often small (0 to 10%). For ester probes this differed by 5 minutes due to their susceptibility toward dialkylation, whereas for amide probes intervals of 30 minutes were used. Reaction monitoring by analytical HPLC was facile and required as little as 2 µL of the reaction mixture to identify the relative intensity of starting material to product such as 36:56 (**Figure 58A,** 30 min).

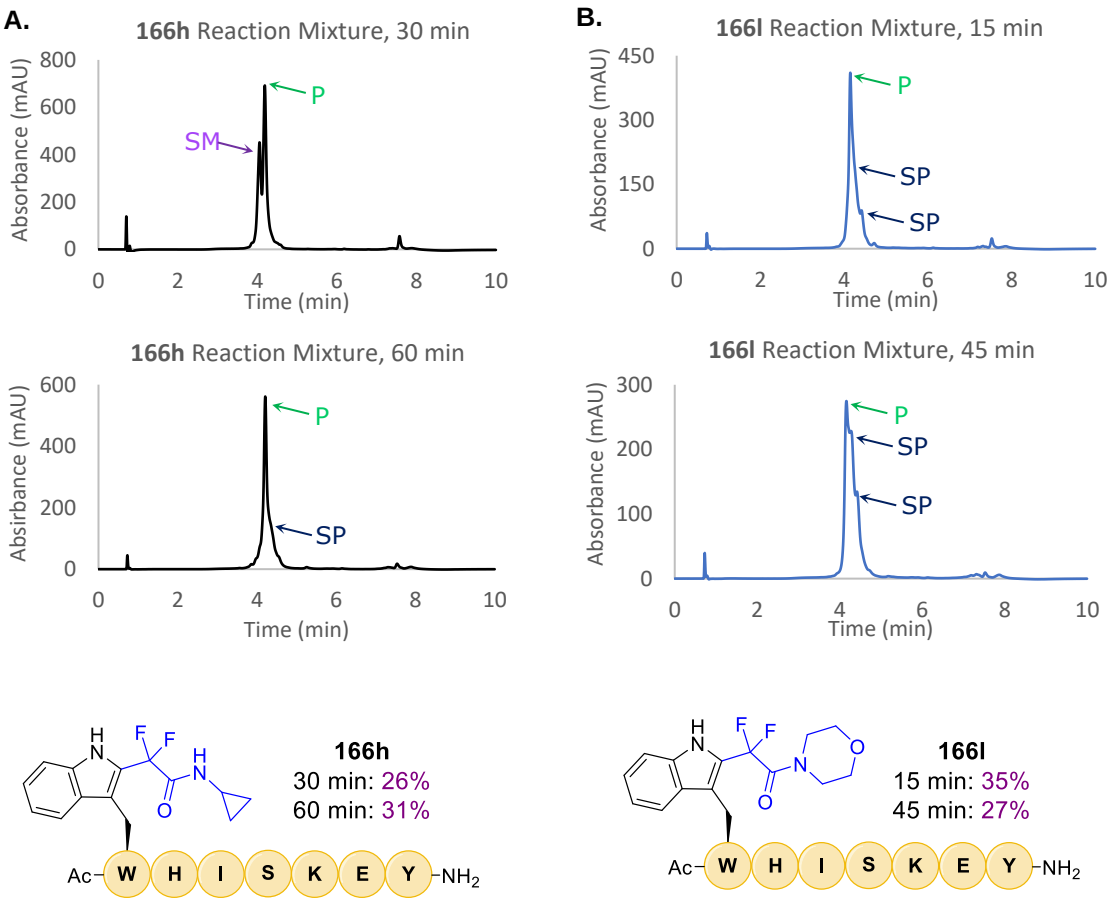

Figure 58. Reaction mixture HPLC chromatograms for **166h** and **166l** highlighting the effect of increased irradiation times. 2-95% B over 5 min, 280 nm.

When the value of starting material was greater than or equal to 10% the reaction was placed back into the PhotoRedOx box for further irradiation. However extended irradiation times can enhance side product (SP) formation which demonstrates the importance of stopping irradiation at the optimum time (**Figure 58B**).

The accuracy of quantitative NMR yields were again validated by the comparable isolated yields obtained for WHISKEY alkylation products. In most cases isolation provided a slightly higher yield between 3 and 7%, which was unexpected because small unavoidable losses would be associated with reaction mixture transfer and purification. Therefore, it could be suggested that the acquired NMR yields slightly underestimated the reaction success potentially due to inherent measuring errors associated with micropipettes when TFT (internal standard) stock solutions were made and transferred to the reaction mixture. If at any point the internal standard TFT was overestimated when added to the reaction mixture the ratio of TFT:product would no longer be 1:1, hence a lower quantitative product yield would be calculated. Alternatively, errors are also associated with NMR analysis itself where the average accuracy will be $\pm$5% and to improve this to <1% factors such as signal to noise, resolution and isotopic satellites must be optimised.[179] Due to the 5.0 μmol reaction scale it was important to be mindful of such equipment and measuring errors because these can become significant. Therefore, stock solutions, micropipettes and the NMR spectrometer used were kept as constant as possible throughout experimental analysis to provide reliable data which allowed comparisons to be made and reaction trends to be rationalised.

Exceptions to the Trends

Even though most product isolated yields were marginally greater than the corresponding ^{19}F NMR yields, this was not the case for ethyl- and 4-bromo benzyl ester products **166a** and **166c** where instead a 5-12% reduction was observed. This could potentially result from product instability due to the labile ester linker. It was shown previously that in a 1:1 DMSO:H_2O solvent mixture, hydrolysis of ethyl ester probe **94a** was observed to give $BrCF_2CO_2H$ **115**. Before purification was carried out, the 500 µL reaction mixtures were diluted with 2.6 mL of 0.1% TFA in H_2O, approximately 5 times the reaction volume, to prevent compounds co-eluting with DMSO at the beginning of the purification. This excess, slightly acidic, water content can encourage ester hydrolysis and was supported by mass spectrometry data obtained from certain fractions isolated after purification where mass ions corresponding to **168** were observed (**Figure 59**).

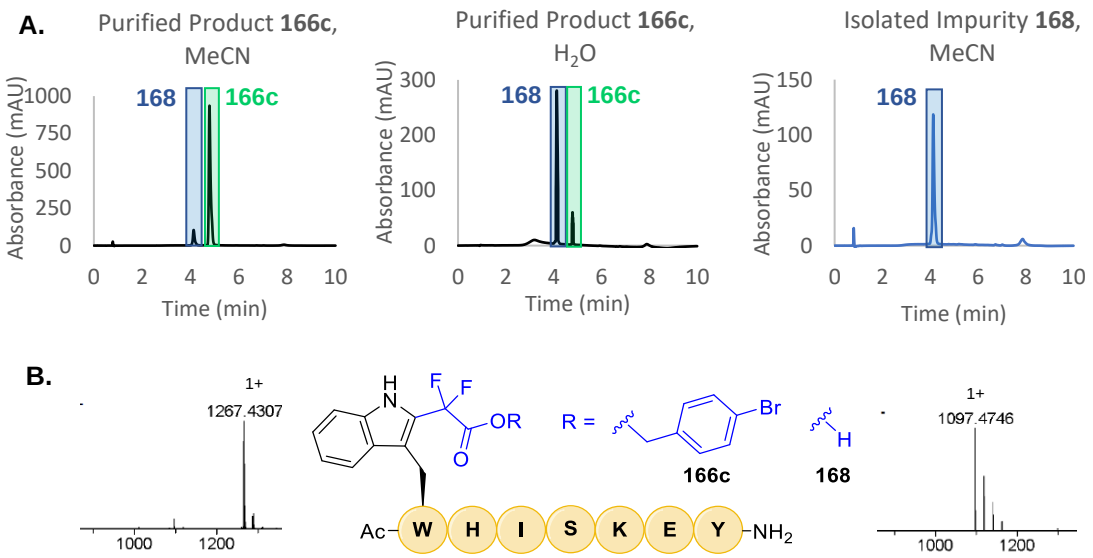

Figure 59. A. HPLC chromatograms showing the instability of difluoroalkylated product **166c** in H_2O. 2-95% B, over 5 min, 280 nm. B. Mass spectrometry data supporting the formation of hydrolysed product **168**.

Hydrolysis had to occur after the radical addition reaction because it was known that $BrCF_2CO_2H$ **115** cannot alkylate Trp under these conditions (2.3 Photocatalytic Difluoroalkylation Conditions) due to its reduction potential (−1.27 V vs SCE).[124] Therefore, the lower isolated yields obtained for **166a** and **166c** compared to the corresponding yields determined by ^{19}F NMR spectroscopy can be explained by product hydrolysis, which was supported by the isolation of such product (**168**) which eluted 6 minutes before the desired product **166c** during preparative HPLC purification. For analytical HPLC a distinct retention time (Rt) of 4.13 minutes was provided by **168** compared to a Rt of 4.78 min for **166c** (**Figure 59**) and this was supported by the observation of hydrolysed product mass ions by mass spectrometry. Pleasingly, side product formation was minor (< 0.5 mg), but after bromo-benzyl product **166c** was dissolved in H_2O almost complete hydrolysis was observed (**Figure 59**), providing access to carboxylic acid conjugated products if required.

Continuing the discussion of examples which did not follow general trends, hexyne **94e** and biotin **94m** radical precursors provided poor product yields (15% and 19% respectively), yet this was consistent with the below average performance observed for the analogous amino acid conjugation reactions. As discussed in 3.2, a side reaction involving 4CzIPN and probe **94e** (in the absence of a biomolecule) can occur and is represented by a broad singlet signal at approximately −102.0 ppm in the ^{19}F NMR spectrum. Therefore, the lower yield does not correspond to chemoselectivity concerns for the peptide conjugation reaction, in fact both Ac-Trp-OEt **93** and Ac-WHISKEY-NH_2 **163** performed comparably: spectroscopic product yields were almost within 5% of each other.

Because the side reaction reduces the equivalents of probe **94e** available for alkylation, a large excess (10 eq.) and portion-wise addition was investigated (**Table 14**); however, the difference in product **166e** yield was minor.

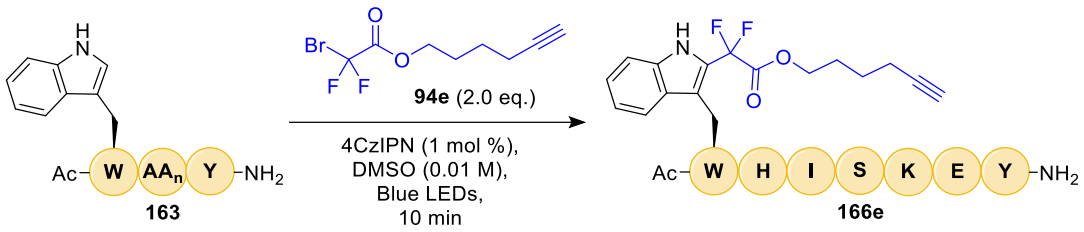

Entry	Deviation from standard conditions	Yield[a]
1	none	15%
2	30 min	19%
3	10 eq. **94e**, 30 min	20%
4	2 × (2 eq. **94e**, 10 min)	17%

Table 14. Photocatalytic alkylation of Ac-WHISKEY-NH_2 on a 5.00 μmol scale in position A of the PhotoRedOx box using EvoluChem™ LED spotlights (455 nm). [a]Yields determined by ^{19}F NMR spectroscopy using TFT as an internal standard.

The product signals were of low intensity hence similar to baseline noise; therefore, it is more likely that the integrations/yields obtained are within NMR error of each other (15-20%). Despite the poor isolated yield (17%), the product was obtained with high purity, which would allow a subsequent reaction to be carried out for product derivatisation if desired.

For biotin conjugation it should be noted that using the standard photocatalytic difluoroalkylation conditions (4CzIPN (1 mol%), **94m** (2.0 eq.)), coelution of unreacted probe was observed with product **166m**. This was highlighted by the presence of a singlet signal around −60 ppm (**Figure 60B**) in the product ^{19}F NMR spectrum, therefore, slightly modified conditions were used to promote complete consumption of the probe which in turn would aid the isolation of pure product: 5 mol% 4CzIPN and 1.5 eq. **94m**.

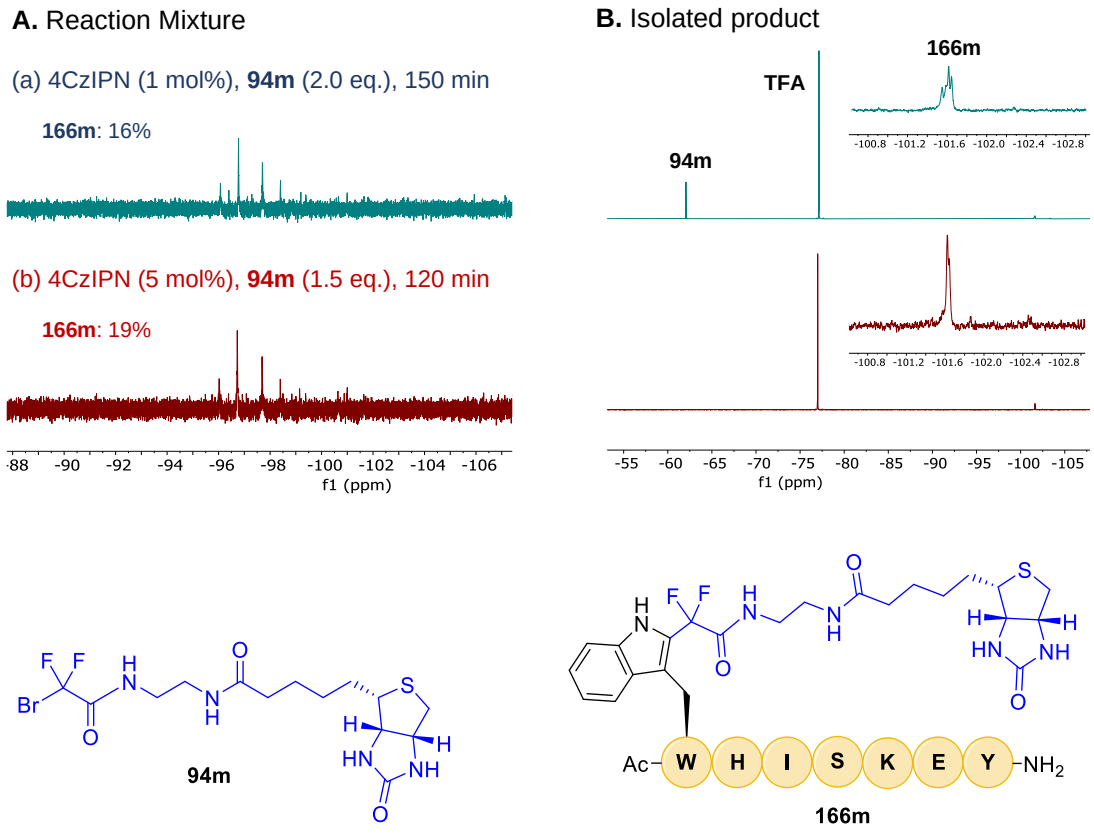

Figure 60. A. Reaction mixture ^{19}F NMR spectra for **166m** showing the product region. Yields determined by using TFT as an internal standard. B. Isolated product ^{19}F NMR spectra.

Pleasingly, similar yields determined by ^{19}F NMR spectroscopy were obtained for WHISKEY conjugation product **166m** using either the standard or modified conditions: 16% and 19% respectively (**Figure 60A**), which demonstrated an alternative set of conditions if probe co-elution is problematic or if the probe synthesised is precious.

There was reason to believe that the yields obtained for a couple of Ac-WHISKEY-NH_2 **163** difluoroalkylation products could be improved due to unusually large amounts of unreacted probe being observed at the end of the reaction (revealed by ^{19}F NMR spectroscopy). For WHISKEY-biotin conjugation 0.95 eq. of **94m** remained compared to 0.42 eq. for the corresponding amino acid reaction and similarly for cyclopropyl conjugation: 1.05 eq. and 0.48 eq. of **94h** was left unreacted for Ac-WHISKEY-NH_2 **163**

and Ac-Trp-OEt **93** difluoroalkylation respectively. This suggested that radical formation was lower for the peptide reaction, implying that the amino acid side chains on Ac-WHISKEY-NH_2 **163** may interact with the probe or the photocatalyst hindering the desired reaction between the two. However, it was discovered that a stock solution of 4CzIPN could lose activity over time, which may cause poorer radical formation as less than 1 mol% would be present in the reaction mixture. Unfortunately, this hypothesis was based on results from a subsequent project (chapter 4: Peptide Stapling), therefore it was only upon reflection that the stock solution used for Ac-WHISKEY-NH_2 **163** difluoroalkylation with biotin probe **94m** was identified as being 2.5 months old.

Aside from signals in the ^{19}F NMR spectra corresponding to probe **94m**, TFT and product **166m**, there was also a distinct doublet signal around −125 ppm. This doublet signal was also observed in other reaction mixtures, albeit less significantly, suggesting the α-carbonyl radical **169** had abstracted a hydrogen atom to from side product **171** instead of the desired indole alkylation product (**Scheme 45**). This side reaction pathway was presumably enhanced for biotin probe **94m** due to the additional amide/carbamide functionality increasing the number of H−bond opportunities. The hydrogen atom may be provided by DMSO (which is in large excess)[167] or the peptide itself allowing side product formation to occur at an appreciable extent.

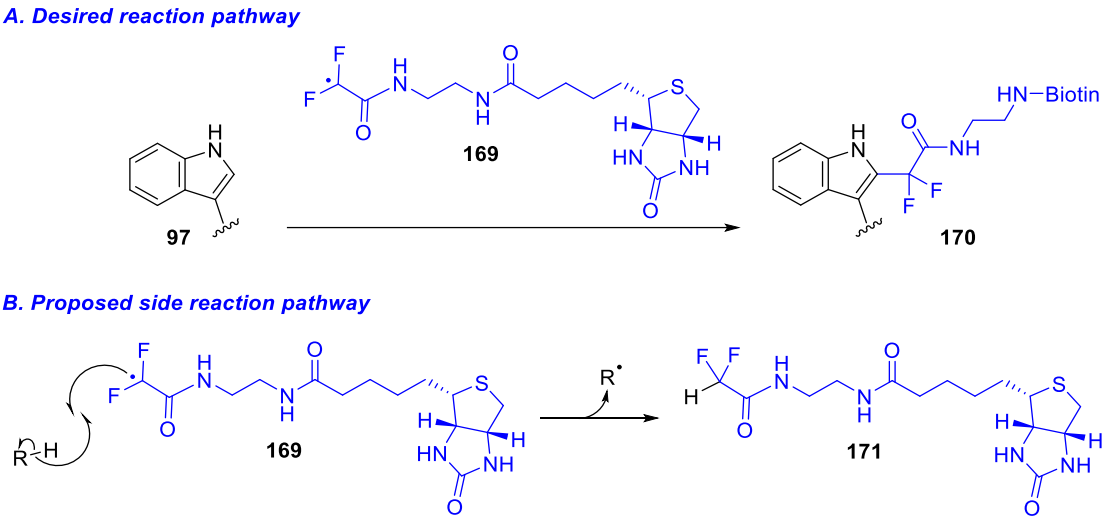

Scheme 45. Reactions involving radical intermediate **169**. A. Photocatalytic difluoroalkylation of Trp. B. Hydrogen atom abstraction (HAA).

Purification was carried out for the peptide conjugation reactions therefore this proposed structure was confirmed by isolation and characterisation using both ^{1}H and ^{19}F NMR spectroscopy (**Figure 61**). The ^{1}H NMR spectrum showed a triplet signal with a large coupling constant of 53.9 Hz (**Figure 61A**) which agreed with literature values reported for the coupling between geminal hydrogen and fluorine nuclei,[161] and the rest of the ^{1}H spectrum was assignable. It should be noted that the triplet is more likely an overlapped doublet of doublets signal because the fluorine atoms are diasterotopic.

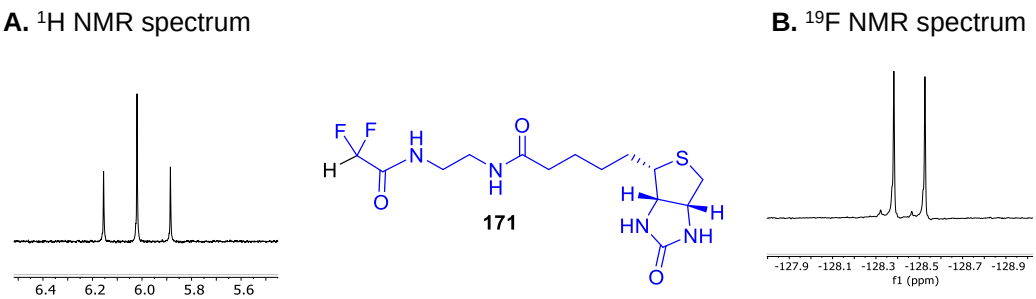

Figure 61. Distinctive NMR signals observed for the characterisation of side product **171**. A. ^{1}H NMR spectrum. B. ^{19}F NMR spectrum.

Additionally, a doublet at −128.5 ppm in the ^{19}F NMR spectrum with the same coupling constant (53.9 Hz) was the only signal present (ignoring TFA)

further characterising side product **171** (**Figure 61B**). Finally, both the $[M+H]^+$ and $[M+Na]^+$ mass ions were the only species observed in the mass spectrum, confirming that HAA had occurred during the reaction. Unfortunately, any attempts to improve the product yield for alkyne and biotin conjugation reactions were unsuccessful: increasing the probe equivalents to try offset the loss *via* competing side reactions also enhanced these side reactions. The reaction mixture profiles in figure 62 showed a significant amount of unreacted starting material, but unfortunately this could not be reduced due to the inherent properties/side reactions associated with probes **94m** and **94e**.

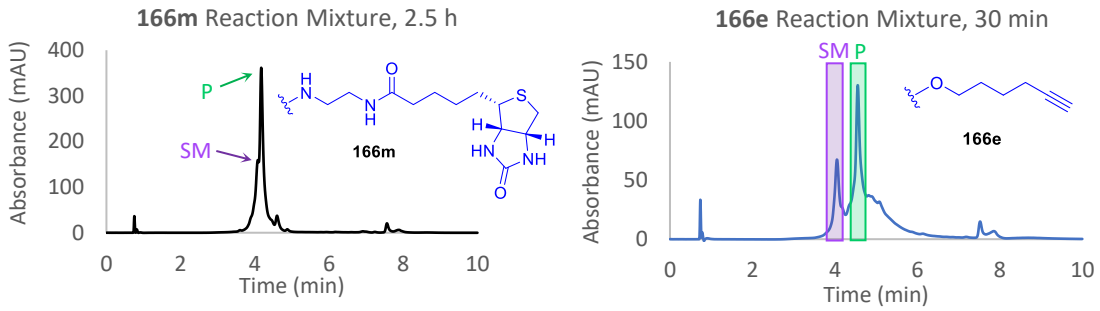

Figure 62. Reaction mixture HPLC chromatograms for Ac-WHISKEY-NH_2 difluoroalkylated products **166m** and **166e**. 2-95% over 5 min, 280 nm.

Reactivity and Selectivity for Amide and Ester Radical Precursors

During the scope exploration for Ac-WHISKEY-NH_2 **163** difluoroalkylation, general trends were identified for reaction times and product yields along with radical precursors that underperformed. A direct comparison was made between benzyl ester **94b** and benzyl amide **94i**, hence any reactivity differences associated with these two radical precursors likely resulted from the type of carbonyl. Similarly to Ac-Trp-OEt **93** conjugation, reaction endpoints and product yields were impacted. Different reaction times of 10- and 60 minutes were required, providing product yields of 42% and 28%

for **166b** and **166i** respectively. This lower product conversion was perhaps due to reduced reactivity and/or poorer selectivity of the α-amide radical which was supported by analytical HPLC and fluorine NMR spectroscopic analysis.

For example, the reaction mixture for benzyl amide product **166i**, showed a greater proportion of side products with retention times at approximately 4.5 – 5.5 minutes, compared to the analogous ester product **166b** (**Figure 63**). In an attempt to reduce these side products, the reaction time was decreased to 30 minutes of irradiation however a lower product yield of 24% was obtained for **166i**. This was accompanied by a significant amount of unreacted starting material observed by analytical HPLC at the end of the reaction (**Figure 63**), which presumably accounted for this minor drop in yield and emphasized once again that these alkylation reactions require a balance between starting material consumption and side product formation to acquire the optimum yield.

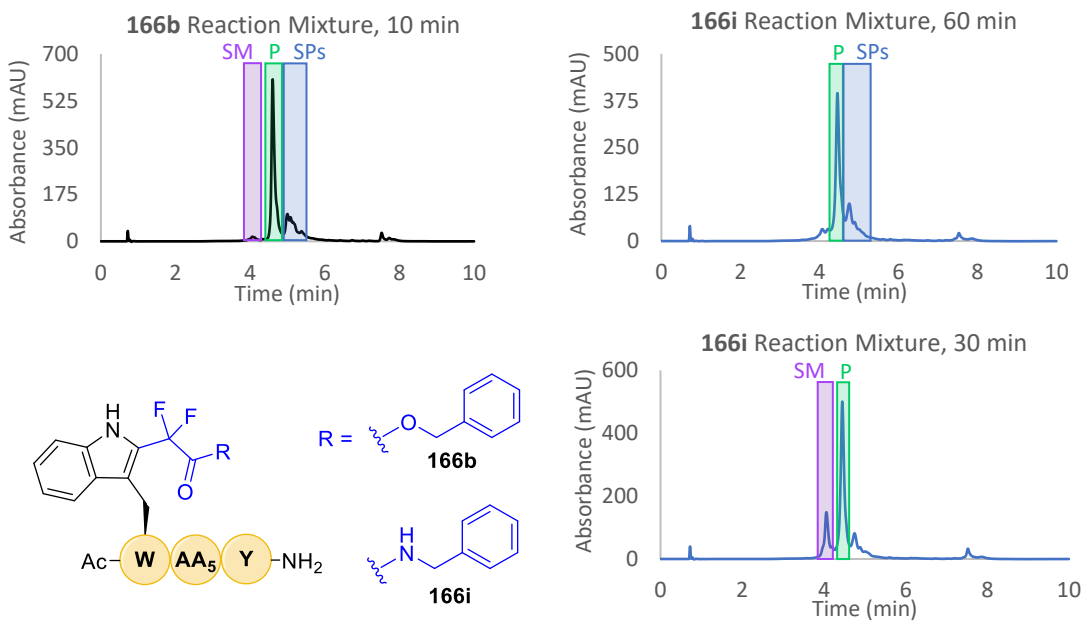

Figure 63. Reaction mixture HPLC chromatograms for Ac-WHISKEY-NH_2 difluoroalkylation products **166b** and **166i**. 2-95% B over 5 min, 280 nm.

Analysis of the reaction mixture ^{19}F NMR spectra for **166b** and **166i** revealed that within the product region (**Figure 64**, −94 → −101 ppm) a similar number of impurity signals were observed, but like the HPLC chromatogram suggested these were slightly more intense for the amide conjugation reaction. This suggested that the amide did not undergo any unique side reactions which was confirmed by MS data: ions observed in both reaction mixtures corresponded to mono- and dialkylated WHISKEY products.

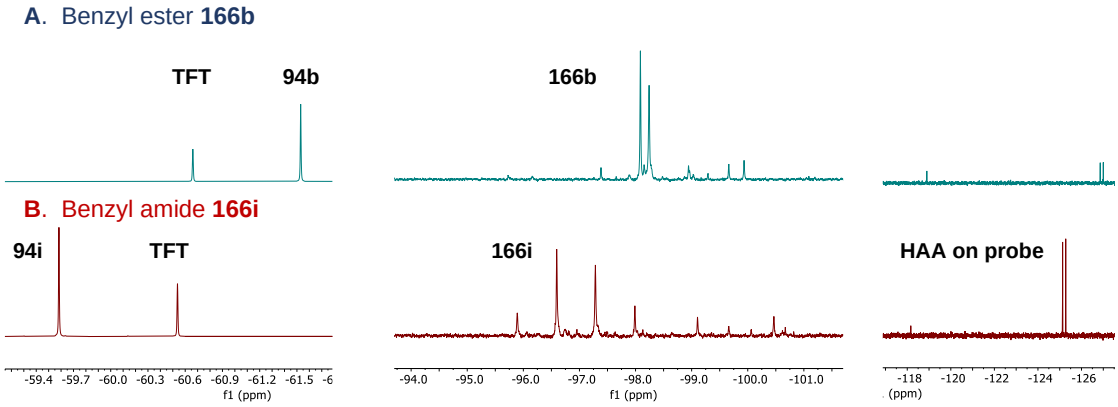

Figure 64. Reaction mixture ^{19}F NMR spectra for **166b** and **166i** syntheses, showing specific regions associated with the radical precursor (left), product (centre) and side product (right).

Additionally, the amount of ester- and amide probe **94b, 94i** left at the end of each reaction was approximately 1.0 eq. (**Figure 64**, left), even though the difference in irradiation time was 50 minutes. This indicated that α-amide radical formation was much slower than the corresponding α-ester radical, potential explanations for which were discussed in 3.3 Reaction Rates.

So far, the evaluation of product yields and reaction times acquired during photocatalytic Ac-WHISKEY-NH_2 **163** difluoroalkylation has been discussed. Many similarities were observed between Ac-Trp-OEt **93** and Ac-WHISKEY-NH_2 **163** substrates including consistent reaction conditions and times highlighting the robustness of the functionalisation strategy. A diverse

library of small molecule-WHISKEY conjugation products (**166a-e; h-n**) were synthesised and characterised using ^{1}H and ^{19}F NMR spectroscopy, allowing the site of difluoroalkylation to be determined.

3.5 Chemoselectivity for Trp

Likewise with the amino acid substrate, the small molecule-peptide products gave distinct and quantifiable signals in their reaction mixture ^{19}F NMR spectra: usually two high intensity roofed doublets (with matching coupling constants) and multiple minor impurity signals (**Figure 65A**). Due to the low intensity of impurity signals characterisation was not possible as negligeable mass was isolated after purification. Therefore, it was assumed that other amino acid residues on the Ac-WHISKEY-NH_2 **163** peptide did not undergo any significant side reactions. Further confirmation was obtained when the peptide substrate Ac-HISKEY-NH_2 **172** (with the Trp residue omitted) was exposed to the photocatalytic difluoroalkylation conditions, using ethyl ester probe **94a**. Only three baseline signals: two singlets and an almost negligible doublet signal corresponding to the HAA product **173**, were observed in the reaction mixture ^{19}F NMR spectrum (**Figure 65**).

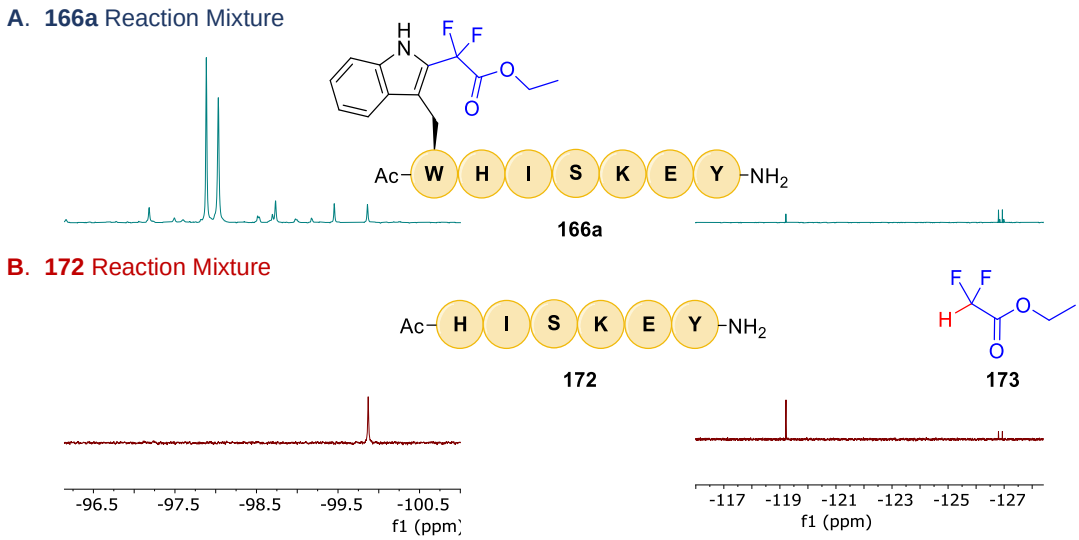

Figure 65. Reaction mixture ^{19}F NMR spectra for Ac-WHiSKEY-NH_2 **163** and Ac-HISKEY-NH_2 **172** photocatalytic difluoroalkylation with $BrCF_2CO_2Et$ **94a**.

These signals were also observed in the reaction mixture when Trp is present (Ac-WHISKEY-NH_2 **163**) but of similarly low intensity (**Figure 65**), therefore, alternative amino acid difluoroalkylation products were not observed in the presence of Trp, and equally not promoted in its absence, highlighting the chemoselectivity of this transformation.

Both reaction mixture analyses (^{19}F NMR spectroscopy and HPLC) identified the formation of a major product for all WHISKEY-conjugation products, however, purification was required to confirm that the doublets corresponded to difluoroalkylation on Trp. Generally, it was easy to identify the site of alkylation using ^{1}H NMR spectroscopy (**Figure 66**). The C–2 proton on the indole ring corresponded to a singlet at 7.14 ppm and is highlighted in green on Figure 66 (H^a), along with the assignment of some other aromatic signals for clarity. In most cases, the disappearance of this singlet was clear, identifying that the site of alkylation was regioselective on the Trp residue.

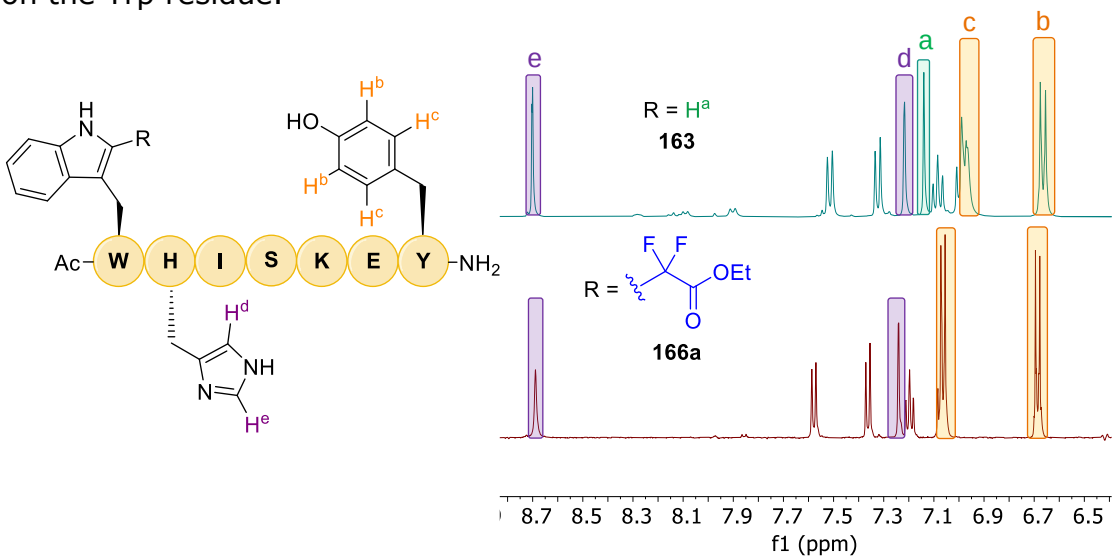

Figure 66. Stacked ^{19}F NMR spectra highlighting the aromatic region for Ac-WHISKEY-NH_2 **163** and alkylated Ac-WHISKEY-NH_2 product **166a**.

For some peptide examples however, ambiguity arose when singlet signals remained in the product spectra with similar chemical shifts to the C–2

proton or the aromatic region was more complicated, therefore, further analysis was necessary for these peptide examples. The His side chain bears an imidazole heterocycle which gave two singlet signals in the ^{1}H NMR spectrum (**Figure 66,** H^{d} and H^{e}), one of which is adjacent to the C−2 singlet of interest: 7.22 ppm and 7.14 ppm respectively. Slight shifts of the proton signals, hence ppm values, can be caused by the presence of salts i.e. TFA, or conformational changes, both of which can vary from starting peptide to product as a result of small molecule conjugation. Therefore, it would not be accurate to solely base the confirmation of chemoselectivity on the disappearance of a singlet at a specific ppm.

Instead, clarity would result from the identification of a cross-peak between the remaining two broad singlets using 2D NMR spectroscopy experiments, proving they correspond to His. Similarly for examples incorporating other aromatic moieties, provided by the probe or peptide sequence, the disappearance of the Trp singlet was unclear due to an increased number of overlapping signals in the aromatic region (**Figure 67**). Consequently, an additional ^{1}H NMR experiment was run for all small molecule-peptide conjugation products: total correlation spectroscopy (TOCSY). A TOCSY shows the coupling between all pairs of hydrogen nuclei when a continuous chain of coupled spins are present: the coupling between all benzene hydrogen atoms on the indole ring are observed due to the aromatic delocalisation (**Figure 67**).

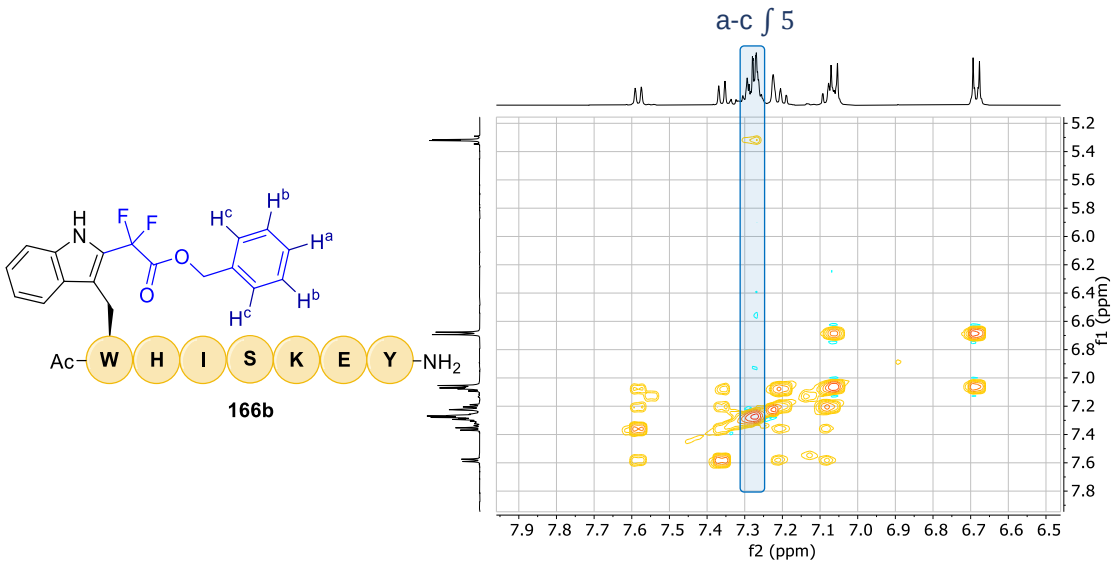

Figure 67. TOCSY spectrum for Ac-WHISKEY-NH_2 difluoroalkylation product **166b** showing the overlap of aromatic protons but the absence of the C−2 proton on Trp was confirmed.

The TOCSY spectrum shown in figure 67 corresponds to benzyl ester product **166b**, which confirmed that the multiplet signal highlighted in blue, with an integral of 5, did not contain the Trp C−2 proton. This multiplet only coupled one benzylic CH_2 signal, assigned to the probe moiety, not the indole benzylic hydrogen atoms. Therefore, it was confirmed that the C−2 proton was not masked within the multiplet, hence difluoroalkylation had occurred at the desired site. A TOCSY is analogous to a COSY experiment in the sense that the *J*-coupling between two hydrogen nuclei appears as a cross-peak in the spectrum but is not restricted to the closest neighbours.

Each experiment has its merits, for example a TOCSY spectrum can be quite overwhelming for assignments, whereas the COSY spectrum is simpler. This was used to determine which hydrogen signals on the indole ring neighboured each other using ethyl ester conjugation product **166a** (**Figure 68**). For example, the doublet at approximately 7.6 ppm coupled to the double doublet (hidden under the Tyr doublet signal) at 7.1 ppm, showing that these two hydrogen atoms are adjacent to one another.

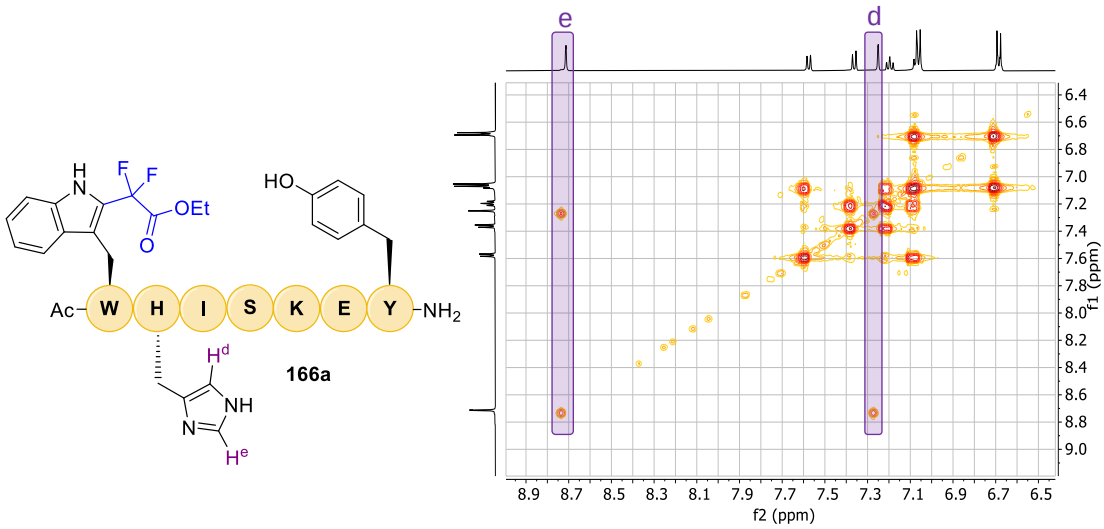

Figure 68. COSY spectrum for Ac-WHISKEY-NH_2 difluoroalkylation product **166a** showing that the broad singlet signals couple.

The presence of His singlets could cause confusion when confirming chemoselectivity but highlighted in purple on figure 68 are the cross-peaks showing that the two singlets observed at approximately 8.7- and 7.3 ppm couple, therefore cannot be assigned to the Trp C−2 singlet. Unfortunately, due to the sensitivity of the NMR probe and the set parameters used for the COSY experiment it was not possible to resolve the His cross-peaks for all conjugation products, whereas this was achieved using a TOCSY experiment providing clarity. With a greater insight into coupling partners, a better understanding hence interpretation of the aromatic region of the product spectra was possible. These experiments were carried out for all products which proved that site of alkylation was at the desired C−2 position, demonstrating a rapid and chemoselective peptide functionalisation method.

Dialkylation of Ac-WHISKEY-NH₂

After the chemoselectivity was confirmed, attempts were made to identify the second site of alkylation of Ac-WHISKEY-NH_2 **163**, associated with the dialkylated side products (**Figure 69A**).

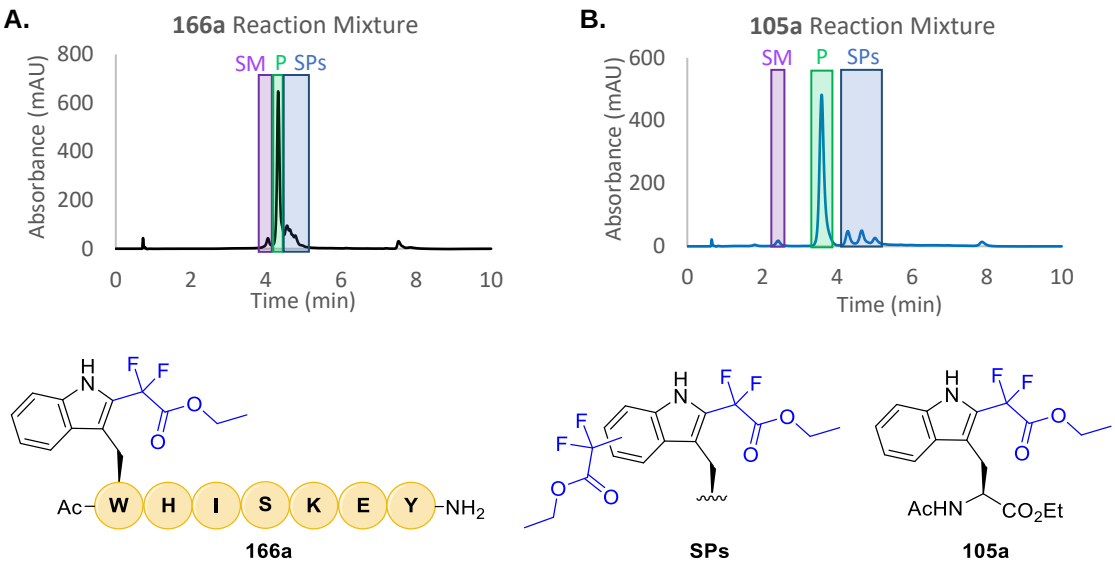

Figure 69. Reaction mixture HPLC chromatograms for Ac-WHISKEY-NH_2 **163** and Ac-Trp-OEt **93** difluoroalkylation with $BrCF_2CO_2Et$ **94a**.

For peptide substrates, dialkylation observed by mass spectrometry could suggest monoalkylation on Trp along with monoalkylation on a competing amino acid residue. This was unlikely because the reaction was known to undergo dialkylation on the indole ring when Ac-Trp-OEt **93** was used as the substrate (**Figure 69B**) and unsuccessful difluoroalkylation was observed using the peptide Ac-HISKEY-NH_2 **172.** Therefore, for Ac-WHISKEY-NH_2 **163** a valid assumption is that the second site of alkylation was once again on Trp.

During purification of the reaction mixture for Ac-WHISKEY-NH_2 **163** and ethyl ester **94a** conjugation, an isocratic gradient was held at approximately 30% MeCN and numerous fractions were collected in an attempt to obtain

pure samples. Due to the very similar retention times observed for the regioisomeric side products, co-elution of compounds was mostly observed, however one fraction primarily showed one species. It should be reiterated that the formation of each side product (SP) was minor; at least three compounds gave a combined relative intensity of 34% (by analytical HPLC). Therefore, the data collected after separating side products encountered sensitivity issues; the ^{19}F NMR spectra only showed a TFA signal (peptide counterion) which potentially drowned out any side product signals. Nonetheless, the TOCSY experiment was ran over 17 h, aiding signal detection (**Figure 70**).

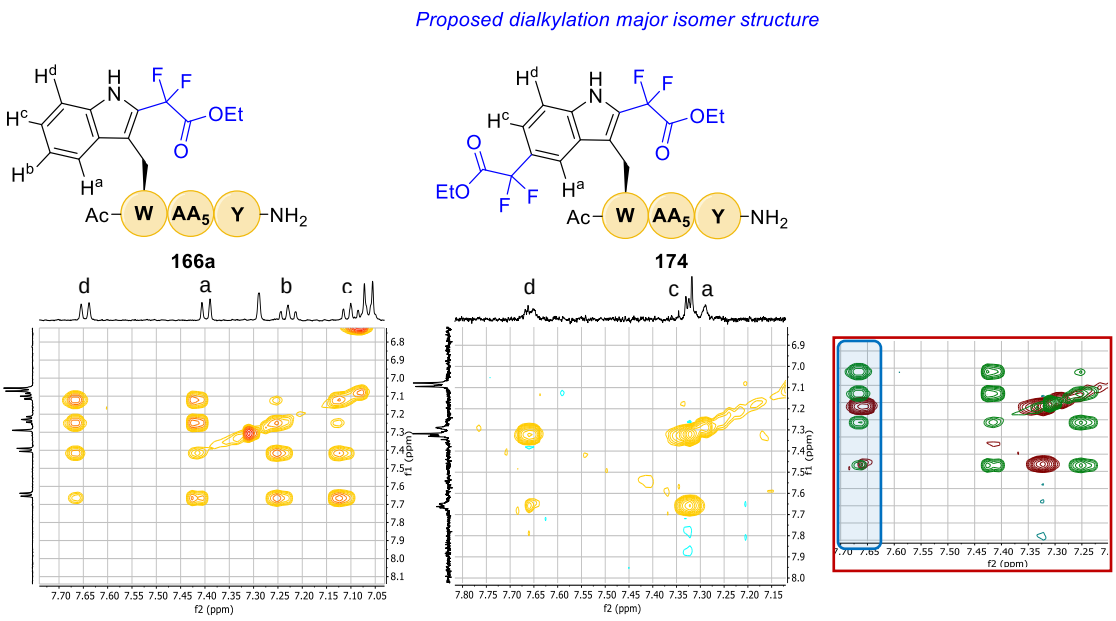

Figure 70. TOCSY spectra highlighting the region of interest for mono- and dialkylated Ac-WHISKEY-NH_2 products **166a** and **174** with a proposed structure for the latter based on the overlapped TOCSY spectra shown in the red box.

The mono- and dialkylated product (**166a** and **174**) TOCSY spectra have been shown in figure 70, focussing on the aromatic region of the ^{1}H NMR spectrum. Signals believed to correspond to the indole ring have been assigned, showing a clear disappearance of an indole hydrogen when comparing the two spectra. A break in the continuous chain of coupled spins

is suggested by the fact that there are fewer cross-peaks observed. This implied that the second site of alkylation had occurred on the indole ring. For the assignment, coupling was observed between two of the three signals suggesting the following multiplicities: doublet, doublet and singlet which would imply that the second alkylation site was on the C−5 or C−6 carbon. The chemical shift for the doublet at 7.67 ppm is constant in both mono- and dialkylated products, which may suggest that this is not influenced by, hence neighbouring the alkylation site, because the chemical environment is unchanged. Based on this assumption and 2D NMR spectroscopic data (HSQC, HMBC, COSY) recorded for similar examples, the assignment of this signal was suggested to be H^b, hence a reasonable prediction is that the second site of alkylation occurred at C−5.

3.6 Difluoroalkylation of Other Trp-Containing Peptides

Encouraged by the successful photocatalytic difluoroalkylation of Ac-WHISKEY-NH_2 **163**, an additional six peptides were synthesised (using SPPS) to further explore the reaction's functional group tolerance in the presence of all native amino acids, assessing chemoselectivity for Trp and any side chain incompatibilities.

To begin the peptide scope Ac-WHISKEY-NH_2 **163** derivates were synthesised to specifically incorporate moieties that have been known to inhibit other photocatalytic Trp modification reactions: a Cys residue (Ac-CWHISKEY-NH_2 **175**) and free peptide termini (H-WHISKEY-OH **176**). For these peptide models reactions were carried out using the ethyl ester probe **94a** (2.0 eq.) and standard conditions (1 mol% 4CzIPN in 0.01 M DMSO) which gave products **177a** and **178a** with a 36% and 38% ^{19}F NMR yield respectively (**Scheme 46**).

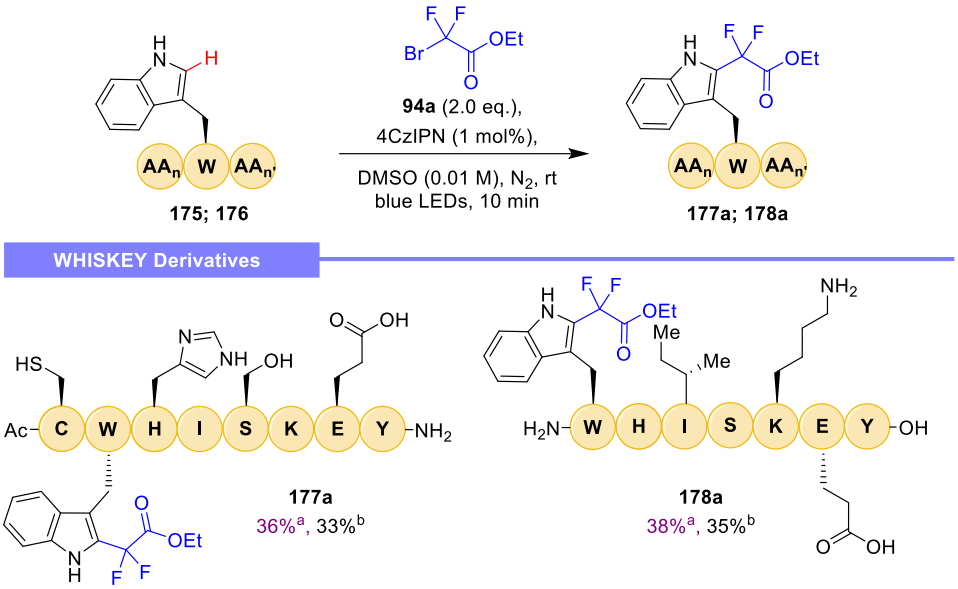

Scheme 46. Photochemical chemoselective alkylation of Trp-containing peptides; reactions performed on a 5.00 μmol scale. [a]Yields determined by ^{19}F NMR spectroscopy using TFT as the internal standard. [b]Isolated yields.

Despite the quantitative yields being lower than the corresponding WHISKEY product **166a** (55%), the isolated yields were all within 10% of each other and were obtained using rapid irradiation times of 10 minutes. Both **177a** and **178a** reaction mixtures showed baseline impurity signals in the product region of the ^{19}F NMR spectra (−97 → −100 ppm) but this was comparable to Ac-WHISKEY-NH_2 **163**, therefore suggested that the presence of Cys or free peptide termini did not compete with the desired reaction by creating a novel side-product. This was supported by MS data which only revealed mass ions associated with desired product and the known dialkylation impurity. The relative intensity of desired product (P) to side products (SPs) by analytical HPLC could potentially account for the reduced yield observed: approximately 33% and 29% SP was shown for **177a** and **178a** respectively (**Figure 71**), whereas for the analogous Ac-WHISKEY-NH_2 product **166a** this was 15%.

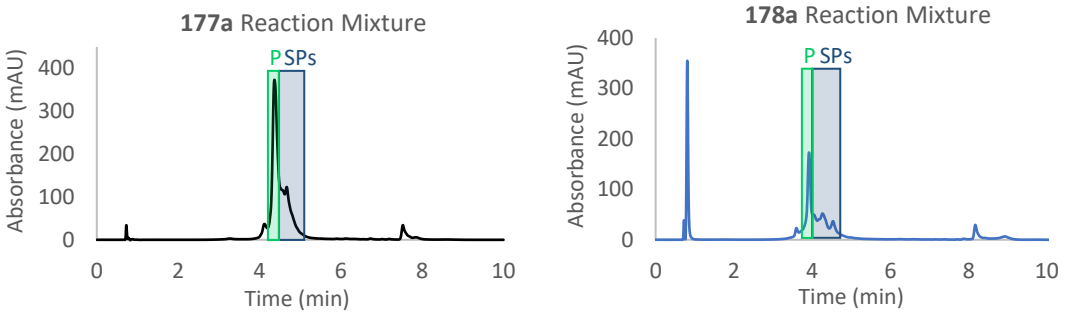

Figure 71. Reaction mixture HPLC chromatograms for Ac-CWHISKEY-NH_2 and H-WHISKEY-OH conjugation products **177a** and **178a** respectively. 2-95% B and 10-80% B over 5 min, 280 nm.

The same ethyl ester conjugation reaction using previously optimised conditions (1 mol% 4CzIPN, 2.0 eq. **94a**, 0.01 M DMSO, blue LEDs, 10 min) was carried out using peptide sequences based on biologically relevant examples: Ac-WLAHKAL-NH_2 **179** is a dipeptidyl peptidase-4 (DPP-4) inhibitor and peptides Ac-VVYPWYQ-NH_2 **180** and Ac-DKVGINYW-NH_2 **181** are angiotensin converting enzyme (ACE) inhibitors.[17] Following photocatalytic difluoroalkylation of these peptides, good yields between 40-50% were obtained for products **182a**, **183a** and **184a**. These yields were more consistent than the above examples to the corresponding Ac-WHISKEY-NH_2 **163** reaction, highlighting the reaction's tolerance to most amino acids. Another interesting feature of these substrates is the location of Trp within the peptide sequences: N-terminus (**179**), internal (**180**), and C-terminus (**181**), which could affect the conversion to product by altering the accessibility of Trp. However, isolated product yields were within 5% of one another, hence it can be assumed that the local steric and electronic environment surrounding the Trp residue had little effect on the desired reaction, demonstrating reaction robustness. Due to the limited peptide scope and similarity in yields, general trends cannot be extrapolated, especially because an 8% difference in yield (**Figure 72**) corresponds to as little as 0.4 mg therefore may not represent the efficiency of the reaction.

Instead, inherent weighing errors of the balance and/or water content in the peptide substrate can often be responsible for variations in yields. This was potentially supported by the reaction mixture analytical HPLC and MS data for **182a** and **184a** (**Figure 72**) showing a similar intensity of side product signals.

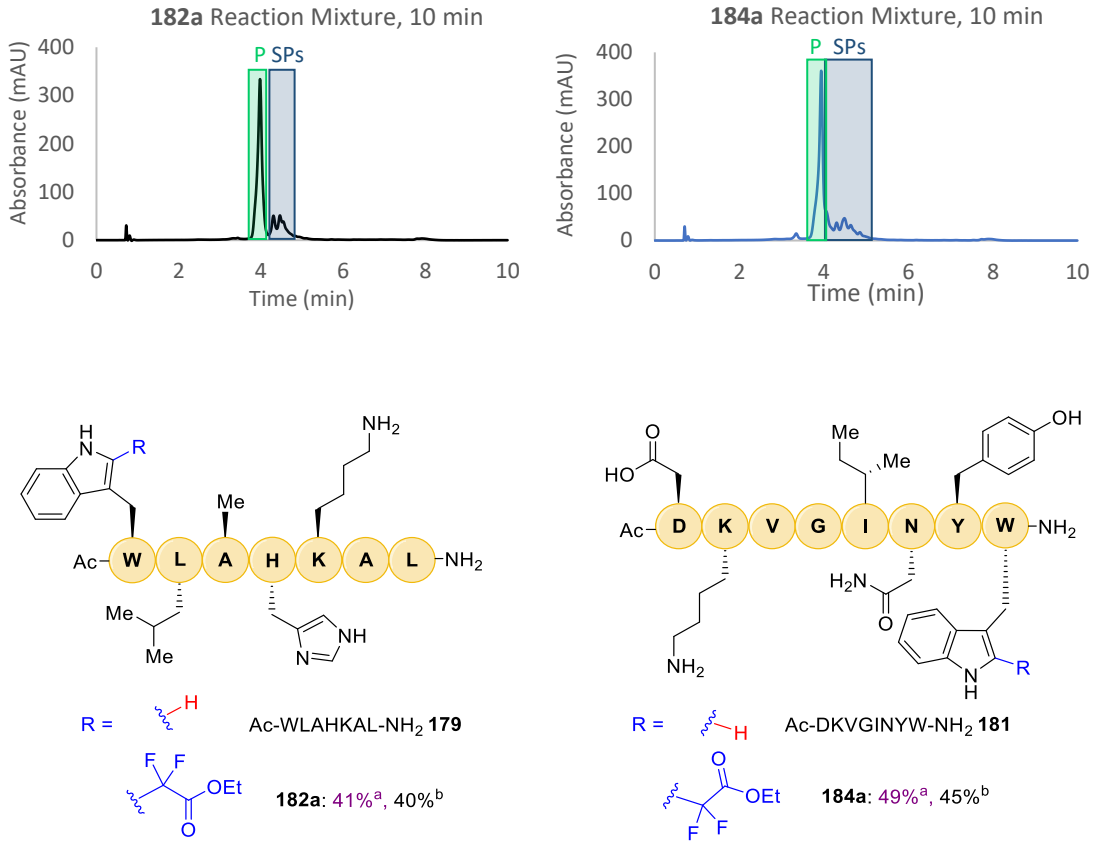

Figure 72. Reaction mixture HPLC chromatograms for peptide conjugation products **182a** and **184a**. 2-95% B over 5 min, 280 nm.

Overall rapid reaction times of 10-15 minutes were observed for the biologically relevant peptides. When Trp was located at the peptide termini (Ac-WLAHKAL-NH_2 **179** and Ac-DKVGINYW-NH_2 **181**) moderate product yields were also obtained after only 5 minutes of irradiation for example peptide **184a** was synthesised in a 43% ^{19}F NMR yield (**Figure 73A**). For these substrates a reaction time of 10 minutes was optimal: any longer was detrimental to the product yield due to dialkylation, whereas when Trp was

embedded within the peptide chain, 15 minutes was favourable because lower starting material consumption was observed (**Figure 73B**).

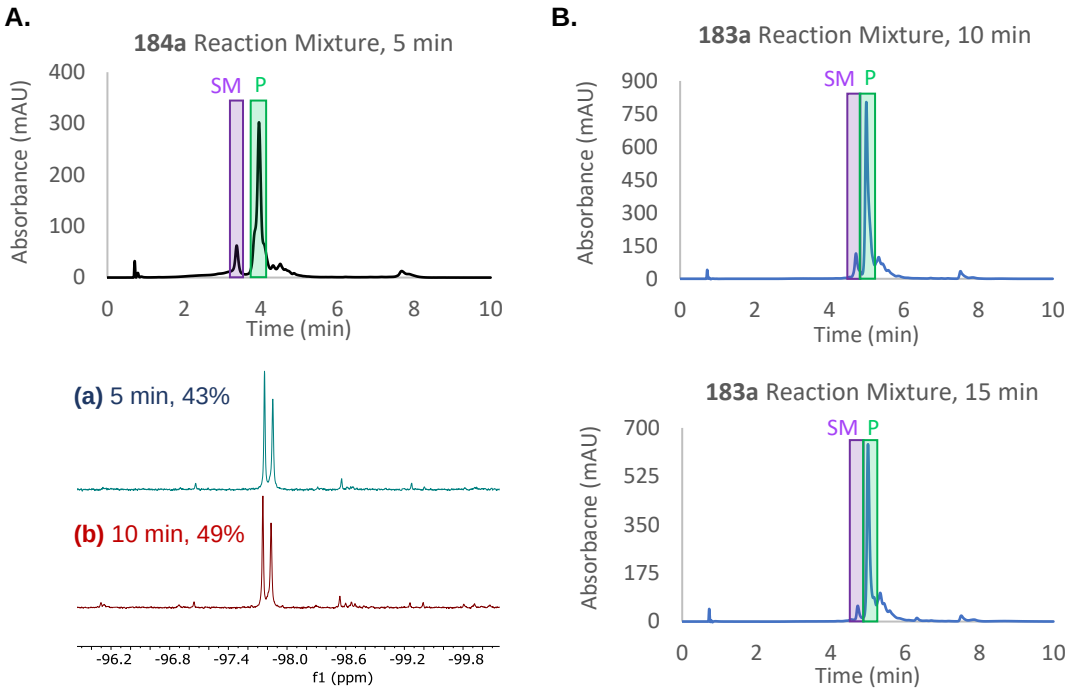

Figure 73. A. Reaction mixture HPLC chromatogram and corresponding ^{19}F NMR spectra for Ac-DKVGINYW-NH_2 **181** difluoroalkylation with $BrCF_2CO_2Et$ **94a**. 2-95% over 5 min, 280 nm and yields determined using TFT as an internal standard. B. Reaction mixture HPLC chromatograms for Ac-VVYPWYQ-NH_2 **180** difluoroalkylation with $BrCF_2CO_2Et$ **94a**. 2-95% over 5 min, 280 nm.

The longer reaction time required for product **183a** may not definitively be due to the position of Trp, because there are also different amino acid residues incorporated in each peptide sequence. Especially because Trp is adjacent to a proline residue, which is known to kink the peptide chain (**Figure 74**),[180] resulting in a potentially different peptide conformation compared to other examples with difficult access to Trp.

Even though any effects resulting from the location of Trp within a peptide sequence could not be determined from the peptide scope explored in this research, the important outcome was that comparable product yields were obtained when amino acid sequences and the position of Trp were changed

(within 1-8%), showcasing the broad ability of this photocatalytic Trp difluoroalkylation strategy.

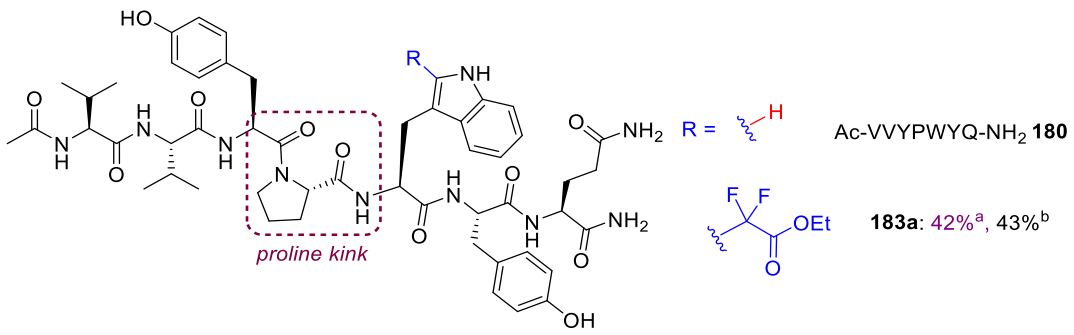

Figure 74. Structure of Ac-VVYPWYQ-NH_2 **180** showing how proline can kink the peptide chain. [a]Yield determined by ^{19}F NMR spectroscopy using TFT as the internal standard. [b]Isolated yield.

The final peptide substrate to undergo the reaction with ethyl ester probe **94a** was Ac-WFMTREY-NH_2 **185** which was synthesised to incorporate the remaining untested canonical amino acids. Pleasingly a 49% ^{19}F NMR yield for product **186a** was obtained after 10 minutes of irradiation, along with consistent reaction mixture data as other examples: minor starting material and side product signals in the HPLC chromatogram and baseline impurity signals in the ^{19}F NMR spectrum (**Figure 75**).

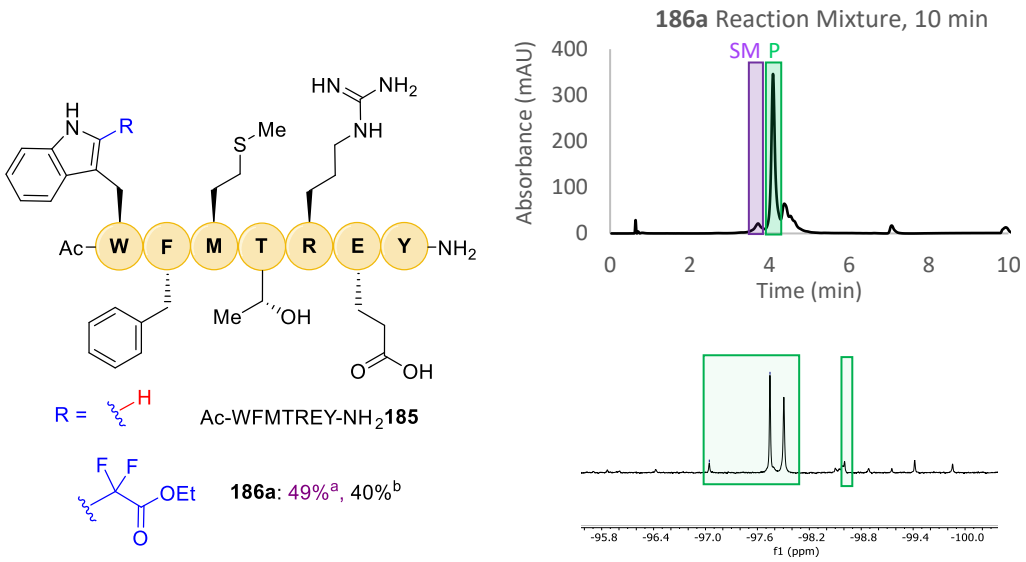

Figure 75. Reaction mixture data for product **186a**: HPLC chromatogram, 2-95% over 5 min, 280 nm and the corresponding ^{19}F NMR spectrum, yield determined using TFT as the internal standard.

Therefore, all functionalities presented by native amino acids residues were tolerated in this novel photocatalytic bioconjugation reaction and chemoselectivity for Trp was observed for every product. Mostly consistent product yields were obtained for ethyl ester-peptide conjugation between 40-50% despite varying the location of Trp in the sequence, but in the presence of Cys and/or unprotected peptide termini a minor reduction in product yield will likely be observed.

Subsequent peptide alkylation reactions were carried out following the success of ethyl ester conjugation, to showcase the ability of the methodology for the synthesis of products which may have useful applications. The biologically relevant peptides (**179**-**181**) were chosen as substrates, due to their inherent bioactivities, and an additional reaction was carried out for each with a different radical precursor: picolyl **94j**, PEG **94d** or biotin **94m**. Incorporation of a pyridine ring could be useful because it can enhance properties associated with small molecule drugs such as biochemical potency and cellular permeability which are just two of the reasons why the pyridine ring is present in an abundance of commercially available drugs.[181] Whereas a PEG chain or biotin moiety are more commonly conjugated to biomolecules; PEGylation is the most common strategy employed for half-life extension,[6] and biotin can aid targeted delivery.[153]

Moderate to good product yields were obtained for the final few photocatalytic difluoroalkylation reactions (**Scheme 47**), with the highest being 46% for PEG conjugated Ac-VVYPWYQ-NH_2 **183d**.

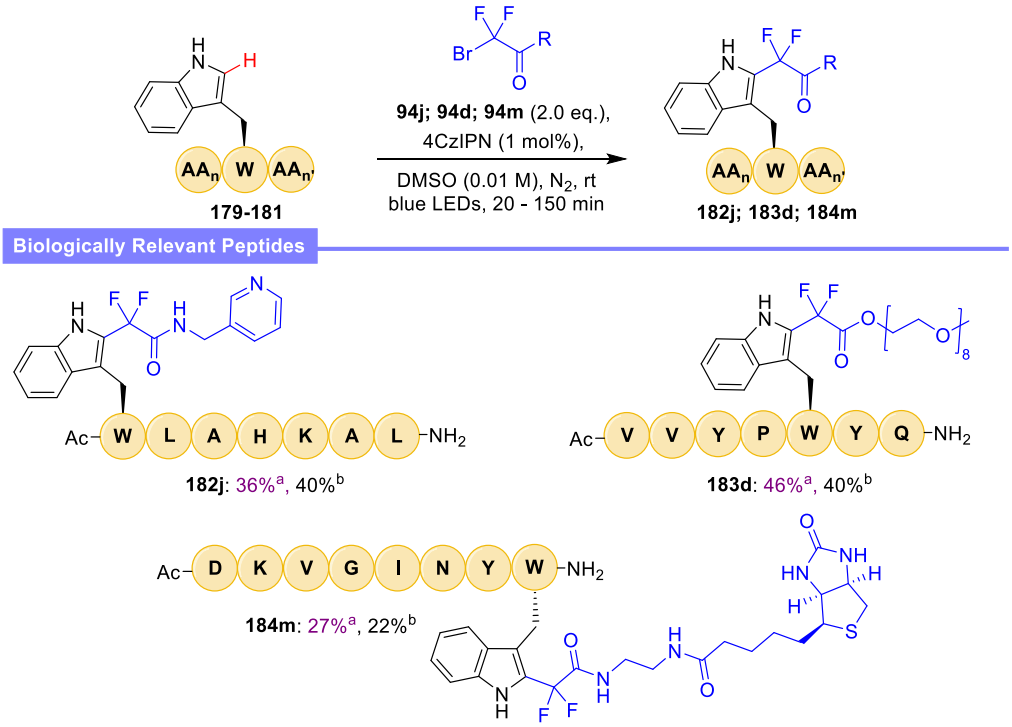

Scheme 47. Photochemical chemoselective alkylation of Trp-containing peptides; reactions performed on a 5.00 μmol scale. [a]Yields determined by ^{19}F NMR spectroscopy using TFT as the internal standard. [b]Isolated yields.

Once again product yields were comparable with the analogous Ac-WHISKEY-NH_2 **163** conjugation reactions. A promising result was associated with biotin conjugation which gave product **184m** in a 27% yield as determined by ^{19}F NMR spectroscopy. This result provided an 8% increase compared to biotin-WHISKEY product **166m** and, because the yield for this reaction is generally poor, this was a significant improvement. Furthermore, the standard reaction conditions were used for Ac-DKVGINYW-NH_2 **181** difluoroalkylation, in contrast to Ac-WHISKEY-NH_2 **163** which required modified conditions for biotin conjugation due to probe coelution during product purification.

Similar reaction times were required as previously mentioned for the difluoroalkylation of Ac-WHISKEY-NH_2 **163** suggesting that the probe mostly dictated the reaction time. However, PEG-conjugated product **183d** benefited from an additional 5 minutes giving ^{19}F NMR yields of 42% and 46% for 15- and 20 minutes of irradiation respectively. This slight extension of reaction time was characteristic for the Ac-VVYPWYQ-NH_2 **180** peptide substrate to enhance starting material consumption, likely due to the presence of the Pro residue rendering Trp less accessible (**Figure 76**).

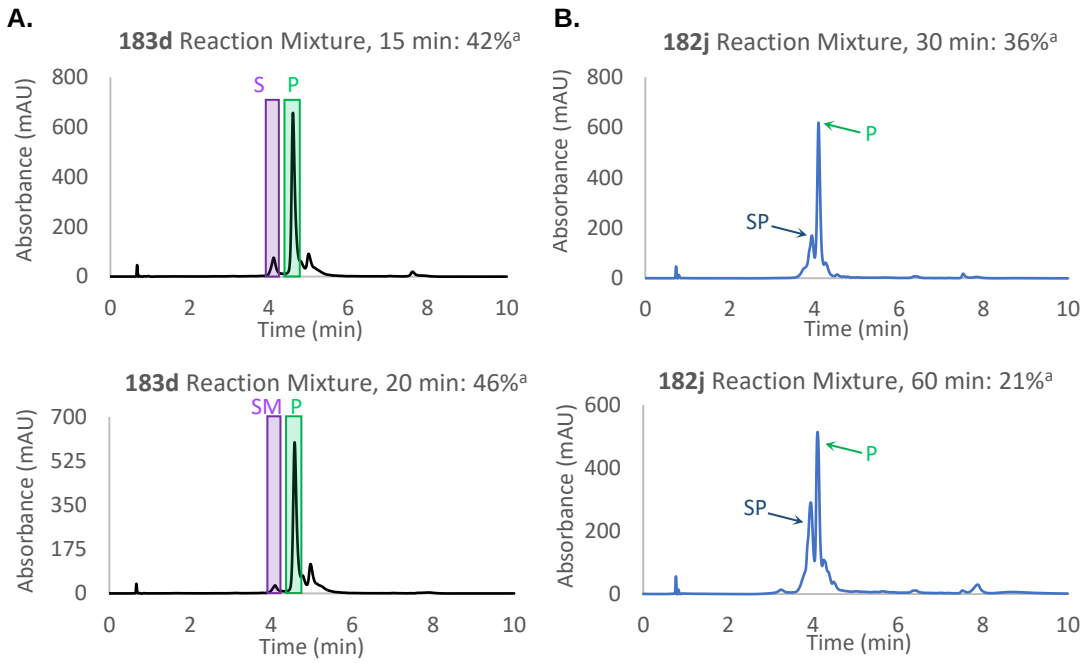

Figure 76. Reaction mixture HPLC chromatograms for **183d** and **182j** highlighting the effect of different reaction times. [a]Yields determined by ^{19}F NMR spectroscopy using TFT as the internal standard.

As before, analysis was carried out at a minimum of two time points for each substrate to ensure the optimum yield was reported. Mentioned throughout this research is that longer irradiation times can be beneficial as exhibited for the example above (**183d**), however, they can also be unfavourable due to enhanced dialkylation. Two common reaction times associated with amide conjugation reactions were 30- and 60 minutes, and for picolyl-WLAHKAL product **182j** a 5% reduction in yield was observed

with the longer reaction time presumably due to increased side product formation (**Figure 76**). This trend was consistent with the analogous Ac-Trp-OEt **93** conjugation reaction shown by an 8% reduction in product yield.

Similar product yields (mostly within 10%) were collected throughout the peptide substrate scope varying the amino acid sequence, chain length and position of Trp. Therefore, it appeared that the most significant influence on product yield, in addition to reaction time, was the radical precursor, specifically the carbonyl moiety (ester or amide).

Product Hydrolysis/Instability

One challenge faced throughout the project was product analysis as some examples were unstable when dissolved in certain solvents, such as Ac-WHISKEY-NH_2 **163** conjugation products: ethyl- and 4-bromo benzyl ester **166a** and **166c** (previously discussed in 3.4. Difluoroalkylation of Ac-WHISKEY-NH_2). To recap, the ester bond can be particularly labile when 50% water (v/v) is present and a water content higher than this was often used to dilute the reaction mixture for purification and to dissolve the isolated products for HPLC analysis. Therefore, the difference between quantitative ^{19}F NMR- and isolated yields was greatest for these examples obtaining a lower yield for the latter. Additionally, products were believed to be contaminated with impurities when in fact over-dilution formed the hydrolysed product within the HPLC/ NMR sample highlighting the product sensitivity to hydrolysis for analysis.

To further investigate this a study was carried out using PEG conjugated product **183d** and HPLC-MS analysis because, similarly to the above examples, the yield determined by ^{19}F NMR spectroscopy dropped by 6%

upon isolation. Appreciably this is not a significant reduction, but the majority of products provided marginally higher isolated yields (compared to their spectroscopic yields) therefore this was an unusual observation. Because water was believed to initiate probe hydrolysis (generating side product **187**), alternative solvents MeCN and MeOH were used to dissolve product **183d**. In MeCN a relatively pure HPLC chromatogram was obtained with a retention time of 4.54 min for the desired mass 1455 Da, and a minor impurity signal at 3.95 min which corresponded to hydrolysed product (1089 Da), however, when this sample was spiked with MeOH, an additional impurity signal was observed at 4.35 min (**Figure 77**).

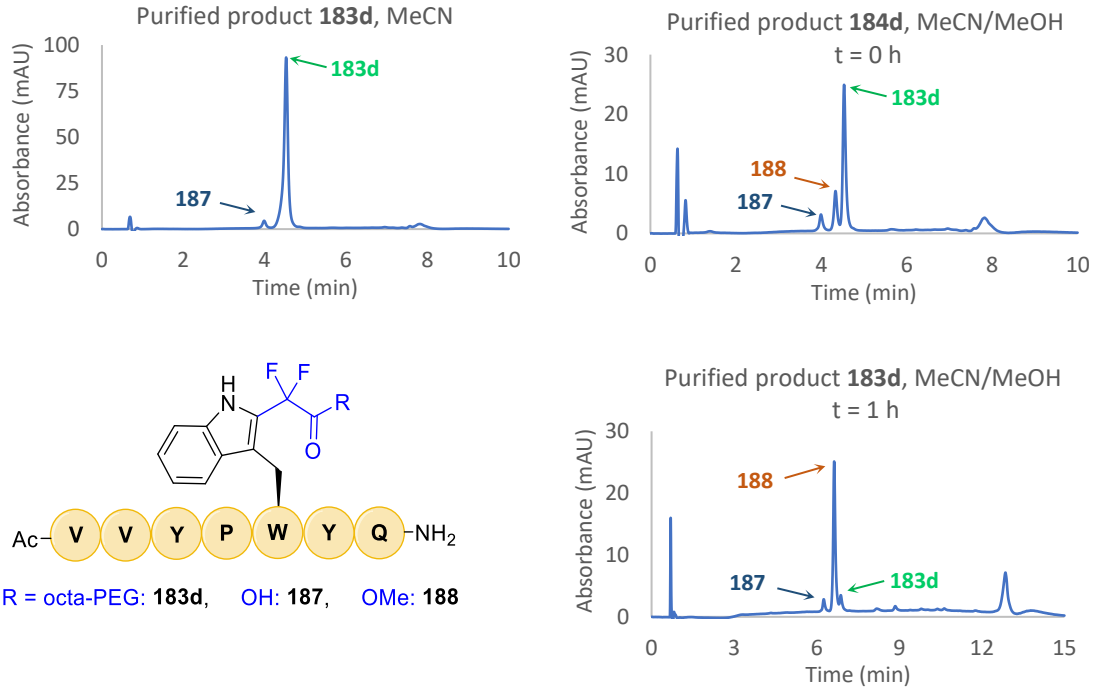

Figure 77. Analytical HPLC chromatograms for **183d** highlighting product instability when dissolved in MeOH. 20-80% B over 5 min, 280 nm and 2-95% B over 10 min, 280 nm.

The mass associated with this new signal was 1103 Da, which corresponded to the methyl ester product **188**, presumably *via* nucleophilic attack of MeOH. This substitution, hence side product **188** signal, increased over time eventually becoming the major product within an hour (**Figure 77**)

demonstrating facile displacement of the PEG chain. Therefore, for ester conjugated products, analysis carried out in MeOH or H_2O could be problematic showing a mixture of products which are not representative of the photocatalytic difluoroalkylation reaction or the purification. This discovery was critical because data would appear less pure than in reality and attempts to further purify material and repeat reactions were made which was an unnecessary waste of material and time. This was equally concerning for NMR spectroscopy data as MeOD was the primary solvent choice for solubility and product recovery after analysis. Instead, sensitive product samples were dissolved in DMSO-d_6 for NMR experiments and MeCN for analytical HPLC, with the minimum amount of water if solubility was causing problems. Alternatively, the most efficient way to obtain an accurate product HPLC chromatogram and avoid impurities caused by solvents was to run the analysis of the sample before lyophilization i.e. after elution from the column already dissolved in an MeCN/H_2O solvent ratio, however sometimes this was very dilute therefore it was ideal to identify multiple options for product analysis. This ester linker instability in certain solvents and concentrations was not ideal but could be minimised with the correct precautions. Alternatively, this was not observed for the amide linkers.

Peptide Conformation

Another challenge faced during peptide photocatalytic difluoroalkylation was identifying and understanding conformational effects on NMR spectra. Amino acid side chains can exist in different conformations called rotamers,

due to single bond rotation (**Figure 78**), and can be influenced by the peptide backbone, secondary structure and amino acid sequence.[182]

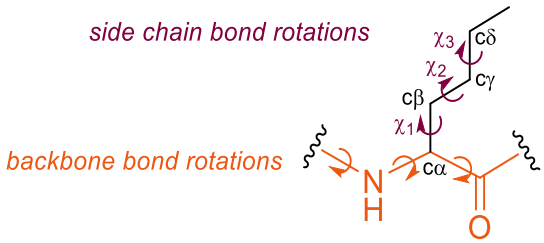

Figure 78. A simplified representation of possible bond rotations within a peptide.

When two (or more) conformational isomers were present, additional signals were observed in both the ^{1}H and ^{19}F NMR spectra. These complications arose for bioactive peptide substrates but were previously unseen for Ac-WHISKEY-NH_2 **163** and its derivatives hence why impurities were believed to be the cause. It was important to identify the true identity of the 'impurity' signals and one strategy was to dissolve the product in different solvent systems observe whether the integration of signals differed. For example, Ac-VVYPWYQ-NH_2 conjugation product **183a** in MeOD showed a 24% 'impurity' doublet in the ^{19}F NMR spectrum, whereas in DMSO-d_6 this was reduced to 8% (**Figure 79**, left). If this were a true impurity, the relative intensity of signals would remain the same, but conformation is influenced by solvent therefore the variable integration values suggested isomer formation.

A similar effect was observed for numerous Ac-WHISKEY-NH_2 **163** difluoroalkylation products, for example cyclopropyl-WHISKEY product **166h** provided a 'singlet' signal in MeOD whereas in DMSO-d_6 the expected two doublet signals were observed (**Figure 79**, right). For all Ac-WHISKEY-NH_2 difluoroalkylated products either a singlet signal or two doublet signals

were visible in the spectra, hence the purity was not questioned, whereas for ethyl ester-Ac-VVYPWYQ-NH_2 product **183a** a mixture of the two were present.

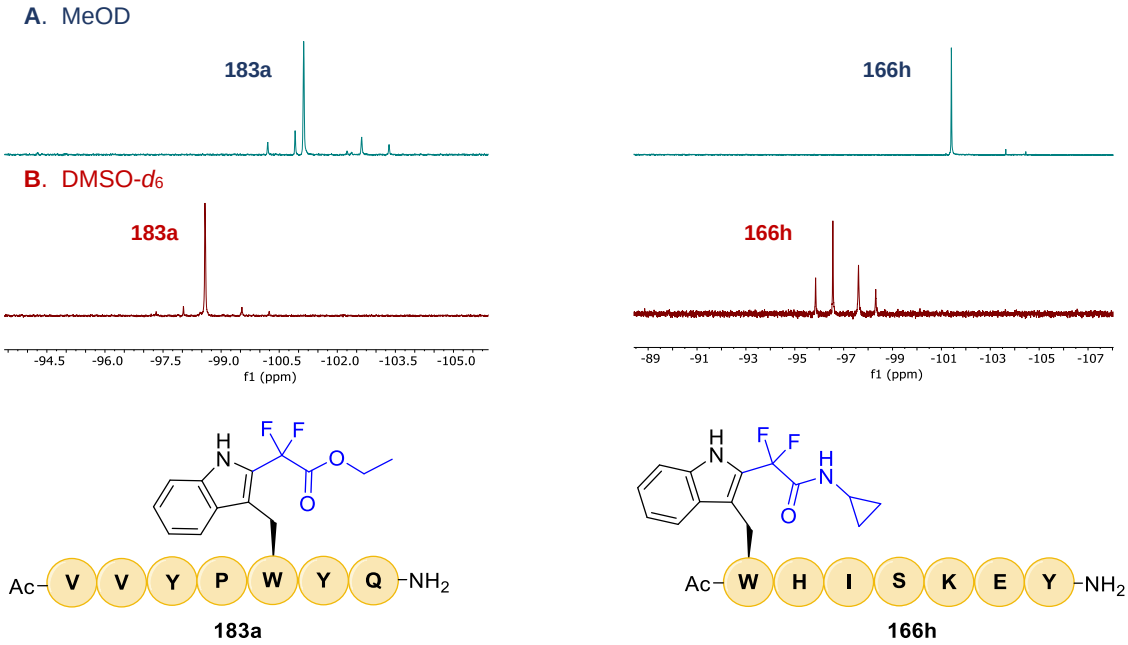

Figure 79. Purified product ^{19}F NMR spectra for **183a** (left) and **166h** (right) suggesting different conformation preferences in different solvents.

Peptide conjugation products were preferentially dissolved in MeOD for ^{1}H NMR analysis because this solvent provided a less complicated spectrum compared to DMSO-d_6: deuterium-hydrogen exchange occurs with heteroatom−hydrogen bonds (N−H and O−H) therefore fewer signals were shown. Whereas in DMSO-d_6 the amide N−H signals often overlapped with the aromatic signals between 7.5 ppm and 8.2 ppm (**Figure 80**), making interpretation of the aromatic region, which was crucial to confirm chemoselectivity for Trp, more challenging.

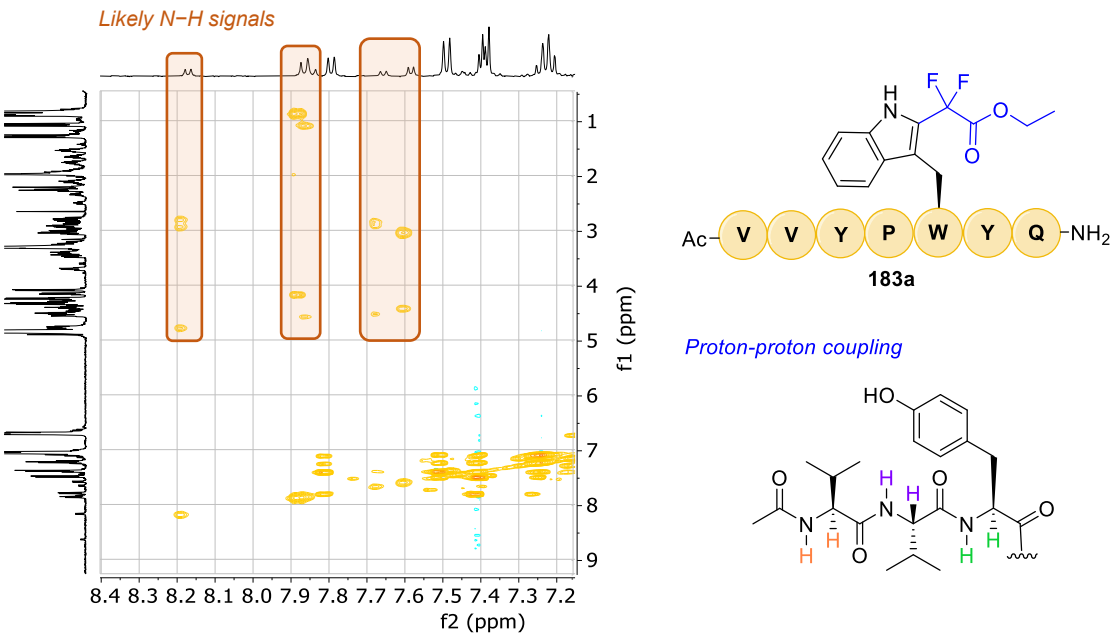

Figure 80. TOCSY spectrum for product **183a** dissolved in DMSO-d_6 highlighting the presence of amide N−H signals by their coupling cross peaks with aliphatic protons.

Proline exhibits *cis* and *trans* forms which are almost isoenergetic and the rate of isomerisation is generally much slower than conformational folding (0-35 °C) resulting in small peptides existing as distinct isomeric species.[54] The solvent present can affect the rate of interconversion with nonpolar solvents and/or the presence of strong acid allowing faster rates.[54] Therefore, it is not uncommon for a change in solvent i.e. MeOD to DMSO-d_6 to affect the ease of peptide interconversion hence the number- and splitting of signals present in the NMR spectra. Pleasingly this was only exhibited for Ac-VVYPWYQ-NH_2 **180** both in the peptide starting material and its difluoroalkylated products (**183a** and **183d**), further implying that the proline residue was responsible for peptide conformational isomers. Despite the added complexity, the site of alkylation in DMSO-d_6 could be confirmed with the aid of a TOCSY experiment, as amide N−H signals showed coupling cross-peaks with ^{1}H signals in the aliphatic region, whereas aromatic signals did not (**Figure 80**).

Other than isomers, the rate of deuterium-hydrogen exchange also caused initial analysis concerns; this was surprisingly low for the other biologically relevant peptide examples Ac-DKVGINYW-NH_2 **181** and Ac-WLAHKAL-NH_2 **179** shown by the ^{1}H NMR spectra in figure 81.

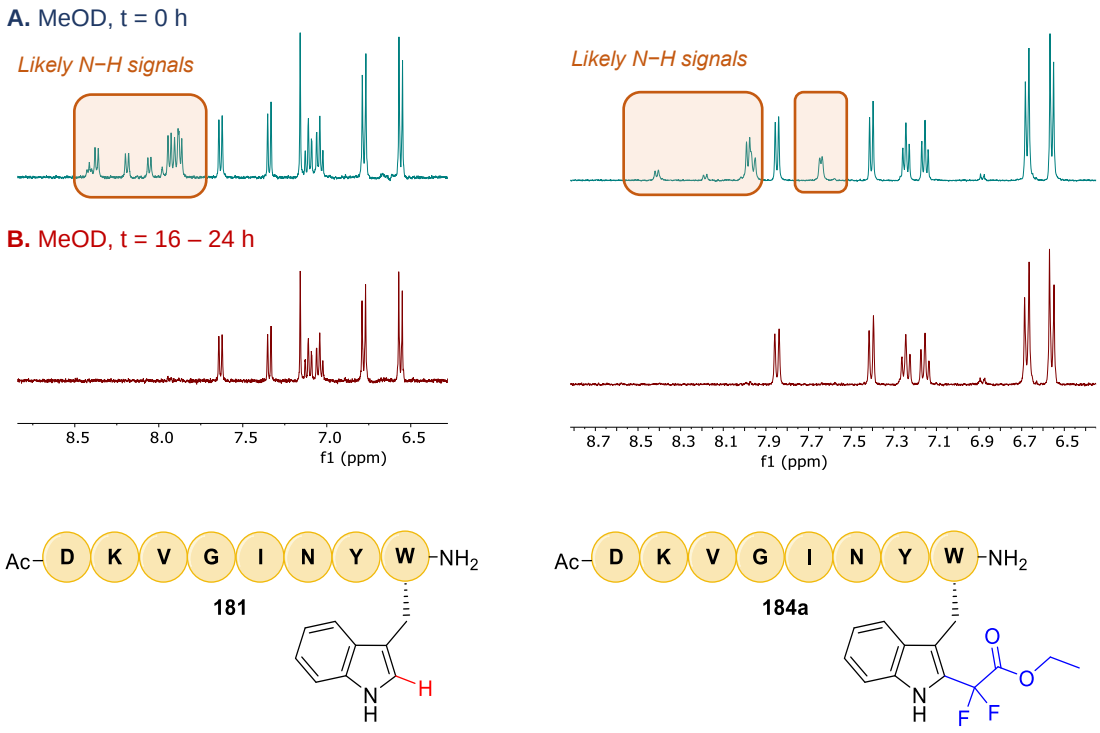

Figure 81. ^{1}H NMR spectra for Ac-DKVGINYW-NH_2 **181** and difluoroalkylated product **184a** highlighting the disappearance of amide N−H signals over time.

The exchange rate of amide N−H bonds are dependent on solvent exposure and hydrogen bonding where folded structures can often have an exchange rate up to eight orders of magnitude lower than the analogous unfolded sequence.[183] For peptides **181** and **179**, hydrogen−bonding was potentially present which buried the protons so they were less exposed to solvent (MeOD), hence poor deuterium exchange was observed. This led to additional unexpected signals shown in the aromatic region of the ^{1}H NMR spectra, however, running the NMR experiment 16-24 hours later provided

enough time for full exchange, hence disappearance of N−H signals (**Figure 81**).

Initially, it was thought that this low exchange was also accountable for the additional signals observed in the ^{1}H spectrum for Ac-VVYPWYQ-NH_2 conjugation product **183a**, however the signals did not disappear after three days, and most overlapped considerably with the Trp aromatic signals (**Figure 82**). The presence of isomers was supported by integration values of signals which were believed to correspond to the same hydrogen atom but on two different conformational isomers: the doublets at 7.8 ppm and 7.5 ppm provided a value of 1 once added together (highlighted by a green box on figure 82). This was also confirmed by the heteronuclear single quantum coherence (HSQC) 2D spectrum which revealed that these doublets were both attached to the same carbon at 119.1 ppm (**Figure 82**).

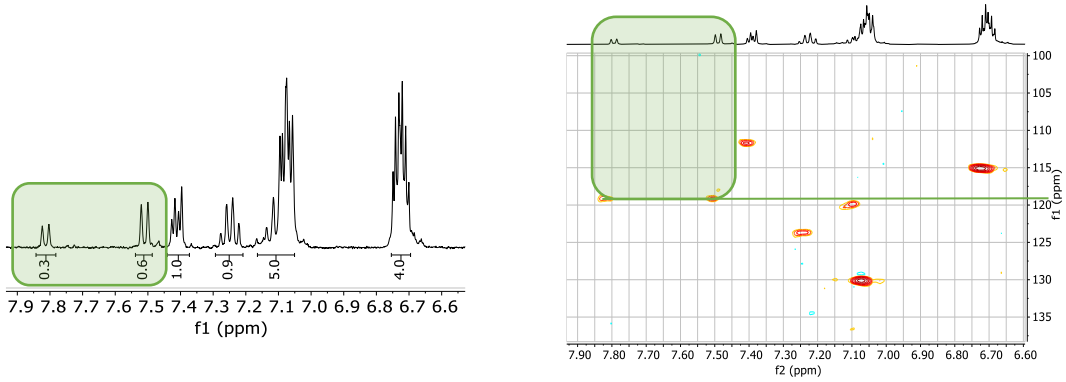

Figure 82. A. ^{1}H NMR spectrum for ethyl ester−Ac-VVYPWYQ-NH_2 product **183a** highlighting the isomeric proton signals in green. B. The corresponding HSQC spectrum showing these protons are on the same carbon atom.

Unfortunately, due to the low concentration of the product sample a ^{13}C spectrum was not obtained (y axis) however the cross-peak sensitivity provided sufficient evidence. Other data collected also supported the presence of isomers: a single mass ion in the mass spectrum and a single peak in the analytical HPLC chromatogram. Therefore, it is predicted that

the additional signals are not associated with an impurity, instead they correspond to *cis*- and *trans*- conformations on the proline residue. Unfolded proteins are known to exist as a mixture of the two,[54] and the presence of isomers was only observed for the peptide containing Pro, further supporting this.

Conclusion

This completes the discussion on peptide substrates used in the photocatalytic difluoroalkylation reaction. Initially the small molecule scope was explored using the model peptide Ac-WHISKEY-NH_2 **163**, which demonstrated reaction versatility; a library of 12 peptide products was synthesised successfully with yields between 15-55% (**Scheme 48**). Consistent reaction times were reported as those obtained for amino acid conjugation reactions highlighting a robust methodology where the rate is mostly dictated by the radical precursor used, not the biomolecular substrate.

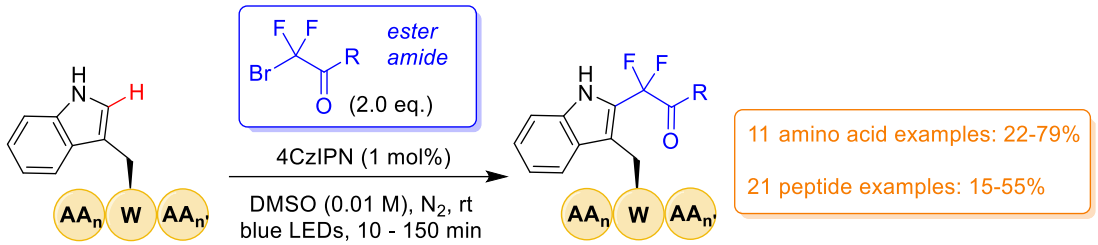

Scheme 48. Photocatalytic difluoroalkylation of biomolecules.

Chemoselectivity for Trp was confirmed for all products using ^{1}H NMR spectroscopy and TOCSY experiments which highlighted the disappearance of the indole C−2 proton and expected coupling between remaining signals. Additional proof was provided by the peptide substrate Ac-HISKEY-NH_2

172, with the Trp residue omitted, which revealed that competition reactions with other amino acid residues were not observed.

Further exploration into amino acid compatibility was carried out using ethyl ester probe **94a** and six new peptides, which were deliberately chosen to ensure that all native amino acids were exposed to the photocatalytic difluoroalkylation reaction. Generally rapid reaction times (10-15 minutes) and consistent product yields were observed between 40-50%, showcasing high functional group compatibility with all proteinogenic functionality and reinforcing the chemoselectivity for Trp. The final few reactions demonstrated the applicability of the methodology by synthesizing products using bioactive peptides and radical precursors bearing pharmaceutically relevant moieties: a pyridine ring, PEG chain and biotin. Using complex peptide substrates in this research was unique compared to most current photochemical Trp modification strategies (discussed previously) and the use of ^{19}F NMR spectroscopy to obtain accurate product yields was another novelty of this research.

3.7 Photocatalytic Modification of β-Casein

After the robustness of photocatalytic peptide alkylation was demonstrated using seven peptide substrates varying in amino acid sequence and length (7 - 8 mer), a brief exploration into protein modification was carried out. Previously all native amino acids showed compatibility with the developed photo-bioconjugation conditions and chemoselectivity for Trp was observed, which showed promise for protein functionalisation. Although the principle focus of this research was peptide modification, β-casein is a relatively cheap, commercially available protein (£73 for 250 mg) carrying a single Trp residue, therefore presented the opportunity for facile protein

investigation. Three probes were trialled for β-casein photocatalytic difluoroalkylation: ethyl ester **94a**, PEG ester **94d** and biotin amide **94m** (**Scheme 49**) and analysis was carried out using various techniques including protein digestion and MS/MS spectroscopy.

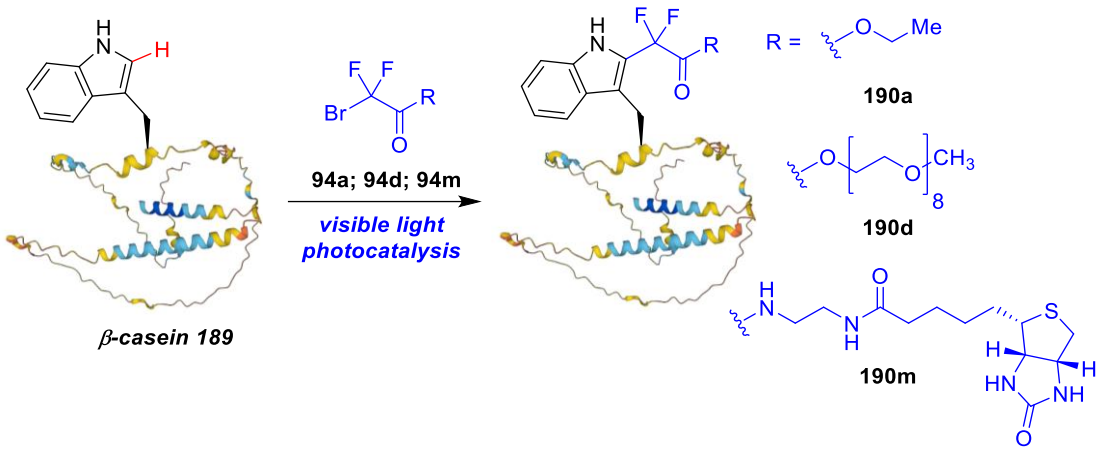

Scheme 49. Photocatalytic difluoroalkylation of β-casein.

Similarly to peptides, protein functionalisation can aid developments in the pharmaceutical industry: typically longer half-lives and specific distribution is observed for protein conjugation products (compared to small molecules) which can be utilised for therapeutic or diagnostic purposes.[13] For example, antibodies are commonly utilised as targeted protein conjugates such as **191** where folic acid is tethered to the biomolecule *via* a chemoselective reaction between ABNO and Trp.[93] The generated folic acid-mAb conjugate selectively targets certain cancer cells which overexpress the folate receptor-α, inducing antibody-dependent cellular cytotoxicity (ADCC).[184] Additionally, interferons are proteins that have numerous biological activities including immunomodulatory, antiviral and antiproliferative,[185] but require conjugation to enhance their properties for therapeutic purposes. This was shown by PEGASYS® **192**: a PEGylated interferon α-2a used to

treat hepatitis C,[186] because this modification increased the protein's half-life by decreasing the rate of proteolytic degradation and renal clearance.[187]

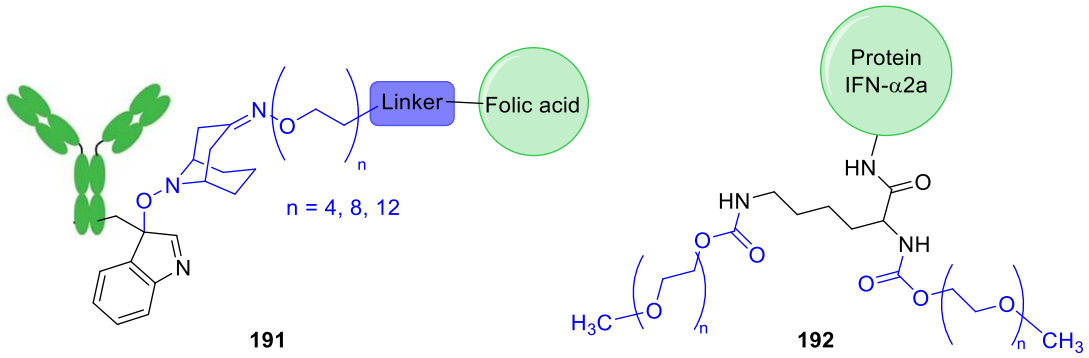

Figure 83. Protein conjugation products with therapeutic applications.[184,186]

β-Casein

Aside from the ready availability of β-casein it was also chosen as the protein substrate because it contained over 200 amino acids (209) and one Trp residue. The protein is commonly found in milk and has a relatively open, flexible conformation for two reasons: the absence of Cys residues, hence disulfide bridges, and many Pro residues creating kinks in the chain.[188] Additionally, β-casein has a tendency to form micelles due to the hydrophobic, globular region at the C–terminal but a hydrophilic N–terminal (**Figure 84**).[189] From a pharmaceutical perspective, this property could be utilised for drug delivery *via* encapsulation: hydrophobic interactions would entrap the drug and following self-assembly of the micelles improved bioavailability could be achieved.[190] However, for photo-bioconjugation micelle formation may lead to a unique solubility and reactivity profile compared to other protein substrates.

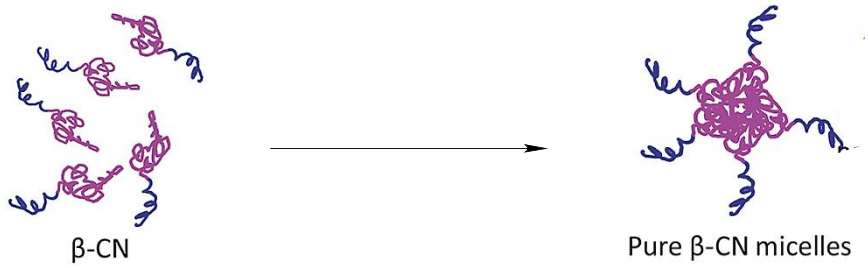

Figure 84. Micelle structure associated with β-casein (β-CN) reported by Kleijn and co-workers.[189]

Reaction Development

Initially β-casein was exposed to the optimised conditions used for photocatalytic Trp difluoroalkylation in peptides (**Scheme 50A**), however this did not solubilise the protein substrate. A 0.01 M solvent concentration, used for peptide reactions, is high for protein substrates and typically protein precipitation and/or aggregation is observed for concentrations > 1 mM.[191] With the addition of 10% water (v/v) and 30 × the initial dilution, β-casein was successfully dissolved in a 0.333 mM solution of 9:1 DMSO:H_2O (**Figure 50B**). Using water as a co-solvent was crucial as neat DMSO, even at lower concentrations, provided a precipitate. The required volume (10%) was also encouraging because it was discussed previously (2.3 Photocatalytic Difluoroalkylation Conditions) that this is tolerated in the reaction.

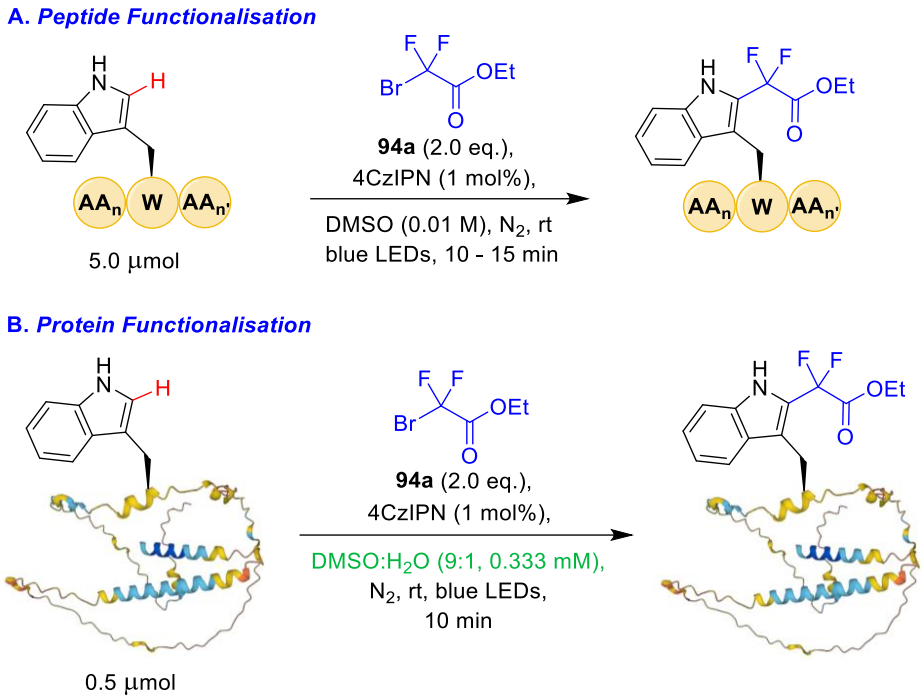

Scheme 50. Photochemical difluoroalkylation of biomolecules using ethyl ester probe **94a**. A. Peptide functionalisation B. β-casein functionalisation.

It was also important to allow the protein to dissolve over 1 h before the reagents were added and the reaction mixture was irradiated. Prior to this time point the protein had not fully solubilised, existing as precipitate (**Figure 85**).

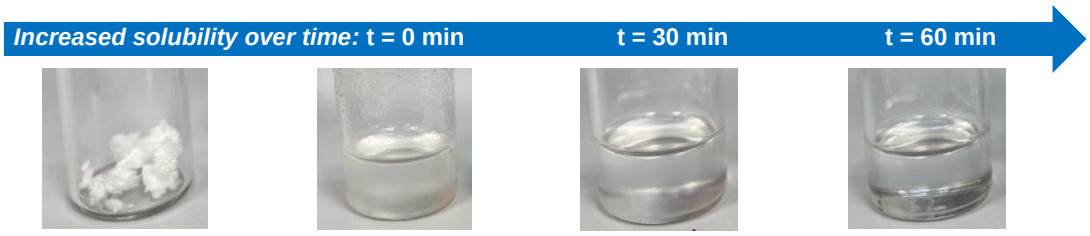

Figure 85. β-casein solubility in 9:1 DMSO:H_2O (0.333 mM) over time.

β-Casein Analysis

Initially three photocatalytic difluoroalkylation reactions were carried out for the conjugation of β-casein **189** and ethyl ester probe **94a**, with minor variations regarding the conditions: 1 mol% 4CzIPN, 10 min (optimised conditions), 1 mol% 4CzIPN, 30 min (longer irradiation time) and 2 mol%

4CzIPN, 10 min (increased photocatalyst concentration). These precautionary measures were to encourage desired product formation assuming that protein functionalisation would be more challenging due to enhanced complexity and reduced access to Trp. All reaction mixtures were then analysed simultaneously to assess the effects, if any, of different conditions.

Unfortunately, the previously used analytical techniques were not successful in identifying product formation. First analytical HPLC presented identical chromatograms for β-casein starting material and the reaction mixture, suggesting product formation had not occurred. However, as the biomolecule increases in size, the addition of a small molecule i.e. a $-CF_2CO_2Et$ moiety approximately 122 Da, will unlikely have a significant effect on the overall molecule's polarity, hence elution time. Therefore, it is plausible that the desired conjugation product would exhibit the same retention time as unmodified β-casein providing inconclusive results.

Additionally, reaction mixture analysis using ^{19}F NMR spectroscopy did not provide evidence of product formation. This was potentially due to the small reaction scale (0.5 μmol) and dilute reaction concentration leading to an approximately 30 × less concentrated sample compared to the peptide substrates. Therefore, any desired product signals could be masked by the spectrum baseline due to the sensitivity of the spectrometer.

Furthermore, proteins can be associated with broad, low intensity signals in NMR spectra due to slow interchange between two or more populated conformations,[192] and considering β-casein can self-assemble into micelles,[189] very large structures will be present potentially with varying

conformations. Alternatively, the broad signals could arise due to protein–fluorine interactions,[57] causing the fluorine nuclei to adopt the protein's shorter relaxation time which decreases the intensity of the NMR signals.[193] This is commonly observed for protein and ligand binding interactions with molecular weights > 5000 Da and < 500 Da respectively,[193] hence protein-fluorine interactions combined with the high molecular weight of β-casein, approximately 24 kDa, could explain why product signals were not detected in the reaction mixture ^{19}F NMR spectra. This contrasts with the sharp, doublets observed for peptide difluoroalkylated products, however data that will be discussed in chapter 4 (Peptide Stapling) involving cyclised difluoroalkylated peptide products, supports this theory because broad, unquantifiable fluorine NMR signals were provided. Therefore, the absence of fluorine signals does not necessarily indicate an unsuccessful reaction.

Instead, the ^{19}F NMR spectrum, could identify and quantify the singlet at −61.4 ppm associated with $BrCF_2CO_2Et$ **94a** and any side-reactions involving the probe including hydrolysis and HAA to give $BrCF_2CO_2H$ **115** at −52.6 ppm and HCF_2CO_2Et **173** at −125 ppm respectively (previously discussed) (**Figure 86**). For example, before irradiation approximately 2.2 eq. of $BrCF_2CO_2Et$ **94a** were present in the reaction mixture shown by a sample containing only **94a** and TFT in 9:1 DMSO:H_2O (**Figure 86A**). For all reaction mixtures minor hydrolysed probe **115** was observed (approximately 0.17 eq.), the HAA side-product **173** was absent, and the amount of unreacted probe **94a** was quantified (**Figure 86**). Using the optimised conditions for β-casein conjugation (**Figure 86B**), approximately 1.00 eq. of probe **94a** had been consumed but only 0.17 eq. were converted into side-product **115** which implied that protein-conjugation had occurred

for the remaining ~ 0.83 eq. Increased amount of probe consumption was observed for the reactions with slightly modified conditions (**Figure 86C** and **D**) which indicated enhanced protein difluoroalkylation, however because both mono- and di-alkylated products can result from the reaction, this may not necessarily be favorable.

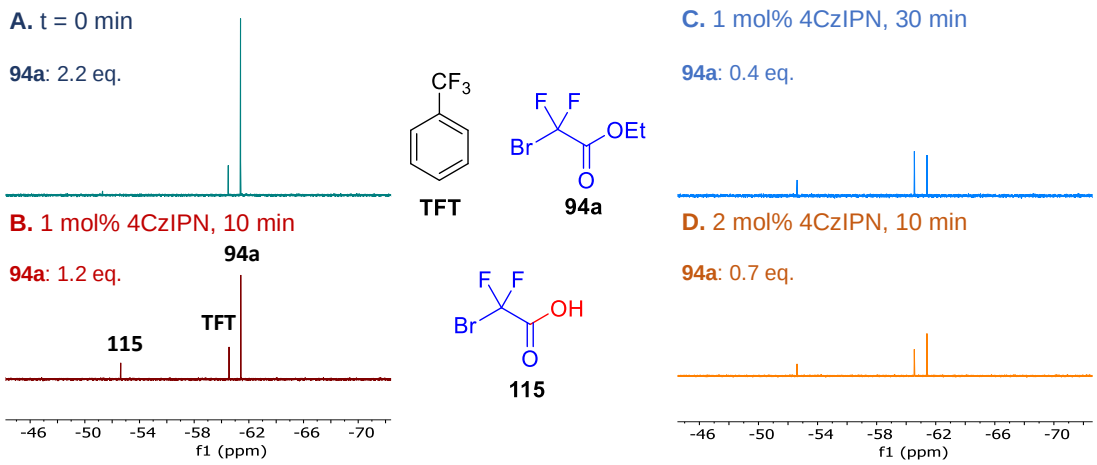

Figure 86. ^{19}F NMR spectra for β-casein ethyl ester conjugation reaction mixtures showing unreacted $BrCF_2CO_2Et$ **94a** which is used to determine probe consumption.

Consequently, MALDI-TOF spectroscopy was also utilised for reaction mixture analysis. Numerous attempts were carried out to obtain mass ions of adequate intensity because a lot of parameters can be varied such as the matrix solution and sample concentration as well as relative ratios of MeCN and H_2O for dilution. The starting material spectrum shown in figure 87 was acquired using a sinapinic acid matrix, ensuring this was saturated to aid ionisation, and β-casein was dissolved in 0.1% TFA in 1:1 MeCN:H_2O (0.055 mM). A number of mass ions were obtained, displayed by a distribution curve, ranging from 23600 and 24000 with 23815.239 being the most intense ion (**Figure 87**), comparable with the molecular weight of β-casein which is approximately 24 kDa.[189]

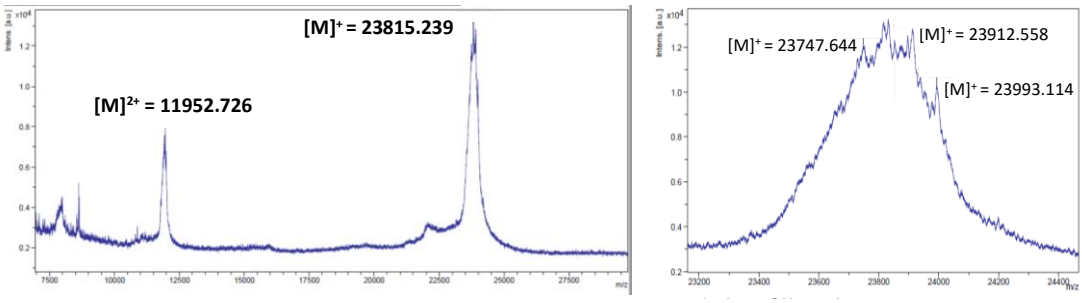

Figure 87. MALDI-TOF-MS spectrum obtained for unmodified β-casein.

For β-casein the observed range for mass ions was ~ 400 Da, which is greater than the expected mass addition for ethyl ester conjugation (122 Da), therefore it would be difficult to prove desired product formation. Nonetheless, reaction mixture analysis was carried out for each reaction (**Figure 88A**): optimised conditions (1 mol% 4CzIPN, 10 min, red line), longer irradiation time (1 mol% 4CzIPN, 30 min, green line) and increased photocatalyst concentration (2 mol% 4CzIPN, 10 min, purple line). Despite the slightly different conditions, consistent MALDI spectra were obtained showing the single- and double charged mass ions, and when overlapped with unmodified β-casein a potential shift in mass ion distribution was observed (**Figure 88B**).

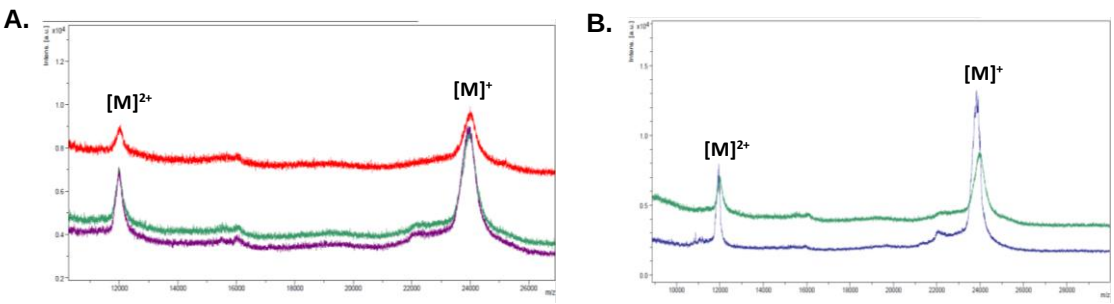

Figure 88. MALDI-TOF-MS spectra: A. Overlapped β-casein-ethyl ester conjugation reaction mixtures: 10 min (red), 30 min (green), 2 mol% 4CzIPN (purple). B. Overlapped reaction mixture (green) and unmodified β-casein (blue).

Scope of β-Casein Photocatalytic Difluoroalkylation

Based on this slightly promising result a brief exploration in β-casein photo-bioconjugation scope was carried out using PEG **94d** and biotin **94m** probes (**Scheme 51**). These reagents were chosen to give functionalised protein products with biological relevance and to explore both ester- and amide-conjugation. Each reaction was carried out with two irradiation times: the one used previously for peptide substrates and a longer time to encourage protein functionalisation.

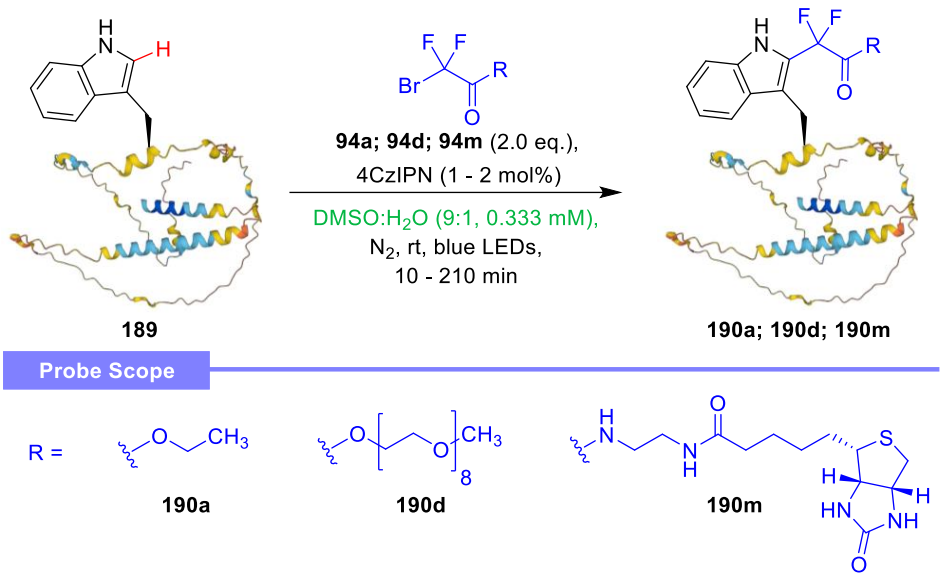

Scheme 51. Photochemical difluoroalkylation β-casein.

Analysis of the reaction mixtures associated with PEG- and biotin-β-casein conjugation products **190d** and **190m** was poor due to sensitivity issues resulting from the MALDI. Repeating the analysis of ethyl ester conjugation reaction mixtures (**190a**) also provided less intense mass spectra (**Figure 89A,** blue line), which highlighted reproducibility concerns. Consequently, broad, low intensity mass ion distributions were obtained for **190d** (orange) and **190m** (burgundy) (**Figure 89B**). Once overlapped with unmodified β-casein it may be suggested that conjugation had occurred by a shift in

protein ions the extent of which was consistent with the size of the small molecule being attached i.e. ethyl < biotin < PEG (**Figure 89B**), however the data reported is inconclusive due to the poor signal to noise ratio.

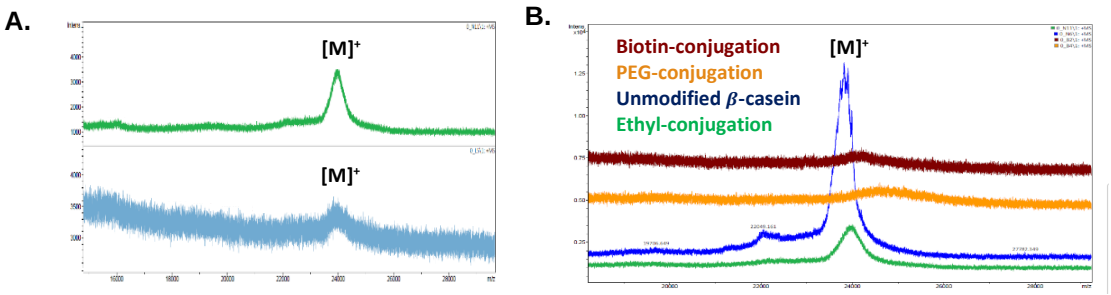

Figure 89. MALDI-TOF-MS spectra for: A. Stacked ethyl ester conjugation reaction mixtures. B. Overlapped reaction mixtures with unmodified β-casein.

Data obtained using ^{19}F NMR spectroscopy also suggested successful protein conjugation had occurred to give PEG **190d** and biotin **190m** products based on probe consumption (**Figure 90**). However, a significant amount of side product formation had also occurred in these reactions including HAA for **94m** (~ −125 ppm, 0.8 eq.). This implied challenging radical addition, but this side product was also observed in peptide difluoroalkylation. Whereas for **94d**, hydrolysed probe **115** (~ −52 ppm) was the major side-product (1.0 eq.) potentially highlighting the lability of this ester linkage.

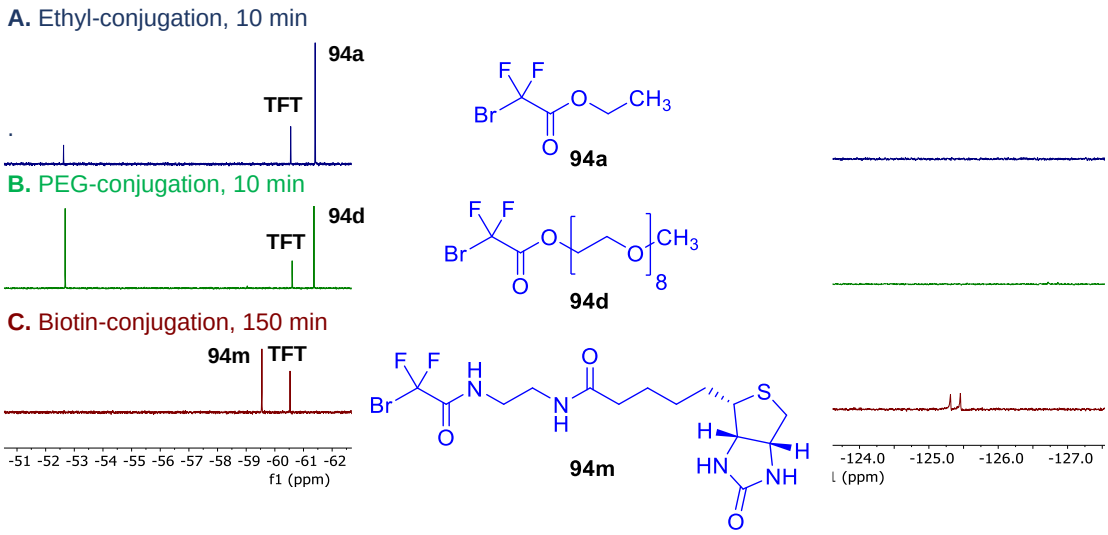

Figure 90. Stacked ^{19}F NMR spectra for β-casein photocatalytic difluoroalkylation reaction mixtures.

Overall, it was more difficult than expected to analyse the reaction mixtures for β-casein functionalisation and determine whether desired product formation had occurred. A lot of variables contributed to this including the scale of the reactions (0.5 μmol), the sensitivity of the instruments carrying out the analyses and challenging sample preparation due to protein insolubility. Therefore, a collaboration was formed with Cameron Bains, a PhD student in Neil Oldham's research group, who carried out protein digestion and tandem mass spectrometry (MS/MS) to obtain more conclusive, accurate data.

β-Casein Protein Digestion and MS/MS

The protein samples were digested using in silico ProAlanase digest to give the peptide fragment 139-LPLLQSWMHQP-146 **193**, with Trp in the middle of the sequence (**Figure 91**). The desired modified fragment ions were found using nanoHPLC-MS analysis for both ethyl- and PEG-conjugation products **194a** and **194d**, but not for the analogous biotin peptide **194m**, which wasn't unsurprising considering this was low yielding for peptide difluoroalkylation (~ 20%).

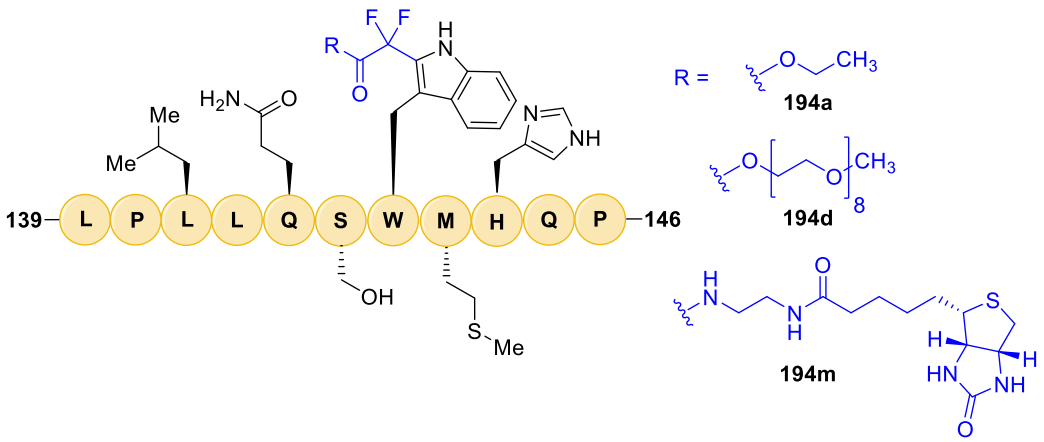

Figure 91. Peptide fragment resulting from β-casein digestion, performed, and analysed by Cameron Bains.

Along with product identification, MS/MS fragments peptides and proteins to determine their amino acid sequence which is often used to identify the specific site of post-translational modifications (PTMs).[194] Therefore MS/MS analysis was used in this research to determine whether the reaction was chemoselective for Trp, by assessing the mass ions of peptide fragments with and without the Trp residue (**Table 15**). For example, the average difference between non-Trp containing fragments for PEG-β-casein conjugation was −0.25 ± 0.12 Da whereas for Trp-containing fragments it was 460.06 ± 0.07 Da.

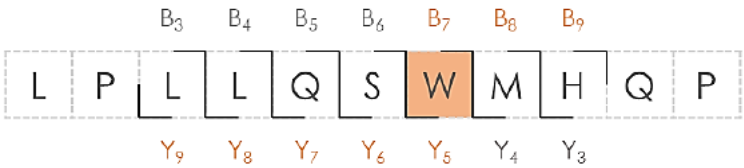

Fragment	Unmodified	Modified	Delta	Fragment	Unmodified	Modified	Delta
B3	324.92	324.17	−0.75	B3	324.50	324.25	−0.25
B4	437.17	437.17	0	B4	437.50	437.25	−0.25
B5	565.83	565.25	−0.58	B5	565.67	565.33	−0.34
B6	652.58	652.42	−0.16	B6	652.42	652.42	0
B7	838.50	960.25	121.75	B7	838.50	1298.42	459.92
B8	969.50	1091.41	121.92	B8	969.42	1429.5	460.08
B9	1106.50	1228.33	121.83	B9	1106.50	1566.67	460.17
Y3	381.75	381.17	−0.58	Y3	381.50	381.17	−0.33
Y4	512.75	512.17	−0.58	Y4	512.50	512.17	−0.33
Y5	698.42	820.17	121.75	Y5	698.33	1158.42	460.09
Y6	785.42	907.17	121.75	Y6	785.33	1245.42	460.09
Y7	913.42	1035.42	122	Y7	913.42	1373.50	460.08
Y8	1026.42	1148.33	121.91	Y8	1026.50	1486.50	460.00
Y9	1139.42	1261.42	122	Y9	1139.50	1599.58	460.08

Table 15. Targeted MS/MS of unmodified and modified peptide for ethyl ester-conjugate **194a** (left) and PEG-conjugate **194d** (right); expected delta 122.01 and 460.21 respectively. This data was obtained and analysed by Cameron Bains.

Furthermore, this data can often be interpreted quantitatively to determine product yields, but to digest the protein the samples were acidified to pH 1.5 (32 mM HCl) and left at rt for 2 h before being stirred at 95 °C for 10

min. To determine the effects of these harsh conditions, ethyl ester-WHISKEY conjugation product **166a** was exposed to the same procedure and the product stability was monitored using analytical HPLC (**Figure 92**). After 2 h under acidic conditions, an impurity signal at 4.21 minutes had developed (**Figure 92A**), likely corresponding to hydrolysed product **168** (by MS). Additionally, after the peptide was exposed to 95 °C, at least 3 impurity signals were formed (**Figure 92B**) along with unidentifiable mass ions. This suggested a labile modification linker (ester) and potential peptide degradation under these protein digestion conditions which would have affected the amount of photodifluoroalkylated β-casein detected; hence the data could not be interpreted quantitatively.

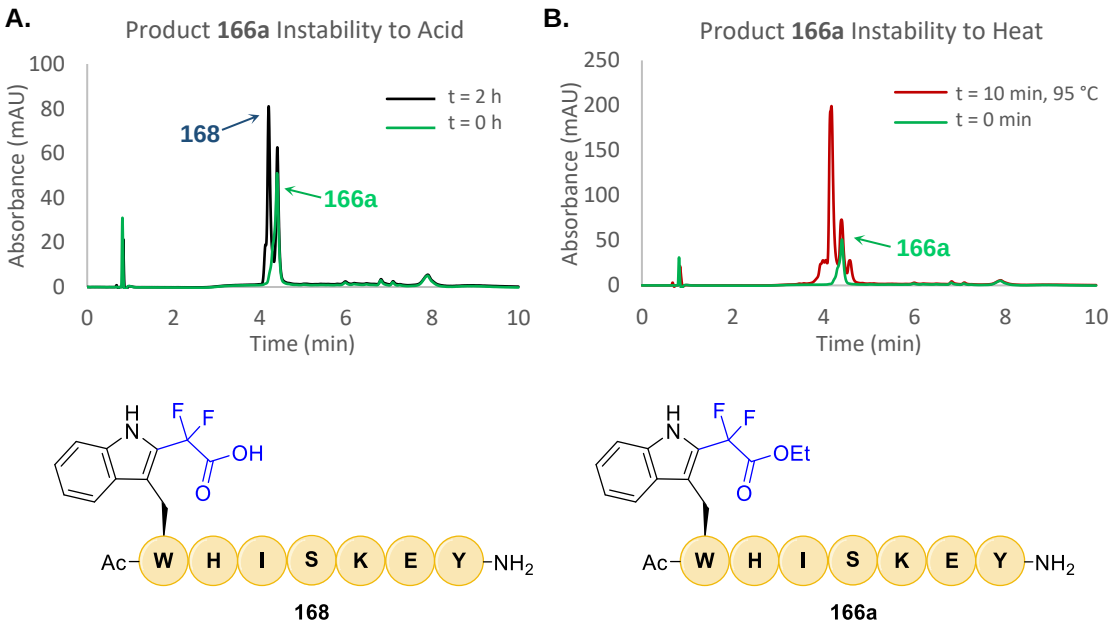

Figure 92. Analytical HPLC chromatograms showing the instability of Ac-WHISKEY-NH_2 conjugated product **166a** under digestion conditions. 2-95% B over 5 min, 280 nm.

To avoid product degradation, attempts were made to obtain intact protein ESI spectra but unfortunately, mass ions were not detected. This was potentially due to the formation of micelles; poor ionisation could be an

inherent property of β-casein, hence intact protein data would be unattainable.

Conclusion

In conclusion, chemoselective functionalisation of β-casein, at the Trp position was suggested for PEG- and ethyl ester conjugation using protein digestion and tandem mass spectrometry. However, the yield for such transformations could not be acquired due to product instability under ProAlanase digestion conditions.

4 Peptide Stapling

In addition to protein functionalisation, a second application explored for photocatalytic difluoroalkylation was peptide stapling. Instead of intermolecular radical addition using an external reagent, when the radical precursor was embedded into the peptide sequence *via* a modified Lys residue (K*) (**Scheme 1**) intramolecular radical addition was possible. The same Trp C–2 difluoroalkylation mechanism occurred to give cyclised peptide products and the number of amino acids between Trp and K* influenced the size of macrocycle formed. This reaction had previously shown compatibility with all native amino acids and functionalisation of the indole does not require any protecting groups or pre-functionalisation, therefore it provided an advantageous peptide stapling strategy.

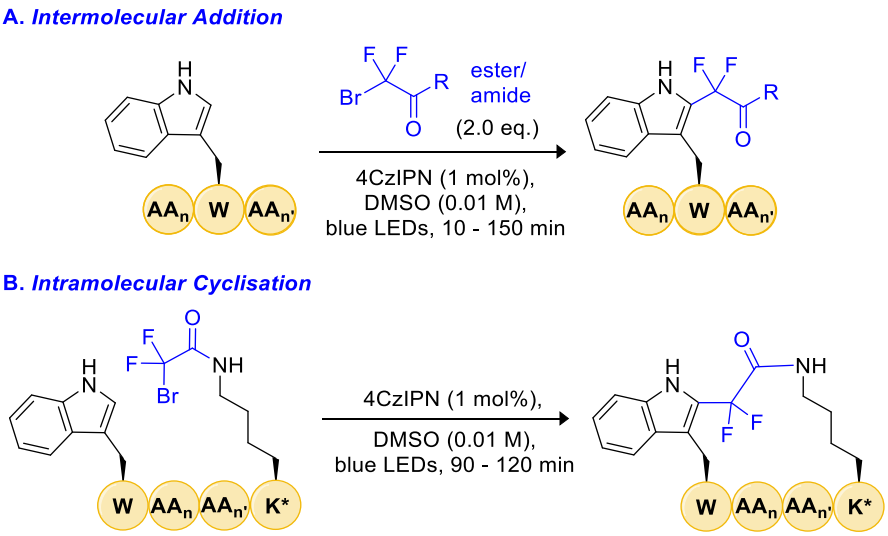

Scheme 1. Photocatalytic difluoroalkylation of Trp: A. Intermolecular addition to give small molecule-peptide conjugates. B. Intramolecular cyclisation to give peptide macrocycles.

4.1 Reaction Development

It was proposed that the photocatalytic difluoroalkylation methodology reported in chapter 2 could be further developed to enable intramolecular peptide cyclisation. If successful, this would be an advantageous peptide stapling strategy utilising an organic photocatalyst and additive free conditions with relatively fast reaction times, overcoming current literature limitations. Furthermore, an inherent property of intramolecular reactions is the 1:1 relationship between the coupling partners undergoing the transformation (Trp and radical precursor), whereas previously the probe was added in a slight excess of 2.0 equivalents. Therefore stoichiometric 'reagents' combined with the beneficial conditions mentioned above would provide a more sustainable, novel macrocyclization technique.

The proof-of-concept reaction was carried out using model peptide: Ac-WAMLK*-NH_2 **195** where K* represents an unnatural amino acid, comparable to the amide probes used previously for intermolecular difluoroalkylation. Therefore, a new C–C bond between a Trp and Lys amino acid would generate the peptide macrocycle **195a** *via* a $-CF_2CO-$ linker (**Scheme 52**).

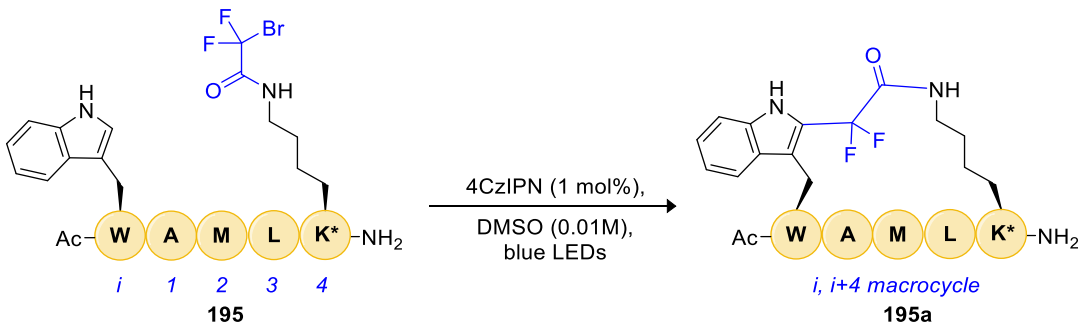

Scheme 52. Photocatalytic stapling of Ac-WAMLK*-NH_2 **195** to give macrocycle **195a**.

Key features of model peptide **195** include: the distance between Trp and Lys* along with specific amino acids chosen for the peptide sequence. The

distance is referred to as i, i+4 and this was to encourage the peptide to be locked in an α-helical shape as there are approximately 3.6 amino acids per turn.[195] Peptides naturally coil into a right-handed spiral which is conformationally rigid and stabilised by hydrogen bonding between amide N−H and C=O groups in the backbone.[59] Furthermore alanine (Ala, A), methionine (Met, M) and leucine (Leu, L) show a high tendency to be part of α-helix structures, in contrast to proline (Pro) and glycine (Gly), based on conformational restrictions for the former amino acids.[196]

Before linear peptide substrates could be synthesised, using SPPS, Lys (K) was functionalised to incorporate the bromodifluoro moiety, and hence provide a radical precursor reagent (K*) (**Scheme 53**). Amide bond formation was achieved using commercially available bromodifluoroacetyl chloride **123** and Fmoc-Lys-OH **196** with a slight modification of literature conditions reported by by Jin and co-workers (**Scheme 53**),[148] the same protocol used previously for probe synthesis.

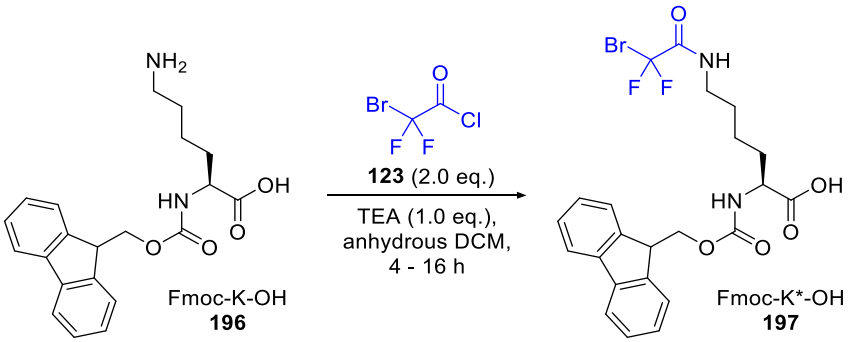

Scheme 53. Synthesis of Fmoc-K*-NH_2 **197**.

The reaction was carried out numerous times and generally similar product yields (48-63%) were obtained highlighting its robustness. Reaction monitoring by analytical HPLC showed both Fmoc-K-OH **196** and Fmoc-K*-OH **197** with retention times of 3.80 min and 5.41 min respectively (**Figure**

93), therefore facile identification of **196** was possible to determine whether subsequent portions of **123** needed to be added. For example, an additional equivalent of $BrCF_2COCl$ **123** after a 2 h time point facilitated full consumption of Fmoc-K-OH **196**, enhancing product formation (**Figure 93**).

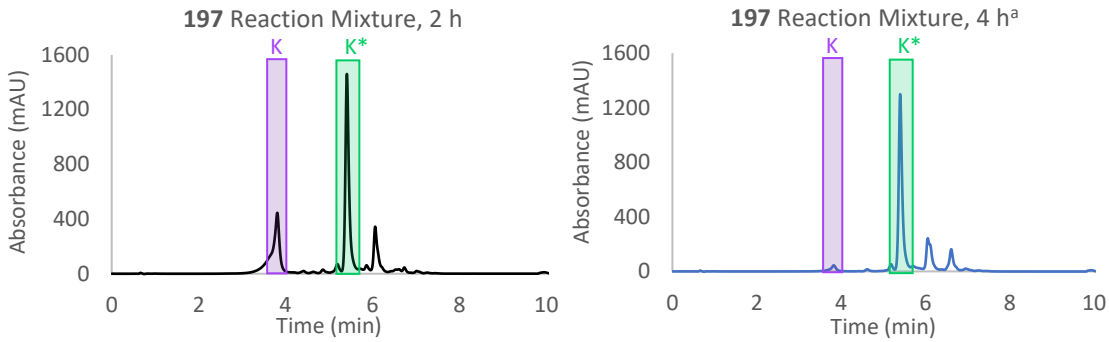

Figure 93. Reaction mixture HPLC chromatograms for Fmoc-K*-OH **197** synthesis. 20-100% B over 5 min, 280 nm. [a]Additional equivalent of $BrCF_2COCl$ **123** added after 2 h.

Once the reaction was complete, preparative HPLC purification was carried out but due to the maximum loading of the column (approximately 200 mg) the crude material had to be separated into multiple batches for isolation. Nonetheless, moderate yields were obtained for the desired unnatural amino acid Fmoc-K*-OH **197**, which was subsequently extended on the solid phase to generate linear peptides such as model peptide Ac-WAMLK*-NH_2 **195**. Standard conditions for SPPS include 4.0 eq. of amino acid (0.5 M, in DMF) and 75 °C MW heating for the coupling reaction, however, to prevent excess waste of the more valuable K* amino acid **197**, this was reduced to 2.0 eq. and because the stability of the $BrCF_2CO-$ moiety was unknown, the coupling temperature was reduced to 50 °C MW heating. Additionally, double coupling was set for all amino acids, to enhance successful coupling and improve the yield of the desired peptide. A pleasing 15% yield was obtained for linear peptide **195** which provided sufficient

material for five initial reactions. The same protocol was followed for all other peptide substrates in this chapter with varying product yields between 3-15%.

Reaction Analysis

It became clear that the use of ^{19}F NMR spectroscopy to determine quantitative NMR product yields was not possible for macrocyclic peptides. Unlike the distinctive, high intensity doublets observed for linear difluoroalkylated peptides (**Figure 94A**), broad and almost negligeable signals were associated with cyclised peptide products lowering the accuracy and ability to quantitatively integrate the signals. (**Figure 94B**). This was further confirmed by an almost 50% discrepancy between the quantitative NMR- and isolated yield for macrocyclic product **195a**, whereas previously these yields were comparable for WHISKEY-conjugated products such as **166k**.

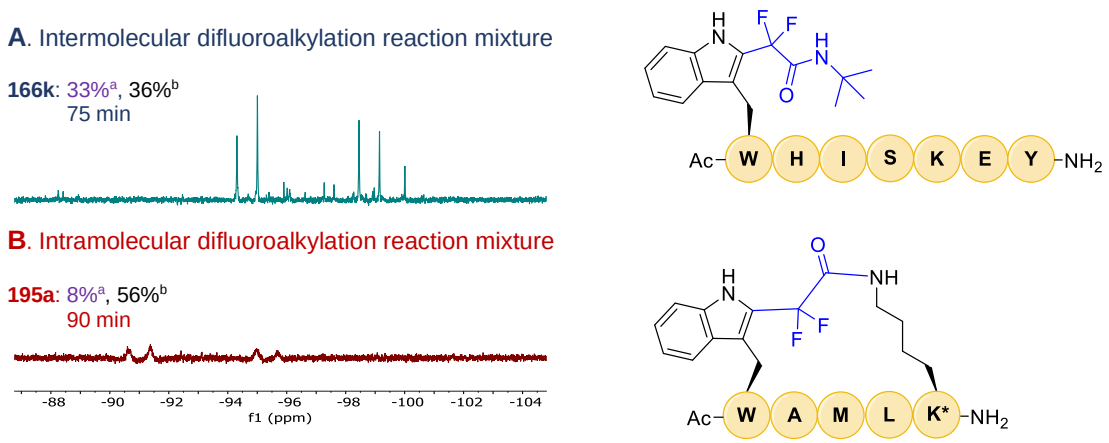

Figure 94. Reaction mixture ^{19}F NMR spectra for **166k** and **195a**. [a]Yield determined by using TFT as the internal standard. [b]Isolated yields.

Numerous factors can cause line broadening in an NMR spectrum including conformational changes, molecular tumbling and peptide-ligand interactions.[197] If the interconversion between two or more conformational

isomers is slow broad signals can arise. In theory stapling is designed to lock the peptide structure in an α-helix but this isn't always the case which was discussed by Johannes and co-workers who cross-linked two Trp residues using an aryl aldehyde.[94] They identified successful cyclisation using ^{1}H NMR spectroscopy however the circular dichroism (CD) spectrum suggested a non-helical/disordered conformation: it was predicted that the fixed stapling linker prevented interactions which encourage the helical structure i.e. indole ring $\pi - \pi$ stacking. A small cluster of α-helical conformations (2%) was determined,[94] which highlights the possibility of macrocycle conformational mixtures: disordered- and α-helical.

On a similar note, molecular tumbling, which encompasses the rotation, vibration and translation of the molecule is slower for larger molecules.[198] Because the slower tumbling causes faster relaxation times compared to smaller biomolecules, line broadening and low signal-to-noise ratios is often observed in NMR spectra, therefore it is not uncommon for signals to be undetected after spin manipulations.[198] Admittedly these peptides aren't larger than the successfully detected linear peptide examples in chapter 3, which suggests that cyclisation had significant effects on peptide conformation and/or the tumbling rate. Alternatively, the broad signals could arise due to peptide-fluorine interactions,[57] causing the fluorine nuclei to adopt the macrocycle's shorter relaxation time which decreases the intensity of the NMR signals.[193]

Despite this, the cyclisation reaction mixture spectra could be utilised for a different purpose: quantification of the linear peptide starting material because these compounds were comparable to intermolecular

difluoroalkylation peptide products and previous radical precursors which integrated accurately and quantitatively. A sharp singlet signal was observed for Ac-WAMLK*-NH_2 **195** at −59.3 ppm and after the addition of TFT (internal standard) the percentage of unreacted peptide **195** can be determined (**Figure 95**).

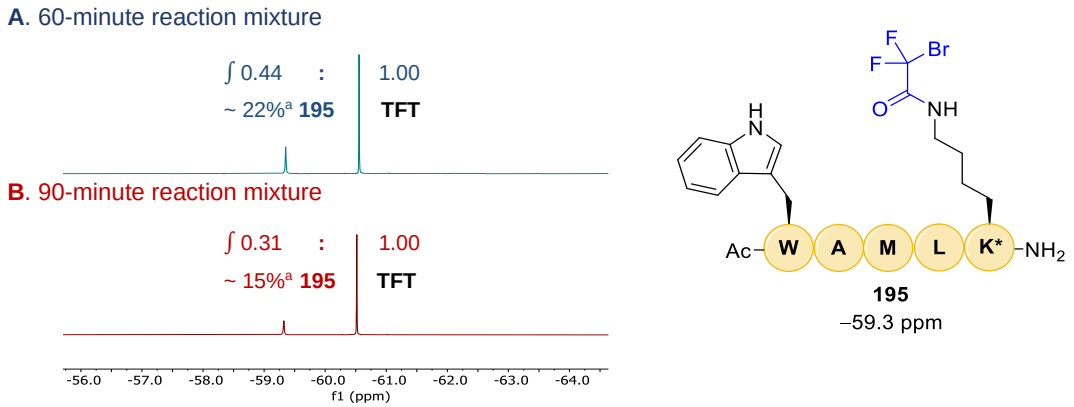

Figure 95. Reaction mixture ^{19}F NMR spectra for the cyclisation of **195** showing unreacted **195** at the end of 60- and 90-minute time points. ªYields determined by using TFT as the internal standard.

Additionally, much like the intermolecular reactions, HPLC analysis was also carried out for peptide stapling, allowing further insight into the reaction mixtures. Complementary information could be obtained from each technique: ^{19}F NMR spectroscopic analysis quantified unreacted starting material and analytical HPLC provided the relative intensity between linear and cyclic peptides along with the visualisation of multiple minor side product signals (**Figure 96**). It was pleasing to observe a significant, distinct signal for macrocycle **195a**, showing that UV absorbance was not hindered by cyclisation, therefore this became the principal technique to identify product formation which was also confirmed by mass spectrometry.

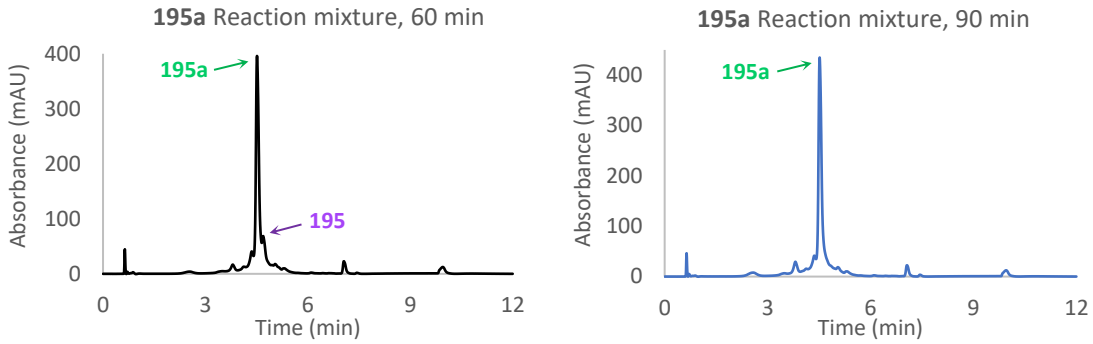

Figure 96. Reaction mixture HPLC chromatograms for Ac-WAMLK*-NH_2 **195** cyclisation to give macrocycle **195a**. 20-100% B over 5 min, 280 nm.

For reaction monitoring, analytical HPLC was more rapid and convenient compared to NMR spectroscopy, especially due to the small reaction volume (500 µL). However, due to the similarity of linear peptide **195** and macrocycle **195a** retention times (4.68 min and 4.52 min respectively) in combination with the impurity signals, this was not always accurate. For example, **195** had seemingly reached full consumption after 90 minutes of blue light irradiation, suggested by the lack of absorbance signal (**Figure 96**), but this was contradicted by the reaction mixture ^{19}F NMR spectrum. At this same time point, approximately 15% of Ac-WAMLK*-NH_2 **195** had not cyclised which implied that its UV absorbance signal was potentially masked by other high intensity signals in the chromatogram or hidden underneath the tail end of the product signal.

After purification, isolated yields for cyclised product **195a** were obtained and a 90-minute irradiation time gave a considerably higher yield than 60 minutes: 56% and 42% respectively (**Figure 97**). This was presumably due to enhanced linear peptide **195** consumption (identified by ^{19}F NMR spectroscopy). Therefore, in an attempt to achieve full consumption of **195** the reaction was repeated using 120 minutes of LED irradiation; however a poorer isolated yield was obtained for macrocycle **195a**: 47% despite there

being no evidence of increased side product formation. Instead, the lower yield could result from weighing errors which are more influential for small-scale reactions. Accurately weighing out starting material can be problematic when the peptide batch has been stored over time as they are known to be hygroscopic therefore the last sample in the batch will likely have a greater water content that the first, causing a lower product yield.[199]

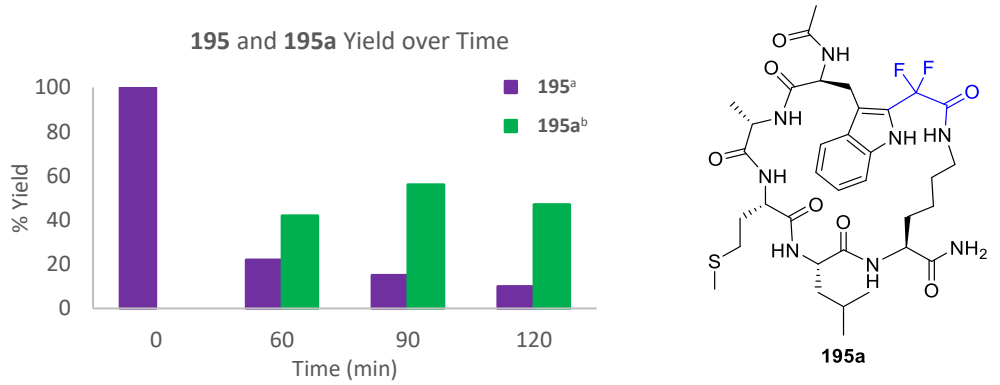

Figure 97. Bar chart to show how yield varied over time for both linear **195** and cyclised **195a** Ac-WAMLK*-NH_2. [a]Yields determined by ^{19}F NMR spectroscopy using TFT as the internal standard. [b]Isolated yields.

Furthermore 10% of unreacted linear peptide **195** was observed, suggesting that prolonged irradiation times were no longer aiding the reaction, instead, perhaps a higher catalyst loading of 2 mol% may be required to enable full consumption of **195**. Unfortunately, due to time constraints, this was not explored, however it would be beneficial to repeat photocatalytic Ac-WAMLK*-NH_2 **195** cyclisation using 2 mol% of 4CzIPN and 120 minutes of blue LED irradiation.

Overall reaction monitoring was challenging for intramolecular cyclisation as the use of analytical HPLC was potentially less reliable than originally expected due to compounds in the reaction mixture showing similar, overlapping retention times. Alternatively, reaction monitoring by ^{19}F NMR spectroscopy may have been more beneficial with regard to identifying the

presence of starting material **195**, however the reaction volume was 500 µL and the minimum volume required for NMR spectroscopy experiments is 600 µL, not to mention the losses upon transfer to and from an NMR tube. Consequently, NMR analysis was carried out following the addition of TFT (101 µL, 16.5 mM in DMSO) to enable quantification before purification; the reaction mixture could not be accurately irradiated further in the presence of TFT (discussed in 3.3 Reaction Rates).

4.2 Synthesis of macrocycles

Following initial studies using model peptide Ac-WAMLK*-NH_2 **195**, reaction conditions were successfully developed for photocatalytic peptide stapling: 4CzIPN (1 mol%) in DMSO (0.01 M) with blue LED irradiation (90 – 120 min). Likewise with intermolecular photocatalytic difluoroalkylation, reaction mixture analysis and final product characterisation was determined using NMR spectroscopy and analytical HPLC. Because this section of research was carried out toward the end of the PhD, the macrocycle scope is relatively small (six examples), however significant progress was made, and additional examples will be suggested for future work.

Synthesis of 23-membered macrocycles

The peptide scope began with four i, i+4 linear peptide substrates (**Figure 98**), including model peptide Ac-WAMLK*-NH_2 **195**, to investigate (i) stapling at opposite ends of the peptide the sequence: Ac-K*AMLW-NH_2 **198** (ii) an internal staple: Ac-EWAMLK*R-NH_2 **199** and (iii) cyclisation without the help of amino acids known to encourage α-helical conformations: Ac-WGFIK*-NH_2 **200**. Following reaction development, an optimum reaction

time for macrocyclization was not determined, therefore for most examples at least two reaction times were investigated.

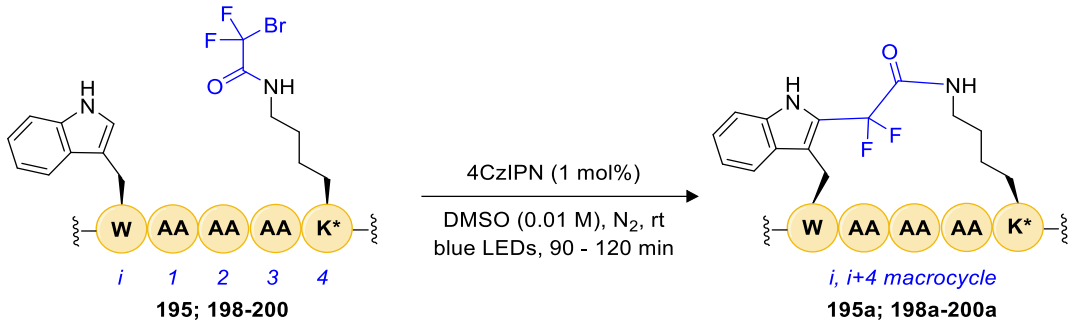

Figure 98. Photocatalytic peptide stapling to generate 23-membered macrocycles.

Cyclisation of Ac-WAMLK*-NH_2 **195** and Ac-K*AMLW-NH_2 **198** provided product yields of 56% and 42% for macrocycles **195a** and **198a** respectively. Similar ^{19}F NMR yields were obtained for unreacted peptide starting material (~ 15%), whereas comparison of analytical HPLC chromatograms suggested that more intense side product (SP) signals were observed for the cyclisation of Ac-K*AMLW-NH_2 **198** (**Figure 99**), potentially accounting for the lower product yield obtained.

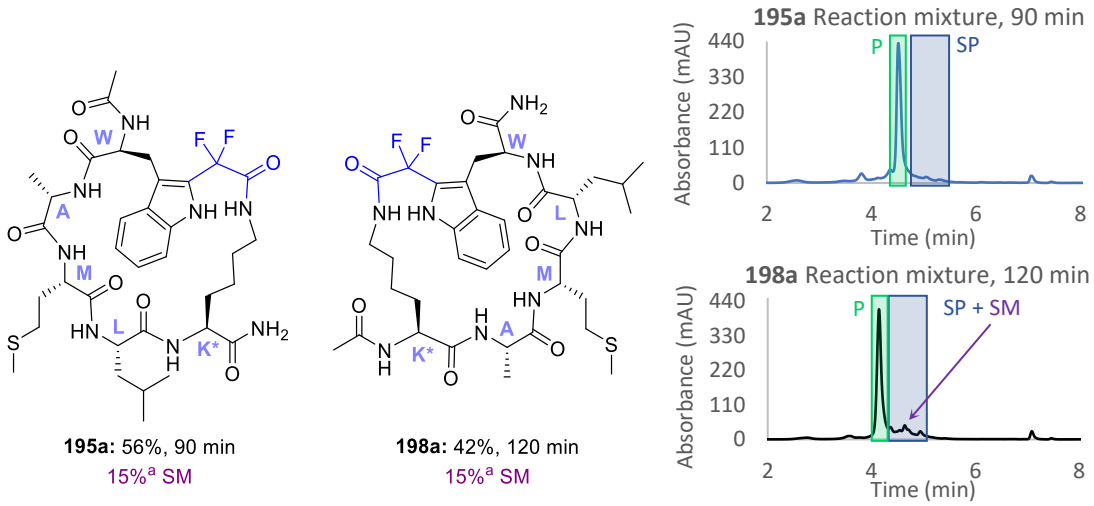

Figure 99. Isolated yields for 23-membered macrocycles synthesised. [a]Yields determined by ^{19}F NMR spectroscopy using TFT as the internal standard. Reaction mixture HPLC chromatograms for the corresponding macrocycles. 20-100% B over 5 min, 280 nm.

Despite this, side product formation in both cases was minor and negligeable material was isolated upon purification leading to impossible identification. Therefore it seemed unlikely that these impurity signals led to the 14% lower isolated yield for macrocyle **198a** compared to **195a**. As mentioned previously this mass difference is small (0.5 mg), and practical challenges, irrespective of reaction capability and unique to each peptide example, could account for the lower yield obtained. For example the crude reaction mixture for **198a** was saponaceous after 0.1 % TFA in H_2O (2.6 mL) was added to aid purification, which led to incomplete transfer to the column. Additionally for both reaction mixtures, the macrocycle and side-products exhibit similar retention times therefore co-elution was often observed for certain isolated fractions, and the extent of this contamination varied significantly.

The reaction time for Ac-K*AMLW-NH_2 **198** cyclization was 120 minutes, and a shorter reaction time of 90 minutes did not appear to reduce the side product formation, instead a 10% poorer yield was obtained for **198a** (32%) due to a greater amount of unreacted linear peptide **198** (34%). For this peptide substrate, increasing the reaction time by 30 minutes reduced the amount of unreacted **198** by 20%, determined by quantitative ^{19}F NMR spectroscopy, therefore a reaction time of 150 minutes should be explored aiming for complete starting material consumption. This was not attempted for numerous reasons: the linear peptide batch was limited, multiple reaction times had already been carried out, and priority was given to investigate the scope of peptide cyclisation over obtaining the best yield.

The final two 23-membered macrocycles were synthesised using linear substrates Ac-EWAMLK*R-NH_2 **199** and Ac-WGFIK*-NH_2 **200** which highlighted the applicability of the methodology for internal peptide cyclisation **199a** and for end-to-end cyclisation in the absence of amino acids known to aid cyclisation **200a**.

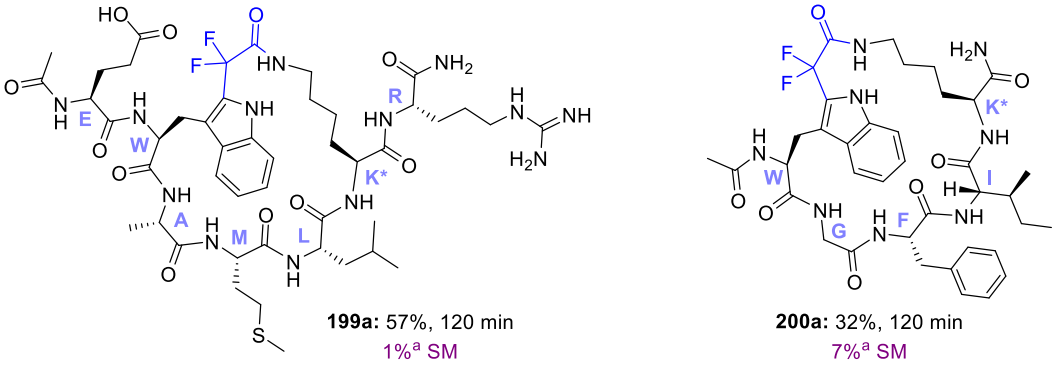

Figure 100. 23-membered macrocycles synthesised.

For both peptide substrates the unreacted linear peptide was minor after 120 minutes of irradiation (1-7% determined by ^{19}F NMR spectroscopy), in contrast to the above examples (15%) (**Figure 101A**). Essentially full consumption was observed for internal stapling to generate macrocycle **199a** accompanied by a product yield of 57%, which was consistent with the analogous end-to-end cyclised product **195a** highlighting the robustness of this methodology.

Conversely, a relatively low yield of 32% was obtained for macrocycle **200a** despite the presence of only 7% unreacted Ac-WGFIK*-NH_2 **200** and few, low intensity side product signals observed by HPLC (**Figure 101B**). This was consistent with other peptide substrates and side product recovery was negligible after purification, therefore it did not seem likely that a significant side reaction was occurring.

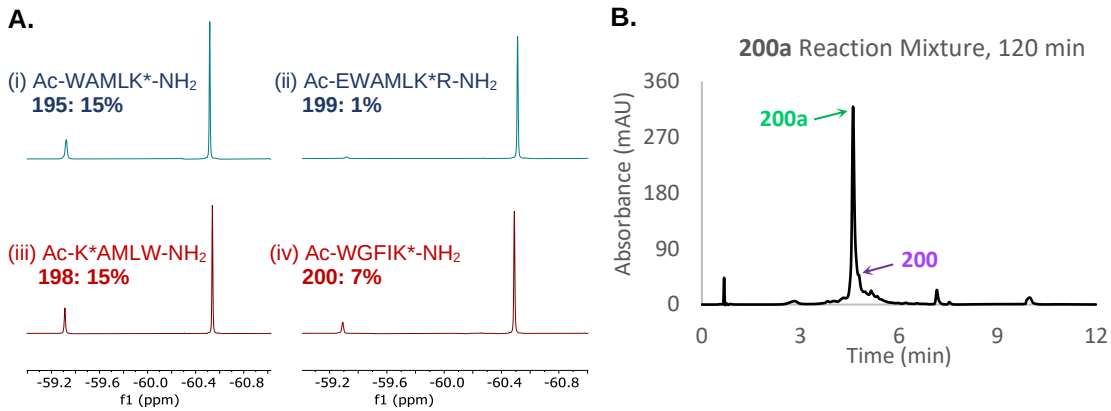

Figure 101. A. Reaction mixture ^{19}F NMR spectra with quantified unreacted linear peptide at the end of the cyclisation reaction determined using TFT (−60.5 ppm) as the internal standard. B. Reaction mixture HPLC chromatogram for macrocycle **200a** synthesis. 20-100% B over 5 min, 280 nm.

Once again, the reaction mixture was saponaceous after dilution which led to incomplete transfer to the column for purification. When the reaction was repeated the volume loaded onto the column differed by 400 µL (approximately 13%), highlighting the inconsistency of transfer even for the same reaction mixture, which can have a significant impact on overall product yield. Furthermore, before the mass of purified material was calculated, transfer to an Eppendorf and lyophilization was carried out. Unique to macrocycle **200a**, rapid melting was observed on the freeze dryer causing product loss due to material leaking out of the Eppendorf and despite thorough freezing, a higher water content and larger Eppendorf this occurred both times. Nonetheless, moderate to good isolated yields of 32-57% were obtained for the above macrocyclic peptide products following additive free photocatalytic cyclisation conditions with relatively short reaction times (2 h).

For each 23-membered macrocycle the fluorine NMR spectrum varied significantly regarding the shape and intensity of signals. Initial macrocycle **195a** (Ac-WAMLK*-NH_2) required the more sensitive Bruker AV(III) 600 spectrometer combined with greater number of scans (2K) to obtain visible

doublets at −91.9 ppm and −95.6 ppm, due to these being broad signals (**Figure 102A**). Whereas much sharper signals were observed for **198a** (Ac-K*AMLW-NH_2) and **199a** (Ac-EWAMLK*R-NH_2) using the more accessible Bruker AV(III) 400 (**Figure 102B and C**). Interestingly for macrocycle **200a** (Ac-WGFIK*-NH_2) a combination of broad (−96.2 ppm) and sharp doublets were shown (−102.1 ppm) along with additional splitting for the latter.

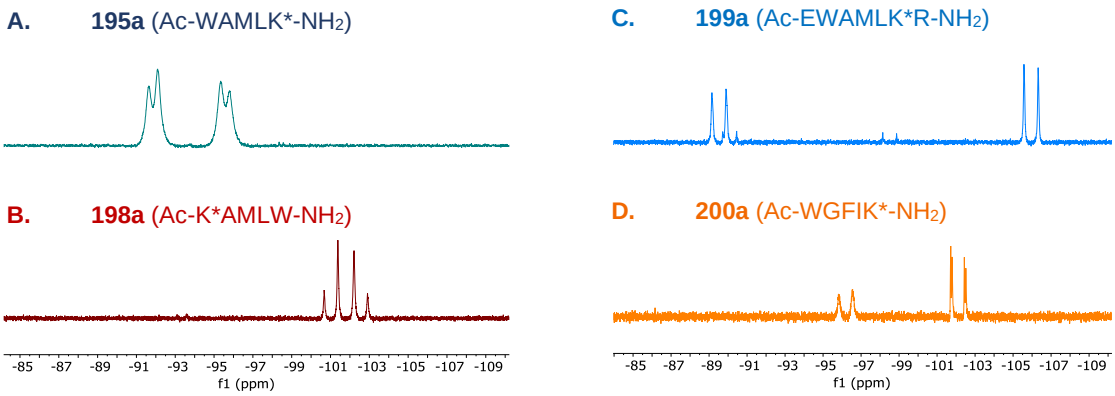

Figure 102. Isolated macrocycle ^{19}F NMR spectra zoomed into the region −85 ppm to −109 ppm.

Broad signals could suggest interactions between the fluorine atoms and other functionality on the macrocycle,[57] where stronger interactions may provide lower intensity, broad NMR signals due to faster relaxation times.[193] This is based on similar observations resulting from protein-ligand interactions: the degree of line broadening is influenced by the fraction of ligand bound to the protein or in the free state,[192] therefore for macrocycle **200a**, potentially one fluorine atom is interacting with the peptide whereas the other is free creating broad and sharp signals respectively. For example, Suryaprakash and Mishra observed through space coupling between fluorine and hydrogen nuclei on compound **201**, suggesting that organic fluorine can participate in intermolecular hydrogen bonding (**Figure 103**).[58] This same interaction (N−H···F−C hydrogen bond) could occur for macrocycles

synthesised in this research, where the ability to interact is influenced by the conformation that the peptide has been locked into and whether this positions an amide moiety nearby with the right orientation.

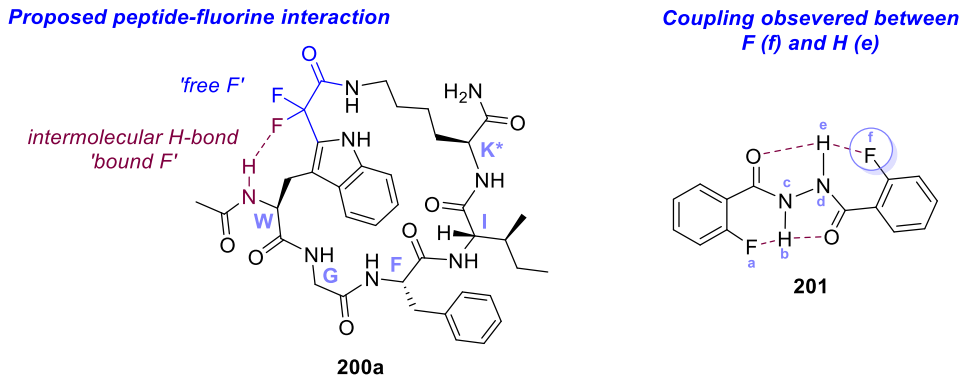

Figure 103. Proposed fluorine-hydrogen interaction for macrocycle **200a** based on literature evidence showing through space coupling between F and H nuclei for compound **201**.[58]

Macrocycle chemical shift values were generally consistent between −90 ppm and −106 ppm, however the separation between the two doublet signals in each spectrum varied greatly from 0.5 ppm to ~ 15 ppm shown by figure 102. A greater difference in chemical shift implied that the fluorine atom environments were more chemically inequivalent. Based on the assumption that only one fluorine atom can participate in intermolecular hydrogen bonding for **200a**, suggested by the broader signal at −96 ppm, the electrons around this fluorine nucleus will be less tightly bound, hence a less negative chemical shift value. Additionally, other factors including the number of fluorine atoms participating in intermolecular interactions such as **195a** or the functional group providing the δ+ hydrogen such as **199a** may influence the chemical shift of each fluorine atom. The exact conformation of macrocycles is not known therefore representative structures have been shown for visualisation purposes only.

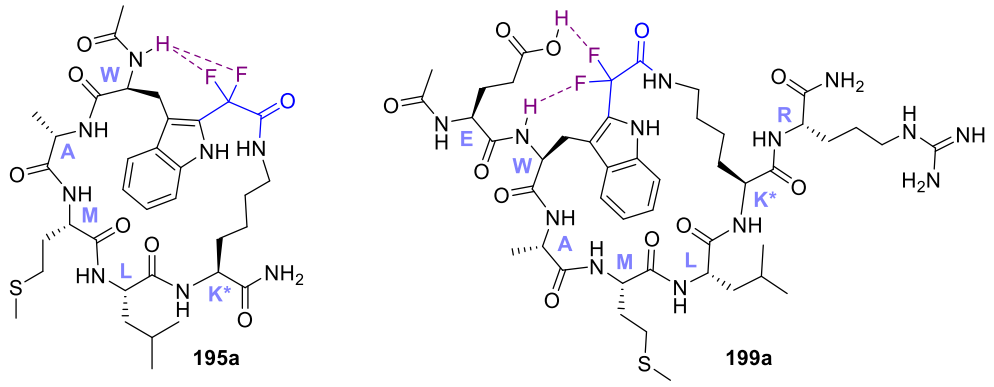

Figure 104. Proposed fluorine-hydrogen interactions for macrocycle **195a** and **199a**.

Unfortunately, secondary structures such as an α-helix cannot be determined using ^{19}F NMR spectroscopy alone, but the variability in chemical shift, signal broadening and splitting can suggest the presence of peptide-fluorine interactions hence macrocyclic structures. It could be hypothesised that the broad signals indicate stronger interactions between the fluorine atom(s) and other functionality on the macrocycle, but also that the fluorine atoms are tightly bound perhaps within an α-helix.[193] Whereas sharper doublet signals, especially those observed for **198a** (Ac-K*AMLW-NH_2) are comparable with linear product signals resulting from intermolecular difluoroalkylation which could imply a disordered macrocycle conformation. To more easily identify whether the macrocycles exist as an α-helix, and time permitting, circular dichroism (CD) could have been carried out. This is a type of absorption spectroscopy which utilises the optically active property of peptide bonds and characteristic spectra can be acquired depending on the local conformation such as α-helices, β-sheets and random coils (**Figure 105**). For example, an α-helix shows negative bands at 222 nm and 208 nm, along with a positive band at 193 nm.[200]

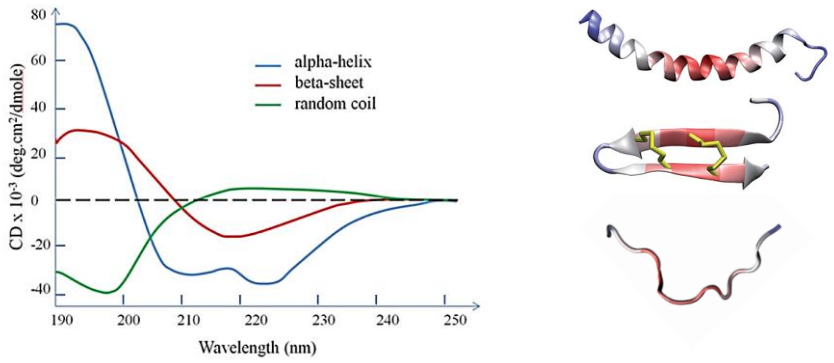

Figure 105. A CD spectrum showing a characteristic trace for three basic secondary structures of a polypeptide chain (α-helix, β-sheet and random coil).[201,202]

Synthesis of 31- and 44-membered macrocycles

Following the peptide scope mostly based on analogues of Ac-WAMLK*-NH_2 further investigation into amino acid compatibility was carried out using longer peptide sequences. End-to-end cyclisation was prioritised because this is generally more common and the ability to form an internal staple had already shown comparable success. The distance between Trp and Lys* was also varied using peptide sequences H-WHASPYVK*-NH_2 **202** (i, i+7) and Ac-WQDECKSNTAGK*-NH_2 **203** (i, i+11) deliberately synthesised to position the residues approximately 2 and 3 α-helical turns apart[195] and to generate larger 31- and 44-membered macrocyclic peptide products. All remaining untested amino acids were incorporated into these two peptide sequences but unfortunately, due to peptide synthesiser complications, these peptide substrate examples were not 100% pure by HPLC (**Figure 106**). Relatively broad signals were observed for peptides **202** and **203** along with multiple minor impurity signals, hence the estimated purity by HPLC was 89% and 70% respectively, which resulted from challenging synthesis and purification. Pleasingly the corresponding ^{1}H and ^{19}F NMR spectroscopic data suggested higher purity; therefore, the reactions were

carried out, however it is recommended that repeating these reactions with pure linear peptides would be beneficial.

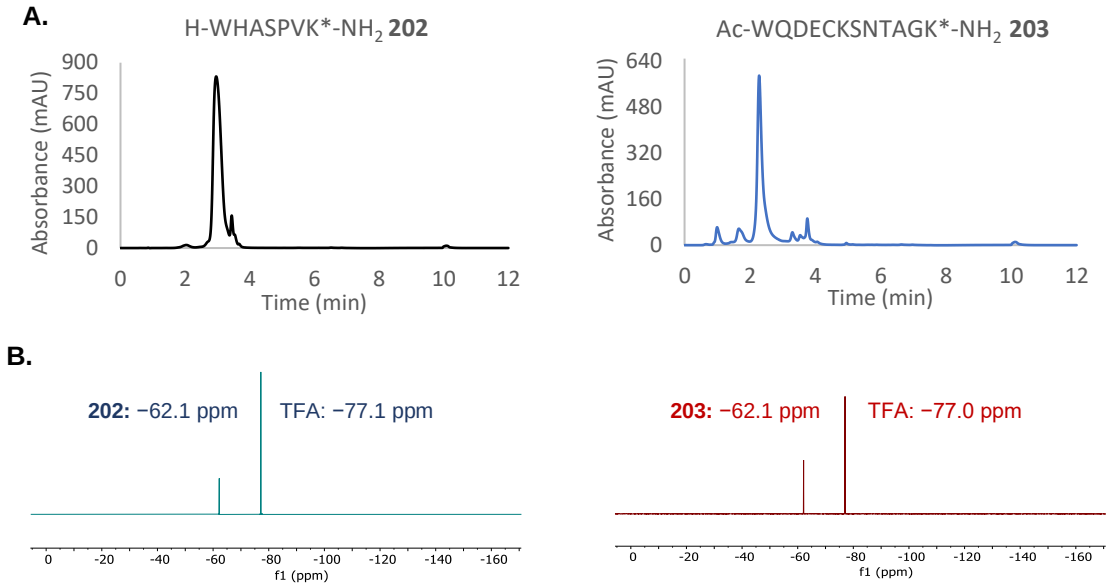

Figure 106. Linear peptide data for H-WHASPYVK*-NH_2 **202** and Ac-WQDECKSNTAGK*-NH_2 **203**. A. HPLC chromatograms, 20-100% B over 5 min, 280 nm. B. ^{19}F NMR spectra.

Despite the lower linear peptide purity, promising results were obtained for 31-membered macrocycle **202a** which was isolated in a 43% yield after 120 minutes of irradiation. This sequence included most aromatic amino acids: Trp, Tyr and His along with a proline (Pro) residue which could cause complications due to its propensity to kink the peptide chain. The free amine N-terminal was also tolerated highlighting the robustness of this cyclisation strategy toward functional groups. Approximately 14% linear peptide remained at the end of the reaction (comparable with Ac-WAMLK*-NH_2 **195** and Ac-K*AMLW-NH_2 **198**) therefore a longer reaction time or 2 mol% of 4CzIPN may enhance starting material consumption improving the product yield. Alternatively, after purification good mass recovery was observed for multiple fractions which contained product contaminated with unidentified side-products (by mass spectrometry) therefore improving product isolation

using an isocratic gradient could also improve the yield for macrocycle **202a**.

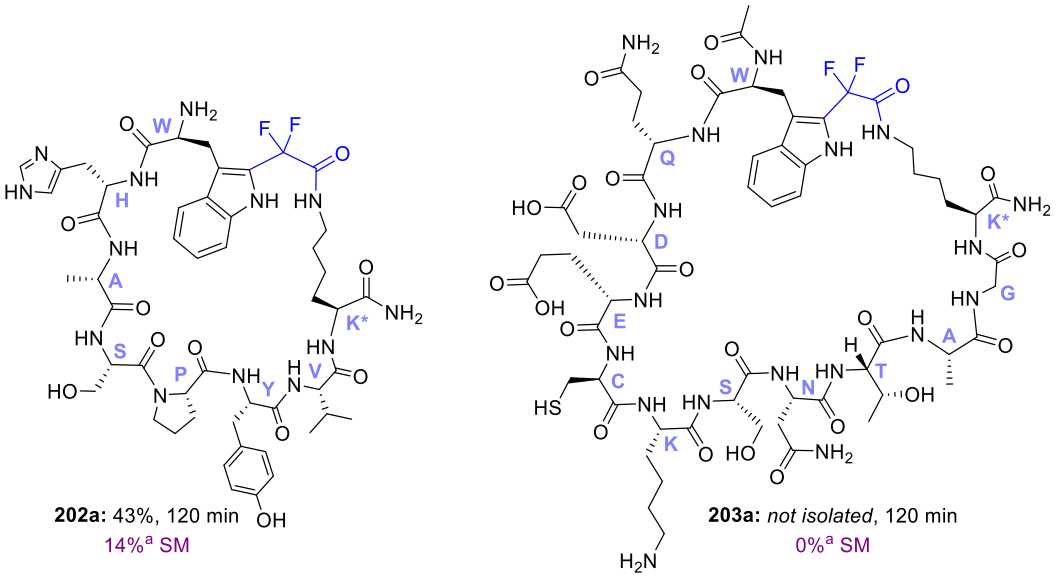

Figure 107. Macrocyclic peptides resulting from H-WHASPYVK*-NH_2 **202** and Ac-WQDECKSNTAGK*-NH_2 **203** peptide stapling.

Unfortunately for Ac-WQDECKSNTAGK*-NH_2 **203** cyclisation, the expected 44-membered macrocycle **203a** was not isolated, despite reaction mixture analysis suggesting successful formation. The desired mass ion for **203a** was observed as the most intense signal in the mass spectrum, with approximately a 1:1 ratio with side product **204**, which forms by the radical intermediate undergoing HAA. As the distance between Trp and Lys* increases, the cyclisation becomes more challenging because the probability of interaction between the ·CF_2R radical and C−2 carbon on Trp is reduced and hydrogen atoms present in the system become preferentially accessible. This was supported by the reaction mixture ^{19}F NMR spectrum which showed a distinctive doublet at −125.1 ppm characteristic of HCF_2− moieties, with an integral of 1.08 corresponding to 54%. Desired macrocycle formation was also indicated by a broad signal in the desired

macrocycle product region −96.4 ppm, similar to **202a** (−96.9 ppm) (**Figure 108A**). This cannot be interpreted quantitatively, as mentioned previously, therefore the low intensity does not necessarily correspond to a low yield. Unfortunately, analytical HPLC could not provide any further insight because the compounds present within the reaction mixture eluted with the injection signal. This was usually avoided by starting the eluent gradient at a lower MeCN concentration i.e. 2% instead of 20%, however time and material restraints prevented the repeat reaction from being attempted.

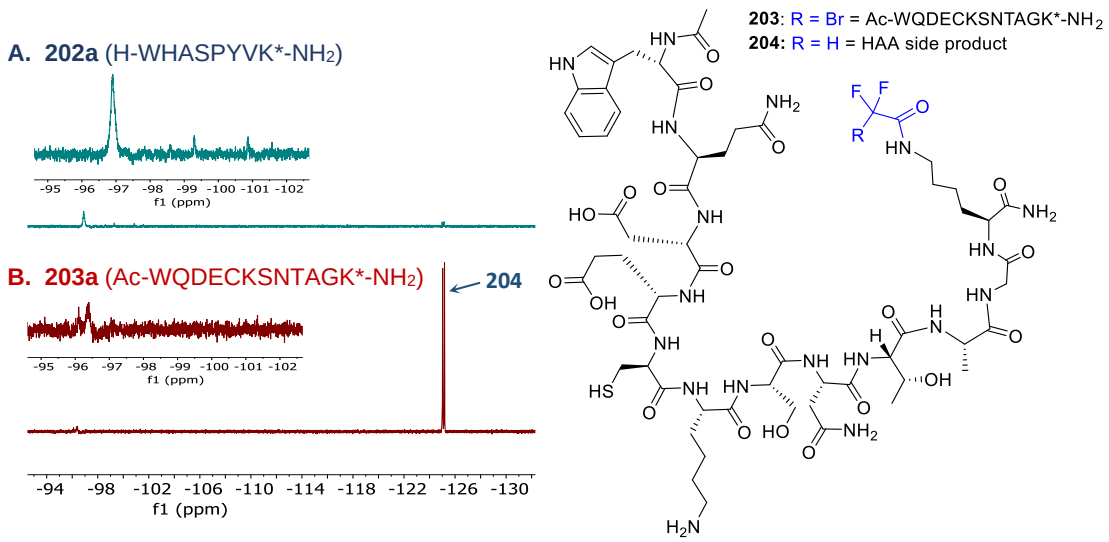

Figure 108. Reaction mixture ^{19}F NMR spectra highlighting the broad low intensity signal for macrocycles **202a** and **203a** and the presence of side-product **204**.

Sufficient data was collected to support macrocycle formation, therefore poor isolation and potential product solubility challenges were likely responsible for the lack of characterisation. After purification, all isolated fractions which showed macrocycle **203a** ions (by mass spectrometry) were also contaminated with the side product **204**. However, using NMR spectroscopy, a mixture of products was not suggested instead only distinctive signals associated with **204** were observed: a doublet and triplet

signal in the ^{19}F and ^{1}H spectrum respectively with matching coupling constants J = 53.8 Hz (**Figure 109**). After the analysis experiments were conducted using either MeOD or DMSO-d_6 as the sample solvent, material precipitated out of the solution which could suggest that macrocycle **203a** was poorly soluble, hence product signals were absent from the spectra.

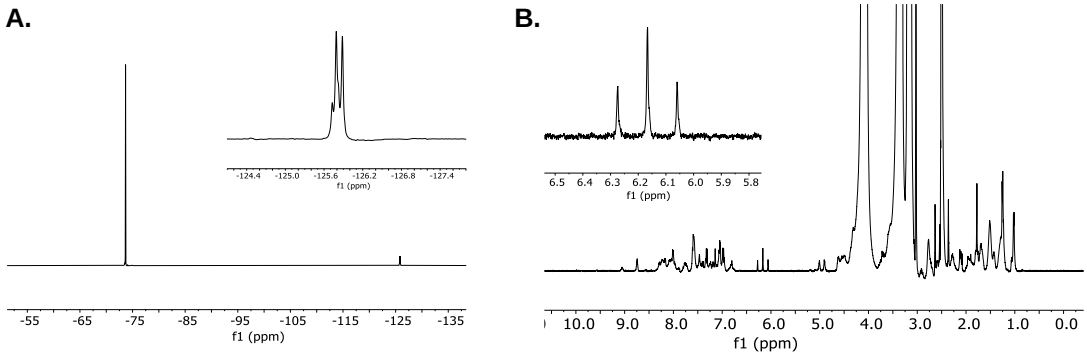

Figure 109. NMR data collected for an isolated product mixture of **203a** and **204** suggested by mass spectrometry. A. ^{19}F NMR spectrum. B. ^{1}H NMR spectrum

It is predicted that with pure starting material and an improved purification gradient isolation of the 44-membered macrocycle **203a** can be obtained by enhancing yield and purity. Product analysis in D_2O may be more successful due to the presence of three charged amino acids (D,E,K) and only one hydrophobic residue (W). The poor solubility in organic solvents may also encourage macrocycle **203a** aggregation,[203] hence the precipitation observed. If solubility, or availability of the solvent to H−bond, is poor interpeptide hydrogen bond formation becomes favourable because it provides an energy gain, subsequently assembling the peptide into aggregates.[203] Dimer formation was also suggested by mass spectrometry when the desired mass ion was observed but as a 2+ charge.

Amino Acid Cyclisation

In contrast to larger 44-membered macrocycles where the i, i+11 separation between the reactive components is likely to be responsible for

poor product yields, smaller ring systems also proved difficult to form. Therefore, successful cyclisation was limited to a specific range of macrocycle size. This was highlighted when the amino acid substrate **205** was exposed to the photocatalytic peptide stapling conditions (**Scheme 54**).

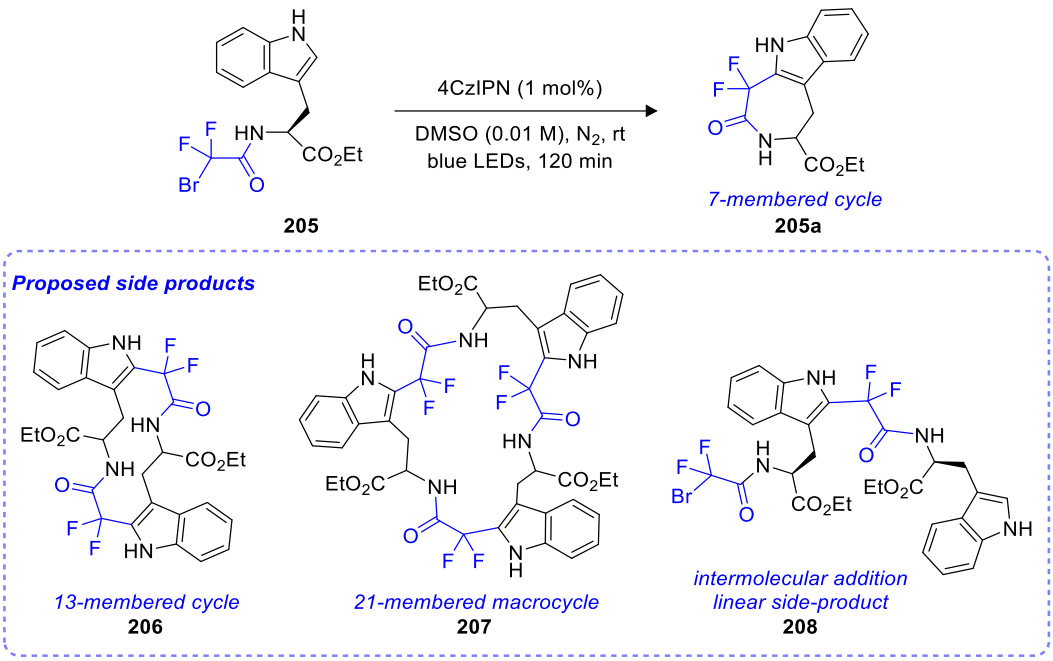

Scheme 54. Photocatalytic cyclisation of (BrCF$_2$CO)HN-Trp-OEt **205**.

Amino acid cyclisation was more complex than expected highlighted by the presence of numerous signals in the reaction mixture HPLC chromatogram (**Figure 110**). Along with the desired 7-membered cyclic product **205a**, potential side-products have been proposed: 13- and 21-membered macrocycles **206** and **207** along with the linear product **208** based on ions observed in the mass spectrum. The 7-membered lactam is highly substituted which may have contributed to the difficulty of formation,[204] therefore intermolecular addition can also occur favourably (side-product **110**), which was not observed for the peptide substrates. Larger

macrocycles can then form following this addition but can perhaps be limited by diluting the reaction mixture further (< 0.01 M).

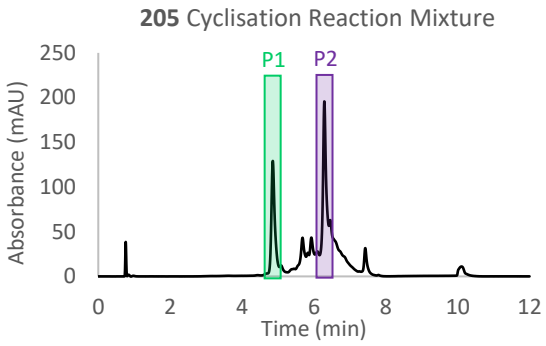

Figure 110. Reaction mixture HPLC chromatogram for the cyclisation of **205**. 20-100% B over 5 min, 280 nm.

The two 'major' products observed in figure 110 with retention times of 4.87- and 6.29 minutes will be referred to as P1 and P2 respectively and were successfully isolated by column chromatography to give relatively pure product HPLC chromatograms (**Figure 111A**). However, NMR and MS data provided conflicting information and were more complicated to interpret, suggesting that more than one compound was present in the sample. For example, P1 reportedly contained the desired product mass ion (309) with 100% intensity, however the ^{1}H spectrum revealed the presence of Trp's C−2 proton singlet. The ^{19}F NMR spectrum suggested that either two fluorinated compounds were present or one existing in two conformational states (**Figure 111B**), which had previously been responsible for singlet signals observed in the desired product region (discussed in 3.6 Difluoroalkylation of Other Trp-Containing Peptides). Unfortunately for these products only ^{1}H, ^{19}F and COSY NMR experiments were carried out, therefore further 2D experiments such as a HSQC would be required to investigate the presence of conformational isomers.

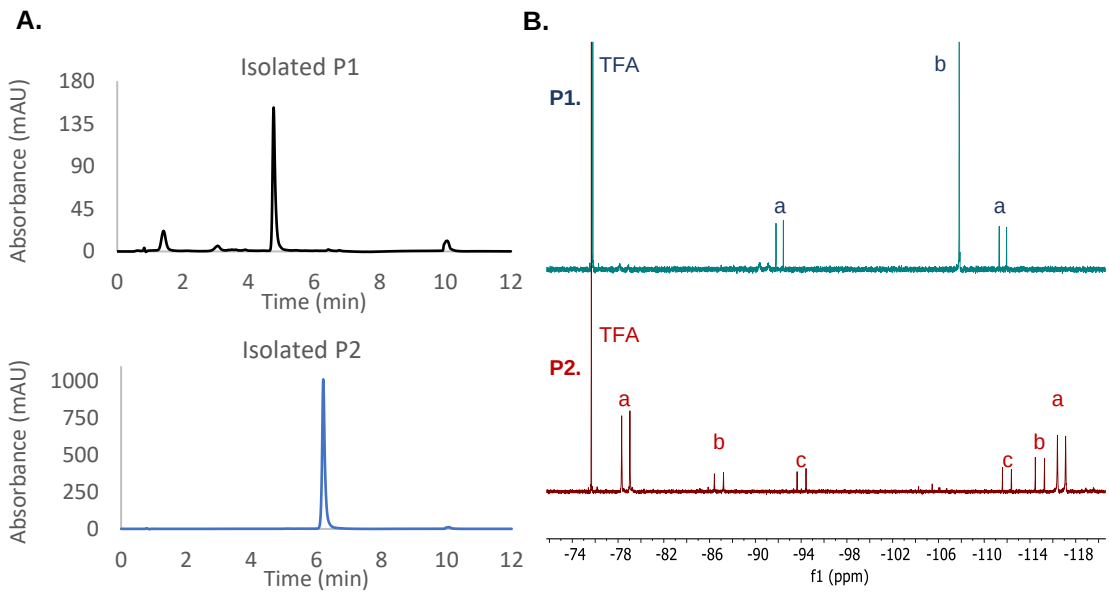

Figure 111. Isolated product data for P1 and P2. A. HPLC chromatograms, 20-100% B over 5 min, 280 nm. B. ^{19}F NMR spectra with labelled signals which display the same coupling constant.

The challenge for P2 analysis was that higher mass ions of 617 ([M+H]$^+$) and 639 ([M+Na]$^+$) were reported which suggested that the 13-membered macrocycle **206** had been isolated. However, dimerization of the 7-membered heterocycle to give the proposed structure **205a*** would also provide these mass ions, and this may be favourable due to an energy gain resulting from enhanced stability *via* hydrogen-bonding (**Figure 112**).[205] Pleasingly analysis of the ^{1}H NMR spectrum, specifically the aromatic region, showed identifiable indole protons and the C–2 singlet was absent, suggesting that cyclisation had occurred. Additional multiplet signals were also present (30-40%) in contrast to the 'pure' HPLC chromatogram. The ^{19}F NMR spectrum also showed more doublet signals than expected, corresponding to three RCF_2 environments based on their coupling constants. The intensity of signals suggested a 1:0.2:0.14 ratio which could imply that the major product contains one CF_2 moiety (a) and the minor product contains two CF_2 moieties (b, c) such as desired product **205a** (or dimerised product **205a***) and macrocycle **206** respectively. Confident

characterisation of P1 and P2 could not be determined due to likely co-elution of compounds, potential dimerization, multiple compounds having the same mass ion and insufficient NMR data. Therefore, further investigation is required to determine the outcome of photocatalytic (BrCF$_2$CO)HN-Trp-OEt **205** cyclisation and due to the complexity of the reaction mixture, tweaking of conditions is likely required.

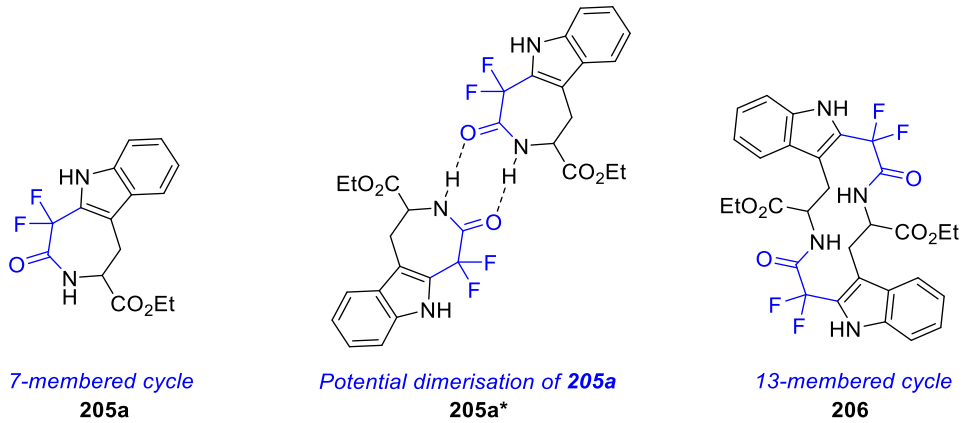

Figure 112. Potential structures of compounds isolated in P1 and P2.

Conclusion

A novel photocatalytic peptide stapling strategy has been developed utilising an organic photocatalyst (4CzIPN) to enable the synthesis of 23- and 31-membered macrocycles (**Scheme 55**).

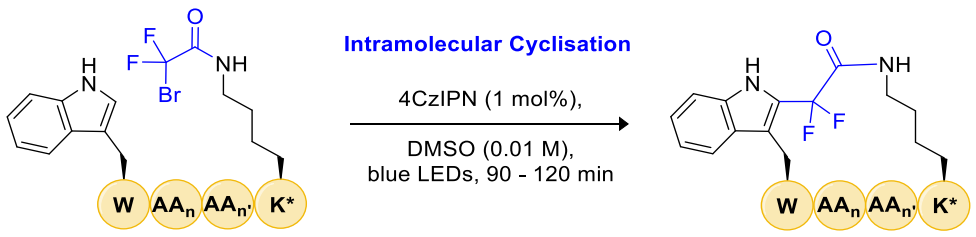

Scheme 55. Photocatalytic peptide stapling to give different sized macrocycles.

Initial investigations using Ac-WAMLK*-NH$_2$ and several analogues demonstrated successful end-to-end- and internal cyclisation after short

irradiation times without the use of additives. All native amino acids along with a free N-terminal were tolerated in the peptide sequence highlighting broad applicability of this methodology, also avoiding the requirement for protecting groups; a limitation associated with several current literature techniques.[106] Furthermore, synthesis of the non-native Lys residue (bearing the $BrCF_2CO-$ moiety) utilises known chemistry and installation into the linear peptide sequence is facile.

Application of the stapling technique to provide larger 44-membered macrocycles but also smaller 7-membered lactams has been briefly explored. However, further investigation and potential reaction development is required to successfully obtain these products.

5 Overall Conclusions and Future Work

In summary, two peptide functionalisation strategies have been reported involving photocatalytic difluoroalkylation of Trp: intermolecular addition and intramolecular cyclisation expanding the underdeveloped area of photo-bioconjugation chemistry (**Scheme 1**). The development of mild, more sustainable conditions using visible light, short reaction times and organic photocatalysis provided an innovative strategy for C–H functionalisation of biomolecules.

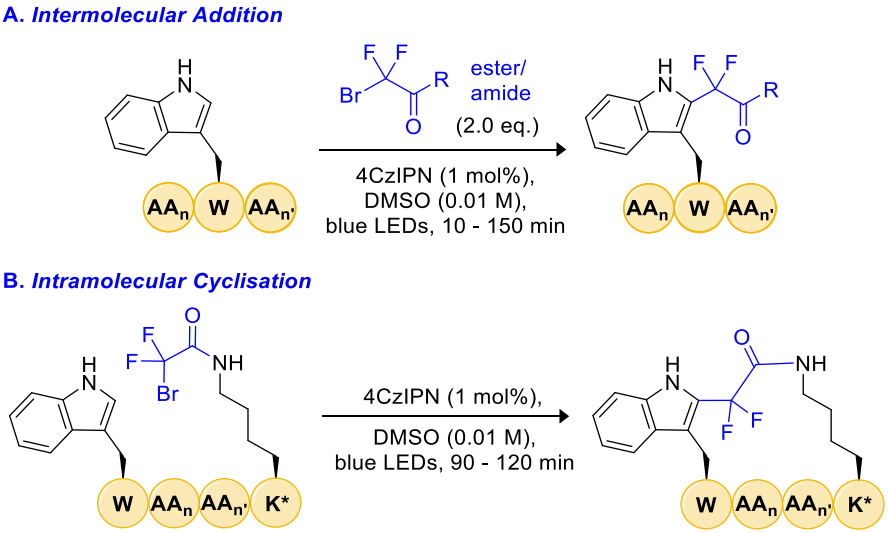

Scheme 1. Photocatalytic difluoroalkylation of Trp: A. Intermolecular addition to give small molecule-peptide conjugates. B. Intramolecular cyclisation to give peptide macrocycles.

For intermolecular addition the scope of the alkylating agent was demonstrated through straightforward derivatization to synthesise a range of amide and ester probes. Such probes were successfully conjugated to Trp at amino acid level and on complex peptide models including Ac-WHISKEY-NH_2, which highlighted the reaction's chemoselectivity for Trp.

An additional six peptides were exposed to the photocatalytic difluoroalkylation conditions generating a modest library of 21 small molecule-peptide conjugates. Such products contained moieties of interest

such as bio-orthogonal linkers or biologically relevant groups (PEG, biotin) therefore the methodology has the potential to further enable the discovery of therapeutic peptides. Application of the methodology to protein modification was briefly explored using β-casein, and potential conjugation was suggested, however this was unquantifiable due to ester linker instability under degradation conditions. This area of research was concluded and published in Organic Letters (8. Appendix).

Another application of photocatalytic Trp difluoroalkylation was to develop a novel peptide stapling technique. Cyclisation was enabled by incorporation of the radical precursor (Lys*) into the peptide sequence which subsequently reacted with Trp (**Scheme 1B**). The successful synthesis of five macrocycles such as **199a** and **202a** (**Figure 113**) highlighted reaction compatibility for different cycle sizes (23- and 31-membered) by extending the distance between W and K* (i, i+4 and i, i+7). Different stapling capabilities (end-to-end and internal) were also demonstrated with high amino acid tolerance showing the versatility and robustness of this transformation.

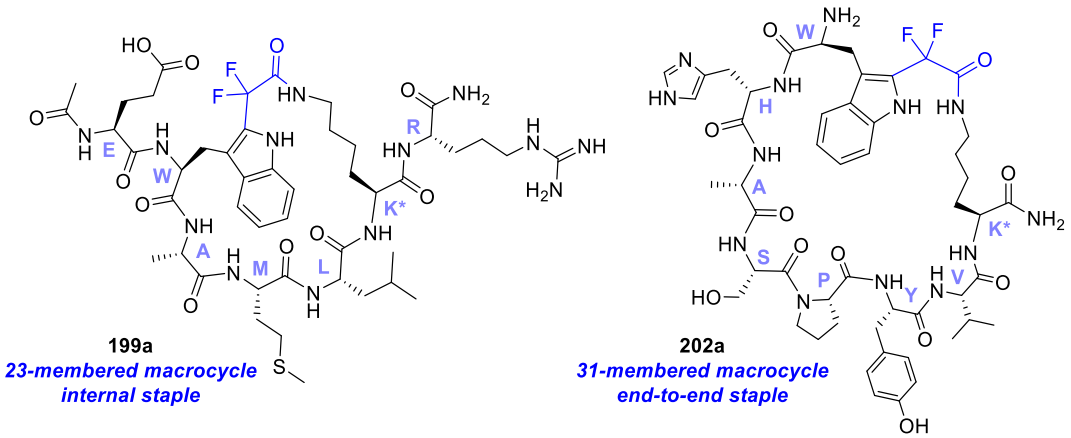

Figure 113. Two of the macrocycles synthesised using photocatalytic Trp difluoroalkylation.

Future Work

The future of peptide cyclisation involves scope expansion of the linear peptide substrates combined with potential investigation into macrocycle secondary structures and/or their biological properties.

Along with repeating the examples previously discussed, in particular the i, i+11 stapling of Ac-WQDECKSNTAGK*-NH_2 **203**, additional peptide substrates should be explored to expand the scope of macrocycle products. For example Ac-WRGDK*-NH_2 **209** and Ac-WANGRELK*-NH_2 **210**, which incorporate tumour signaling sequences: -RGD- and -NGR-.[108,109]

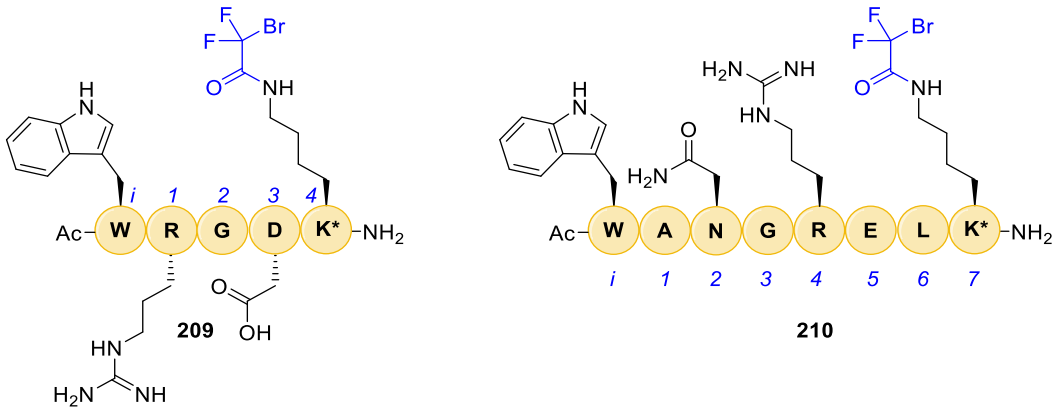

Figure 114. Linear peptide substrates containing tumour-hormone signalling sequences.

It would be of interest to carry out circular dichroism (CD) measurements and 2D NMR spectroscopy experiments to characterise the macrocycle products and identify any secondary structures such as α-helices and β-sheets or whether a random coil is the preferred conformation.

Following this, comparing the results with the product ^{19}F NMR spectra may be able to provide further insight into the doublet signal line width and chemical shift. It should be noted that an α-helical structure is not crucial in providing enhanced peptide properties, for example Johannes and co-

workers discovered that macrocycle **78d** had a non-helical conformation, however showed resistance toward enzymatic degradation (**Figure 18**): a significant improvement compared to the linear analogue **77d**.[94] Therefore, whether the macrocycles exhibit α-helical conformations or not, it would be beneficial to investigate their stability when treated with enzymes investigating proteolytic resistance.

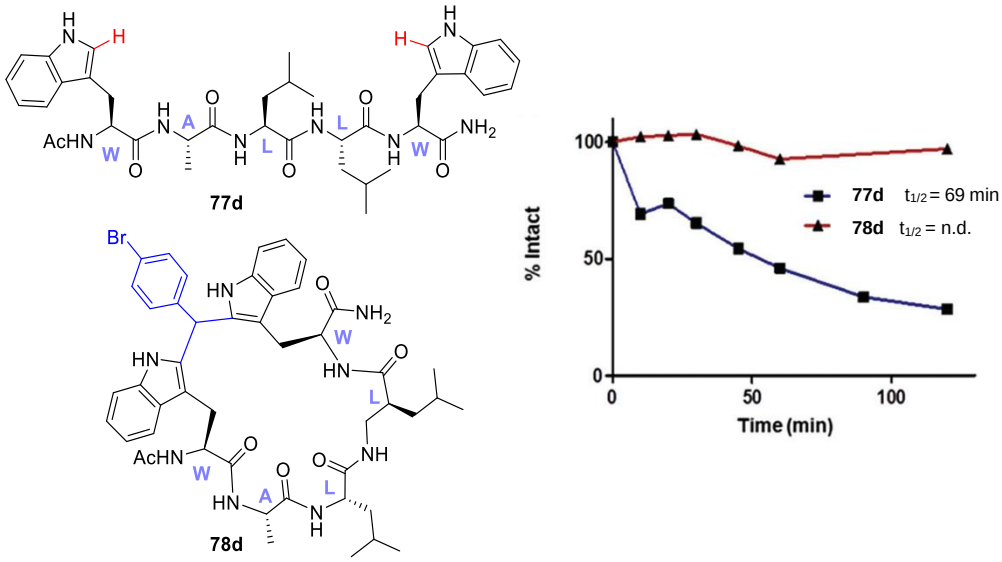

Figure 18. Chymotrypsin proteolysis highlighting the stability difference toward degradation between linear **77d** and cyclised peptide **78d** analogues.[94]

Finally, biologically active peptide substrates should be exposed to the photocatalytic stapling strategy to not only expand the scope of peptide macrocycles but to also compare the properties (stability and activity) of linear and stapled peptides. Macrocycles **211a** and **212a** would result from the cyclisation of linear bioactive peptides based on a dipeptidyl peptidase III inhibitor and neurostimulating peptide respectively (**Figure 115**).[104,105]

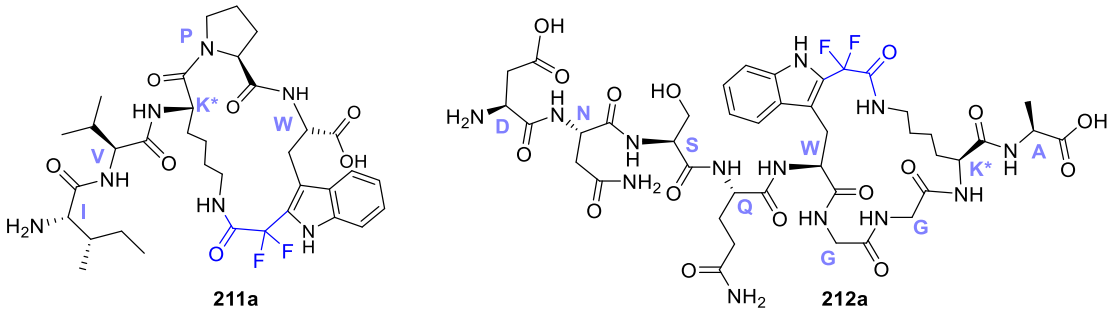

Figure 115. Potentially bioactive macrocyclic peptides.

6 Experimental

General information

^{1}H, ^{13}C and ^{19}F NMR spectra were recorded on a Bruker DPX 400, Bruker AV400, Bruker AV(III)400, Bruker AV(III)400HD, Bruker AV(III)500 or Bruker AV(III)600 spectrometer. Chemical shifts (δ) are reported in parts per million (ppm); coupling constants (*J*) are quoted in Hertz (Hz) and are reported to the nearest 0.1 Hz. ^{1}H, ^{13}C and ^{19}F chemical shifts are reported relative to tetramethylsilane and are referenced to the appropriate residual solvent peaks: $CDCl_3$ (δ 7.26 ppm [^{1}H]/ δ 77.16 ppm [^{13}C]), CD_3OD (δ 3.31 [^{1}H]/ δ 49.00 [^{13}C]), DMSO-d_6 (δ 2.50 [^{1}H]/ δ 39.52 [^{13}C]. ^{1}H NMR spectral data are reported as follows; chemical shift, multiplicity, number of protons and coupling constant. The following abbreviations (and combinations of) are used to label multiplicities: s (singlet), d (doublet), t (triplet), q (quartet), dd (doublet of doublets), ddd (doublet of doublet of doublets), and m (multiplet). HSQC, DEPT, TOCSY, and COSY experiments were used to assist structural assignments.

Analytical RP-HPLC: Performed on a Thermo Ultimate 3000 uHPLC system equipped with PDA eλ detector (λ = 210 – 400 nm). Amino acids and peptides were analysed using a Waters SunFire 5 µm, 2.1 × 150 mm column (C-18) at a flow rate of 0.6 mL min^{-1}. The mobile phase composed of 0.1% trifluoroacetic acid in H_2O (Solvent A) and 0.1% trifluoroacetic acid in acetonitrile (Solvent B). The analysis of the chromatograms was conducted using Chromeleon 7 software.

Preparative RP-HPLC: Performed using a Waters 1525 binary pump HPLC equipped with a dual wavelength UV detector set to 210 nm and 280 nm. Peptides were purified on a Waters SunFire 5 µm (C-18) preparative column with 5 µm particle size, 19 × 150 mm, operating at a flow rate of 6 mL min^{-1} using a mobile phase of 0.1% trifluoroacetic acid in H_2O (Solvent A) and 0.1% trifluoroacetic acid in MeCN (Solvent B) using the gradient specified for each specific compound. Semi-preparative reverse-phase HPLC was performed using the same HPLC and solvent system. The column used was a Waters SunFire 5 µm (C-18) preparative column, 10 × 250 mm, operating

at a flow rate of 5 mL min^{-1} using the gradient specified for each specific compound.

High-resolution mass spectra: Recorded on a Bruker MicroTOF II spectrometer (ESI) and Bruker Ultraflex III (MALDI). Electron ionisation (EI) mass spectra were recorded on a JEOL AccuTOF GCX with the MS ion source conditions: temperature (270°C), ionisation energy (70eV) and mass calibration by PFTBA.

HPLC-MS: Performed on a Thermo Ultimate 3000 uHPLC system equipped with PDA eλ detector (λ = 210 – 400 nm). Amino acids and peptides were analysed using a Waters SunFire 5 µm, 2.1 × 150 mm column (C-18) at a flow rate of 0.6 mL min^{-1}. The mobile phase composed of 0.1% formic acid in H_2O (Solvent A) and 0.1% formic acid in acetonitrile (Solvent B). The analysis of the chromatograms was conducted using Chromeleon 7 software and the sample was then subjected to the Bruker MicroTOF II spectrometer (ESI).

MALD-TOF: Recorded on a Bruker Autoflex Max, the protein sample was mixed with a matrix solution of sinapinic acid in a 1:1 acetonitrile and H_2O mixture containing 0.1% trifluoroacetic acid. The mixture was spotted on the MALDI target plate and a laser intensity of 100% was fired at the sample.

Liquid chromatography-mass spectrometry: Peptide digests were analysed with Dionex UltiMate 3000 RSLCnano HPLC system coupled to a ThermoFisher LTQ FT Ultra Hybrid Mass Spectrometer fitted with a nano-ESI source. Peptide injections (DDA, 2 µL; MS/MS 4 µL) were loaded onto a C18 Pepmap300 loading column (10 mm, 300 Å, 5 µm particle size) followed by separation through a C18 Pepmap300 column (150 mm × 75 µm, 300 Å, 5 µm particle size). A dual mobile-phase gradient was used composed of phase A (5% acetonitrile, 0.1% formic acid) and phase B (95% acetonitrile, 0.1% formic acid). The mass spectrometer was operated in positive ion mode, with the nESI source fitted with a fused silica emitter tip (MSWIL). Protease coverage was assessed using data-dependent acquisition (DDA), and individual peptides of interest with ion-trap CID MS/MS of designated precursor peptides.

Protein Analyses: DDA RAW files were analysed in SearchGUI through a database search against 580,590 unique protein sequences.[206] Analyses using PeptideShaker[207] identified β-casein as the top hit and revealed a peptide (137-LPLLQSWMHQP-147) containing the tryptophan of interest, with identity confirmed through assignment of B and Y fragment ions. Full scan RAW files of modified β-casein were analysed in XCalibur (Thermo Fisher), where peaks corresponding to modified peptides were identified through the expected mass shifts corresponding to the modification. MS/MS data was processed in XCalibur, with B and Y fragment ions manually assigned.

Infrared spectra (IR): Recorded on a Bruker Alpha platinum-ATR with diamond window. Melting points were measured on a Gallenkamp melting point apparatus.

Analytical TLC: Carried out on aluminium-backed silica gel plates (Merck/EMD Millipore, 60 Å pore size, pre-coated with 254 nm-responsive fluorescent dye), and spots were visualised with UV irradiation (254 and 366 nm). Flash column chromatography was accomplished using silica gel 60 Å (40-63 μm particle size), used as purchased from Sigma-Aldrich, eluting with the solvents listed.

Cyclic voltammetry: Performed in 0.1 M $TBAPF_6$ in anhydrous MeCN, at a scan rate of 100 mV/s (unless otherwise stated). Working electrode: Glassy Carbon (CH Instruments Part No. CHI104). Counter electrode: Pt wire (CH Instruments Part No. CHI115). Reference electrode: $Ag/AgNO_3$ (Ag wire in 10 mM $AgNO_3$, 0.1 M $TBAPF_6$ in anhydrous MeCN) (CH Instruments Part No. CHI 112). Measurements were taken using a CHi-1140c potentiostat.

Materials

Starting materials and reagents were obtained from commercial sources and were used without further purification unless stated otherwise. Reagents that were not commercially available were synthesised as outlined for each specific compound.

Automated Solid-Phase Peptide Synthesis (SPPS)

Automated Fmoc-SPPS was carried out on a Biotage Initiator+ Alstra microwave peptide synthesizer. General synthetic procedures for Fmoc-deprotection and capping were carried out in accordance with the manufacturer's specifications. Standardized amino acid couplings were performed for 15 min at 50 °C under microwave irradiation in the presence of amino acid (0.5 M in DMF, 4.00 equiv.), Oxyma (0.5 M in DMF, 4.00 equiv.) and diisopropylcarbodiimide (0.5 M in DMF, 4.00 equiv.).

Cleavage: For peptides containing Cys/Met: A mixture of TFA, thioanisole, triisopropylsilane (TIPS) and water (85:5:5:5 v/v/v/v) was added to the resin. After 3 h, the resin was washed with TFA (3 × 2 mL). For all other peptides: A mixture of TFA, triisopropylsilane (TIPS) and water (90:5:5 v/v/v) was added to the resin. After 3 h, the resin was washed with TFA (3 × 2 mL).

Work-up: The combined solutions were concentrated under a stream of nitrogen to < 5 mL. Diethyl ether (40 mL) was added to precipitate the peptide and the suspension centrifuged. The pellet was then dissolved in water containing 0.1% TFA, filtered and purified by preparative HPLC and analysed by LC-MS and ESI mass spectrometry.

Photoredox Reaction Setups

A *Standard setup:* The photoredox setup used standard iNextStation blue LED strip lights (60 W) wrapped inside a Pyrex dish. Reaction vessels were chosen based on the reaction volume, using either 8 mL or 20 mL screw top vials. The temperature inside the dish was within the range of 23 - 43 °C.

B *PhotoRedOx box:* The EvoluChem™ PhotoRedOx Box is a multi-format photo reactor compatible with vial formats 0.3 mL, 2 mL, 8 mL and 20 mL vials and flow reactor. It is equipped with several mirrors that direct and distribute the light toward the samples. The geometry of the box enables parallel reaction with homogenous light exposure. The position of the light source on the side of the samples reduces the amount of heat directed to samples. The embedded fan circulated any remaining heat. EvoluChem™ LED spotlights (18 W) were used - 455 nm (blue) and 6200K (white).

The reactions were set up inside a standard fume hood, then transferred to the specified photoredox reaction setup.

Stock Solutions

Where necessary stock solutions of known concentration were made by dissolving a quantity of the substrate/reagent/catalyst in anhydrous DMSO.

Quantitative NMR Spectroscopy Analysis of Reaction Mixtures

After irradiating the reaction mixture with blue LEDs for the specified amount of time, α,α,α-trifluorotoluene (0.333 eq.) was added, then a sample (600 µL) was taken for analysis by ^{19}F NMR spectroscopy. The delay and number of scans for this experiment were set to 15 s and 32 scans respectively. Inversion recovery experiments showed that the t0 was 2.5 s. The integral of the α,α,α-trifluorotoluene (TFT) singlet was set to 1, and due to the 1:1 relationship between the standard and product doublets, integration of a product doublet represented the quantitative NMR spectroscopic yield.

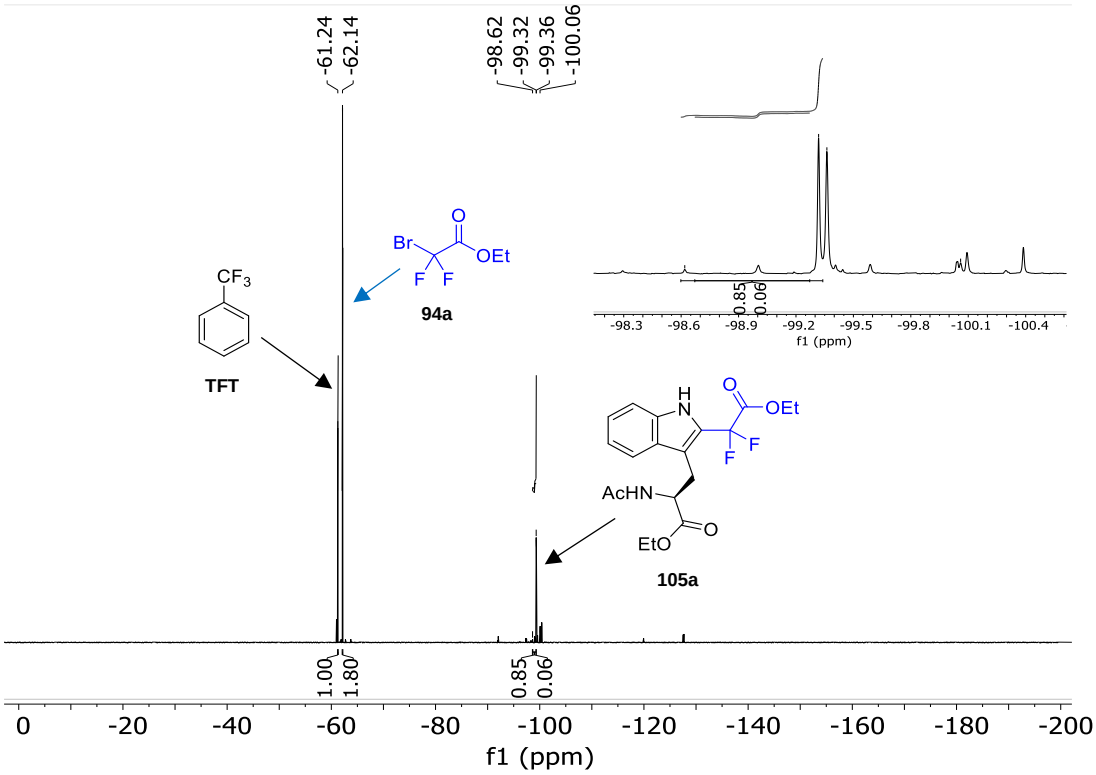

Figure 116. Representative ^{19}F NMR spectrum of an unpurified amino acid reaction mixture.

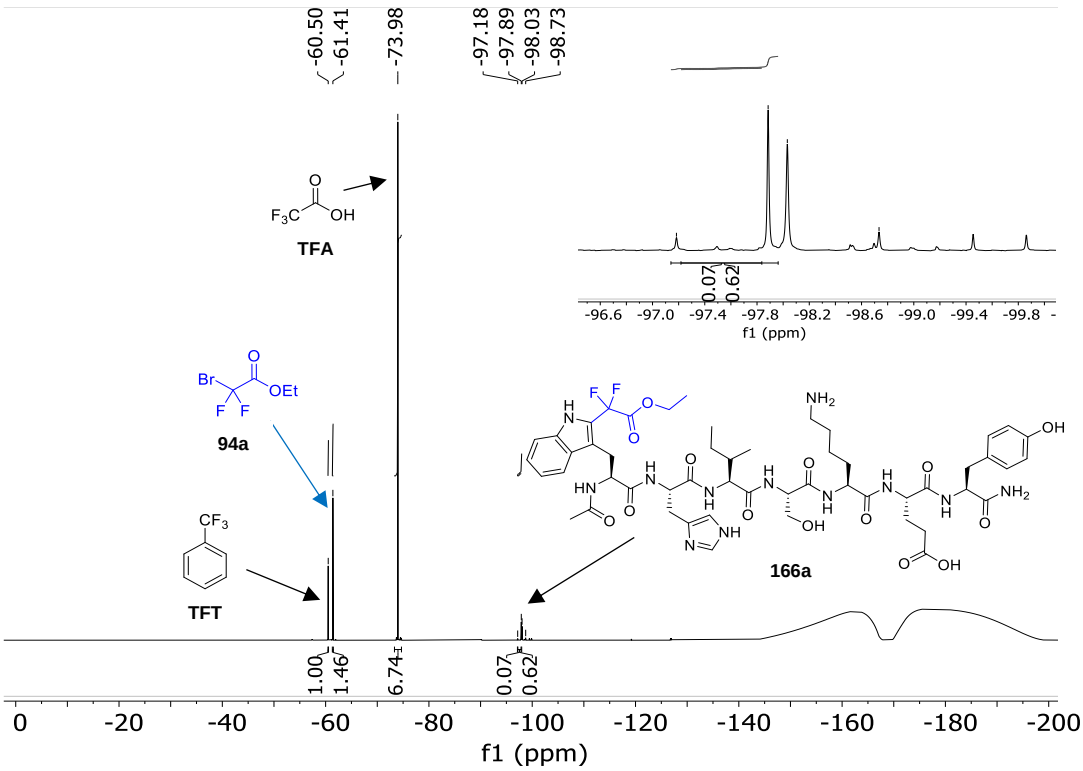

Figure 117. Representative ^{19}F NMR spectrum of an unpurified peptide reaction mixture.

6.1 Optimisation studies with Ac-Trp-OEt

_N_-Acetyl-L-tryptophan ethyl ester (93)

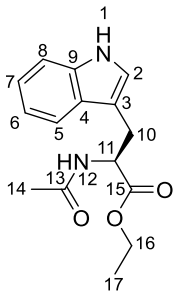

To a stirred suspension of L-tryptophan ethyl ester hydrochloride (1.27 g, 4.73 mmol, 1.00 eq.) in DCM (10 mL, 0.5 M) were added DIPEA (1.80 mL, 10.0 mmol, 2.00 eq.) and acetic anhydride (0.470 mL, 5.00 mmol, 1.00 eq.) under an argon atmosphere and stirred for 3 h. The solution was diluted with water (10 mL) and extracted with DCM (3 × 10 mL). The combined organic extracts were washed with 1 M aq. HCl (10 mL), sat. aq. $NaHCO_3$ (10 mL) and brine (10 mL), dried over $MgSO_4$ and concentrated *in vacuo*. The crude residue was purified by recrystallisation from ethyl acetate and petroleum ether to give the title compound **93** as an off-white crystalline solid (1.13 g, 4.12 mmol, 87%). Mp 105-107 °C (lit.[208] 109-110 °C); υ_{max}/cm^{-1} (ATR) 3288, 3079, 3059, 3011, 2993, 2965, 2926, 2910, 2857, 1742, 1638, 1614, 1552, 1481, 1458; ^{1}H NMR (400 MHz, $CDCl_3$) δ 8.50 (1H, s, H-1), 7.54 (1H, dd, *J* = 7.9, 1.5 Hz, H-8), 7.35 (1H, dd, *J* = 8.2, 1.5 Hz, H-5), 7.18 (1H, ddd, *J* = 8.2, 7.0, 1.2 Hz, H-6), 7.11 (1H, ddd, *J* = 7.9, 7.0, 1.3 Hz, H-7), 6.96 (1H, s, H-2), 6.13 (1H, d, *J* = 7.9 Hz, H-12), 4.93 (1H, ddd, *J* = 7.9, 5.4, 5.3 Hz, H-11), 4.22 – 4.05 (2H, m, H-16), 3.34 (1H, dd, *J* = 14.8, 5.4 Hz, H-10), 3.29 (1H, dd, *J* = 14.8, 5.3 Hz, H-10), 1.94 (3H, s, H-14), 1.22 (3H, t, *J* = 7.1 Hz, H-17); ^{13}C{^{1}H} NMR (101 MHz, $CDCl_3$) δ 172.1 (C, C-15), 170.0 (C, C-13), 136.2 (C, C-9), 127.9 (C, C-4), 122.9 (CH, C-2), 122.2 (CH, C-6), 119.7 (CH, C-7), 118.6 (CH, C-8), 111.4 (CH, C-5), 110.0 (C, C-3), 61.6 (CH_2, C-16), 53.3 (CH, C-11), 27.7 (2 x CH, C-10), 23.3 (CH_3, C14), 14.2 (CH_3, C-17); HRMS (ESI) Exact mass calcd. for $C_{15}H_{19}N_2O_3$ $[M + H]^+$: 275.1390; found: 275.1398 (2.9 ppm error). Characterization data were in accordance with those previously reported.[209]

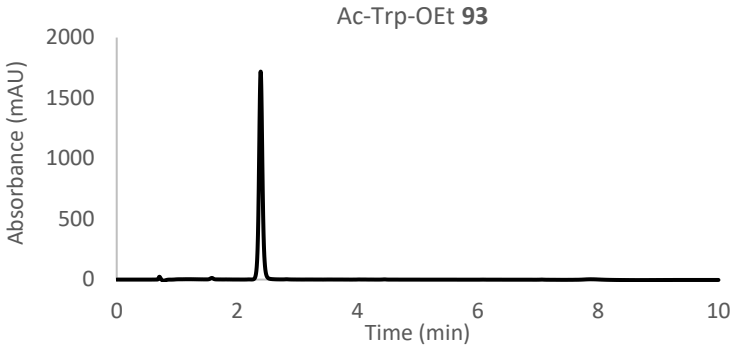

Figure 118. Pure analytical HPLC chromatogram for Ac-Trp-OEt **93**. Rt = 2.39 min on analytical gradient 40-80% B over 5 min, 0.6 mL min^{-1}, 280 nm.

Optimisation General Procedure

A solution of Ac-Trp-OEt **93** (16.5 mg, 60.0 µmol, 1.00 eq.), photocatalyst, base and ethyl bromodifluoroacetate **94a** in solvent was purged with N_2 (5 min) and irradiated with blue LEDs (PhotoRedOx box, 18 W) for 10 min at room temperature. α,α,α-Trifluorotoluene (20 µL, 1.0 M in DMSO, 20.0 µmol, 0.333 eq.) was added to the reaction mixture before quantitative NMR spectroscopy, analytical HPLC and MS analysis was carried out.

6.2 Synthesis of Radical Precursors

General Procedure A: Synthesis of Bromodifluoroacetates and Bromodifluoroacetamides

Using a modification of the procedure reported by Jin and co-workers.[2] Under an inert atmosphere (N_2) a solution of alcohol or amine (1.00 mmol, 1.00 eq.) and triethylamine (279 µL, 2.00 mmol, 2.00 eq.) in anhydrous DCM (3 mL, 0.333 M) was cooled to 0 °C. A solution of bromodifluoroacetyl chloride (188 µL, 2.00 mmol, 2.00 eq.) in anhydrous DCM (1 mL, 2.00 M) was added dropwise. The reaction was allowed to warm to room temperature and stirring was continued for 16 - 18 h. The reaction mixture was diluted with water (5 mL) and washed with sat. aq. NH_4Cl (2 × 10 mL), sat. aq. $NaHCO_3$ (2 × 10 mL) and brine (10 mL), dried ($MgSO_4$) and concentrated *in vacuo*. The resulting residue was purified by flash column chromatography.

General Procedure B: Synthesis of Bromodifluoroacetamides[152]

Prepared according to the procedure reported by Ohshima and co-workers.[3] To a glass vial, equipped with a stirrer bar, lanthanum trifluoromethanesulfonate (26.4 mg, 45.0 µmol, 5 mol%) was added then the vial was sealed with a silicone septum screw-cap and purged with N_2 (5 min). Ethyl bromodifluoroacetate **2a** (139 µL, 1.08 mmol, 1.20 eq.) and amine (0.900 mmol, 1.00 eq.) were added, then the mixture was stirred at rt for 17-20 h. The reaction was monitored by TLC analysis and once complete consumption of the starting material was observed, the crude mixture was directly purified by flash column chromatography.

Bromodifluoroacetates

Benzyl 2-bromo-2,2-difluoroacetate (94b)

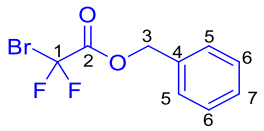

Prepared according to general procedure A using benzyl alcohol (104 µL, 1.00 mmol, 1.00 eq.), triethylamine (279 µL, 2.00 mmol, 2.00 eq.) and bromodifluoroacetyl chloride (188 µL, 2.00 mmol, 2.00 eq.). The crude material was purified by flash column chromatography (SiO_2, pentane/EtOAc, 9:1) to give the title compound **94b** (152 mg, 0.573 mmol, 57%) as a colourless oil. R_f = 0.80 (pentane/EtOAc, 9:1), υ_{max}/cm^{-1} (ATR) 3092, 3068, 3036, 2964, 2926, 2857, 1774, 1498; ^{1}H NMR (400 MHz, $CDCl_3$) δ 7.41 (5H, m, H-5-7), 5.36 (2H, s, H-3); ^{13}C {^{1}H} NMR (101 MHz, $CDCl_3$) δ 159.6 (C, t, *J* = 31.5 Hz, C-2), 133.6 (C, C-4), 129.3 (CH, C-7), 129.0 (2 × CH, C-6), 128.7 (2 × CH, C-5), 108.9 (C, t, *J* = 314 Hz, C-1), 69.9 (CH_2, C-3); ^{19}F NMR (376 MHz, $CDCl_3$) δ −60.7 (2F, s, F–1); HRMS (EIMS, 70 eV) m/z: $[M]^+$ Calcd for $C_9H_7{}^{79}BrF_2O_2$ 263.95920; Found: 263.9594 (0.6 ppm error). Characterization data were in accordance with those previously reported.[4]

4-Bromobenzyl 2-bromo-2,2-difluoroacetate (94c)

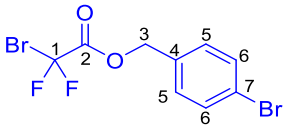

Prepared according to general procedure A using 4-bromo benzyl alcohol (187 µL, 1.00 mmol, 1.00 eq.), triethylamine (279 µL, 2.00 mmol, 2.00 eq.) and bromodifluoroacetyl chloride (188 µL, 2.00 mmol, 2.00 eq.). The crude material was purified by flash column chromatography (SiO_2, pentane/EtOAc, 9:1) to give the title compound **94c** (167 mg, 0.485 mmol, 49%) as a colourless oil; R_f = 0.93 (pentane/EtOAc, 9:1), υ_{max}/cm^{-1} (ATR) 2964, 2928, 2895, 2854, 1773, 1595, 1490; ^{1}H NMR (400 MHz, $CDCl_3$) δ 7.54 (2H, ddd, *J* = 8.4, 2.3, 1.8 Hz, H-6, H-6′), 7.28 (2H, ddd, *J* = 8.4, 2.3, 1.8 Hz, H-5, H-5′), 5.31 (2H, s, H-3); ^{13}C {^{1}H} NMR (101 MHz, $CDCl_3$) δ

159.5 (C, t, *J* = 31.6 Hz, C-2), 132.5 (C, C-4), 132.2 (2 × CH, C-6), 130.3 (2 × CH, C-5), 123.6 (C, C-7), 108.7 (C, t, *J* = 314 Hz, C-1), 69.0 (CH_2, C-3); ^{19}F NMR (376 MHz, $CDCl_3$) δ −60.8 (2F, s, F-1); HRMS (EIMS, 70 eV) m/z: $[M]^+$ Calcd for $C_9H_6{}^{79}Br_2F_2O_2$ 341.8684; Found: 341.8697 (3.7 ppm error).

2,5,8,11,14,17,20,23-Octaoxapentacosan-25-yl 2-bromo-2,2-difluoroacetate (94d)

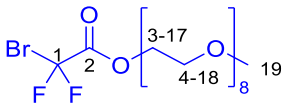

Prepared according to general procedure A using 2,5,8,11,14,17,20,23-octaoxapentacosan-25-ol (353 µL, 1.00 mmol, 1.00 eq.), triethylamine (279 µL, 2.00 mmol, 2.00 eq.) and bromodifluoroacetyl chloride (188 µL, 2.00 mmol, 2.00 eq.). The crude material was purified by flash column chromatography (SiO_2, DCM/MeOH, 95:5) to give the title compound **94d** (237 mg, 0.439 mmol, 44%) as a yellow oil; R_f = 0.46 (DCM/MeOH, 95:5), υ_{max}/cm^{-1} (ATR) 2913, 2870, 1774, 1740, 1579, 1452; ^{1}H NMR (400 MHz, $CDCl_3$) δ 4.52 – 4.45 (2H, m, H-3), 3.82 – 3.76 (2H, m, H-4), 3.70 – 3.60 (26H, m, OCH_2CH_2O), 3.57 – 3.51 (2H, m, H-X), 3.37 (3H, s, H-19); ^{13}C {^{1}H} NMR (101 MHz, $CDCl_3$) δ 159.7 (C, t, *J* = 31.3 Hz, C-2), 108.8 (C, t, *J* = 314 Hz, C-1), 72.1 (CH_2, C-X), 71.0 (CH_2, C-PEG), 70.8 (CH_2, C-PEG), 70.7 (CH_2, C-PEG), 70.7 (9 × CH_2, C-PEG), 70.7 (CH_2, C-PEG), 68.4 (CH_2, C-4), 67.3 (CH_2, C-3), 59.2 (CH_3, C-19); ^{19}F NMR (376 MHz, $CDCl_3$) δ −60.7 (2F, s, F-1); HRMS (ESI) m/z: $[M + Na]^+$ Calcd for $C_{19}H_{35}{}^{79}BrF_2NaO_{10}$ 563.1274; Found 563.1267 (1.2 ppm error).

Hex-5-yn-1-yl 2-bromo-2,2-difluoroacetate (94e)

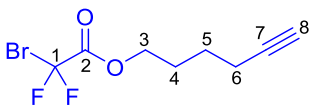

Prepared according to general procedure A using 5-hexyn-1-ol (110 µL, 1.00 mmol, 1.00 eq.), triethylamine (279 µL, 2.00 mmol, 2.00 eq.) and bromodifluoroacetyl chloride (188 µL, 2.00 mmol, 2.00 eq.). The crude material was purified by flash column chromatography (SiO_2, pentane/EtOAc, 9:1) to give the title compound **94e** (158 mg, 0.620 mmol,

62%) as a pale yellow oil; R_f = 0.87 (pentane/EtOAc, 9:1), υ_{max}/cm^{-1} (ATR) 3305, 2939, 2870, 2117, 1773; ^{1}H NMR (400 MHz, $CDCl_3$) δ 4.39 (2H, t, *J* = 6.4 Hz, H-3), 2.27 (2H, td, *J* = 6.9, 2.6 Hz, H-6), 1.98 (1H, t, *J* = 2.6 Hz, H-8), 1.96 – 1.84 (2H, m, H-4), 1.71 – 1.61 (2H, m, H-5); ^{13}C {^{1}H} NMR (101 MHz, $CDCl_3$) δ 160.1 (C, t, *J* = 31.3 Hz, C-2), 109.2 (C, t, *J* = 314 Hz, C-1), 83.8 (C, C-7), 69.5 (CH, C-8), 68.3 (CH_2, C-3), 27.6 (CH_2, C-4), 24.9 (CH_2, C-5), 18.4 (CH_2, C-6); ^{19}F NMR (376 MHz, $CDCl_3$) δ −60.7 (2F, s, F-1); HRMS (ESI) m/z: [carboxylate fragment]$^-$ Cacld for $^{79}BrCF_2CO_2$ 172.9055; Found 172.9069 (8.1 ppm error).

Methyl *O*-(2-bromo-2,2-difluoroacetyl)-*N*-(*tert*-butoxycarbonyl)-D-serinate (94f)

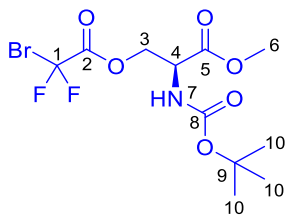

Prepared according to general procedure A using *N*Boc-D-Ser-OMe (219 mg, 1.00 mmol, 1.00 equiv.). The crude material was purified by flash column chromatography (SiO_2, pentane/EtOAc, 9:1) to give the title compound **94f** (130 mg, 0.344 mmol, 35%) as a pale yellow oil; R_f = 0.35 (pentane/EtOAc, 9:1), υ_{max}/cm^{-1} (ATR) 3389, 2979, 2959, 2937, 1781, 1746, 1689; ^{1}H NMR (400 MHz, $CDCl_3$) δ 5.32 (1H, d, *J* = 5.4 Hz, H-7), 4.79 – 4.54 (3H, m, H-3, H-4), 3.81 (3H, s, H-6), 1.46 (9H, s, H-10); ^{13}C {^{1}H} NMR (101 MHz, $CDCl_3$) δ 169.3 (C, C-5), 159.2 (C, t, *J* = 31.9 Hz, C-2), 155.1 (C, C-8), 108.3 (C, t, *J* = 315 Hz, C-1), 81.0 (C, C-9), 67.5 (CH_2, C-3), 53.3 (CH_3, C-6), 52.8 (CH, C-4), 28.4 (CH_3, C-10); ^{19}F NMR (377 MHz, $CDCl_3$) δ −60.8 (F-1); HRMS (ESI) m/z: [M + Na]$^+$ Calcd for $C_{11}H_{16}{}^{79}BrF_2NNaO_6$ 398.0021; Found 398.0024 (0.8 ppm error).

2-((*tert*-Butoxycarbonyl)amino)ethyl 2-bromo-2,2-difluoroacetate (94g)

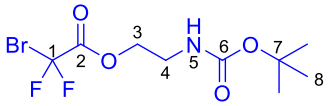

Prepared according to general procedure A (2 × the scale) using *N*-Boc ethanolamine (309 µL, 2.00 mmol, 2.00 equiv.). The crude material was purified by flash column chromatography (SiO_2, pentane/EtOAc, 9:1) to give the title compound **94g** (509 mg, 1.60 mmol, 80%) as a pale yellow oil; R_f = 0.32 (pentane/EtOAc, 9:1), υ_{max}/cm^{-1} (ATR) 3337, 2979, 2933, 1776, 1685; ^{1}H NMR (400 MHz, $CDCl_3$) δ 4.81 (1H, s, H-5), 4.41 (2H, t, *J* = 5.3 Hz, H-3), 3.50 (2H, dt, *J* = 5.3, 4.9 Hz, H-4), 1.45 (9H, s, H-8); ^{13}C {^{1}H} NMR (101 MHz, $CDCl_3$) δ 159.66 (C, t, *J* = 31.9 Hz, C-2), 155.87 (C, C-6), 108.63 (C, t, *J* = 314 Hz, C-1), 80.32 (C, C-7), 67.44 (CH_2, C-3), 39.31 (CH_2, C-4), 28.45 (CH_3, C-8); ^{19}F NMR (376 MHz, $CDCl_3$) δ −60.8 (F-1); HRMS (ESI) m/z: [M + Na]$^+$ Calcd for $C_9H_{14}{}^{79}BrF_2NNaO_4$ 339.9966; Found 339.9969 (0.9 ppm error).

2-Bromo-*N*-cyclopropyl-2,2-difluoroacetamide (94h)

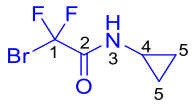

Prepared according to general procedure B using cyclopropylamine (187 µL, 2.70 mmol, 1.00 eq.), $BrCF_2CO_2Et$ **94a** (417 µL, 3.24 mmol, 1.20 eq.) and $La(OTf)_3$ (79.2 mg, 135 µmol, 5 mol%). The crude material was purified by flash column chromatography (SiO_2, pentane/EtOAc, 9:1) to give the title compound **94h** (469 mg, 2.19 mmol, 81%) as a colourless crystalline solid. Mp 60-62 °C; R_f = 0.37 (pentane/EtOAc, 9:1); υ_{max}/cm^{-1} (ATR) 3241, 3064, 2845, 1706, 1682, 1547; ^1H NMR (400 MHz, $CDCl_3$) δ 6.45 (1H, s, H-3), 2.95 – 2.50 (1H, m, H-4), 0.94 – 0.79 (2H, m, H-5), 0.72 – 0.58 (2H, m, H-5); ^{13}C {^1H} NMR (101 MHz, $CDCl_3$) δ 161.3 (C, t, *J* = 27.2 Hz, C-2), 111.8 (C, t, *J* = 317 Hz, C-1), 23.2 (CH, C-4), 6.7 (CH, C-5); ^{19}F NMR (376 MHz, $CDCl_3$) δ −60.6 (2F, s, F-1); HRMS (ESI) m/z: $[M + Na]^+$ Calcd for $C_5H_6{}^{79}BrF_2NNaO$ 235.9493; Found 235.9486 (3.0 ppm error). Characterization data were in accordance with those previously reported.[5]

2-Bromo-*N*-benzyl-2,2-difluoroacetamide (94i)

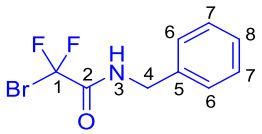

Prepared according to general procedure B using benzylamine (98.3 µL, 0.900 mmol, 1.00 eq.), $BrCF_2CO_2Et$ **94a** (139 µL, 1.08 mmol, 1.20 eq.) and $La(OTf)_3$ (26.4 mg, 45.0 µmol, 5 mol%). The crude material was purified by flash column chromatography (SiO_2, pentane/EtOAc, 9:1) to give the title compound **94i** (199 mg, 0.75 mmol, 84%) as a colourless crystalline solid. R_f = 0.42 (pentane/EtOAc, 9:1); Mp 38-40 °C (lit.[210] 44-45 °C); υ_{max}/cm^{-1} (ATR) 3316, 3244, 3067, 3034, 2957, 2929, 2855, 1687, 1543; ^1H NMR (400 MHz, $CDCl_3$) δ 7.44 – 7.27 (5H, m, H-6, H-7, H-8), 6.56 (1H, s, H-3), 4.53 (2H, d, *J* = 5.8 Hz, H-4); ^{13}C {^1H} NMR (101 MHz, $CDCl_3$) δ 160.1 (C, t, *J* = 27.5 Hz, C-2), 136.2 (C, C-5), 129.2 (CH, C-7), 128.4 (CH, C-8), 128.0 (CH, C-6), 111.9 (C, t, *J* = 316 Hz, C-1), 44.3 (CH_2, C-4); ^{19}F NMR

(376 MHz, $CDCl_3$) δ −60.5 (2F, s, F-1); HRMS (ESI) m/z: $[M + H]^+$ Calcd for $C_9H_9{}^{79}BrF_2NO$ 263.9830; Found 263.9832 (0.8 ppm error). Characterization data were in accordance with those previously reported.[6]

2-Bromo-2,2-difluoro-*N*-(pyridin-3-ylmethyl)acetamide (94j)

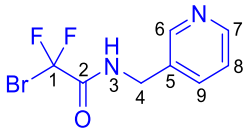

Prepared according to general procedure B using 3-picolylamine (91.6 µL, 0.900 mmol, 1.00 eq.), $BrCF_2CO_2Et$ **94a** (139 µL, 1.08 mmol, 1.20 eq.) and $La(OTf)_3$ (26.4 mg, 45.0 µmol, 5 mol%). The crude material was purified by flash column chromatography (SiO_2, EtOAc) to give the title compound **94j** (80.2 mg, 0.303 mmol, 34%) as a colourless crystalline solid; R_f = 0.34 (EtOAc); mp 73-75 °C; υ_{max}/cm^{-1} (ATR) 3169, 2923, 2851, 2817, 1701, 1559; ^1H NMR (400 MHz, $CDCl_3$) δ 8.50 (1H, dd, *J* = 4.9, 2.0 Hz, H-7), 8.45 (1H, d, *J* = 2.1 Hz, H-6), 7.66 (1H, ddd, *J* = 7.8, 2.1 Hz, H-9), 7.58 (1H, s, H-3), 7.30 (1H, dd, *J* = 7.9, 4.8 Hz, H-8), 4.53 (2H, d, *J* = 6.0 Hz, H-4); $^{13}C\ \{^1H\}$ NMR (101 MHz, $CDCl_3$) δ 160.5 (C, t, *J* = 27.9 Hz, C-2), 149.4 (CH, C-7), 149.1 (CH, C-6), 136.0 (CH, C-9), 132.4 (C, C-4), 124.1 (CH, C-6), 111.7 (C, t, *J* = 316 Hz, C-1), 41.6 (CH_2, C-4); ^{19}F NMR (377 MHz, $CDCl_3$) δ −60.6 (2F, s, F-1); HRMS (ESI) m/z: $[M + H]^+$ Calcd for $C_8H_8{}^{79}BrF_2N_2O$ 264.9783; Found 264.9785 (0.8 ppm error).

2-Bromo-*N*-(*tert*-butyl)-2,2-difluoroacetamide (94k)

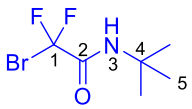

Prepared according to general procedure B using *tert*-butylamine (94.6 µL, 0.900 mmol, 1.00 eq.), $BrCF_2CO_2Et$ **94a** (139 µL, 1.08 mmol, 1.20 eq.) and $La(OTf)_3$ (26.4 mg, 45.0 µmol, 5 mol%). The crude material was purified by flash column chromatography (SiO_2, pentane/EtOAc, 9:1) to give the title compound **94k** (111 mg, 0.483 mmol, 54%) as a colourless crystalline solid. Rf = 0.71 (pentane/EtOAc, 9:1); Mp 53-55 °C; υ_{max}/cm^{-1} (ATR) 3340, 3322, 3056, 2977, 2938, 2921, 2875, 2851, 1710, 1695, 1535; ^1H NMR (400 MHz, $CDCl_3$) δ 5.97 (1H, s, H-3), 1.41 (9H, s, H-5); $^{13}C\ \{^1H\}$ NMR (101

MHz, $CDCl_3$) δ 158.9 (C, t, *J* = 26.3 Hz, C-2), 112.2 (C, t, *J* = 318 Hz, C-1), 52.9 (C, C-4), 28.3 (CH_3, C-5); ^{19}F NMR (376 MHz, $CDCl_3$) δ −60.3 (2F, s, F-1); HRMS (ESI) m/z: $[M + H]^+$ Calcd for $C_6H_{11}{}^{79}BrF_2NO$ 229.9987; Found 229.9985 (3.0 ppm error). Characterization data were in accordance with those previously reported.[5]

2-Bromo-2,2-difluoro-1-morpholinoethan-1-one (94l)

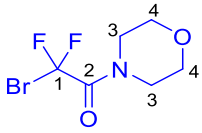

Prepared according to general procedure B using morpholine (78.7 µL, 0.900 mmol, 1.00 eq.), $BrCF_2CO_2Et$ **94a** (139 µL, 1.08 mmol, 1.20 eq.) and $La(OTf)_3$ (26.4 mg, 45.0 µmol, 5 mol%). The crude material was purified by flash column chromatography (SiO_2, pentane/EtOAc, 4:1) to give the title compound **94l** (129 mg, 0.526 mmol, 59%) as a colourless liquid. R_f = 0.55 (pentane/EtOAc, 4:1); υ_{max}/cm^{-1} (ATR) 2970, 2925, 2859, 1680; ^1H NMR (400 MHz, $CDCl_3$) δ 3.83 – 3.72 (4H, m, H-3 or H-4), 3.72 – 3.64 (4H, m, H-3 or H-4); ^{13}C {^1H} NMR (101 MHz, $CDCl_3$) δ 158.0 (C, t, *J* = 26.6 Hz, C-2), 110.6 (C, t, *J* = 314 Hz, C-1), 66.6 (CH), 66.2 (CH), 47.4 (CH, t, *J* = 4.0 Hz), 44.0 (CH); ^{19}F NMR (376 MHz, $CDCl_3$) δ −54.5 (2F, s, F-1); [HRMS (ESI) Exact mass calcd. for $C_6H_8{}^{79}BrF_2NNaO_2$ $[M + Na]^+$: 265.9598; found: 265.9600 (0.8 ppm error)]. Characterization data were in accordance with those previously reported.[5]

Methyl 5-((3a*S*,4*S*,6a*R*)-2-oxohexahydro-1*H*-thieno[3,4-d]imidazol-4-yl)pentanoate (Biotin-OMe, 134)

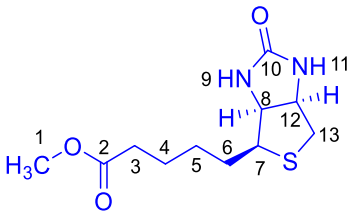

Biotin-OMe **134** was prepared according to previous reports.[7] To methanol (10 mL) cooled to 0 °C was added acetyl chloride (1.46 mL, 20.5 mmol, 5.01 eq.) dropwise. This was stirred for 5 min before a suspension of biotin (1.0 g, 4.09 mmol, 1.00 eq.) in methanol (10 mL) was added dropwise at 0 °C. The resulting solution was stirred for 1 hour whilst warming to room

temperature to give a colourless solution. The reaction mixture was concentrated *in vacuo*, then redissolved in 2% methanol in DCM (50 mL). This solution was extracted with sat. aq. $NaHCO_3$ (3 x 10 mL), water (10 mL) and brine (10 mL), dried over $MgSO_4$ and concentrated *in vacuo* to give the title compound **134** (594 mg, 2.30 mmol, 56% yield) as a colourless solid. ^{1}H NMR (400 MHz, DMSO-d_6) δ 6.43 (1H, s, H-9/11), 6.36 (1H, s, H-9/11), 4.33 – 4.27 (1H, m, H-8), 4.18 – 4.07 (1H, m, H-7), 3.58 (3H, s, H-1), 3.14 – 3.05 (1H, m, H-12), 2.82 (1H, dd, *J* = 12.4, 5.1 Hz, H-13), 2.57 (1H, d, *J* = 12.4 Hz, H-13), 2.30 (2H, t, *J* = 7.4 Hz), 1.68 – 1.24 (6H, m); HRMS (ESI) m/z: $[M + Na]^+$ Calcd for $C_{11}H_{18}N_2O_3SNa$; Found 281.0929 (2.5 ppm error). Characterization data were in accordance with those previously reported.[7] Biotin-OMe **134** was an intermediate species, carried through to the next step to synthesise biotin-EDA **136**.

N-(2-aminoethyl)-5-((3a*S*,4*S*,6a*R*)-2-oxohexahydro-1*H*-thieno[3,4-d]imidazol-4-yl)pentanamide (Biotin-EDA, 136)

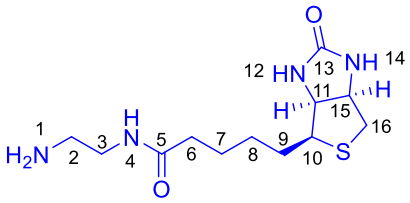

Biotin-EDA **136** was prepared according to previous reports.[7] To Biotin-OMe **134** (588 mg, 2.28 mmol, 1.00 eq.) in methanol (25 mL) was added ethylenediamine (3.80 mL, 57.0 mmol, 25.0 eq.). The resulting precipitate was stirred at 60 °C (heating mantle) for 16 h. The reaction mixture was concentrated *in vacuo*, with excess ethylenediamine being co-evaporated with toluene (3 x 20 mL). The resulting solid was washed with ethyl acetate (3 x 25 mL) and dried in vacuo to give the title compound **136** (636 mg, 2.22 mmol, 97% yield) as an off-white solid. ^{1}H NMR (400 MHz, DMSO-d_6) δ 7.78 (1H, t, *J* = 5.9 Hz, H-4), 6.43 (1H, s, H-12/14), 6.36 (1H, s, H-12/14), 4.30 (1H, dd, *J* = 7.6, 5.0 Hz, H-11), 4.16 – 4.08 (1H, m, H-10), 3.16 – 3.06 (1H, m, H-15), 3.03 (q, 2H, *J* = 5.9 Hz, H-3), 2.82 (1H, dd, *J* = 12.4, 5.1 Hz, H-16), 2.60 (1H, d, *J* = 12.4 Hz, H-16), 2.61 – 2.51 (m, 2H, H-2), 2.06 (2H, t, *J* = 7.4 Hz), 1.73 – 1.13 (6H, m); HRMS (ESI) m/z: $[M + H]^+$ Calcd for $C_{12}H_{23}N_4O_2S$ 287.1542; Found 287.1546 (1.4 ppm error). Characterization data were in accordance with those previously reported.[7]

Biotin-EDA **136** was an intermediate species, carried through to the next step to synthesise biotin probe **94m**.

_N_-(2-(2-bromo-2,2-difluoroacetamido)ethyl)-5-((3a_S_,4_S_,6a_R_)-2-oxohexahydro-1_H_-thieno[3,4-d]imidazol-4-yl)pentanamide (94m)

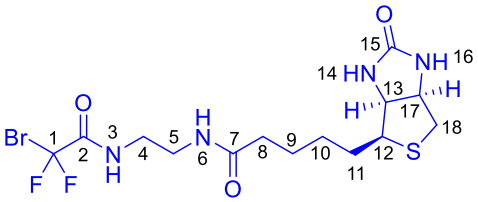

Prepared according to general procedure A using Biotin-NH_2 **136** (623 mg, 2.18 mmol, 1.00 eq.), bromodifluoroacetyl chloride (410 µL, 4.35 mmol, 2.00 eq.) and triethylamine (606 µL, 4.35 mmol, 2.00 eq.). The crude material was purified by preparative HPLC (2 – 95% B ov. 30 min) to give the title compound **94m** (504 mg, 1.14 mmol, 52%) as a colourless solid; mp = 175-177 °C; υ_{max}/cm^{-1} (ATR) 3289, 3080, 2932, 2863, 1694, 1649, 1550; ^{1}H NMR (400 MHz, DMSO-d_6) δ 9.16 (1H, t, J = 5.3 Hz, H-3), 7.90 (1H, t, J = 5.5 Hz, H-6), 6.41 (1H, s, H-14/16), 6.35 (1H, s, H-14/16), 4.30 (1H, dd, J = 7.8, 5.0 Hz, H-13), 4.16 – 4.08 (1H, m, H-12), 3.24 – 3.13 (4H, m, H-4, H-5), 3.13 – 3.02 (1H, m, H-17), 2.82 (1H, dd, J = 12.4, 5.0 Hz, H-18), 2.57 (1H, d, J = 12.4 Hz, H-18), 2.05 (2H, t, J = 7.4 Hz), 1.70 – 1.21 (6H, m); ^{13}C {^{1}H} NMR (101 MHz, DMSO-d_6) δ 173.0 (C, C-7), 163.2 (C, C-15), 160.2 (C, t, J = 27.1 Hz, C-2), 112.4 (C, t, J = 315.1 Hz, C-1), 61.5 (CH, C-12), 59.7 (CH, C-13), 55.9 (CH, C-17), 40.3 (CH_2, C-18), 39.6 (CH_2), 37.9 (CH_2), 35.7 (CH_2), 28.7 (CH_2), 28.5 (CH_2), 25.6 (CH_2); ^{19}F NMR (376 MHz, DMSO-d_6) δ −60.0 (s, 2F), −74.9 (s, TFA); HRMS (ESI) m/z: [M + H]$^+$ Cacld for $C_{14}H_{22}{}^{79}BrF_2N_4O_3S$ 443.0564; Found 443.0567 (0.7 ppm error).

***N*-((2*R*,3*R*,4*R*,5*S*,6*R*)-3-acetamido-4,5-dihydroxy-6-(hydroxymethyl)tetrahydro-2*H*-pyran-2-yl)-2-bromo-2,2-difluoroacetamide (94n)**

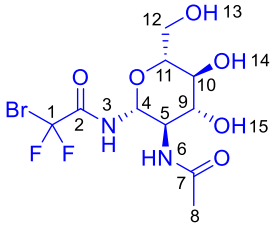

Prepared according to general procedure A using 2-acetamido-2-deoxy-beta-D-glucopyranosylamine (220 mg, 1.00 mmol, 1.00 eq.), triethylamine (140 µL, 1.00 mmol, 1.00 eq.) and bromodifluoroacetyl chloride (188 µL, 2.00 mmol, 2.00 eq.). The crude material was purified by preparative HPLC (2 – 95% B ov. 30 min then 2 – 70% B ov. 30 min) to give the title compound **94n** (23.6 mg, 0.063 mmol, 6%) as a colourless solid; mp = 208 - 210 °C (decomposed); υ_{max}/cm^{-1} (ATR) 3361, 3281, 3080, 2953, 2928, 2873, 2852, 1213, 1659, 1539; ^{1}H NMR (400 MHz, DMSO-d_6) δ 9.50 (1H, d, *J* = 8.8 Hz, H-3), 7.90 (1H, d, *J* = 8.5 Hz, H-6), 5.09 – 5.03 (2H, m, H-14, H-15), 4.86 (1H, t, *J* = 8.8 Hz, H-4), 4.71 – 4.49 (1H, m, H-13), 3.73 – 3.59 (2H, m, H-5, H-12), 3.49 – 3.35 (2H, m, H-9, H-12), 3.23 – 3.14 (1H, m, H-11), 3.13 – 3.04 (1H, m, H-10), 1.80 (3H, s, H-8); ^{13}C NMR {^{1}H} (126 MHz, DMSO-d_6) δ 170.2 (C, C-7), 159.7 (C, t, *J* = 27.9 Hz, C-2), 111.3 (C, t, *J* = 314.3 Hz, C-1), 79.8 (CH, C-4), 79.3 (CH, C-11), 74.0 (CH, C-9), 70.3 (CH, C-10), 60.8 (CH_2, C-12), 54.4 (CH, C-5), 22.8 (CH_3, C-8); ^{19}F NMR (376 MHz, DMSO-d_6) δ −61.1 (1F, d, *J* = 158.0 Hz), −61.5 (1F, d, *J* = 158.0 Hz); HRMS (ESI) m/z: [M + Na]$^{+}$ Calcd for $C_{10}H_{15}{}^{79}BrF_2N_2O_6Na$ 398.9979; Found 398.9975 (1.00 ppm error).

6.3 Biomolecule Synthesis

Ac-WHISKEY-NH_2 (163)

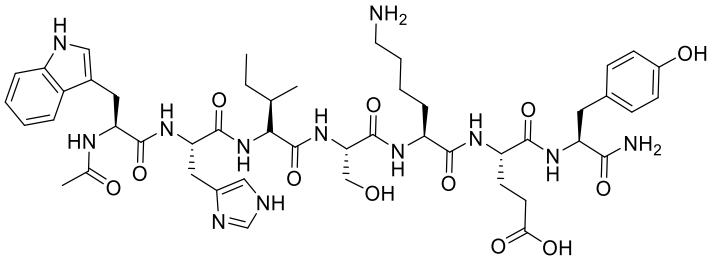

Prepared using rink amide resin and SPPS (250 µmol). The crude peptide was cleaved from the resin using mixture of TFA, TIPS and water (90:5:5 v/v/v) and purified by preparative RP-HPLC (2-95% B over 30 min) to give the title compound **163** (50.0 mg, 49.9 µmol, 20%) as a colourless powder; ^{1}H NMR (400 MHz, CD_3OD) δ 8.70 (d, 1H, *J* = 1.4 Hz), 7.51 (d, 1H, *J* = 7.9 Hz), 7.32 (d, 1H, *J* = 8.1 Hz), 7.22 (d, 1H, *J* = 1.4 Hz), 7.14 (s, 1H), 7.08 (dd, 1H, *J* = 8.1, 7.6 Hz), 7.03 – 6.94 (m, 3H), 6.67 (d, 2H, *J* = 8.4 Hz), 4.65 (dd, 1H, *J* = 7.2, 5.5 Hz), 4.56 (dd, 1H, *J* = 8.2, 6.1 Hz), 4.51 – 4.42 (m, 2H), 4.42 – 4.29 (m, 2H), 4.23 (d, 1H, *J* = 7.4 Hz), 3.88 (dd, 1H, *J* = 10.9, 5.5 Hz), 3.79 (dd, 1H, *J* = 10.9, 5.9 Hz), 3.30 – 2.95 (m, 5H), 2.91 – 2.81 (m, 2H), 2.77 – 2.67 (m, 1H), 2.40 – 2.22 (m, 2H), 2.07 – 1.95 (m, 1H), 1.94 (s, 3H), 1.92 – 1.82 (m, 3H), 1.79 – 1.67 (m, 1H), 1.67 – 1.57 (m, 2H), 1.57 – 1.49 (m, 1H), 1.49 – 1.36 (m, 2H), 1.26 – 1.12 (m, 1H), 0.96 (d, 3H, *J* = 6.8 Hz), 0.91 (t, 3H, *J* = 7.4 Hz); HRMS (ESI) m/z: $[M + H]^+$ Calcd for $C_{48}H_{67}N_{12}O_{12}$ 1003.4996; Found 1003.5022 (2.6 ppm error).

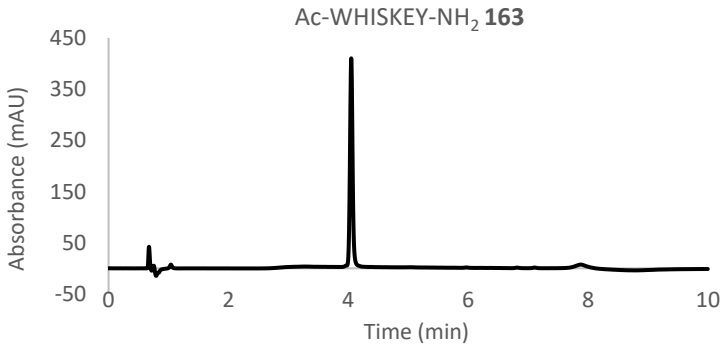

Figure 119. Analytical HPLC chromatogram for purified Ac-WHISKEY-NH_2 **163** Rt = 4.04 min on analytical gradient 2-95% B over 5 min, 0.6 mL min^{-1}, 280 nm.

Ac-HISKEY-NH$_2$ (172)

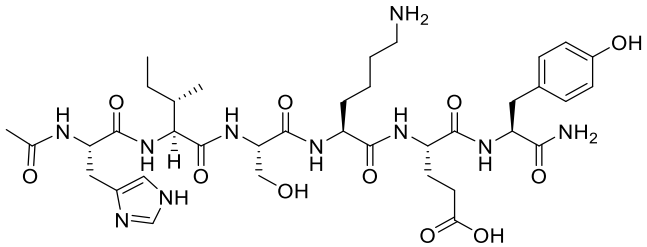

Prepared using rink amide resin and SPPS (200 µmol). The crude peptide was cleaved from the resin using mixture of TFA, TIPS and water (90:5:5 v/v/v) and purified by preparative RP-HPLC (2-70% B over 30 min) to give the title compound **172** (72.4 mg, 88.6 µmol, 44%) as a colourless powder; ^{1}H NMR (400 MHz, CD_3OD) δ 8.77 (d, 1H, *J* = 1.4 Hz), 7.33 (d, 1H, *J* = 1.4 Hz), 7.07 (d, 2H, *J* = 8.5 Hz), 6.69 (d, 2H, *J* = 8.6 Hz), 4.73 (dd, 1H, *J* = 7.5, 6.9 Hz), 4.51 (dd, 1H, *J* = 8.5, 5.6 Hz), 4.45 (dd, 1H, *J* = 6.1, 5.7 Hz) 4.33 – 4.25 (m, 2H), 4.22 (d, 1H, *J* = 7.4 Hz), 3.89 (dd, 1H, *J* = 10.9, 5.7 Hz), 3.79 (dd, 1H, *J* = 10.9, 6.1 Hz), 3.24 (dd, 1H, *J* = 15.3, 6.7 Hz), 3.13 – 3.02 (m, 2H), 2.92 (dd, *J* = 8.5, 7.5 Hz, 2H), 2.86 (dd, 1H, *J* = 14.0, 8.6 Hz), 2.41 – 2.23 (m, 2H), 2.07 – 1.99 (m, 1H), 1.98 (s, 3H), 1.94 – 1.80 (m, 3H), 1.80 – 1.63 (m, 3H), 1.62 – 1.40 (m, 3H), 1.28 – 1.12 (m, 1H), 0.95 (d, 3H, *J* = 6.8 Hz), 0.91 (t, 3H, *J* = 7.4 Hz); HRMS (ESI) m/z: [M + H]$^+$ Calcd for $C_{37}H_{57}N_{10}O_{11}$ 817.4208; Found 817.4168 (4.9 ppm error).

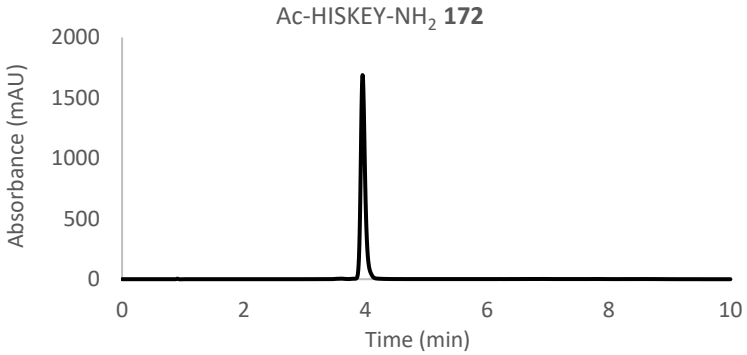

Figure 120. Analytical HPLC chromatogram for purified Ac-HISKEY-NH$_2$ **172** Rt = 3.95 min on analytical gradient 2-70% B over 5 min, 0.6 mL min^{-1}, 280 nm.

Ac-CWHISKEY-NH_2 (175)

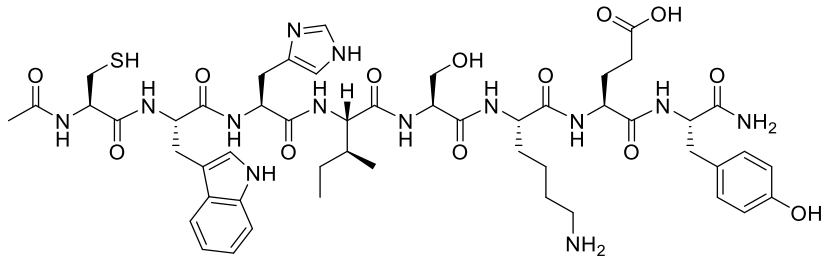

Prepared using rink amide resin and SPPS (250 µmol). The crude peptide was cleaved from the resin using mixture of TFA, TIPS, thioanisole and water (85:5:5:5 v/v/v) and purified by preparative RP-HPLC (2-95% B over 30 min) to give the title compound **175** (48.6 mg, 43.9 µmol, 18%) as a colourless powder; ^{1}H NMR (400 MHz, CD_3OD) δ 8.72 (s, 1H), 7.52 (d, 1H, *J* = 7.7 Hz), 7.35 (d, 1H, *J* = 8.1 Hz), 7.17 (s, 1H), 7.14 (s, 1H), 7.13 – 7.04 (m, 3H), 7.01 (dd, 1H, *J* = 7.7, 7.3 Hz), 6.69 (d, 2H, *J* = 8.1 Hz), 4.61 (dd, 2H, J = 8.1, 6.6 Hz), 4.50 (dd, 1H, *J* = 8.8, 5.5 Hz), 4.42 (t, 1H, J = 5.7 Hz), 4.36 – 4.22 (m, 3H), 4.15 (d, 1H, *J* = 7.7 Hz), 3.91 (dd, 1H, *J* = 11.0, 5.7 Hz), 3.82 (dd, 1H, *J* = 11.0, 5.7 Hz), 3.27 – 3.15 (m, 3H), 3.12 – 2.98 (m, 2H), 2.97 – 2.67 (m, 5H), 2.39 – 2.26 (m, 2H), 2.07 – 1.80 (m, 7H), 1.80 – 1.71 (m, 1H), 1.71 – 1.59 (m, 2H), 1.59 – 1.51 (m, 1H), 1.50 – 1.39 (m, 2H), 1.24 – 1.16 (m, 1H), 0.96 (d, 3H, *J* = 6.8 Hz), 0.91 (t, 3H, *J* = 7.4 Hz); HRMS (ESI) m/z: $[M + H]^+$ Calcd for $C_{51}H_{71}N_{12}O_{14}S$ 1107.4933; Found 1107.4940 (0.6 ppm error).

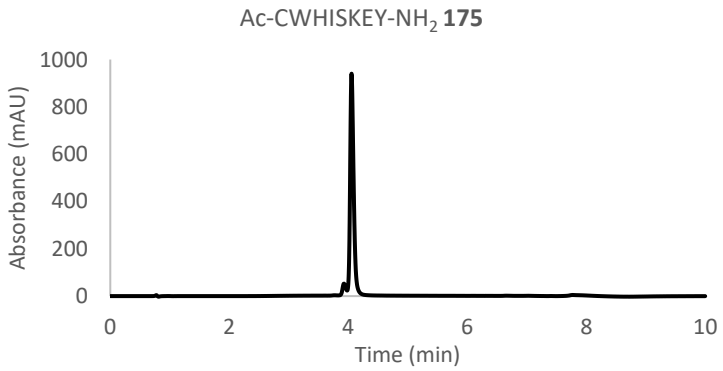

Figure 121. Analytical HPLC chromatogram for purified Ac-CWHISKEY-NH_2 **175** Rt = 4.06 min on analytical gradient 10-70% B over 5 min, 0.6 mL min^{-1}, 280 nm.

H-WHISKEY-OH (176)

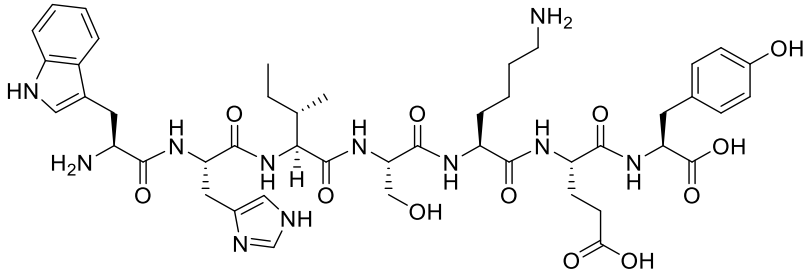

Prepared using 2-chlorotrityl chloride resin and SPPS (250 µmol). The crude peptide was cleaved from the resin using mixture of TFA, TIPS and water (90:5:5 v/v/v) and purified by preparative RP-HPLC (10-80% B over 30 min) to give the title compound **176** (74.6 mg, 77.5 µmol, 31%) as a colourless powder; ^{1}H NMR (400 MHz, CD_3OD) δ 8.60 (s, 1H), 7.63 (d, 1H, *J* = 7.9 Hz), 7.38 (d, 1H, *J* = 8.1 Hz), 7.27 (s, 1H), 7.20 (s, 1H), 7.14 (dd, 1H, *J* = 8.1, 7.3 Hz), 7.10 – 7.01 (m, 3H), 6.77 – 6.65 (m, 2H), 4.75 (dd, 1H, *J* = 7.4, 6.5 Hz), 4.54 – 4.44 (m, 2H), 4.34 – 4.26 (m, 2H), 4.25 – 4.17 (m, 2H), 3.88 (dd, 1H, *J* = 10.9, 5.6 Hz), 3.81 (dd, 1H, *J* = 10.9, 6.0 Hz), 3.41 (dd, 1H, *J* = 15.0, 5.6 Hz), 3.29 – 2.99 (m, 4H), 2.94 – 2.81 (m, 3H), 2.42 – 2.24 (m, 2H), 2.10 – 1.97 (m, 1H), 1.96 – 1.81 (m, 3H), 1.80 – 1.61 (m, 3H), 1.61 – 1.51 (m, 1H), 1.51 – 1.38 (m, 2H), 1.31 – 1.14 (m, 1H), 0.96 (d, 3H, *J* = 6.9 Hz), 0.93 (t, 3H, *J* = 7.5 Hz); HRMS (ESI) m/z: $[M + H]^+$ Calcd for $C_{46}H_{64}N_{11}O_{12}$ 962.4736; Found 962.4805 (7.2 ppm error).

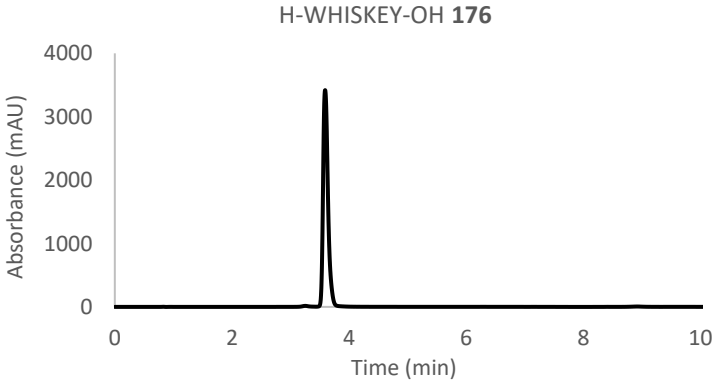

Figure 122. Analytical HPLC chromatogram for purified H-WHISKEY-OH **176** Rt = 3.59 min on analytical gradient 10-80% B over 5 min, 0.6 mL min^{-1}, 280 nm.

Ac-WLAHKAL-NH_2 (179)

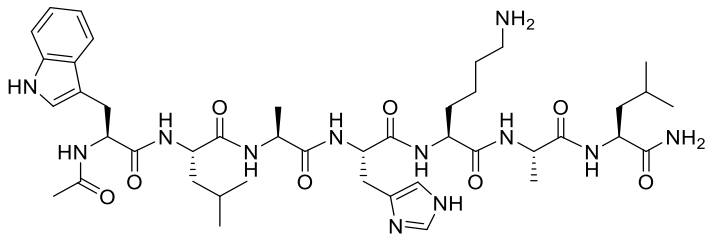

Prepared using rink amide resin and SPPS (250 µmol). The crude peptide was cleaved from the resin using mixture of TFA, TIPS and water (90:5:5 v/v/v) and purified by preparative RP-HPLC (20-80% B over 30 min) to give the title compound **179** (61.6 mg, 70.1 µmol, 28%) as a colourless powder; ^{1}H NMR (400 MHz, CD_3OD) δ 8.73 (d, 1H, *J* = 1.4 Hz), 7.53 (ddd, 1H, *J* = 7.9, 1.2, 1.0 Hz), 7.38 – 7.31 (m, 2H), 7.18 (s, 1H), 7.10 (ddd, 1H, *J* = 8.2, 7.0, 1.2 Hz), 6.99 (ddd, 1H, *J* = 7.9, 7.0, 1.0 Hz), 4.63 – 4.45 (m, 2H), 4.44 – 4.22 (m, 3H), 4.21 – 4.07 (m, 2H), 3.31 – 3.12 (m, 4H), 2.93 (dd, 2H, *J* = 8.8, 7.4 Hz), 2.01 (s, 3H), 1.95 – 1.80 (m, 1H), 1.80 – 1.55 (m, 6H), 1.55 – 1.42 (m, 5H), 1.39 (d, 3H, *J* = 7.2 Hz), 1.34 (d, 3H, *J* = 7.2 Hz), 0.96 – 0.87 (m, 9H), 0.82 (d, 3H, *J* = 6.1 Hz); HRMS (ESI) m/z: $[M + H]^+$ Calcd for $C_{43}H_{67}N_{12}O_8$ 879.5205; Found 879.5190 (1.7 ppm error).

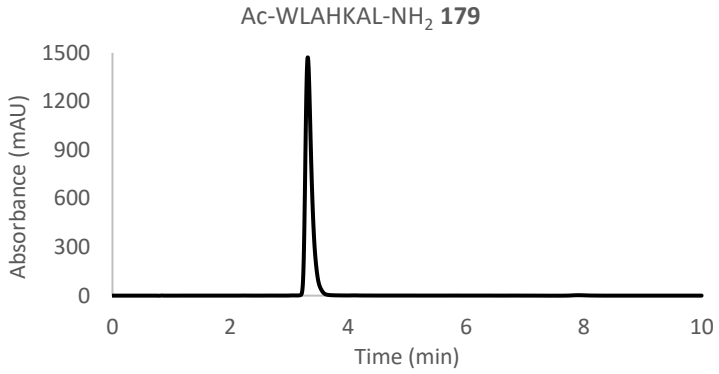

Figure 123. Analytical HPLC chromatogram for purified Ac-WLAHKAL-NH_2 **179** Rt = 3.32 min on analytical gradient 20-80% B over 5 min, 0.6 mL min^{-1}, 280 nm.

Ac-VVYPWYQ-NH$_2$ (180)

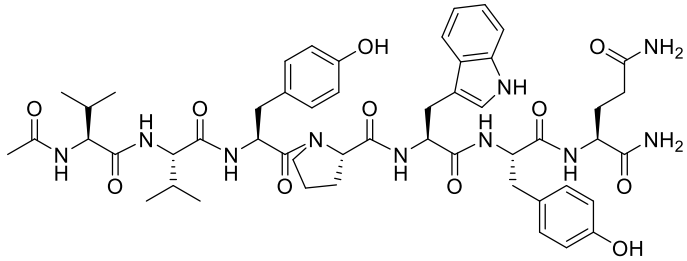

Prepared using rink amide resin and SPPS (200 µmol). The crude peptide was cleaved from the resin using mixture of TFA, TIPS and water (90:5:5 v/v/v) and purified by preparative RP-HPLC (20-70% B over 30 min) to give the title compound **180** (26.0 mg, 26.1 µmol, 14%) as a colourless powder; ^{1}H NMR (400 MHz, DMSO-d_6) δ 10.78 (d, 1H, *J* = 2.4 Hz), 9.13 (d, 2H, *J* = 13.7 Hz), 8.05 (d, 1H, *J* = 8.0 Hz), 7.96 – 7.82 (m, 3H), 7.70 (d, 1H, *J* = 7.7 Hz), 7.62 (d, 1H, *J* = 9.1 Hz), 7.51 (d, 1H, *J* = 7.8 Hz), 7.30 (d, 1H, *J* = 8.1 Hz), 7.25 (s, 1H), 7.14 – 7.05 (m, 3H), 7.05 – 7.00 (m, 3H), 6.99 – 6.92 (m, 3H), 6.78 (s, 1H), 6.67 – 6.54 (m, 4H), 4.64 – 4.53 (m, 1H), 4.49 – 4.33 (m, 2H), 4.30 – 4.23 (m, 1H), 4.20 – 4.06 (m, 3H), 3.59 – 3.52 (m, 1H), 3.38 – 3.33 (m, 1H), 3.17 – 3.01 (m, 1H), 3.01 – 2.90 (m, 1H), 2.88 – 2.59 (m, 4H), 2.18 – 2.02 (m, 2H), 1.97 – 1.79 (m, 7H), 1.79 – 1.60 (m, 4H), 0.86 – 0.68 (m, 12H); HRMS (ESI) m/z: [M + Na]$^+$ Calcd for $C_{51}H_{66}N_{10}O_{11}Na$ 1017.4810; Found 1017.4774 (3.5 ppm error).

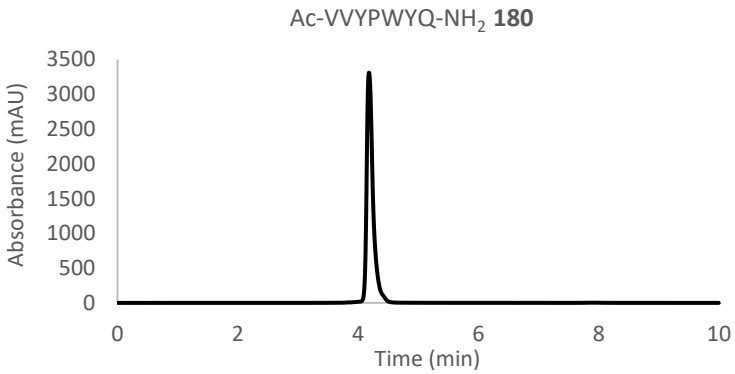

Figure 124. Analytical HPLC chromatogram for purified Ac-VVYPWYQ-NH$_2$ **180** Rt = 4.18 min on analytical gradient 20-80% B over 5 min, 0.6 mL min^{-1}, 280 nm.

Ac-DKVGINYW-NH$_2$ (181)

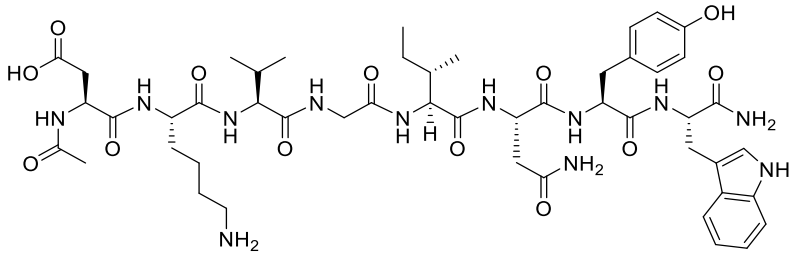

Prepared using rink amide resin and SPPS (250 μmol). The crude peptide was cleaved from the resin using mixture of TFA, TIPS and water (90:5:5 v/v/v) and purified by preparative RP-HPLC (20-80% B over 30 min then 2-70% B over 30 min) to give the title compound **181** (35.3 mg, 34.1 μmol, 14%) as a colourless powder; ^{1}H NMR (400 MHz, CD_3OD) δ 7.63 (dd, 1H, *J* = 7.8, 0.9 Hz), 7.34 (dd, 1H, *J* = 8.1, 0.9 Hz), 7.16 (s, 1H), 7.11 (ddd, 1H, *J* = 8.1, 7.3, 0.9 Hz), 7.04 (ddd, 1H, *J* = 7.8, 7.4, 0.9 Hz), 6.78 (d, 2H, *J* = 8.4 Hz), 6.56 (d, 2H, *J* = 8.4 Hz), 4.68 – 4.60 (m, 2H), 4.57 (dd, 1H, *J* = 9.7, 4.7 Hz), 4.39 (dd, 1H, *J* = 9.2, 5.2 Hz), 4.24 (dd, 1H, *J* = 7.8, 6.6 Hz), 4.13 (dd, 2H, *J* = 10.0, 7.2 Hz), 3.99 (d, 1H, *J* = 16.4 Hz, 1H), 3.76 (d, 1H, *J* = 16.4 Hz), 3.37 (dd, 1H, *J* = 14.7, 4.5 Hz), 3.22 – 3.14 (m, 1H), 2.96 – 2.83 (m, 3H), 2.82 – 2.62 (m, 6H), 2.18 – 2.06 (m, 1H), 1.98 (s, 3H), 1.92 – 1.80 (m, 2H), 1.74 – 1.55 (m, 2H), 1.52 – 1.37 (m, 2H), 1.25 – 1.11 (m, 1H), 1.00 – 0.93 (m, 7H), 0.89 (t, 3H, *J* = 7.5 Hz), 0.85 (d, 3H, *J* = 6.9 Hz); HRMS (ESI) m/z: $[M + H]^+$ Calcd for $C_{49}H_{71}N_{12}O_{13}$ 1035.5264; Found 1035.5168 (9.3 ppm error).

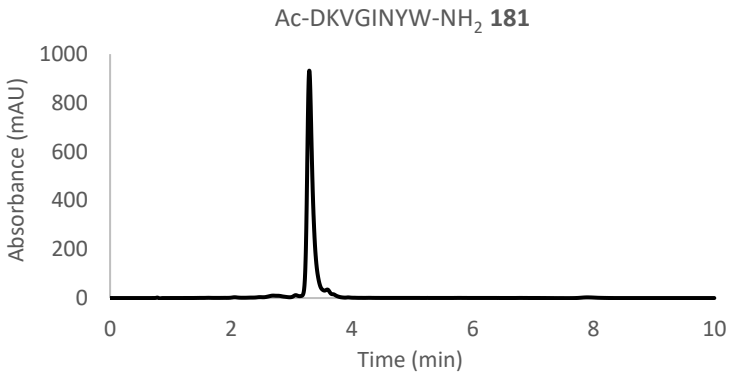

Figure 125. Analytical HPLC chromatogram for purified Ac-DKVGINYW-NH$_2$ **181** Rt = 3.30 min on analytical gradient 20-80% B over 5 min, 0.6 mL min^{-1}, 280 nm.

Ac-WFMTREY-NH$_2$ (185)

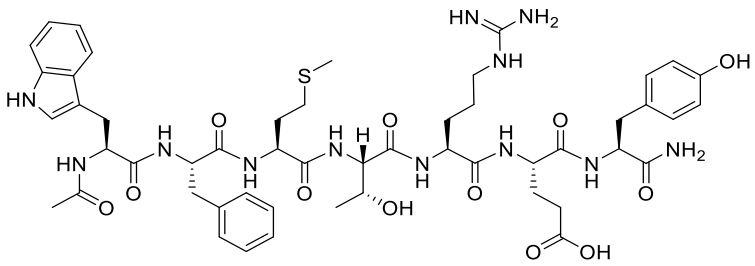

Prepared using rink amide resin and SPPS (250 μmol). The crude peptide was cleaved from the resin using mixture of TFA, TIPS, thioanisole and water (85:5:5:5 v/v/v) and purified by preparative RP-HPLC (20-80% B over 30 min then 2-95% B over 30 min) to give the title compound **185** (19.6 mg, 18.3 μmol, 7%) as a colourless powder; ^{1}H NMR (400 MHz, CD_3OD) δ 7.49 (d, 1H, *J* = 7.9 Hz), 7.36 (d, 1H, *J* = 8.2 Hz), 7.32 – 7.20 (m, 3H), 7.18 – 7.09 (m, 2H), 7.08 (d, 2H, *J* = 8.5 Hz), 7.06 – 6.98 (m, 3H), 6.69 (d, 2H, *J* = 8.5 Hz), 4.56 – 4.37 (m, 3H), 4.35 – 4.29 (m, 1H), 4.29 – 4.18 (m, 4H), 3.19 – 3.11 (m, 4H), 3.11 – 3.03 (m, 1H), 2.93 (dd, 1H, *J* = 14.0, 7.3 Hz), 2.86 (dd, 1H, *J* = 14.1, 9.0 Hz), 2.75 (dd, 1H, *J* = 14.0, 5.8 Hz), 2.43 – 2.26 (m, 3H), 2.16 – 2.08 (m, 1H), 2.07 (s, 3H), 2.03 – 1.88 (m, 3H), 1.87 (s, 3H), 1.85 – 1.67 (m, 2H), 1.67 – 1.56 (m, 2H), 1.24 (d, 3H, *J* = 6.1 Hz); HRMS (ESI) m/z: $[M + H]^+$ Calcd for $C_{51}H_{69}N_{12}O_{12}S$ 1073.4879; Found 1073.4798 (7.5 ppm error).

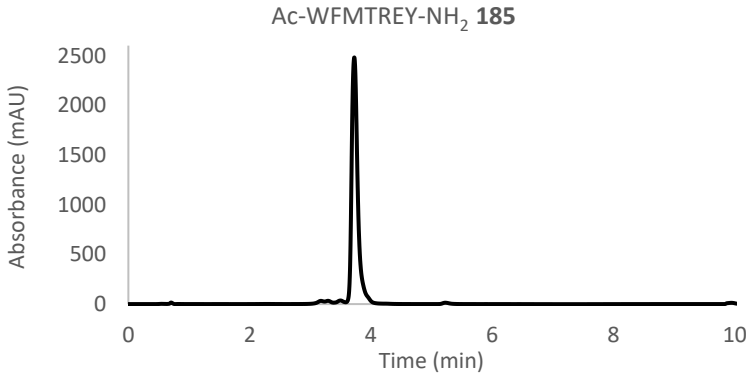

Figure 126. Analytical HPLC chromatogram for purified Ac-WFMTREY-NH$_2$ **185** Rt = 3.73 min on analytical gradient 20-100% B over 5 min, 0.6 mL min^{-1}, 280 nm.

β-Casein (189)

β-casein (250 mg) was purchased from Sigma-Aldrich with a reported ≥ 98% purity.

1 **10** **20**
Arg- Glu- Leu- Glu- Glu- Leu-Asn- Val- Pro- Gly- Glu- Ile- Val- Glu- *SerP*- Leu- *SerP*-*SerP*-*SerP*- Glu-
21 **30** **40**
Glu- Ser- Ile- Thr- Arg- Ile- Asn- Lys- Lys- Ile- Glu- Lys- Phe- Gln- *SerP*- Glu- Glu- Gln- Gln- Gln-
41 **50** **60**
Thr- Glu-Asp- Glu- Leu- Gln- Asp- Lys- Ile- His- Pro- Phe- Ala- Gln- Thr- Gln- Ser- Leu- Val- Tyr-
61 **70** **80**
Pro- Phe- Pro- Gly- Pro- Ile- Pro- Asn- Ser- Leu- Pro- Gln- Asn- Ile- Pro- Pro- Leu- Thr- Gln- Thr-
81 **90** **100**
Pro- Val- Val- Val- Pro- Pro- Phe- Leu- Gln- Pro- Glu- Val- Met- Gly- Val- Ser- Lys- Val- Lys- Glu-
101 **110** **120**
Ala- Met- Ala- Pro-Lys- His- Lys- Glu- Met- Pro- Phe- Pro- Lys- Tyr- Pro- Val- Glu- Pro- Phe- Thr-
121 **130** **140**
Glu- Ser- Gln- Ser-Leu- Thr- Leu- Thr- Asp- Val- Glu- Asn- Leu- His- Leu- Pro- Leu- Pro- Leu- Leu-
141 **150** **160**
Gln- Ser- Trp-Met- His- Gln- Pro- His- Gln- Pro- Leu- Pro- Pro- Thr- Val- Met- Phe- Pro- Pro- Gln-
161 **170** **180**
Ser- Val- Leu- Ser-Leu- Ser- Gln- Ser- Lys- Val- Leu- Pro- Val- Pro- Gln- Lys- Ala- Val- Pro- Tyr-
181 **190** **200**
Pro- Gln- Arg- Asp- Met- Pro- Ile- Gln- Ala- Phe- Leu- Leu- Tyr- Gln- Glu- Pro- Val- Leu- Gly- Pro-
201
Val- Arg- Gly- Pro- Phe- Pro- Ile- Ile- Val

Figure 127. Amino acid sequence of β-casein.[211]

N^2-(((9*H*-fluoren-9-yl)methoxy)carbonyl)-N^6-(2-bromo-2,2-difluoroacetyl)-*L*-lysine (Fmoc-K*-OH, 197)

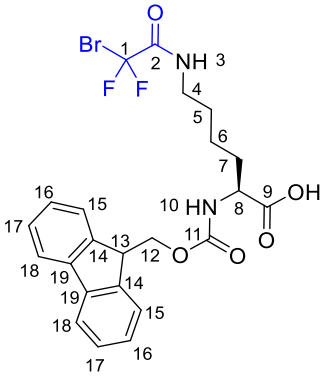

To a heterogeneous mixture of Fmoc-Lys-OH (368 mg, 1.00 mmol, 1.00 eq.) in anhydrous DCM (15 mL) was added triethylamine (0.140 mL, 2.00 mmol, 1.00 eq.) before the mixture was cooled to 0 °C. A solution of bromodifluoroacetyl chloride (0.190 mL, 2.02 mmol, 2.0 eq.) in anhydrous DCM (1 mL) was added to the mixture dropwise and stirred warming to room temperature (2 h). The reaction was monitored using analytical HPLC and if Fmoc-Lys-OH was observed, further bromodifluoroacetyl chloride (0.100 mL, 1.06 mmol, 1.00 eq.) in anhydrous DCM (1 mL) was added dropwise at 0 °C and then stirred for 2 h. The colourless precipitate was concentrated *in vacuo,* dissolved in a 4:7 mixture of 0.1% TFA in H_2O : 0.1% TFA in MeCN and purified by preparative RP-HPLC (20-100% B over 30 min) to give the title compound **197** (328 mg, 0.624 mmol, 63%) as a colourless powder; mp 150-152 °C; υ_{max}/cm^{-1} (ATR) 3294, 3067, 3043, 3016, 2945, 2864, 2359, 1696, 1530, 1449; ^{1}H NMR (400 MHz, MeOD) δ 7.80 (2H, d, *J* = 7.5 Hz, H-18), 7.68 (2H, dd, *J* = 7.5, 6.9 Hz, H-15), 7.39 (2H, dd, *J* = 7.9, 7.5 Hz, H-17), 7.31 (2H, dd, *J* = 7.9, 7.5 Hz, H-16), 4.42 – 4.30 (2H, m, H-12), 4.23 (1H, dd, *J* = 7.3, 6.9 Hz, H-13), 4.14 (1H, dd, *J* = 9.3, 4.7 Hz, H-8), 3.29 – 3.25 (2H, m, H-4), 1.95 – 1.82 (1H, m, H-7), 1.79 – 1.66 (1H, m, H-7), 1.65 – 1.53 (2H, m, H-5), 1.53 – 1.38 (2H, m, H-6); ^{13}C {^{1}H} NMR (101 MHz, MeOD) δ 175.9 (C, C=O), 162.2 (C, C=O), 158.7 (C, C=O), 145.4 (C), 145.2 (C), 142.6 (C), 128.80 (CH, C-17), 128.2 (CH, C-16), 126.3 (CH, C-15), 120.9 (CH, C-18), 113.2 (C, t, *J* = 313.9 Hz, C-1), 68.0 (CH_2, C-12), 55.2 (CH, C-8), 48.4 (CH, C-13), 40.7 (CH_2, C-4), 32.3 (CH_2, C-7), 29.4 (CH_2, C-5), 24.2 (CH_2, C-6); ^{19}F NMR (376 MHz, MeOD) δ

−62.2 (2F, s, F-1), −77.2 (TFA); HRMS (ESI) m/z: $[M - H]^-$ Calcd for $C_{23}H_{22}{}^{79}BrF_2N_2O_5$ 523.0680; Found 523.0688 (1.5 ppm error).

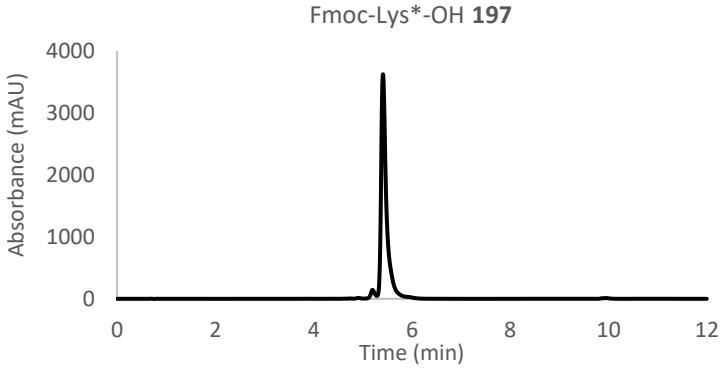

Figure 128. Analytical HPLC chromatogram for purified Fmoc-Lys*-OH **197** Rt = 5.41 min on analytical gradient 20-100% B over 5 min, 0.6 mL min^{-1}, 280 nm.

Ac-WAMLK*-NH$_2$ (195)

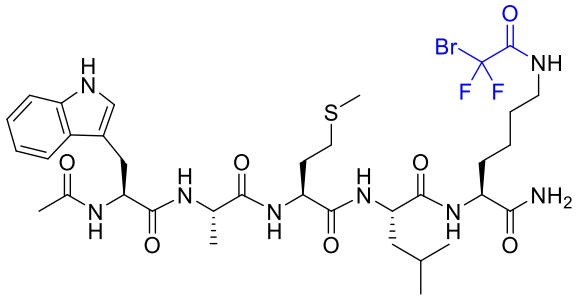

Prepared using Fmoc-K*-OH **197** (200 mg, 381 µmol, 1.90 eq.), rink amide resin and SPPS (200 µmol). The crude peptide was cleaved from the resin using mixture of TFA, TIPS, thioanisole and water (85:5:5:5 v/v/v/v) and purified by preparative RP-HPLC (20-100% B over 30 min) to give the title compound **195** (24 mg, 28.4 µmol, 15%) as a colourless powder; ^{1}H NMR (400 MHz, MeOD) δ 7.55 (d, *J* = 7.9 Hz, 1H), 7.34 (d, *J* = 8.1 Hz, 1H), 7.17 (s, 1H), 7.10 (ddd, *J* = 8.1, 7.0, 0.9 Hz, 1H), 7.01 (ddd, *J* = 7.9, 7.0, 1.0 Hz, 1H), 4.51 (dd, *J* = 7.6, 5.8 Hz, 1H), 4.40 – 4.28 (m, 2H), 4.25 (dd, *J* = 9.5, 4.6 Hz, 1H), 4.11 (q, *J* = 7.2 Hz, 1H), 3.28 – 3.15 (m, 4H), 2.63 – 2.40 (m, 2H), 2.08 (s, 3H), 2.06 – 1.98 (m, 2H), 1.96 (s, 3H), 1.92 – 1.79 (m, 1H), 1.80 – 1.66 (m, 3H), 1.65 – 1.51 (m, 2H), 1.50 – 1.32 (m, 3H), 1.25 (d, *J* = 7.2 Hz, 3H), 0.95 (d, *J* = 6.2 Hz, 3H), 0.90 (d, *J* = 6.3 Hz, 3H); ^{19}F NMR (376 MHz, MeOD) δ −62.1 (s, 2F), −77.0 (s, TFA); HRMS (ESI) m/z: [M + H]$^{+}$ Calcd for $C_{35}H_{52}{}^{79}BrF_2N_8O_7S$ 845.2831; Found 845.2872 (4.9 ppm error).

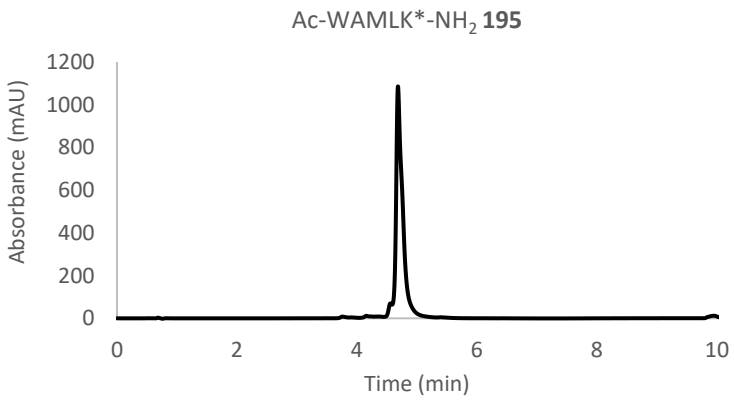

Figure 129. Analytical HPLC chromatogram for purified Ac-WAMLK*-NH$_2$ **195** Rt = 4.68 min on analytical gradient 20-100% B over 5 min, 0.6 mL min^{-1}, 280 nm.

Ac-K*AMLW-NH$_2$ (198)

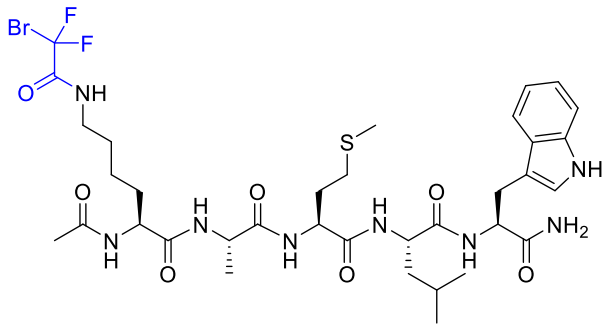

Prepared using Fmoc-K*-OH **197** (200 mg, 381 µmol, 1.90 eq.), rink amide resin and SPPS (200 µmol). The crude peptide was cleaved from the resin using mixture of TFA, TIPS, thioanisole and water (85:5:5:5 v/v/v/v) and purified by preparative RP-HPLC (20-100% B over 30 min) to give the title compound **198** (30.8 mg, 36.5 µmol, 10%) as a colourless powder; ^{1}H NMR (500 MHz, MeOD) δ 7.60 (d, *J* = 7.9 Hz, 1H), 7.32 (d, *J* = 8.1 Hz, 1H), 7.12 (s, 1H), 7.07 (ddd, *J* = 8.1, 7.1, 0.8 Hz, 1H), 7.00 (ddd, *J* = 7.9, 7.1, 0.8 Hz, 1H), 4.62 (dd, *J* = 8.7, 5.3 Hz, 1H), 4.36 (dd, *J* = 9.1, 5.1 Hz, 1H), 4.25 (dd, *J* = 10.3, 4.8 Hz, 1H), 4.21 – 4.05 (m, 2H), 3.39 – 3.32 (m, 1H), 3.17 (dd, *J* = 14.7, 8.8 Hz, 1H), 2.62 – 2.40 (m, 2H), 2.06 (s, 3H), 2.01 (s, 3H), 2.04 – 1.93 (m, 3H), 1.85 – 1.75 (m, 1H), 1.74 – 1.64 (m, 1H), 1.64 – 1.51 (m, 4H), 1.50 – 1.27 (m, 4H), 1.35 (d, *J* = 7.2 Hz, 3H), 0.89 (d, *J* = 6.4 Hz, 3H), 0.84 (d, *J* = 6.4 Hz, 3H); ^{19}F NMR (376 MHz, MeOD) δ −62.1 (s, 2F), −76.9 (s, TFA); HRMS (ESI) m/z: [M + H]$^{+}$ Calcd for $C_{35}H_{52}{}^{79}BrF_2N_8O_7S$ 845.2831; Found 845.2812 (2.2 ppm error).

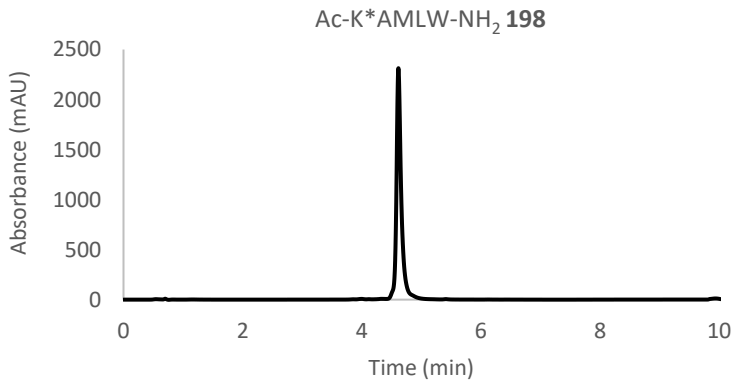

Figure 130. Analytical HPLC chromatogram for purified Ac-K*AMLW-NH$_2$ **198** Rt = 4.62 min on analytical gradient 20-100% B over 5 min, 0.6 mL min^{-1}, 280 nm.

Ac-EWAMLK*R-NH$_2$ (199)

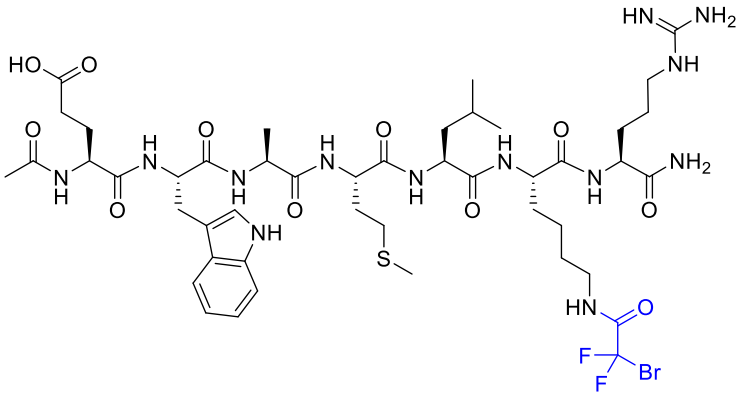

Prepared using Fmoc-K*-OH **197** (200 mg, 381 µmol, 1.90 eq.), rink amide resin and SPPS (200 µmol). The crude peptide was cleaved from the resin using mixture of TFA, TIPS, thioanisole and water (85:5:5:5 v/v/v/v) and purified by preparative RP-HPLC (20-100% B over 30 min) to give the title compound **199** (39.4 mg, 34.9 µmol, 9%) as a colourless powder; ^{1}H NMR (500 MHz, MeOD) δ 7.49 (1H, d, *J* = 8.0 Hz), 7.37 (1H, d, *J* = 8.2 Hz), 7.21 (1H, s), 7.13 (1H, dd, *J* = 8.2, 7.0 Hz), 7.03 (1H, dd, *J* = 8.0, 7.0 Hz), 4.38 (1H, dd, *J* = 7.1, 6.0 Hz), 4.33 – 4.22 (2H, m), 4.22 – 4.12 (2H, m), 4.09 (1H, dd, *J* = 8.4, 7.4 Hz), 3.98 (1H, dd, *J* = 7.6 Hz), 3.29 – 3.13 (5H, m), 2.68 – 2.59 (1H, m), 2.56 – 2.46 (1H, m), 2.44 – 2.30 (2H, m), 2.21 – 2.07 (2H, m), 2.05 (3H, s), 2.02 – 1.92 (3H, m), 1.91 – 1.78 (8H, m), 1.79 – 1.35 (8H, m), 1.17 (3H, d, *J* = 7.4 Hz), 0.95 (3H, d, *J* = 6.5 Hz), 0.91 (3H, d, *J* = 6.4 Hz); ^{19}F NMR (376 MHz, MeOD) δ −62.0 (s, 2F), −77.0 (s, TFA); HRMS (ESI) m/z: $[M + H]^+$ Calcd for $C_{46}H_{71}{}^{79}BrF_2N_{13}O_{11}S$ 1130.4268; Found: 1130.4268 (0.0 ppm error).

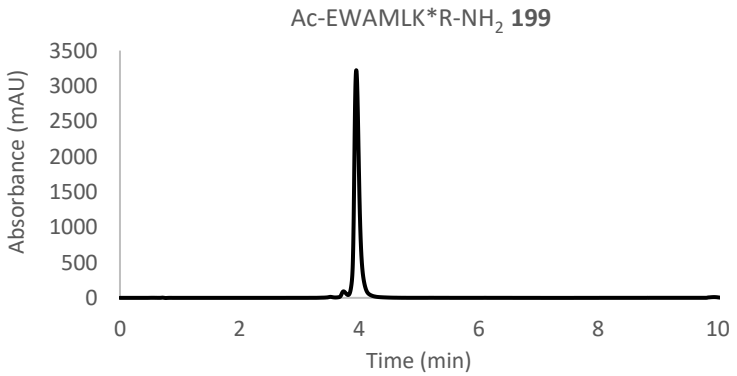

Figure 131. Analytical HPLC chromatogram for purified Ac-K*AMLW-NH$_2$ **199** Rt = 3.95 min on analytical gradient 20-100% B over 5 min, 0.6 mL min^{-1}, 280 nm.

Ac-WGFIK*-NH$_2$ (200)

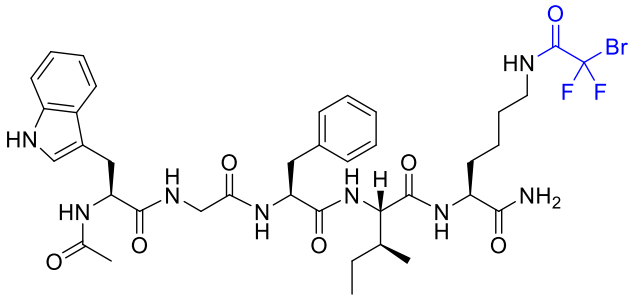

Prepared using Fmoc-K*-OH **197** (200 mg, 381 µmol, 1.90 eq.), rink amide resin and SPPS (200 µmol). The crude peptide was cleaved from the resin using mixture of TFA, TIPS and water (90:5:5 v/v/v) and purified by preparative RP-HPLC (20-100% B over 30 min with an isocratic hold at 45% B) to give the title compound **200** (10.4 mg, 12.3 µmol, 6%) as a colourless powder; ^{1}H NMR (500 MHz, MeOD) δ 7.56 (dd, *J* = 7.8, 1.0 Hz, 1H), 7.33 (dd, *J* = 8.2, 1.0 Hz, 1H), 7.29 – 7.15 (m, 5H), 7.12 (s, 1H), 7.09 (ddd, *J* = 8.2, 7.0, 1.0 Hz, 1H), 7.01 (ddd, *J* = 7.8, 7.0, 1.0 Hz, 1H), 4.60 (dd, *J* = 9.8, 4.8 Hz, 1H), 4.49 (t, *J* = 7.1 Hz, 1H), 4.28 (dd, *J* = 8.9, 5.1 Hz, 1H), 4.18 (d, *J* = 7.9 Hz, 1H), 3.81 (d, *J* = 16.8 Hz, 1H), 3.51 (d, *J* = 16.7 Hz, 1H), 3.28 – 3.19 (m, 3H), 3.19 – 3.09 (m, 2H), 2.98 – 2.93 (m, 1H), 1.98 (s, 3H), 1.96 – 1.88 (m, 1H), 1.85 – 1.74 (m, 1H), 1.72 – 1.61 (m, 1H), 1.60 – 1.49 (m, 3H), 1.43 – 1.32 (m, 2H), 1.27 – 1.17 (m, 1H), 0.94 (d, *J* = 6.8 Hz, 3H), 0.89 (t, *J* = 7.4 Hz, 3H); ^{19}F NMR (376 MHz, MeOD) δ −62.1 (s, 2F), −77.0 (s, TFA); HRMS (ESI) m/z: [M – H]$^{-}$ Calcd for $C_{38}H_{48}{}^{79}BrF_2N_8O_7$ 845.2797; Found: 845.2811 (1.7 ppm error).

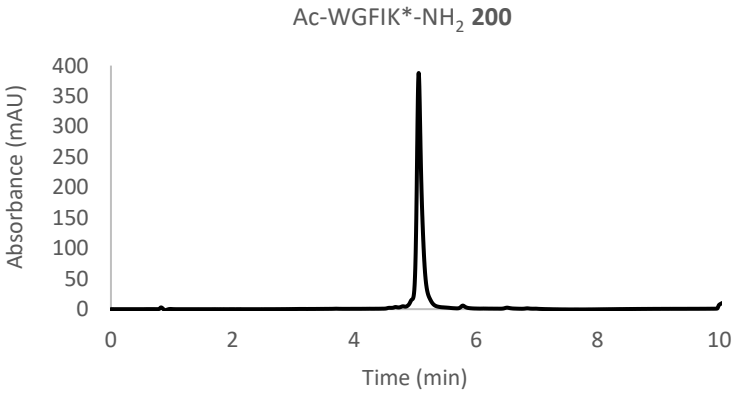

Figure 132. Analytical HPLC chromatogram for purified Ac-WGFIK*-NH$_2$ **200** Rt = 5.06 min on analytical gradient 20-100% B over 5 min, 0.6 mL min^{-1}, 280 nm.

H-WHASPYVK*-NH₂ (202)

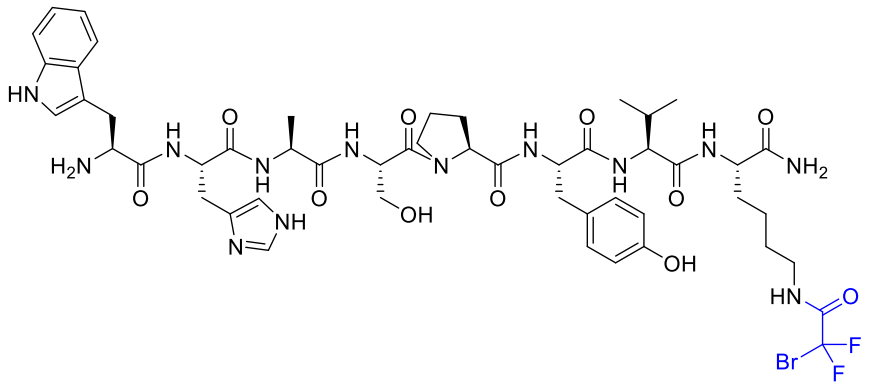

Prepared using Fmoc-K*-OH **197** (200 mg, 381 µmol, 1.90 eq.), rink amide resin and SPPS (200 µmol). The crude peptide was cleaved from the resin using mixture of TFA, TIPS and water (90:5:5 v/v/v) and purified by preparative RP-HPLC (10-80% B over 30 min) to give the title compound **202** (20.8 mg, 18.2 µmol, 5%) as a colourless powder; ^{1}H NMR (500 MHz, MeOD) δ 8.79 (d, *J* = 1.4 Hz, 1H), 7.57 (dd, *J* = 8.0, 1.1 Hz, 1H), 7.37 (dd, *J* = 8.2, 0.9 Hz, 1H), 7.35 (d, *J* = 1.4 Hz, 1H), 7.20 (s, 1H), 7.14 (ddd, *J* = 8.2, 7.0, 1.1 Hz, 1H), 7.07 – 7.00 (m, 3H), 6.71 (d, *J* = 8.5 Hz, 2H), 4.61 (dd, *J* = 7.2, 5.2 Hz, 1H), 4.53 (dd, *J* = 10.7, 4.6 Hz, 1H), 4.39 (dd, *J* = 8.7, 4.4 Hz, 1H), 4.33 – 4.22 (m, 2H), 4.22 – 4.15 (m, 2H), 3.96 (dd, *J* = 10.3, 5.9 Hz, 1H), 3.81 (dd, *J* = 10.3, 8.2 Hz, 1H), 3.79 – 3.71 (m, 2H), 3.38 (dd, *J* = 14.8, 6.5 Hz, 1H), 3.29 – 3.23 (m, 4H), 3.24 – 3.20 (m, 1H), 3.20 – 3.11 (m, 2H), 2.72 (dd, *J* = 14.2, 10.7 Hz, 1H), 2.21 – 2.02 (m, 2H), 1.89 – 1.79 (m, 2H), 1.77 – 1.53 (m, 5H), 1.49 – 1.39 (m, 2H), 1.37 (d, *J* = 7.2 Hz, 3H), 0.99 (dd, *J* = 6.8, 1.8 Hz, 6H); ^{19}F NMR (376 MHz, MeOD) δ −62.1 (s, 2F), −77.1 (s, TFA); HRMS (ESI) m/z: $[M + 2H]^{2+}$ Calcd for $C_{50}H_{68}{}^{79}BrF_2N_{13}O_{11}$ 571.7157; Found: 571.7170 (2.3 ppm error).

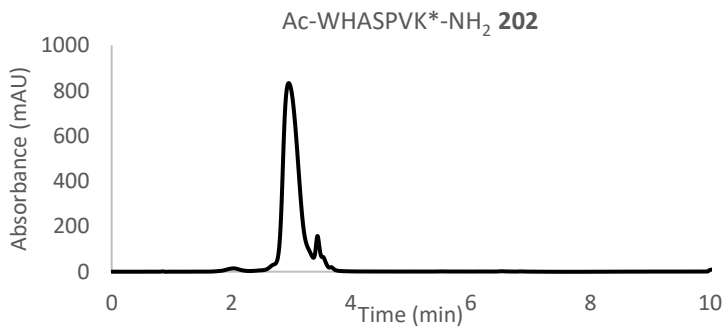

Figure 133. Analytical HPLC chromatogram for purified Ac-WHASPYVK*-NH₂ **202** Rt = 2.96 min on analytical gradient 20-100% B over 5 min, 0.6 mL min^{-1}, 280 nm.

Ac-WQDECKSNTAGK*-NH_2 (203)

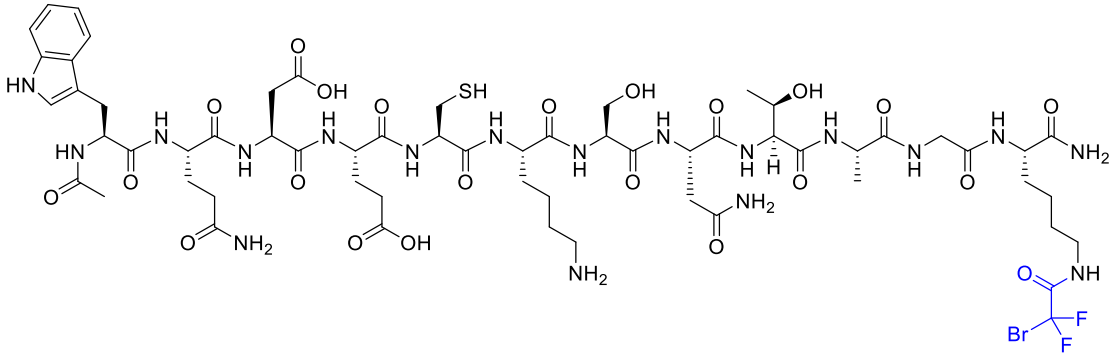

Prepared using Fmoc-K*-OH **197** (200 mg, 381 µmol, 1.90 eq.), rink amide resin and SPPS (200 µmol). The crude peptide was cleaved from the resin using mixture of TFA, TIPS and water (90:5:5 v/v/v) and purified by preparative RP-HPLC (10-80% B over 30 min) to give the title compound **203** (10.7 mg, 6.84 µmol, 3%) as a colourless crystalline solid; ^{1}H NMR (400 MHz, MeOD) δ 7.54 (d, *J* = 7.9 Hz, 1H), 7.34 (d, *J* = 8.1 Hz, 1H), 7.21 (s, 1H), 7.10 (dd, *J* = 8.1, 7.4 Hz, 1H), 7.02 (dd, *J* = 7.9, 7.4 Hz, 1H), 4.80 – 4.70 (m, 1H), 4.63 – 4.53 (m, 1H), 4.53 – 4.47 (m, 1H), 4.39 – 4.17 (m, 7H), 4.00 – 3.85 (m, 3H), 3.85 – 3.76 (m, 2H), 3.29 – 3.21 (m, 3H), 2.97 – 2.76 (m, 8H), 2.59 – 2.39 (m, 2H), 2.23 – 2.10 (m, 3H), 2.04 (s, 3H), 2.01 – 1.74 (m, 7H), 1.72 – 1.49 (m, 7H), 1.49 – 1.36 (m, 6H), 1.23 (d, *J* = 6.4 Hz, 3H); ^{19}F NMR (376 MHz, MeOD) δ −62.1 (s, 2F), -77.0 (s, TFA); HRMS (ESI) m/z: $[M + 2H]^{2+}$ Calcd for $C_{60}H_{91}{}^{79}BrF_2N_{18}O_{22}S$ 782.2714; Found: 782.2746 (4.1 ppm error).

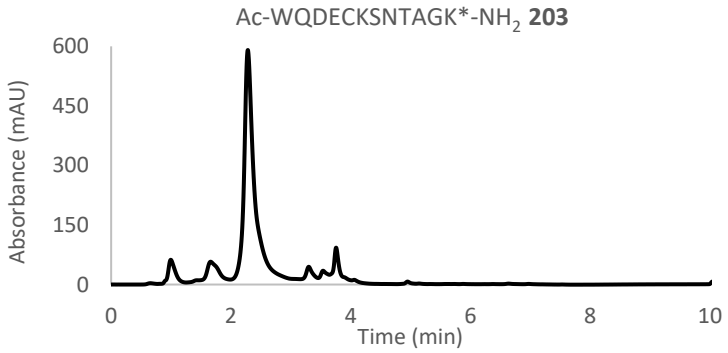

Figure 134. Analytical HPLC chromatogram for purified Ac-WQDECKSNTAGK*-NH_2 **203** Rt = 2.28 min on analytical gradient 20-100% B. over 5 min, 0.6 mL min^{-1}, 280 nm.

Ethyl (2-bromo-2,2-difluoroacetyl)tryptophanate (205)

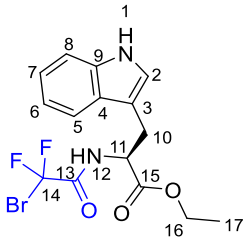

To a suspension of L-tryptophan ethyl ester hydrochloride (134 mg, 0.50 mmol, 1.00 eq.) in anhydrous DCM (8 mL) was added triethyl amine (0.07 mL, 0.50 mmol, 1.00 eq.) before the mixture was cooled to 0 °C. A solution of bromodifluoroacetyl chloride (0.10 mL, 1.00 mmol, 2.00 eq.) in anhydrous DCM (1 mL) was added to the mixture dropwise. The resultant colourless solution was stirred for 2 h while warming to room temperature. The solution was diluted with water (10 mL) and extracted with DCM (3 × 10 mL). The combined organic extracts were washed with 1 M aq. HCl (10 mL) and brine (10 mL), dried over $MgSO_4$ and concentrated *in vacuo* to give the title compound **205** (185 mg, 0.475 mmol, 95%) as colourless powder; mp 116-118 °C; υ_{max}/cm^{-1} (ATR) 3409, 3386, 3301, 3080, 2989, 2875, 2856, 1755, 1735, 1687, 1547, 1457; ^{1}H NMR (400 MHz, $CDCl_3$) δ 8.11 (1H, s, H-1), 7.53 (1H, d, *J* = 7.9 Hz, H-8), 7.37 (1H, d, *J* = 8.1 Hz, H-5), 7.21 (1H, dd, *J* = 8.1, 7.5 Hz, H-6), 7.13 (1H, dd, *J* = 7.9, 7.5 Hz, H-7), 7.02 (1H, s, H-2), 6.79 (1H, d, *J* = 7.7 Hz, H-12), 4.89 (1H, dd, *J* = 7.7, 5.3 Hz, H-11), 4.31 – 4.00 (2H, m, H-16), 3.42 (2H, d, *J* = 5.3 Hz, H-10), 1.24 (3H, t, *J* = 7.1 Hz, H-17); ^{13}C NMR (101 MHz, $CDCl_3$) δ 170.5 (C, C-15), 159.6 (C, t, *J* = 28.2 Hz, C-13), 136.2 (C, C-9), 127.5 (C, C-4), 123.1 (CH, C-2), 122.7 (CH, C-6), 120.1 (CH, C-7), 118.6 (CH, C-8), 111.6 (C, t, *J* = 316.4 Hz, C-14), 111.5 (CH, C-5), 109.2 (C, C-3), 62.3 (CH_2, C-16), 53.7 (CH, C-11), 27.3 (CH_2, C-10), 14.2 (CH_3, C-17); ^{19}F NMR (376 MHz, $CDCl_3$) δ −60.6 (2F, s, F-1); HRMS (ESI) m/z: $[M + Na]^+$ Calcd for $C_{15}H_{15}BrF_2N_2O_3Na$ 411.0132; Found 411.0135 (0.7 ppm error).

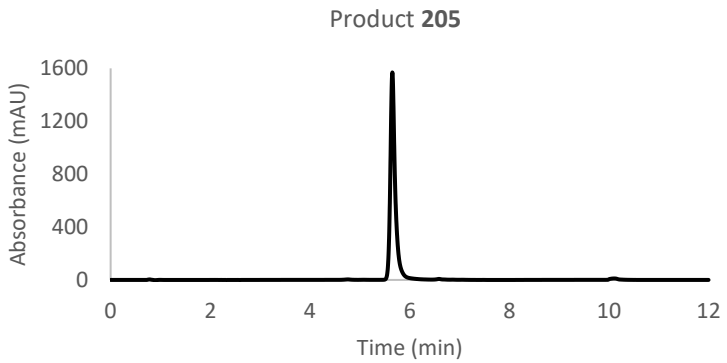

Figure 135. Analytical HPLC chromatogram for product **205** Rt = 5.65 min on analytical gradient 20-100% B. over 5 min, 0.6 mL min^{-1}, 280 nm.

6.4 Photochemical Alkylation of Ac-Trp-OEt

General Procedure C: Analytical Scale Photocatalytic Difluoroalkylation of Ac-Trp-OEt

A solution of Ac-Trp-OEt **93** (0.1 M in DMSO, 200 µL, 20.0 µmol, 1.00 eq.), 4CzIPN (0.01 M in DMSO, 20 µL, 0.200 µmol, 1 mol%) and bromodifluoroalkyl reagent (0.1 M in DMSO, 400 µL, 40.0 µmol, 2.00 eq.) in DMSO (1.380 mL, total solvent volume 2 mL) was purged with N_2 (5 min) and then irradiated with blue LEDs (PhotoRedOx box, 18 W) for 10 – 150 min at room temperature. α,α,α-Trifluorotoluene (0.0165 M in DMSO, 404 µL, 6.67 µmol, 0.333 equiv.) was added, then the reaction mixture was analysed by quantitative NMR spectroscopy, analytical HPLC, and mass spectrometry.

General procedure D: Scale-up of the Photocatalytic Difluoroalkylation of Ac-Trp-OEt

A solution of Ac-Trp-OEt **93** (54.9 mg, 200 µmol, 1.00 eq.), 4CzIPN (1.6 mg, 2.00 µmol, 1 mol%) and bromodifluoroalkyl reagent (400 µmol, 2.00 eq.) in DMSO (20 mL, 0.01 M) was purged with N_2 (5 min) and then irradiated with blue LEDs (PhotoRedOx box, 18 W) for 10 - 30 min at room temperature. α,α,α-Trifluorotoluene (8.20 µL, 66.7 µmol, 0.333 eq.) was added to the reaction mixture, then quantitative NMR spectroscopy and analytical HPLC analysis were carried out. The reaction mixture was diluted with water (10 mL) and extracted with ethyl acetate (3 × 10 mL). The combined organic extracts were washed with brine (30 mL), dried over $MgSO_4$ and concentrated *in vacuo*. The resulting residue was purified by flash column chromatography.

Ethyl (*S*)-2-acetamido-3-(2-(2-ethoxy-1,1-difluoro-2-oxoethyl)-1*H*-indol-3-yl)propanoate (105a) - analytical scale

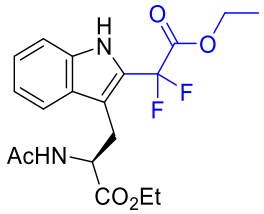

Prepared according to general procedure C using Ac-Trp-OEt **93** (0.1 M in DMSO, 200 µL, 20.0 µmol, 1.00 eq.), 4CzIPN (0.01 M in DMSO, 20 µL, 0.200 µmol, 1 mol%) and ethyl bromodifluoroacetate **94a** (0.1 M in DMSO, 400 µL, 40.0 µmol, 2.00 eq.). The reaction mixture was irradiated with blue LEDs for 15 min then the yield was determined by quantitative ^{19}F NMR spectroscopy (79% yield); ^{19}F NMR (376 MHz, DMSO) δ −99.0 (d, 1F, *J* = 264 Hz), −99.7 (d, 1F, *J* = 264 Hz); HRMS (ESI) m/z: [M + H]$^+$ Calcd for $C_{19}H_{23}F_2N_2O_5$ 397.1567; Found 397.1548 (4.0 ppm error).

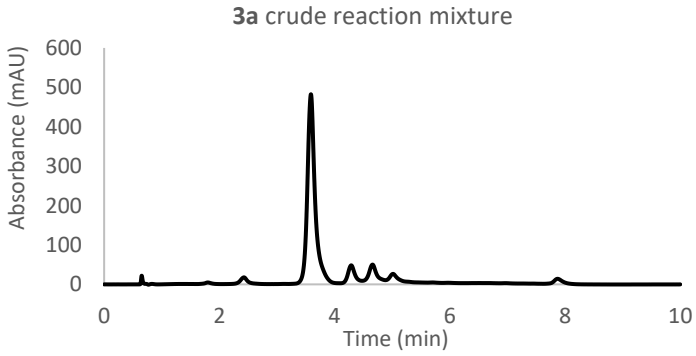

Figure S12. Reaction mixture analytical HPLC chromatogram for product **3a** Rt = 3.59 min on analytical gradient 40-80% B over 5 min, 0.6 mL min^{-1}, 280 nm.

Ethyl (*S*)-2-acetamido-3-(2-(2-ethoxy-1,1-difluoro-2-oxoethyl)-1*H*-indol-3-yl)propanoate (105a)

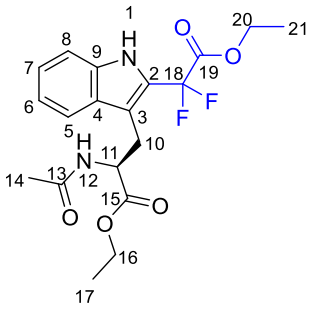

Prepared according to general procedure D using Ac-Trp-OEt **93** (54.9 mg, 200 µmol, 1.00 eq.), 4CzIPN (1.6 mg, 2.00 µmol, 1 mol%) and ethyl

bromodifluoroacetate **94a** (51.3 µL, 400 µmol, 2.00 eq.). The reaction mixture was irradiated with blue LEDs for 10 min then was analysed by quantitative ^{19}F NMR spectroscopy (65% yield) and analytical HPLC. The crude material was purified by flash column chromatography (SiO_2, pentane/EtOAc, 1:1) to give the title compound **105a** (51.5 mg, 0.130 mmol, 65%) as an off white crystalline solid; R_f = 0.31 (pentane/EtOAc, 1:1); mp = 33-35 °C; υ_{max}/cm^{-1} (ATR) 2984, 2921, 2870, 2851, 1761, 1736, 1656, 1526, 1446, 1372; ^{1}H NMR (400 MHz, $CDCl_3$) δ 8.77 (1H, s, H-1), 7.70 (1H, d, *J* = 8.0 Hz, H-8), 7.37 (1H, d, *J* = 8.2 Hz, H-5), 7.28 (1H, ddd, *J* = 8.2, 7.0, 0.8 Hz, H-6), 7.17 (1H, ddd, *J* = 8.0, 7.0, 1.0 Hz, H-7), 6.20 (1H, d, *J* = 7.6 Hz, H-12), 4.90 (1H, ddd, *J* = 7.6, 7.4, 6.0 Hz, H-11), 4.34 (2H, q, *J* = 7.2 Hz, H-20), 4.21 – 4.01 (2H, m, H-16), 3.45 – 3.30 (2H, m, H-10), 1.92 (3H, s, H-14), 1.34 (3H, t, *J* = 7.2 Hz, H-21), 1.17 (3H, t, *J* = 7.4 Hz, H-17); ^{13}C {^{1}H} NMR (101 MHz, $CDCl_3$) δ 172.0 (C, C-15), 170.1 (C, C-13), 163.6 (C, t, *J* = 35.5 Hz, C-19), 135.9 (C, C-9), 127.9 (C, C-4) 124.8 (CH, C-6), 124.6 (C, t, *J* = 30.1 Hz, C-2), 120.8 (CH, C-7), 120.0 (CH, C-8), 112.6 (C, t, *J* = 2.7 Hz, C-3), 111.91 (CH, C-5) , 111.4 (C, t, *J* = 252 Hz, C-18), 64.0 (CH_2, C-20), 61.6 (CH_2, C-16), 53.0 (CH, C-11), 27.1 (CH_2, C-10), 23.1 (CH_3, C-14), 14.0 (CH_3, C-17), 14.0 (CH_3, C-21); ^{19}F NMR (377 MHz, $CDCl_3$) δ −99.6 (1F, d, *J* = 267.0 Hz, F-18), −101.3 (1F, d, *J* = 267.0 Hz, F-18); HRMS (ESI) m/z: [M + Na]$^+$ Calcd for $C_{19}H_{22}F_2N_2NaO_5$ 419.1389; Found 419.1408 (4.5 ppm error).

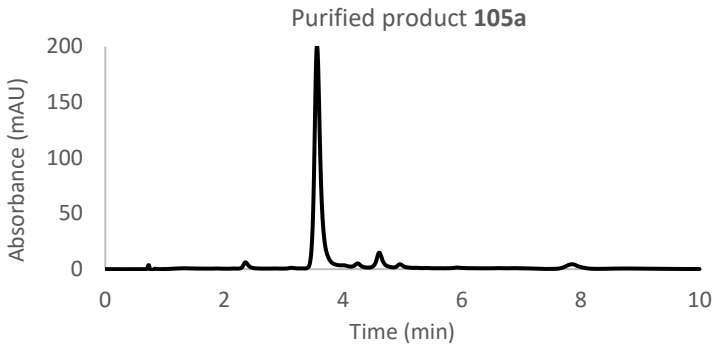

Figure 136. Analytical HPLC chromatogram for purified product **105a** Rt = 3.56 min on analytical gradient 40-80% B over 5 min, 0.6 mL min^{-1}, 280 nm.

Ethyl (*S*)-2-acetamido-3-(2-(2-(benzyloxy)-1,1-difluoro-2-oxoethyl)-1*H*-indol-3-yl)propanoate (105b) - analytical scale

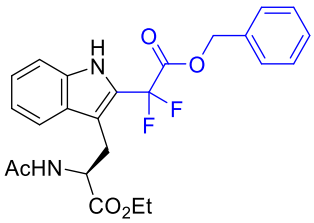

Prepared according to general procedure C using Ac-Trp-OEt **93** (0.1 M in DMSO, 200 µL, 20.0 µmol, 1.00 eq.), 4CzIPN (0.01 M in DMSO, 20 µL, 0.200 µmol, 1 mol%) and benzyl 2-bromo-2,2-difluoroacetate **94b** (0.1 M in DMSO, 400 µL, 40.0 µmol, 2.00 eq.). The reaction mixture was irradiated with blue LEDs for 10 min then the yield was determined by quantitative ^{19}F NMR spectroscopy (66% yield); ^{19}F NMR (376 MHz, DMSO) δ −98.8 (d, 1F, *J* = 263 Hz), −99.6 (d, 1F, *J* = 263 Hz); HRMS (ESI) m/z: $[M + H]^+$ Calcd for $C_{24}H_{25}F_2N_2O_5$ 459.1732; Found 459.1730 (0.4 ppm error).

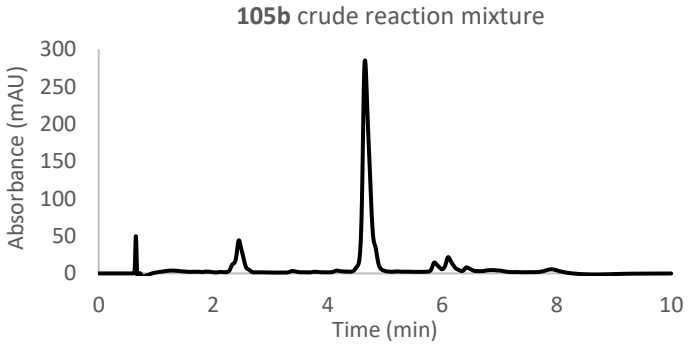

Figure 137. Reaction mixture analytical HPLC chromatogram for product **105b** Rt = 4.65 min on analytical gradient 40-80% B over 5 min, 0.6 mL min^{-1}, 280 nm.

Ethyl (*S*)-2-acetamido-3-(2-(2-(benzyloxy)-1,1-difluoro-2-oxoethyl)-1*H*-indol-3-yl)propanoate (105b)

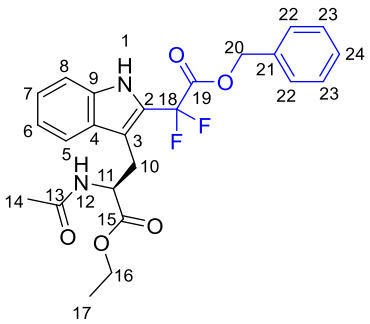

Prepared according to general procedure D using Ac-Trp-OEt **93** (54.9 mg, 200 µmol, 1.00 eq.), 4CzIPN (1.6 mg, 2.00 µmol, 1 mol%) and benzyl 2-

bromo-2,2-difluoroacetate **94b** (106 mg, 400 μmol, 2.00 eq.). The reaction mixture was irradiated with blue LEDs for 10 min then was analysed by quantitative ^{19}F NMR spectroscopy (70% yield) and analytical HPLC. The crude material was purified by flash column chromatography (SiO_2, pentane/EtOAc, 6:4) to give the title compound **105b** (59.5 mg, 0.130 mmol, 65%) as an off white crystalline solid; R_f = 0.28 (pentant/EtOAc, 6:4); mp = 40-42 °C; υ_{max}/cm^{-1} (ATR) 3065, 3037, 2955, 2918, 2849, 1763, 1734, 1657; ^{1}H NMR (400 MHz, $CDCl_3$) δ 7.69 (1H, d, *J* = 8.1 Hz, H-8), 7.37 – 7.20 (7H, m, H-22-24, H-5, H-6), 7.16 (1H, ddd, *J* = 8.1, 6.9, 1.2 Hz, H-7), 6.21 (1H, d, *J* = 7.9 Hz, H-12), 5.28 (2H, s, H-20), 4.90 (1H, ddd, J = 7.9, 7.6, 6.1 Hz, H-11), 4.18 – 3.99 (2H, m, H-16), 3.38 (1H, dd, *J* = 14.6, 6.1 Hz, H-10), 3.30 (1H, dd, *J* = 14.6, 7.6 Hz, H-10), 1.87 (3H, s, H-14), 1.15 (3H, t, *J* = 7.1 Hz, H-17); ^{13}C {^{1}H} NMR (101 MHz, $CDCl_3$) δ 172.0 (C, C-15), 170.2 (C, C-13), 163.4 (C, t, *J* = 35.9 Hz, C-19), 136.0 (C, C-9), 133.9 (C, C-21), 129.1 (CH, C-24), 128.9 (2×CH, C-22), 128.5 (2×CH, C-23), 127.8 (C, C-4), 124.7 (CH, C-6), 124.24 (C, t, *J* = 29.8 Hz, C-2), 120.7 (CH, C-7), 119.9 (CH, C-8), 112.6 (C, t, *J* = 2.8 Hz, C-3), 112.0 (CH, C-5), 111.5 (C, t, *J* = 252 Hz, C-18), 69.2 (CH_2, C-20), 61.6 (CH_2, C-16) , 53.0 (CH C-11), 27.0 (CH_2, C-10), 23.0 (CH_3, C-14), 14.0 (CH_3, C-17); ^{19}F NMR (376 MHz, $CDCl_3$) δ −99.6 (1F, d, *J* = 266.8 Hz, F-18), −101.1 (1F, d, *J* = 267 Hz, F-18); HRMS (ESI) m/z: [M + Na]$^+$ Calcd for $C_{24}H_{24}F_2N_2NaO_5$ 481.1545; Found 481.1548 (0.6 ppm error).

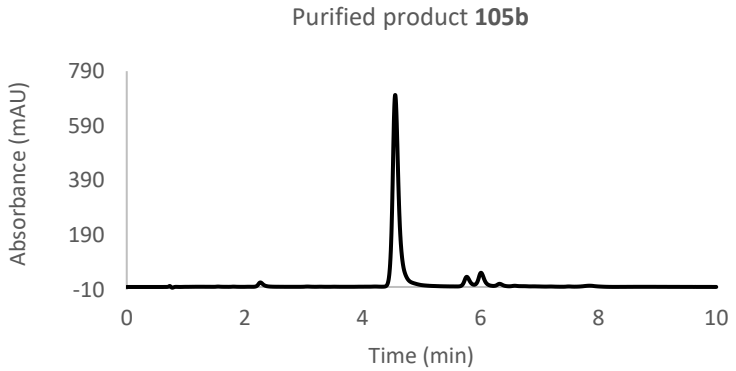

Figure 138. Analytical HPLC chromatogram for purified product **105b** Rt = 4.55 min on analytical gradient 40-80% B over 5 min, 0.6 mL min^{-1}, 280 nm.

Ethyl (*S*)-2-acetamido-3-(2-(2-((4-bromobenzyl)oxy)-1,1-difluoro-2-oxoethyl)-1*H*-indol-3-yl)propanoate (105c) - analytical scale

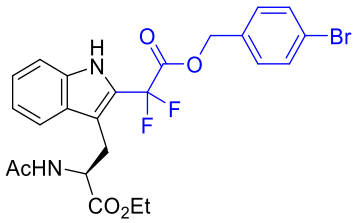

Prepared according to general procedure C using Ac-Trp-OEt **93** (0.1 M in DMSO, 200 µL, 20.0 µmol, 1.00 eq.), 4CzIPN (0.01 M in DMSO, 20 µL, 0.200 µmol, 1 mol%) and 4-bromobenzyl 2-bromo-2,2-difluoroacetate **105c** (0.1 M in DMSO, 400 µL, 40.0 µmol, 2.00 eq.). The reaction mixture was irradiated with blue LEDs for 10 min then the yield was determined by quantitative ^{19}F NMR spectroscopy (62% yield); ^{19}F NMR (376 MHz, DMSO) δ −98.0 (d, 1F, *J* = 264 Hz), −99.0 (d, 1F, *J* = 264 Hz); HRMS (ESI) m/z: $[M + H]^+$ Calcd for $C_{24}H_{24}{}^{79}BrF_2N_2O_5$ 537.0831; Found 537.0817 (2.7 ppm error).

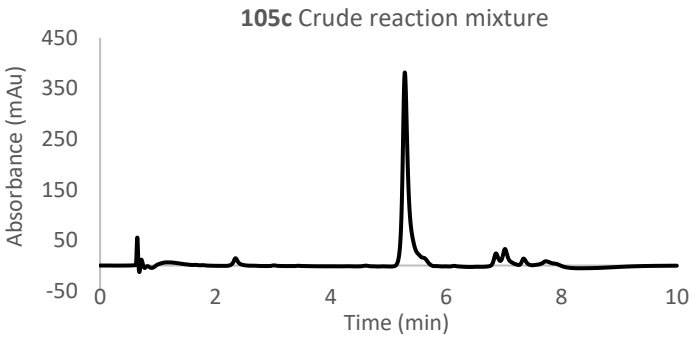

Figure 139. Reaction mixture analytical HPLC chromatogram for product **105c** Rt = 5.28 min on analytical gradient 40-80% B over 5 min, 0.6 mL min^{-1}, 280 nm.

Ethyl (*S*)-2-acetamido-3-(2-(28,28-difluoro-27-oxo-2,5,8,11,14,17,20,23,26-nonaoxaoctacosan-28-yl)-1*H*-indol-3-yl)propanoate (105d) - analytical scale

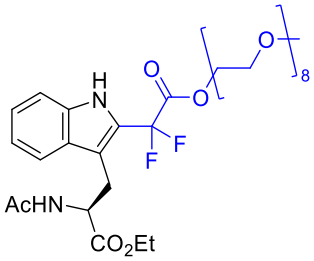

Prepared according to general procedure C using Ac-Trp-OEt **93** (0.1 M in DMSO, 200 µL, 20.0 µmol, 1.00 eq.), 4CzIPN (0.01 M in DMSO, 20 µL, 0.200 µmol, 1 mol%) and 2,5,8,11,14,17,20,23-octaoxapentacosan-25-yl 2-bromo-2,2-difluoroacetate **94d** (0.1 M in DMSO, 400 µL, 40.0 µmol, 2.00 eq.). The reaction mixture was irradiated with blue LEDs for 10 min then the yield was determined by quantitative ^{19}F NMR spectroscopy (60% yield); ^{19}F NMR (376 MHz, DMSO) δ −98.6 (s, 2F); HRMS (ESI) m/z: $[M + H]^+$ Calcd for $C_{34}H_{53}F_2N_2O_{13}$ 735.3516; Found 735.3535 (2.6 ppm error).

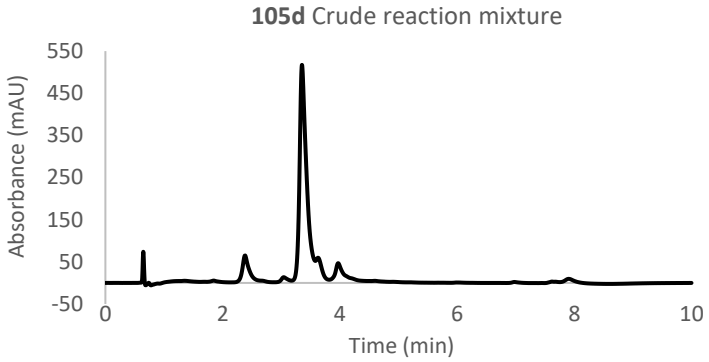

Figure 140. Reaction mixture analytical HPLC chromatogram for product **105d** Rt = 3.35 min on analytical gradient 40-80% B over 5 min, 0.6 mL min^{-1}, 280 nm.

Ethyl (*S*)-2-acetamido-3-(2-(1,1-difluoro-2-(hex-5-yn-1-yloxy)-2-oxoethyl)-1*H*-indol-3-yl)propanoate (105e) - analytical scale

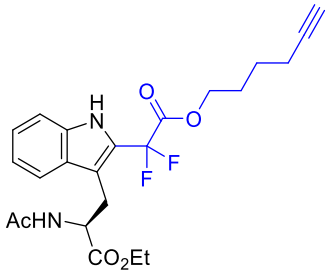

Prepared according to general procedure C using Ac-Trp-OEt **93** (0.1 M in DMSO, 200 µL, 20.0 µmol, 1.00 eq.), 4CzIPN (0.01 M in DMSO, 20 µL, 0.200 µmol, 1 mol%) and hex-5-yn-1-yl 2-bromo-2,2-difluoroacetate **94e** (0.1 M in DMSO, 400 µL, 40.0 µmol, 2.00 eq.). The reaction mixture was irradiated with blue LEDs for 30 min then the yield was determined by quantitative ^{19}F NMR spectroscopy (21% yield); ^{19}F NMR (376 MHz, DMSO) δ −98.7 (s, 2F); HRMS (ESI) m/z: $[M + H]^+$ Calcd for $C_{23}H_{27}F_2N_2O_5$ 449.1888; Found 449.1871 (3.8 ppm error).

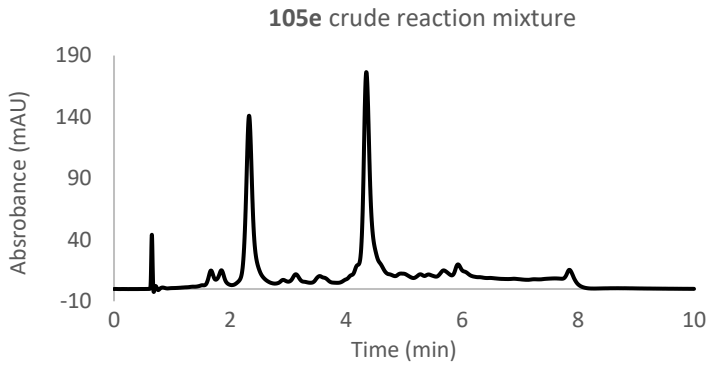

Figure 141. Reaction mixture analytical HPLC chromatogram for product **105e** Rt = 4.35 min on analytical gradient 40-80% B over 5 min, 0.6 mL min^{-1}, 280 nm.

Ethyl (*S*)-2-acetamido-3-(2-(2-(cyclopropylamino)-1,1-difluoro-2-oxoethyl)-1*H*-indol-3-yl)propanoate (105h) - analytical scale

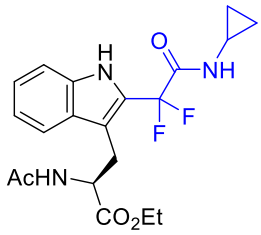

Prepared according to general procedure C using Ac-Trp-OEt **93** (0.1 M in DMSO, 200 µL, 20.0 µmol, 1.00 eq.), 4CzIPN (0.01 M in DMSO, 20 µL, 0.200 µmol, 1 mol%) and 2-bromo-N-cyclopropyl-2,2-difluoroacetamide **94h** (0.1 M in DMSO, 400 µL, 40.0 µmol, 2.00 eq.). The reaction mixture was irradiated with blue LEDs for 60 min then the yield was determined by quantitative ^{19}F NMR spectroscopy (65% yield); ^{19}F NMR (376 MHz, DMSO) δ −96.1 (d, 1F, *J* = 265 Hz), −97.0 (d, 1F, *J* = 265 Hz); HRMS (ESI) m/z: $[M + H]^+$ Calcd for $C_{20}H_{24}F_2N_3O_4$ 408.1735; Found 408.1719 (3.9 ppm error).

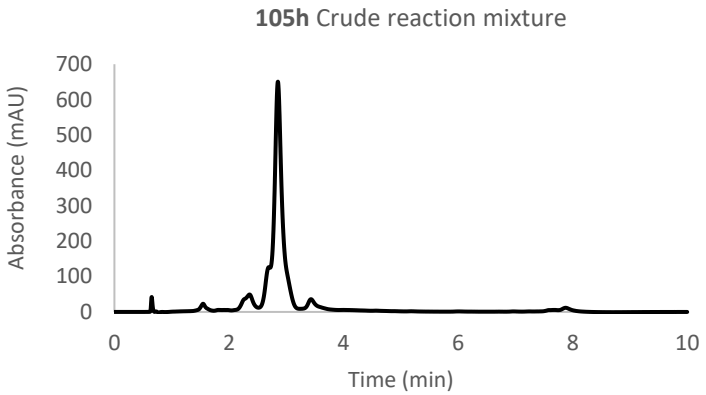

Figure 142. Reaction mixture analytical HPLC chromatogram for product **105h** Rt = 2.85 min on analytical gradient 40-80% over 5 min, 0.6 mL min^{-1}, 280 nm.

Ethyl (*S*)-2-acetamido-3-(2-(2-(benzylamino)-1,1-difluoro-2-oxoethyl)-1*H*-indol-3-yl)propanoate (105i) - analytical scale

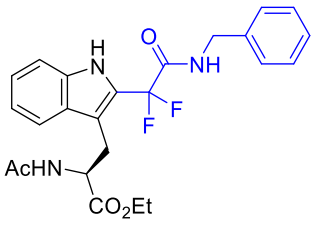

Prepared according to general procedure C using Ac-Trp-OEt **93** (0.1 M in DMSO, 200 µL, 20.0 µmol, 1.00 eq.), 4CzIPN (0.01 M in DMSO, 20 µL, 0.200

μmol, 1 mol%) and 2-bromo-*N*-benzyl-2,2-difluoroacetamide **94i** (0.1 M in DMSO, 400 μL, 40.0 μmol, 2.00 eq.). The reaction mixture was irradiated with blue LEDs for 60 min then the yield was determined by quantitative ^{19}F NMR spectroscopy (53% yield); ^{19}F NMR (376 MHz, DMSO) δ −96.4 (d, 1F, *J* = 266 Hz), −97.3 (d, 1F, *J* = 266 Hz); HRMS (ESI) m/z: [M − H]$^-$ Calcd for $C_{24}H_{24}F_2N_3O_4$ 456.1735; Found 456.1731 (0.9 ppm error).

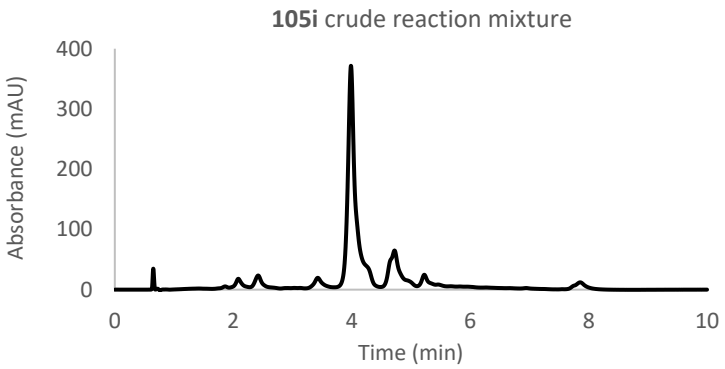

Figure 143. Reaction mixture analytical HPLC chromatogram for product **105i** Rt = 3.99 min on analytical gradient 40-80% B over 5 min, 0.6 mL min^{-1}, 280 nm.

Ethyl (*S*)-2-acetamido-3-(2-(2-(benzylamino)-1,1-difluoro-2-oxoethyl)-1*H*-indol-3-yl)propanoate (105i)

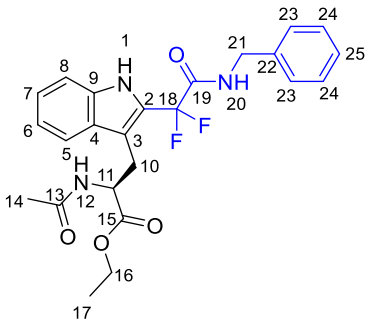

Prepared according to general procedure D using Ac-Trp-OEt **93** (54.9 mg, 200 μmol, 1.00 eq.), 4CzIPN (1.6 mg, 2.00 μmol, 1 mol%) and 2-bromo-N-benzyl-2,2-difluoroacetamide **94i** (106 mg, 400 μmol, 2.00 eq.). The reaction mixture was irradiated with blue LEDs for 30 min then was analysed by quantitative ^{19}F NMR spectroscopy (51% yield) and analytical HPLC. The crude material was purified by flash column chromatography (SiO_2, pentane/EtOAc, 1:1) to give the title compound **105i** (48.1 mg, 0.105 mmol, 53%) as a colourless crystalline solid; R_f = 0.48 (pentane/EtOAc, 1:1); mp = 60-62 °C; υ_{max}/cm^{-1} (ATR) 3283, 3112, 3064, 3032, 2980, 2921, 2850, 1731, 1688, 1650; ^{1}H NMR (400 MHz, $CDCl_3$) δ 9.19 (1H, s, H-

1), 7.80 (t, *J* = 5.0 Hz, 1H, H-20), 7.58 (1H, d, *J* = 8.0 Hz, H-8), 7.35 (1H, d, *J* = 8.2 Hz, H-5), 7.32 – 7.19 (6H, m, H-23,24,25, H-6), 7.13 (1H, ddd, *J* = 8.0, 6.9, 0.9 Hz, H-7), 6.71 (1H, d, *J* = 7.3 Hz, H-12), 4.73 (1H, ddd, *J* = 7.3, 7.2, 7.2 Hz, H-11), 4.64 – 4.39 (2H, m, H-21), 4.12 – 3.87 (2H, m, H-16), 3.42 – 3.23 (2H, m, H-10), 1.85 (3H, s, H-14), 1.03 (3H, t, *J* = 7.1 Hz, H-17); $^{13}C\ \{^{1}H\}$ NMR (101 MHz, $CDCl_3$) δ 172.2 (C, C-15), 170.8 (C, C-13), 163.7 (C, t, *J* = 31.2 Hz, C-19), 136.7 (C, C-9), 135.8 (C, C-22), 128.9 (CH, C-24), 128.1 (CH, C-23), 128.1 (C, C-4), 127.8 (C, C-25), 125.3 (C, t, *J* = 29.9 Hz, C-2), 124.5 (CH, C-6), 120.6 (CH, C-7), 119.6 (CH, C-8), 112.8 (C, t, *J* = 251 Hz, C-18), 112.1 (CH, C-5), 111.8 (C, t, *J* = 2.0 Hz, C-3), 61.8 (CH_2, C-16), 53.6 (CH, C-11), 44.0 (CH_2, C-21), 27.2 (CH_2, C-10), 22.8 (CH_3, C-14), 13.9 (CH_3, C-17); ^{19}F NMR (376 MHz, $CDCl_3$) δ −97.7 (1F, d, *J* = 268.0 Hz, F-18), −101.6 (1F, d, *J* = 268.0 Hz, F-18); HRMS (ESI) m/z: $[M + Na]^+$ Calcd for $C_{24}H_{25}F_2N_3NaO_4$ 480.1705; Found 480.1706 (0.2 error).

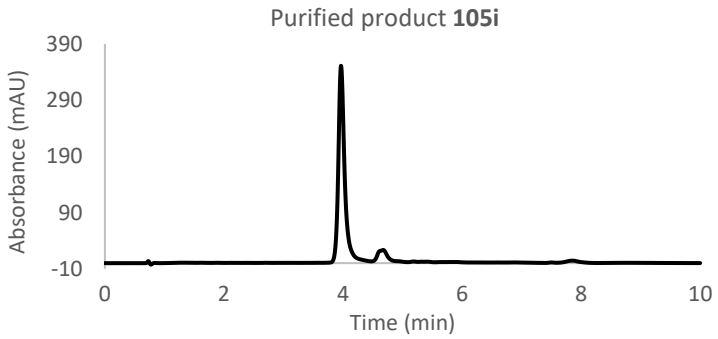

Figure 144. Analytical HPLC chromatogram for purified product **105i** Rt = 3.97 min on analytical gradient 40-80% B over 5 min, 0.6 mL min^{-1}, 280 nm.

Ethyl (*S*)-2-acetamido-3-(2-(1,1-difluoro-2-oxo-2-((pyridin-3-ylmethyl)amino)ethyl)-1*H*-indol-3-yl)propanoate (105j) - analytical scale

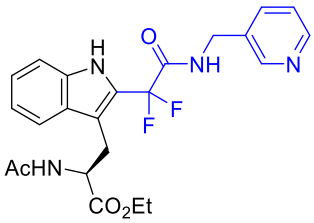

Prepared according to general procedure C using Ac-Trp-OEt **93** (0.1 M in DMSO, 200 µL, 20.0 µmol, 1.00 eq.), 4CzIPN (0.01 M in DMSO, 20 µL, 0.200 µmol, 1 mol%) and 2-bromo-2,2-difluoro-*N*-(pyridin-3-ylmethyl)acetamide **94j** (0.1 M in DMSO, 400 µL, 40.0 µmol, 2.00 eq.). The reaction mixture was irradiated with blue LEDs for 30 min then the yield was determined by quantitative ^{19}F NMR spectroscopy (48%); ^{19}F NMR (376 MHz, DMSO) δ −96.5 (d, 1F, *J* = 267 Hz), −97.2 (d, 1F, *J* = 267 Hz); HRMS (ESI) m/z: [M + H]$^+$ Calcd for $C_{23}H_{25}F_2N_4O_4$ 459.1838; Found 459.1846 (1.6 ppm error).

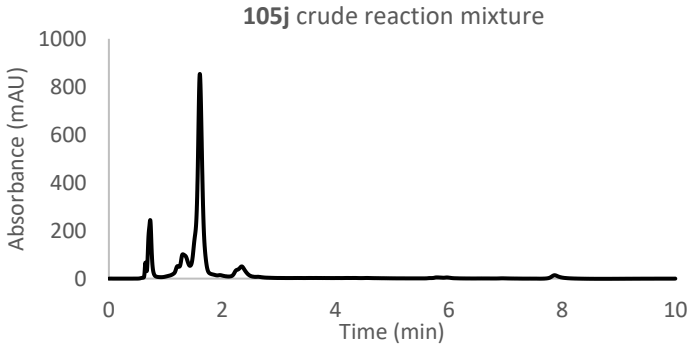

Figure 145. Reaction mixture analytical HPLC chromatogram for product **105j** Rt = 1.61 min on analytical gradient 40-80% B over 5 min, 0.6 mL min^{-1}, 280 nm.

Ethyl (*S*)-2-acetamido-3-(2-(2-(*tert*-butylamino)-1,1-difluoro-2-oxoethyl)-1*H*-indol-3-yl)propanoate (105k) - analytical scale

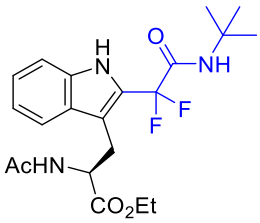

Prepared according to general procedure C using Ac-Trp-OEt **93** (0.1 M in DMSO, 200 µL, 20.0 µmol, 1.00 eq.), 4CzIPN (0.01 M in DMSO, 20 µL, 0.200 µmol, 1 mol%) and *2*-bromo-*N*-(*tert*-butyl)-2,2-difluoroacetamide **94k** (0.1

M in DMSO, 400 µL, 40.0 µmol, 2.00 eq.). The reaction mixture was irradiated with blue LEDs for 75 min then the yield was determined by quantitative ^{19}F NMR spectroscopy (50% yield); ^{19}F NMR (376 MHz, DMSO) δ −95.4 (d, *J* = 262 Hz), −97.4 (d, *J* = 262 Hz); HRMS (ESI) m/z: $[M + H]^+$ Calcd for $C_{21}H_{28}F_2N_3O_4$ 424.2048; Found 424.2057 (2.1 ppm error).

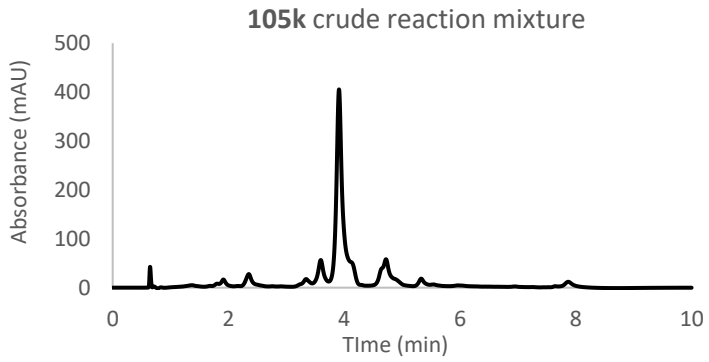

Figure 146. Reaction mixture analytical HPLC chromatogram for product **105k** Rt = 3.91 min on analytical gradient 40-80% B over 5 min, 0.6 mL min^{-1}, 280 nm.

Ethyl (*S*)-2-acetamido-3-(2-(1,1-difluoro-2-morpholino-2-oxoethyl)-1*H*-indol-3-yl)propanoate (105l) - analytical scale

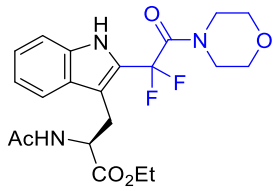

Prepared according to general procedure C using Ac-Trp-OEt **93** (0.1 M in DMSO, 200 µL, 20.0 µmol, 1.00 eq.), 4CzIPN (0.01 M in DMSO, 20 µL, 0.200 µmol, 1 mol%) and 2-bromo-2,2-difluoro-1-morpholinoethan-1-one **94l** (0.1 M in DMSO, 400 µL, 40.0 µmol, 2.00 eq.). The reaction mixture was irradiated with blue LEDs for 15 min then the yield was determined by quantitative ^{19}F NMR spectroscopy (39% yield); ^{19}F NMR (376 MHz, DMSO) δ −88.7 (d, *J* = 274 Hz), −89.8 (d, *J* = 274 Hz); HRMS (ESI) m/z: $[M + H]^+$ Calcd for $C_{21}H_{26}F_2N_3O_5$ 438.1841; Found 438.1838 (0.7 ppm error).

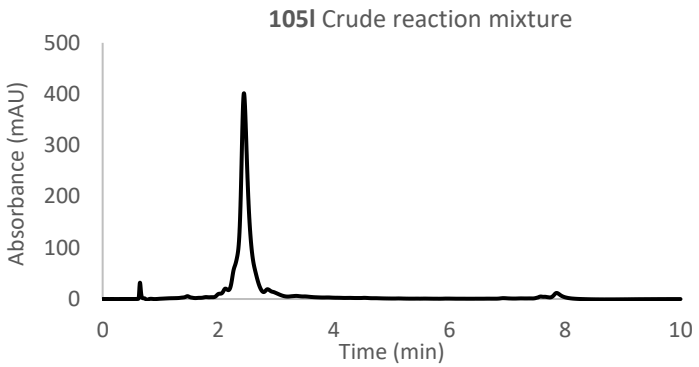

Figure 147. Reaction mixture analytical HPLC chromatogram for product **105l** Rt = 2.45 min on analytical gradient 40-80% B over 5 min, 0.6 mL min^{-1}, 280 nm.

Ethyl (*S*)-2-acetamido-3-(2-(1,1-difluoro-2-oxo-2-((2-(5-((3a*S*,4*S*,6a*R*)-2-oxohexahydro-1*H*-thieno[3,4-d]imidazol-4-yl)pentanamido)ethyl)amino)ethyl)-1*H*-indol-3-yl)propanoate (105m) -analytical scale

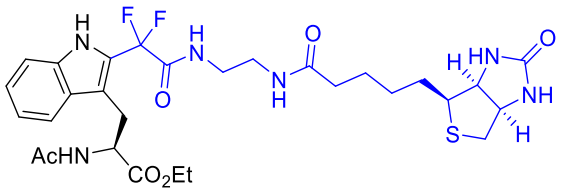

Prepared according to general procedure C using Ac-Trp-OEt **93** (0.1 M in DMSO, 200 µL, 20.0 µmol, 1.00 eq.), 4CzIPN (0.01 M in DMSO, 20 µL, 0.200 µmol, 1 mol%) and *N*-(2-(2-bromo-2,2-difluoroacetamido)ethyl)-5-((3a*S*,4*S*,6a*R*)-2-oxohexahydro-1*H*-thieno[3,4-d]imidazol-4-yl)pentanamide **94m** (0.1 M in DMSO, 400 µL, 40.0 µmol, 2.00 eq.). The reaction mixture was irradiated with blue LEDs for 150 min then the yield was determined by quantitative ^{19}F NMR spectroscopy (40% yield); ^{19}F NMR (376 MHz, DMSO) δ −97.4 (s, 2F); HRMS (ESI) m/z: $[M + H]^+$ Calcd for $C_{29}H_{39}F_2N_6O_6S$ 637.2620; found: 637.2591 (4.6 ppm error).

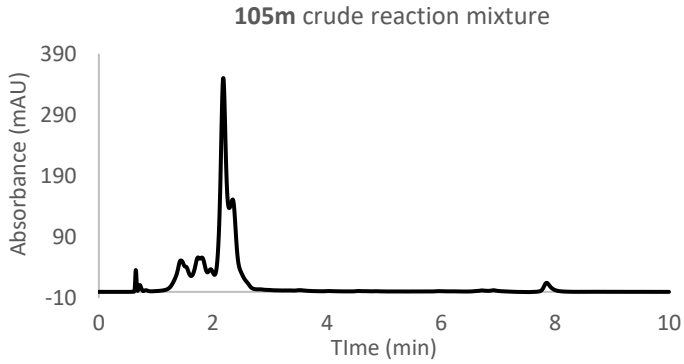

Figure 148. Reaction mixture analytical HPLC chromatogram for product **105m** Rt = 2.18 min on analytical gradient 40-80% B over 5 min, 0.6 mL min^{-1}, 280 nm.

6.5 Photochemical Alkylation of Trp-containing Peptides and Protein

General Procedure E: Photocatalytic Difluoroalkylation of Trp-containing peptides

A solution of peptide (25 mM in DMSO, 200 µL, 5.00 µmol, 1.00 eq.), 4CzIPN (2.5 mM in DMSO, 20 µL, 0.0500 µmol, 1 mol%) and bromodifluoroalkyl reagent (100 mM in DMSO, 100 µL, 10.0 µmol, 2.00 eq.) in DMSO (180 µL, total solvent volume 500 µL) was purged with N_2 (5 min) and then irradiated with blue LEDs (PhotoRedOx box, 18 W) for 10 - 150 min at room temperature. α,α,α-Trifluorotoluene (101 µL, 16.5 mM in DMSO, 1.65 µmol, 0.333 eq.) was added to the reaction mixture, then quantitative NMR spectroscopy and analytical HPLC analysis were carried out. The reaction mixture was diluted with 0.1% TFA in H_2O (2.60 mL) and then purified by semi-preparative HPLC.

Ac-WHISKEY-NH_2 conjugated with ethyl bromodifluoroacetate (166a)

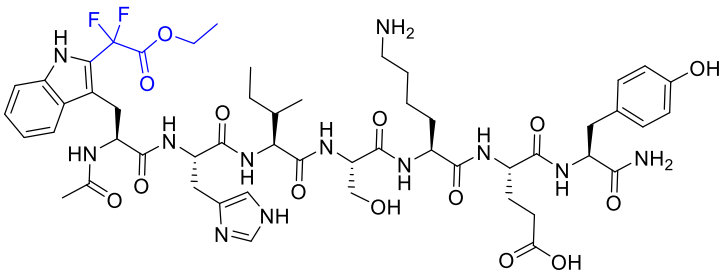

Prepared according to general procedure E using Ac-WHISKEY-NH_2 **163** (25.0 mM in DMSO, 200 µL, 5.00 µmol, 1.00 eq.), 4CzIPN (2.50 mM in DMSO, 20 µL, 0.0500 µmol, 1 mol%) and ethyl bromodifluoroacetate **94a** (0.1 M in DMSO, 100 µL, 10.0 µmol, 2.00 eq.). The reaction mixture was irradiated with blue LEDs for 10 min, then was analysed by quantitative ^{19}F NMR spectroscopy (55% yield). The reaction mixture was then purified by semi-preparative RP-HPLC (2-70% B over 30 min) to give the title compound **5a** (2.4 mg, 2.13 µmol, 43%) as a colourless powder; ^{1}H NMR (500 MHz, CD_3OD) δ 8.69 (d, 1H, *J* = 1.4 Hz), 7.58 (dd, 1H, *J* = 8.2, 1.1 Hz), 7.36 (dd, 1H, *J* = 8.3, 1.0 Hz), 7.24 (d, 1H, *J* = 1.4 Hz), 7.20 (ddd, 1H, *J* = 8.3, 6.9, 1.1 Hz), 7.11 – 7.00 (m, 3H), 6.69 (d, 2H, *J* = 8.5 Hz), 4.50 (dd, 1H, *J* = 8.7, 5.6 Hz), 4.46 – 4.39 (m, 3H), 4.38 – 4.31 (m, 2H), 4.31 – 4.23 (m, 2H), 4.04 (d, 1H, *J* = 7.3 Hz), 3.83 (dd, 1H, *J* = 10.9, 5.7 Hz), 3.77 (dd, 1H, *J* = 10.9, 6.0 Hz), 3.28 – 3.21 (m, 2H), 3.08 – 3.00 (m, 2H), 2.94 – 2.88 (m, 2H), 2.88 – 2.80 (m, 1H), 2.40 – 2.23 (m, 2H), 2.07 – 1.97 (m, 1H), 1.96 (s, 3H), 1.93 – 1.77 (m, 3H), 1.76 – 1.68 (m, 1H), 1.68 – 1.58 (m, 2H), 1.54 – 1.46 (m, 1H), 1.47 – 1.38 (m, 2H), 1.33 – 1.26 (m, 4H), 1.22 – 1.10 (m, 1H), 1.00 – 0.86 (m, 6H); ^{19}F NMR (376 MHz, CD_3OD) δ −77.0 (s, TFA), −101.4 (d, 1F, *J* = 266 Hz), −103.5 (d, 1F, *J* = 266 Hz); HRMS (ESI) m/z: $[M + H]^+$ Calcd for $C_{52}H_{71}F_2N_{12}O_{14}$ 1125.5181; Found 1125.5141 (3.6 ppm error).

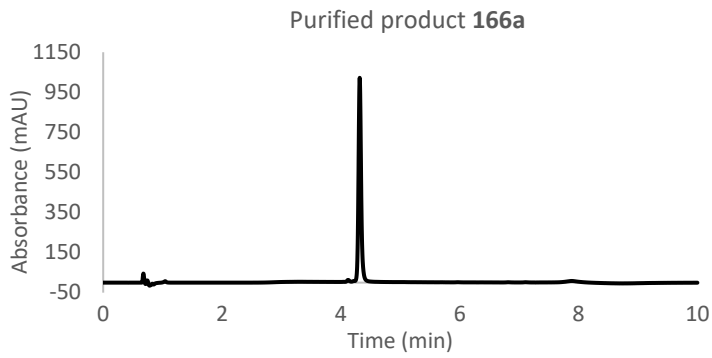

Figure 149. Analytical HPLC chromatogram for purified product **166a** Rt = 4.32 min on analytical gradient 2-95% B over 5 min, 0.6 mL min^{-1}, 280 nm.

Confirmation of regioselectivity and chemoselectivity was carried out using ^{1}H NMR spectroscopy to show the disappearance of the C−2 proton on Trp. COSY/ TOCSY experiments were carried out to show that the two signals in the aromatic region of the product spectrum (8.69 and 7.24 ppm) are coupling which proved that they correspond to the histidine proton signals. This was carried out for every alkylated peptide product and a representative example is shown below.

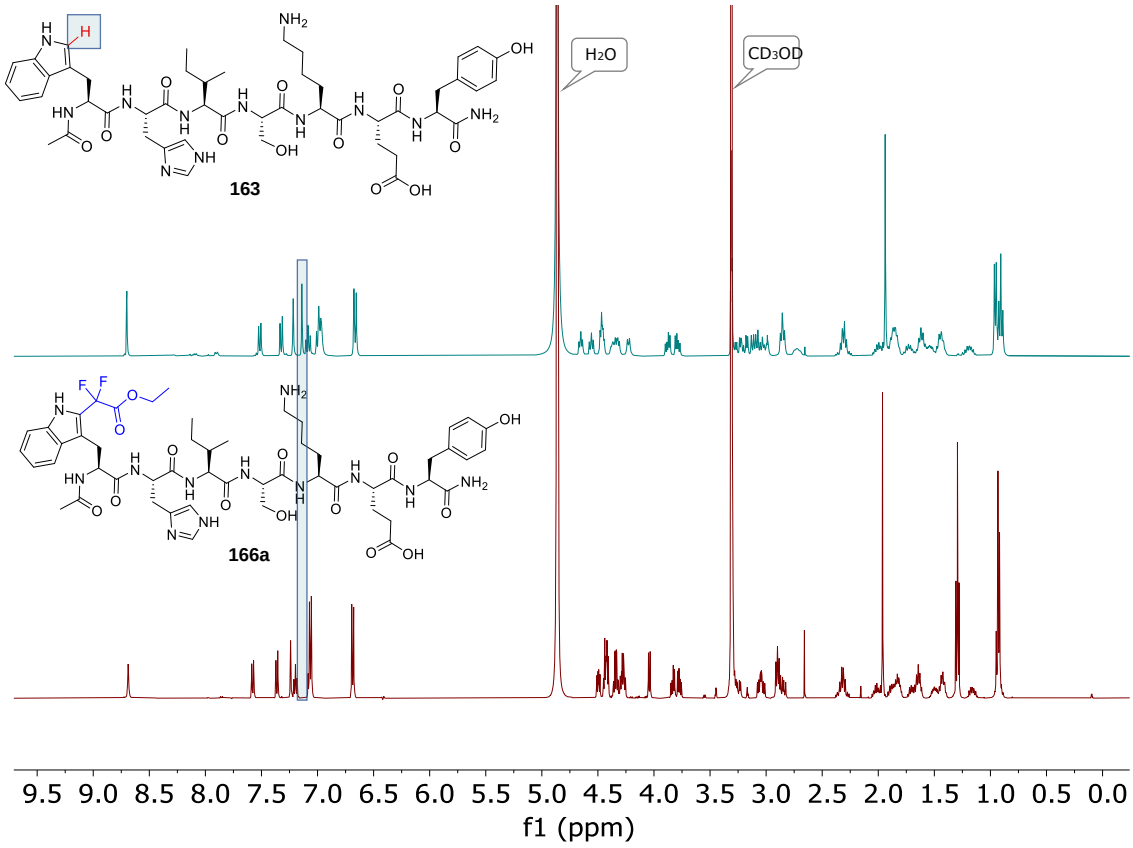

Figure 150. Stacked ^{1}H NMR spectrum of peptide **163** and product **166a** (400/500 MHz, CD_3OD).

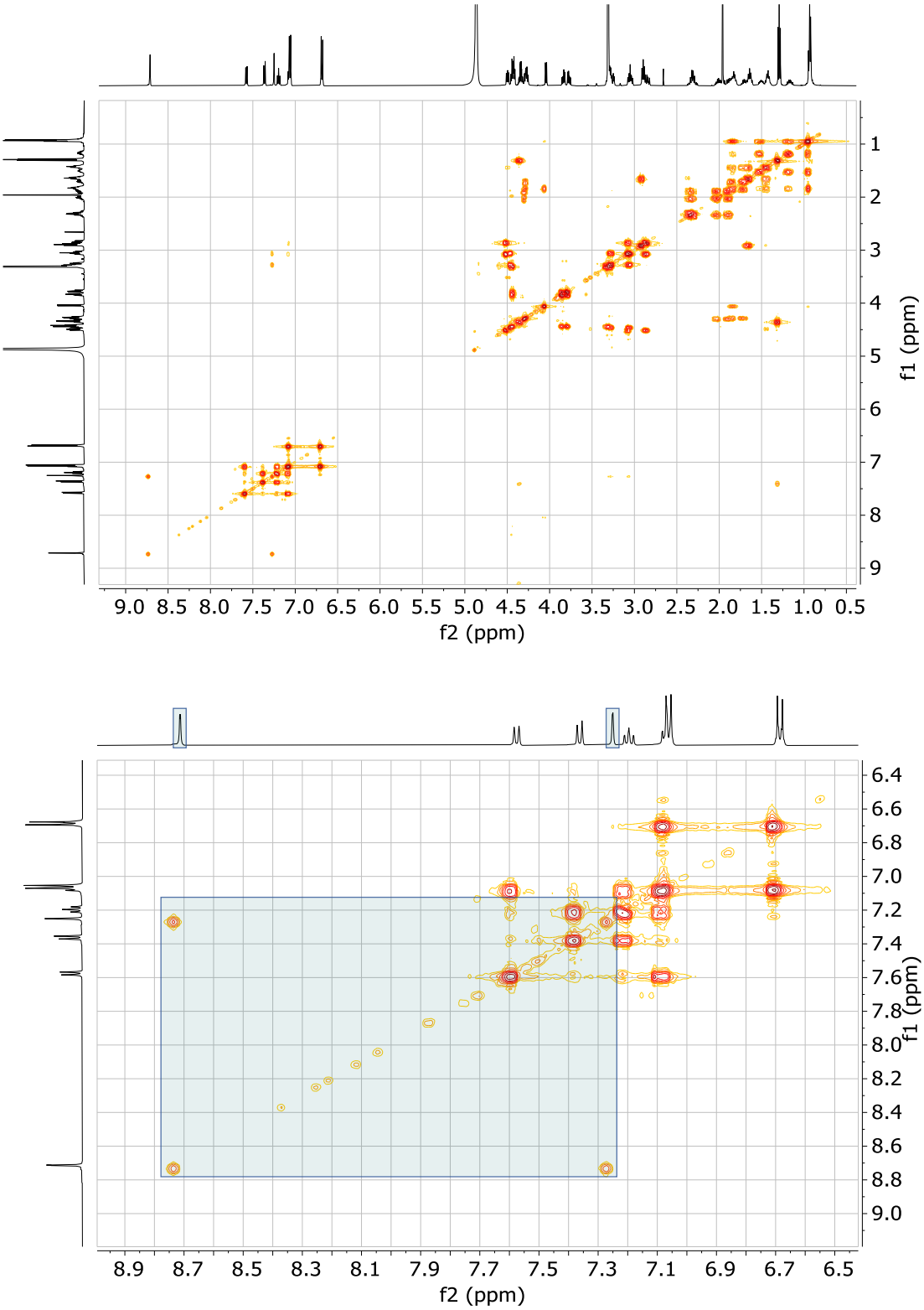

Figure 151. COSY spectrum of product **166a** (500 MHz, CD_3OD).

Ac-WHISKEY-NH_2 conjugated with benzyl 2-bromo-2,2-difluoroacetate (166b)

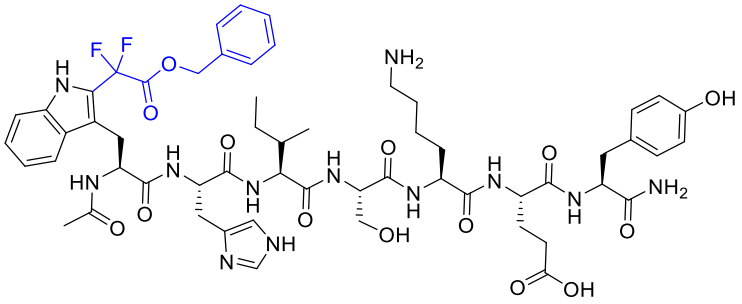

Prepared according to general procedure E using Ac-WHISKEY-NH_2 **163** (25.0 mM in DMSO, 200 µL, 5.00 µmol, 1.00 eq.), 4CzIPN (2.50 mM in DMSO, 20 µL, 0.0500 µmol, 1 mol%) and benzyl 2-bromo-2,2-difluoroacetate **94b** (0.1 M in DMSO, 100 µL, 10.0 µmol, 2.00 eq.). The reaction mixture was irradiated with blue LEDs for 10 min, then was analysed by quantitative ^{19}F NMR spectroscopy (42% yield). The reaction mixture was purified by semi-preparative RP-HPLC (2-70% B over 30 min) to give the title compound **166b** (2.80 mg, 2.36 µmol, 47%) as a colourless powder; ^{1}H NMR (400 MHz, CD_3OD) δ 8.55 (s, 1H), 7.57 (dd, 1H, *J* = 8.2, 0.6 Hz), 7.36 (dd, 1H, *J* = 8.3, 0.9 Hz), 7.35 – 7.24 (m, 5H), 7.24 – 7.16 (m, 2H), 7.12 – 7.00 (m, 3H), 6.68 (d, 2H, *J* = 8.4 Hz), 5.32 (d, 1H, *J* = 12.2 Hz), 5.32 (d, 1H, *J* = 12.2 Hz), 4.53 – 4.46 (m, 1H), 4.46 – 4.34 (m, 3H), 4.31 – 4.20 (m, 2H), 4.03 (d, 1H, *J* = 7.2 Hz), 3.90 – 3.74 (m, 2H), 3.28 – 3.14 (m, 3H), 3.11 – 2.98 (m, 2H), 2.96 – 2.79 (m, 3H), 2.39 – 2.24 (m, 2H), 2.07 – 1.96 (m, 1H), 1.94 (s, 3H), 1.92 – 1.76 (m, 3H), 1.75 – 1.66 (m, 1H), 1.66 – 1.57 (m, 2H), 1.54 – 1.45 (m, 1H), 1.45 – 1.35 (m, 2H), 1.23 – 1.06 (m, 1H), 1.00 – 0.82 (m, 6H); ^{19}F NMR (377 MHz, CD_3OD) δ −76.9 (s, TFA), −102.2 (d, 1F, *J* = 266 Hz), −103.1 (d, 1F, *J* = 266 Hz); HRMS (ESI) m/z: $[M + H]^+$ Calcd for $C_{57}H_{73}F_2N_{12}O_{14}$ 1187.5337; Found 1187.5307 (2.5 ppm error).

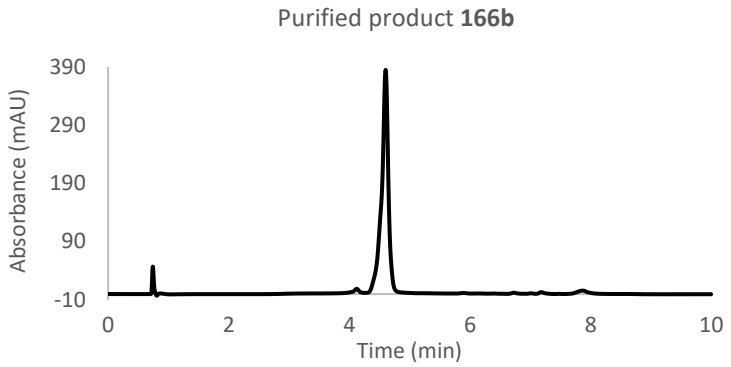

Figure 152. Analytical HPLC chromatogram for purified product **166b** Rt = 4.60 min on analytical gradient 2-95% B over 5 min, 0.6 mL min^{-1}, 280 nm.

Ac-WHISKEY-NH_2 conjugated with 4-bromobenzyl 2-bromo-2,2-difluoroacetate (166c)

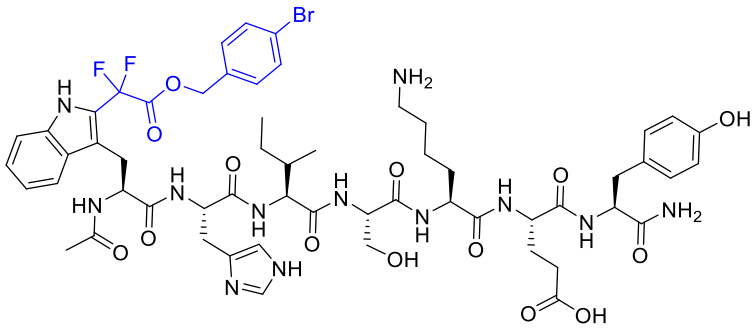

Prepared according to general procedure E using Ac-WHISKEY-NH_2 **163** (25.0 mM in DMSO, 200 µL, 5.00 µmol, 1.00 eq.), 4CzIPN (2.50 mM in DMSO, 20 µL, 0.0500 µmol, 1 mol%) and 4-bromobenzyl 2-bromo-2,2-difluoroacetate **94c** (0.1 M in DMSO, 100 µL, 10.0 µmol, 2.00 eq.). The reaction mixture was irradiated with blue LEDs for 10 min, then was analysed by quantitative ^{19}F NMR spectroscopy (43% yield). The reaction mixture was purified by semi-preparative RP-HPLC (2-70% B over 30 min) to give to give the title compound **166c** (2.4 mg, 1.90 µmol, 38%) as a colourless powder; ^{1}H NMR (500 MHz, DMSO-d_6) δ 14.20 – 13.70 (m, 1H), 12.09 (s, 1H), 11.64 (s, 1H), 9.16 (s, 1H), 8.94 (s, 1H), 8.16 (d, 1H, *J* = 7.4 Hz), 8.08 (d, 1H, *J* = 7.8 Hz), 8.03 – 7.93 (m, 3H), 7.82 (d, 1H, *J* = 8.3 Hz), 7.76 (d, 1H, *J* = 8.1 Hz), 7.69 (d, 1H, *J* = 8.1 Hz), 7.64 – 7.56 (m, 3H), 7.53 (d, 2H, *J* = 8.4 Hz), 7.37 (d, 1H, *J* = 8.2 Hz), 7.35 – 7.31 (m, 1H), 7.29 (d, 2H, *J* = 8.4 Hz), 7.27 – 7.23 (m, 1H), 7.20 (dd, 1H, *J* = 8.2, 7.6 Hz), 7.07 – 7.03 (m, 2H), 6.99 (d, 2H, *J* = 8.5 Hz), 6.63 (d, 2H, *J* = 8.5 Hz), 5.32 (s, 2H), 4.63 – 4.53 (m, 1H), 4.45 – 4.37 (m, 1H), 4.37 – 4.27

(m, 2H), 4.26 – 4.11 (m, 3H), 3.66 – 3.50 (m, 2H), 3.23 – 3.14 (m, 1H), 3.13 – 3.05 (m, 1H), 3.05 – 2.91 (m, 2H), 2.91 – 2.81 (m, 1H), 2.77 – 2.67 (m, 3H), 2.23 – 2.13 (m, 2H), 1.91 – 1.81 (m, 1H), 1.73 – 1.62 (m, 6H), 1.54 – 1.45 (m, 3H), 1.45 – 1.35 (m, 1H), 1.33 – 1.23 (m, 2H), 1.10 – 1.02 (m, 1H), 0.85 – 0.71 (m, 6H); ^{19}F NMR (376 MHz, DMSO-d_6) δ −73.5 (s, TFA), −98.3 (d, 1F, *J* = 265 Hz), −99.1 (d, 1F, *J* = 265 Hz); HRMS (ESI) m/z: [M + H]$^+$ Calcd for $C_{57}H_{72}{}^{79}BrF_2N_{12}O_{14}$ 1265.4442; Found 1265.4322 (9.5 ppm error).

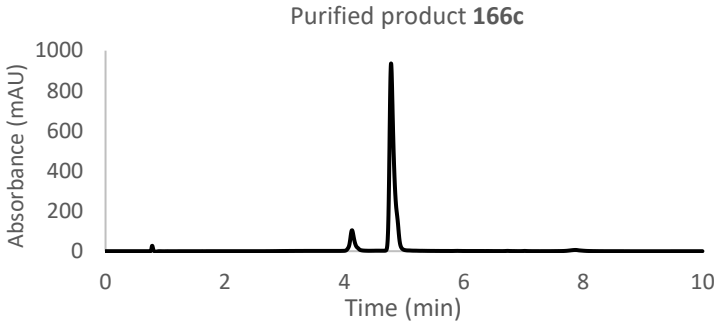

Figure 153. Analytical HPLC chromatogram for purified product **166c** Rt = 4.78 min on analytical gradient 2-95% B over 5 min, 0.6 mL min^{-1}, 280 nm.

Ac-WHISKEY-NH$_2$ conjugated with 2,5,8,11,14,17,20,23-octaoxapentacosan-25-yl 2-bromo-2,2-difluoroacetate (166d)

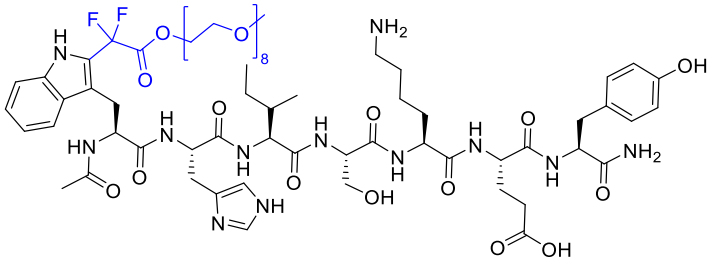

Prepared according to general procedure E using Ac-WHISKEY-NH$_2$ **163** (25.0 mM in DMSO, 200 µL, 5.00 µmol, 1.00 eq.), 4CzIPN (2.50 mM in DMSO, 20 µL, 0.0500 µmol, 1 mol%) and 2,5,8,11,14,17,20,23-octaoxapentacosan-25-yl 2-bromo-2,2-difluoroacetate **94d** (0.1 M in DMSO, 100 µL, 10.0 µmol, 2.00 eq.). The reaction mixture was irradiated with blue LEDs for 10 min, then was analysed by quantitative ^{19}F NMR spectroscopy (42% yield). The reaction mixture was purified by semi-preparative RP-HPLC (2-70% B over 30 min) to give the title compound **166d** (3.5 mg, 2.39 µmol, 48%) as a colourless powder; ^{1}H NMR (400 MHz, CD$_3$OD) δ 8.71 (d, 1H, *J* = 1.0 Hz), 7.59 (d, 1H, *J* = 8.0 Hz), 7.38 (d, 1H, *J*

= 8.2 Hz), 7.25 (d, 1H, *J* = 1.0 Hz), 7.21 (ddd, 1H, *J* = 8.2, 6.9, 1.1 Hz), 7.12 – 7.03 (m, 3H), 6.68 (d, 2H, *J* = 8.3 Hz), 4.56 – 4.36 (m, 5H), 4.34 – 4.22 (m, 2H), 4.05 (d, 1H, *J* = 7.2 Hz), 3.84 (dd, 1H, *J* = 10.9, 5.6 Hz), 3.77 (dd, 1H, *J* = 10.9, 6.0 Hz), 3.71 (dd, 2H, *J* = 5.3, 4.5 Hz), 3.69 – 3.57 (m, 20H), 3.57 – 3.47 (m, 8H), 3.46 – 3.41 (m, 2H), 3.34 (s, 3H), 3.25 – 3.20 (m, 1H), 3.11 – 2.97 (m, 2H), 2.94 – 2.87 (m, 2H), 2.87 – 2.78 (m, 1H), 2.48 – 2.20 (m, 2H), 2.10 – 1.98 (m, 1H), 1.96 (s, 3H), 1.94 – 1.78 (m, 3H), 1.77 – 1.68 (m, 1H), 1.68 – 1.58 (m, 2H), 1.56 – 1.47 (m, 1H), 1.48 –1.38 (m, 2H), 1.37 – 1.23 (m, 2H), 1.22 – 1.10 (m, 1H), 0.97 – 0.87 (m, 6H); ^{19}F NMR (376 MHz, CD_3OD) δ −77.0 (s, TFA) −101.2 (d, 1F, J = 265 Hz), −103.8 (d, 1F, J = 265 Hz); HRMS (ESI) m/z: $[M - H + C_2HF_3O_2]^-$ Calcd for $C_{67}H_{99}F_2N_{12}O_{22}$ 1575.6894; Found 1575.6959 (4.1 ppm error).

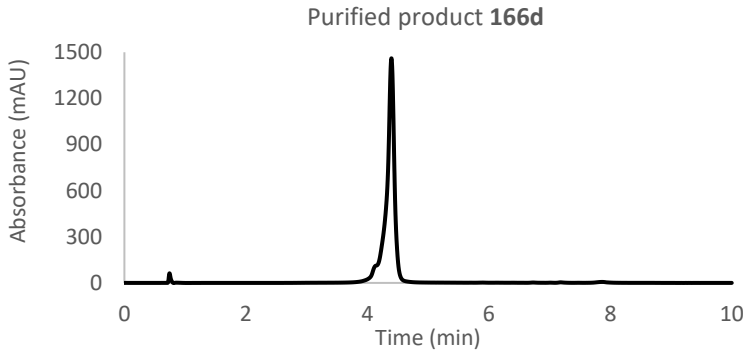

Figure 154. Analytical HPLC chromatogram for purified product **166d** Rt = 4.40 min on analytical gradient 2-95% B over 5 min, 0.6 mL min^{-1}, 280 nm.

Ac-WHISKEY-NH$_2$ conjugated with hex-5-yn-1-yl 2-bromo-2,2-difluoroacetate (5e)

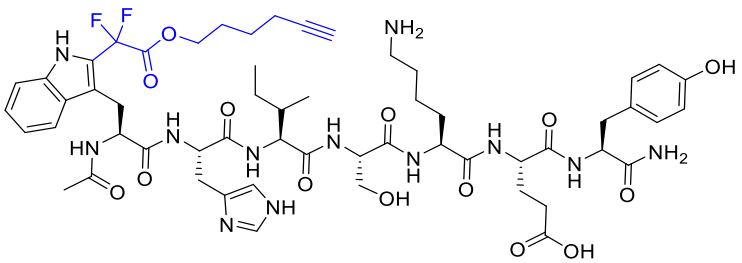

Prepared according to general procedure E using Ac-WHISKEY-NH$_2$ **163** (25.0 mM in DMSO, 200 µL, 5.00 µmol, 1.00 eq.), 4CzIPN (2.50 mM in DMSO, 20 µL, 0.0500 µmol, 1 mol%) and hex-5-yn-1-yl 2-bromo-2,2-difluoroacetate **94e** (0.100 M in DMSO, 100 µL, 10.0 µmol, 2.00 eq.). The reaction mixture was irradiated with blue LEDs for 30 min, then was

analysed by quantitative ^{19}F NMR spectroscopy (15% yield). The reaction mixture was purified by semi-preparative RP-HPLC (2-70% B over 30 min) to give the title compound **166e** (1.0 mg, 0.85 μmol, 17%) as a colourless powder; ^{1}H NMR (400 MHz, CD_3OD) δ 8.59 (s, 1H), 7.58 (d, 1H, *J* = 8.2 Hz), 7.37 (d, 1H, *J* = 8.2 Hz), 7.22 (s, 1H), 7.21 – 7.16 (m, 1H), 7.09 – 6.98 (m, 3H), 6.69 (d, 2H, *J* = 8.4 Hz), 4.58 – 4.44 (m, 1H), 4.47 – 4.36 (m, 3H), 4.33 (dd, 2H, *J* = 6.9, 6.4 Hz), 4.30 – 4.18 (m, 2H), 4.04 (d, 1H, *J* = 7.2 Hz), 3.84 (dd, 1H, *J* = 10.9, 5.7 Hz), 3.78 (dd, 1H, *J* = 10.9, 5.8 Hz), 3.27 – 3.16 (m, 2H), 3.11 – 2.99 (m, 2H), 2.93 – 2.86 (m, 3H), 2.86 – 2.80 (m, 1H), 2.39 – 2.26 (m, 2H), 2.18 (dd, 1H, *J* = 3.0, 2.6 Hz), 2.13 (td, 2H, *J* = 6.9, 2.6 Hz), 2.07 – 1.85 (m, 3H), 1.97 (s, 3H), 1.85 – 1.74 (m, 3H), 1.74 – 1.57 (m, 3H), 1.55 – 1.39 (m, 5H), 1.22 – 1.10 (m, 1H), 0.96 – 0.90 (m, 6H); ^{19}F NMR (376 MHz, CD_3OD) δ −77.0 (s, TFA), −101.7 (d, 1F, *J* = 266 Hz), −103.3 (d, 1F, *J* = 266 Hz); HRMS (ESI) m/z: $[M - H + CF_3CO_2H]^-$ Calcd for $C_{56}H_{73}F_2N_{12}O_{14}$ 1289.5266; Found 1289.5311 (3.5 ppm error).

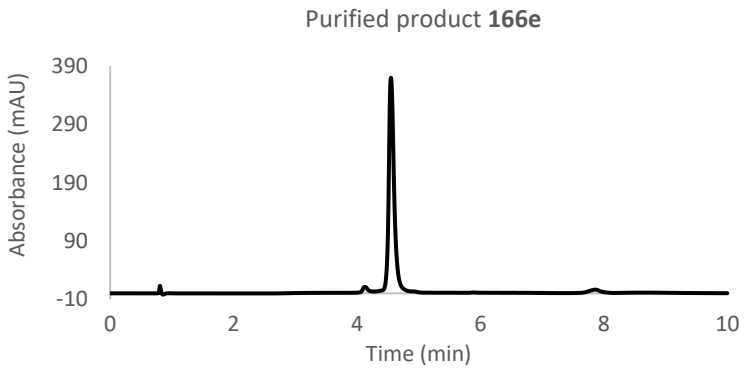

Figure 155. Analytical HPLC chromatogram for purified product **166e** Rt = 4.55 min on analytical gradient 2-95% B over 5 min, 0.6 mL min^{-1}, 280 nm.

Ac-WHISKEY-NH_2 conjugated with 2-bromo-*N*-cyclopropyl-2,2-difluoroacetamide (166h)

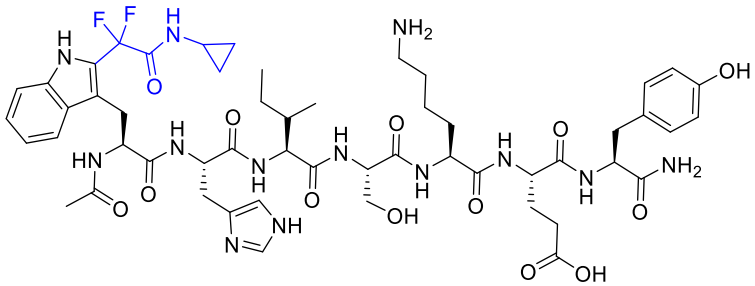

Prepared according to general procedure E using Ac-WHISKEY-NH_2 **163** (25.0 mM in DMSO, 200 µL, 5.00 µmol, 1.00 eq.), 4CzIPN (2.50 mM in DMSO, 20 µL, 0.0500 µmol, 1 mol%) and 2-bromo-*N*-cyclopropyl-2,2-difluoroacetamide **94h** (0.1 M in DMSO, 100 µL, 10.0 µmol, 2.00 eq.). The reaction mixture was irradiated with blue LEDs for 60 min, then was analysed by quantitative ^{19}F NMR spectroscopy (31% yield). The reaction mixture was then purified by semi-preparative RP-HPLC (2-70% B over 30 min) to give the title compound **166h** (2.10 mg, 1.85 µmol, 37%) as a colourless powder; ^{1}H NMR (500 MHz, CD_3OD) δ 8.71 (d, 1H, *J* = 1.4 Hz), 7.65 (d, 1H, *J* = 8.1 Hz), 7.37 (d, 1H, *J* = 8.3 Hz), 7.28 (d, 1H, *J* = 1.4 Hz), 7.21 (ddd, 1H, *J* = 8.3, 7.0, 1.1 Hz), 7.11 – 7.00 (m, 3H), 6.69 (d, 2H, *J* = 8.5 Hz), 4.61 – 4.53 (m, 2H), 4.50 (dd, 1H, *J* = 8.3, 5.7 Hz), 4.43 (dd, 1H, *J* = 6.1, 5.6 Hz), 4.29 (dd, 2H, *J* = 8.9, 5.5 Hz), 4.16 – 4.05 (m, 1H), 3.86 (dd, 1H, *J* = 10.9, 5.6 Hz), 3.79 (dd, 1H, *J* = 10.9, 6.1 Hz), 3.30 – 3.23 (m, 3H), 3.10 – 3.01 (m, 2H), 2.90 (dd, 2H, *J* = 8.7, 7.5 Hz), 2.88 – 2.80 (m, 2H), 2.40 – 2.25 (m, 2H), 2.09 – 1.97 (m, 1H), 1.95 (s, 3H), 1.93 – 1.81 (m, 3H), 1.77 – 1.69 (m, 1H), 1.66 (dd, 2H, *J* = 8.7, 7.4 Hz), 1.57 – 1.49 (m, 1H), 1.49 – 1.39 (m, 2H), 1.25 – 1.12 (m, 1H), 0.98 – 0.87 (m, 6H), 0.85 – 0.73 (m, 2H), 0.73 – 0.61 (m, 2H); ^{19}F NMR (376 MHz, DMSO) δ −73.5 (s, TFA), −96.2 (d, 1F, *J* = 266 Hz), −98.0 (d, 1F, *J* = 266 Hz); HRMS (ESI) m/z: $[M + H]^+$ Calcd for $C_{53}H_{72}F_2N_{13}O_{13}$ 1136.5341; Found 1136.5301 (3.5 ppm error).

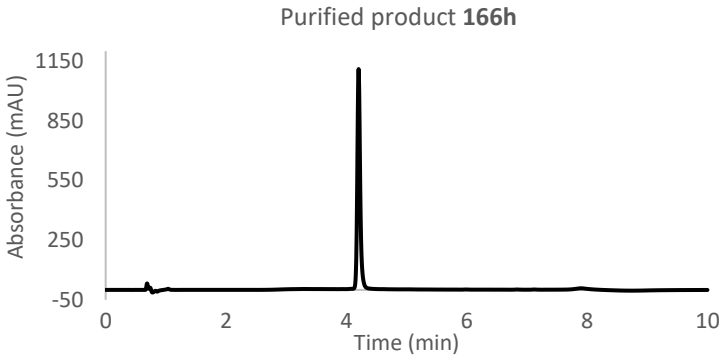

Figure 156. Analytical HPLC chromatogram for purified product **166h** Rt = 4.20 min on analytical gradient 2-95% B over 5 min, 0.6 mL min^{-1}, 280 nm.

Ac-WHISKEY-NH_2 conjugated with 2-bromo-*N*-benzyl-2,2-difluoroacetamide (166i)

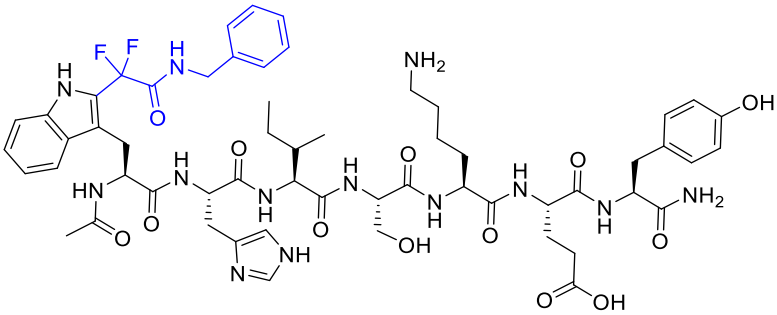

Prepared according to general procedure E using Ac-WHISKEY-NH_2 **163** (25.0 mM in DMSO, 200 µL, 5.00 µmol, 1.00 eq.), 4CzIPN (2.50 mM in DMSO, 20 µL, 0.0500 µmol, 1 mol%) and 2-bromo-*N*-benzyl-2,2-difluoroacetamide **94i** (0.1 M in DMSO, 100 µL, 10.0 µmol, 2.00 eq.). The reaction mixture was irradiated with blue LEDs for 60 min, then was analysed by quantitative ^{19}F NMR spectroscopy (28% yield). The reaction mixture was then purified by semi-preparative RP-HPLC (2-70% B over 30 min) to give the title compound **166i** (1.90 mg, 1.60 µmol, 32%) as a colourless powder; ^{1}H NMR (500 MHz, CD_3OD) δ 8.67 (s, 1H), 7.67 (d, 1H, *J* = 8.1 Hz), 7.39 (d, 1H, *J* = 8.2 Hz), 7.34 – 7.18 (m, 7H), 7.12 – 7.01 (m, 3H), 6.68 (d, 2H, *J* = 8.4 Hz), 4.63 – 4.54 (m, 2H), 4.53 – 4.46 (m, 3H), 4.43 (dd, 1H, *J* = 6.2, 5.8 Hz), 4.29 (dd, 2H, *J* = 8.8, 5.5 Hz), 4.11 (d, 1H, *J* = 7.3 Hz), 3.87 (dd, 1H, *J* = 10.9, 5.8 Hz), 3.80 (dd, 1H, *J* = 10.9, 6.2 Hz), 3.28 – 3.21 (m, 1H), 3.10 – 3.01 (m, 2H), 2.93 – 2.81 (m, 3H), 2.39 – 2.24 (m, 2H), 2.06 – 1.91 (m, 2H), 1.92 – 1.81 (m, 5H), 1.77 – 1.69 (m, 1H), 1.69 – 1.60 (m, 2H), 1.56 – 1.48 (m, 1H), 1.49 – 1.40 (m, 2H), 1.24 – 1.11 (m, 1H), 0.96 – 0.88 (m, 6H); ^{19}F NMR (376 MHz, DMSO-d_6) δ −73.4

(s, TFA), −96.6 (d, 1F, *J* = 266 Hz), −98.0 (d, 1F, *J* = 266 Hz); HRMS (ESI) m/z: [M + H]$^+$ Calcd for $C_{57}H_{74}F_2N_{13}O_{13}$1186.5497; Found 1186.5465 (2.7 ppm error).

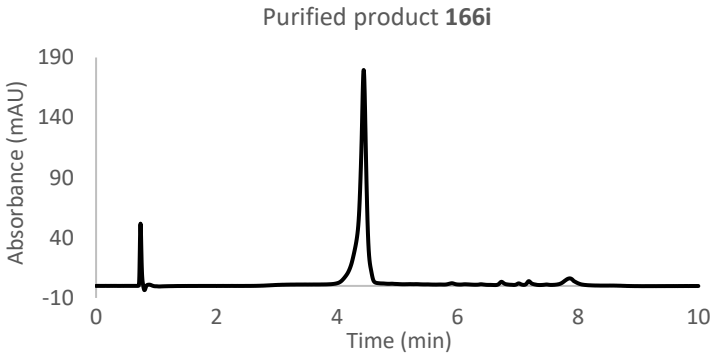

Figure 157. Analytical HPLC chromatogram for purified product **166i** Rt = 4.44 min on analytical gradient 2-95% B over 5 min, 0.6 mL min^{-1}, 280 nm.

Ac-WHISKEY-NH$_2$ conjugated with 2-bromo-2,2-difluoro-*N*-(pyridin-3-ylmethyl)acetamide (166j)

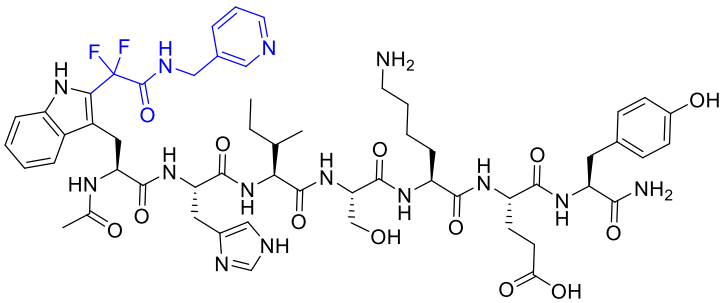

Prepared according to general procedure E using Ac-WHISKEY-NH$_2$ **163** (25.0 mM in DMSO, 200 µL, 5.00 µmol, 1.00 eq.), 4CzIPN (2.50 mM in DMSO, 20 µL, 0.0500 µmol, 1 mol%) and 2-bromo-2,2-difluoro-*N*-(pyridin-3-ylmethyl)acetamide **94j** (0.1 M in DMSO, 100 µL, 10.0 µmol, 2.00 eq.). The reaction mixture was irradiated with blue LEDs for 60 min, then was analysed by quantitative ^{19}F NMR spectroscopy (34% yield). The reaction mixture was then purified by semi-preparative RP-HPLC (2-70% B over 30 min) to give the title compound **166j** (2.50 mg, 2.10 µmol, 42%) as a colourless powder; ^{1}H NMR (500 MHz, CD$_3$OD) δ 8.72 (d, 1H, *J* = 1.4 Hz), 8.58 (d, 1H, *J* = 2.1 Hz), 8.51 (dd, 1H, *J* = 5.1, 1.6 Hz), 7.91 (ddd, 1H, *J* = 8.0, 2.1, 1.6 Hz), 7.65 (d, 1H, *J* = 8.2 Hz), 7.50 (dd, 1H, *J* = 8.0, 5.1 Hz), 7.37 (d, 1H, *J* = 8.3 Hz), 7.28 (d, 1H, *J* = 1.4 Hz), 7.21 (ddd, 1H, *J* = 8.3, 7.0, 1.1 Hz), 7.13 – 7.02 (m, 3H), 6.68 (d, 2H, *J* = 8.5 Hz), 4.68 – 4.47 (m, 6H), 4.44 (dd, 1H, *J* = 6.1, 5.7 Hz), 4.33 – 4.25 (m, 2H), 4.11 (d, 1H,

J = 7.4 Hz), 3.85 (dd, 1H, *J* = 10.9, 5.7 Hz), 3.78 (dd, 1H, *J* = 10.9, 6.1 Hz), 3.28 – 3.21 (m, 2H), 3.10 – 2.99 (m, 2H), 2.90 (dd, 2H, *J* = 8.9, 7.6 Hz), 2.84 (dd, 1H, *J* = 14.0, 8.5 Hz), 2.40 – 2.23 (m, 2H), 2.10 – 1.97 (m, 1H), 1.90 (s, 3H), 1.89 – 1.79 (m, 3H), 1.77 – 1.69 (m, 1H), 1.67 – 1.58 (m, 2H), 1.55 – 1.40 (m, 3H), 1.23 – 1.09 (m, 1H), 0.96 – 0.86 (m, 6H); ^{19}F NMR (376 MHz, DMSO-d_6) δ −73.5 (s, TFA), −96.7 (d, 1F, *J* = 267 Hz), −98.1 (d, 1F, *J* = 267 Hz); HRMS (ESI) m/z: $[M + H]^+$ Calcd for $C_{56}H_{73}F_2N_{14}O_{13}$ 1187.5450; Found 1187.5459 (0.8 ppm error).

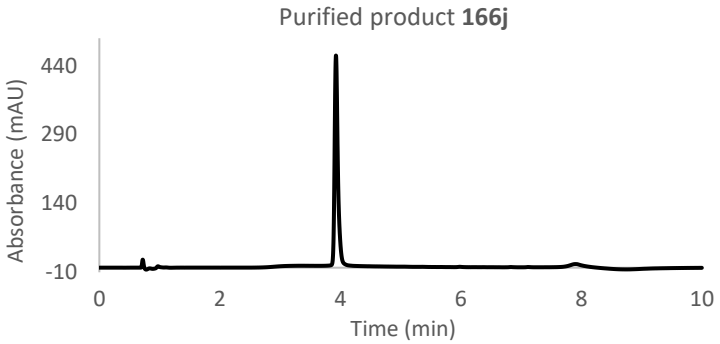

Figure 158. Analytical HPLC chromatogram for purified product **166j** Rt = 3.93 min on analytical gradient 2-95% B over 5 mins 0.6 mL min^{-1}, 280 nm.

Ac-WHISKEY-NH$_2$ conjugated with 2-bromo-*N*-(*tert*-butyl)-2,2-difluoroacetamide (166k)

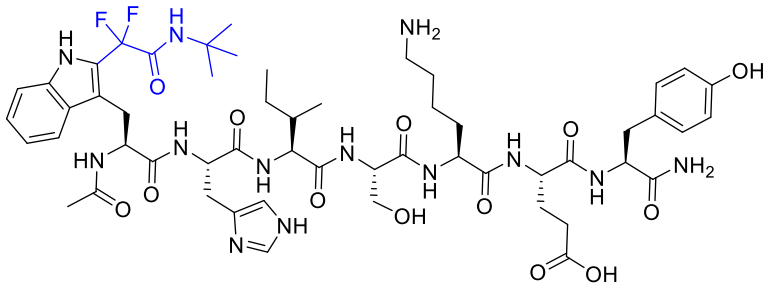

Prepared according to general procedure E using Ac-WHISKEY-NH$_2$ **163** (25.0 mM in DMSO, 200 µL, 5.00 µmol, 1.00 eq.), 4CzIPN (2.50 mM in DMSO, 20 µL, 0.0500 µmol, 1 mol%) and 2-bromo-*N*-(*tert*-butyl)-2,2-difluoroacetamide **94k** (0.1 M in DMSO, 100 µL, 10.0 µmol, 2.00 eq.). The reaction mixture was irradiated with blue LEDs for 75 min, then was analysed by quantitative ^{19}F NMR spectroscopy (33% yield). The reaction mixture was purified by semi-preparative RP-HPLC (2-70% B over 30 min) to give the title compound **166k** (2.1 mg, 1.82 µmol, 36%) as a colourless powder; ^{1}H NMR (500 MHz, CD_3OD) δ 8.63 (s, 1H), 7.67 (d, 1H, *J* = 8.1

Hz), 7.38 (d, 1H, *J* = 8.2 Hz), 7.26 (s, 1H), 7.22 (dd, 1H, *J* = 8.2, 7.6 Hz), 7.13 – 7.00 (m, 3H), 6.69 (d, 2H, *J* = 8.5 Hz), 4.63 – 4.57 (m, 1H), 4.55 (dd, 1H, *J* = 8.3, 7.5 Hz), 4.50 (dd, 1H, *J* = 8.5, 5.7 Hz), 4.41 (dd, 1H, *J* = 6.0, 5.6 Hz), 4.32 – 4.25 (m, 2H), 4.12 (d, 1H, *J* = 7.4 Hz), 3.87 (dd, 1H, *J* = 10.9, 5.6 Hz), 3.81 (dd, 1H, *J* = 10.9, 6.0 Hz), 3.34 – 3.32 (m, 2H), 3.27 – 3.20 (m, 1H), 3.11 – 3.03 (m, 2H), 2.94 – 2.88 (m, 2H), 2.85 (dd, 1H, *J* = 13.9, 8.5 Hz), 2.40 – 2.25 (m, 2H), 2.06 – 1.98 (m, 1H), 1.96 (s, 3H), 1.93 – 1.82 (m, 3H), 1.79 – 1.70 (m, 1H), 1.70 – 1.61 (m, 2H), 1.52 – 1.44 (m, 2H), 1.42 (s, 9H), 1.39 – 1.35 (m, 1H), 1.22 – 1.13 (m, 1H), 0.98 – 0.89 (m, 6H); ^{19}F NMR (377 MHz, CD_3OD) δ −76.9 (s, TFA), −100.4 (d, 1F, *J* = 266 Hz), −102.1 (d, 1F, *J* = 266 Hz); HRMS (ESI) m/z: $[M + H]^+$ Calcd for $C_{54}H_{76}F_2N_{13}O_{13}$ 1152.5648; Found 1152.5646 (0.2 ppm error).

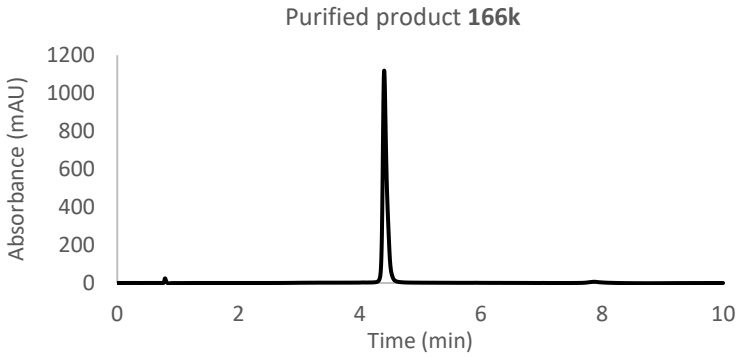

Figure 159. Analytical HPLC chromatogram for purified product **166k** Rt = 4.41 min on analytical gradient 2-95% B over 5 min, 0.6 mL min^{-1}, 280 nm.

Ac-WHISKEY-NH$_2$ conjugated with 2-bromo-2,2-difluoro-1-morpholinoethan-1-one (166l)

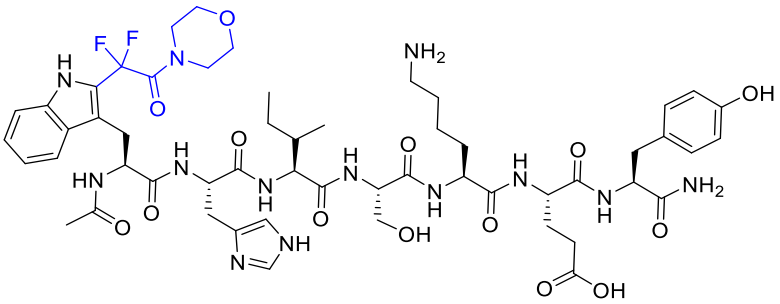

Prepared according to general procedure E using Ac-WHISKEY-NH$_2$ **163** (25.0 mM in DMSO, 200 µL, 5.00 µmol, 1.00 eq.), 4CzIPN (2.50 mM in DMSO, 20 µL, 0.0500 µmol, 1 mol%) and 2-bromo-2,2-difluoro-1-morpholinoethan-1-one **94l** (0.1 M in DMSO, 100 µL, 10.0 µmol, 2.00 eq.).

The reaction mixture was irradiated with blue LEDs for 15 min, then was analysed by quantitative ^{19}F NMR spectroscopy (35% yield). The reaction mixture was then purified by semi-preparative RP-HPLC (2-70% B over 30 min) to give the title compound **166l** (2.20 mg, 1.89 μmol, 38%) as a colourless powder; ^{1}H NMR (500 MHz, CD_3OD) δ 8.71 (s, 1H), 7.65 (d, 1H, *J* = 8.1 Hz), 7.40 (d, 1H, *J* = 8.2 Hz), 7.29 (d, 1H, *J* = 1.4 Hz), 7.23 (dd, 1H, *J* = 8.2, 7.6 Hz), 7.10 (dd, 1H, *J* = 8.1, 7.6 Hz), 7.06 (d, 2H, *J* = 8.5 Hz), 6.69 (d, 2H, *J* = 8.5 Hz), 4.54 (dd, 1H, *J* = 6.9, 6.1 Hz), 4.50 (dd, 1H, *J* = 8.5, 5.7 Hz), 4.47 – 4.39 (m, 2H), 4.34 – 4.26 (m, 2H), 4.11 (d, 1H, *J* = 7.2 Hz), 3.86 (dd, 1H, *J* = 10.9, 5.7 Hz), 3.79 (dd, 1H, *J* = 10.9, 6.0 Hz), 3.77 – 3.63 (m, 4H), 3.58 – 3.51 (m, 2H), 3.50 – 3.42 (m, 2H), 3.28 – 3.20 (m, 2H), 3.19 – 3.01 (m, 3H), 2.94 – 2.87 (m, 2H), 2.88 – 2.79 (m, 1H), 2.46 – 2.23 (m, 2H), 2.13 – 1.98 (m, 1H), 1.89 (s, 3H), 1.88 – 1.80 (m, 3H), 1.78 – 1.70 (m, 1H), 1.70 – 1.60 (m, 2H), 1.57 – 1.49 (m, 1H), 1.48 – 1.38 (m, 2H), 1.25 – 1.12 (m, 1H), 0.99 – 0.87 (m, 6H); ^{19}F NMR (376 MHz, CD_3OD) δ −77.0 (s, TFA), −92.2 (d, 1F, *J* = 279 Hz), −93.3 (d, 1F, *J* = 279 Hz); HRMS (ESI) m/z: $[M + H]^+$ Calcd for $C_{54}H_{74}F_2N_{13}O_{14}$ 1166.5446; Found 1166.5426 (1.7 ppm error).

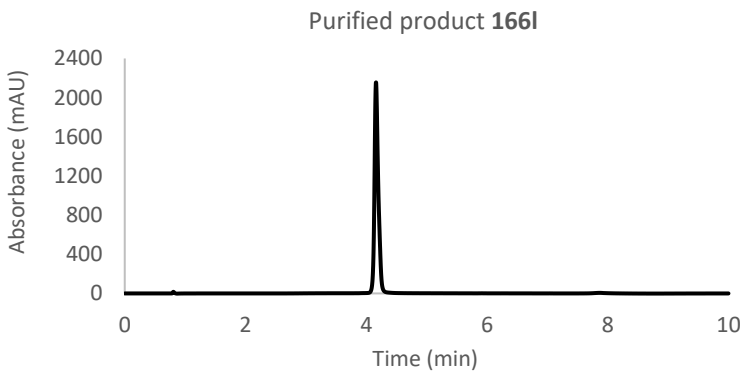

Figure 160. Analytical HPLC chromatogram for purified product **166l** Rt = 4.16 min on analytical gradient 2-95% B over 5 min, 0.6 mL min^{-1}, 280 nm.

Ac-WHISKEY-NH_2 conjugated with *N*-(2-(2-bromo-2,2-difluoroacetamido)ethyl)-5-((3a*S*,4*S*,6a*R*)-2-oxohexahydro-1*H*-thieno[3,4-d]imidazol-4-yl)pentanamide (166m)

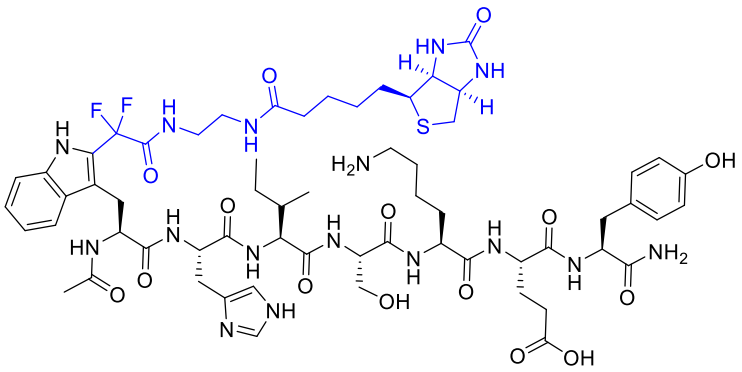

Prepared according to general procedure E using Ac-WHISKEY-NH_2 **163** (25.0 mM in DMSO, 200 µL, 5.00 µmol, 1.00 eq.), 4CzIPN (12.5 mM in DMSO, 100 µL, 0.250 µmol, 5 mol%) and *N*-(2-(2-bromo-2,2-difluoroacetamido)ethyl)-5-((3a*S*,4*S*,6a*R*)-2-oxohexahydro-1*H*-thieno[3,4-d]imidazol-4-yl)pentanamide **94m** (0.1 M in DMSO, 75 µL, 7.50 µmol, 1.50 eq.). The reaction mixture was irradiated with blue LEDs for 120 min, then was analysed by quantitative ^{19}F NMR spectroscopy (19% yield). The reaction mixture was then purified by semi-preparative RP-HPLC (2-70% B over 30 min with an isocratic hold at 23% B) to give the title compound **166m** (1.20 mg, 0.89 µmol, 18%) as a colourless powder; ^{1}H NMR (400 MHz, CD_3OD) δ 8.70 (s, 1H), 7.68 (d, 1H, *J* = 8.1 Hz), 7.40 (d, 1H, *J* = 8.3 Hz), 7.29 (s, 1H), 7.22 (dd, 1H, *J* = 8.3, 7.6 Hz), 7.13 – 7.03 (m, 3H), 6.69 (d, 2H, *J* = 8.5 Hz), 4.64 – 4.55 (m, 2H), 4.53 – 4.46 (m, 2H), 4.46 – 4.40 (m, 1H), 4.35 – 4.22 (m, 3H), 4.12 (d, 1H, *J* = 7.3 Hz), 3.87 (dd, 1H, *J* = 10.8, 5.6 Hz), 3.80 (dd, 1H, *J* = 10.8, 5.9 Hz), 3.46 – 3.36 (m, 7H), 3.11 – 3.02 (m, 3H), 2.95 – 2.89 (m, 2H), 2.90 – 2.81 (m, 2H), 2.69 (d, 1H, *J* = 12.9 Hz), 2.37 – 2.28 (m, 2H), 2.18 – 2.06 (m, 2H), 2.01 – 1.97 (m, 1H), 1.93 (s, 3H), 1.91 – 1.80 (m, 3H), 1.75 – 1.62 (m, 3H), 1.58 – 1.38 (m, 7H), 1.36 – 1.25 (m, 2H), 1.23 – 1.03 (m, 1H), 0.98 – 0.90 (m, 6H); ^{19}F NMR (376 MHz, CD_3OD) δ −77.0 (s, TFA), −101.6 (s, 2F); HRMS (ESI) m/z: $[M + 2H]^{2+}$ Calcd for $C_{62}H_{88}F_2N_{16}O_{15}S$683.3152; Found 683.3148 (0.6 ppm error).

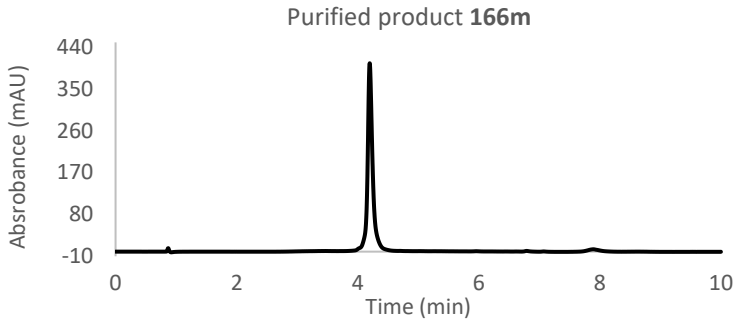

Figure 161. Analytical HPLC chromatogram for purified product **166m** Rt = 4.20 min on analytical gradient 2-95% B over 5 mins,0.6 mL min^{-1}, 280 nm.

Ac-WHISKEY-NH$_2$ conjugated with *N*-((2*R*,3*R*,4*R*,5*S*,6*R*)-3-acetamido-4,5-dihydroxy-6-(hydroxymethyl)tetrahydro-2*H*-pyran-2-yl)-2-bromo-2,2-difluoroacetamide (166n)

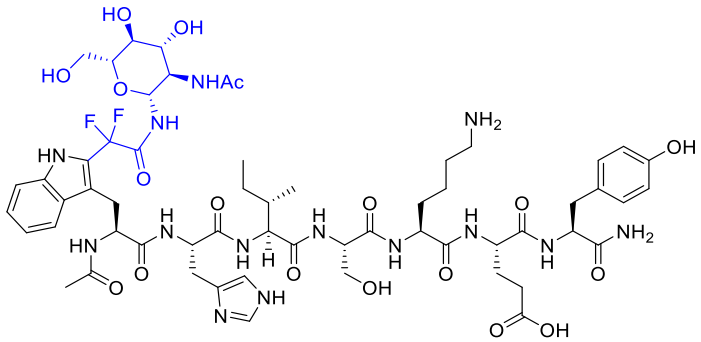

Prepared according to general procedure E using Ac-WHISKEY-NH$_2$ **163** (25.0 mM in DMSO, 200 µL, 5.00 µmol, 1.00 eq.), 4CzIPN (2.50 mM in DMSO, 20 µL, 0.0500 µmol, 1 mol%) and *N*-((2*R*,3*R*,4*R*,5*S*,6*R*)-3-acetamido-4,5-dihydroxy-6-(hydroxymethyl) tetrahydro-2*H*-pyran-2-yl)-2-bromo-2,2-difluoroacetamide **94n** (0.1 M in DMSO, 100 µL, 10.0 µmol, 2.00 eq.). The reaction mixture was irradiated with blue LEDs for 90 min, then was analysed by quantitative ^{19}F NMR spectroscopy (31% yield). The reaction mixture was purified by semi-preparative RP-HPLC (2-70% B over 30 min) to give the title compound **166n** (2.50 mg, 1.92 µmol, 38%) as a colourless powder; ^{1}H NMR (500 MHz, CD$_3$OD) δ 8.61 (s, 1H), 7.64 (d, 1H, *J* = 8.2 Hz), 7.38 (d, 1H, *J* = 8.3 Hz), 7.24 (s, 1H), 7.21 (dd, 1H, *J* = 8.3, 7.6 Hz), 7.13 – 7.00 (m, 3H), 6.69 (d, 1H, *J* = 8.5 Hz), 5.05 (d, 1H, *J* = 9.7 Hz), 4.62 – 4.52 (m, 2H), 4.54 – 4.45 (m, 1H), 4.41 (dd, 1H, *J* = 6.6, 5.7 Hz), 4.35 – 4.17 (m, 2H), 4.11 (d, 1H, *J* = 7.3 Hz), 3.92 – 3.77 (m, 4H), 3.75 – 3.62 (m, 1H), 3.58 – 3.48 (m, 1H), 3.38 – 3.33 (m, 3H), 3.26 – 3.19 (m, 2H), 3.12 – 2.99 (m, 2H), 2.98 – 2.79 (m, 3H), 2.40 – 2.25 (m, 2H),

2.02 – 1.97 (m, 1H), 1.91 (s, 3H), 1.88 – 1.79 (m, 3H), 1.76 (s, 3H), 1.74 – 1.68 (m, 1H), 1.68 – 1.59 (m, 2H), 1.55 – 1.47 (m, 1H), 1.46 – 1.38 (m, 2H), 1.23 – 1.07 (m, 1H), 0.98 – 0.87 (m, 6H); ^{19}F NMR (376 MHz, CD_3OD) δ −77.0 (s, TFA), −102.1 (d, 1F, *J* = 267 Hz), −103.5 (d, 1F, *J* = 267 Hz); HRMS (ESI) m/z: $[M + H]^+$ Calcd for $C_{58}H_{81}F_2N_{14}O_{18}$ 1299.5821; Found 1299.5795 (2.08 ppm error).

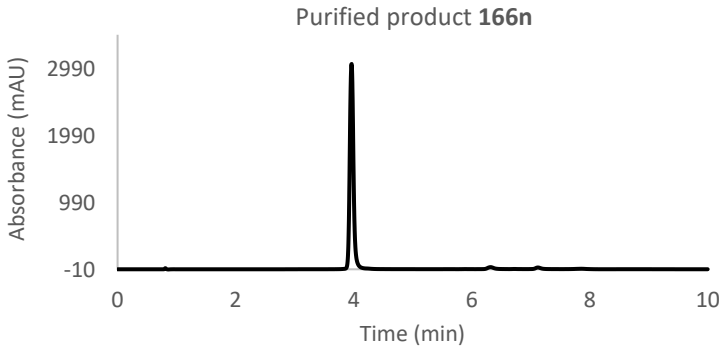

Figure 162. Analytical HPLC chromatogram for purified product **166n** Rt = 3.97 min on analytical gradient 2-95% B over 5 mins,0.6 mL min^{-1}, 280 nm.

Ac-HISKEY-NH_2 conjugated with ethyl bromodifluoroacetate (172)

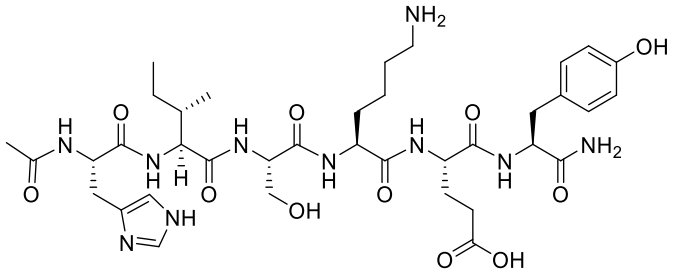

Prepared according to general procedure E using Ac-HISKEY-NH_2 **172** (25.0 mM in DMSO, 200 µL, 5.00 µmol, 1.00 eq.), 4CzIPN (2.50 mM in DMSO, 20 µL, 0.0500 µmol, 1 mol%) and ethyl bromodifluoroacetate **94a** (0.100 M in DMSO, 100 µL, 10.0 µmol, 2.00 eq.). The reaction mixture was irradiated with blue LEDs for 10 min, then was analysed by quantitative ^{19}F NMR spectroscopy (0% yield).

Ac-CWHISKEY-NH_2 conjugated with ethyl bromodifluoroacetate (177a)

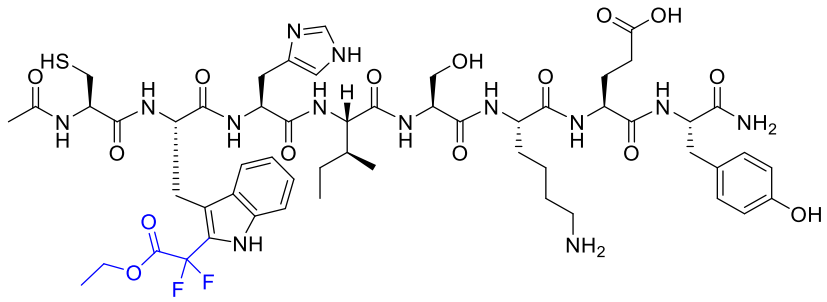

Prepared according to general procedure E using Ac-CWHISKEY-NH_2 **175** (25.0 mM in DMSO, 200 µL, 5.00 µmol, 1.00 eq.), 4CzIPN (2.50 mM in DMSO, 20 µL, 0.0500 µmol, 1 mol%) and ethyl bromodifluoroacetate **94a** (0.100 M in DMSO, 100 µL, 10.0 µmol, 2.00 eq.). The reaction mixture was irradiated with blue LEDs for 10 min, then was analysed by quantitative ^{19}F NMR spectroscopy (36% yield). The reaction mixture was then purified by semi-preparative RP-HPLC (2-70% B over 30 min) to give the title compound **177a** (2.00 mg, 1.62 µmol, 33%) as a colourless powder; ^{1}H NMR (500 MHz, CD_3OD) δ 8.71 (s, 1H), 7.60 (d, 1H, *J* = 8.2 Hz), 7.39 (d, 1H, *J* = 8.3 Hz), 7.30 (s, 1H), 7.23 (dd, 1H, *J* = 8.3, 7.6 Hz), 7.12 – 7.02 (m, 3H), 6.69 (d, 2H, *J* = 8.5 Hz), 4.59 – 4.47 (m, 3H), 4.43 – 4.37 (m, 1H), 4.37 – 4.37 – 4.31 (m, 3H), 4.30 – 4.22 (m, 2H), 4.08 (d, 1H, *J* = 7.5 Hz), 3.86 (dd, 1H, *J* = 11.0, 5.7 Hz), 3.80 (dd, 1H, *J* = 11.0, 5.8 Hz), 3.43 – 3.35 (m, 2H), 3.28 – 3.23 (m, 1H), 3.14 – 3.03 (m, 2H), 2.94 – 2.81 (m, 3H), 2.77 – 2.68 (m, 2H), 2.40 – 2.24 (m, 2H), 2.06 – 2.00 (m, 1H), 1.99 (s, 3H), 1.93 – 1.80 (m, 3H), 1.77 – 1.68 (m, 1H), 1.68 – 1.60 (m, 2H), 1.58 – 1.51 (m, 1H), 1.48 – 1.40 (m, 2H), 1.30 (t, 3H, *J* = 7.1 Hz), 1.24 – 1.16 (m, 1H), 0.97 – 0.88 (m, 6H); ^{19}F NMR (376 MHz, CD_3OD) δ −77.0 (s, TFA), −100.9 (d, 1F, *J* = 266 Hz), −102.2 (1F, d, *J* = 266 Hz); HRMS (ESI) m/z: $[M]^+$ Calcd for $C_{55}H_{74}F_2N_{12}O_{16}S$: 1228.5035; Found 1228.5118 (6.8 ppm error).

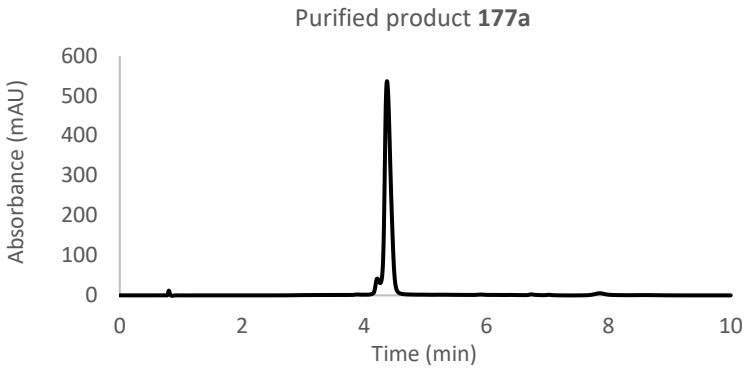

Figure 163. Analytical HPLC chromatogram for purified product **177a** Rt = 4.37 min on analytical gradient 2-95% B over 5 min, 0.6 mL min^{-1}, 280 nm.

H-WHISKEY-OH conjugated with ethyl bromodifluoroacetate (178a)

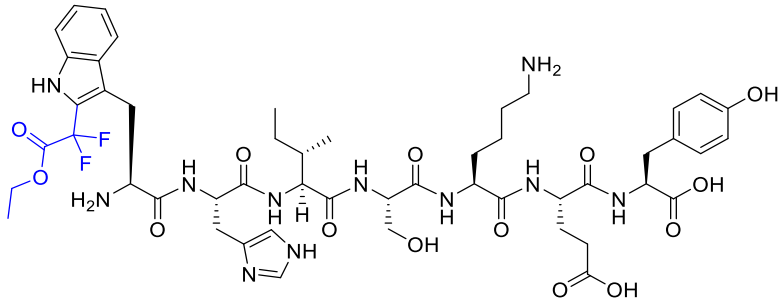

Prepared according to general procedure E using H-WHISKEY-OH **176** (25.0 mM in DMSO, 200 µL, 5.00 µmol, 1.00 eq.), 4CzIPN (2.50 mM in DMSO, 20 µL, 0.0500 µmol, 1 mol%) and ethyl bromodifluoroacetate **94a** (0.100 M in DMSO, 100 µL, 10.0 µmol, 2.00 eq.). The reaction mixture was irradiated with blue LEDs for 10 min, then was analysed by quantitative ^{19}F NMR spectroscopy (38% yield). The reaction mixture was then purified by semi-preparative RP-HPLC (2-70% B over 30 min) to give the title compound **178a** (1.90 mg, 1.75 µmol, 35%) as a colourless powder; ^{1}H NMR (500 MHz, CD_3OD) δ 8.62 (s, 1H), 7.59 (d, 1H, *J* = 8.0 Hz), 7.40 (d, 1H, *J* = 8.3 Hz), 7.27 – 7.20 (m, 2H), 7.11 (dd, 1H, *J* = 8.0, 7.0 Hz), 7.06 (d, 2H, *J* = 8.5 Hz), 6.69 (d, 2H, *J* = 8.5 Hz), 4.53 – 4.42 (m, 3H), 4.38 – 4.26 (m, 4H), 4.22 (dd, 1H, *J* = 9.0, 6.9 Hz), 3.98 (d, 1H, *J* = 6.8 Hz), 3.81 (dd, 1H, *J* = 10.9, 5.6 Hz), 3.76 (dd, 1H, *J* = 10.9, 6.1 Hz), 3.45 – 3.36 (m, 2H), 3.23 – 3.16 (m, 1H), 3.11 – 3.01 (m, 2H), 2.94 – 2.82 (m, 3H), 2.40 – 2.25 (m, 2H), 2.08 – 1.97 (m, 1H), 1.91 – 1.82 (m, 2H), 1.80 – 1.74 (m, 1H), 1.73 – 1.61 (m, 3H), 1.56 – 1.48 (m, 1H), 1.47 – 1.38 (m, 2H), 1.29 (t, 3H, *J* = 7.1 Hz), 1.22 – 1.11 (m, 1H), 1.01 – 0.89 (m, 6H); ^{19}F NMR (376

MHz, CD_3OD) δ −76.9 (s, TFA), −101.9 (d, 1F, *J* = 266 Hz), −104.3 (d, 1F, *J* = 266 Hz); HRMS (ESI) m/z: $[M + H]^+$ Calcd for $C_{50}H_{68}F_2N_{11}O_{14}$ 1084.4915; Found 1084.4980 (6.0 ppm error).

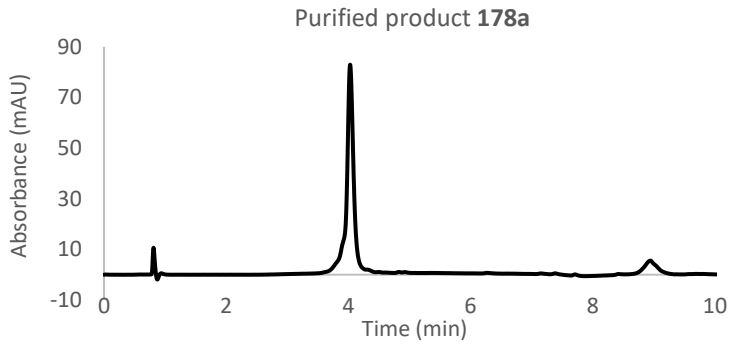

Figure 164. Analytical HPLC chromatogram for purified product **178a** Rt = 4.03 min on analytical gradient 10-80% B over 5 min, 0.6 mL min^{-1}, 280 nm.

Ac-WLAHKAL-NH_2 conjugated with ethyl bromodifluoroacetate (182a)

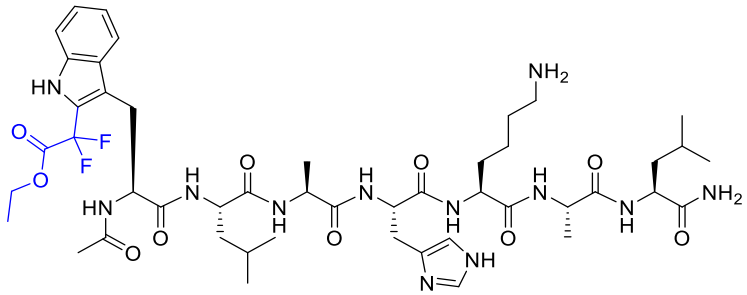

Prepared according to general procedure E using Ac-WLAHKAL-NH_2 **179** (25.0 mM in DMSO, 200 µL, 5.00 µmol, 1.00 eq.), 4CzIPN (2.50 mM in DMSO, 20 µL, 0.0500 µmol, 1 mol%) and ethyl bromodifluoroacetate **94a** (0.100 M in DMSO, 100 µL, 10.0 µmol, 2.00 eq.). The reaction mixture was irradiated with blue LEDs for 10 min, then was analysed by quantitative ^{19}F NMR spectroscopy (41% yield). The reaction mixture was then purified by semi-preparative RP-HPLC (2-70% B over 30 min) to give the title compound **182a** (2.00 mg, 2.00 µmol, 40%) as a colourless powder; ^1H NMR (500 MHz, CD_3OD) δ 8.69 (s, 1H), 7.62 (d, 1H, *J* = 8.0 Hz), 7.40 (d, 1H, *J* = 8.2 Hz), 7.28 (s, 1H), 7.23 (ddd, 1H, *J* = 8.2, 7.0, 1.1 Hz), 7.07 (ddd, 1H, *J* = 8.0, 7.0, 1.0 Hz), 4.49 – 4.41 (m, 2H), 4.39 – 4.31 (m, 3H), 4.27 (q, 1H, *J* = 7.2 Hz), 4.22 – 4.02 (m, 3H), 3.43 – 3.33 (m, 2H), 3.23 (dd, 1H, *J* = 15.4, 5.7 Hz), 3.10 (dd, 1H, *J* = 15.4, 8.2 Hz), 2.91 (dd, 2H, *J* = 8.2, 7.5 Hz), 2.00 (s, 3H), 1.84 – 1.75 (m, 1H), 1.74 – 1.53 (m, 9H),

1.44 – 1.38 (m, 5H), 1.36 (d, 3H, *J* = 7.2 Hz), 1.30 (t, 3H, *J* = 7.1 Hz), 0.98 – 0.89 (m, 12H); ^{19}F NMR (376 MHz, CD_3OD) δ −77.0 (s, TFA), −101.4 (d, 1F, *J* = 265 Hz), −102.5 (d, 1F, *J* = 265 Hz); HRMS (ESI) m/z: [M + H]$^+$ Calcd for $C_{47}H_{71}F_2N_{12}O_{10}$ 1001.5384; Found 1001.5333 (5.1 ppm error).

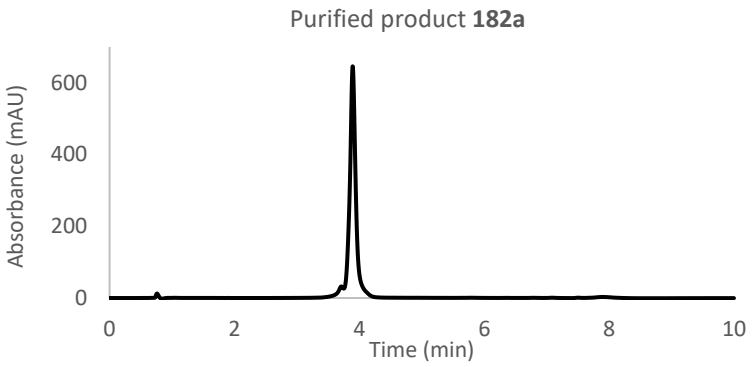

Figure 165. Analytical HPLC chromatogram for purified product **182a** Rt = 3.89 min on analytical gradient 20-80% B over 5 min, 0.6 mL min^{-1}, 280 nm.

Ac-VVYPWYQ-NH$_2$ conjugated with ethyl bromodifluoroacetate (183a)

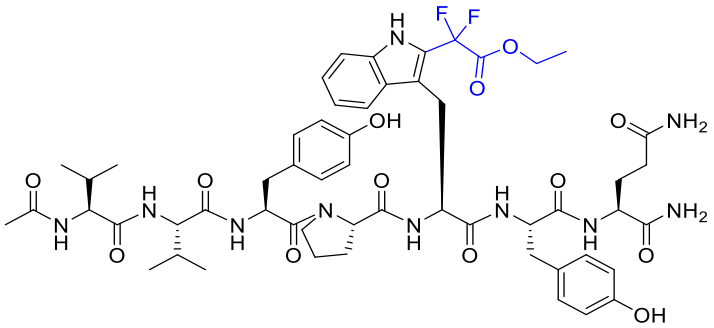

Prepared according to general procedure E using Ac-VVYPWYQ-NH$_2$ **180** (25.0 mM in DMSO, 200 µL, 5.00 µmol, 1.00 eq.), 4CzIPN (2.50 mM in DMSO, 20 µL, 0.0500 µmol, 1 mol%) and ethyl bromodifluoroacetate **94a** (0.100 M in DMSO, 100 µL, 10.0 µmol, 2.00 eq.). The reaction mixture was irradiated with blue LEDs for 15 min, then was analysed by quantitative ^{19}F NMR spectroscopy (42% yield). The reaction mixture was then purified by semi-preparative RP-HPLC (2-70% B over 30 min) to give the title compound **183a** (2.40 mg, 2.15 µmol, 43%) as a colourless powder; ^{1}H NMR (500 MHz, DMSO-d_6) δ 11.63 (s, 1H), 9.13 (d, 2H, *J* = 6.6 Hz), 8.08 (d, 1H, *J* = 7.9 Hz), 7.88 (d, 2H, *J* = 8.4 Hz), 7.75 (d, 1H, *J* = 8.0 Hz), 7.63 (d, 1H, *J* = 9.0 Hz), 7.50 (d, 1H, *J* = 7.3 Hz), 7.45 (d, 1H, *J* = 8.0 Hz), 7.37 (d, 1H, *J* = 8.2 Hz), 7.23 – 7.14 (m, 2H), 7.06 – 6.98 (m, 5H), 6.98 – 6.91

(m, 1H), 6.75 (s, 1H), 6.69 – 6.56 (m, 4H), 6.54 (s, 1H), 4.68 – 4.57 (m, 1H), 4.41 – 4.28 (m, 3H), 4.27 – 4.21 (m, 1H), 4.19 – 4.09 (m, 3H), 4.08 – 4.00 (m, 1H), 3.63 – 3.53 (m, 1H), 3.53 – 3.46 (m, 1H), 3.25 – 3.17 (m, 1H), 3.13 – 3.04 (m, 1H), 3.01 – 2.93 (m, 1H), 2.92 – 2.79 (m, 2H), 2.75 – 2.66 (m, 1H), 2.14 – 1.99 (m, 2H), 1.92 – 1.80 (m, 7H), 1.79 – 1.59 (m, 3H), 1.60 – 1.50 (m, 1H), 1.22 (t, 3H, *J* = 7.1 Hz), 0.79 – 0.68 (m, 12H); ^{19}F NMR (376 MHz, DMSO-d_6) δ −73.6 (s, TFA), −98.6 (s, 2F); HRMS (ESI) m/z: [M + H]$^+$ Calcd for $C_{55}H_{71}F_2N_{10}O_{13}$ 1117.5170; Found 1117.5201 (2.8 ppm error).

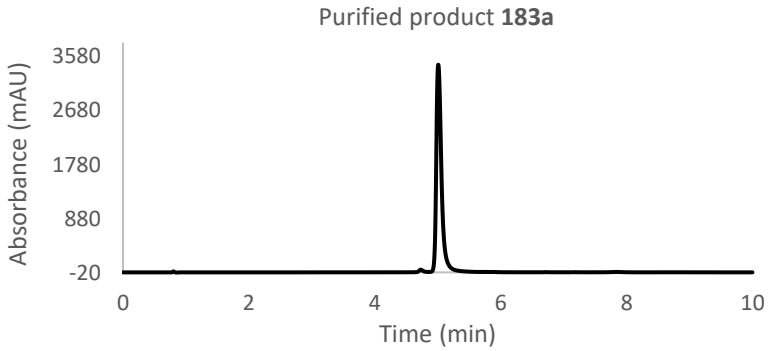

Figure 166. Analytical HPLC chromatogram for purified product **183a** Rt = 5.00 min on analytical gradient 2-95% B over 5 min, 0.6 mL min^{-1}, 280 nm.

Ac-DKVGINYW-NH$_2$ conjugated with ethyl bromodifluoroacetate (184a)

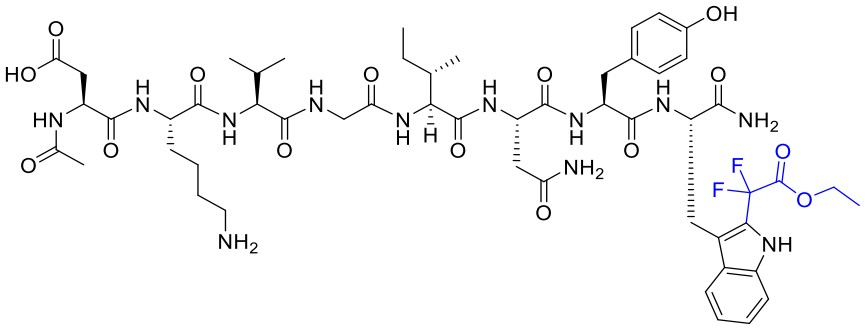

Prepared according to general procedure D using Ac-DKVGINYW-NH$_2$ **181** (25.0 mM in DMSO, 200 µL, 5.00 µmol, 1.00 eq.), 4CzIPN (2.50 mM in DMSO, 20 µL, 0.0500 µmol, 1 mol%) and ethyl bromodifluoroacetate **94a** (0.100 M in DMSO, 100 µL, 10.0 µmol, 2.00 eq.). The reaction mixture was irradiated with blue LEDs for 10 min, then was analysed by quantitative ^{19}F NMR spectroscopy (49% yield). The reaction mixture was then purified by semi-preparative RP-HPLC (2-70% B over 30 min) to give the title compound **184a** (2.60 mg, 2.25 µmol, 45%) as a colourless powder; ^{1}H

NMR (400 MHz, CD_3OD) δ 7.85 (d, 1H, *J* = 8.0 Hz), 7.41 (d, 1H, *J* = 8.2 Hz), 7.24 (dd, 1H, *J* = 8.2, 7.6 Hz), 7.15 (dd, 1H, *J* = 8.0, 7.6 Hz), 6.68 (d, 2H, *J* = 8.4 Hz), 6.56 (d, 2H, *J* = 8.4 Hz), 4.73 – 4.60 (m, 3H), 4.46 – 4.39 (m, 1H), 4.35 (q, 2H, *J* = 7.1 Hz), 4.18 (d, 1H, *J* = 7.2 Hz), 4.13 (dd, 2H, *J* = 7.7, 6.3 Hz), 4.01 (d, 1H, *J* = 16.3 Hz), 3.75 (d, 1H, *J* = 16.3 Hz), 3.61 – 3.53 (m, 1H), 3.26 – 3.16 (m, 1H), 2.89 (t, 2H, *J* = 7.4 Hz), 2.85 – 2.62 (m, 4H), 2.50 (dd, 1H, *J* = 14.0, 6.8 Hz), 2.41 (dd, 1H, *J* = 14.0, 8.1 Hz), 2.16 – 2.06 (m, 1H), 1.97 (s, 3H), 1.93 – 1.79 (m, 2H), 1.75 – 1.55 (m, 3H), 1.55 – 1.37 (m, 3H), 1.30 (t, 3H, *J* = 7.1 Hz), 1.24 – 1.11 (m, 1H), 0.97 (dd, 7H, *J* = 7.3, 6.3 Hz), 0.89 (dd, 3H, *J* = 8.0, 7.4 Hz), 0.83 (d, 3H, *J* = 7.2 Hz); ^{19}F NMR (376 MHz, CD_3OD) δ −77.1 (s, TFA), −101.0 (d, 1F, *J* = 266 Hz), −102.0 (d, 1F, *J* = 266 Hz); HRMS (ESI) m/z: $[M + 2H]^{2+}$ Calcd for $C_{53}H_{76}F_2N_{12}O_{15}$ 579.2761; Found 579.2775 (2.4 ppm error).

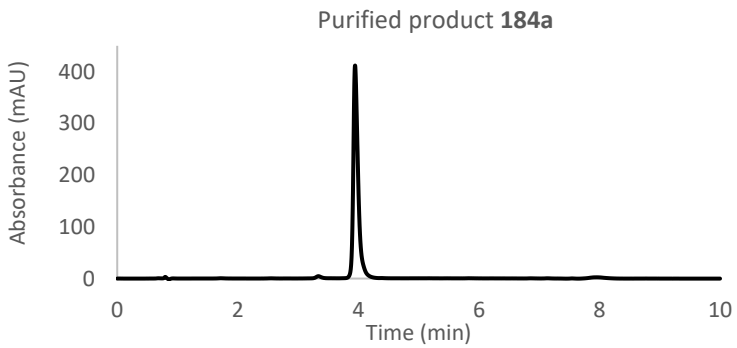

Figure 167. Analytical HPLC chromatogram for purified product **184a** Rt = 3.95 min on analytical gradient 20-80% B over 5 min, 0.6 mL min^{-1}, 280 nm.

Ac-WFMTREY-NH_2 conjugated with ethyl bromodifluoroacetate (186a)

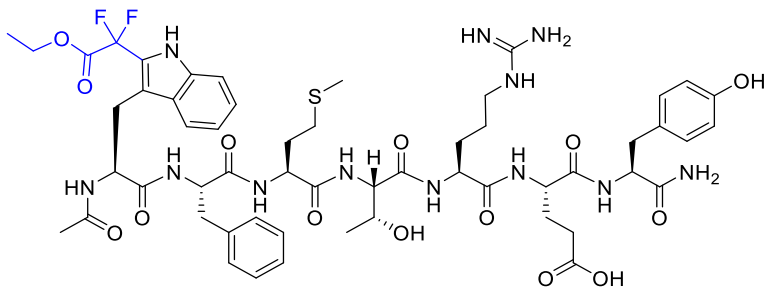

Prepared according to general procedure E using Ac-WFMTREY-NH_2 **185** (25.0 mM in DMSO, 200 µL, 5.00 µmol, 1.00 eq.), 4CzIPN (2.50 mM in DMSO, 20 µL, 0.0500 µmol, 1 mol%) and ethyl bromodifluoroacetate **94a** (0.100 M in DMSO, 100 µL, 10.0 µmol, 2.00 eq.). The reaction mixture was

irradiated with blue LEDs for 10 min, then was analysed by quantitative ^{19}F NMR spectroscopy (49% yield). The reaction mixture was then purified by semi-preparative RP-HPLC (2-70% B over 30 min) to give the title compound **186a** (2.40 mg, 2.01 μmol, 40%) as a colourless powder; ^{1}H NMR (400 MHz, CD_3OD) δ 7.52 (d, 1H, *J* = 8.1 Hz), 7.39 (d, 1H, *J* = 8.3 Hz), 7.35 – 7.27 (m, 2H), 7.27 – 7.17 (m, 4H), 7.12 – 7.02 (m, 3H), 6.69 (d, 2H, *J* = 8.6 Hz), 4.50 (dd, 1H, *J* = 9.0, 5.1 Hz), 4.44 (dd, 1H, *J* = 8.1, 7.5 Hz), 4.40 – 4.28 (m, 4H), 4.27 – 4.06 (m, 4H), 3.18 – 2.95 (m, 6H), 2.86 (dd, 1H, *J* = 14.0, 9.2 Hz), 2.59 – 2.37 (m, 2H), 2.36 – 2.22 (m, 2H), 2.14 – 2.03 (m, 2H), 2.09 (s, 3H), 2.03 – 1.91 (m, 3H), 1.91 – 1.83 (m, 4H), 1.80 – 1.59 (m, 2H), 1.59 – 1.48 (m, 2H), 1.30 (t, 3H, *J* = 7.1 Hz), 1.17 (d, 3H, *J* = 5.7 Hz); ^{19}F NMR (376 MHz, CD_3OD) δ −77.1 (s, TFA), −101.4 (d, 1F, *J* = 266 Hz), −102.4 (d, 1F, *J* = 266 Hz); HRMS (ESI) m/z: $[M + 2H]^{2+}$ Calcd for $C_{55}H_{74}F_2N_{12}O_{14}S$ 598.2568; Found 598.2576 (1.3 ppm error).

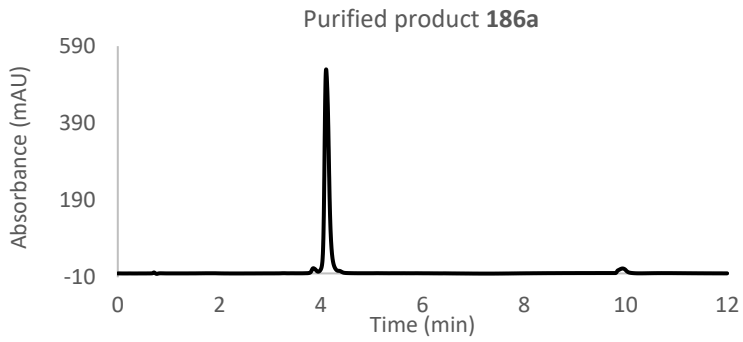

Figure 168. Analytical HPLC chromatogram for purified product **186a** Rt = 4.10 min on analytical gradient 20-100% B over 5 min, 0.6 mL min^{-1}, 280 nm.

Ac-WLAHKAL-NH_2 conjugated with 2-Bromo-2,2-difluoro-*N*-(pyridin-3-ylmethyl)acetamide (182j)

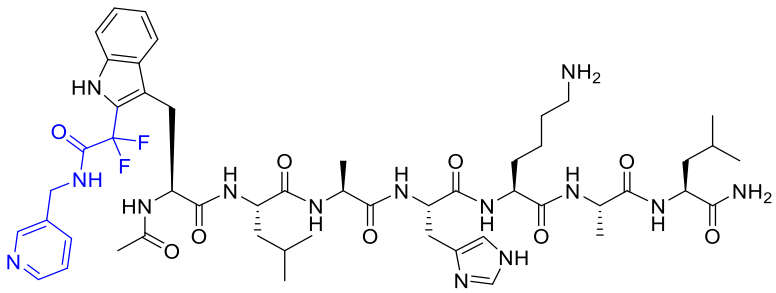

Prepared according to general procedure E using Ac-WLAHKAL-NH_2 **179** (25.0 mM DMSO, 200 μL, 5.00 μmol, 1.00 eq.), 4CzIPN (2.50 mM in DMSO,

20 μL, 0.0500 μmol, 1 mol%) and 2-Bromo-2,2-difluoro-*N*-(pyridin-3-ylmethyl)acetamide **94j** (0.1 M in DMSO, 100 μL, 10.0 μmol, 2.00 eq.). The reaction mixture was irradiated with blue LEDs for 30 min, then was analysed by quantitative ^{19}F NMR spectroscopy (36% yield). The reaction mixture was then purified by semi-preparative RP-HPLC (2-70% B over 30 min) to give the title compound **182j** (2.10 mg, 1.98 μmol, 40%) as a colourless powder; ^{1}H NMR (400 MHz, CD_3OD) δ 8.76 (d, 1H, *J* = 1.4 Hz), 8.58 (d, 1H, *J* = 2.2 Hz), 8.54 (dd, 1H, *J* = 5.1, 1.6 Hz), 7.98 (ddd, 1H, *J* = 8.0, 2.2, 1.6 Hz), 7.67 (d, 1H, *J* = 8.0 Hz), 7.57 (dd, 1H, *J* = 8.0, 5.1 Hz), 7.41 (d, 1H, *J* = 8.2 Hz), 7.35 (d, 1H, *J* = 1.4 Hz), 7.24 (ddd, 1H, *J* = 8.2, 7.0, 1.1 Hz), 7.07 (ddd, 1H, *J* = 8.0, 7.0, 1.0 Hz), 4.61 (dd, 2H, *J* = 22.7, 15.1 Hz), 4.58 – 4.44 (m, 2H), 4.40 – 4.32 (m, 1H), 4.32 – 4.28 (m, 1H), 4.28 – 4.22 (m, 1H), 4.22 – 4.10 (m, 2H), 3.42 (dd, 1H, *J* = 14.6, 5.8 Hz), 3.39 – 3.34 (m, 1H), 3.18 (dd, 1H, *J* = 15.4, 8.1 Hz), 2.94 (dd, 2H, *J* = 8.7, 7.2 Hz), 1.94 (s, 3H), 1.91 – 1.79 (m, 1H), 1.78 – 1.53 (m, 9H), 1.52 – 1.43 (m, 2H), 1.39 (d, 3H, *J* = 7.2 Hz), 1.35 (d, 3H, *J* = 7.3 Hz), 1.03 – 0.84 (m, 12H); ^{19}F NMR (376 MHz, CD_3OD) δ −77.2 (s, TFA), −101.1 (d, 1F, *J* = 269 Hz), −101.9 (d, 1F, *J* = 269 Hz); HRMS (ESI) m/z: $[M + 2H]^{2+}$ Calcd for $C_{51}H_{74}F_2N_{14}O_9$ 532.2866; Found 532.2878 (2.3 ppm error).

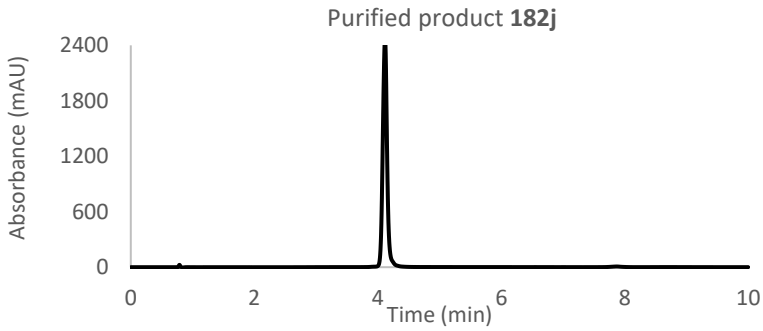

Figure 169. Analytical HPLC chromatogram for purified product **182j** Rt = 4.12 min on analytical gradient 2-95% B over 5 min, 0.6 mL min^{-1}, 280 nm.

Ac-VVYPWYQ-NH_2 conjugated with 2,5,8,11,14,17,20,23-Octaoxapentacosan-25-yl 2-bromo-2,2-difluoroacetate (183d)

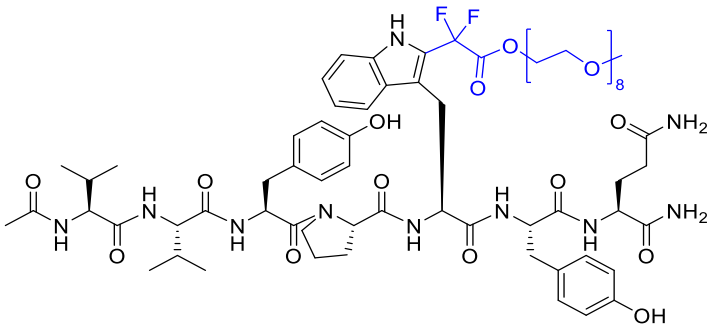

Prepared according to general procedure E using Ac-VVYPWYQ-NH_2 **180** (25.0 mM in DMSO, 200 µL, 5.00 µmol, 1.00 eq.), 4CzIPN (2.50 mM in DMSO, 20 µL, 0.0500 µmol, 1 mol%) and 2,5,8,11,14,17,20,23-octaoxapentacosan-25-yl 2-bromo-2,2-difluoroacetate **94d** (0.1 M in DMSO, 100 µL, 10.0 µmol, 2.00 eq.). The reaction mixture was irradiated with blue LEDs for 20 min, then was analysed by quantitative ^{19}F NMR spectroscopy (46% yield). The reaction mixture was then purified by semi-preparative RP-HPLC (2-70% B over 30 min) to give the title compound **183d** (2.9 mg, 1.99 µmol, 40%) as a colourless powder; ^{1}H NMR (500 MHz, DMSO-d_6) δ 11.62 (s, 1H), 9.13 (d, 2H, J = 7.3 Hz), 8.08 (d, 1H, J = 8.0 Hz), 7.88 (d, 2H, J = 8.7 Hz), 7.75 (d, 1H, J = 8.1 Hz), 7.63 (d, 1H, J = 9.0 Hz), 7.51 (d, 1H, J = 7.1 Hz), 7.46 (d, 1H, J = 7.9 Hz), 7.37 (d, 1H, J = 8.3 Hz), 7.22 – 7.14 (m, 2H), 7.05 – 6.98 (m, 5H), 6.95 (s, 1H), 6.66 – 6.59 (m, 4H), 6.56 – 6.47 (m, 2H), 4.69 – 4.54 (m, 1H), 4.46 – 4.35 (m, 2H), 4.35 – 4.27 (m, 1H), 4.28 – 4.20 (m, 1H), 4.19 – 4.08 (m, 2H), 4.09 – 4.01 (m, 1H), 3.63 (t, 2H, J = 4.6 Hz), 3.61 – 3.55 (m, 1H), 3.52 – 3.45 (m, 22H), 3.44 – 3.39 (m, 8H), 3.23 (s, 3H), 3.26 – 3.30 (m, 1H), 3.13 – 3.05 (m, 1H), 2.99 – 2.93 (m, 1H), 2.92 – 2.78 (m, 2H), 2.76 – 2.67 (m, 1H), 2.08 – 2.00 (m, 2H), 1.93 – 1.79 (m, 7H), 1.79 – 1.59 (m, 3H), 1.60 – 1.50 (m, 1H), 0.80 – 0.75 (m, 6H), 0.74 – 0.68 (m, 6H); ^{19}F NMR (376 MHz, DMSO-d_6) δ −73.4 (s, TFA), −98.7 (s, 2F); HRMS (ESI) m/z: $[M + H + Na]^{2+}$ Calcd for $C_{70}H_{101}F_2N_{10}O_{21}Na$ 739.3505; Found 739.3518 (1.8 ppm error).

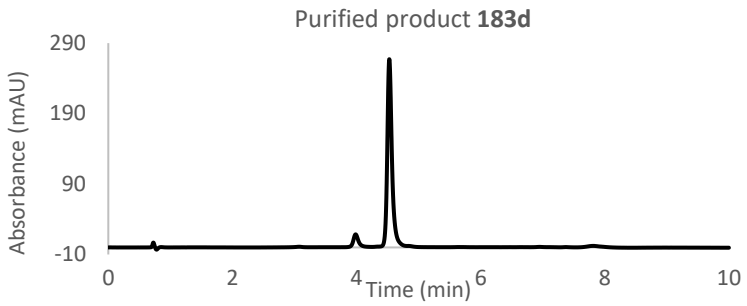

Figure 170. Analytical HPLC chromatogram for purified product **183d** Rt = 4.53 min on analytical gradient 20-80% B over 5 min, 0.6 mL min^{-1}, 280 nm.

183d Product Instability in MeOH shown by HPLC-MS

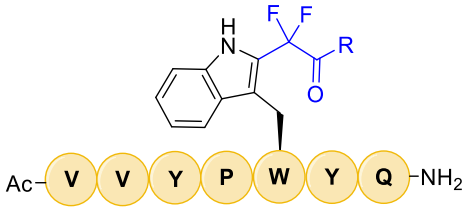

R = octa-PEG: **183d**, OH: **187**, OMe: **188**

After purification, **183d** was dissolved in MeCN to give the chromatogram in figure 170. HPLC-MS of this sample showed that the major signal at 4.53 corresponded to desired product **183d** (**Figure 171A**) and the minor signal at 3.95 min corresponded to hydrolysed product **187** (**Figure 171B**).

A

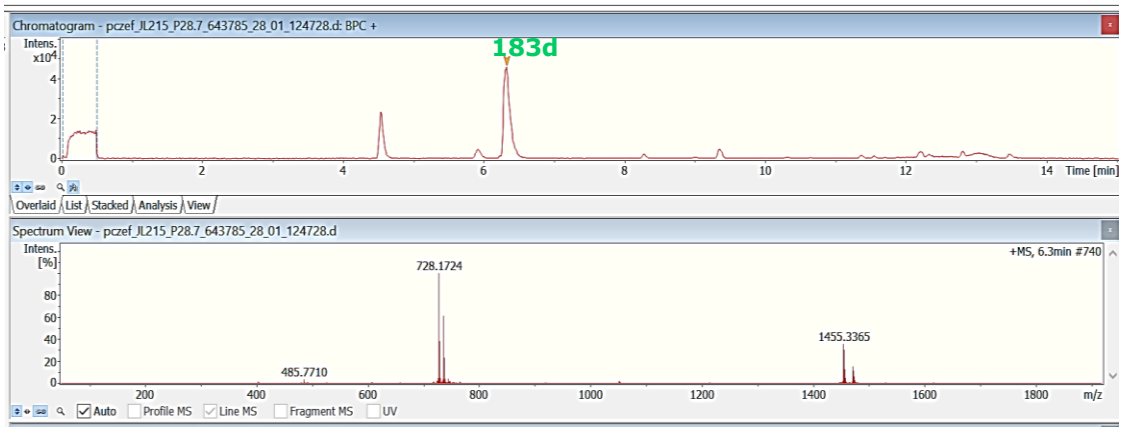

B

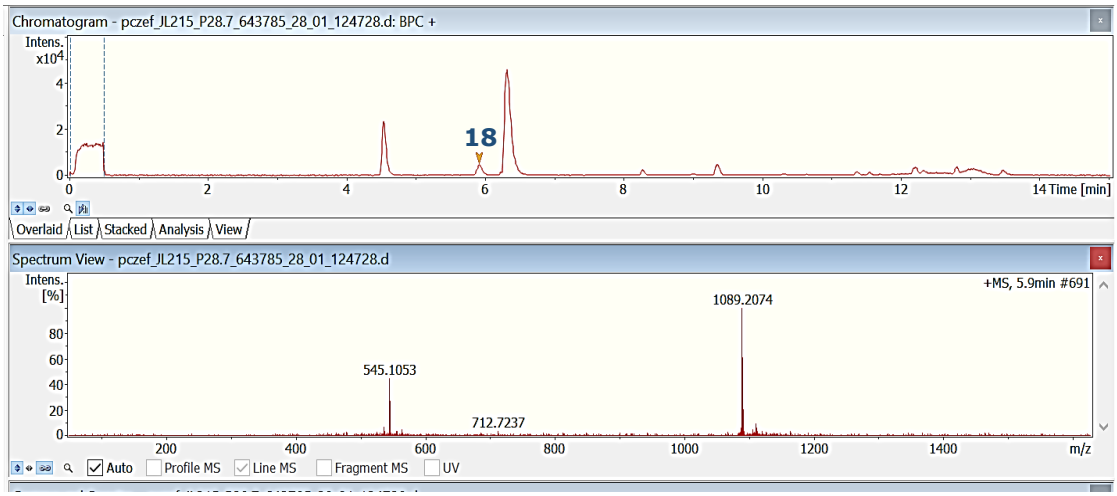

Figure 171. HPLC-MS Base Peak Chromatogram (BPC) and the corresponding mass spectra for **183d** and **187**.

The same sample was spiked with MeOH (3 drops) which formed the methyl ester product **188** (**Figure 172A**). This side-product signal increased over time eventually becoming the major compound in the sample (**Figure 172B**).

A

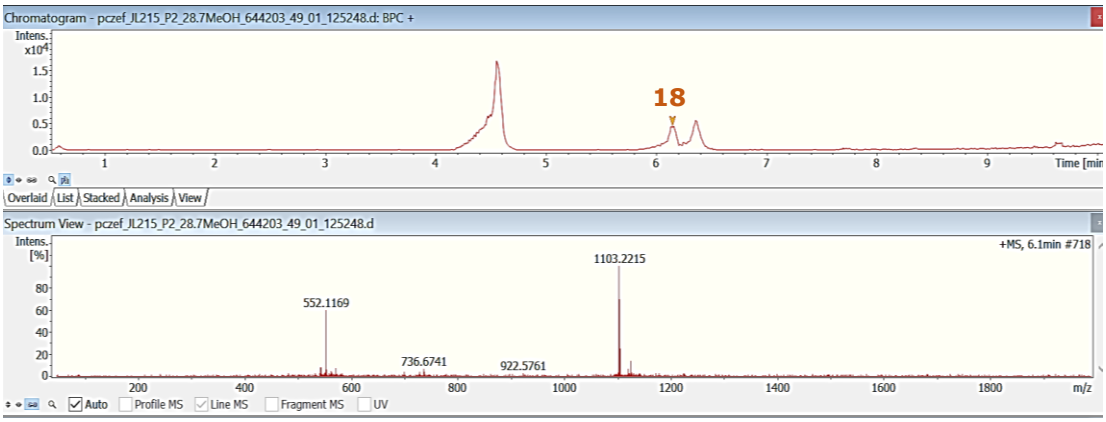

B

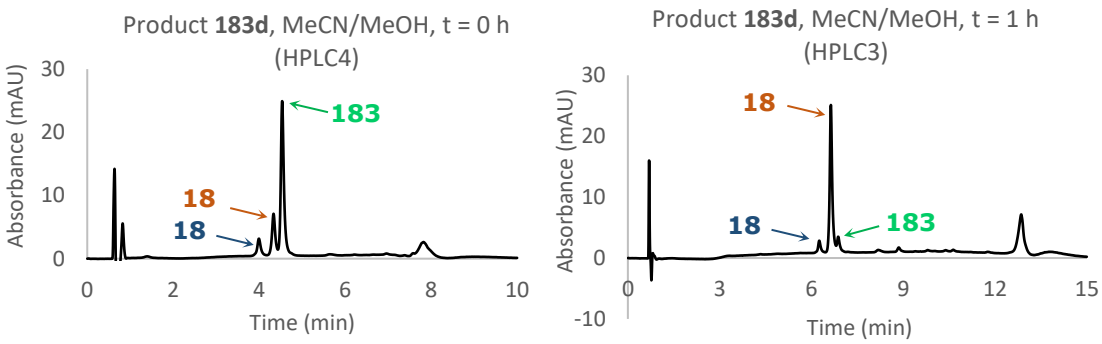

Figure 172. A. HPLC-MS BPC and the corresponding mass spectrum showing side product **188**. B. HPLC chromatograms showing enhanced **188** formation over time. HPLC4 conditions 2-95% B (0.1% TFA) over 5 min, 280 nm, HPLC3 2-95% (0.1% formic acid) over 10 min, 280 nm.

Ac-DKVGINYW-NH_2 conjugated with *N*-(2-(2-bromo-2,2-difluoroacetamido)ethyl)-5-((3a*S*,4*S*,6a*R*)-2-oxohexahydro-1*H*-thieno[3,4-d]imidazol-4-yl)pentanamide (184m)

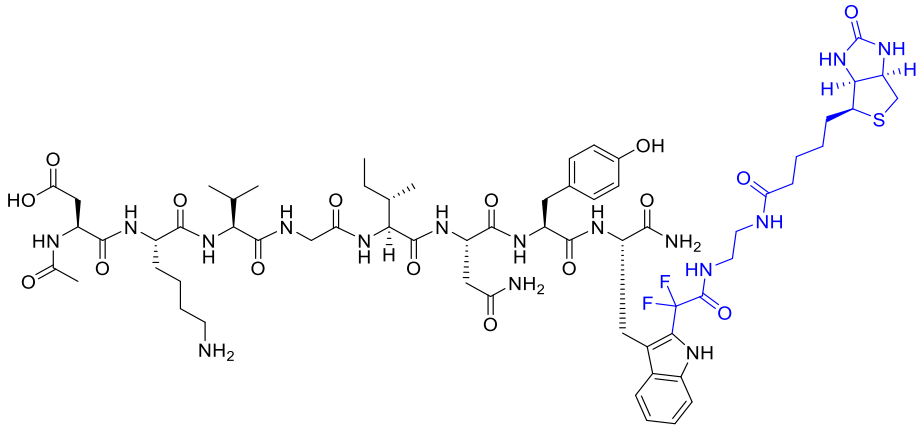

Prepared according to general procedure E using Ac-DKVGINYW-NH_2 **181** (25.0 mM in DMSO, 200 µL, 5.00 µmol, 1.00 eq.), 4CzIPN (2.50 mM in DMSO, 20 µL, 0.0500 µmol, 1 mol%) and *N*-(2-(2-bromo-2,2-difluoroacetamido)ethyl)-5-((3a*S*,4*S*,6a*R*)-2-oxohexahydro-1*H*-thieno[3,4-d]imidazol-4-yl)pentanamide **94m** (0.1 M in DMSO, 100 µL, 10.0 µmol, 2.00 eq.). The reaction mixture was irradiated with blue LEDs for 150 min, then was analysed by quantitative ^{19}F NMR spectroscopy (27% yield). The reaction mixture was then purified by semi-preparative RP-HPLC (2-70% B over 30 min) to give the title compound **184m** (1.6 mg, 1.14 µmol, 22%) as a colourless powder; ^{1}H NMR (400 MHz, CD_3OD) δ 7.84 (d, 1H, *J* = 8.0 Hz), 7.44 (d, 1H, *J* = 8.3 Hz), 7.26 (dd, 1H, *J* = 8.3, 7.5 Hz), 7.16 (dd, 1H, *J* = 8.0, 7.5 Hz), 6.68 (d, 2H, *J* = 8.5 Hz), 6.54 (d, 2H, *J* = 8.5 Hz), 4.75 – 4.70 (m, 1H), 4.69 – 4.60 (m, 2H), 4.53 – 4.38 (m, 2H), 4.33 – 4.22 (m, 2H), 4.19 (d, 1H, *J* = 7.5 Hz), 4.14 (d, 1H, *J* = 7.2 Hz), 4.01 (d, 1H, *J* = 16.4 Hz), 3.78 (d, 1H, *J* = 16.4 Hz), 3.60 – 3.40 (m, 3H), 3.25 – 3.16 (m, 1H), 3.11 – 3.02 (m, 1H), 2.96 – 2.76 (m, 6H), 2.75 – 2.63 (m, 4H), 2.58 – 2.45 (m, 2H), 2.39 – 2.31 (m, 1H), 2.17 – 2.08 (m, 1H), 2.08 – 2.02 (m, 2H), 1.98 (s, 3H), 1.91 – 1.80 (m, 2H), 1.78 – 1.56 (m, 2H), 1.56 – 1.34 (m, 6H), 1.32 – 1.10 (m, 3H), 0.97 (dd, 7H, *J* = 7.2, 6.3 Hz), 0.88 (dd, *J* = 7.6, 7.4 Hz, 3H), 0.84 (d, 3H, *J* = 7.5 Hz); ^{19}F NMR (376 MHz, CD_3OD) δ −77.0 (s, TFA), −99.2 (d, 1F, *J* = 269 Hz), −102.0 (d, 1F, *J* = 269 Hz); HRMS (ESI) m/z: $[M + H + Na]^{2+}$ Calcd for $C_{63}H_{91}F_2N_{16}O_{16}SNa$ 710.3193; Found 710.3207 (2.0 ppm error).

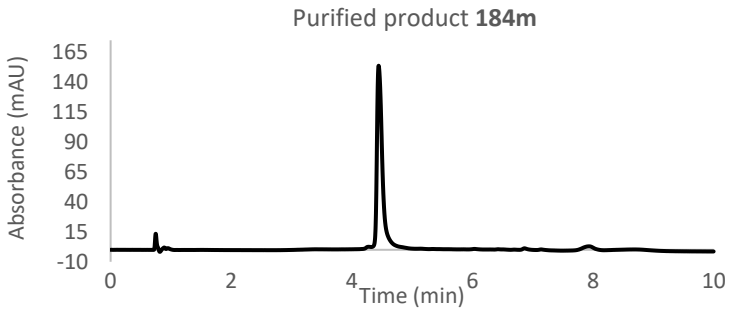

Figure 173. Analytical HPLC chromatogram for purified product **184m** Rt = 4.45 min on analytical gradient 2-95% B over 5 min, 0.6 mL min^{-1}, 280 nm.

General Procedure F: Photocatalytic Difluoroalkylation of β-Casein

A solution of β-casein **189** (12 mg, 0.509 μmol, 1.00 eq.) in a DMSO (1344 μL) H_2O (153 μL) mix was left to dissolve at rt (1 h) before 4CzIPN (0.254 mM in DMSO, 20 μL, 0.00509 μmol, 1 mol%) and bromodifluoroalkyl reagent (50.9 mM in DMSO, 20 μL, 1.02 μmol, 2.00 eq.) were added. The solution was purged with N_2 (5 min) and then irradiated with blue LEDs (PhotoRedOx box, 18 W) for 10 - 210 min at room temperature. α,α,α-Trifluorotoluene (20 μL, 8.48 mM in DMSO, 0.170 μmol, 0.333 eq.) was added to the reaction mixture, then ^{19}F NMR spectroscopy, analytical HPLC and MALDI-TOF analysis were carried out. One third of the reaction mixture (500 μL) was diluted with 0.1% TFA in H_2O (3.0 mL) and then purified by semi-preparative HPLC.

Protein Digestion and Analysis

Samples were suspended in ultra-pure water (Milli-Q, 18.2 MΩcm-1) to approximately 25 μM and digested using ProAlanase (enzyme:substrate 1:50). The digests (β-casein, 10 μL, approx. 5 μg; ProAlanase, 0.5 μL, 0.1 μg; water, 26.94 μL; hydrochloric acid, 2.56 μL, 32 mM final concentration) were incubated at 37°C for 2 h, followed by 95°C for 10 min. Digest solutions were centrifuged (5000 × g, 2 min) and transferred to autosampler vials for nanoHPLC-MS analysis.

Proteolysis of unmodified β-casein to give peptide 136-LPLLQSWMHQPHQP-151 (213)

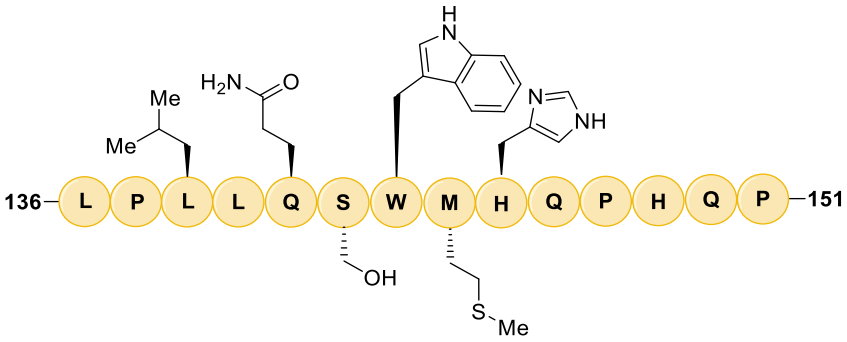

Unmodified β-casein **189** was suspended in ultra-pure water (Milli-Q, 18.2 MΩcm^{-1}) to approximately 25 μM and digested using ProAlanase (enzyme:substrate 1:50). The digests (β-casein, 10 μL, approx. 5 μg; ProAlanase, 0.5 μL, 0.1 μg; water, 26.94 μL; hydrochloric acid, 2.56 μL, 32 mM final concentration) were incubated at 37°C for 2 h, followed by 95°C for 10 min. Digest solutions were centrifuged (5000 × g, 2 min) and transferred to autosampler vials for nanoHPLC-MS analysis; MS/MS (ESI) m/z: $[M+2H]^{2+}$ Calcd for $C_{79}H_{118}N_{22}O_{19}S$ 856.4410; Found 856.44 (1.1 ppm error).

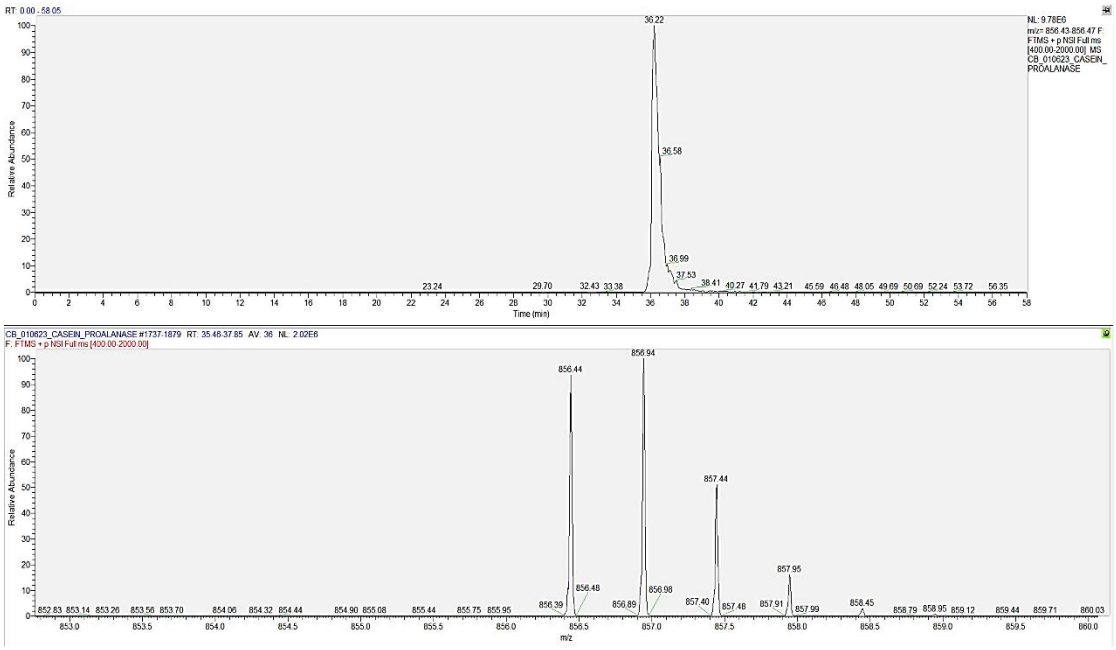

Figure 174. A. Mass chromatogram of range 856.43 – 856.47 showing a single chromatographic peak B. Mass ions within the chromatographic peak showed $[M+2H]^{2+}$ = 856.44 for peptide **213**. Data obtained and analysed by Cameron Bains.

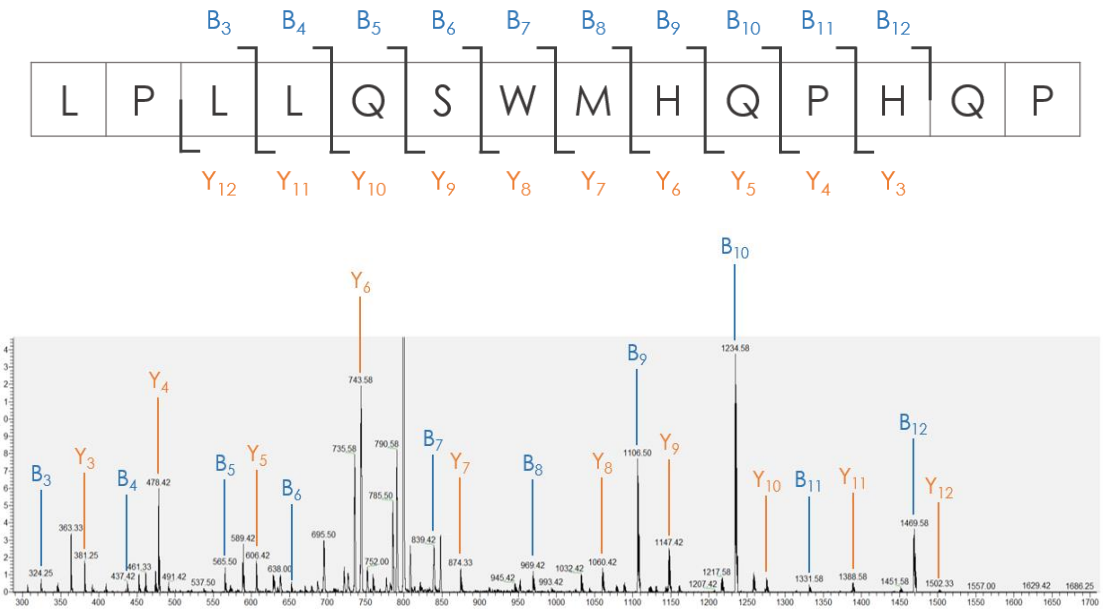

Figure 175. MS/MS spectrum of fragmented peptide LPLLQSWMHQPHQP **213** annotated with the peaks corresponding to B and Y ions from the parent. Data obtained and analysed by Cameron Bains.

β-Casein conjugated with ethyl bromodifluoroacetate (190a)

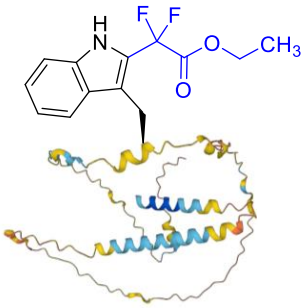

Prepared according to general procedure F using β-casein **189** (12 mg, 0.509 μmol, 1.00 eq.), 4CzIPN (0.254 mM in DMSO, 20 μL, 0.00509 μmol, 1 mol%) and ethyl bromodifluoroacetate **94a** (50.9 mM in DMSO, 20 μL, 1.02 μmol, 2.00 eq.). The reaction mixture was irradiated with blue LEDs for 10 min, then was analysed by ^{19}F NMR spectroscopy, analytical HPLC and MALDI-TOF. The reaction mixture (1/3 volume) was then purified by semi-preparative RP-HPLC (2-70% B over 30 min) to give a mixture of the title compound **190a** and unreacted starting material as a colourless powder (2.2 mg).

Proteolysis of β-casein conjugated with ethyl bromodifluoroacetate to give fragment (194a)

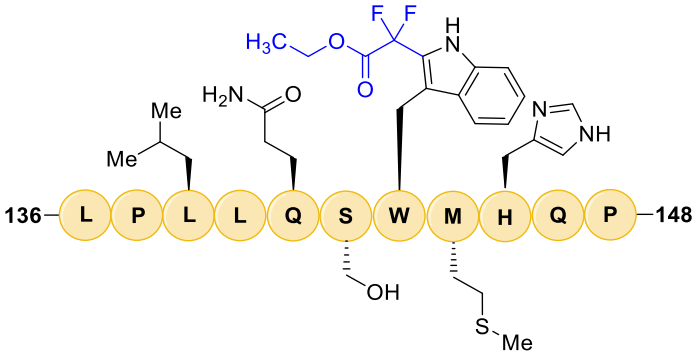

β-Casein conjugated with ethyl bromodifluoroacetate **190a** was suspended in in ultra-pure water (Milli-Q, 18.2 MΩcm^{-1}) to approximately 25 μM and digested using ProAlanase (enzyme:substrate 1:50). The digests (β-casein, 10 μL, approx. 5 μg; ProAlanase, 0.5 μL, 0.1 μg; water, 26.94 μL; hydrochloric acid, 2.56 μL, 32 mM final concentration) were incubated at 37°C for 2 h, followed by 95°C for 10 min. Digest solutions were centrifuged (5000 x g, 2 min) and transferred to autosampler vials for nanoHPLC-MS analysis; MS/MS (ESI) m/z: $[M+2H]^{2+}$ Calcd for $C_{67}H_{102}F_2N_{16}O_{17}S$ 736.3649; Found 736.3700 (6.9 ppm error).

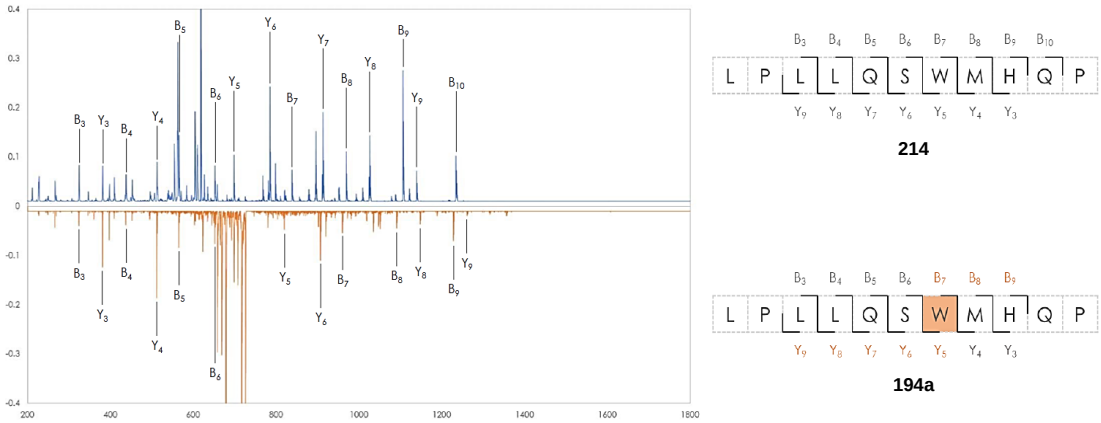

Figure 176. Targeted MS/MS of unmodified (top) **214** modified (bottom) **194a** peptide LPLLQSWMHQP. Data obtained and analysed by Cameron Bains.

Fragment	Unmodified	Modified	Delta
B3	324.92	324.17	−0.75
B4	437.17	437.17	0
B5	565.83	565.25	−0.58
B6	652.58	652.42	−0.16
B7	838.50	960.25	121.75
B8	969.50	1091.41	121.92
B9	1106.50	1228.33	121.83

Fragment	Unmodified	Modified	Delta
Y3	381.75	381.17	−0.58
Y4	512.75	512.17	−0.58
Y5	698.42	820.17	121.75
Y6	785.42	907.17	121.75
Y7	913.42	1035.42	122
Y8	1026.42	1148.33	121.91
Y9	1139.42	1261.42	122

Table 16. Table of mass ions for unmodified **214** modified **194a** peptide LPLLQSWMHQP confirming modification on the Trp residue. Data obtained and analysed by Cameron Bains.

β-Casein conjugated with 2,5,8,11,14,17,20,23-octaoxapentacosan-25-yl 2-bromo-2,2-difluoroacetate (190d)

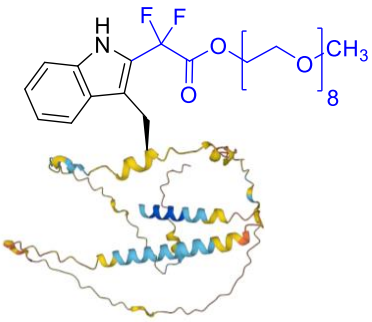

Prepared according to general procedure F using β-casein **189** (12 mg, 0.509 μmol, 1.00 eq.), 4CzIPN (0.254 mM in DMSO, 20 μL, 0.00509 μmol, 1 mol%) and 2,5,8,11,14,17,20,23-Octaoxapentacosan-25-yl 2-bromo-2,2-difluoroacetate **94d** (50.9 mM in DMSO, 20 μL, 1.02 μmol, 2.00 eq.). The reaction mixture was irradiated with blue LEDs for 10 min, then was analysed by ^{19}F NMR spectroscopy, analytical HPLC and MALDI-TOF. The reaction mixture (1/3 volume) was then purified by semi-preparative RP-HPLC (2-70% B over 30 min) to give a mixture of the title compound **190d** and unreacted starting material as a colourless powder (3.4 mg).

Proteolysis of β-casein conjugated with 2,5,8,11,14,17,20,23-Octaoxapentacosan-25-yl 2-bromo-2,2-difluoroacetate to give fragment (194d)

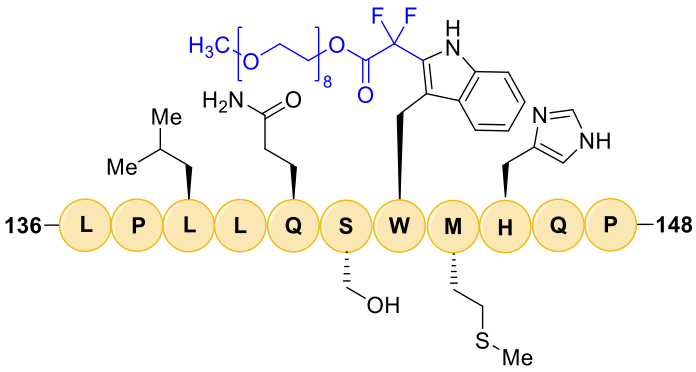

β-Casein conjugated with 2,5,8,11,14,17,20,23-octaoxapentacosan-25-yl 2-bromo-2,2-difluoroacetate **190d** was suspended in in ultra-pure water (Milli-Q, 18.2 MΩcm^{-1}) to approximately 25 μM and digested using ProAlanase (enzyme:substrate 1:50). The digests (β-casein, 10 μL, approx. 5 μg; ProAlanase, 0.5 μL, 0.1 μg; water, 26.94 μL; hydrochloric acid, 2.56 μL, 32 mM final concentration) were incubated at 37°C for 2 h, followed by 95°C for 10 min. Digest solutions were centrifuged (5000 x g, 2 min) and transferred to autosampler vials for nanoHPLC-MS analysis; MS/MS (ESI) m/z: $[M+2H]^{2+}$ Calcd for $C_{82}H_{132}F_2N_{16}O_{25}S$ 905.4619; Found 905.4618 (0.1 ppm error).

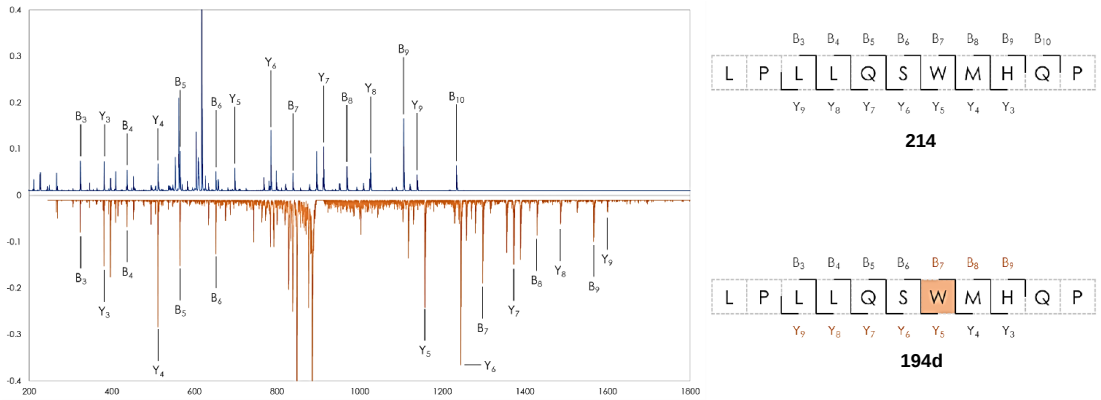

Figure 177. Targeted MS/MS of unmodified (top) **214** modified (bottom) **194d** peptide LPLLQSWMHQP. Data obtained and analysed by Cameron Bains.

Fragment	Unmodified	Modified	Delta
B3	324.50	324.25	−0.25
B4	437.50	437.25	−0.25
B5	565.67	565.33	−0.34
B6	652.42	652.42	0
B7	838.50	1298.42	459.92
B8	969.42	1429.5	460.08
B9	1106.50	1566.67	460.17

Fragment	Unmodified	Modified	Delta
Y3	381.50	381.17	−0.33
Y4	512.50	512.17	−0.33
Y5	698.33	1158.42	460.09
Y6	785.33	1245.42	460.09
Y7	913.42	1373.50	460.08
Y8	1026.50	1486.50	460.00
Y9	1139.50	1599.58	460.08

Table 17. Table of mass ions for unmodified **214** modified **194d** peptide LPLLQSWMHQP confirming modification on the Trp residue. Data obtained and analysed by Cameron Bains.

β-Casein conjugated with *N*-(2-(2-bromo-2,2-difluoroacetamido)ethyl)-5-((3a*S*,4*S*,6a*R*)-2-oxohexahydro-1*H*-thieno[3,4-d]imidazol-4-yl)pentanamide (190m)

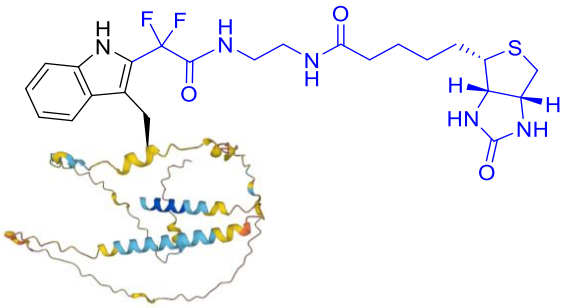

Prepared according to general procedure F using β-casein **189** (12 mg, 0.509 μmol, 1.00 eq.), 4CzIPN (0.254 mM in DMSO, 20 μL, 0.00509 μmol, 1 mol%) *N*-(2-(2-bromo-2,2-difluoroacetamido)ethyl)-5-((3a*S*,4*S*,6a*R*)-2-oxohexahydro-1*H*-thieno[3,4-d]imidazol-4-yl)pentanamide **94m** (50.9 mM in DMSO, 20 μL, 1.02 μmol, 2.00 eq.). The reaction mixture was irradiated with blue LEDs for 10 min, then was analysed by ^{19}F NMR spectroscopy, analytical HPLC and MALDI-TOF. The reaction mixture (1/3 volume) was then purified by semi-preparative RP-HPLC (2-70% B over 30 min) to give a mixture of the title compound **190m** and unreacted starting material as a colourless powder (2.9 mg) as a colourless powder. Identification and characterisation of modified peptide by proteolysis was unsuccessful.

6.6 Photochemical Stapling of Trp-Containing Peptides

General Procedure G: Photocatalytic Stapling of Trp-containing Peptides

A solution of peptide (25 mM in DMSO, 200 µL, 5.00 µmol, 1.00 eq.) and 4CzIPN (2.5 mM in DMSO, 20 µL, 0.0500 µmol, 1 mol%) in DMSO (280 µL, total solvent volume 500 µL) was purged with N_2 (5 min) and then irradiated with blue LEDs (PhotoRedOx box, 18 W) for 90 - 120 min at room temperature. α,α,α-Trifluorotoluene (101 µL, 16.5 mM in DMSO, 1.65 µmol, 0.333 eq.) was added to the reaction mixture, then quantitative NMR spectroscopy and analytical HPLC analysis were carried out. The reaction mixture was diluted with 0.1% TFA in H_2O (2.60 mL) and then purified by semi-preparative HPLC.

Cyclised Ac-WAMLK*-NH_2 (195a)

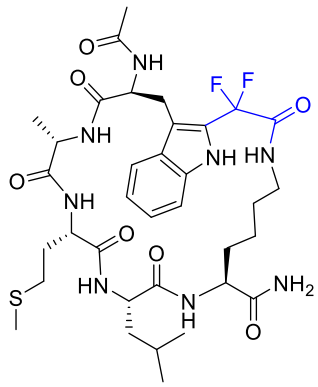

Prepared according to general procedure G using Ac-WAMLK*-NH_2 **195** (25.0 mM in DMSO, 200 µL, 5.00 µmol, 1.00 eq.) and 4CzIPN (2.50 mM in DMSO, 20 µL, 0.0500 µmol, 1 mol%). The reaction mixture was irradiated with blue LEDs for 90 min. The reaction mixture was then purified by semi-preparative RP-HPLC (2-95% B over 30 min with an isocratic hold at 43% B) to give the title compound **195a** (2.1 mg, 2.75 µmol, 56%) as a colourless powder; ^{1}H NMR (500 MHz, MeOD) δ 7.64 (d, *J* = 8.1 Hz, 1H), 7.42 (d, *J* = 8.3 Hz, 1H), 7.23 (dd, *J* = 8.3, 7.6 Hz, 1H), 7.10 (dd, *J* = 8.1, 7.6 Hz, 1H), 4.54 – 4.43 (m, 1H), 4.30 – 4.22 (m, 1H), 4.22 – 4.12 (m, 2H), 4.05 (q, *J* = 7.3 Hz, 1H), 3.43 – 3.38 (m, 1H), 3.38 – 3.33 (m, 2H), 3.27 – 3.25 (m, 1H), 2.65 – 2.57 (m, 1H), 2.58 – 2.48 (m, 1H), 2.09 (s, 3H), 2.12 – 2.06 (m, 2H), 1.96 (s, 3H), 1.92 – 1.84 (m, 1H), 1.74 – 1.63 (m, 1H), 1.63 – 1.49 (m, 4H), 1.44 (d, *J* = 7.3 Hz, 3H), 1.47 – 1.35 (m, 3H), 0.76 (d, *J* = 6.3 Hz, 3H), 0.61 (d, *J* = 6.3 Hz, 3H); ^{19}F NMR (565 MHz, DMSO-d_6) δ −74.2 (s, TFA), −91.9 (d, 1F, *J* = 255.5 Hz), −95.6 (d, 1F, *J* = 255.5 Hz); HRMS (ESI) m/z: $[M + H]^+$ Calcd for $C_{35}H_{51}F_2N_8O_7S$ 765.3569; Found 765.3572 (0.4 ppm error).

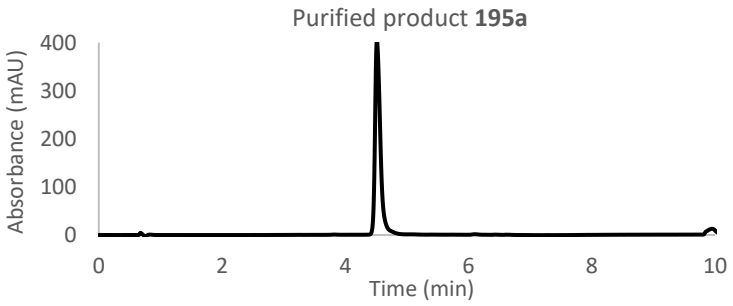

Figure 178. Analytical HPLC chromatogram for purified product **195a** Rt = 4.41 min on analytical gradient 20-100% B over 5 min, 0.6 mL min^{-1}, 280 nm.

Cyclised Ac-K*AMLW-NH$_2$ (198a)

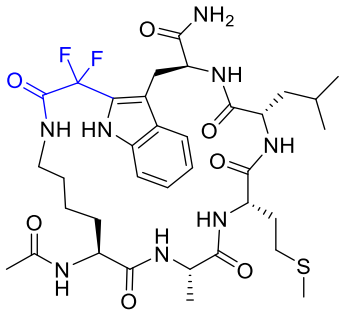

Prepared according to general procedure G using Ac-K*AMLW-NH$_2$ **198** (25.0 mM in DMSO, 200 µL, 5.00 µmol, 1.00 eq.) and 4CzIPN (2.50 mM in DMSO, 20 µL, 0.0500 µmol, 1 mol%). The reaction mixture was irradiated with blue LEDs for 120 min. The reaction mixture was then purified by semi-preparative RP-HPLC (2-70% B over 30 min) to give the title compound **198a** (1.6 mg, 2.09 µmol, 42%) as a colourless powder; ^{1}H NMR (400 MHz, MeOD) δ 7.82 (d, *J* = 8.1 Hz, 1H), 7.39 (d, *J* = 8.2 Hz, 1H), 7.23 (dd, *J* = 8.2, 7.7 Hz, 1H), 7.10 (dd, *J* = 8.1, 7.7 Hz, 1H), 4.67 (dd, *J* = 8.2, 7.6 Hz, 1H), 4.61 – 4.50 (m, 1H), 4.43 – 4.35 (m, 1H), 4.33 – 4.19 (m, 2H), 3.60 – 3.52 (m, 1H), 3.38 (d, *J* = 7.6 Hz, 2H), 3.29 – 3.23 (m, 1H), 2.37 – 2.29 (m, 2H), 1.98 (s, 3H), 1.95 – 1.86 (m, 1H), 1.92 (s, 3H), 1.87 – 1.77 (m, 2H), 1.76 – 1.62 (m, 3H), 1.62 – 1.51 (m, 1H), 1.51 – 1.39 (m, 4H), 1.36 (d, *J* = 7.3 Hz, 3H), 0.93 – 0.82 (m, 6H); ^{19}F NMR (376 MHz, MeOD) δ −77.4 (s, TFA), −101.0 (d, 1F, *J* = 265.0 Hz), −102.6 (d, 1F, *J* = 265.0 Hz); HRMS (ESI) m/z: [M + H]$^+$ Calcd for $C_{35}H_{51}F_2N_8O_7S$ 765.3569; Found 765.3556 (1.7 ppm error).

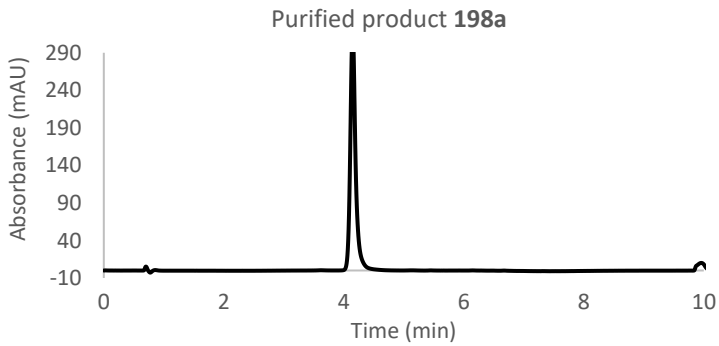

Figure 179. Analytical HPLC chromatogram for purified product **198a** Rt = 4.15 min on analytical gradient 20-100% B over 5 min, 0.6 mL min^{-1}, 280 nm.

Cyclised Ac-EWAMLK*R-NH$_2$ (199a)

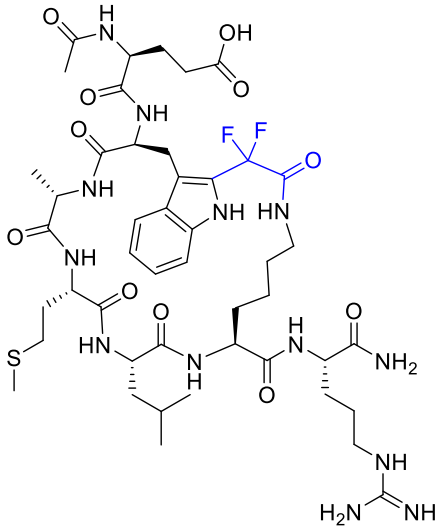

Prepared according to general procedure G using Ac-EWAMLK*R-NH$_2$ **199** (25.0 mM in DMSO, 200 µL, 5.00 µmol, 1.00 eq.) and 4CzIPN (2.50 mM in DMSO, 20 µL, 0.0500 µmol, 1 mol%). The reaction mixture was irradiated with blue LEDs for 120 min. The reaction mixture was then purified by semi-preparative RP-HPLC (2-70% B over 30 min) to give the title compound **199a** (3.0 mg, 2.86 µmol, 57%) as a colourless powder; ^{1}H NMR (500 MHz, MeOD) δ 7.66 (dd, *J* = 8.0, 1.1 Hz, 1H), 7.45 (dd, *J* = 8.3, 1.0 Hz, 1H), 7.26 (ddd, *J* = 8.3, 6.9, 1.1 Hz, 1H), 7.15 (ddd, *J* = 8.0, 6.9, 1.0 Hz, 1H), 4.44 (t, *J* = 7.9 Hz, 1H), 4.25 (dd, *J* = 10.0, 4.4 Hz, 1H), 4.21 (dd, *J* = 9.5, 5.4 Hz, 1H), 4.16 – 4.07 (m, 3H), 4.01 (q, *J* = 7.3 Hz, 1H), 3.36 (d, *J* = 7.9 Hz, 2H), 3.25 – 3.14 (m, 3H), 2.73 – 2.62 (m, 1H), 2.62 – 2.50 (m, 1H), 2.30 – 2.18 (m, 2H), 2.20 – 2.09 (m, 2H), 2.08 (s, 3H), 2.00 (s, 3H), 1.98 – 1.93 (m, 1H), 1.91 – 1.82 (m, 4H), 1.81 – 1.72 (m, 2H), 1.71 – 1.63 (m, 3H), 1.63 – 1.52 (m, 4H), 1.49 (d, *J* = 7.3 Hz, 3H), 1.46 – 1.32 (m, 2H), 0.77 (d, *J* = 6.4 Hz, 3H), 0.72 (d, *J* = 6.3 Hz, 3H); ^{19}F NMR (376 MHz, MeOD) δ −77.2 (s, TFA), −89.5 (d, 1F, *J* = 280.7 Hz), −106.0 (d, 1F, *J* = 280.7 Hz); HRMS (ESI) m/z: [M + H]$^+$ Calcd for $C_{46}H_{70}F_2N_{13}O_{11}S$ 1050.5007; Found 1050.4996 (1.0 ppm error).

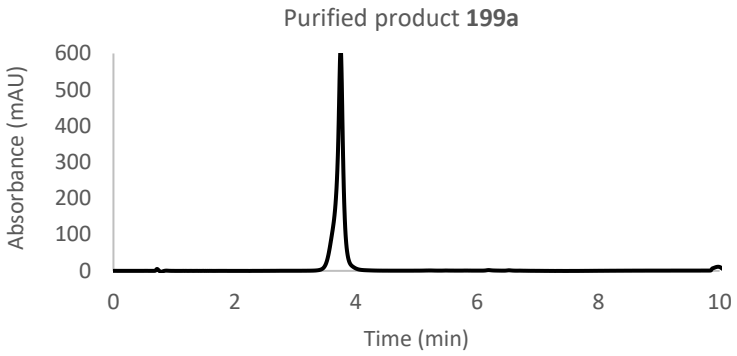

Figure 180. Analytical HPLC chromatogram for purified product **199a** Rt = 3.75 min on analytical gradient 20-100% B over 5 min, 0.6 mL min^{-1}, 280 nm.

Cyclised Ac-WGFIK*-NH$_2$ (200a)

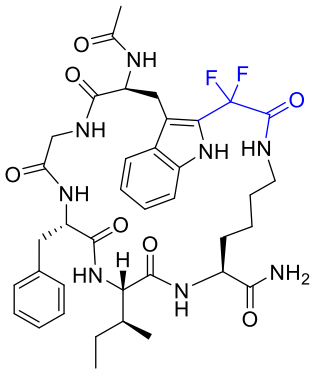

Prepared according to general procedure G using Ac-WGFIK*-NH$_2$ **200** (4.2 mg, 5.00 µmol, 1.00 eq.) and 4CzIPN (2.50 mM in DMSO, 20 µL, 0.0500 µmol, 1 mol%). The reaction mixture was irradiated with blue LEDs for 120 min. The reaction mixture was then purified by semi-preparative RP-HPLC (2-70% B over 30 min with an isocratic hold at 41% B) to give the title compound **200a** (1.2 mg, 1.56 µmol, 32%) as a colourless powder; ^{1}H NMR (500 MHz, MeOD) δ 7.62 (d, *J* = 8.1 Hz, 1H), 7.40 (d, *J* = 8.3 Hz, 1H), 7.29 – 7.25 (m, 4H), 7.25 – 7.17 (m, 2H), 7.09 (ddd, *J* = 8.1, 7.0, 1.0 Hz, 1H), 4.58 – 4.48 (m, 2H), 4.25 (dd, *J* = 9.6, 4.1 Hz, 1H), 4.08 (d, *J* = 8.0 Hz, 1H), 3.80 (d, *J* = 16.6 Hz, 1H), 3.46 (d, *J* = 16.6 Hz, 1H), 3.42 – 3.33 (m, 3H), 3.25 – 3.13 (m, 2H), 3.04 – 2.92 (m, 1H), 1.96 (s, 3H), 1.89 – 1.78 (m, 2H), 1.73 – 1.64 (m, 1H), 1.63 – 1.53 (m, 2H), 1.51 – 1.41 (m, 1H), 1.42 – 1.32 (m, 2H), 1.21 – 1.14 (m, 1H), 0.86 (d, *J* = 6.9 Hz, 3H), 0.83 (dd, *J* = 8.0, 7.4 Hz, 3H); ^{19}F NMR (376 MHz, MeOD) δ −77.3 (s, TFA), −96.2 (d, 1F, *J* = 273.0 Hz), −102.1 (dd, 1F, *J* = 273.0, 29.3 Hz); HRMS (ESI) m/z: [M + H]$^+$ Calcd for $C_{38}H_{49}F_2N_8O_7$ 767.3692; Found 767.3688 (0.5 ppm error).

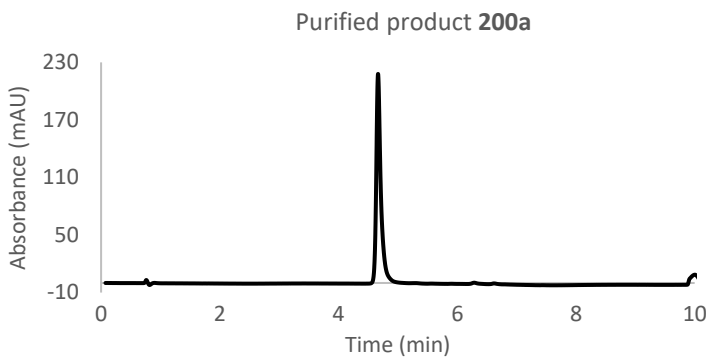

Figure 181. Analytical HPLC chromatogram for purified product **200a** Rt = 4.67 min on analytical gradient 20-100% B over 5 min, 0.6 mL min^{-1}, 280 nm.

Cyclised H-WHASPYVK*-NH$_2$ (202a)

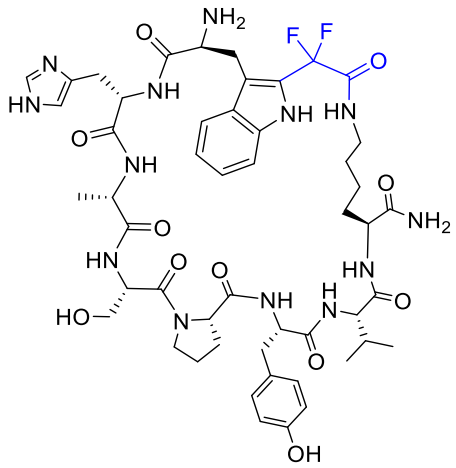

Prepared according to general procedure G using H-WHASPYVK*-NH$_2$ **202** (5.7 mg, 5.00 µmol, 1.00 eq.) and 4CzIPN (2.50 mM in DMSO, 20 µL, 0.0500 µmol, 1 mol%). The reaction mixture was irradiated with blue LEDs for 120 min. The reaction mixture was then purified by semi-preparative RP-HPLC (2-70% B over 30 min) to give the title compound **202a** (2.3 mg, 2.17 µmol, 43%) as a colourless powder; ^{1}H NMR (500 MHz, MeOD) δ 8.75 (s, 1H), 7.56 (d, *J* = 8.1 Hz, 1H), 7.45 – 7.38 (m, 1H), 7.31 (s, 1H), 7.26 (ddd, *J* = 8.2, 6.9, 1.1 Hz, 1H), 7.11 (ddd, *J* = 8.0, 7.0, 1.1 Hz, 1H), 7.06 – 7.00 (m, 2H), 6.70 (d, *J* = 8.5 Hz, 2H), 4.73 (dd, *J* = 8.3, 5.6 Hz, 1H), 4.50 – 4.44 (m, 1H), 4.42 (dd, *J* = 11.3, 4.3 Hz, 1H), 4.30 – 4.18 (m, 2H), 4.11 (d, *J* = 7.6 Hz, 1H), 4.03 – 3.95 (m, 1H), 3.89 (dd, *J* = 10.3, 5.6 Hz, 1H), 3.77 – 3.69 (m, 1H), 3.69 – 3.61 (m, 2H), 3.52 – 3.35 (m, 3H), 3.28 – 3.21 (m, 2H), 3.19 – 3.10 (m, 2H), 3.02 (dd, *J* = 15.3, 5.8 Hz, 1H), 2.74 (dd, *J* = 14.2, 11.3 Hz, 1H), 2.23 – 2.13 (m, 1H), 2.06 – 1.92 (m, 1H), 1.92

– 1.81 (m, 1H), 1.77 – 1.67 (m, 1H), 1.65 – 1.48 (m, 5H), 1.47 – 1.33 (m, 2H), 1.24 (d, *J* = 7.1 Hz, 3H), 1.02 – 0.96 (m, 6H); ^{19}F NMR (565 MHz, MeOD) δ – 77.0 (s, TFA), −104.0 (2F, d, *J* = 265.0 Hz); HRMS (ESI) m/z: [M + H]$^+$ Calcd for $C_{50}H_{66}F_2N_{13}O_{11}$ 1062.4973; Found 1062.4986 (1.2 ppm error).

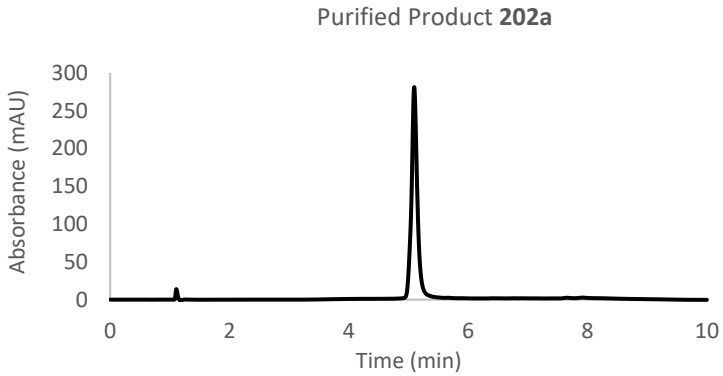

Figure 182. Analytical HPLC chromatogram for purified product **202a** Rt = 5.10 min on analytical gradient 2-70% B over 5 min, 0.6 mL min^{-1}, 280 nm.

Cyclised Ac-WQDECKSNTAGK*-NH$_2$ (203a)

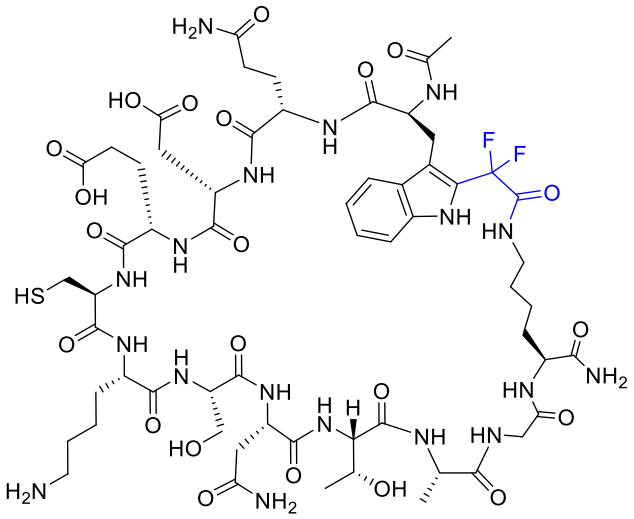

Prepared according to general procedure G using Ac-WQDECKSNTAGK*-NH$_2$ **203** (7.8 mg, 5.00 µmol, 1.00 eq.) and 4CzIPN (2.50 mM in DMSO, 20 µL, 0.0500 µmol, 1 mol%). The reaction mixture was irradiated with blue LEDs for 120 min. The reaction mixture was then purified by semi-preparative RP-HPLC (2-70% B over 30 min) to give a mixture of the title compound **203a** and HAA linear peptide side product **204** as a colourless powder (1.6 mg). Characterisation of **203a** by NMR spectroscopy was unsuccessful due

to solubility challenges. HRMS (ESI) m/z: $[M + 2Na]^{2+}$ Calcd for $C_{60}H_{88}F_2N_{18}O_{22}S$ 764.2903; Found 764.2903 (1.0 ppm error).

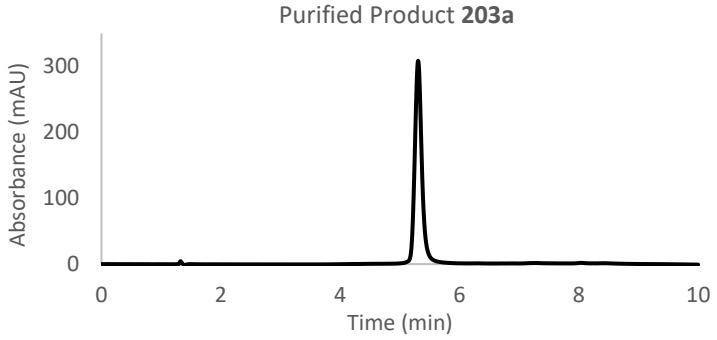

Figure 183. Analytical HPLC chromatogram for purified product **203a** Rt = 5.31 min on analytical gradient 2-70% B over 5 min, 0.6 mL min^{-1}, 280 nm.

7 References

1 J. C. Lee, J. D. Cuthbertson and N. J. Mitchell, *Org. Lett.*, 2023, **25**, 5459–5464.

2 T. Dang and R. D. Süssmuth, *Acc. Chem. Res.*, 2017, **50**, 1566–1576.

3 D. J. Craik, D. P. Fairlie, S. Liras and D. Price, *Chem. Biol. \& Drug Des.*, 2013, **81**, 136–147.

4 L. Wang, N. Wang, W. Zhang, X. Cheng, Z. Yan, G. Shao, X. Wang, R. Wang and C. Fu, *Signal Transduct. Target. Ther.*, 2022, **7**, 48.

5 N. Krall, F. P. da Cruz, O. Boutureira and G. J. L. Bernardes, *Nat. Chem.*, 2016, **8**, 103–113.

6 J. K. Dozier and M. D. Distefano, *Int. J. Mol. Sci.*, 2015, **16**, 25831–25864.

7 S. B. Gunnoo and A. Madder, *Org. Biomol. Chem.*, 2016, **14**, 8002–8013.

8 S. V. Moradi, W. M. Hussein, P. Varamini, P. Simerska and I. Toth, *Chem. Sci.*, 2016, **7**, 2492–2500.

9 M. Lelle, S. Kaloyanova, C. Freidel, M. Theodoropoulou, M. Musheev, C. Niehrs, G. Stalla and K. Peneva, *Mol. Pharm.*, 2015, **12**, 4290–4300.

10 M. Nahrwold, C. Weiß, T. Bogner, F. Mertink, J. Conradi, B. Sammet, R. Palmisano, S. Royo Gracia, T. Preuße and N. Sewald, *J. Med. Chem.*, 2013, **56**, 1853–1864.

11 J. Burggraaf, I. M. C. Kamerling, P. B. Gordon, L. Schrier, M. L. de Kam, A. J. Kales, R. Bendiksen, B. Indrevoll, R. M. Bjerke, S. A. Moestue, S. Yazdanfar, A. M. J. Langers, M. Swaerd-Nordmo, G. Torheim, M. V Warren, H. Morreau, P. W. Voorneveld, T. Buckle, F. W. B. van Leeuwen, L.-I. Ødegårdstuen, G. T. Dalsgaard, A. Healey and J. C. H. Hardwick, *Nat. Med.*, 2015, **21**, 955–961.

12 M. Staderini, A. Megia-Fernandez, K. Dhaliwal and M. Bradley, *Bioorganic Med. Chem.*, 2018, **26**, 2816–2826.

13 B. Bumbaca, Z. Li and D. K. Shah, *Drug Metab. Pharmacokinet.*, 2019, **34**, 42–54.

14 A. Tantipanjaporn and M.-K. Wong, *Molecules*, 2023, **28**, 1083.

15 S. Iyengar, M. H. Ossipov and K. W. Johnson, *Pain*, 2017, **158**, 543–559.

16 S. C. Peterson and A. R. Barry, *Curr. Diabetes Rev.*, 2018, **14**, 273–279.

17 S. Sharma, R. Singh and S. Rana, *Int. J. Bioautomation*, 2011, **15**, 223–250.

18 F. K. Knop, A. Brønden and T. Vilsbøll, *Expert Opin. Pharmacother.*, 2017, **18**, 555–571.

19 R. Polt, F. Porreca, L. Z. Szabò, E. J. Bilsky, P. Davis, T. J. Abbruscato, T. P. Davis, R. Harvath, H. I. Yamamura and V. J. Hruby, *Proc. Natl. Acad. Sci. U. S. A.*, 1994, **91**, 7114–7118.

20 Geoffrey M Cooper, *The Cell: A Molecular Approach. 2nd edition.*, Sunderland (MA), 2nd edn., 2000.

21 F. D. Makurvet, *Med. Drug Discov.*, 2021, **9**, 100075.

22 P. B. John Gooch, Frank Cordes, Frank Bressau, What Does—and Does Not—Drive Biopharma Cost Performance, https://www.bcg.com/publications/2017/biopharmaceuticals-operations-what-does-and-does-not-drive-biopharma-cost-performance, (accessed 12 October 2023).

23 R. He, B. Finan, J. P. Mayer and R. D. DiMarchi, *Molecules*, 2019, **24**, 11–14.

24 F. Spada and M. Valente, *J. Cancer Metastasis Treat.*, 2016, **2**, 313–320.

25 M. de Jong, R. Valkema, F. Jamar, L. K. Kvols, D. J. Kwekkeboom, W. A. P. Breeman, W. H. Bakker, C. Smith, S. Pauwels and E. P. Krenning, *Semin. Nucl. Med.*, 2002, **32**, 133–140.

26 J. C. Reubi, J.-C. Schär, B. Waser, S. Wenger, A. Heppeler, J. S.

Schmitt and H. R. Mäcke, *Eur. J. Nucl. Med.*, 2000, **27**, 273–282.

27 FDA approves lutetium Lu 177 dotatate for treatment of GEP-NETS, https://www.fda.gov/drugs/resources-information-approved-drugs/fda-approves-lutetium-lu-177-dotatate-treatment-gep-nets, (accessed 8 August 2023).

28 C. Gründker and G. Emons, *Front. Endocrinol. (Lausanne).*, 2017, **8**, 187.

29 G. Emons, G. Gorchev, P. Harter, P. Wimberger, A. Stähle, L. Hanker, F. Hilpert, M. W. Beckmann, P. Dall, C. Gründker, H. Sindermann and J. Sehouli, *Int. J. Gynecol. cancer Off. J. Int. Gynecol. Cancer Soc.*, 2014, **24**, 260–265.

30 M. Akbarian, A. Khani, S. Eghbalpour and V. N. Uversky, *Int. J. Mol. Sci.*, 2022, **23**, 1445.

31 J. Tang, Y. He, H. Chen, W. Sheng and H. Wang, *Chem. Sci.*, 2017, **8**, 4565–4570.

32 C. Jo, F. F. Khan, M. I. Khan and J. Iqbal, *Food Rev. Int.*, 2017, **33**, 44–61.

33 M. Broggini, S. V Marchini, E. Galliera, P. Borsotti, G. Taraboletti, E. Erba, M. Sironi, J. Jimeno, G. T. Faircloth, R. Giavazzi and M. d'Incalci, *Leukemia*, 2003, **17**, 52–59.

34 K. M. White, R. Rosales, S. Yildiz, T. Kehrer, L. Miorin, E. Moreno, S. Jangra, M. B. Uccellini, R. Rathnasinghe, L. Coughlan, C. Martinez-Romero, J. Batra, A. Rojc, M. Bouhaddou, J. M. Fabius, K. Obernier, M. Dejosez, M. J. Guillén, A. Losada, P. Avilés, M. Schotsaert, T. Zwaka, M. Vignuzzi, K. M. Shokat, N. J. Krogan and A. García-Sastre, *Science*, 2021, **371**, 926–931.

35 P. W. Ford, K. R. Gustafson, T. C. McKee, N. Shigematsu, L. K. Maurizi, L. K. Pannell, D. E. Williams, E. Dilip de Silva, P. Lassota, T. M. Allen, R. Van Soest, R. J. Andersen and M. R. Boyd, *J. Am. Chem. Soc.*, 1999, **121**, 5899–5909.

36 K. J. Wesson and M. T. Hamann, *J. Nat. Prod.*, 1996, **59**, 629–631.

37 A. A. Zaky, J. Simal-Gandara, J.-B. Eun, J.-H. Shim and A. M. Abd El-Aty, *Front. Nutr.*, 2022, **8**, 815640.

38 J. Lee, J. N. Currano, P. J. Carroll and M. M. Joullié, *Nat. Prod. Rep.*, 2012, **29**, 404–424.

39 S. E. Dmitriev, D. O. Vladimirov and K. A. Lashkevich, *Biochem.*, 2020, **85**, 1389–1421.

40 J. Adrio, C. Cuevas, I. Manzanares and M. M. Joullié, *J. Org. Chem.*, 2007, **72**, 5129–5138.

41 G. Hong, A. L. Antaris and H. Dai, *Nat. Biomed. Eng.*, 2017, **1**, 10.

42 A. D. Warren, S. T. Gaylord, K. C. Ngan, M. Dumont Milutinovic, G. A. Kwong, S. N. Bhatia and D. R. Walt, *J. Am. Chem. Soc.*, 2014, **136**, 13709–13714.

43 L. Mendive-Tapia, C. Zhao, A. R. Akram, S. Preciado, F. Albericio, M. Lee, A. Serrels, N. Kielland, N. D. Read, R. Lavilla and M. Vendrell, *Nat. Commun.*, 2016, **7**, 10940.

44 A. Glas, D. Bier, G. Hahne, C. Rademacher, C. Ottmann and T. N. Grossmann, *Angew. Chem. Int. Ed. Engl.*, 2014, **53**, 2489–2493.

45 D. M. Rissin, C. W. Kan, T. G. Campbell, S. C. Howes, D. R. Fournier, L. Song, T. Piech, P. P. Patel, L. Chang, A. J. Rivnak, E. P. Ferrell, J. D. Randall, G. K. Provuncher, D. R. Walt and D. C. Duffy, *Nat. Biotechnol.*, 2010, **28**, 595–599.

46 M. Rahiminejad, A. Rastogi, S. Prabhudesai, D. Mcclinton, P. MacCallum, S. Platton and E. Friedman, *ISRN Radiol.*, 2014, **2014**, 519875.

47 M. Whitney, E. N. Savariar, B. Friedman, R. A. Levin, J. L. Crisp, H. L. Glasgow, R. Lefkowitz, S. R. Adams, P. Steinbach, N. Nashi, Q. T. Nguyen and R. Y. Tsien, *Angew. Chem. Int. Ed. Engl.*, 2013, **52**, 325–330.

48 E. C. Smyth and M. A. Shah, *World J. Gastroenterol.*, 2011, **17**, 5059–5074.

49 O. Jacobson, D. O. Kiesewetter and X. Chen, *Bioconjug. Chem.*, 2015, **26**, 1–18.

50 E. N. G. Marsh and Y. Suzuki, *ACS Chem. Biol.*, 2014, **9**, 1242–1250.

51 J. T. Gerig, *Prog. Nucl. Magn. Reson. Spectrosc.*, 1994, **26**, 293–370.

52 M. Arias, J. M. Aramini, N. D. Riopel and H. J. Vogel, *Biochim. Biophys. Acta - Biomembr.*, 2020, **1862**, 183260.

53 L. T. Nguyen, E. F. Haney and H. J. Vogel, *Trends Biotechnol.*, 2011, **29**, 464–472.

54 W. J. Wedemeyer, E. Welker and H. A. Scheraga, *Biochemistry*, 2002, **41**, 14637–14644.

55 G. Esposito, A. M. Lesk, H. Molinari, A. Motta, N. Niccolai and A. Pastore, *Biopolymers*, 1993, **33**, 839–846.

56 M. B. Ulmschneider and M. S. P. Sansom, *Biochim. Biophys. Acta - Biomembr.*, 2001, **1512**, 1–14.

57 P. Zhou, J. Zou, F. Tian and Z. Shang, *J. Chem. Inf. Model.*, 2009, **49**, 2344–2355.

58 S. K. Mishra and N. Suryaprakash, *Molecules*, 2017, **22**, 423.

59 J. M. Monkovic, H. Gibson, J. W. Sun and J. K. Montclare, *Pharmaceuticals*, 2022, **15**, 1201.

60 F. Jia, Y. Zhang, J. Wang, J. Peng, P. Zhao, L. Zhang, H. Yao, J. Ni and K. Wang, *Peptides*, 2019, **112**, 56–66.

61 M. Mardirossian, M. Rubini, M. F. A. Adamo, M. Scocchi, M. Saviano, A. Tossi, R. Gennaro and A. Caporale, *Molecules*, 2021, **26**, 7401.

62 J. N. DeGruyter, L. R. Malins and P. S. Baran, *Biochemistry*, 2017, **56**, 3863–3873.

63 S. B. Gunnoo and A. Madder, *ChemBioChem*, 2016, **17**, 529–553.

64 J. M. Chalker, G. J. L. Bernardes, Y. A. Lin and B. G. Davis, *Chem. Asian J.*, 2009, **4**, 630–640.

65 O. Boutureira and G. J. L. Bernardes, *Chem. Rev.*, 2015, **115**, 2174–2195.

66 F.-J. Chen and J. Gao, *Chem. Eur. J.*, 2022, **28**, e202201843.

67 J. M. Ravasco, H. Faustino, A. Trindade and P. M. P. Gois, *Chem. Eur. J.*, 2019, **25**, 43–59.

68 Q. Luo, Y. Tao, W. Sheng, J. Lu and H. Wang, *Nat. Commun.*, 2019, **10**, 1–9.

69 Y. Zhang, X. Zhou, Y. Xie, M. M. Greenberg, Z. Xi and C. Zhou, *J. Am. Chem. Soc.*, 2017, **139**, 6146–6151.

70 Y. Zhang, C. Zang, G. An, M. Shang, Z. Cui, G. Chen, Z. Xi and C. Zhou, *Nat. Commun.*, 2020, **11**, 1015.

71 B. Bernardim, M. J. Matos, X. Ferhati, I. Compañón, A. Guerreiro, P. Akkapeddi, A. C. B. Burtoloso, G. Jiménez-Osés, F. Corzana and G. J. L. Bernardes, *Nat. Protoc.*, 2019, **14**, 86–99.

72 D. Abegg, M. Tomanik, N. Qiu, D. Pechalrieu, A. Shuster, B. Commare, A. Togni, S. B. Herzon and A. Adibekian, *J. Am. Chem. Soc.*, 2021, **143**, 20332–20342.

73 N. J. Smith, K. Rohlfing, L. A. Sawicki, P. M. Kharkar, S. J. Boyd, A. M. Kloxin and J. M. Fox, *Org. Biomol. Chem.*, 2018, **16**, 2164–2169.

74 G. Wu, J. R. Lupton, N. D. Turner, Y.-Z. Fang and S. Yang, *J. Nutr.*, 2004, **134**, 489–492.

75 O. Koniev and A. Wagner, *Chem. Soc. Rev.*, 2015, **44**, 5495–5551.

76 M. A. Robinson, S. T. Charlton, P. Garnier, X. Wang, S. S. Davis, A. C. Perkins, M. Frier, R. Duncan, T. J. Savage, D. A. Wyatt, S. A. Watson and B. G. Davis, *Proc. Natl. Acad. Sci.*, 2004, **101**, 14527–14532.

77 K. Tanaka, Y. Fujii and K. Fukase, *ChemBioChem*, 2008, **9**, 2392–2397.

78 H. Sun, M. Xi, Q. Jin, Z. Zhu, Y. Zhang, G. Jia, G. Zhu, M. Sun, H. Zhang, X. Ren, Y. Zhang, Z. Xu, H. Huang, J. Shen, B. Li, G. Ge, K. Chen and W. Zhu, *J. Med. Chem.*, 2022, **65**, 11840–11853.

79 K. F. Tanaka Koichi; Katsumura, Shigeo, *Synlett*, 2011, **2011**, 2115–2139.

80 K. Tanaka and K. Fukase, *Org. Biomol. Chem.*, 2008, **6**, 815–828.

81 Y. Weng, C. Song, C.-W. Chiang and A. Lei, *Commun. Chem.*, 2020, **3**, 171.

82 P. Y. Chou and G. D. Fasman, *Biochemistry*, 1974, **13**, 222–245.

83 C. M. Santiveri and M. A. Jiménez, *Biopolymers*, 2010, **94**, 779–790.

84 Y. Zhu, M. Bauer and L. Ackermann, *Chem. Eur. J.*, 2015, **21**, 9980–9983.

85 A. J. Reay, T. J. Williams and I. J. S. Fairlamb, *Org. Biomol. Chem.*, 2015, **13**, 8298–8309.

86 H. Dong, C. Limberakis, S. Liras, D. Price and K. James, *Chem. Commun.*, 2012, **48**, 11644–11646.

87 N. Kaplaneris, T. Rogge, R. Yin, H. Wang, G. Sirvinskaite and L. Ackermann, *Angew. Chemie Int. Ed.*, 2019, **58**, 3476–3480.

88 A. D. Roy, R. J. M. Goss, G. K. Wagner and M. Winn, *Chem. Commun.*, 2008, 4831–4833.

89 E. S. T. Asakura,K. Adachi, *J. Biol. Chem.*, 1978, **253**, 6423–6425.

90 T. J. Williams, A. J. Reay, A. C. Whitwood and I. J. S. Fairlamb, *Chem. Commun.*, 2014, **50**, 3052–3054.

91 L. R. Malins, K. M. Cergol and R. J. Payne, *Chem. Sci.*, 2014, **5**, 260–266.

92 M. Imiołek, G. Karunanithy, W.-L. Ng, A. J. Baldwin, V. Gouverneur and B. G. Davis, *J. Am. Chem. Soc.*, 2018, **140**, 1568–1571.

93 Y. Seki, T. Ishiyama, D. Sasaki, J. Abe, Y. Sohma, K. Oisaki and M. Kanai, *J. Am. Chem. Soc.*, 2016, **138**, 10798–10801.

94 E. Y.-L. Hui, B. Rout, Y. S. Tan, C. S. Verma, K.-P. Chan and C. W. Johannes, *Org. Biomol. Chem.*, 2018, **16**, 389–392.

95 L. Mendive-Tapia, S. Preciado, J. García, R. Ramón, N. Kielland, F. Albericio and R. Lavilla, *Nat. Commun.*, 2015, **6**, 7160.

96 Y. H. Lau, P. de Andrade, Y. Wu and D. R. Spring, *Chem. Soc. Rev.*, 2015, **44**, 91–102.

97 M. Góngora-Benítez, J. Tulla-Puche and F. Albericio, *Chem. Rev.*, 2014, **114**, 901–926.

98 H. Jo, N. Meinhardt, Y. Wu, S. Kulkarni, X. Hu, K. E. Low, P. L. Davies, W. F. DeGrado and D. C. Greenbaum, *J. Am. Chem. Soc.*, 2012, **134**, 17704–17713.

99 H. E. Blackwell and R. H. Grubbs, *Angew. Chemie Int. Ed.*, 1998, **37**, 3281–3284.

100 A.-C. Carbonnelle and J. Zhu, *Org. Lett.*, 2000, **2**, 3477–3480.

101 S. A. Kawamoto, A. Coleska, X. Ran, H. Yi, C.-Y. Yang and S. Wang, *J. Med. Chem.*, 2012, **55**, 1137–1146.

102 D. Gilis, S. Massar, N. J. Cerf and M. Rooman, *Genome Biol.*, 2001, **2**, research0049.1.

103 N. Lebrasseur and I. Larrosa, *J. Am. Chem. Soc.*, 2008, **130**, 2926–2927.

104 T. Chiba, Y.-H. Li, T. Yamane, O. Ogikubo, M. Fukuoka, R. Arai, S. Takahashi, T. Ohtsuka, I. Ohkubo and N. Matsui, *Peptides*, 2003, **24**, 773–778.

105 D. R. Nassel, M. G. S. Persson and J. E. Muren, *J. Comp. Neurol.*, 2000, **422**, 267–286.

106 M. M. Lorion, N. Kaplaneris, J. Son, R. Kuniyil and L. Ackermann, *Angew. Chemie Int. Ed.*, 2019, **58**, 1684–1688.

107 P. Gandeepan, T. Müller, D. Zell, G. Cera, S. Warratz and L. Ackermann, *Chem. Rev.*, 2019, **119**, 2192–2452.

108 R. Huang, P. S. Conti and K. Chen, *Methods Mol. Biol.*, 2016, **1444**, 73–84.

109 S. Jackson, W. DeGrado, A. Dwivedi, A. Parthasarathy, A. Higley, J. Krywko, A. Rockwell, J. Markwalder and G. Wells, *J. Am. Chem. Soc.*, 1994, **116**, 3220–3230.

110 C. Bottecchia and T. Noël, *Chem. Eur. J.*, 2019, **25**, 26–42.

111 E. Speckmeier, T. G. Fischer and K. Zeitler, *J. Am. Chem. Soc.*, 2018, **140**, 15353–15365.

112 T. A. King, J. Mandrup Kandemir, S. J. Walsh and D. R. Spring, *Chem. Soc. Rev.*, 2021, **50**, 39–57.

113 S. Sato, K. Hatano, M. Tsushima and H. Nakamura, *Chem. Commun.*, 2018, **54**, 5871–5874.

114 B. Ding, Y. Weng, Y. Liu, C. Song, L. Yin, J. Yuan, Y. Ren, A. Lei and C.-W. Chiang, *European J. Org. Chem.*, 2019, **2019**, 7596–7605.

115 N. Ichiishi, J. P. Caldwell, M. Lin, W. Zhong, X. Zhu, E. Streckfuss, H. Y. Kim, C. A. Parish and S. W. Krska, *Chem. Sci.*, 2018, **9**, 4168–4175.

116 S. Tower, W. Hetcher, T. Myers, N. Kuehl and M. Taylor, *J. Am. Chem. Soc.*, 2020, **142**, 9112–9118.

117 M. F. Lin, C. M. Tzeng, Y. A. Dyakov and C. K. Ni, *J. Chem. Phys.*

118 M. S. Hamdy, E. L. Scott, R. H. Carr and J. P. M. Sanders, *Catal. Letters*, 2012, **142**, 338–344.

119 R. N. Lima, J. A. C. Delgado, D. I. Bernardi, R. G. S. Berlinck, N. Kaplaneris, L. Ackermann and M. W. Paixão, *Chem. Commun.*, 2021.

120 B. Laroche, X. Tang, G. Archer, R. Di Sanza and P. Melchiorre, *Org. Lett.*, 2021, **23**, 285–289.

121 Z. Pan, Y. Liu, F. Hu, Q. Liu, W. Shang and C. Xia, *Chem. Commun.*, 2020, **56**, 4930–4933.

122 C.-W. Huang, Z. Li and P. S. Conti, *J. Nucl. Med.*, 2011, **52**, 1979 LP – 1986.

123 J. Jung, E. Kim, Y. You and E. J. Cho, *Adv. Synth. Catal.*, 2014, **356**,

2741–2748.

124 A. Lemos, C. Lemaire and A. Luxen, *Adv. Synth. Catal.*, 2019, **361**, 1500–1537.

125 C. D. Spicer and B. G. Davis, *Nat. Commun.*, 2014, **5**, 4740.

126 O. M. Musa, S.-Y. Choi, J. H. Horner and M. Newcomb, *J. Org. Chem.*, 1998, **63**, 786–793.

127 R. Wei, C. L. Dickson, D. Uhrín and G. C. Lloyd-Jones, *J. Org. Chem.*, 2021, **86**, 9023–9029.

128 R. Rey-Rodriguez, P. Retailleau, P. Bonnet and I. Gillaizeau, *Chem. Eur. J.*, 2015, **21**, 3572–3575.

129 Y. Li, R. J. Vaz, S. H. Olson, M. Munson, N. A. Paras and J. Conrad, *European J. Org. Chem.*, 2020, **2020**, 5828–5832.

130 C. C. Le, M. K. Wismer, Z. C. Shi, R. Zhang, D. V. Conway, G. Li, P. Vachal, I. W. Davies and D. W. C. MacMillan, *ACS Cent. Sci.*, 2017, **3**, 647–653.

131 T. D. Svejstrup, A. Chatterjee, D. Schekin, T. Wagner, J. Zach, M. J. Johansson, G. Bergonzini and B. König, *ChemPhotoChem*, 2021, **5**, 808–814.

132 D. A. Nagib and D. W. C. MacMillan, *Nature*, 2011, **480**, 224–228.

133 STREM in collaboration with HepatoChem, EvoluChem ™ PhotoRedOx Products, https://www.strem.com/uploads/resources/documents/evoluchem_photoredox_products_copy1.pdf, (accessed 11 November 2023).

134 E. Calce, R. M. Vitale, A. Scaloni, P. Amodeo and S. De Luca, *Amino Acids*, 2015, **47**, 1507–1515.

135 C. M. Alder, J. D. Hayler, R. K. Henderson, A. M. Redman, L. Shukla, L. E. Shuster and H. F. Sneddon, *Green Chem.*, 2016, **18**, 3879–3890.

136 Y. Yu, J. Wang, Q. Shao, J. Shi and W. Zhu, *Sci. Rep.*, 2016, **6**, 19500.

137 M. Quevedo, H. P. Karbstein and M. A. Emin, *Food Hydrocoll.*, 2021,

118, 106745.

138 M. K. Etherington, N. A. Kukhta, H. F. Higginbotham, A. Danos, A. N. Bismillah, D. R. Graves, P. R. McGonigal, N. Haase, A. Morherr, A. S. Batsanov, C. Pflumm, V. Bhalla, M. R. Bryce and A. P. Monkman, *J. Phys. Chem. C. Nanomater. Interfaces*, 2019, **123**, 11109–11117.

139 A. Vega-Peñaloza, J. Mateos, X. Companyó, M. Escudero-Casao and L. Dell'Amico, *Angew. Chemie Int. Ed.*, 2021, **60**, 1082–1097.

140 K. C. Harper, E. G. Moschetta, S. V. Bordawekar and S. J. Wittenberger, *ACS Cent. Sci.*, 2019, **5**, 109–115.

141 M. Zhou, C. Ni, Z. He and J. Hu, *Org. Lett.*, 2016, **18**, 3754–3757.

142 P. L. da Silva, L. Guimarães and J. R. J. Pliego, *J. Phys. Chem. B*, 2013, **117**, 6487–6497.

143 J. W. Beatty and C. R. J. Stephenson, *Acc. Chem. Res.*, 2015, **48**, 1474–1484.

144 Y. Kwon, J. Lee, Y. Noh, D. Kim, Y. Lee, C. Yu, J. C. Roldao, S. Feng, J. Gierschner, R. Wannemacher and M. S. Kwon, *Nat. Commun.*, 2023, **14**, 92.

145 M. Chakraborty and A. K. Panda, *Spectrochim. Acta Part A Mol. Biomol. Spectrosc.*, 2011, **81**, 458–465.

146 C. K. Prier, D. A. Rankic and D. W. C. MacMillan, *Chem. Rev.*, 2013, **113**, 5322–5363.

147 N. A. Romero and D. A. Nicewicz, *Chem. Rev.*, 2016, 116.

148 J. Yang, B. Sun, H. Ding, P.-Y. Huang, X.-L. Tang, R.-C. Shi, Z.-Y. Yan, C.-M. Yu and C. Jin, *Green Chem.*, 2021, **23**, 575–581.

149 F. M. Veronese and G. Pasut, *Drug Discov. Today*, 2005, **10**, 1451–1458.

150 A. A. H. Ahmad Fuaad, F. Azmi, M. Skwarczynski and I. Toth, *Molecules*, 2013, **18**, 13148–13174.

151 M. S. Kang, T. W. S. Kong, J. Y. X. Khoo and T.-P. Loh, *Chem. Sci.*,

2021, **12**, 13613–13647.

152 H. Morimoto, R. Fujiwara, Y. Shimizu, K. Morisaki and T. Ohshima, *Org. Lett.*, 2014, **16**, 2018–2021.

153 W. X. Ren, J. Han, S. Uhm, Y. J. Jang, C. Kang, J. H. Kim and J. S. Kim, *Chem. Commun.*, 2015, **51**, 10403–10418.

154 M. Tsushima, S. Sato and H. Nakamura, *Chem. Commun.*, 2017, **53**, 4838–4841.

155 L. Biancalana, L. K. Batchelor, S. A. P. Pereira, P. J. Tseng, S. Zacchini, G. Pampaloni, L. M. F. S. Saraiva, P. J. Dyson and F. Marchetti, *Chem. Eur. J.*, 2020, **26**, 17525–17535.

156 R. C. Griffiths, F. R. Smith, J. E. Long, H. E. L. Williams, R. Layfield and N. J. Mitchell, *Angew. Chemie Int. Ed.*, 2020, **59**, 23659–23667.

157 J. Z. Wang Ru-Yan; Wang, Ya-Cong; Chen, Xiang-Zhao; Yin, Xu-Guang; Du, Jing-Jing; Lei, Ze; Xin, Ling-Ming; Gao, Xiao-Fei; Liu, Zheng; Guo, Jun, *Synlett*, 2017, **28**, 1934–1938.

158 M. K. O'Reilly, B. E. Collins, S. Han, L. Liao, C. Rillahan, P. I. Kitov, D. R. Bundle and J. C. Paulson, *J. Am. Chem. Soc.*, 2008, **130**, 7736–7745.

159 A. Biffis, P. Centomo, A. Del Zotto and M. Zecca, *Chem. Rev.*, 2018, **118**, 2249–2295.

160 C.-J. Wallentin, J. D. Nguyen, P. Finkbeiner and C. R. J. Stephenson, *J. Am. Chem. Soc.*, 2012, **134**, 8875–8884.

161 P. J. Czerwiński, B. Grzeszczyk and B. Furman, *Org. Lett.*, 2022, **24**, 9269–9274.

162 L. Wang, X.-J. Wei, W.-L. Jia, J.-J. Zhong, L.-Z. Wu and Q. Liu, *Org. Lett.*, 2014, **16**, 5842–5845.

163 M. C. Pirrung, ed. M. C. B. T.-H. of S. O. C. (Second E. Pirrung, Academic Press, 2017, pp. 35–54.

164 A. L. J. Beckwith and J. S. Poole, *J. Am. Chem. Soc.*, 2002, **124**, 9489–9497.

165 J. Q. Wu, I. Beranek and H. Fischer, *Helv. Chim. Acta*, 1995, **78**, 194–214.

166 K. Héberger and H. Fischer, *Int. J. Chem. Kinet.*, 1993, **25**, 913–920.

167 M. Salamone, G. A. DiLabio and M. Bietti, *J. Org. Chem.*, 2012, **77**, 10479–10487.

168 F. Tureček and E. A. Syrstad, *J. Am. Chem. Soc.*, 2003, **125**, 3353–3369.

169 D. B. McConnell, *J. Med. Chem.*, 2021, **64**, 16319–16327.

170 N. Elgrishi, K. J. Rountree, B. D. McCarthy, E. S. Rountree, T. T. Eisenhart and J. L. Dempsey, *J. Chem. Educ.*, 2018, **95**, 197–206.

171 M. Tariq, 2020, **234**, 295–312.

172 N. Elgrishi, K. J. Rountree, B. D. McCarthy, E. S. Rountree, T. T. Eisenhart and J. L. Dempsey, *J. Chem. Educ.*, 2018, **95**, 197–206.

173 H. Liang, G.-Q. Xu, Z.-T. Feng, Z.-Y. Wang and P.-F. Xu, *J. Org. Chem.*, 2019, **84**, 60–72.

174 V. V Pavlishchuk and A. W. Addison, *Inorganica Chim. Acta*, 2000, **298**, 97–102.

175 Y.-N. Zhao, Y.-C. Luo, Z.-Y. Wang and P.-F. Xu, *Chem. Commun.*, 2018, **54**, 3993–3996.

176 D. Song, C.-M. Wang, Z.-P. Ye, P.-J. Xia, Z.-X. Deng, J.-A. Xiao, H.-Y. Xiang and H. Yang, *J. Org. Chem.*, 2019, **84**, 7480–7487.

177 J.-J. Zhong, C. Yang, X.-Y. Chang, C. Zou, W. Lu and C.-M. Che, *Chem. Commun.*, 2017, **53**, 8948–8951.

178 S. Minakata, S. Manabe, Y. Inai, M. Ikezaki, K. Nishitsuji, Y. Ito and Y. Ihara, *Molecules*, 2021, **26**, 5258.

179 Anasazi instruments, How to Reduce 1H NMR – Quantitative Evaluation Errors, https://www.aiinmr.com/nmr-spectroscopy-articles-case-studies/how-to-reduce-1h-nmr-quantitative-evaluation-errors, (accessed 9 November 2023).

180 A. A. Morgan and Edward Rubenstein, *PLoS One*, 2013, **8**, 1–9.

181 S. De, A. Kumar S K, S. K. Shah, S. Kazi, N. Sarkar, S. Banerjee and S. Dey, *RSC Adv.*, 2022, **12**, 15385–15406.

182 L. Dicks and D. J. Wales, *J. Phys. Chem. B*, 2022, **126**, 8381–8390.

183 J. R. Engen, *Anal. Chem.*, 2009, **81**, 7870–7875.

184 H. Tagawa, K. Maruyama, K. Sasaki, N. Konoue, A. Kishimura, M. Kanai, T. Mori, K. Oisaki and Y. Katayama, *RSC Adv.*, 2020, **10**, 16727–16731.

185 G. R. Stark, I. M. Kerr, B. R. Williams, R. H. Silverman and R. D. Schreiber, *Annu. Rev. Biochem.*, 1998, **67**, 227–264.

186 S. Foser, A. Schacher, K. A. Weyer, D. Brugger, E. Dietel, S. Marti and T. Schreitmüller, *Protein Expr. Purif.*, 2003, **30**, 78–87.

187 T. Yamaoka, Y. Tabata and Y. Ikada, *J. Pharm. Sci.*, 1994, **83**, 601–606.

188 A. Cieślińska, E. Fiedorowicz, D. Rozmus, E. Sienkiewicz-Szłapka, B. Jarmołowska and S. Kamiński, *Int. J. Mol. Sci.*, 2022, **23**, 15637.

189 M. Li, R. Fokkink, Y. Ni and J. M. Kleijn, *Food Hydrocoll.*, 2019, **96**, 653–662.

190 J. M. van der Schaaf, S. V Crowley, A. L. Kelly and J. A. O'Mahony, eds. P. L. H. McSweeney and J. P. B. T.-E. of D. S. (Third E. McNamara, Academic Press, Oxford, 2022, pp. 31–39.

191 A. P. Golovanov, G. M. Hautbergue, S. A. Wilson and L.-Y. Lian, *J. Am. Chem. Soc.*, 2004, **126**, 8933–8939.

192 N. G. Sharaf and A. M. Gronenborn, in *Isotope Labeling of Biomolecules - Labeling Methods*, ed. Z. B. T.-M. in E. Kelman, Academic Press, 2015, vol. 565, pp. 67–95.

193 M. D. Shortridge, D. S. Hage, G. S. Harbison and R. Powers, *J. Comb. Chem.*, 2008, **10**, 948–958.

194 A.-N. Neagu, M. Jayathirtha, E. Baxter, M. Donnelly, B. A. Petre and

C. C. Darie, *Molecules*, 2022, **27**, 2411.

195 K. Beck and B. Brodsky, *J. Struct. Biol.*, 1998, **122**, 17–29.

196 P. C. Lyu, J. C. Sherman, A. Chen and N. R. Kallenbach, *Proc. Natl. Acad. Sci. U. S. A.*, 1991, **88**, 5317–5320.

197 M. A. Danielson and J. J. Falke, *Annu. Rev. Biophys. Biomol. Struct.*, 1996, **25**, 163–195.

198 D. P. Frueh, *Prog. Nucl. Magn. Reson. Spectrosc.*, 2014, **78**, 47–75.

199 N. K. Bordeerat, N. I. Georgieva, D. G. Klapper, L. B. Collins, T. J. Cross, C. H. Borchers, J. A. Swenberg and G. Boysen, *Proteomics*, 2009, **9**, 3939–3944.

200 N. J. Greenfield, *Nat. Protoc.*, 2006, **1**, 2876–2890.

201 Y. Wei, A. Thyparambil and R. Latour, *Biochim. Biophys. Acta*, 2014, **1844**, 2331–2337.

202 M. Zhang, J. Zhao and J. Zheng, *Soft Matter*, 2014, **10**, 7425–7451.

203 A. Del Giudice, A. Rüter, N. V. Pavel, L. Galantini and U. Olsson, *Langmuir*, 2020, **36**, 8451–8460.

204 M. A. Battiste, P. M. Pelphrey and D. L. Wright, *Chem. Eur. J.*, 2006, **12**, 3438–3447.

205 R. Guttmann and A. F. Sax, *ChemistryOpen*, 2017, **6**, 571–584.

206 H. Barsnes and M. Vaudel, *J. Proteome Res.*, 2018, **17**, 2552–2555.

207 M. Vaudel, J. M. Burkhart, R. P. Zahedi, E. Oveland, F. S. Berven, A. Sickmann, L. Martens and H. Barsnes, *Nat. Biotechnol.*, 2015, 33, 22–24.

208 J. R. Spies, *J. Am. Chem. Soc.*, 1948, **70**, 3717–3719.

209 I. Karlsson, E. Persson, A. Ekebergh, J. Mårtensson and A. Börje, *Chem. Res. Toxicol.*, 2014, **27**, 1294–1303.

210 Y. Lv, W. Pu, Q. Chen, Q. Wang, J. Niu and Q. Zhang, *J. Org. Chem.*, 2017, **82**, 8282–8289.

211 T. Huppertz, P. F. Fox and A. L. Kelly, in *Woodhead Publishing Series in Food Science, Technology and Nutrition*, ed. R. Y. B. T.-P. in F. P. (Second E. Yada, Woodhead Publishing, 2018, pp. 49–92.

8 Appendix

OL | Organic Letters

pubs.acs.org/OrgLett

Letter

Chemoselective Late-Stage Functionalization of Peptides via Photocatalytic C2-Alkylation of Tryptophan

Published as part of the Organic Letters virtual special issue "Chemoselective Methods for Labeling and Modification of Peptides and Proteins".

Joanna C. Lee, James D. Cuthbertson,* and Nicholas J. Mitchell*

Cite This: *Org. Lett.* 2023, 25, 5459−5464

Read Online

ACCESS | Metrics & More | Article Recommendations | Supporting Information

ABSTRACT: Across eukaryotic proteomes, tryptophan is the least abundant of the 20 canonical amino acids, which makes it an ideal chemical handle for the late-stage functionalization of peptide and protein scaffolds with minimal production of undesired isoforms. Herein, we report the photocatalytic C2-alkylation of tryptophan using bromodifluoroacetate/acetamide-derived radical precursors. This rapid visible-light-mediated reaction is additive-free, operationally simple, and tolerates diverse functionality. We demonstrate the late-stage modification of a variety of complex peptides, including examples of biological significance.

Chemistry that targets the canonical amino acids enables the late-stage functionalization of peptides and the site-selective modification of proteins.[1−3] Such techniques facilitate the installation of groups to modulate the activity and/or stability of polypeptide tools and therapeutics.[4] An extensive array of reactions has been developed to target the canonical amino acids.[5] The majority of these chemoselective methods focus on the amino acids lysine (Lys)[1] or cysteine (Cys)[6,7] due to the inherent nucleophilicity of their side chain functional groups. While reactions selective for alternative amino acids have been developed, many of these are less effective on (or cannot be applied to) complex peptides and proteins.[5]

Key considerations when developing methods that target the canonical residues include the inherent reactivity of the side chain and relative proteinogenic abundance of the residue. A broad reactivity profile allows for the application of milder and more varied methods of functionalization, thereby facilitating the development of chemoselective chemistry that is likely to be effective on large and complex peptides and proteins. Techniques that target residues with higher natural abundance, such as Lys, often produce multiple isoforms, which can be challenging to separate from the desired product in larger polypeptide systems. Because of the inherent reactivity of its electron-rich indole side chain and its low natural abundance, tryptophan (Trp) is an ideal proteinogenic chemical handle. This residue accounts for just 1.1% of eukaryotic proteomes,[8] the lowest of the 20 canonical amino acids. Thus, the sequence of any given target protein is likely to have no more than one Trp residue. If the protein target does not contain this amino acid, then a non-native Trp mutant can be recombinantly expressed.

Previous efforts to target this residue draw on the wealth of indole chemistry reported in the literature. A significant amount of work has focused on transition metal (TM)-catalyzed C−H activation of Trp, including rhodium,[9−11] manganese,[12,13] and ruthenium[14,15] C2-alkylation; palladium-catalyzed C2-arylation[16−19] and peptide olefination;[20] gold-catalyzed C2-ethynylation;[21] and palladium/cobalt-catalyzed macrocyclization.[22−24] Metal-free strategies toward C2-sulfenylation,[25] trifluoromethylation,[26,27] and arylation[28] have also been explored, as well as the modification of Trp using persistent radical traps.[29] Over the past decade, photocatalytic C−H functionalization has come to the forefront in this field.[30,31] Many of these methods have achieved greater success when applied to the functionalization of complex peptides and proteins compared with transition-metal-catalyzed approaches. Examples include alkylation at the C2[32] and β-positions of Trp.[33] More recently, electron donor−acceptor (EDA) pyridinium salts have been applied to great effect to target Trp in both peptides and proteins.[34−36]

In 2014, Cho et al. reported a method for the photocatalytic difluoroalkylation of aromatic and heteroaromatic compounds, which included two examples of indole C2-alkylation (Figure 1A).[37] Considering the success of photocatalytic methods in this field and the advantages of utilizing Trp as a chemical

Received: June 1, 2023
Published: July 18, 2023

ACS Publications

© 2023 The Authors. Published by American Chemical Society

https://doi.org/10.1021/acs.orglett.3c01795
Org. Lett. 2023, 25, 5459−5464

Downloaded via 92.28.149.64 on November 18, 2023 at 19:33:59 (UTC).
See https://pubs.acs.org/sharingguidelines for options on how to legitimately share published articles.

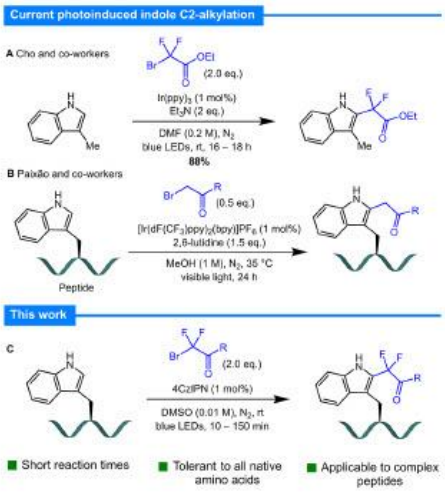

Figure 1. Selected photocatalytic methods for C2-alkylation of indole/tryptophan.

handle, we reasoned that photocatalytic C2-alkylation could potentially be leveraged as an effective peptide modification strategy. During the course of our studies, Paixão and co-workers reported a similar photocatalytic method for Trp C2-alkylation using α-bromo carbonyl compounds (Figure 1B).[38] However, despite the utility of Paixão et al.'s method, their chemistry relies on a precious metal photocatalyst and requires extended reaction times (24 h), as well as an additive (2,6-lutidine). In order to broaden the scope and extend the applications of Trp C2-alkylation as a bioconjugation strategy, we sought to develop a method that overcomes these limitations. Herein, we report the development of a mild and operationally simple strategy using electron-deficient radicals[39] for the late-stage alkylation of Trp-containing biomolecules that achieves these goals (Figure 1C). The reaction tolerates diverse functionalities and can be applied to complex peptides. Furthermore, the incorporation of a difluoroalkyl moiety enables the modulation of key physicochemical properties that impact the pharmacokinetics of the molecule and allows the progression and conversion of the reaction to be accurately quantified by ^{19}F NMR spectroscopy.

We initially chose to explore the radical functionalization of amino acid Ac-Trp-OEt (**1**) using ethyl bromodifluoroacetate (**2a**) as the radical precursor; irradiation was achieved using a PhotoRedOx Box (Hepatochem) equipped with a 34 mW cm^{-2} LED 450 nm bulb. Reactions run under the conditions reported by the Cho group {0.25 M in DMF, 1 mol % *fac*-[Ir(ppy)$_3$], 2 equiv of TEA, blue LEDs[37]} afforded 30% yield by ^{19}F NMR over a 17 h period. Following optimization, we identified suitable conditions using the organic photocatalyst 4-CzIPN [1,2,3,5-tetrakis(carbazol-9-yl)-4,6-dicyanobenzene 2,4,5,6-tetrakis(9*H*-carbazol-9-yl) isophthalonitrile][40] in DMSO (Table 1, entry 1). Pleasingly, under these conditions, near-complete consumption of starting amino acid **1** was observed (via analytical HPLC) within 10 min. The product

Table 1. Optimization Studies and Control Reactions[a]

entry	deviation from standard conditions	% yield[b]
1	none	71
2	aerobic	61
3	DMF	61
4	MeCN	23
5	DMSO:H_2O (9:1)	71
6	DMSO:H_2O (1:1)	2
7	DMSO (0.25 M)	45[c]
8	Ir(ppy)$_3$	56
9	blue LED strip -60 min	53
10	60 min	45
11	0.2 mmol "scale-up"	65 [64[d]]
12	no PC/no light	0

[a]Reactions performed under a nitrogen atmosphere on a 60.0 μmol scale. [b]Yield of product 3a determined by ^{19}F NMR spectroscopy using α,α,α-trifluorotoluene as the internal standard. [c]60 min, 120 μmol scale. [d]Isolated yield.

was obtained in 71% yield, as determined by ^{19}F NMR spectroscopy. Interestingly, stirring was found to have no impact on the reaction and, in some early studies, even resulted in reduced yields because of the formation of a greater proportion of side products; thus, all further reactions were carried out without agitation. Running the reaction under an atmosphere of air gave similar results to an inert atmosphere, highlighting the robustness of the chemistry (Table 1, entry 2). However, to avoid undesired oxidation of residues, such as Cys and methionine (Met), in more complex starting materials, an inert atmosphere was preferred. The reaction was observed to proceed similarly when run in DMF (Table 1, entry 3); however, running the reaction in MeCN severely affected the conversion, with a significant proportion of starting material **1** left unreacted after 10 min (Table 1, entry 4). The reaction tolerates an organic/aqueous solvent mixture up to 10% aqueous (Table 1, entry 5). However, increasing the amount of water further (50% aqueous DMSO) resulted in minimal product formation (Table 1, entry 6). Increasing the concentration of the reaction from 0.01 to 0.25 M reduced the yield to 8% after 10 min and 45% after 60 min with approximately 1 equiv. of **2a** left unreacted (Table 1, entry 7). Switching to an iridium(III) photocatalyst [Ir(ppy)$_3$] decreased the yield of the reaction (Table 1, entry 8). The use of inexpensive, lower intensity blue LED strips in place of the PhotoRedOx Box resulted in a lower yield and an increase in reaction time (Table 1, entry 9). Leaving the reaction for longer durations (60 min) resulted in a lower yield because of the formation of undesired side products (overalkylation of the indole ring, Table 1, entry 10). Scale-up of the reaction from 60 μmol of amino acid **1** to 0.2 mmol had a negligible effect on the yield of product **3a** (Table 1, entry 11). Following isolation and purification by flash chromatography, the desired product was obtained in a yield that was comparable with the yield determined spectroscopically. Finally, it was confirmed that the

https://doi.org/10.1021/acs.orglett.3c01795
Org. Lett. 2023, 25, 5459−5464

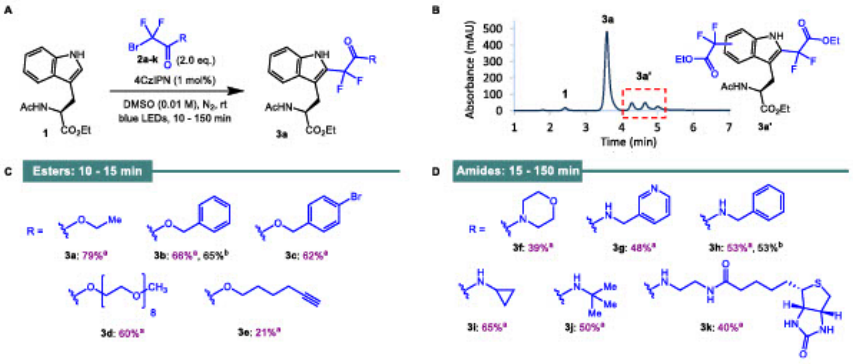

Figure 2. Photochemical alkylation of Ac-Trp-OEt **1**. (A) Reactions performed on a 20.0 μmol scale. [a]Yields were determined by ^{19}F NMR spectroscopy using α,α,α-trifluorotoluene as the internal standard. [b]Isolated yield was on a 200 μmol scale. (B) Analytical HPLC chromatogram of the crude reaction mixture for the photochemical alkylation of Ac-Trp-OEt **1** using probe **2a** (40–80% gradient over 5 min). (C) Ester series of products produced using standard conditions. (D) Amide series of products produced using standard conditions.

reaction does not proceed in the absence of photocatalyst or light (Table 1, entry 12).

With optimized conditions in hand, we sought to explore the scope of the alkylating agent **2**. Several bromodifluoroacetates (**2b–e**) and bromodifluoroacetamides (**2f–l**) carrying a range of sterically and electronically different groups, including aliphatic, aromatic, cyclic, and heterocyclic moieties, were prepared [Figure 2, see the Supporting Information (SI) for experimental details]. Radical precursors bearing functionality applicable within the context of chemical biology, such as a PEG chain, an alkyne, a biotin reporter tag, and a sugar moiety, were included in this series. Applying the standard conditions developed for bromide **2a**, we repeated the reaction using these compounds to alkylate amino acid **1** (Figure 2A). The "*esterseries*" of radical precursors (**2a–d**) gave the product in yields ranging from 60 to 79% (**3a–d**), as determined by ^{19}F NMR spectroscopy. Reaction monitoring via analytical HPLC indicated that the reactions were very close to completion within 10–15 min for this series. Past this time point range, further undesired overalkylation of the indole was observed, which resulted in lower yields (Figure 2B). Notably, the reaction using radical precursor **2e** bearing an alkyne group gave a lower yield (21%), even after extended reaction times, which was attributed to undesired radical addition to the alkyne. The "*amide series*" of radical precursors gave yields from 39 to 65% as determined by ^{19}F NMR spectroscopy (**3f–k**). Reaction monitoring indicated that the reactions were complete within 15–150 min. The reactions with benzyl derivatives **2b** and **2h** were repeated on a larger scale (0.2 mmol) to enable isolation and full characterization of the products. Both **3b** and **3h** were isolated in the same yields as those determined by ^{19}F NMR spectroscopy for the smaller-scale reactions.

Having investigated how the steric and electronic properties of alkylating agent **2** govern reactivity, we progressed on to an assessment of our strategy on complex peptides. The sequence Ac-WHISKEY-NH_2 **4** was synthesized via Fmoc-SPPS (solid-phase peptide synthesis). Carrying the majority of proteinogenic chemical functionality displayed across the proteome, this model enables a thorough interrogation of the tolerance and chemoselectivity of our reaction (Figure 3). The standard conditions optimized for Ac-Trp-OEt (**1**) were applied to peptide **4** (5 μmol) using radical precursor **2a**. HPLC analysis revealed that the reaction was complete within 10 min; product **5a** was obtained in 55% yield, as determined by quantitative ^{19}F NMR spectroscopy. Following purification by preparative RP-HPLC, the product was isolated in 43% yield. Characterization of the product by ^{1}H NMR spectroscopy confirmed selective functionalization of Trp, as evidenced by the disappearance of the C2 proton signal.

The reaction was repeated with the remaining ester-derived radical precursors (**2b–d**) affording yields in the range 42–43% (**5b–d**) with comparable isolated yields. The hexyne radical precursor (**2e**) again gave a lower yield (**5e**) with a comparable isolated yield (17%). The *amide series* (**2f–l**), including the *N*-acetylglucosamine (GlcNAc) radical precursor acetamide, **2l**, employed to explore C2-glycosylation, afforded yields in the range 19–35% (**5f–l**), with the isolated yields mirroring the yields determined spectroscopically. Analysis of the crude reaction mixtures for the *amide series* showed the generation of a greater proportion of alkylated side-products compared with the *ester series* compounds (Figure 3A). However, by monitoring the reaction (HPLC) and controlling the end point, overalkylation of the indole could be minimized. While these yields are lower than those acquired for the functionalization of Ac-Trp-OEt (**1**), they do demonstrate rapid and chemoselective alkylation of Trp on a complex polypeptide. Importantly, when the substrate Ac-HISKEY-NH_2 **6** (with the Trp residue omitted) was exposed to the reaction conditions, no undesired modification of the alternative amino acids was observed.

Encouraged by these results, we prepared model peptides **7–9** to probe the reaction in the presence of a free N-terminus and carboxy C-terminus (**7**; H-WHISKEY-OH), a Cys residue (**8**; Ac-CWHISKEY-NH_2), and additional canonical amino acids with untested reactive functionality (**9**; Ac-WFMTREY-NH_2). The reaction of these models with radical precursor **2a** was undertaken, and yields similar to those observed for peptide **4** were confirmed (**13–15**; Figure 3B). In all cases these translated into comparable isolated yields. In addition to

https://doi.org/10.1021/acs.orglett.3c01795
Org. Lett. 2023, 25, 5459−5464

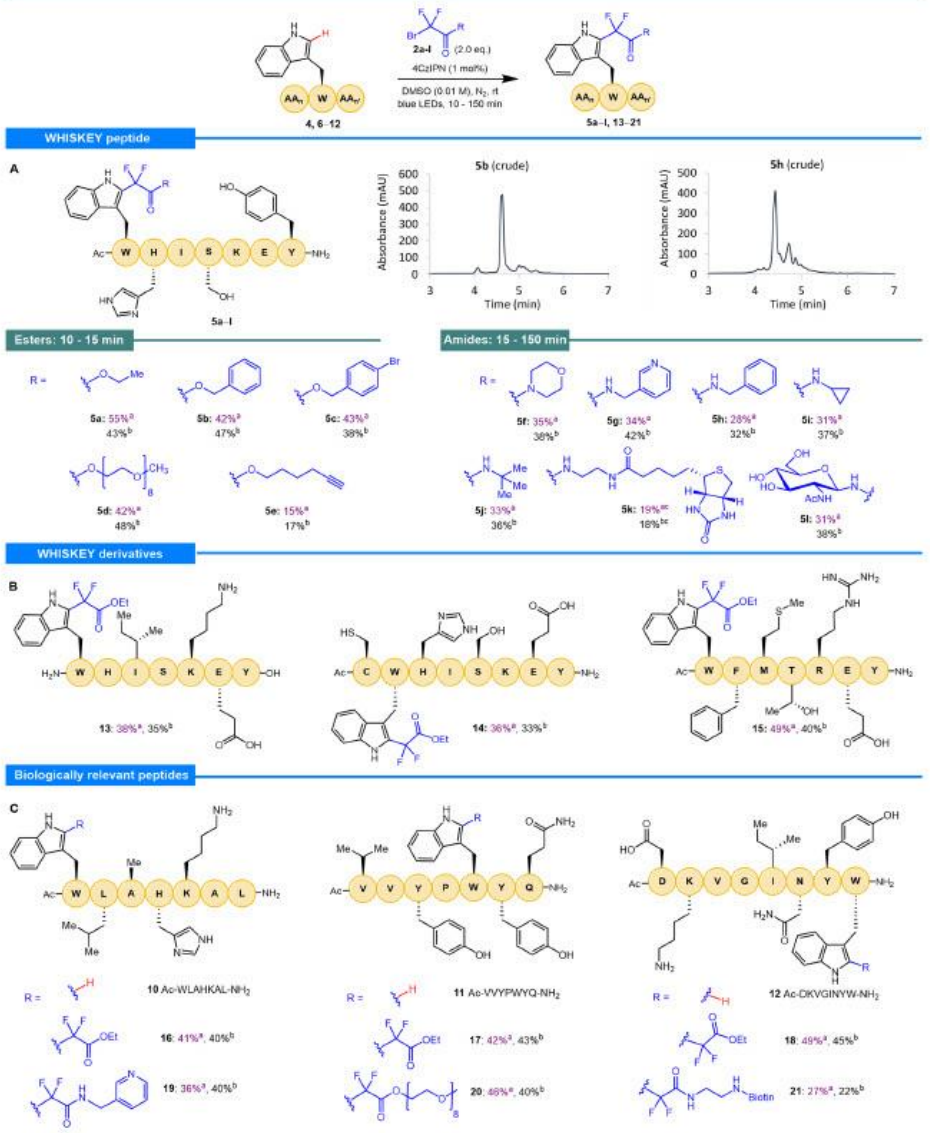

Figure 3. (A–C) Photochemical chemoselective alkylation of Trp-containing peptides (4, 6–12); reactions performed on a 5.00 μmol scale. [a]Yields determined by ^{19}F NMR spectroscopy using α,α,α-trifluorotoluene as the internal standard. [b]Isolated yields. [c]4CzIPN (5 mol %), bromodifluoroacetamide 2k (1.5 equiv).

these models, peptides 10–12 were synthesized as biologically relevant examples (Figure 3C). Peptide 10 is a dipeptidyl peptidase-4 (DPP-4) inhibitor, and peptides 11 and 12 are angiotensin converting enzyme (ACE) inhibitors. Further-

https://doi.org/10.1021/acs.orglett.3c01795
Org. Lett. 2023, 25, 5459−5464

more, the lone Trp residue in these models is located at different positions in each sequence: N-terminus (**10**), internal (**11**), and C-terminus (**12**), thereby enabling assessment of the effect that the positioning of the Trp residue has on conversion to the product. The reaction of radical precursor **2a** with these sequences under standard conditions gave yields comparable with those of reactions using model peptide **4** (**16**−**18**; Figure 3C). These results suggest that the positioning and local steric and electronic environment surrounding the Trp residue have a negligible effect on the formation of the desired product. Alkylation of the biologically relevant peptides **10**−**12** with radical precursor **2g**, and the more chemically diverse peptides **2d** and **2k**, respectively, was also demonstrated on these models (**19**−**21**; Figure 3C). Pleasingly, the yields were broadly consistent with those achieved using model peptide **4**. The consistency of the yields across the peptide models illustrates the tolerance of this reaction to all proteinogenic functionality.

In conclusion, we have developed a rapid, functional-group-tolerant, and operationally simple photocatalytic difluoroalkylation reaction that enables the chemoselective functionalization of Trp residues in complex peptides. For the majority of the radical precursors explored, the reactions are complete within minutes, regardless of the position of the target residue. The precursors can be readily synthesized using simple, established chemistry, which enables diverse functionality to be introduced into valuable peptide targets at a late stage.

■ ASSOCIATED CONTENT

Data Availability Statement

The data underlying this study are available in the published article and its Supporting Information.

Supporting Information

The Supporting Information is available free of charge at https://pubs.acs.org/doi/10.1021/acs.orglett.3c01795.

Experimental details and full characterization data of all compounds (PDF)

■ AUTHOR INFORMATION

Corresponding Authors

Nicholas J. Mitchell − *School of Chemistry, University of Nottingham, Nottingham NG7 2RD, United Kingdom;* orcid.org/0000-0002-9041-1852; Email: nicholas.mitchell@nottingham.ac.uk

James D. Cuthbertson − *School of Chemistry, University of Nottingham, Nottingham NG7 2RD, United Kingdom; School of Chemistry, GlaxoSmithKline Carbon Neutral Laboratories for Sustainable Chemistry, University of Nottingham, Nottingham NG7 2TU, United Kingdom;* orcid.org/0000-0003-3820-6816; Email: james.cuthbertson@nottingham.ac.uk

Author

Joanna C. Lee − *School of Chemistry, University of Nottingham, Nottingham NG7 2RD, United Kingdom; School of Chemistry, GlaxoSmithKline Carbon Neutral Laboratories for Sustainable Chemistry, University of Nottingham, Nottingham NG7 2TU, United Kingdom*

Complete contact information is available at: https://pubs.acs.org/10.1021/acs.orglett.3c01795

Notes

The authors declare no competing financial interest.

■ ACKNOWLEDGMENTS

The authors gratefully acknowledge funding from the UKRI (EP/S028323/1; EP/S017739/1) and the Royal Society (URF awarded to J.D.C. − UF160532). We gratefully acknowledge the support of the EPSRC through the Centre for Doctoral Training in Sustainable Chemistry (PhD studentship for J.C.L. − EP/L015633/1). We thank Kevin Butler for assistance with NMR analysis, and Ben Pointer-Gleadhill, Cameron Baines and Prof. Neil J. Oldham for assistance with MS analysis.

■ REFERENCES

(1) Boutureira, O.; Bernardes, G. J. L. Advances in chemical protein modification. *Chem. Rev.* **2015**, *115* (5), 2174−2195.

(2) Koniev, O.; Wagner, A. Developments and recent advancements in the field of endogenous amino acid selective bond forming reactions for bioconjugation. *Chem. Soc. Rev.* **2015**, *44* (15), 5495−5551.

(3) Hoyt, E. A.; Cal, P. M. S. D.; Oliveira, B. L.; Bernardes, G. J. L. Contemporary approaches to site-selective protein modification. *Nat. Rev. Chem.* **2019**, *3* (3), 147−171.

(4) Krall, N.; Da Cruz, F. P.; Boutureira, O.; Bernardes, G. J. L. Site-selective protein-modification chemistry for basic biology and drug development. *Nat. Chem.* **2016**, *8* (2), 103−113.

(5) deGruyter, J. N.; Malins, L. R.; Baran, P. S. Residue-specific peptide modification: a chemist's guide. *Biochemistry* **2017**, *56* (30), 3863−3873.

(6) Gunnoo, S. B.; Madder, A. Chemical protein modification through cysteine. *ChemBioChem.* **2016**, *17* (7), 529−553.

(7) Chalker, J. M.; Bernardes, G. J. L.; Lin, Y. A.; Davis, B. G. Chemical modification of proteins at cysteine: opportunities in chemistry and biology. *Chem.—Asian J.* **2009**, *4* (5), 630−640.

(8) Gilis, D.; Massar, S.; Cerf, N. J.; Rooman, M. Optimality of the genetic code with respect to protein stability and amino-acid frequencies. *Genome Biol.* **2001**, *2*, research0049.1.

(9) Antos, J. M.; McFarland, J. M.; Iavarone, A. T.; Francis, M. B. Chemoselective tryptophan labeling with rhodium carbenoids at mild pH. *J. Am. Chem. Soc.* **2009**, *131* (17), 6301−6308.

(10) Antos, J. M.; Francis, M. B. Selective tryptophan modification with rhodium carbenoids in aqueous solution. *J. Am. Chem. Soc.* **2004**, *126* (33), 10256−10257.

(11) Popp, B. V.; Ball, Z. T. Structure-selective modification of aromatic side chains with dirhodium metallopeptide catalysts. *J. Am. Chem. Soc.* **2010**, *132* (19), 6660−6662.

(12) Ruan, Z.; Sauermann, N.; Manoni, E.; Ackermann, L. Manganese-Catalyzed C-H Alkynylation: Expedient Peptide Synthesis and Modification. *Angew. Chem., Int. Ed.* **2017**, *56* (12), 3172−3176.

(13) Kaplaneris, N.; Rogge, T.; Yin, R.; Wang, H.; Sirvinskaite, G.; Ackermann, L. Late-Stage Diversification through Manganese-Catalyzed C-H Activation: Access to Acyclic, Hybrid, and Stapled Peptides. *Angew. Chem., Int. Ed.* **2019**, *58* (11), 3476−3480.

(14) Schischko, A.; Ren, H.; Kaplaneris, N.; Ackermann, L. Bioorthogonal Diversification of Peptides through Selective Ruthenium (II)-Catalyzed C-H Activation. *Angew. Chem., Int. Ed.* **2017**, *56* (6), 1576−1580.

(15) Schischko, A.; Kaplaneris, N.; Rogge, T.; Sirvinskaite, G.; Son, J.; Ackermann, L. Late-stage peptide C-H alkylation for bioorthogonal C-H activation featuring solid phase peptide synthesis. *Nat. Commun.* **2019**, *10* (1), 3553.

(16) Ruiz-Rodríguez, J.; Albericio, F.; Lavilla, R. Postsynthetic modification of peptides: chemoselective C-arylation of tryptophan residues. *Chem.—Eur. J.* **2010**, *16* (4), 1124−1127.

(17) Reay, A. J.; Williams, T. J.; Fairlamb, I. J. S. Unified mild reaction conditions for C2-selective Pd-catalysed tryptophan

arylation, including tryptophan-containing peptides. *Org. Biomol. Chem.* **2015**, *13* (30), 8298−8309.
(18) Zhu, Y.; Bauer, M.; Ackermann, L. Late-Stage Peptide Diversification by Bioorthogonal Catalytic C-H Arylation at 23°C in H_2O. *Chem.—Eur. J.* **2015**, *21* (28), 9980−9983.
(19) Williams, T. J.; Reay, A. J.; Whitwood, A. C.; Fairlamb, I. J. S. A mild and selective Pd-mediated methodology for the synthesis of highly fluorescent 2-arylated tryptophans and tryptophan-containing peptides: a catalytic role for Pd^0 nanoparticles? *Chem. Commun.* **2014**, *50* (23), 3052−3054.
(20) Terrey, M. J.; Holmes, A.; Perry, C. C.; Cross, W. B. C-H olefination of tryptophan residues in peptides: Control of residue selectivity and peptide-amino acid cross-linking. *Org. Lett.* **2019**, *21* (19), 7902−7907.
(21) Hansen, M. B.; Hubálek, F.; Skrydstrup, T.; Hoeg-Jensen, T. Chemo-and regioselective ethynylation of tryptophan-containing peptides and proteins. *Chem.—Eur. J.* **2016**, *22* (5), 1572−1576.
(22) Mendive-Tapia, L.; Preciado, S.; García, J.; Ramón, R.; Kielland, N.; Albericio, F.; Lavilla, R. New peptide architectures through C-H activation stapling between tryptophan-phenylalanine/tyrosine residues. *Nat. Commun.* **2015**, *6* (1), 7160.
(23) Dong, H.; Limberakis, C.; Liras, S.; Price, D.; James, K. Peptidic macrocyclization via palladium-catalyzed chemoselective indole C-2 arylation. *Chem. Commun.* **2012**, *48* (95), 11644−11646.
(24) Lorion, M. M.; Kaplaneris, N.; Son, J.; Kuniyil, R.; Ackermann, L. Late-Stage Peptide Diversification through Cobalt-Catalyzed C-H Activation: Sequential Multicatalysis for Stapled Peptides. *Angew. Chem. Int. Ed.* **2019**, *58* (6), 1684−1688.
(25) Malins, L. R.; Cergol, K. M.; Payne, R. J. Chemoselective sulfenylation and peptide ligation at tryptophan. *Chem. Sci.* **2014**, *5* (1), 260−266.
(26) Imiolek, M.; Karunanithy, G.; Ng, W.-L.; Baldwin, A. J.; Gouverneur, V.; Davis, B. G. Selective radical trifluoromethylation of native residues in proteins. *J. Am. Chem. Soc.* **2018**, *140* (5), 1568−1571.
(27) Rahimidashaghoul, K.; Klimánková, I.; Hubálek, M.; Matoušek, V.; Fílgas, J.; Slavíček, P.; Slanina, T.; Beier, P. Visible-Light-Driven Fluoroalkylation of Tryptophan Residues in Peptides. *ChemPhotoChem.* **2021**, *5* (1), 43−50.
(28) Zhu, Y.; Bauer, M.; Ploog, J.; Ackermann, L. Late-Stage Diversification of Peptides by Metal-Free C-H Arylation. *Chem.—Eur. J.* **2014**, *20* (41), 13099−13102.
(29) Seki, Y.; Ishiyama, T.; Sasaki, D.; Abe, J.; Sohma, Y.; Oisaki, K.; Kanai, M. Transition metal-free tryptophan-selective bioconjugation of proteins. *J. Am. Chem. Soc.* **2016**, *138* (34), 10798−10801.
(30) King, T. A.; Kandemir, J. M.; Walsh, S. J.; Spring, D. R. Photocatalytic methods for amino acid modification. *Chem. Soc. Rev.* **2021**, *50* (1), 39−57.
(31) Bottecchia, C.; Noël, T. Photocatalytic modification of amino acids, peptides, and proteins. *Chem.—Eur. J.* **2019**, *25* (1), 26−42.
(32) Furst, L.; Matsuura, B. S.; Narayanam, J. M. R.; Tucker, J. W.; Stephenson, C. R. J. Visible light-mediated intermolecular C-H functionalization of electron-rich heterocycles with malonates. *Org. Lett.* **2010**, *12* (13), 3104−3107.
(33) Yu, Y.; Zhang, L.-K.; Buevich, A. V.; Li, G.; Tang, H.; Vachal, P.; Colletti, S. L.; Shi, Z.-C. Chemoselective peptide modification via photocatalytic tryptophan β-position conjugation. *J. Am. Chem. Soc.* **2018**, *140* (22), 6797−6800.
(34) Laroche, B.; Tang, X.; Archer, G.; Di Sanza, R.; Melchiorre, P. Photochemical chemoselective alkylation of tryptophan-containing peptides. *Org. Lett.* **2021**, *23* (2), 285−289.
(35) Tower, S. J.; Hetcher, W. J.; Myers, T. E.; Kuehl, N. J.; Taylor, M. T. Selective modification of tryptophan residues in peptides and proteins using a biomimetic electron transfer process. *J. Am. Chem. Soc.* **2020**, *142* (20), 9112−9118.
(36) Hoopes, C. R.; Garcia, F. J.; Sarkar, A. M.; Kuehl, N. J.; Barkan, D. T.; Collins, N. L.; Meister, G. E.; Bramhall, T. R.; Hsu, C.-H.; Jones, M. D.; Schirle, M.; Taylor, M. T. Donor-Acceptor Pyridinium Salts for Photo-Induced Electron-Transfer-Driven Modification of Tryptophan in Peptides, Proteins, and Proteomes Using Visible Light. *J. Am. Chem. Soc.* **2022**, *144* (14), 6227−6236.
(37) Jung, J.; Kim, E.; You, Y.; Cho, E. J. Visible Light-Induced Aromatic Difluoroalkylation. *Adv. Synth. Catal.* **2014**, *356* (13), 2741−2748.
(38) Lima, R. N.; Delgado, J. A. C.; Bernardi, D. I.; Berlinck, R. G. S.; Kaplaneris, N.; Ackermann, L.; Paixão, M. W. Post-synthetic functionalization of tryptophan protected peptide sequences through indole (C-2) photocatalytic alkylation. *Chem. Commun.* **2021**, *57* (47), 5758−5761.
(39) Li, Y.; Vaz, R. J.; Olson, S. H.; Munson, M.; Paras, N. A.; Conrad, J. Selectivity in the Addition of Electron-Deficient Radicals to the C2 Position of Indoles. *Eur. J. Org. Chem.* **2020**, *2020* (36), 5828−5832.
(40) Shang, T.-Y.; Lu, L.-H.; Cao, Z.; Liu, Y.; He, W.-M.; Yu, B. Recent advances of 1, 2, 3, 5-tetrakis (carbazol-9-yl)-4, 6-dicyanobenzene (4CzIPN) in photocatalytic transformations. *Chem. Commun.* **2019**, *55* (38), 5408−5419.

https://doi.org/10.1021/acs.orglett.3c01795
Org. Lett. 2023, 25, 5459−5464